



UNIVERSIDADE DE BRASÍLIA
INSTITUTO DE GEOCIÊNCIAS

DEPARTAMENTO DE MINERALOGIA E PETROLOGIA

TESE DE DOUTORADO

Nº 083

**PETROGÊNESE E EVOLUÇÃO DO OFIOLITO DE ABURRÁ,
CORDILHEIRA CENTRAL DOS ANDES COLOMBIANOS**

Autora:
ANA MARÍA CORREA MARTÍNEZ

Orientador:
Prof. Dr. Aripílínio A. Nilson

Co-orientador:
Prof. Dr. Márcio M. Pimentel

Brasília-DF
Dezembro de 2007



**UNIVERSIDADE DE BRASÍLIA
INSTITUTO DE GEOCIÊNCIAS**

DEPARTAMENTO DE MINERALOGIA E PETROLOGIA

**TESE DE DOUTORADO
Nº 083**

**PETROGÊNESE E EVOLUÇÃO DO OFIOLITO DE ABURRÁ,
CORDILHEIRA CENTRAL DOS ANDES COLOMBIANOS**

Autora:
ANA MARÍA CORREA MARTÍNEZ

Tese de Doutorado apresentada em 17 de dezembro de 2007, visando a obtenção do grau de Doutor em Mineralogia e Petrologia pelo Programa de Pós-Graduação em Geologia da UnB.

Comissão Examinadora:

Prof. Dr. Márcio M. Pimentel (UnB, Co-orientador)
Prof. Dr. Hardy Jost (UnB)
Prof. Dr. Reinhardt Adolfo Fuck (UnB)
Profa. Dra. Maria da Glória da Silva (UFBA)
Prof. Dr. Umberto G. Cordani (USP)

Brasília-DF/ Dezembro de 2007

ÍNDICE

Agradecimentos	vi
Resumo.....	viii
Abstract.....	xi
Capítulo 1.- Introdução.....	1
1.1 Apresentação.....	1
1.2 . Localização.....	3
1.3 .Objetivos.....	3
1.4 Métodos de trabalho.....	4
1.4.1 Petrografia.....	4
1.4.2 Análises químicas de minerais por microssonda electrônica.....	4
1.4.3 Pulverização de amostras e separação de minerais.....	5
1.4.4 Análises químicas de rocha.....	5
1.4.5 Geoquímica isotópica Sr-Nd.....	6
1.4.6 Geocronologia U-Pb.....	6
1.4.7 Análises Isotópicas Re-Os.....	7
1.5 Revisão temática sobre ofiolitos.....	7
1.6 Contexto geológico.....	11
1.6.1 Arcabouço geotectonico das Cordilheiras Central e Ocidental.....	12
Complexo Polimetamórfico da Cordilheira Central.....	12
Corpos intrusivos.....	15
1.6.2 Associações de rochas máficas e ultramáficas oceânicas nos Andes Colombianos	15
1.6.2.1 Associações máficas-ultramáficas a oeste da falha Cauca-Almaguer....	15
Província Litosférica Oceânica Cretácea Ocidental.....	16
1.6.2.2 Associações máficas-ultramáficas a leste da falha Cauca-Almaguer....	17
Complexo Arquia.....	18
Complexo máfico-ultramáfico de Heliconia.....	19
Complexo Quebradagrande.....	19
Complexo Ofiolítico de Yarumal.....	20
Complexo Ofiolítico de Aburrá.....	21
Capítulo 2. The nature of the ultramafic section of the Aburrá Ophiolite, Medellín region, Colombian Andes.....	27
Abstract.....	28
Resumo.....	28
2.1. Introduction.....	29
2.2. Regional Geological Setting	30
2.3. The Medellín Ultramafic Massif.....	31
2.4. Geology and petrography of the ultramafic massif.....	33
2.4.1. I-type harzburgite.....	33
2.4.2. II-type harzburgite and dunite.....	35
2.4.3. II-type harzburgite with concordant bands of dunite	35
2.4.4. Ultramafic dykes.....	38
2.4.5. Wehrlite	38
2.4.6. Banded or layered peridotites.....	39
2.5. Analytical Methods.....	40
2.5.1. Mineral chemistry.....	40

2.6. Mineral chemistry.....	40
2.6.1. Olivine.....	40
2.6.2. Spinel	41
2.6.3. Pyroxenes.....	48
2.6.4. Amphibole.....	49
2.6.5. Chlorite.....	50
2.6.6. Ni-Fe-S mineral assemblage.....	50
2.7. Discussion.....	51
2.7.1. Origin of peridotites	51
Origin of harzburgite.....	51
Origin of dunite.....	52
Origin of wehrlite.....	54
2.7.2. Primary spinel composition and nature of the percolating melts.....	55
2.7.3. Tectonic implications	57
2.8. Concluding remarks.....	59
Acknowledgments.....	59
References.....	60

Capítulo 3. The chromite deposits of the Aburrá Ophiolite, Colombian Andes: Constraints from mineral chemistry and Re-Os isotopes.....	67
Abstract.....	68
3.1. Introduction.....	68
3.2. Previous work.....	69
3.3. Geological Setting.....	70
3.4. Field relationships.....	73
3.4.1. Chromite deposits.....	73
Chromite deposits of the Southern Sector.....	73
Chromite deposits of the Northern Sector.....	75
3.4.2. The reaction zone peridotites	76
3.5. Samples and analytical methods.....	79
3.5.1. Mineral chemistry.....	79
3.5.2. Re-Os method.....	79
Re-Os analytical procedures.....	80
3.6. Petrography.....	81
3.6.1. Chromitites.....	81
3.6.2. Surrounding peridotites.....	82
3.6.3. Reaction zone.....	83
3.7. Mineral chemistry.....	83
3.7.1. Chromitites.....	83
Ore composition.....	83
Associated silicates.....	89
3.7.2. Surrounding peridotites.....	89
3.7.3. Reaction zone.....	90
3.8. Re-Os systematic.....	90
3.9. Discussion.....	92
3.9.1. Constraints on chromitites composition.....	93
Parental magma composition.....	94
3.9.2. Re-Os constraints.....	96
3.9.3. Origin of the chromitites.....	96
3.9.4. Tectonic setting implications.....	97
3.10. Conclusions.....	98

Acknowledgments.....	99
References.....	99
Capítulo 4. Age and petrogenesis of the metamafic rocks of the Medellín area, Colombian Central Cordillera: Constraints on their relationships with the Aburrá Ophiolite.....	108
Abstract.....	109
4.1. Introduction.....	110
4.2. Geological context.....	111
4.3. Nomenclature, field occurrence and petrography.....	114
4.3.1 El Picacho Metagabbro.....	114
4.3.1.1 Metagabbros.....	114
4.3.1.2 Plagiogranites.....	117
4.3.1.3 Garnet-epidote-plagioclase metasomatite (or Rodingite-like rock).....	118
4.2. Boquerón Metagabbro	118
4.3. Santa Elena Amphibolite.....	119
4.4 Analytical Methods.....	120
4.4.1. Mineral chemistry.....	120
4.4.2. Litogegeochemistry.....	120
4.4.3. U-Pb procedures.....	121
4.4.4. Sr-Nd procedures.....	121
4.5. Mineral chemistry.....	122
4.5.1. Amphibole	122
4.5.1.1 El Picacho metagabbros.....	122
4.5.1.2 Boquerón metagabbros.....	123
4.5.1.3 Santa Elena amphibolites.....	126
4.5.2. Plagioclase.....	126
4.5.2.1 El Picacho metagabbros.....	126
4.5.2.2 Boquerón metagabbros.....	126
4.5.2.3 Santa Elena amphibolites.....	126
4.5.3. Garnet.....	128
4.5.4. Ilmenite.....	128
4.6. Geothermobarometry	129
4.7. Geochemistry.....	131
4.8. Zircon U-Pb age.....	139
4.9. Sr-Nd Isotopic compositions.....	140
4.10. Discussion.....	142
4.10.1 Constraints on the origin of the mafic rocks.....	142
4.10.2. Constraints on metamorphism.....	142
4.10.3. The origin of the plagiogranites and the age of syn-oceanic deformation....	144
4.11. Conclusions.....	145
Acknowledgments.....	146
References.....	147
Capítulo 5. Discussões e Modelo evolutivo.....	153
5.1 Características do ophiolito da área do Vale de Aburrá.....	153
5.2 Correlação com outros complexos da região e proposta de modelo evolutivo....	156
Capítulo 6. Recomendações.....	168
Referências dos Capítulos 1 e 5.....	170

INDICE DE FIGURAS

CAPITULO 1

Figura 1. Mapa de localização da área de estudo.....	3
Figura 2. Seqüência ideal de um ofiolito segundo a Conferência Penrose de 1972. <i>Apud:</i> Moores & Twiss (1995).....	8
Figura 3. Ambientes de geração de ofiolitos. a). Zonas relacionadas a subducção. b) Dorsais meso-oceânicas.....	9
Figura 4. Modelos de empurrão oceânico reproduzidos de Nicolas e LePichon (1980) <i>in</i> Boudier et al. 1988. a) descolamento ao longo de um limite elástico-plástico num ambiente de zona de subducção. b) descolamento ao longo do limite listosfera-astenosfera num ambiente de dorsal.....	11
Figura 5. a) Províncias fisiográficas da Colômbia. Modificado de Ordoñez (2001). b) Unidades litoestratigráficas das Cordilheiras Central e Ocidental, e falhas do Sistema Romeral. <i>Apud</i> Nivia et al. 1996.....	13
Figura 6. Geologia regional do setor norte das Cordilheiras Central e Ocidental da Colômbia perto da cidade de Medellín, mostrando o Complexo polimetamórfico da Cordilheira Central e os complexos máficos e ultramáficos. Adaptado de Botero (1963), González (2001), Montoya e Peláez (1993), Correa e Martens (2000), Nivia e Gómez (2005).....	14
Figura 7. Distribuição das associações máficas-ultramáficas nas Cordilheiras de afinidade oceânica nas Cordilheiras Central e Ocidental da Colômbia. Modificado de Restrepo & Toussaint (1973), Toussaint (1996), Kerr et al.(1997).....	16
Figura 8. Geologia do Complexo ofiolítico de Yarumal, eixo da Cordilheira Central. <i>Apud</i> Hall et al. (1972) <i>in</i> Bourgois et al. (1987).....	21
Figura 9. Mapa da geologia local do Vale de Aburrá. Modificado de Botero (1963), Rendón (1999), Correa e Martens (2000), Rodríguez et al. (2005).....	23

CAPÍTULO 5

Figura 1. Esquema do modelo evolutivo dos complexos máficos e ultramáficos de Aburrá, Heliconia e Arquia. Desenho adaptado de Gribble et al. (1998).....	159
Figura 2. Modelos de reconstrução paleogeográfica dos Andes do Norte, América do Centro e da região Caribe no Permo-Triássico. a) Reproduzido de Cardona et al. (2006). b).Esquema para começos do Triássico reproduzido de Toussaint (1995).....	161

Figura 3. Esquema do alojamento intra-oceânico das unidades de Aburrá e aproximação do conjunto oceânico à borda continental.....	162
Figura 4. Esquema de alojamento dos complexos máfico-ultramáficos Triássicos na borda continental.....	163
Figura 5. Esquema mostrando a zona subdução no Jurássico após alojamento dos complexos ofiolíticos Triássicos no Terreno Tahami. Modificado de Toussaint e Restrepo (1994) e Ordóñez-Carmona (2001).....	163
Figura 6. Diagrama esquemático que mostra a evolução da bacia marginal do Complexo Quebradagrande e sua relação espacial com os complexos máfico-ultramáficos Triássicos e o Terreno Tahami. Modificado de Nivia et al. (1996, 2006).....	164
Figura 7. Representação esquemática da configuração da borda continental na porção NW de América do Sul a finais do Cretáceo Inferior. Modificado de Naranjo (2001).....	165

INDICE DE ANEXOS

Anexo 1. Artigo publicado na Revista de la Academia Colombiana de Ciencias Exactas, Físicas y Naturales.

Anexo 2. Tabela de localização dos pontos

Anexo 3. Resultados de análises de química mineral

Anexo 4. Métodos de análises químicos de rocha total

AGRADECIMENTOS

Agradeço ao professor Ariplínio A. Nilson por ser o orientador da tese e pela sua ajuda valiosa durante o tempo de estudos do mestrado e doutorado. Aproveito para fazer um reconhecimento a sua coragem porque apesar do estado de saúde, sempre fez um esforço enorme para acompanhar o desenvolvimento da pesquisa.

Agradeço ao professor Márcio M. Pimentel por ter aceitado ser o co-orientador, pelo apoio acadêmico e econômico que ofereceu para o desenvolvimento da investigação ainda antes de ser co-orientador.

Ao Conselho Nacional de Desenvolvimento Científico e Tecnológico-CNPq pelas bolsas de Mestrado (Convênio PEC-PG) e de Doutorado.

À FINATEC pelos apoios financeiros para participar de congressos e simpósios geológicos.

Aos colegas e amigos colombianos que me acompanharam nos trabalhos de campo, aos geólogos Juan Guillermo Cano, Jairo Herrera, Milton Alvarez, Javier Buitrago e Mauricio Valencia. Aos amigos Jhon Gallego, Leonardo Alvarez, Alejandro Perañez. A meu tio Jairo e aos meus irmãos Juan Pablo e Andrés Felipe.

À professora Marion Weber da Facultad de Minas da Universidade Nacional de Colômbia (UNAL-Medellín) por me acompanhar ao campo, permitir o uso do laboratório de laminação da Faculdade de Minas e por me ajudar no processo de preparação de amostras. À funcionária Martha Salazar. Aos geólogos Pablo E. Mejía H., Mônica A. Santa E., César Maya Y. e a Milton Alvarez pela preparação de várias amostras. À professora Inês Carmona pela amizade.

Ao professor Jorge Julián Restrepo da UNAL-Medellín pelas discussões, pela companhia em algumas excursões de campo e por me brindar uma amostra de harzburgito.

Um agradecimento especial ao geólogo Oswaldo Ordóñez da UNAL-Medellín por me acompanhar ao campo a locais onde outras pessoas não tinham coragem de ir e por me ajudar na preparação de algumas amostras. Por gestionar na Faculdade de Minas a liberação de um veículo para trabalhos de campo.

Ao professor Humberto González por me brindar amostras de cromita e fazer o contato com o Senhor Manuel Diaz para conhecer dois depósitos de cromita. Ao senhor Manuel Diaz por sua gentileza e disposição para me acompanhar nas visitas dos depósitos de cromita que está explorando.

À empresa INDURAL por me permitir amostrar sua pedreira. À geóloga Patrícia Angel e à empresa SOLINGRAL por me ceder testemunhos de sondagem.

A todos os professores do Instituto de Geociências da UnB que de alguma maneira me transmitiram seus conhecimentos e contribuíram para meu crescimento intelectual, em especial a Nilson Francisquini Botelho, José Affonso Brod, Márcia Abrahão, Mônica P. Escayola e Sylvia Araújo. A Hardy Jost e Tereza Cristina Junqueira Brod pela revisão de alguns manuscritos. À professora Edi Guimarães pela realização de análises de difração de raios-x em algumas amostras de rocha e pela interpretação dos resultados.

À professora Maria da Glória da Silva da Universidade Federal da Bahia pela ajuda na interpretação petrográfica de algumas amostras.

A todo o pessoal do Laboratório de Geocronologia sempre disposto a ajudar. Aos professores Márcio M. Pimentel e Elton Luiz Dantas. Agradeço enormemente a Sérgio Junges pela ajuda na preparação de amostras e na obtenção de concentrados de minerais. A Jorge E. Laux pela realização de várias datações radiométricas e a Bárbara Alcantara, Sandrine Ferraz e Simone Gioia pela assistência nas análises de Sr-Nd.

A Francisca das Chagas e Adalgisa Ferreira do laboratório de laminação do IG-UnB pela disposição e boa vontade para a confecção das lâminas polidas.

A Abel Nunes de O. Filho e Rogério Lourenço do CPD do Instituto pela presteza e pela ajuda em tudo o relacionado com informática.

A Onésio Rodrigues Filho do Laboratório de Microssonda eletrônica do IG-UnB pela suas explicações para manipular a microssonda e assistência durante a realização das análises.

A todos os funcionários da Secretaria do Instituto de Geociências por estarem sempre dispostos a solucionar dúvidas e ajudar nos processos burocráticos e administrativos relacionados com meu período de estudos neste Instituto. Francisca de Rodrigues Freitas, Maristela Menezes, Lusilene Leal e Valdeci da Silva Reis.

À geóloga Juliana Marques da UFRGS pela realização de análises isotópicas pelo método RE-Os de amostras de cromititos e peridotitos no Department of Terrestrial Magnetism da Carnegie Institution of Washington nos Estados Unidos. Ao professor José Carlos Frantz pelas análises no MEV da Universidade Federal do Rio Grande do Sul.

Ao Dr. Pierre Sabaté do IRD pelos contatos com a Universidade de Montpellier. Ao pessoal do Laboratoire de Tectonophysique da Université de Montpellier por me permitir realizar análises de microssonda nesse laboratório e pelas interessantes discussões geológicas. Em especial agradeço a: Jean-Louis Bodinier, Françoise Boudier, Andréa Tommasi, Delphine Bosch e Alain Vauchez. A Jean Marie Peiris e Claude Merlet pela assistência durante a realização das análises de microssonda. A Bernadette Marie-Hurson pela sua gentileza e ajuda que me brindou durante a minha estada em Montpellier.

A meus amigos e colegas do Instituto de Geociências da UnB: Natalia Hauser, Gloria Obando, Mássimo Matteini, Luciana Melo, Márcia Gaspar, Carlos Rendón, Miriela Ulloa, Cecília Ártica, Fátima Leite e Oscar Omar Guevara H. por todas as experiências vividas dentro e fora da universidade. A minhas colegas de sala Lys Mattos, Giana Marcia dos Santos e Stella Bijos.

A Uwe Martens, Beatriz Elena Ramírez e Paola Andrea Buitrago pela amizade durante todos estes anos e a Uwe por analisar uma amostra na microssonda eletrônica da Stanford University.

A Reinaldo Brito pelo seu apoio constante, sua companhia, sua ajuda técnica, correção dos manuscritos e por me brindar com seu amor.

A minha mãe, irmãos e tio o meu muito obrigado por todo o amor, a compreensão e a força com que me brindaram durante todo este tempo, apesar da distância.

RESUMO

Estudos petrográficos, geoquímicos, geocronológicos e isotópicos realizados nesta pesquisa permitiram estabelecer relações genéticas entre corpos de rochas ultramáficas e um conjunto de unidades maficas que ocorrem na cidade de Medellín e adjacências, na região do vale de Aburrá, setor noroeste da Cordilheira Central da Colômbia. As rochas ultramáficas compõem o Maciço Ultramáfico de Medellín e as unidades maficas são conhecidas como Metagabro de El Picacho, Metagabro de Boqueron e Anfibolito de Santa Elena.

O Maciço Ultramáfico de Medellín consiste principalmente de dunito e em menor proporção de cromititos, harzburgito, diques ultramáficos e wehrlito. Peridotito intensamente recristalizado ocorre na base dos corpos ultramáficos. Há harzburgito com ortopiroxênio preservado (Tipo-I) e harzburgito onde o ortopiroxênio foi totalmente substituído por pseudomorfos (Tipo-II). Dunito ocorre em corpos extensos e também em bandas dentro de harzburgito Tipo-II. Os cromititos podiformes com envelopes de dunito estão associados com harzburgito Tipo-II. Wehrlito ocorre em corpos pequenos e esparsos na parte mais superior da seção ultramáfica próximo ao limite com a crosta mafica.

Harzburgito Tipo-I é interpretado como peridotito residual após aproximadamente 15 a 17% de fusão parcial do manto lherzolítico. Dunito em bandas intercaladas com harzburgito Tipo-II é interpretado como resultante da interação fusão/rocha, ou seja, da reação do harzburgito com fusões percolantes dos tipos MORB ou BABB. Wehrlito é interpretado como peridotito impregnado resultante da interação de dunito com fusões do tipo MORB (ou BABB) e provavelmente também com fusões hidratadas.

Os cromititos podiformes são principalmente concordantes e, em menor proporção, discordantes dos peridotitos hospedeiros. Os cromititos são do tipo rico em alumínio e exibem diferenças composticionais entre alguns depósitos. Estas diferenças são interpretadas como devidas a históricos de cristalização distintos ou à precipitação a partir de magmas com composições variáveis devido à mistura de magmas. Os resultados isotópicos de Re-Os em cromititos, dunito e harzburgito confirmam a existência de magmas com composição isotópica distinta. Há evidências de que processos de reação entre fusões percolantes e o harzburgito hospedeiro foram importantes no maciço peridotítico e provavelmente estas interações permitiram a formação dos cromititos. Desta maneira muitas das concentrações de cromita provavelmente cristalizaram como resultado da saturação em cromo dos magmas percolantes depois da sua interação com os peridotitos.

O conjunto de dunito, harzburgito Tipo-II, cromititos e wehrlito é interpretado como a Zona de Transição do Ofiolito de Aburrá, onde aconteceram reação e impregnação. O oxiolito é classificado como do tipo Harzburgito.

A evolução tectonomagmática do maciço peridotítico compreendeu pelo menos dois estágios. Durante o primeiro estágio uma suite composta de espinélio harzburgito foi formada durante a fusão parcial do manto. No segundo estágio o espinélio harzburgito foi afetado pela percolação de fusões tipo MORB ou BABB.

O Metagabro de El Picasso preserva estruturas, texturas e composição ígneas dos protólitos que permitem classificá-las como cumulatos gabróicos. São equivalentes aos gabros acamados ou inferiores de outros oxiolitos como o de Omã. A presença de pargasita nos metagabros e nos wehrlitos adjacentes sugere processo tardi-magmático comum entre a parte superior da zona de transição do manto e a crosta máfica inferior do oxiolito. Esta unidade apresenta evidência de recristalização na crosta oceânica produzida por deformação dinâmica e alteração hidrotermal em temperaturas decrescentes desde ~850 até ~550° C em condições de baixa pressão (<2 kbar). Plagiogranitos associados aos metagabros possivelmente se formaram a partir da fusão parcial dos gabros sob regime de alteração hidrotermal de alta temperatura ou deformação sin-alojamento.

O Metagabro de Boquerón consiste em rochas metagabroicas cujo protólito tinha uma razão La_N/Yb_N (0.89-1.48) maior do que o protólito dos metagabros de El Picasso ($\text{La}_N/\text{Yb}_N < 0.64$). Estes gabros apresentam semelhanças com os gabros isotrópicos, varitexturados e superiores do oxiolito de Omã. Exibem evidências de alteração hidrotermal de fundo oceânico ocorrida a temperaturas (~680 e 550° C) menores do que nas rochas de El Picasso e novamente deformados provavelmente após alojamento no continente.

Os Anfibolitos de Santa Elena correspondem principalmente a lavas máficas ou também a metagabros. Suas características químicas indicam que foram líquidos do tipo MORB que guardam semelhanças com as lavas e diques de Omã. Exibem evidências de ter atingido equilíbrio metamórfico na fácie anfibolito, mas as paragêneses metamórficas registram diferenças de pressão e temperatura ao longo da unidade. Essas diferenças podem ser atribuídas em parte à sua proximidade ao contato com os peridotitos e a corpos intrusivos, os quais podem ter afetado termicamente as associações metamórficas pretéritas.

Idade U-Pb obtida em zircão de um plagiogranito é de aproximadamente $216,6 \pm 0,4$ Ma e é interpretada como o evento de deformação e fusão parcial dos gabros na crosta oceânica, ou seja, que indica a idade mínima do oxiolito.

As composições isotópicas de neodímio nas três unidades máficas são semelhantes e indicam derivação dos magmas originais de manto empobrecido. Alguns resultados de isótopos de Sr indicam possível interação com água do mar.

Enquanto nos metagabros foram preservadas evidências de metamorfismo de fundo oceânico, nos anfibolitos as características de alteração hidrotermal adquiridas no ambiente oceânico foram obliteradas. Esta maior deformação nos anfibolitos possivelmente aconteceu durante o empurrão intra-oceânico e alojamento na margem continental.

Os resultados obtidos nesta pesquisa permitem concluir que as unidades máficas, félscica, e o maciço ultramáfico representam um ofiolito, para o qual se propõe o nome de Ofiolito de Aburrá.

As características geológicas e geoquímicas de todas as unidades estudadas são consistentes com uma evolução conjunta num mesmo sistema oceânico do tipo retro-arco.

ABSTRACT

Petrographic, geochemical, isotopic and geochronological studies carried out in this research aimed to establish the genetic relationships between a group of ultramafic bodies and a set of mafic belts that occur around the city of Medellín along the Aburrá Valley in the northwestern sector of the Colombian Central Cordillera.

The ultramafic rocks are part of the Medellín Ultramafic Massif, whereas the mafic units are named El Picacho Metagabbro, Boquerón Metagabbro and Santa Elena Amphibolite.

The Medellín Ultramafic Massif consists mainly of dunite and in less proportion of chromitites, harzburgite, ultramafic dykes and wehrlite. Strongly recrystallized peridotite occurs at the base such ultramafic bodies. Harzburgite with preserved orthopyroxene is denominated as I-Type, whereas harzburgite with pseudomorphs after orthopyroxene is denominated as II-Type. Dunite forms extensive bodies, but also occurs as milimetric to centimetric bands within II-Type harzburgite. Chromitite bodies with dunite envelopes are associated with II-Type harzburgite. Wehrlite are barely found in the uppermost part of the ultramafic section close to the limit of the mafic crust.

I-Type harzburgite corresponds to the lower peridotite within this mantle portion and it probably represents a residual peridotite after ~15-17% partial melting of lherzolite mantle. Dunite bands within II-Type harzburgite are interpreted as the result of melt/rock interaction of harzburgite with MORB or BABB melts. Wehrlite is interpreted as impregnated peridotite, resulting from the interaction between dunite and hydrous MORB (or BABB) melts.

Podiform chromitites are generally Al-rich and lie conformably within the host peridotite. They exhibit compositional differences among individual deposits, which are attributed to different crystallization histories or to slight differences in parent magma composition. Re-Os isotopic results obtained from chromitites, dunite and harzburgite also confirm the occurrence of melts with different Re-Os isotopic compositions. Reactions between host harzburgite and percolating melts with composition varying between mid-ocean ridge basalt (MORB) and back-arc basalt (BABB) types coupled with magma mixing probably played an important role in the formation of most chromitite bodies in the Aburrá Ophiolite. At least part of the chromitites crystallized owing to chrome saturation in the percolating melts after interaction with peridotites.

The group consisting of dunite, II-Type harzburgite, chromitites and wehrlite is interpreted as the Transition Zone of the Aburrá Ophiolite, and represent the loci where most of the impregnation and reactions took place. The overwhelming abundance of harzburgite

among other lithotypes within the Aburrá Ophiolite lead to its classification as Harzburgite-Type.

At least two stages of tectonomagmatic evolution of the peridotites were identified. During the first stage, a suite of spinel harzburgite was formed after partial melting of the mantle. In the second stage, spinel harzburgite was affected by percolating MORB- or BABB-type melts. These processes probably took place in an oceanic back-arc environment.

El Picacho Metagabbro locally preserves most of its igneous structures, textures, and geochemical composition, which permits to consider as gabbroic cumulates. They are equivalent to the lower gabbros from other ophiolite such as Oman Ophiolite. Igneous pargasite have been identified in these metagabbros, as well as in the adjacent wehrlites. This is an indication that these amphiboles were produced through a post-magmatic process that usually take place between the upper part of the transition zone of the mantle and the lower part of the mafic crust of the ophiolites. This unit presents evidences of recrystallization within the oceanic crust produced by dynamic deformation and hydrothermal alteration at decreasing temperatures from ~850 to ~550° C and low pressure (<2 kbar). Plagiogranites occur associated within these metagabbros, which might have been formed by partial melting of the gabbros promoted by high temperature hydrothermal alteration coupled with sin obduction deformation.

Boquerón Metagabbro might have had a much more fractionated protholith ($\text{La}_\text{N}/\text{Yb}_\text{N} = 0.89\text{-}1.48$) than El Picacho metagabbros ($\text{La}_\text{N}/\text{Yb}_\text{N} < 0.64$). The Boquerón unit resembles those varied-textured upper gabbros from Oman Ophiolite. They exhibit typical ocean floor-type hydrothermal alteration, and another metamorphism with temperatures range from~680 to 550° C, which were lower than those from El Picacho. This metamorphism might have taken place after emplacement upon the continent.

Santa Elena Amphibolite might represent recrystallized mafic lavas or it may also correspond to metagabbros. The geochemical signatures indicate that they were MORB-Type magmas, which are similar to those from lavas and dykes from Oman Ophiolite. They exhibit metamorphic paragenesis which has equilibrated under the amphibolite facies conditions. Variations of pressure and temperatures were observed along this unit, which is ascribed to the thermal effect of the nearby intrusive bodies that may have modified the original metamorphic assemblage.

U-Pb dating carried out on zircon grains from the plagiogranite yielded a concordant age of 216.6 ± 0.4 Ma, which is interpreted as the age of the deformation and partial melting of

the gabbros within the oceanic crust, i.e. it can be considered as the minimum age of the ophiolite.

Neodymium isotopic compositions are very similar among the three mafic units, which indicate an origin from the same parental magma type which was derived from a depleted mantle source. Some strontium isotopic results indicate interaction with sea water.

Gabbroic rocks preserve most of the evidence of ocean floor metamorphism, whereas amphibolites has their igneous features and ocean floor alteration obliterated. This can be explained possibly because the amphibolite might have undergone stronger deformation rates during intra-ocean thrusting and emplacement upon the continental margin.

The results obtained in this study allow concluding that mafic and felsic rocks, and the ultramafic massif represent an almost complete ophiolite pile, which is named Aburrá Ophiolite.

The geological features and geochemical data shown in this study are consistent with the hypothesis that these ophiolitic units have evolved in an oceanic back arc-type environment.

CAPÍTULO 1. INTRODUÇÃO

1.1 APRESENTAÇÃO

Esta tese consiste no estudo da gênese e evolução geológica do Ofiolito de Aburrá, localizado na Cordilheira Central da Colômbia e apresenta interpretações baseadas em um conjunto de dados de campo, petrografia, química mineral, litogeoquímica, geocronologia e geoquímica isotópica.

Associações de rochas básicas e ultrabásicas de ambientes oceânicos ocorrem nos Andes Colombianos principalmente no flanco ocidental da Cordilheira Central, na Cordilheira Ocidental e na Serrania de Baudó. Alguns desses conjuntos representam ofiolitos (Restrepo & Toussaint 1973, Alvarez 1983, Bourgois et al. 1985, 1987) e outros correspondem a fragmentos de platô oceânico (Millward et al. 1984, Nivia 1987, Kerr et al. 1996). Os ofiolitos da Cordilheira Central não têm sido estudados em detalhe adequado sob o ponto de vista da petrografia, geoquímica, geocronologia e metalogênese. É notório que estas associações são elementos-chave para o entendimento dos processos que ocorrem nas bordas das placas tectônicas, seja em dorsais meso-oceânicas, ou em zonas relacionadas à subducção, e nesse sentido, o estudo do Ofiolito de Aburrá deve representar uma contribuição relevante para a compreensão da história geológica da borda NW da América do Sul.

O conjunto de rochas maficas e ultramáficas do Vale de Aburrá, na cidade de Medellín e adjacências, é interpretado como uma fatia ofiolítica e foi denominado por Correa e Martens (2000) como “Complexo Ofiolítico de Aburrá”. De acordo com esses autores, o ofiolito consiste em duas unidades: o Dunito de Medellín composto por rochas ultramáficas do manto e os Metagabros de El Picacho, com rochas plutônicas maficas. Alguns autores (Restrepo 1986, Toussaint 1996, Pereira & Ortíz 2003) propuseram que a unidade Anfibolito de Medellín e paragnasses associados, que ocorrem a leste dos peridotitos, poderiam constituir parte da mesma seqüência ofiolítica. Este conjunto ofiolítico está localizado a leste do Sistema de Falhas de Romeral, que representa o limite entre os domínios de embasamento continental e oceânico da Colômbia. Esta situação constitui objeto interessante para o estudo do contexto geotectônico das associações máfico-ultramáficas em tela. O estudo deste ofiolito é também de grande importância porque a sua porção ultramáfica hospeda a única ocorrência de cromita podiforme até hoje reconhecida na Colômbia e a contextualização geológica dessa mineralização, neste conjunto ofiolítico, é fundamental para a interpretação da sua gênese e evolução geológica.

A tese está dividida em oito secções. A primeira consiste da parte introdutória, onde são apresentados os objetivos da tese, a localização da área de estudo, os métodos de trabalho, uma breve revisão bibliográfica sobre ofiolitos e por fim uma síntese sobre a geologia regional relacionada com os ofiolitos da Cordilheira Central. Os capítulos 2 a 4 transcrevem os três artigos, um submetido e os outros dois a serão submetidos a periódicos científicos de circulação internacional.

O capítulo 2 abrange a petrografia e química mineral das rochas ultramáficas do Ofiolito de Aburrá. Mostra-se que o maciço peridotítico não consiste só em dunitos como outros autores afirmaram. Também se expõem evidências de processos de reação na zona de transição do ofiolito. A partir da composição petrográfica e química, sugere-se o provável ambiente de geração e/ou modificação da parte superior do manto do ofiolito. Este capítulo corresponde a um artigo submetido para publicação à revista *Journal of South American Earth Sciences*.

No capítulo 3 descreve-se a petrografia e química mineral dos vários depósitos de cromita estudados e das rochas hospedeiras dessas mineralizações. São também apresentados os primeiros dados isotópicos de Re-Os obtidos em cromititos e rochas ultramáficas objeto deste estudo. Conclui-se com discussões relativas ao processo gerador dos cromititos. Este capítulo foi transcrito num artigo que será submetido à revista *Mineralium Deposita*.

O capítulo 4 versa sobre a petrografia, química mineral, litogeoquímica, geocronologia e geoquímica isotópica das rochas máficas e plagiogranitos associados do ofiolito de Aburrá. Neste item apresenta-se a idade radiométrica obtida em rochas do próprio ofiolito, a qual corresponde à idade próxima à da geração do complexo. Discute-se o ambiente mais apropriado de geração das rochas máficas de acordo com os dados químicos e isotópicos e sugere-se o possível processo formador dos plagiogranitos. O conteúdo deste capítulo também será apresentado sob a forma de artigo a ser submetido.

No capítulo 5 é proposto um modelo evolutivo para o Ofiolito de Aburrá. O capítulo 6 trata das recomendações para futuras pesquisas. O Capítulo 7 contem as referências bibliográficas dos capítulos 1 e 5. Nos anexos se apresenta um artigo que foi publicado na Revista de la Academia Colombiana de Ciencias Exactas, Físicas y Naturales, as tabelas de dados locacionais das amostras, os resultados analíticos de química mineral e a descrição dos métodos analíticos de rocha total.

1.2 LOCALIZAÇÃO

A região de estudo localiza-se na porção norte da Cordilheira Central da Colômbia, no estado de Antioquia, sobre os flancos do Vale de Aburrá, na cidade de Medellín e arredores (Figura 1). Possui aproximadamente 920 km² e está contida entre as coordenadas geográficas 6°30'16" N e 75°39'45" W no extremo noroeste e 6°8'5" N e 75°26'10" W no extremo sudeste.

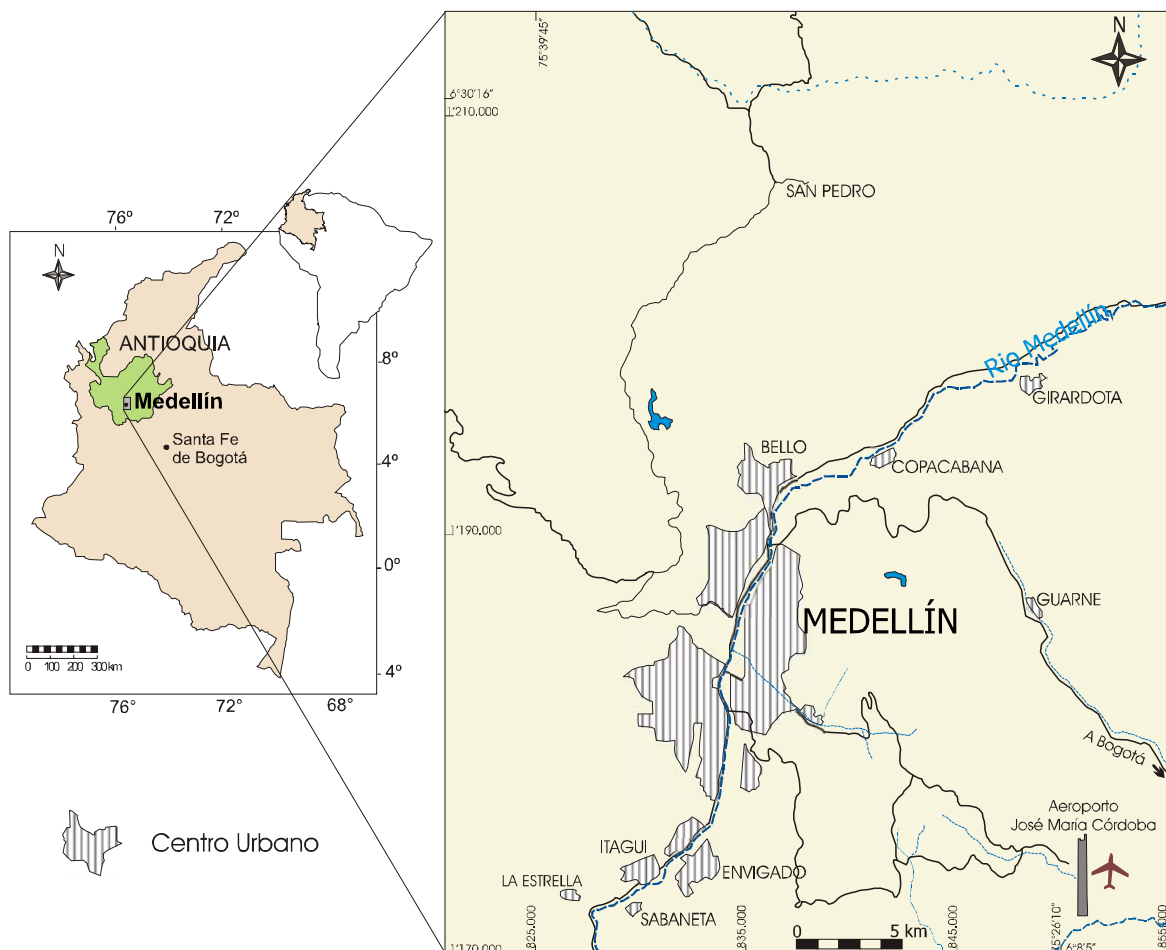


Figura 1. Mapa de localização da área de estudo.

1.3 OBJETIVOS

Esta pesquisa teve como objetivo geral:

- Estudar as rochas do ofiolito de Aburrá (Medellín-Colômbia) e algumas unidades de rochas relacionadas sob os pontos de vista geológico, petrológico e isotópico (Sr-Nd e U-Pb).

As finalidades específicas foram:

- Definir o(s) tipo(s) de peridotito de manto presente(s).
- Propor o processo mais provável de geração dos cromititos.

- Determinar a assinatura geoquímica das rochas maficas.
- Estabelecer se os metagabros e anfibolitos fazem parte da mesma seqüência ofiolítica, juntamente com as rochas ultramáficas.
- Definir o tipo de ofiolito e seu possível ambiente tectônico de geração.
- Comparar com ofiolitos de outras partes do mundo ou com conjuntos oceânicos atuais e elaborar modelo de geração e evolução geológica que contribua com o entendimento geológico da porção norte da Cordilheira Central da Colômbia e da porção NW da América do Sul.

1.4 MÉTODOS DE TRABALHO

1.4.1 Petrografia

As lâminas polidas de rocha foram confeccionadas no Laboratório de Laminação do Instituto de Geociências da Universidade de Brasília - UnB. Para descrição usaram-se os microscópios petrográficos de luz transmitida e refletida do Laboratório de Microscopia do Instituto de Geociências da UnB.

1.4.2 Análises Químicas de Minerais por Microssonda Eletrônica

A maior parte das análises se realizaram no Laboratório de Microssonda Eletrônica do Instituto de Geociências da UnB. O equipamento usado é um modelo CAMECA SX-50, cujas condições de operação foram 15 kV e 20 nA, com tempos de contagem entre 10 e 50 segundos e o diâmetro do feixe entre 2 e 5 µm.

As amostras AC77A, AC77B, AC77C, AC78B, AC80B1, AC80B2, AC52E foram analisadas na microssonda eletrônica - JEOL JXA-8600 Superprobe - do Instituto de Geociências da Universidade de São Paulo. As condições de operação do equipamento foram: 15 kV de voltagem de aceleração e 20 nA de corrente. O tempo de contagem para os elementos maiores foi de 10 s e para os menores de 50 s. O diâmetro do feixe foi de 1 µm para análises de óxidos e de 5 µm para os outros minerais.

A química mineral das amostras: AC59B, AC49II, AC20M, AC22B, AC51, AC25, AC78C1, JJ1396, AC53J, AC61T, AC52-0.4, AC52-1.65, AC52-5.02, AC52-19.25, AC52-26.54 foi obtida na Microssonda eletrônica do Laboratório de Tectonofísica da Université de Montpellier II. O equipamento usado foi uma microssonda CAMECA SX-100, sendo que as condições de operação foram: 20 kV, 10 nA, diâmetro do feixe foi de 1-5 µm. O tempo de contagem foi entre 10 e 50 segundos.

A maior parte da química mineral da amostra P2-11.20 foi obtida na Microssonda eletrônica da Universidade de Stanford, que é uma microssonda JEOL Superprobe 733. As condições de trabalho foram: voltagem de aceleração 15 kV, corrente 20 nA e diâmetro do feixe de 1 μ m. Alguns pontos desta amostra foram analisados também na microssonda da Universidade de Montpellier.

Em todos os casos foram usados padrões tanto sintéticos quanto naturais. O cálculo de Fe₂O₃ nos espinélios e nos piroxênios foi feito a partir dos resultados de FeO* fornecidos pela microssonda e por meio de cálculos estequiométricos (equações de Droop 1987). O cálculo de Fe₂O₃ nos anfibólios seguiu o procedimento sugerido por Schumacher (1997) *in* Leake et al. (1997). A nomenclatura usada para os anfibólios e piroxênios corresponde àquela sugerida pela IMA (*International Mineralogical Association*) e que se encontra em Leake et al. (1997) e Morimoto (1989).

O cálculo das fórmulas estruturais dos minerais foi realizado com planilhas do programa EXCEL. Todos os resultados obtidos estão no Anexo 3.

1.4.3 Pulverização de amostras e separação de minerais

As amostras foram pulverizadas a uma granulação menor que 200 malhas, utilizando-se um moinho de bola de carbeto de tungstênio, do Laboratório de Geocronologia, Instituto de Geociências - UnB.

Concentrados de minerais pesados foram obtidos a partir de pré-concentrados com bateia, seguido do separador magnético Frantz do Laboratório de Geocronologia da UnB.

1.4.4 Análises químicas de rocha

As análises químicas de elementos maiores, traços e terras raras foram realizadas no Laboratório comercial ACME Ltd., no Canadá. A preparação das amostras para análises dos elementos maiores, e a maior parte dos traços, foi feita por fusão com LiBO₂, e para metais base e preciosos por digestão com água régia. As análises dos elementos maiores foram efetuadas por espectrometria de emissão com ICP-OES e dos elementos traços por espectrometria de massa com ICP-MS. A descrição completa dos procedimentos laboratoriais seguidos, assim como os limites de detecção dos elementos para cada método, foram fornecidos pelo laboratório ACME Ltd. e encontram-se no Anexo 4.

1.4.5 Geoquímica isotópica de Sr e Nd

As análises isotópicas de Sr e Nd em rocha total foram realizadas no Laboratório de Geocronologia da UnB, em amostras de metagabros, anfibolitos e granítoides. O método Sm-Nd obedeceu aos procedimentos de Gioia & Pimentel (2000). Aproximadamente entre 70 mg e 80 mg de pó das amostras foram misturados a uma solução traçadora mista (Spike) de ^{149}Sm - ^{150}Nd e dissolvidas em cápsulas Savillex. A extração dos lantanídeos foi feita por meio de técnicas convencionais de troca iônica em colunas de quartzo, usando resina BIO-RAD AG-50W-X8. As extrações de Sm e Nd foram realizadas em colunas de teflon empacotadas com resina LN-Spec (resina líquida HDEHP – ácido di-ethylhexil fosfórico impregnada em pó de teflon). As frações de Sr, Sm e Nd foram depositadas em arranjos duplos de filamentos de rênio. As razões isotópicas foram determinadas em espectrômetro de massa multi-coletor Finnigan MAT 262, em modo estático. As incertezas para $^{87}\text{Sr}/^{86}\text{Sr}$ são menores do que 0.01% (2 σ) e para as razões Sm/Nd e $^{143}\text{Nd}/^{144}\text{Nd}$ são melhores do que $\pm 0,1\%$ (1σ) e $\pm 0.005\%$ (1 σ) respectivamente, baseadas em análises repetidas dos padrões BHVO-1 e BCR-1. As razões $^{143}\text{Nd}/^{144}\text{Nd}$ são normalizadas para o valor de $^{146}\text{Nd}/^{144}\text{Nd}$ de 0.7219 e a constante de desintegração (λ) usada é $6.54 \times 10^{-12}\text{a}^{-1}$. Os resultados foram processados utilizando-se o programa ISOPLOT/Ex 3 (Ludwig 2003).

1.4.6 Geocronologia U-Pb

Determinações isotópicas por meio do método U-Pb convencional em zircão foram realizadas no Laboratório de Geocronologia de UnB, de acordo com os procedimentos de diluição isotópica de zircão descritos por Pimentel et al. (2003).

A separação manual dos grãos de zircão, a partir dos concentrados de minerais pesados, se fez com auxílio de lupa binocular. As frações de zircão foram lavadas duas vezes na solução HNO_3 4N, primeiro para dissolver os grãos de pirita e depois por cerca de 45 minutos para limpeza final, seguida de repetidas lavadas com água destilada e acetona. Pequenas frações de zircão foram pesadas em pedaço de alumínio descartável e dissolvidas em mistura de HF 8N e HNO_3 (15:1), usando bombas de teflon do tipo Parr, a 220°C. Foi adicionada pequena quantidade de traçador isotópico (Spike) ^{205}Pb - ^{235}U (Krogh & Davis 1975). A dissolução e a extração química de U e Pb seguiram os procedimentos descritos por Krogh (1973). Pb e U são recuperados como fosfatos com gel de sílica e depositados em filamentos simples de rênio e analisados na forma metálica em modo estático, usando espectrômetro de massa Finnigan MAT-262 multi-coletor.

1.4.7 Análises Isotópicas Re-Os

A preparação e as análises das amostras foram realizadas pela Dra. Juliana Marques. A preparação foi executada na Universidade Federal do Rio Grande do Sul, enquanto as análises foram realizadas no *Department of Terrestrial Magnetism of the Carnegie Institution of Washington, USA*. As amostras analisadas foram três peridotitos e concentrados de cromita de três amostras de cromititos. As técnicas de separação química usadas neste estudo foram similares às descritas por Carlson et al. (1999). O pó da amostra (~2 g) foi colocado em uma cápsula Pyrex™ Carius e depois foi adicionada uma solução traçadora (*spike*). Para dissolução foram colocados também dentro da cápsula aproximadamente 2 g de HCl concentrado e 4 g de HNO₃ concentrado. Após essa mistura estar congelada, a cápsula foi selada e aquecida a 240°C, durante 12 horas. Após a abertura das cápsulas, foi adicionado CCl₄ à mistura de ácidos e Os foi extraído da fase aquosa. OsO₄ foi subsequentemente reduzido por meio da mistura com HBr. A purificação final para Os foi realizada via microdestilação. Re foi purificado por troca iônica. Os óxidos de Re e Os foram depositados em filamentos de Pt. As composições isotópicas de Re e Os foram medidas em espectrômetro de massa multicoletor Triton.

1.5 REVISÃO TEMÁTICA SOBRE OFIOLITOS

O termo ofiolito se refere a um conjunto de rochas maficas e ultramáficas geradas em ambiente oceânico em expansão e que foi alojado tectonicamente sobre bordas continentais ativas ou passivas.

Segundo a definição dada pela conferência Penrose (Anonymous 1972), os ofiolitos apresentam a seguinte distribuição litológica da base para o topo (Figura 2): um complexo ultramáfico que consiste de quantidades variáveis de lherzolito, harzburgito e dunito, com deformação adquirida no manto; um complexo máfico-ultramáfico que contém peridotitos e piroxenitos cumuláticos que gradam para gabros bandados; gabros isotrópicos, dioritos e plagiogranitos; um enxame de diques maficos; complexo vulcânico máfico com basaltos almofadados e uma seção superior sedimentar composta por cherts, folhelhos e calcários.

É importante salientar que nem todos os ofiolitos apresentam esta seqüência ideal, seja como resultado das condições do ambiente de geração do ofiolito que não permite a formação de alguns dos seus componentes, ou devido a desmembramento tectônico durante o alojamento ou em eventos deformativos posteriores.

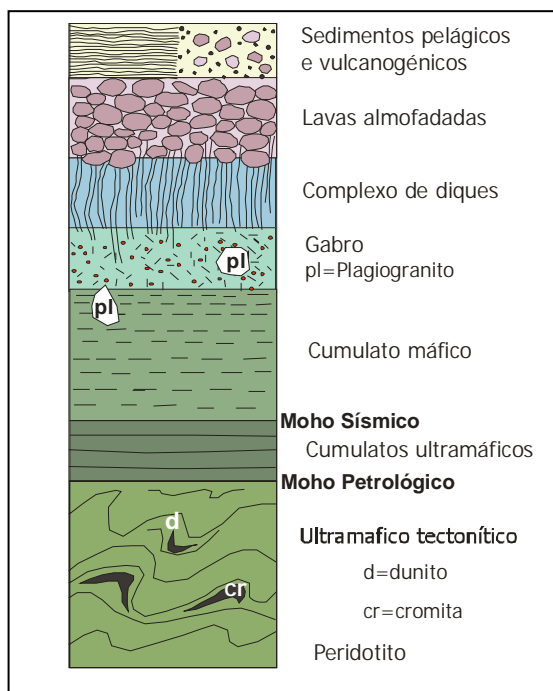


Figura 2. Seqüência ideal de um ofiolito segundo a Conferência Penrose de 1972. *Apud:* Moores & Twiss (1995).

Do ponto de vista da geologia econômica, os ofiolitos são importantes por serem portadores de mineralizações associadas a diferentes litotipos. Depósitos de sulfetos maciços e em *stockwork* ocorrem na parte superior dos ofiolitos relacionados com as rochas vulcânicas e sedimentares. Por outro lado, mineralizações de cobre, níquel e cobalto podem existir em halos de alteração hidrotermal nos gabros. As rochas ultramáficas podem hospedar mineralizações de cromita e platinóides, resultantes de processos magmáticos (Constantinou 1980, O'Hanley 1996) e/ou mineralizações de asbestos, talco, magnesita, níquel laterítico e ouro, produzidas a partir de processos singenéticos e epigenéticos (Vakanjac & Llich 1980, O'Hanley 1996).

Na base de muitos complexos ofiolíticos é comum ocorrer a sola metamórfica sub-ofiolítica que corresponde a fatias delgadas (<500 m) de rochas metamórficas de alto grau fortemente deformadas (Williams & Smyth 1973, Jamieson 1986). As partes superiores das solas metamórficas consistem em rochas metabásicas de afinidade oceânica, com menor quantidade de rochas sedimentares pelágicas metamorfisadas. Muitas exibem gradientes metamórficos inversos de temperatura e pressão e uma seqüência crustal oceânica invertida.

A ampla variedade petrográfica, estrutural e química encontrada nos ofiolitos indica diferentes ambientes tectônicos de origem, ainda que dentro de um mesmo cinturão orogênico (Dilek 2003). Os principais ambientes de geração de ofiolitos correspondem a zonas de supra-subducção (ante-arco, arco e retro-arco ou bacias marginais) (Figura 3a), dorsais meso-

oceânicas (Figura 3b) e falhas transformantes (Miyashiro 1973, Dewey 1976, Moores 1982, Pearce et al. 1984, Shervais 2001, Beccaluva et al. 2004).

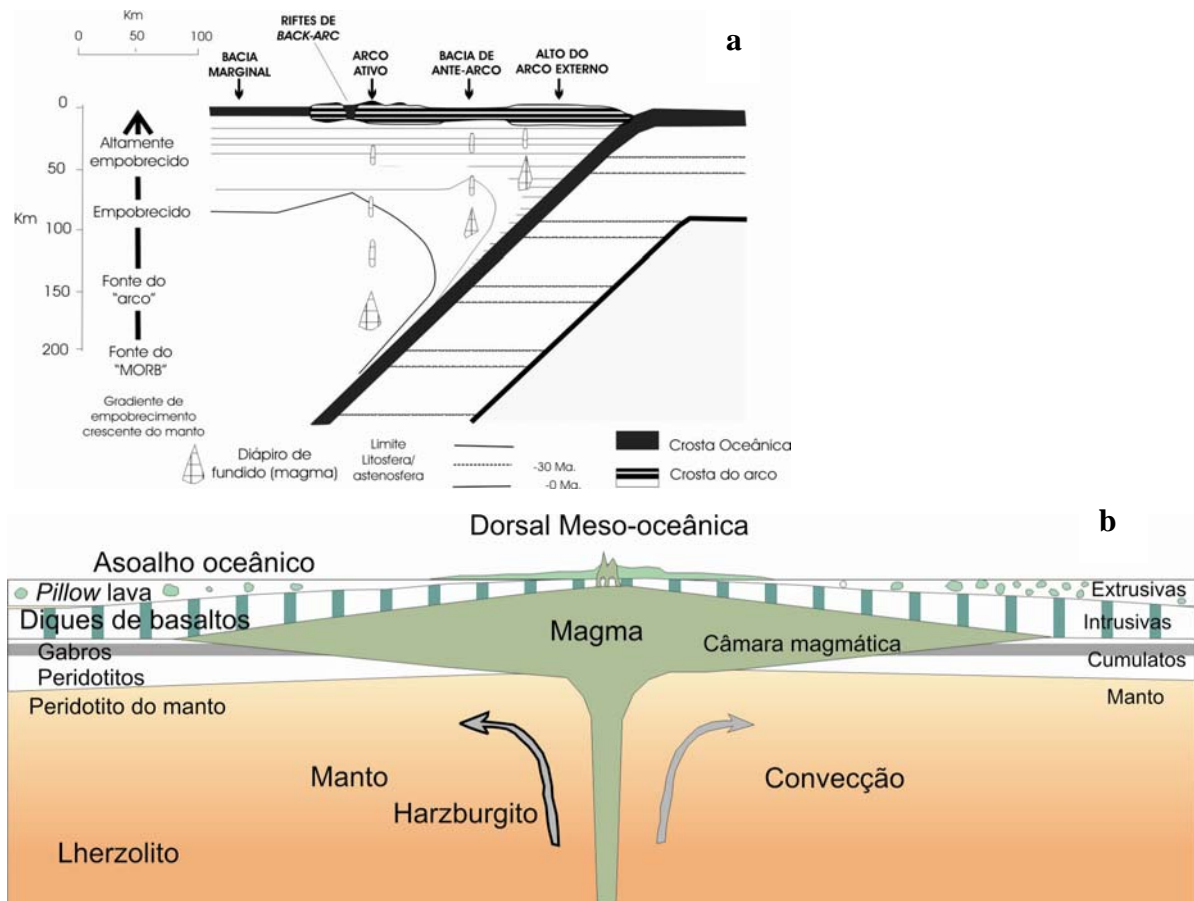


Figura 3. Ambientes de geração de ofiolitos. a) Zonas relacionadas a subducção. b) Dorsais meso-oceânicas.

Alguns fatores intrínsecos ao ambiente de geração determinantes nas feições dos ofiolitos são: (a) a taxa de expansão, tanto nas dorsais meso-oceânicas como nas bacias relacionadas a subducção, que pode variar de ultra-lenta ($<1\text{cm/a}$) a rápida ($\sim 6\text{cm/a}$); (b) o tipo de subducção (longitudinal e retrógrada); e (c) a taxa da subducção (1-10 cm/a). A velocidade da expansão influencia também os mecanismos de deformação e o tipo de alteração hidrotermal da crosta oceânica (Mével & Cannat 1991, Giguère et al. 2003).

A natureza toleítica ou picrítica das fusões primárias do manto em dorsais meso-oceânicas tem sido objeto de debate. Segundo os modelos de Prinzhofer & Allègre (1985) e Klein & Langmuir (1987), as fusões “primárias” integradas são toleíticas e não picríticas, porque a fração de fusão originada em níveis profundos permanece pequena e se mistura com fusões toleíticas menos profundas. As feições magmáticas de ofiolitos de zona de supra-subducção parecem controladas principalmente pela dinâmica e geometria dos processos de

subducção e pela maneira de fusão parcial da cunha do manto (Beccaluva et al. 2004). Os vários tipos de magmas que podem ocorrer em ambientes em uma zona de supra-subducção são: 1) toleitos de arco de ilha-IAT e em menor proporção cálcio-alcalinos de arco de ilha-IAC, 2) boninitos e toleitos de arco, altamente depletados, gerados em ambientes de ante-arco e inter-arco, 3) basaltos de bacia ante-arco (BABB), que exibem feições intermediárias IAT/MORB.

Tentar reconhecer o ambiente de geração de um ofiolito é importante, já que permite reconstruções palinspásticas a escala mais regional. No entanto, há muitos ofiolitos no mundo (por exemplo, Semail, Troodos e Bay of Islands) com características de vários ambientes e, portanto, nem sempre é fácil definir seu ambiente de geração.

Outro tema controverso no estudo dos ofiolitos é o que trata dos mecanismos de colocação (Wakabayashi & Dilek 2003). Os principais estágios envolvidos no alojamento são: descolamento oceânico, início da subducção, geração da sola metamórfica e colocação sobre a margem continental.

Existem dois locais nos oceanos que são os mais prováveis para que ocorra o descolamento e empurrão intra-oceânico (Boudier et al. 1988):

- localizado frente a uma zona de subducção (Figura 4a) onde a superfície de descolamento coincide com uma isoterma de aproximadamente 600º C que separa a litosfera elástica da litosfera plástica.
- no centro de expansão ou próximo deste, ou seja, na própria dorsal (Figura 4b) e a superfície de descolamento é o limite físico entre a litosfera e a astenosfera.

O termo obdução é amplamente usado na literatura e tem dois significados: (a) alojamento de ofiolito por meio de empurrão antitético ao longo de margens continentais ativas (Coleman 1971), (b) qualquer mecanismo de alojamento de ofiolito (p. ex. Dewey 1976). Wakabayashi & Dilek (2003) classificam o alojamento dos ofiolitos nas margens continentais de acordo com quatro protótipos, sendo mais comuns dois tipos. O alojamento de ofiolitos Tethyanos é um processo pontual que resulta da colisão ou empurrão de um ofiolito sobre uma margem continental passiva, enquanto o dos Cordilheiranos é um processo gradual ou acumulativo produzido por acresção tectônica progressiva a margens ativas ou a complexos de acresção-subducção.

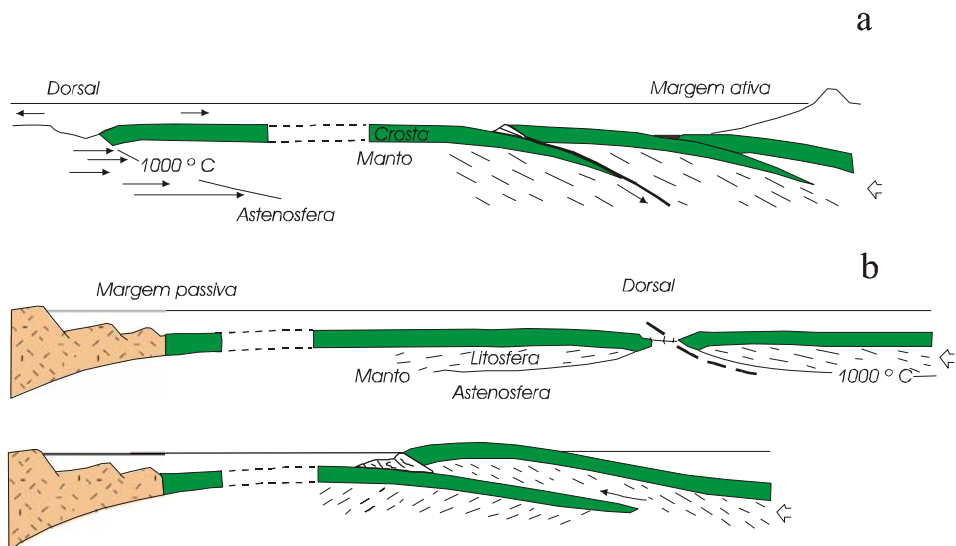


Figura 4. Modelos de empurrão oceânico reproduzidos de Nicolas & LePichon (1980) in Boudier et al. 1988. a) descolamento ao longo de limite elástico-plástico em ambiente de zona de subducção. b) descolamento ao longo do limite listosfera-astenosfera em ambiente de dorsal.

1.6 CONTEXTO GEOLÓGICO

A Colômbia está localizada no extremo noroeste da América do Sul onde interagem as placas Sul-americana, Nazca, Caribe e a micro-placa Panamá. Sua área terrestre divide-se nas seguintes províncias fisiográficas (Figura 5a): Amazônica, Planícies Orientais, Andina, Pacífica e Caribe. Feições geográficas menores na região do Caribe são a Serra Nevada de Santa Marta e a Península de La Guajira. Os Andes Colombianos se dividem nas cordilheiras Oriental, Central e Ocidental, separadas pelos vales interandinos dos rios Magdalena e Cauca, respectivamente. A Serrania do Baudó também faz parte da região andina e situa-se a oeste da Cordilheira Ocidental, da qual está separada pela planície do Pacífico.

As diversas unidades geológicas da Colômbia evidenciam diferentes orogenias, tais como a Grenvilliana, Caledoniana, Acadiana, Herciniana e Andina. Para explicar esta evolução geológica complexa, vários autores têm proposto modelos baseados na tectônica de terrenos, dentre os quais se destacam McCourt et al. (1984), Aspden e McCourt (1986), Etayo et al. (1986), Toussaint & Restrepo (1987, 1989), Restrepo & Toussaint (1988, 1989) e Ordóñez-Carmona (2001).

1.6.1 Arcabouço geotectônico das Cordilheiras Central e Ocidental

As principais unidades litoestratigráficas da Cordilheira Central da Colômbia são cinturões contínuos e descontínuos de rochas metamórficas. Associados a eles ocorrem conjuntos de rochas máficas e ultramáficas classificados como ofiolitos (Restrepo & Toussaint 1973, Alvarez 1985, Bourgois et al. 1985) e alguns corpos intrusivos mesozóicos de arco.

Seqüências de rochas vulcânicas e sedimentares e algumas ocorrências de ultramáficas e máficas plutônicas compõem a Cordilheira Ocidental e o flanco sudoeste da Cordilheira Central (sul da latitude 4° Norte), e correspondem a uma parte de um platô oceânico (Millward et al. 1984, Nivia 1987) da Grande Província Ignea Caribenha-Colombiana (Nivia 1996, Kerr et al. 1997).

Os limites tectônicos entre as unidades litoestratigráficas correspondem a estruturas do Sistema de Falhas Romeral (Figura 5b) que são a falha San Jerónimo a leste, falha Silvia Pijao no centro e falha Cauca-Almaguer a oeste (Maya & González 1995). O sistema é interpretado como um limite entre dois grandes domínios geológicos, um de afinidade continental a leste e outro oceânico a oeste (Case et al. 1971, McCourt et al. 1984). Este sistema também é considerado como uma sutura cretácea (Case et al. 1971, 1973, McCourt et al. 1984, Kerr et al. 1997, Chicangana et al. 2004) ou um conjunto de falhas de dispersão (Toussaint 1996).

As unidades litoestratigráficas, a leste da falha Cauca-Almaguer, são o Complexo Polimetamórfico da Cordilheira Central, o Complexo Quebradagrande, o Complexo Arquia, o Batólito de Santa Bárbara, o Batólito Antioqueno (Figura 5b) e várias fatias e fragmentos ofiolíticos. A seguir será apresentada breve descrição do Complexo Polimetamórfico, do Batólito de Santa Bárbara e do Batólito Antioqueno. Os Complexos Arquia, Quebradagrande e os ofiolíticos serão apresentados no item dedicado às associações máficas e ultramáficas oceânicas dos Andes Colombianos.

O *Complexo Polimetamórfico da Cordilheira Central* consiste em rochas polimetamórficas que afloram na Cordilheira Central, entre a falha Otú-Pericos a leste e a falha San Jerónimo a oeste (Restrepo & Toussaint 1982), e representam o embasamento da Cordilheira (Figura 5b). De maneira mais específica, esta unidade agrupa os granulitos e migmatitos de El Retiro (González 2001), o Complexo Cajamarca, no sentido de unidade litodêmica (Maya & González 1995), corpos extensos de anfibolitos, corpos intrusivos gnáissicos sintectônicos e *stocks* triássicos (Figura 6).

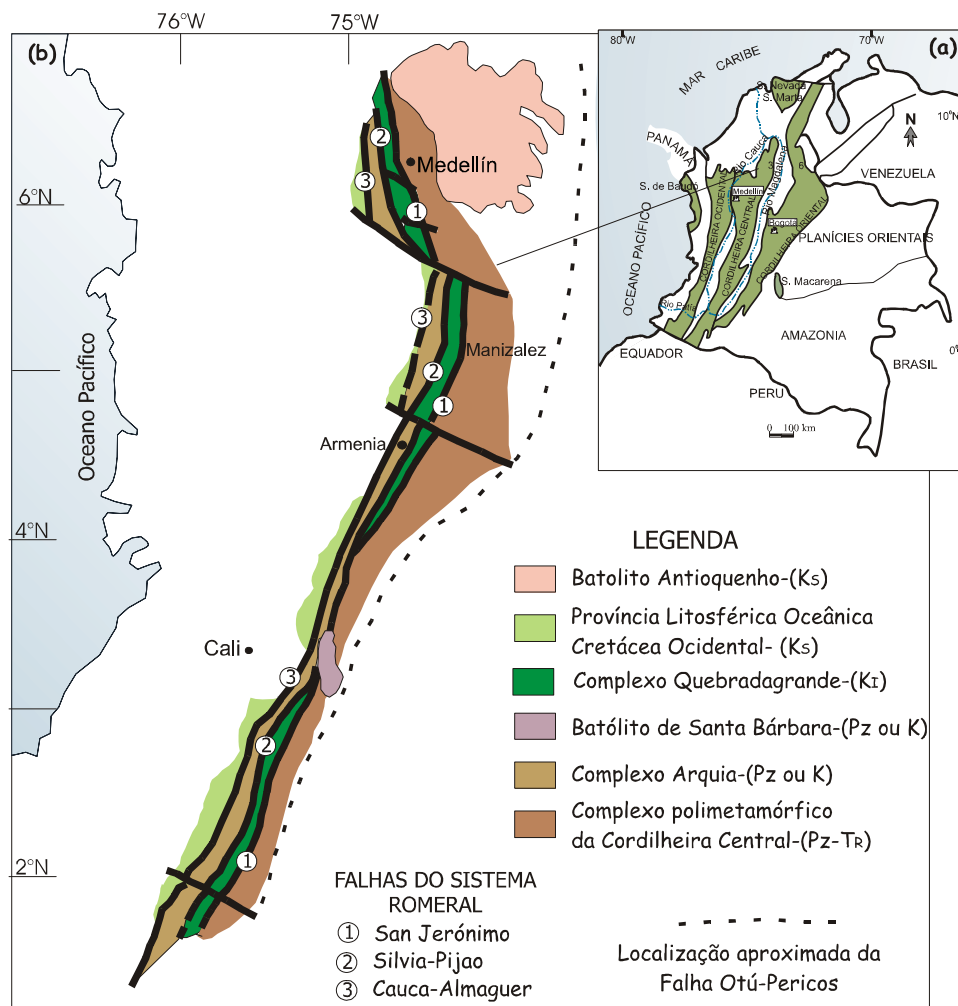


Figura 5. a) Províncias fisiográficas da Colômbia. Modificado de Ordóñez-Carmona (2001). b) Unidades litoestratigráficas das Cordilheiras Central e Ocidental e falhas do Sistema Romeral. Apud Nivia et al. (1996).

É constituído por grande variedade de litotipos tais como xistos, gnaisses, migmatitos, anfibolitos, granulitos e, em alguns locais, mármore, com características metamórficas muito variadas. Nas diferentes unidades do complexo ocorrem evidências de metamorfismo durante os eventos caledoniano, acadiano, herciniano e cretáceo (Restrepo et al. 1991, Ordóñez-Carmona 2001, Vinasco et al. 2003). O ofiolito de Aburrá está localizado geograficamente dentro deste complexo.

Granitos gnáissicos e *stocks* graníticos (Figura 6), com idades permo-triássicas, registram neste complexo diferentes processos durante esse intervalo de tempo (Vinasco et al. 2006), assim: um evento colisional (~280 Ma), magmatismo sintectônico de caráter cortical (~250 Ma) e magmatismo tarditectônico, com apporte juvenil (~228 Ma), que representa o colapso do orógeno.

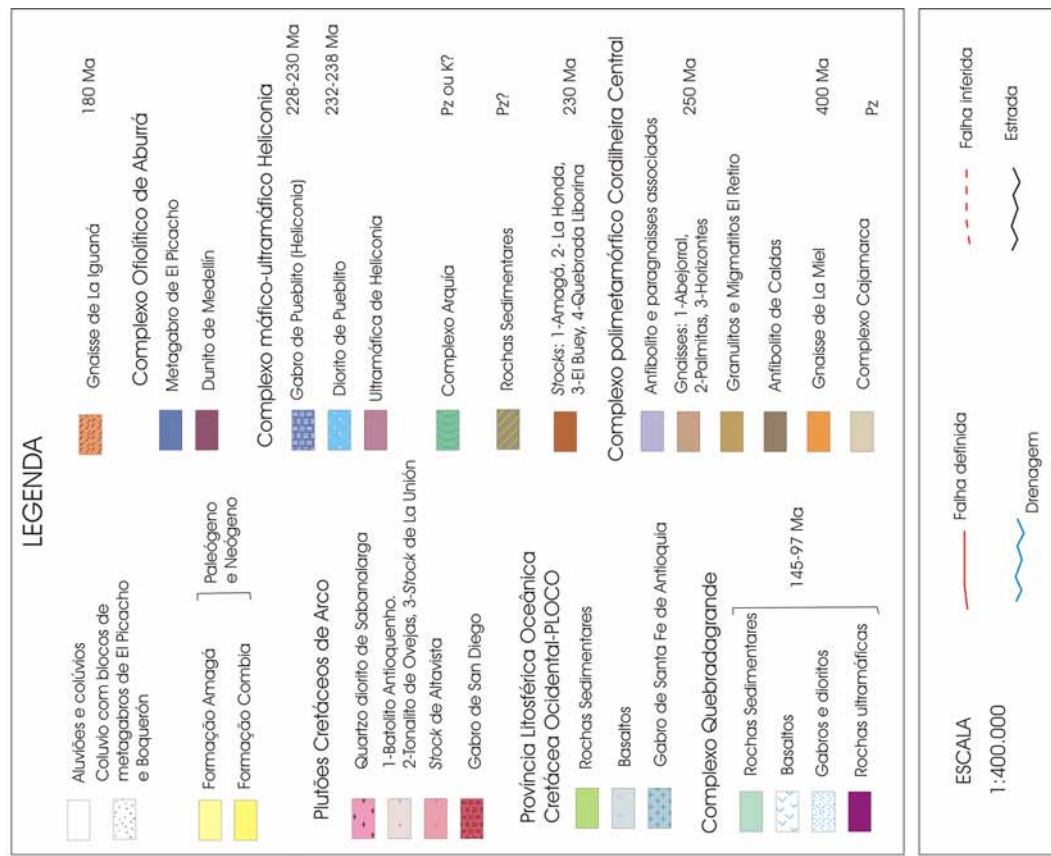
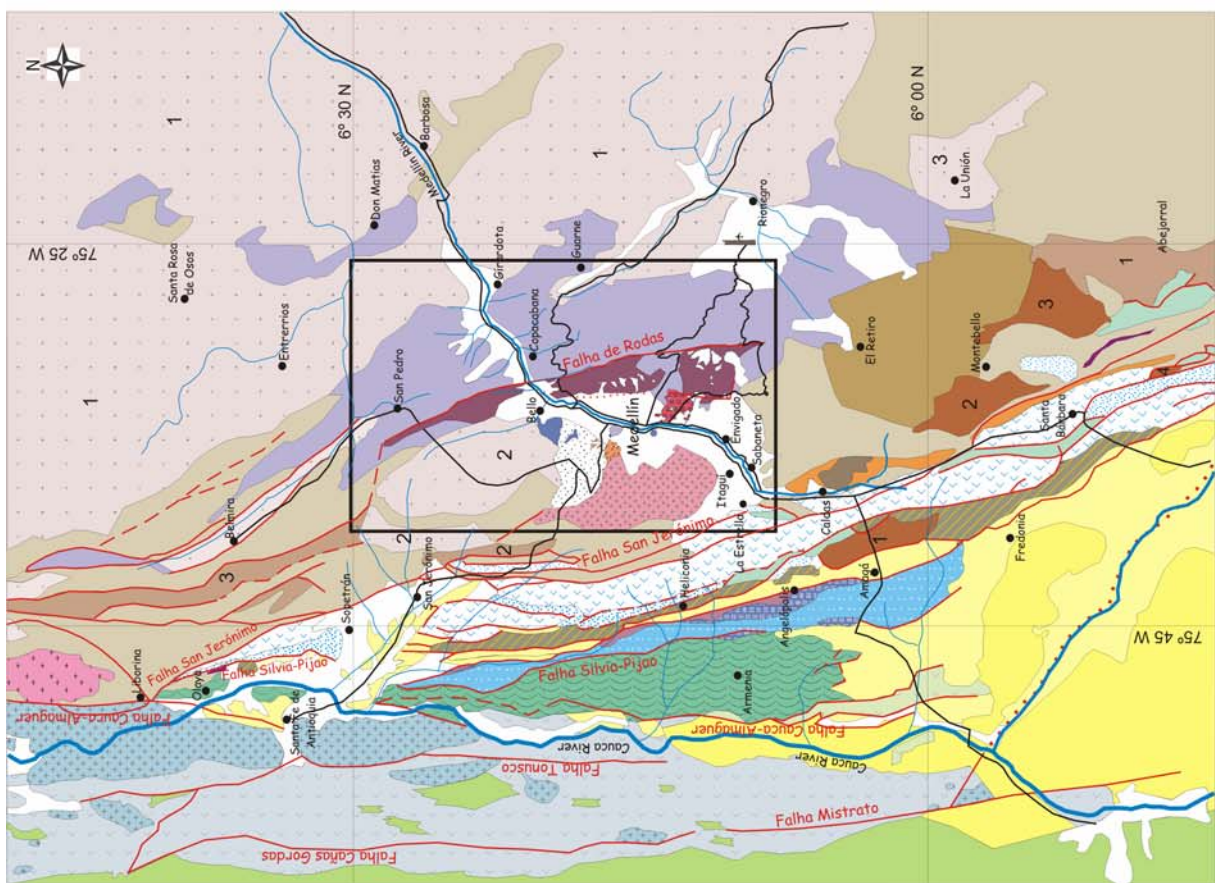


Figura 6. Geologia regional do setor norte da Cordilheira Central e parte da Cordilheira Ocidental, mostrando o Complexo polimetamórfico da Cordilheira Central, os complexos mafíticos e ultramáficos e os plutões cretáceos. Adaptado de Botero (1963), González (2001), Montoya & Paléz (1993), Correa & Martens (2000), Nivia & Gómez (2005). O retângulo define os limites da área de estudo.



Os *corpos intrusivos* de arco, cretáceos, mais importantes na Cordilheira Central, são o Batólito de Santa Bárbara (Figura 5b) e o Batólito Antioqueno, com seus corpos satélites (Figura 6). O Batólito de Santa Bárbara aflora na porção sudoeste da Cordilheira Central, ocupando uma área de 375 km², exibe composição tonalítica e é intrusivo nas rochas metamórficas do Complexo Arquía. A idade pode ser paleozóica (McCourt et al. 1984) ou cretácea (Restrepo et al. 1991). O Batólito Antioqueno aflora no setor setentrional da Cordilheira Central, ocupando área de 7543 km². Apresenta diferentes fácies, sendo que a principal varia entre tonalito e granodiorito, e as fácies subordinadas são uma félscica e outra gabróica (González 1997). Este corpo tem forma trapezoidal e está em contacto intrusivo com as rochas metamórficas do Complexo Polimetamórfico da Cordilheira Central. Idades cretáceas entre 100 Ma e 68 Ma aparecem registradas por vários métodos de datação (Pérez 1967, Ordóñez-Carmona 2001, Ordóñez-Carmona & Pimentel 2001).

1.6.2 Associações de rochas máficas e ultramáficas oceânicas nos Andes Colombianos

As associações de rochas máficas e ultramáficas na Colômbia ocorrem principalmente no eixo e no flanco ocidental da Cordilheira Central, na Cordilheira Ocidental e na Serranía de Baudó (Restrepo & Toussaint 1973, 1974, Alvarez 1985, Bourgois et al. 1985, 1987). Também existem conjuntos menores na região do Caribe (Mejía & Durango 1981, Alvarez 1967, Sepúlveda 2003, Weber et al. 2004).

Bourgois et al. (1985, 1987) explicam a formação da Cordilheira Ocidental a partir de *nappes* do tipo alpino, produzidos por empurrão e dobramento que atingiram, durante seu alojamento, porções da Cordilheira Central. Os autores sugerem que tenham acontecido duas fases de obdução ofiolítica no Mesozóico. Com isto, todos os conjuntos ofiolíticos, em ambas as cordilheiras, seriam cogenéticos. No entanto, trabalhos de detalhe em alguns complexos mostraram que existem diferenças genéticas, metamórficas e temporais, entre as várias associações máfico-ultramáficas de ambos os lados da falha Cauca-Almaguer (Restrepo & Toussaint 1984, Toussaint 1996, Nivia et al. 1996) (Figura 7). A principal característica a ressaltar é que os conjuntos a leste da falha Cauca-Almaguer foram gerados em ambiente de platô oceânico (Millward et al. 1984, Nivia 1987, Kerr et al. 1996) e não correspondem a ofiolitos *sensu stricto*.

1.6.2.1 Associações máficas-ultramáficas a oeste da falha Cauca-Almaguer

As unidades que afloram a oeste da falha Cauca-Almaguer no setor sudoeste da Cordilheira Central e na Cordilheira Ocidental correspondem a rochas ígneas e sedimentares

cretáceas de afinidade oceânica que Nivia (1993) agrupou na Província Litosférica Oceânica Cretácea Ocidental - PLOCO (Figura 6 e 7).

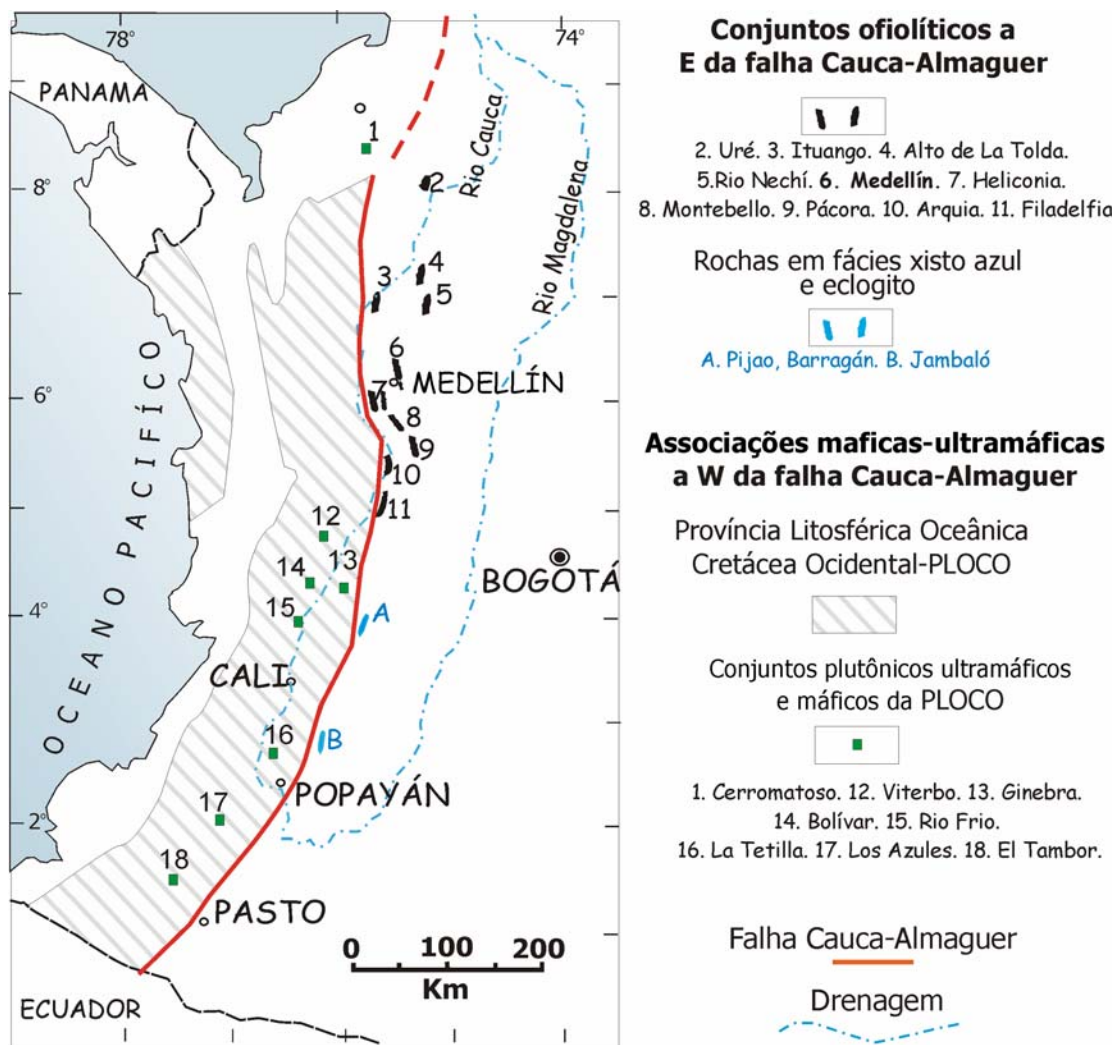


Figura 7. Distribuição das associações mafico-ultramáficas de afinidade oceânica nas cordilheiras Central e Ocidental da Colômbia. Modificado de Restrepo & Toussaint (1973), Toussaint (1996), Kerr et al. (1997).

A *Província Litosférica Oceânica Cretácea Ocidental* consiste de espessas seqüências de rochas vulcânicas básicas com intercalações menores de rochas sedimentares e em menor proporção associações de rochas plutônicas ultramáficas e maficas, que ocorrem em blocos imbricados com deformação variável (Nivia 1996). As vulcânicas básicas ocupam grandes extensões e correspondem a derrames picríticos e basálticos, bem como a *sills* e diques diabásicos. Os diferentes nomes dados por diversos autores ao longo do tempo para os conjuntos vulcânicos são: Grupo Diabásico, Basaltos de la Trinidad e Formações Amaime e Volcánica. As rochas sedimentares são siltitos, grauvacas líticas e cherts, agrupadas nas formações Penderisco, Consólida e Lázaro, Grupo Dagua e Complexo Estrutural Dagua.

Dentre os conjuntos de gabros e peridotitos pertencentes à PLOCO estão (Figura 7) o Complexo Ultramáfico de Bolívar e gabros associados de Riofrio, Rio Volcanes, complexos ofiolíticos de Los Azules, La Tetilla e Ginebra, *stocks* de El Palmar e El Tambor, ultramafita de Puente Umbría-La Isla, Gabro de Anserma, Gabro Uralítico de Belen de Umbría, Plutón de Mistrató e o Gabro Santa Fe de Antioquia, antes conhecido como Batolito de Sabanalarga (Nivia & Gómez 2005).

As rochas ígneas se formaram em ambiente de platô oceânico, associado a uma pluma do manto, enquanto que as sedimentares correspondem a material depositado em deltas progradantes desenvolvidos sobre o platô, durante sua acresção à borda continental (Nivia 1996). Estes terrenos representam a porção sul da grande Província Ígnea Cretácea Colombiana-Caribenha. Kerr et al. (1997) identificam variações geoquímicas nas rochas vulcânicas, sendo que o grau de empobrecimento em elementos traços incompatíveis aumenta de leste para oeste. Também reconhecem três intervalos de idades distintas da atividade vulcânica, que de leste para oeste, são: >100 Ma, 90-82 Ma e 78-73 Ma.

1.6.2.2 Associações máficas-ultramáficas a leste da falha Cauca-Almaguer

Toussaint (1996) fez uma divisão dos conjuntos a leste da falha Cauca-Almaguer (a mais ocidental do sistema de Romeral), em ofiolitos com evidências de metamorfismo de média a alta pressão e baixa temperatura, e ofiolitos sem evidências de metamorfismo regional. Quase todos os ofiolitos a leste da falha Cauca-Almaguer estão desmembrados e ocorrem como fatias e fragmentos. Na borda ocidental da cordilheira, corpos de gabros e peridotitos estão associados, ora com rochas metamórficas cretáceas (?) de pressão alta a média - temperatura baixa do Complexo Arquía, ora com rochas vulcano-sedimentares do Cretáceo Inferior do Complexo Quebradagrande. Ainda no flanco ocidental, na região de Medellín e no eixo da cordilheira, na região de Yarumal, os fragmentos ofiolíticos estão relacionados espacialmente com rochas metamórficas do Paleozóico-Mesozoico Inferior do embasamento da Cordilheira Central.

As associações de rochas ultramáficas e máficas, sem metamorfismo aparente, expostas no flanco ocidental e no eixo da Cordilheira Central, foram agrupadas no Complexo Ofiolítico do Cauca (Restrepo & Toussaint 1974). De forma mais restrita, Alvarez (1983) incluiu no Cinturão Ofiolítico de Romeral só os conjuntos de rochas ultramáficas e máficas associados à zona tectônica de Romeral. O metamorfismo é de baixo grau, fácies xisto verde (Alvarez 1983).

De oeste para leste os conjuntos de *ofiolitos no sistema de falhas de Romeral* são o Complexo Arquia, o complexo máfico-ultramáfico de Heliconia e o Complexo Quebradagrande (Figura 6):

O *Complexo Arquia* é um cinturão metamórfico de pressão média, que aflora na borda leste do Vale do Rio Cauca e está espacialmente associado a corpos ultrabásicos e escamas de rochas de alta pressão. É uma faixa descontínua que se estende de 7°30' N até 4° S (Figura 5b). No sentido de Maya & González (1995), corresponde a um complexo litodémico que agrupa várias unidades previamente definidas por outros autores. Encontra-se em contacto tectônico, a leste, com o Complexo Quebradagrande e, a oeste, com a Província Litosférica Oceânica Cretácea-PLOCO (Figura 6), por meio das falhas Silvia-Pijao e Cauca-Almaguer, respectivamente. Toussaint (1996) interpreta o complexo como ofiolitos metamorfisados em pressão média a alta e temperatura baixa.

O Complexo Arquia consiste em grafita xistos, biotita xistos, quartzitos, actinolita xistos, anfibolitos, granada anfibolitos, serpentinitos, metagabros, metadioritos, hornblenda pegmatitos, hornblenda gnaisses e esparsos corpos ultramáficos. Estas rochas foram metamorfizadas nas fácies xisto verde e anfibolito, sob condições de média a alta pressão. As rochas foram agrupadas em várias unidades que receberam diferentes nomes ao longo da cordilheira: a norte, o grupo Arquia (Restrepo & Toussaint 1975), xistos anfibólicos do Cauca (González, 1976) e, a sul, xisto de Bugalagrande, anfibolito Rosário, metagabro Bolo Azul, e anfibolito e metagabro San Antônio (McCourt et al. 1984).

As fatias, com evidências de metamorfismo nas fácies xisto azul e eclogito, consistem em jadeita-glaucofano xistos, lawsonita-glaucofano xistos e eclogitos, com intercalações menores de mica xistos (Orrego et al. 1980, Feininger 1980, 1982, McCourt & Feininger 1984) e ocorrem de maneira descontínua com *trend* N-NE no flanco ocidental da Cordilheira Central, aproximadamente a 5-10 km a leste da falha Cauca-Almaguer (Figura 7). Os eclogitos e xistos azuis formaram-se em zona de subducção (Feininger 1980, McCourt & Feininger 1984) durante o Jurássico - Eo-Cretáceo e fazem parte de uma *mélange* que resultou da intercalação tectônica com unidades metamórficas paleozóicas (Orrego et al. 1980). Alternativamente, elas foram geradas durante a colocação de ofiolitos ao longo da margem continental (Restrepo & Toussaint 1975).

A idade do complexo é motivo de controvérsia, já que alguns autores o consideram como de idade paleozóica (McCourt et al. 1984) e outros cretácica (Restrepo & Toussaint 1975).

O *Complexo mafico-ultramáfico de Heliconia* é um conjunto que aflora a leste do Complexo Arquia e oeste do Complexo Quebradagrande (Figura 6). Foi estudado inicialmente por Grosse (1926) e denominado por Montoya & Peláez (1993). Corresponde a uma faixa alongada N10°W composta por três corpos: um de peridotito, outro de gабro e outro de diorito. Os nomes de cada um dos membros do complexo são Harzburgito de Heliconia (Montoya & Peláez 1993), Gabro de Pueblito (Toussaint & Restrepo 1978) que depois Montoya & Peláez (1993) propuseram chamar de Gabro de Heliconia e, finalmente, o Diorito de Pueblito (Toussaint & Restrepo 1978). Os contatos com as unidades adjacentes são: a leste a falha Amagá que limita o complexo com a Formação Amagá (Paleógeno-Neógeno) e o Stock de Amagá (Triássico) e, a oeste, a falha Silvia-Pijao, que marca o contato com o Complexo Arquía. O contato entre o diorito e o gabro é a falha Llorasangre e, entre o gabro e o peridotito, a falha Sabaletas. O gabro e o diorito apresentam saussuritização e uralitização parcial e o harzburgito está parcialmente serpentinizado.

Montoya & Peláez (1993) incluem no complexo só os corpos de peridotito e gabro e separam o corpo de diorito do complexo, por considerar que não existem evidências que permitam concluir que o diorito também faz parte do conjunto. Os autores concluem que o modelo mais apropriado para explicar a geração deste complexo é o de um ofiolito.

Vinasco et al. (2001) obtiveram idades Ar-Ar de 230+/-3 Ma e 224+/-2 Ma no gabro e de 238+/-1 Ma e 232+/-1.6 Ma no diorito. Vinasco et al. (2003) interpretam estes resultados como idades magmáticas que definem o Triássico como o limite mínimo para o Complexo Arquía.

O *Complexo Quebradagrande* é um cinturão descontínuo que aflora na porção ocidental da área de estudo, ao longo do flanco ocidental da Cordilheira Central (Figura 5b e 6). Está limitado a leste com o Complexo Cajamarca, por meio da falha San Jerônimo, e a oeste com o Complexo Arquía, por meio da falha Silvia-Pijao (Maya & González 1995). Consiste em rochas meta-vulcânicas (basálticas a andesíticas) e meta-sedimentares cretáceas, de afinidade oceânica (González 1980, Gómez et al. 1995, Mojica et al. 2001). As rochas vulcânicas exibem evidências de metamorfismo dinâmico, na fácie prehnita-pumpellyita, e ocorrem em blocos justapostos. A idade deste conjunto foi determinada por fósseis como sendo do intervalo compreendido entre o Barresiano até o Albiano (González 1980, Gómez et al. 1995). Este complexo pode representar: (i) a parte superior de um ofiolito (Restrepo & Toussaint 1973, 1974), (ii) um arco insular (Restrepo & Toussaint 1975, Nivia et al. 1996, Chicangana et al. 2004), (iii) um rifte oceânico (González 1980), ou (iv) uma bacia marginal

intracratônica (Nivia et al. 1996, 2006). Os últimos autores, a partir de dados geoquímicos, sugerem uma fonte de manto localizada acima de uma zona de subducção para as rochas vulcânicas, e de acordo com esta proposta, o Complexo Quebradagrande não é cogenético com as rochas vulcânicas a oeste da falha Cauca-Almaguer que exibem afinidade de platô oceânico.

Alguns corpos ultramáficos isolados e *conjuntos ofiolíticos afloram a leste da Falha San Jerônimo* (a mais oriental do sistema Romeral). Dentre os maiores são o Complexo Ofiolítico de Yarumal, no eixo da Cordilheira, na área de Yarumal, a norte do Estado de Antioquia (Figura 8) e o Ofiolito de Aburrá, no flanco oeste da Cordilheira, nas adjacências de Medellín (Figura 6 e 9).

Complexo Ofiolítico de Yarumal. Aflora ao norte do Batólito Antioqueno, no município de Yarumal, próximo às localidades de Yarumal e Campamento (Figura 8). Foi definido por Estrada (1967) e também é conhecido como associação de rochas básicas e ultrabásicas del Nechí. Consiste em serpentinitos e peridotitos, intimamente associados a gabros, gabros grossos acamados (bandas entre 10 e 70 cm de espessura), basaltos maciços toleíticos e basaltos almofadados, estes últimos associados com tufos, aglomerados vulcânicos e rochas sedimentares (turbiditos arenosos e pelitos finamente bandados). Não existem idades radiométricas diretas do Complexo, mas o mesmo está intrudido pelo Batólito Antioqueno (80-100 Ma) e em contato falhado com as rochas metamórficas (xistos e gnaisses) do embasamento da Cordilheira Central. Depósitos importantes de talco e asbestos estão associados a este complexo.

O processo de colocação dos ofiolitos que hoje afloram no eixo da Cordilheira Central e a leste da falha San Jerônimo não é claro. Restrepo & Toussaint (1973) propõem grandes *nappes*, com deslocamentos de até 70 km, desde o atual vale do rio Cauca. Bourgois et al. (1987) sugerem que o alojamento ocorreu entre a deposição da Fm. La Soledad (Albiano) e a intrusão do Batólito Antioqueno. Ordóñez-Carmona & Pimentel (2002) sugerem obdução deste ofiolito sobre a porção setentrional da Cordilheira Central, durante a colisão do Complexo de Puqui com a Cordilheira Central, há ~140-120 Ma.

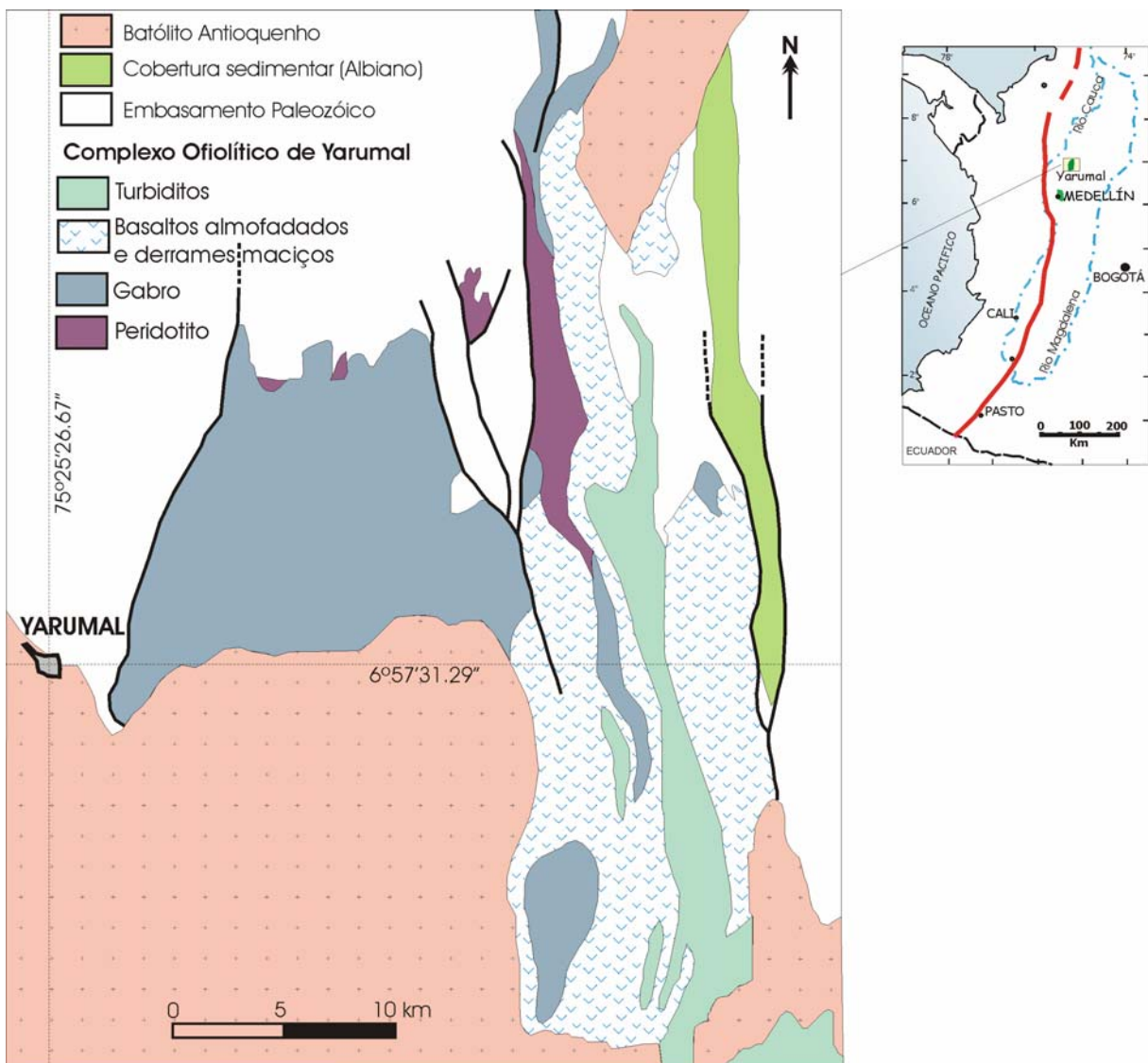


Figura 8. Geologia do Complexo ofiolítico de Yarumal, eixo da Cordilheira Central. *Apud* Hall et al. (1972) *in* Bourgois et al. (1987).

O *Complexo Ofiolítico de Aburrá* ocorre no flanco ocidental da Cordilheira Central, a leste e norte do vale do Rio Medellín ou Vale de Aburrá, na cidade de Medellín e alguns municípios próximos. Foi definido com este nome por Correa & Martens (2000) e consiste de porções do manto e de crosta oceânica (Figura 9). Está em contato tectônico sobre rochas metamórficas mais antigas do que o Triássico Médio e é intrudido por rochas do Jurássico e do Cretáceo.

Rochas metamórficas do embasamento

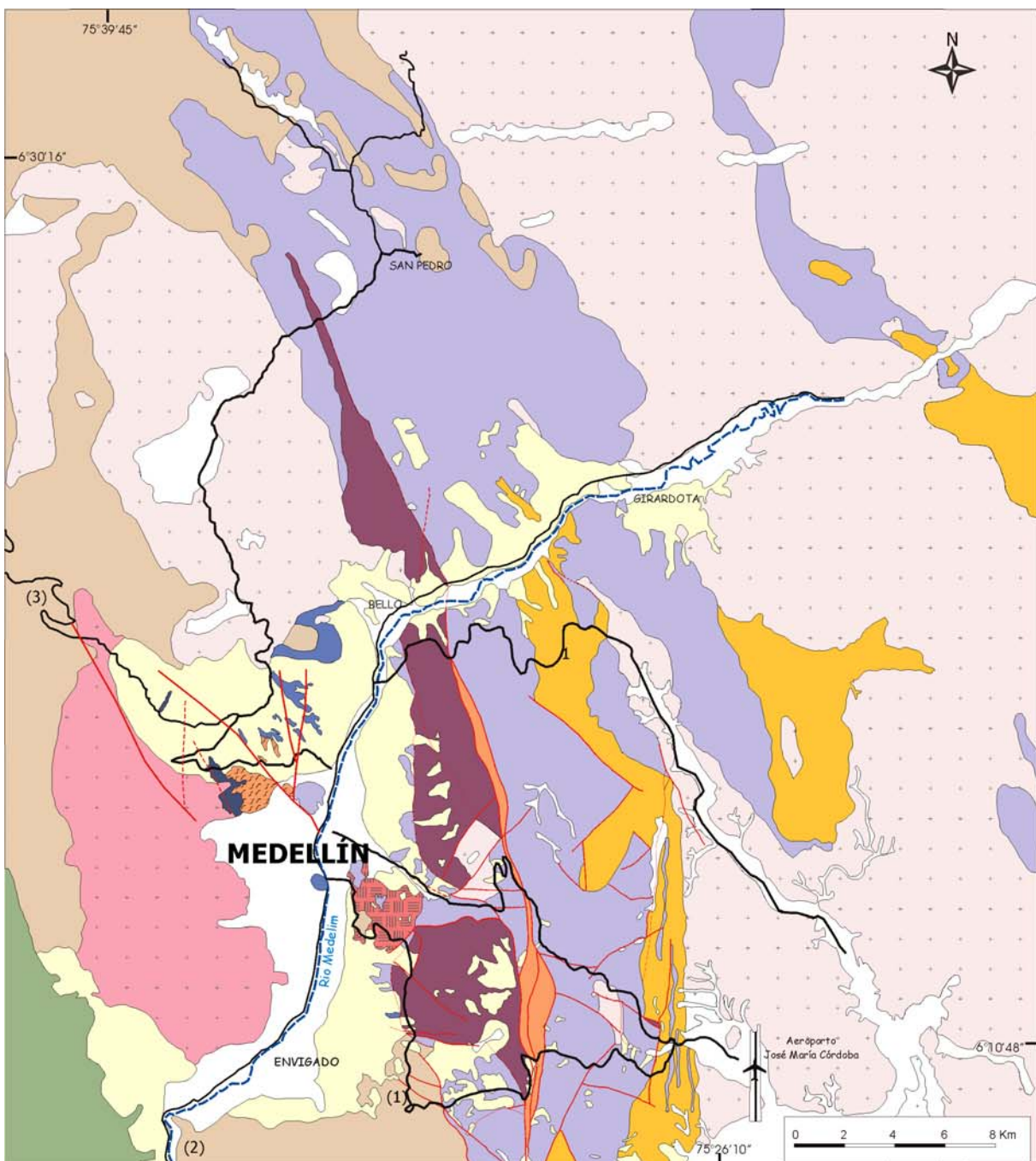
As unidades subjacentes ao ofiolito consistem em rochas metamórficas tais como gnaisses, migmatitos, xistos e anfibolitos e, em menor proporção, granulitos. Estas rochas

foram inicialmente reunidas no Grupo Ayurá-Montebello por Botero (1963) e Echeverría (1973) dividiu o grupo em Zona Montebello, com as rochas de baixo grau, e Zona Ayurá, com as rochas de alto grau. Restrepo & Toussaint (1982) agruparam estas unidades no Complexo Polimetamórfico da Cordilheira Central baseados em evidências geocronológicas dos eventos Devoniano-Carbonífero, Permo-Triássico e Cretáceo.

Algumas denominações informais para as unidades são gnaisses das Palmas e Ayurá (Restrepo & Toussaint 1984), paragnaisse de Las Peñas (Correa & Martens 2000), Anfibolitos de Medellín (Restrepo & Toussaint 1984, Correa & Martens 2000), migmatitos de Puente Peláez (González 1980), granulitos de El Retiro (Restrepo & Toussaint 1984, Ardila 1986), xistos sericíticos de Ancón e Baldías (Restrepo & Toussaint 1984). Grande parte dessas unidades, em especial as que afloram a leste da área de estudo, foi reagrupada e redenominada por Rodríguez et al. (2005), no Complexo El Retiro, enquanto outras unidades novas foram definidas por estes autores. O Complexo El Retiro consiste das unidades: Anfibolitos, Gnaisses e Migmatitos de Puente Peláez, Gnaisse de Las Palmas, Granofelsa de Normandia, Gnaisse Milonítico de Sajonia e os Gnaisses de La Ceja. Nesta nova divisão os Gnaisses de La Ceja incluem a unidade “paragnaisse de Las Peñas” e parte do que antes era conhecido como “granulitos de El Retiro”.

Dados radiométricos indicam que o último metamorfismo orogênico destas unidades aconteceu no intervalo do Permo-Triássico (Toussaint & Restrepo 1976, Ordóñez-Carmona et al. 2001, Vinasco et al. 2006). A maior parte das rochas metamórficas exibe uma componente crustal importante (Ordóñez-Carmona 2001, Vinasco et al. 2006), exceto a unidade Anfibolitos de Medellín, que são rochas derivadas do manto (Correa & Martens 2000).

É importante salientar que muitos autores interpretaram os anfibolitos próximos à cidade de Medellín como parte do embasamento da Cordilheira Central, metamorfizado e erodido antes do alojamento do ofiolito (Echeverría 1973, Restrepo & Toussaint 1973, Rodríguez et al. 2005). No entanto, outros autores (Restrepo 1986, 2003, Pereira & Ortíz 2003) chamaram a atenção sobre a possibilidade destas rochas serem também parte do ofiolito. De acordo com as características petrográficas, químicas e isotópicas, estas rochas representam partes de uma crosta oceânica (Correa & Martens 2000) e, um dos objetivos desta tese é discutir se podem ou não ser parte do ofiolito do Vale de Aburrá.



LEGENDA

Aluvíones	Gnaisse milonítico de Sajonia
Colúvios	Gnisses de La Ceja. 1. Las Peñas
1-Batolito Antioqueno. 2-Stock de Ovejas	Anfibolito de Santa Elena
Diorito de Altavista	Anfibolito de Boquerón
Gabro de San Diego	Metagabro de El Picacho
Complexo Quebradagrande	Dunito de Medellín
Gnaisse de La Iguaná	(1) Gnisses de Las Palmas e Ayurá. (2) Xistos de Ancón. (3) Xistos de Baldías
Complexo Ofiolítico de Aburrá	

Figura 9. Mapa da geologia local do Vale de Aburrá. Modificado de Botero (1963), Rendón (1999), Correa & Martens (2000) e Rodríguez et al. (2005).

Anfibolitos e rochas metassedimentares associadas

O Anfibolito de Medellín (Restrepo & Toussaint 1984) ou Anfibolito de Santa Elena (Restrepo 2005) ocorre na parte leste da área de estudo (Figura 9), como corpo alongado segundo N-S, com aproximadamente 72 km de comprimento e 6 km de largura. Restrepo (2005) sugeriu mudar o nome de Anfibolito de Medellín para Anfibolito de Santa Elena porque a denominação inicial não era mais válida. A unidade Anfibolito de Medellín incluía todos os corpos de metabasitos dos arredores da cidade de Medellín, mas Correa & Martens (2000) propuseram que alguns corpos de rochas maficas deveriam ser excluídos da grande unidade e classificados em unidades diferentes, como é o caso do Metagabro de El Picacho e Anfibolito de Boquerón.

A unidade consiste em metabasitos de alto grau, intercalados em alguns setores, de maneira estratigráfica ou tectônica, com pacotes de xistos e paragnaisse. Os anfibolitos consistem em hornblenda + plagioclásio, acompanhados por titanita +/- quartzo +/- opacos (ilmenita, sulfetos), apatita e zircão acessório. Em alguns locais existe granada e em outros diopsídio. A paragênese metamórfica corresponde à fácie anfibolito, possivelmente de média pressão (Correa et al. 2005a). Os anfibolitos apresentam evidências estruturais de pelo menos três fases tectônicas (Tamayo 1984, Correa & Martens 2000). Do ponto de vista químico, estes anfibolitos exibem características de basaltos tipo MORB (T-MORB) e as assinaturas isotópicas também são compatíveis com rochas derivadas do manto (Correa & Martens 2000). Os ambientes tectônicos mais prováveis para geração desta unidade são uma dorsal meso-oceânica com aporte de sedimentos continentais, ou uma bacia retro-arco evoluída e afastada da zona de subducção (Correa et al. 2005a). A unidade está em contato por falha com a unidade Dunitos de Medellín e é intrudida pelo Batólito Antioqueno.

O anfibolito de Boquerón ocorre a oeste de Medellín, principalmente em blocos métricos (que fazem parte de coluvião) e em poucos afloramentos *in situ* (Correa & Martens 2000). De maneira local, os blocos destes anfibolitos estão misturados com blocos do Metagabro de El Picacho. Os anfibolitos são de grão grosso e consistem em hornblenda e plagioclásio mais titanita, ilmenita, apatita e +/- quartzo. A litogegeoquímica e a química isotópica destes anfibolitos são semelhantes às do Anfibolito de Medellín, enquanto as características estruturais sugerem que se trata de um corpo ígneo fanerítico deformado semelhante ao Metagabro de El Picacho.

A unidade de rochas metassedimentares relacionadas espacialmente com o Anfibolito de Santa Elena tem recebido os seguintes nomes: Paragnaisse associados ao Anfibolito de

Medellín (Restrepo & Toussaint 1984), grupo Medellín que incluía anfibolitos e paragnaisse associados (Restrepo 1986), Paragnaisse de Las Peñas (Correa & Martens 2000; Estrada-Carmona 2003) e Gnaisse de La Ceja (Rodríguez et al. 2005).

Unidades do Ofiolito

A porção do manto do ofiolito conhecida como Dunito de Medellín (Restrepo & Toussaint 1984) está localizada a leste e norte de Medellín, numa faixa de 35 km de comprimento e largura entre 0,2 a 5 km, com direção aproximada N15°W. A faixa está dividida nos corpos sul, central e norte (Figura 9). A rocha predominante no maciço é dunito composto por olivina e cromita acessória, com magnetita e serpentina como minerais de alteração (Alvarez 1982). Em alguns locais dos três corpos há jazidas de cromita podiforme (Geominas 1975, Alvarez 1987). As rochas ultramáficas se sobrepõem, em contato tectônico, ao Anfibolito de Santa Elena (Restrepo 2005). Em alguns setores, o contato caracteriza-se pela presença de clorita e tremolita xistos.

Há outros corpos pequenos de rochas ultramáficas, alguns quilômetros a sul (Botero 1963, Rodríguez et al. 2005), leste (Restrepo & Toussaint 1973) e a norte (Rico 1965), da faixa principal de peridotitos, que podem representar sua continuação.

A porção da crosta oceânica, segundo Correa & Martens (2000), está representada pelo Metagabro de El Picacho (Figura 9). O Metagabro ocorre como blocos no cerro El Picacho e em vários locais do noroeste de Medellín, no centro da cidade, no cerro Nutibara e a leste, em sítios vizinhos aos peridotitos (Correa & Martens 2000). As rochas preservam macroestruturas de rochas gabróicas, mas as microestruturas foram obliteradas devido à deformação dinâmica e alteração hidrotermal em fácies xisto verde ou anfibolito baixo. As rochas consistem em anfibólito, plagioclásio e clinopiroxênio recristalizados, e epidoto de saussuritização. A natureza dos contatos com as unidades adjacentes é mal conhecida devido à sua ocorrência em blocos. Os blocos de metagabro ocorrem em certos locais misturados com os blocos de anfibolitos de Boquerón no mesmo depósito. A unidade de metagabros é possivelmente intrudida pelo gnaisse de La Iguaná (Rendón 1999).

As idades de geração e colocação das unidades do ofiolito não são conhecidas com precisão. Inicialmente, os peridotitos eram interpretados como gerados no Jurássico e alojados no Cretáceo (Restrepo & Toussaint 1973, Alvarez 1985). Restrepo (2003) admite a possibilidade de que tanto os anfibolitos quanto os dunitos se alojaram em um embasamento continental indeterminado e participaram do mesmo metamorfismo durante a orogenia perm-

triássica. Para Pereira & Ortiz (2003) estas unidades foram metamorfisadas, provavelmente, durante o episódio tectono-metamórfico Apalachiano, ocorrido no Devoniano-Carbonífero.

Unidades posteriores ao ofiolito

As unidades mais novas do que o ofiolito correspondem principalmente a plutões que intrudem o ofiolito e extensos depósitos de colúvio (Figura 9), que em muitos locais, cobrem as relações entre os membros do ofiolito. Há também depósitos aluviais, principalmente do Rio Medellín. Os plutões da área são o Gnaisse de La Iguaná (Restrepo & Toussaint 1984), Gabro de San Diego (Restrepo & Toussaint 1984, Machado & Salazar 2000), *Stock* de Altavista (Montoya 1987, Preciado & Vásquez 1987, Rodríguez & Sánchez 1987) e o Batólito Antioqueno (Botero 1963, Feininger & Botero 1982).

O Gnaisse de La Iguaná corresponde a um granitóide milonitizado intrusivo nos anfibolitos de Boquerón, e apresenta idade de cristalização de $180 \pm 1,9$ Ma (Correa et al. 2005b).

O Gabro de San Diego consiste de gабro, e em menor proporção, de diorito, parece ser intrusivo nos dunitos (Rendón 1999) e sua fácie diorítica tem idade de cristalização de 94 ± 0.9 Ma (Correa et al. 2006).

O *Stock* de Altavista é um corpo de composição heterogênea, que apresenta desde dioritos até granitos, intrude o Gnaisse de La Iguaná e, aparentemente, também os anfibolitos de Boquerón. A fácie diorítica tem idade de cristalização de 96 ± 0.39 Ma, enquanto a granítica de 87 ± 0.53 Ma (Correa et al. 2006).

O Batólito Antioqueno é um plutão extenso que consiste em tonalitos e granodioritos com alguns corpos gabrómicos subordinados (Feininger & Botero 1982). Na porção leste da área de estudo, as rochas deste corpo intrudem o embasamento metamórfico da cordilheira, os Anfibolitos de Medellín e os Dunitos de Medellín. Apresenta vários corpos satélites, como o Tonalito de Ovejas e os *Stocks* de Las Estancias e Media Luna. A maior parte das datações, pelos métodos K-Ar, Rb-Sr e U-Pb, têm fornecido idades do Eo-cretáceo, entre 67 a 100 Ma (Pérez 1967, Ordóñez-Carmona & Pimentel 2001).

CAPÍTULO 2

THE NATURE OF THE ULTRAMAFIC SECTION OF THE ABURRÁ OPHIOLITE, MEDELLÍN REGION, COLOMBIAN ANDES

Ana María Correa M

Instituto de Geociências, Universidade de Brasília, Campus Universitário Darcy Ribeiro,
Brasília, Brazil. CEP 70910900, anamacor@unb.br

Ariplínio A. Nilson

Instituto de Geociências, Universidade de Brasília, Campus Universitário Darcy Ribeiro,
Brasília, Brazil. CEP 70910900, aanilson@unb.br

Abstract

The Medellín Ultramafic Massif, previously known as the Medellín Dunite, consists mainly of dunite and, subordinately, of harzburgite, chromitites, ultramafic dykes and wehrlite. Metamorphic peridotite occurs at the base of the ultramafic bodies. Harzburgite is divided into two types, one with preserved orthopyroxene (I-Type) and other with bastite, talc and tremolite pseudomorphs after orthopyroxene (II-Type). Dunite forms extensive bodies, but also occurs as bands within II-Type harzburgite. Chromitite bodies with dunite envelopes are associated with II-Type harzburgite. Wehrlite is scarce and occurs in the uppermost part of the ultramafic section, close to the limit with the mafic unit.

I-Type harzburgite corresponds to the lower peridotite within this mantle portion and it probably represents a residual peridotite after ~15-17% partial melting of lherzolite mantle. Dunite bands within II-Type harzburgite are interpreted as the result of melt/rock interaction of harzburgite with MORB or BABB melts. Wehrlite is interpreted as impregnated peridotite, resulting from the interaction between dunite and hydrous MORB (or BABB) melts. Dunite, II-Type harzburgite, chromitites and wehrlite are interpreted as the Transition Zone of the Harzburgite-Type Aburrá Ophiolite.

The tectonomagmatic evolution of peridotite comprises at least two stages. During the first stage, a suite of spinel harzburgite was formed after partial melting of the mantle. In the second stage, spinel harzburgite was affected by percolating MORB- or BABB-type melts. These processes probably took place in an oceanic back-arc environment.

Key words: peridotite, Moho Transition Zone, melt-rock interaction, Aburrá Ophiolite, Colombian Andes

Resumo

O Maciço Ultramáfico de Medellín, antes conhecido como Dunito de Medellín, consiste principalmente em dunito e em menor proporção de cromititos, harzburgito, diques ultramáficos e wehrlito. Peridotito intensamente deformado e recristalizado ocorre na base dos corpos ultramáficos. O harzburgito é subdividido em dois grupos: Tipo-I, que contém ortopiroxênio preservado e Tipo II, no qual o ortopiroxênio foi totalmente substituído por pseudomorfos de bastita, talco e tremolita. Dunito ocorre em corpos extensos e também em bandas dentro de harzburgito Tipo-II. Os cromititos podiformes com envelopes de dunito estão associados com harzburgito. Wehrlito ocorre em corpos pequenos e esparsos na parte mais superior da seção ultramáfica próximo ao limite com a crosta máfica.

Harzburgito Tipo-I é interpretado como peridotito residual após aproximadamente 15 a 17% de fusão parcial do manto lherzolítico. Dunito em bandas intercaladas com harzburgito Tipo-II é interpretado como resultante da interação fusão/rocha, ou seja, da reação do harzburgito com fusões percolantes dos tipos MORB ou BABB. Wehrilito é interpretado como peridotito impregnado resultante da interação de dunito com fusões do tipo MORB (ou BABB) e provavelmente também com fusões hidratadas. O conjunto formado por dunito, harzburgito tipo II, cromititos e wehrilito é interpretado como a Zona de Transição do ofiolito tipo Harzburgito de Aburrá.

A evolução tectonomagmática do maciço peridotítico compreendeu pelo menos dois estágios. Durante o primeiro estágio uma suite composta de espinélio harzburgito foi formada durante a fusão parcial do manto. No segundo estágio o espinélio harzburgito foi afetado pela percolação de fusões tipo MORB ou BABB. Esses processos ocorreram provavelmente em ambiente oceânico do tipo retro arco.

Palavras-chave: peridotito, Zona de Transição, interação rocha-fusão, ofiolito de Aburrá, Andes Colombianos.

2.1. Introduction

Ophiolitic peridotites may record features resulting from processes such as partial melting, melt-peridotite interaction and melt segregation in the oceanic mantle (Leblanc et al., 1980; Nicolas, 1989; Pearce et al., 2000; Zhou et al., 2005). Therefore, peridotite composition may be used as an indicator of the original tectonic setting as well as of the petrogenetic processes involved in the formation of these rocks (Dick and Bullen, 1984; Boudier and Nicolas, 1985).

In the Colombian Andes, ophiolitic peridotite is located mainly along the western flank of the Central Cordillera, within the Romeral Fault System (Restrepo and Toussaint, 1973; Alvarez, 1985) and, in lesser proportion, to the east of this fault system (Restrepo and Toussaint, 1984) such as peridotite from the Aburrá Ophiolite. Ophiolitic peridotite in Colombia has been only superficially studied and there is not enough data to constrain the genesis and tectonic evolution. This is especially true for the ultramafic unit exposed in the vicinity of the city of Medellín, in the Aburrá Valley.

The ultramafic rocks in the Medellín area were grouped by Botero (1963) in the so-called Medellín serpentinites and by Restrepo and Toussaint (1984) in the Medellín Dunite. This unit represents the upper mantle member of the Aburrá Ophiolitic Complex (Correa and Martens 2000) or Aburrá Ophiolite. According to Alvarez (1982), the massif is formed mainly

by dunite. Although dunite is the dominant lithotype in the massif other types of peridotite have been recognized. Thus the unit is hereafter referred to as the Medellín Ultramafic Massif.

In this paper we present new field, petrographic and mineral chemistry data of representative ultramafic rocks of the Aburrá Ophiolite. The data are used to show that the ultramafic massif is not as compositionally homogeneous as previously thought. Moreover, evidence of melt-mantle peridotite interaction in the Transition Zone is reported for the first time. Finally, inferences are drawn on the original tectonic setting where mantle peridotite uprise took place.

2.2. Regional Geological Setting

The western flank of the Colombian Central Cordillera is cut by the Romeral Fault System (Figure 1) which is interpreted as a major domain boundary in Colombia, broadly separating the domains with Cretaceous oceanic basement to the west from domain with Palaeozoic continental basement to the east (Case et al., 1971, 1973; McCourt et al., 1984). Although most ophiolitic fragments occur along the fault system (Restrepo and Toussaint, 1973; Alvarez, 1985), some oceanic assemblages also occur associated to the continental basement of the Central Cordillera such as the Aburrá Ophiolitic Complex.

The continental basement of the cordillera consists of Palaeozoic to Early Mesozoic metamorphic rocks comprising the Central Cordillera Polymetamorphic Complex (in the sense of Restrepo and Toussaint, 1982) or the Cajamarca Complex (in the sense of Maya and González, 1995). The main types of rocks in the study area are gneisses, schists, amphibolites, migmatites and granulites. With the exception of the amphibolites and some other smaller units, almost all the metamorphic rocks were derived from sources with continental crust affinity (Ordóñez-Carmona, 2001; Vinasco et al., 2006). The last orogenic metamorphism recorded in these units is attributed to a Permian-Triassic continent-continent collision (Toussaint and Restrepo, 1976; Vinasco et al., 2006).

The Aburrá Ophiolitic Complex or Aburrá Ophiolite occurs in the northwestern portion of the Central Cordillera in the Aburrá Valley in the state of Antioquia. This ophiolite exhibits a mantle section represented by peridotites - the “Medellín Dunite” (Restrepo and Toussaint, 1984) hereafter called the Medellín Ultramafic Massif and a crustal section represented by mafic rocks - the El Picacho Metagabbro (Correa and Martens, 2000). The Aburrá Ophiolite also probably includes other members: the Boquerón Metagabbro (previous Boquerón Amphibolite of Correa and Martens, 2000), the Santa Elena Amphibolite (Restrepo, 2005),

the Sajonia Mylonitic Gneiss (Rodríguez et al. 2005) and a large portion of the La Ceja Gneiss (Rodríguez et al. 2005). The ophiolite units are intruded by the Jurassic La Iguaná Orthogneiss (Correa et al. 2005) and by Cretaceous plutons such as the Altavista Stock, the San Diego Gabbro, the Ovejas Tonalite and Antioquean Batholith (Feininger *et al.*, 1972; Restrepo *et al.*, 1991; Ordóñez-Carmona and Pimentel, 2001).

The formation and emplacement ages of the ophiolitic rocks are not well constrained. For some authors, the ophiolites of the Central Cordillera were formed during the Late Jurassic and emplaced during the Early Cretaceous (Restrepo and Toussaint, 1973; Alvarez, 1985). Restrepo et al. (2007) interpreted this ophiolite as Triassic based on an U-Pb age of 228 ± 0.92 Ma obtained in zircon from a pegmatitic gabbro. We obtained an U-Pb age of 217 ± 0.36 Ma in zircon grains from a plagiogranite occurring as irregular pockets and dykes crosscutting the metagabbros. This result is interpreted as the minimum age of formation of the oceanic crust of the ophiolite.

2.3. The Medellín Ultramafic Massif

The Medellín Ultramafic Massif is exposed in the eastern and northern flanks of the Aburrá Valley, to the east and to the north of the city of Medellín (Figure 1). It is a 35 km long and 0.2-5 km wide elongate discontinuous ultramafic belt (Figure 1 and 2) which is divided into three bodies (Restrepo and Toussaint, 1973): the southern body (36 km^2), the central body (25 km^2) and the northern body (10 km^2). The southern and central bodies have a N10°W strike (Rodríguez et al., 2005) and the northern one follows a N24°W strike (Restrepo and Toussaint, 1973). The ultramafic massif is made up mainly of dunite, which locally hosts podiform chromitite bodies (Restrepo and Toussaint, 1984), and in lesser proportion of harzburgite (Correa and Nilson, 2003). The hydrated minerals occurring in the peridotites have been ascribed to regional metamorphism (Restrepo and Toussaint, 1984; Proenza et al., 2004) and to metasomatism (Alvarez, 1982).

Chromitite mineralization occurs in the three ultramafic bodies, but is more conspicuous in the southern and northern ultramafic sectors. Most of the chromite ores were mined out in the past, only some small chromitite bodies are being exploited at present (Geominas, 1975; Alvarez, 1987; Monsalve, 1996).

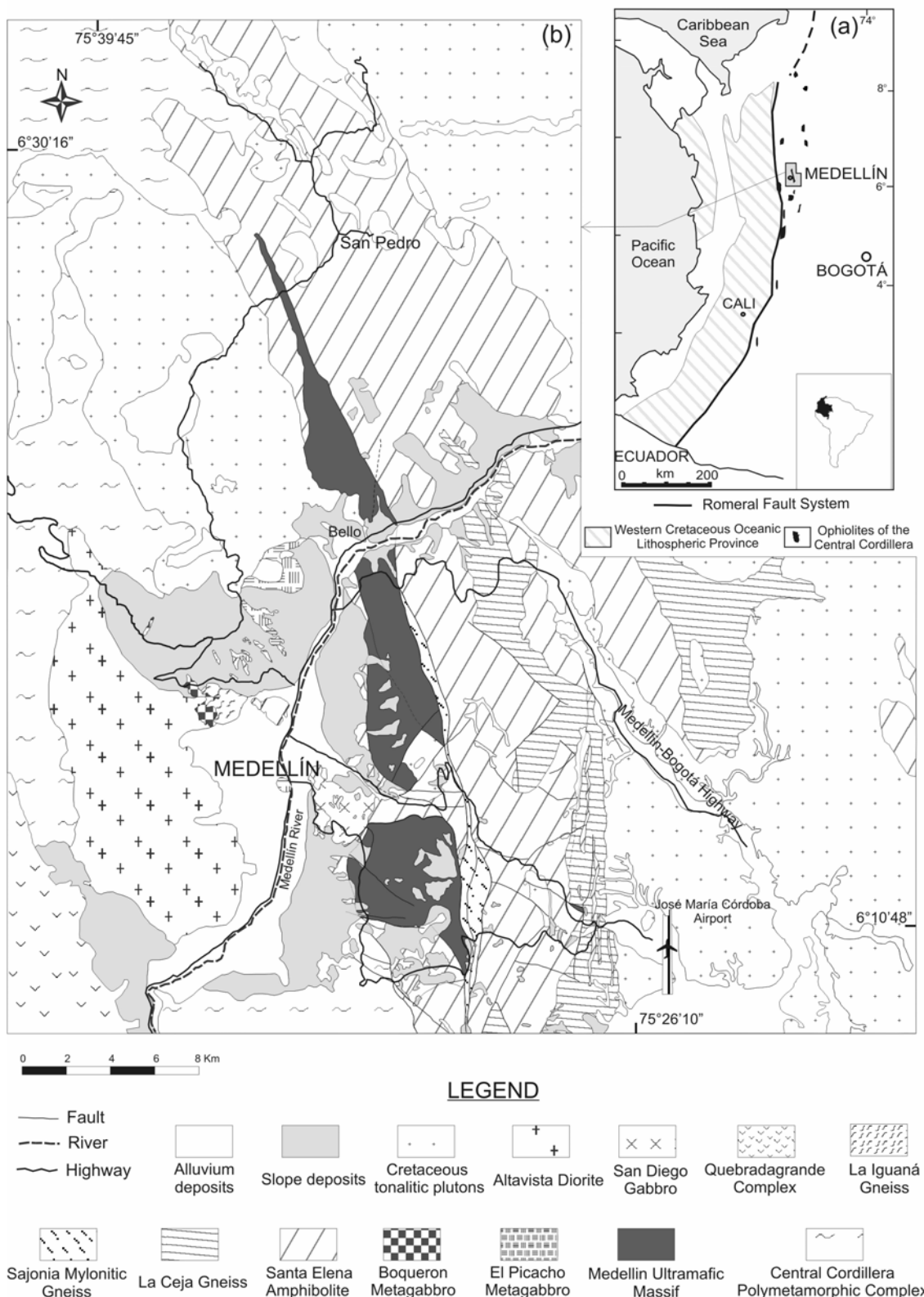


Figure 1. (a) Sketch showing the distribution of the main mafic-ultramafic complexes in the Colombian Andes (after Restrepo and Toussaint, 1973; Kerr et al., 1997). (b) Geological map of the Medellín area. Compiled after Botero (1963); Rendón (1999); Correa and Martens (2000); Rodríguez et al. (2005).

The peridotites lie in tectonic contact over the amphibolite unit. The contact consists of chlorite schist, tremolite rock, metasomatised amphibolite (Restrepo and Toussaint 1973, Alvarez 1982) and garnet-bearing amphibolite. This zone corresponds to the metamorphic sole of the ophiolite.

Restrepo and Toussaint (1973) were the first to interpret the ultramafic rocks as part of an ophiolite obducted over the continent with an emplacement direction towards the east. Alvarez (1982) classified the ultramafic rocks as tectonite dunite similar to Alpine-type ultramafic rocks, representing the upper mantle tectonically emplaced in the core of mountain belt. Correa and Nilson (2003) interpreted the ophiolite as a Harzburgite-type generated probably in an environment related with subduction zone, whereas Proenza et al. (2004) argued that the ophiolite formed or modified in a back-arc environment.

2.4. Geology and petrography of the ultramafic massif

The descriptions and interpretations below refer to outcrops, for which structural and petrographical features have not been previously described. The sample location is displayed in Figure 2.

The IUGS classification which define dunite as a peridotite with 90-100 vol.% of olivine was used for most of cases in this study. The only exception applies to the dunite bands within harzburgite, where we used the following classification: dunite is a peridotite with less than 2 vol.% of orthopyroxene, whilst orthopyroxene depleted harzburgite is a peridotite with 2-10 vol.% of orthopyroxene.

2.4.1. *I*-Type harzburgite

I-Type harzburgite is scarce in the ultramafic massif (point JJ1396, Figure 2). The rock exhibits fresh coarse-grained orthopyroxene porphyroclasts in a dark brown fine-grained matrix.

I-Type harzburgite consists of olivine (87-85%), orthopyroxene (12-14%), spinel (<1%) and rare sulphide grains. They show porphyroclastic to low-temperature mylonitic microstructures. Orthopyroxene occurs as highly deformed porphyroclasts (3-7 mm) (Figure 3a) with kink bands and exsolution lamellae, indicative of high temperature deformation. This mineral defines the metamorphic foliation. It is surrounded by fine olivine neoblasts (0.15-0.75 mm). Red-brown spinel (0.2 to 1.6 mm) occurs outside the pyroxene grains. It displays holly-leaf and anhedral shape, although equant and euhedral grains (0.3 -0.35 mm) are also found in smaller proportions. Locally replacement of orthopyroxene by fine-grained

amphibole indicates a late modification by secondary hydration. No primary clinopyroxene has been found in the harzburgite. Orthopyroxene is partially altered to bastite, whereas the olivine is serpentinized, forming mesh texture.

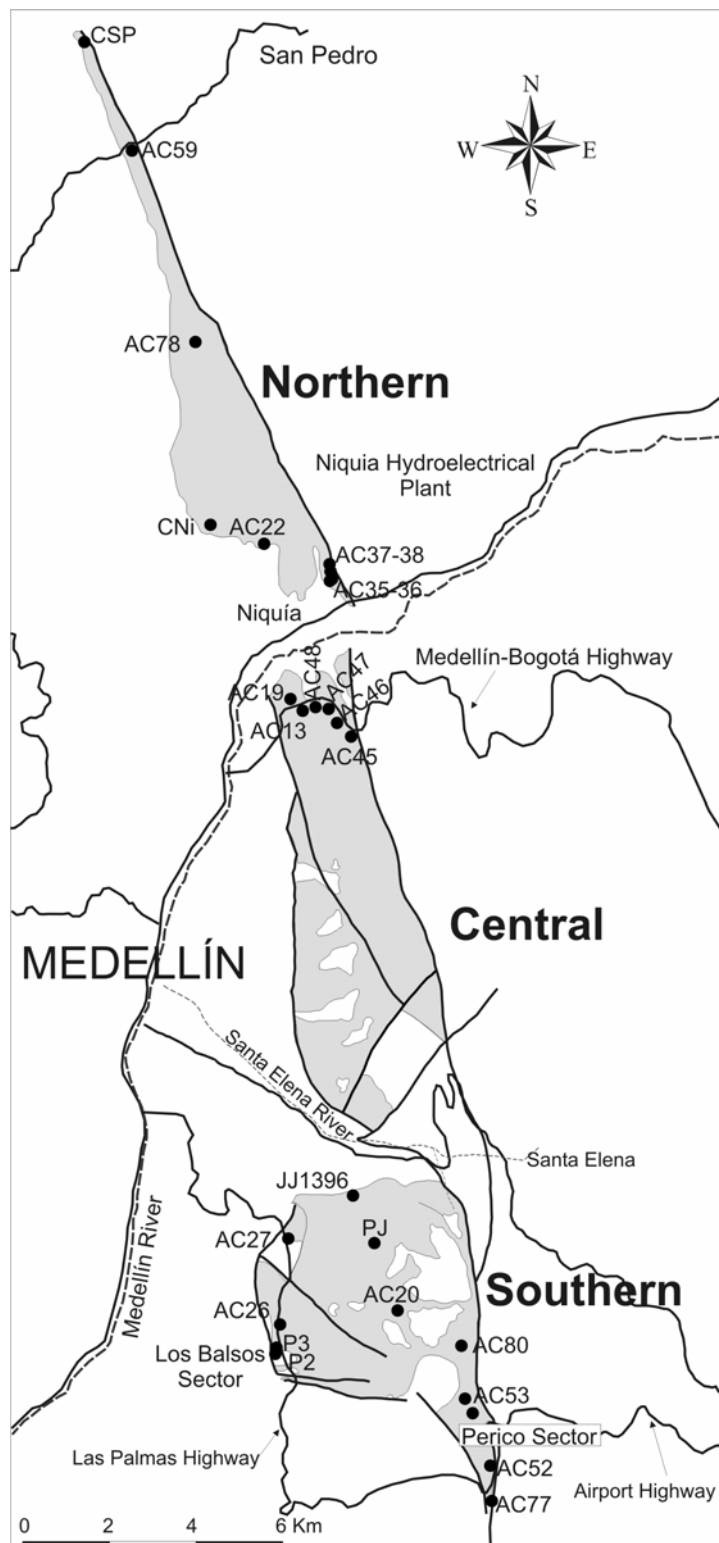


Figure 2. Sketch map of the peridotites bodies of the ultramafic massif of the Aburrá Ophiolite, showing the sampling locations.

2.4.2. II-Type harzburgite and dunite

II-Type harzburgite is characterized by a speckled appearance and was identified in several places of the three ultramafic bodies (*e.g.* points AC22, AC26, AC53A, I, AC77, AC78). The speckles are medium-grained light color aggregates with pearl lustre, which consist of serpentine, talc and tremolite. These aggregates are interpreted as orthopyroxene pseudomorphs. In II-Type harzburgite the orthopyroxene has been completely transformed. Gradation of II-Type harzburgite to dunite is common. Dunite is variably serpentinized and is the dominant peridotite in the massif.

The primary modal composition of harzburgite and dunite consists of 89.0-98.3% olivine, 1.5-11% orthopyroxene, 0.2-0.5% spinel and trace sulphides. Olivine occurs in flattened porphyroclasts (up to 0.8 x 3 mm). Orthopyroxene (up to 4 x 5 mm) is pseudomorphosed by aggregates of bastite plus talc plus tremolite (Figure 3b). Spinel (0.5 mm to 2 mm) occurs in holly-leaf (Figure 3c) and anhedral grains surrounded by chlorite haloes. It is black and shows a completely altered rough surface. Almost all samples exhibit porphyroclastic microstructure in which the foliation is defined by flattened olivine porphyroclasts and trails of spinel grains. Olivine may exhibit undulatory extinction and subgrain boundaries.

The secondary minerals are serpentine, talc, amphibole, chlorite and magnetite. The serpentinization degree varies between 35% and 90%, it occurs in mesh-texture and also in veins. In addition to the small amphibole crystals (< 0.25 mm) associated with talc, some amphibole grains are interstitial to olivine grains and occasionally seem to crosscut olivine. Peridotite occurring close to pyroxenitic dykes contains larger prismatic amphibole crystals (up to 0.3 x 2.5 mm), which occur in poorly defined bands or randomly distributed. Fine veins of chlorite are common in some samples. Carbonate veinlets crosscutting serpentine and/or chlorite veins are also common.

2.4.3. II-Type harzburgite with concordant bands of dunite

II-Type harzburgite interbanded with dunite crops out at the margins of the Las Palmas-Airport Highway in the Perico sector, southeastern portion of the southern ultramafic body (point AC52). The analysed outcrop is 30 m-thick, even though the portion of interbanded peridotites may extend over 150 m. Bands of harzburgite and dunite range from 0.5 cm to 1.0 m in thickness but those thinner than 10 cm are dominant. Harzburgite bands are, in general, continuous, whereas dunite bands are sometimes discontinuous. Harzburgite bands exhibit a surface with speckled appearance, whereas dunite bands show a smooth surface (Figure 3d). The contacts between harzburgite and dunite are both gradational and sharp.

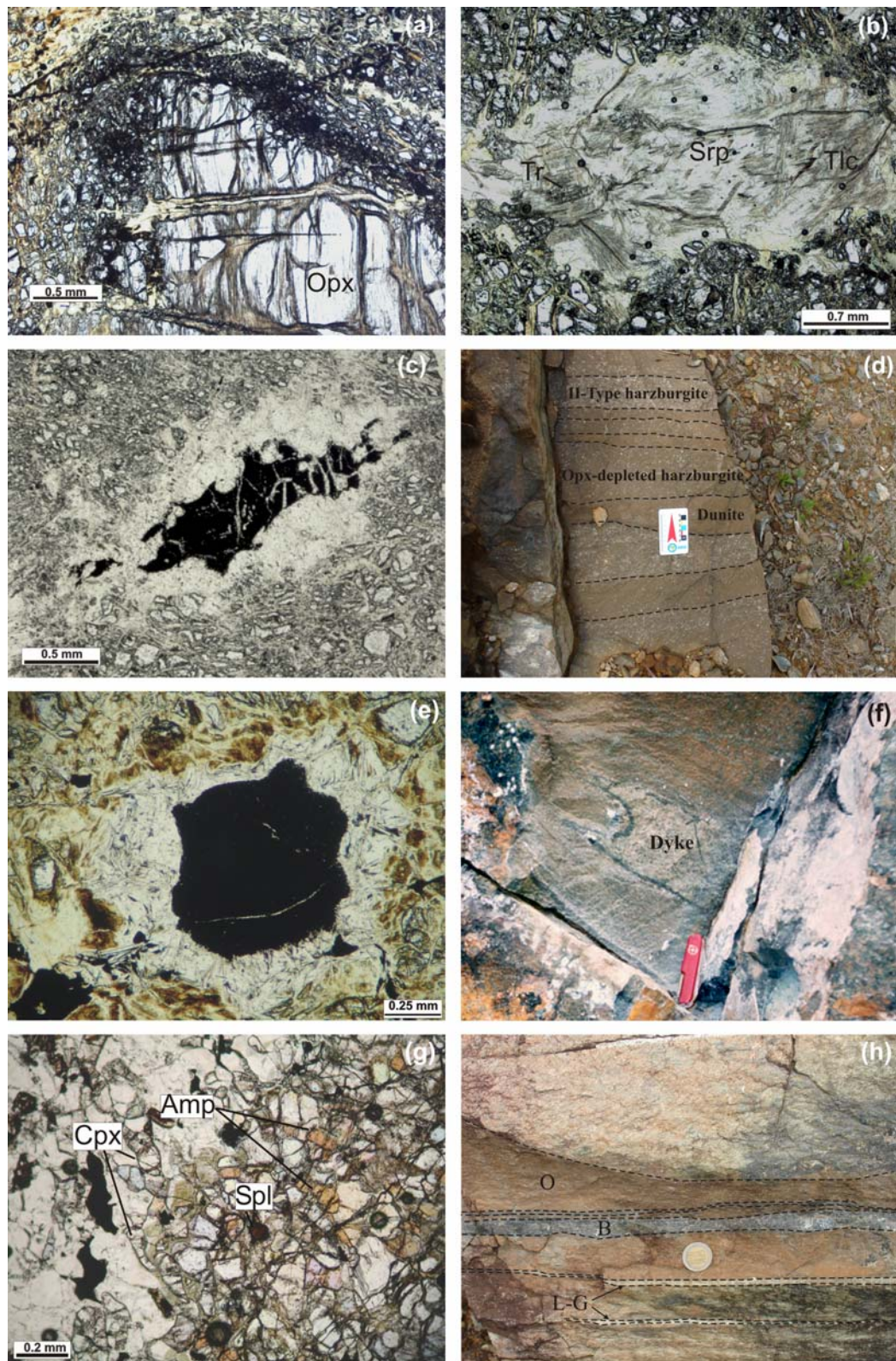


Figure 3. Microscopic and macroscopic features of different peridotites. (a) Orthopyroxene in I-Type harzburgite. (b) Orthopyroxene pseudomorph in II-Type harzburgite. (c) Holly-leaf spinel in II-Type harzburgite. (d) II-Type harzburgite (speckled portion), Opx-depleted harzburgite, dunite (homogeneous portion). (e) Rounded and opaque spinel in dunite. (f) Ultramafic dyke. (g) Olivine, clinopyroxene (cpx), kaersutite-pargasite (amp) and red spinel (sp) in wehrlite. (h) Banded basal peridotite, O: orange bands, B: black bands, L-G: light green bands.

Occasionally, coarse-grained spinel grains form discontinuous, thin (<1cm thick) bands, inside dunite bands. The narrow bands of chromite are parallel to banding.

The foliation is marked by elongated grains or aggregates of chrome spinel. Perpendicular to the foliation numerous serpentine veins are common. The top of the banded unit is in tectonic contact with dunite and metagabbro.

Harzburgite consists of olivine (80-90 %), aggregates of bastite plus talc plus tremolite, pseudomorphs after orthopyroxene (10-20 %), spinel (<1%) and traces of sulphide. Serpentine, magnetite and chlorite are also observed. The microstructure in II-Type harzburgite and Opx-depleted harzburgite is porphyroclastic. Olivine is flattened (1 to 5 mm) with wavy extinction and subgrain boundaries. Orthopyroxene, originally porphyroclastic (2.5 x 4.5 mm) to anhedral, was completely replaced by aggregates of bastite, talc and tremolite. Spinel is holly-leaf (0.5 x 1.0 mm) to anhedral and commonly altered, exhibiting a corroded surface. It is commonly surrounded by chlorite. Foliation is formed by the alignment of flattened olivine and spinel. Sulphide (<0.07 mm) is disseminated in the rocks.

Dunite consists of olivine (98-99), spinel (1-2%) and traces of sulphide. Small proportions (< 2%) of talc or tremolite may be present. It shows less flattened and coarser (3mm x 3.75 mm) olivine grains when compared to the adjacent harzburgite. Olivine microstructure exhibits poor shape fabrics and higher degree of recovery than olivine in harzburgite. Grain boundaries are curved and there are some triple point junctions at 120°. Spinel occurs commonly at the junctions of olivine grains. The microstructure of the rock resembles that of an “adcumulate”. Spinel grains are usually subeuhedral to euhedral (0.9 mm x 0.85 mm in size) (Figure 3e), and sometimes may be elongate (1.0 x 1.5 mm). Spinel in the discontinuous bands of chromite is subeuhedral (up to 5 mm). Fresh spinel exhibits a smooth surface; it is red-brown without a chlorite halo, whereas the abundant altered spinel consists of an opaque Cr-spinel surrounded by chlorite (Figure 3e). Dunite is richer in sulphide than harzburgite. Sulphide, mainly pentlandite with rims of millerite and awaruite, varies in shape from anhedral (0.075 x 0.25 mm) to euhedral grains (0.25 x 0.35 mm). They occur in three ways: (i) along grain boundaries of olivine, sometimes in the triple points junctions of the olivine grains, (ii) close to spinel grains or associated with the chlorite haloes and rarely enclosed by the spinel and (iii) locally in fractures perpendicular to the olivine flattening plane.

2.4.4. Ultramafic dykes

These dykes were recognized in the Perico-El Carmelo roadway, southeast portion of the southern body (AC53G). They are up to 10 cm-thick and are medium-grained, granular, light green with a dark green to black border along the contact zone with the host peridotite (Figure 3f). The dykes are isoclinally folded and the axial plane is apparently parallel to the foliation and banding of the peridotite. Dyke consists of amphibole (92%), formed after original pyroxene, olivine (7%) and opaques (1%). Magnetite, sulphide (pentlandite-pyrrotite) and ilmenite are the opaques. Amphibole is fibrous and randomly oriented (0.75 x 2.5 mm). Olivine grains are smaller than 0.75 mm. Amphibole and olivine are both partially chloritized. The hydrous alteration makes recognition of original microstructure impossible. Towards the contact with the peridotite the amphibole amount decreases and the olivine amount increases. Along the contact (1 cm wide) sulphide (pentlandite-calcopirite-pyrrotite) is more abundant.

2.4.5. Wehrlite

Wehrlite occurs in the southwestern side of the southern body, at the Los Balsos sector, in drill core samples (P2, P3) close to metagabbro outcrops, but the relationship with them and other ultramafic rocks remains unknown. Therefore wehrlite may be an intrusive body or a layer of the ultramafic body.

Wehrlite consists of olivine (79.2%), clinopyroxene (17.5%), brown amphibole (3%), spinels and sulphides (0.3%). Its microstructure is not typical neither of mantle peridotite nor of cumulate. Olivine crystals are generally rounded (0.75 mm), locally embayed and display compositional zoning. Some olivine grains are elongate and exhibit undulatory extinction and sub-boundaries. Clinopyroxene commonly occurs in vermicular and irregular fine grains (0.075 mm - 0.25 mm) (Figure 3g), interstitial to olivine grains and, in a smaller proportion with subeuhedral shape in isolated larger grains. The irregular morphology with curved grain boundaries is more commonly observed in the serpentized bands where clinopyroxene surrounds olivine or orthopyroxene pseudomorphs. The occurrence of intergranular and irregular clinopyroxene is a feature of impregnation.

Brown amphibole (0.1 x 0.3 mm) is interstitial to olivine (Figure 3g) and clinopyroxene and in some places this amphibole exhibits the same irregular shape of the clinopyroxene. Brown amphibole is altered to colorless-light green amphibole. The sharp contacts between olivine, clinopyroxene and brown amphibole suggest that these phases were in equilibrium. Brown amphibole may be igneous or metasomatic in origin, and the colorless amphibole is clearly secondary. Two types of spinel are observed. The first is irregularly elongate (0.5-1.25

mm) opaque and corroded altered spinel surrounded by chlorite; these grains are parallel to the banding. Second occurs in small amount, is smaller than the first, equidimensional, red brownish, fresh grains. It occurs interstitial to the silicate grains or as droplets.

The alteration minerals are serpentine, chlorite, talc, tremolite, magnetite, sulphide, and carbonate. The carbonate occurs in veinlets.

2.4.6. Banded or layered peridotites

This type of peridotite occurs in the roadway to the Niquia Hydroelectrical Plant in the southeast portion of the northern body (AC35 to AC38) and in some blocks exposed along the Medellin-Bogotá Highway (AC48), at the base of the ultramafic bodies close to the amphibolites of the metamorphic sole. Peridotite of basal portion is compositionally banded (Figure 3h) and exhibits mylonitic foliation which is parallel or subparallel to that in the underlying amphibolites. In Niquia, the ultramafic rocks show open metric folds and locally these rocks are cut by a small stockwork of magnesite. Peridotite occurring close to the contact with amphibolites is highly sheared, showing C'- type shear band cleavage.

The dominant orange bands are olivine-rich and have thicknesses varying from a few centimeters to one meter or more. They consist of olivine (80%), amphibole (20%) and spinel (<1%). Olivine occurs as fine grained neoblasts (0.07 - 0.025 mm) and amphibole as prismatic crystals (0.07 x 0.7 mm) randomly oriented. In some portions there are coarser olivine grains (0.4 mm), equant to weakly elongate, which show undulatory extinction. Spinel occurs in small proportions; is black, having homogeneous surface, and may be equidimensional, rounded (up to 3 mm in diameter) or elongate (0.5 mm - 2.0 mm) with chlorite halo. Fine veins of serpentine, chlorite and magnetite and carbonate are common in these rocks. Increase in amount and size of the amphibole crystals characterize the transition to the black amphibole-rich bands. These bands are not as common, are thinner than the orange bands and are often discontinuous. It consists almost entirely of amphibole (0.27 x 2.5 mm) with nematoblastic foliation but also contain randomly oriented interlocking amphibole crystals. Dark millimetric to centimetric porphyroclasts occur in this type of bands and consist of aggregates of amphibole prisms with turbid appearance due to abundant fine magnetite inclusions. Amphiboles are locally altered to talc. The light green bands are chlorite-rich, their thickness varies from one millimeter to a few centimeters.

2.5. Analytical Methods

2.5.1. Mineral chemistry

Electron microprobe analyses were carried out at the Geosciences Institute of the University of Brasília, at the Laboratoire de Tectonophysique of the University of Montpellier II and at the School of Earth Sciences, Stanford University. At the University of Brasília, analyses were performed using a CAMECA SX-50 microprobe operating at 15 kV accelerating voltage and 20 nA sample current. The beam size was variable between 2 and 5 μm and the counting time was 10 s. In Montpellier the data were obtained using a CAMECA SX-100 microprobe operating at 20 kV, 10 nA, beam size of 1-5 μm and counting time between 10 and 50 s. At Stanford University the measurements were performed using a JEOL Superprobe 733 operating at 15 kV and 19 nA, with a beam size of 1 μm .

The samples analyzed in Brasilia were: AC19B, AC35, AC52C, AC53B3, AC53A, AC52E and those in Montpellier were: AC52-0.4, AC52-1.65, AC52-5.02, AC52-19.25, AC52-26.54, AC22B, AC53J, JJ1396, P2-11.20. At Stanford were analyzed the olivine and amphiboles composition from P2-11.20 sample.

Fe^{3+} content of spinel and pyroxene was calculated based on stoichiometry following Droop (1987) equation. The Fe_2O_3 content in the amphiboles was calculated following the procedure suggested by Schumacher (1997) *in* Leake et al. (1997). The nomenclature of pyroxenes and amphiboles is that recommended by the IMA (International Mineralogical Association), which is presented by Morimoto (1989) and Leake et al. (1997), respectively. Mineral compositions presented in this paper are representative analyses. The results are shown in Tables 1 to 8.

2.6. Mineral Chemistry

2.6.1. Olivine

Olivine exhibits compositional variations within the massif, but with the exception of wehrlite, it is relatively uniform in each individual sample. Olivine in I-Type harzburgite displays Fo content of 91.8. NiO content is in the range of mantle peridotites ($\text{NiO} (\%)=0.38\text{-}0.39 \text{ wt\%}$).

II-Type harzburgite olivines exhibit Fo values from 89.7 to 90.8. NiO contents vary from 0.36 to 0.49 wt%. Peridotite with amphibole aggregates (sample AC53J) shows lower Fo contents (88.9-89.0) and also lower NiO tenors (0.26-0.36 wt%).

Olivine from dunite bands within II-Type harzburgite (Tables 1 and 2) shows systematically slightly higher Fo values (90.1-90.9) than those in the harzburgitic portions (Fo=89.5 - 90.0), whereas the NiO values are slightly higher in harzburgites (0.36-0.45 wt%, almost all values are between 0.37 and 0.39) than those in the dunites (0.31-0.40 wt%, most part of values close to 0.36%). In dunite the NiO content exhibits large variation within one single olivine grain. The opx-depleted harzburgites show Fo values from 90.0 to 90.2 and their NiO content is variable, for instance, some core of olivine grains exhibit high NiO (0.45 %), whereas other cores display relatively low NiO (0.34%). For some reason thin section (AC52_26.54), in which dunite and opx-depleted harzburgite are in contact, the NiO content exhibits a reverse trend. Some olivine grains located close to spinel exhibit higher forsterite content. This shift may suggest subsolidus reequilibration.

Olivine in wehrlite is compositionally heterogeneous; it shows Fo 87.0 (core) to Fo 81 (rim). The NiO content is 0.25 wt%. It is not clear whether the compositional zoning of olivine is concentric or irregular.

Basal peridotite and, highly sheared and serpentized peridotite (AC59B) contain more magnesian olivine (Fo 92.1 - 93.9) which can be attributed to metamorphism.

A I-Type harzburgite and two dunite samples plot within the olivine-spinel mantle array (OSMA) of Arai (1994) as shown in Figure 4. It suggests that they are residual peridotites, whereas the wehrlite plots outside this trend towards the right of this field, indicating a cumulate or a melt impregnation origin for this rock type. The plot shows that harzburgite samples overlap the region between abyssal peridotites and passive margin peridotites, whereas the dunites plot mainly in the overlap region between abyssal peridotites and oceanic subduction zone peridotites. If the OSMA is a residual peridotite array as argued by Arai (1994), then one can assume that a cumulate origin can not be postulated for dunite. This question will be discussed later in this paper.

2.6.2 Spinel

Unaltered spinel was identified in just one sample from I-Type harzburgite, which exhibits restricted Cr# [Cr/(Cr+Al)] values between 0.33 and 0.35. Mg# [Mg/(Mg+Fe²⁺)] varies between 0.62 and 0.65. TiO₂ values range from 0.09 to 0.12 wt%. NiO content varies from 0.09 to 0.14 wt%.

In dunite from the concordant bands within II-Type harzburgite, the primary spinel exhibits very restricted Cr#, ranging from 0.42 to 0.45 and Mg# from 0.48 to 0.58. TiO₂

values are not homogeneous along a single grain; in fact TiO_2 varies from 0.13 to 0.35 wt%. NiO content ranges from 0.07 to 0.12 wt%.

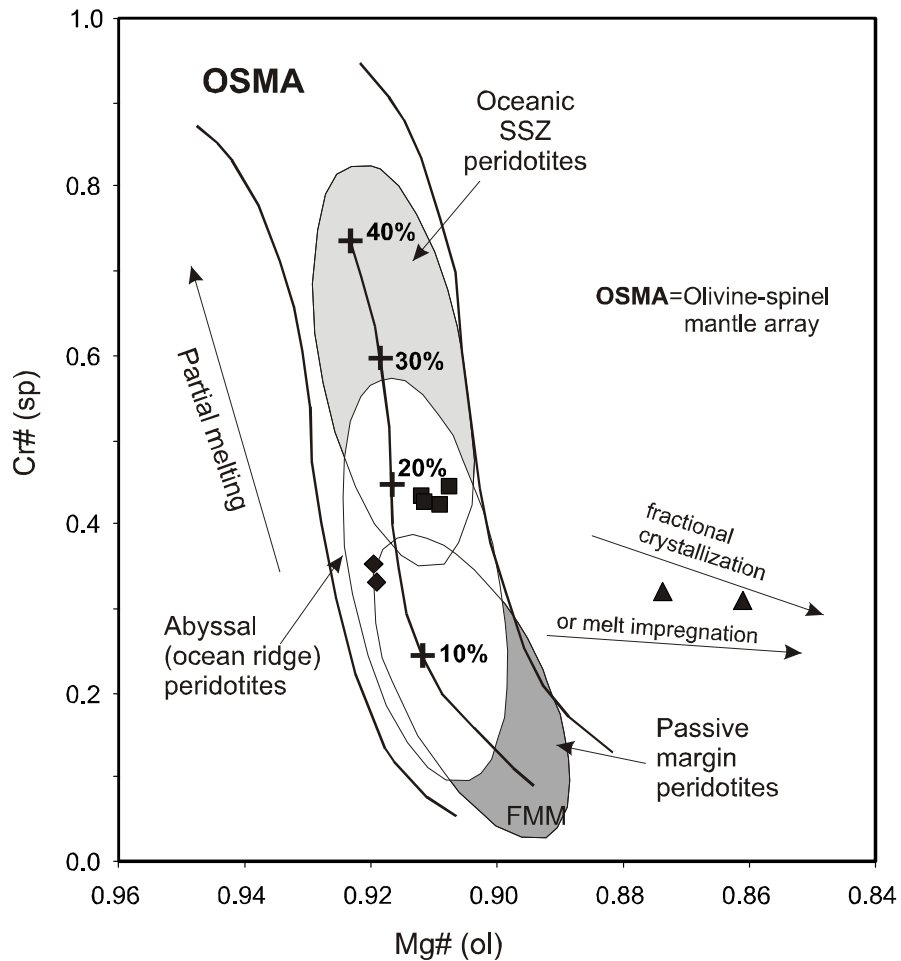


Figure 4. Plot of spinel Cr# versus olivine Mg# of the peridotites of the Aburrá ophiolite. Fields of abyssal peridotite, passive margins peridotite and oceanic supra-subduction peridotite summarized by Pearce et al. (2000), and the olivine-spinel mantle array (OSMA) and melting trend of Arai (1994). FMM Fertile MORB mantle. Diamonds: I-Type harzburgite (JJ1396), Squares: dunite (AC52), Triangles: wehrlite (P2-11.20).

In wehrlite the primary spinel exhibits a constant Cr# of 0.31 and Mg# ranging from 0.50 to 0.53. TiO_2 is 0.18 to 0.23 wt%. NiO ranges from 0.10 to 0.14 wt%.

The primary spinels of I-Type harzburgite and dunite plot within the ophiolite field (Figure 5a), whereas those of the wehrlite plot slightly outside of that field.

The slightly altered spinel in dunite (samples AC52) displays higher Cr # (0.49 to 0.57) and lower Mg# (0.41-0.50) than those from fresh spinels (Figure 5b). TiO_2 content ranges

from 0.07 to 0.23 wt% and NiO content varies from 0.04 to 0.07 wt%, but spinel from sample AC52_0.4 exhibits higher TiO₂ (0.34-0.38 wt%) and NiO (0.14-0.15 wt%) contents.

The completely altered spinels of the II-Type harzburgites exhibit Cr# values ranging from 0.93 to 0.97, Mg# values vary from 0.13 to 0.16, TiO₂ content ranging from 0.27 to 0.73 wt% and NiO content varying from 0.05 to 0.09 wt%. Altered spinel in the amphibole aggregates-rich rock (AC53J) displays Cr# value of 0.99, Mg# of 0.04, TiO₂ of 1.15 wt% and NiO content of 0.43 wt%.

Recrystallized spinel from metamorphic peridotites displays Cr# ranging from 0.98 to 1.00. Mg# values ranges from 0.03 to 0.12. TiO₂ ranges from 0.06 to 0.29 wt% and the NiO content varies between 0.69 and 1.07 wt%. In Figure 5b is shown that all altered spinel grains plot out of any primary field.

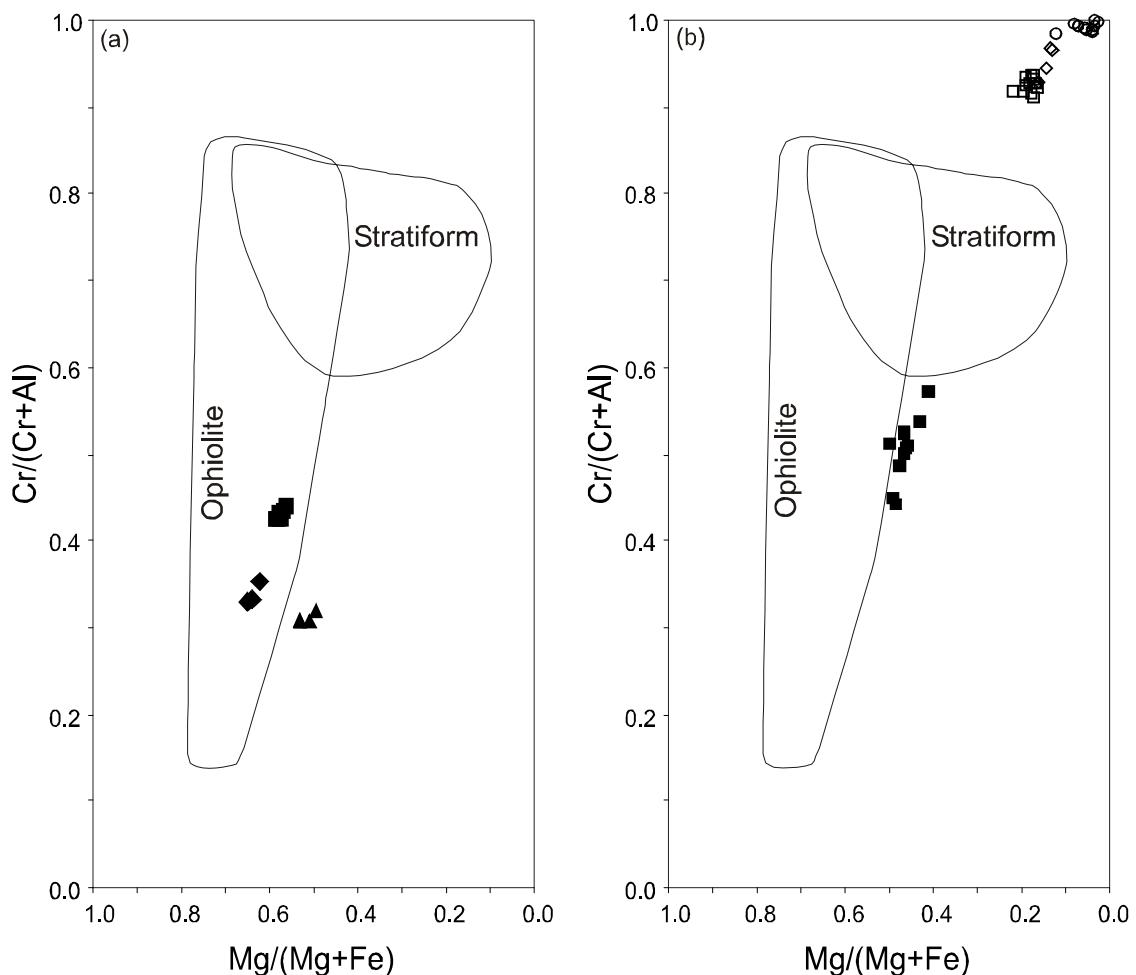


Figure 5. (a) Cr#[Cr/(Cr+Al)] versus Mg#[Mg/(Mg+Fe)] for primary spinel from peridotites. The ophiolite and stratiform fields are from Leblanc and Nicolas (1992). (b) Cr#[Cr/(Cr+Al)] versus Mg#[Mg/(Mg+Fe)] for altered spinels from peridotites. Symbols: Black diamonds =

fresh spinels of I-Type harzburgite, black squares = unaltered spinels of dunite in a), incipient altered spinels of dunite in b), black triangles = fresh spinel in wehrlite, open squares = altered spinels of banded harzburgite-dunite, open diamonds = altered spinel of II-Type harzburgite, open circles = altered spinels of metamorphic basal peridotite.

Table 1. Representative electron microprobe analyses of olivine from the peridotites from the Aburrá Ophiolite.

Rock Sample	Harz JJ1396	Har* AC22B	Har* AC53A	Har* AC53J	A.Perid AC52C	Har* AC52B3	Dun P21120C	Wehr P21120P4	Wehr P21120I	Wehr P21120R	Wehr P21120R	Wehr P21120R	M.Perid AC59B	M.Perid AC19B	M.Perid AC35A
SiO ₂	41.42	40.59	41.59	40.96	41.47	40.45	40.72	40.76	39.77	39.69	39.98	40.01	41.51	41.88	42.49
TiO ₂	0.01			0.01			0.00	0.01	0.00	0.03	0.00	0.00	0.02		
Al ₂ O ₃	0.00	0.01	0.00	0.01	0.00	0.00	0.02	0.01	0.05	0.04	0.08	0.07	0.00	0.01	0.00
Cr ₂ O ₃	0.00		0.03	0.02	0.00	0.00	0.00	0.00	0.02	0.01	0.00	0.00	0.00	0.00	0.03
FeO	7.79	9.74	8.89	10.44	10.00	8.96	12.19	13.16	14.46	16.25	16.91	17.07	7.38	6.28	6.18
MnO	0.14	0.16	0.05	0.20	0.15	0.11	0.17	0.21	0.28	0.30	0.29	0.36	0.24	0.12	0.08
MgO	49.73	48.50	49.54	48.39	48.71	49.31	46.47	45.48	44.62	43.01	42.01	41.60	51.30	51.54	51.86
CaO	0.01	0.00	0.00	0.00	0.02	0.01	0.00	0.01	0.00	0.00	0.01	0.01	0.00	0.04	0.01
NiO	0.39	0.36	0.49	0.34	0.39	0.36		0.25					0.37	0.35	0.32
Total	99.48	99.35	100.59	100.37	100.74	99.20	99.58	99.87	99.20	99.32	99.29	99.12	100.82	100.21	100.97
					Banded dunite-harzburgite				Wehrlite				Metamorphic peridotite		
Si	1.013	1.004	1.009	1.005	1.009	0.999	1.011	1.009	1.016	1.008	1.018	1.021	1.001	1.008	1.013
Ti	0.000			0.000			0.000	0.000	0.000	0.001	0.000	0.000	0.000	0.000	
Al		0.000	0.000	0.000	0.000	0.000	0.001	0.001	0.000	0.001	0.002	0.002	0.000	0.000	0.000
Cr			0.001	0.000	0.000	0.000	0.000	0.001	0.000	0.000	0.000	0.000	0.000	0.000	0.001
Fe	0.159	0.201	0.180	0.214	0.204	0.185	0.253	0.263	0.274	0.345	0.360	0.364	0.149	0.126	0.123
Mn	0.003	0.003	0.001	0.004	0.003	0.002	0.004	0.005	0.004	0.006	0.006	0.008	0.005	0.003	0.002
Mg	1.812	1.787	1.791	1.770	1.767	1.815	1.719	1.711	1.689	1.629	1.594	1.582	1.844	1.848	1.842
Ca	0.000	0.000	0.000	0.000	0.001	0.000	0.000	0.000	0.000	0.000	0.000	0.000	0.000	0.001	0.000
Ni	0.008	0.007	0.009	0.007	0.008	0.007	0.000	0.000	0.005	0.000	0.000	0.000	0.007	0.007	0.006
Mg no	0.919	0.899	0.909	0.892	0.897	0.907	0.872	0.867	0.860	0.825	0.816	0.813	0.925	0.936	0.937
Fo	91.79	89.72	90.80	89.02	89.53	90.64	87.00	86.48	85.84	82.24	81.31	80.96	92.30	93.49	93.66

Notes: cations calculated on the basis of 6 oxygens. Blanks =not determined. Harz= I-Type harzburgite, Harz*= II-Type harzburgite, A.Perid=peridotite with amphibole aggregates, Dun=dunite, Wehr= wehrlite, M.Perid=metamorphic basal peridotite.

Table 2. Representative electron microprobe analyses of olivine from the harzburgite-dunite outcrop in the Perico Sector.

Rock	Dun	Trans	Harz*	Rock	Dun	Dun	Harz*	Harz*	Dun	Dep. Harz	Dun	Dun	Trans	Harz*	Harz*
Sample	AC52E Ol	AC52EOI 9A	AC52E O8	Sample Distance (m)	AC52	AC52	AC52	AC52	AC52	AC52	AC52	AC52	AC52	AC52	AC52
SiO ₂	40.76	40.22	40.51		41.41	41.39	41.50	41.44	41.11	41.21	41.15	41.21	41.56	41.21	41.44
TiO ₂	0.00	0.04	0.01		0.01	0.00	0.00	0.00	0.00	0.00	0.01	0.00	0.00	0.00	0.01
Al ₂ O ₃	0.03	0.01	0		0.00	0.01	0.00	0.01	0.00	0.00	0.01	0.00	0.00	0.00	0.00
Cr ₂ O ₃	0.00	0.00	0.04		0.01	0.00	0.01	0.00	0.00	0.02	0.00	0.00	0.00	0.00	0.00
FeO	8.96	9.15	9.52		8.84	8.38	9.39	9.62	8.92	9.60	9.27	9.34	9.43	9.41	9.35
MnO	0.10	0.15	0.14		0.16	0.16	0.15	0.13	0.14	0.16	0.15	0.18	0.15	0.17	0.14
MgO	49.91	50.44	49.98		48.72	49.42	48.46	48.46	48.95	48.52	48.46	48.18	48.44	48.62	48.22
CaO	0.04	0.00	0.00		0.01	0.02	0.00	0.01	0.01		0.01	0.00	0.00	0.00	0.00
NiO	0.35	0.37	0.39		0.38	0.38	0.39	0.45	0.36	0.39	0.39	0.33	0.36	0.36	0.32
Total	100.15	100.36	100.59		99.53	99.75	99.90	100.11	99.50	99.90	99.45	99.25	99.93	99.77	99.47
Along a single thin section										Within a thin section					
Si	0.997	0.984	0.990		1.016	1.012	1.017	1.015	1.010	1.012	1.013	1.016	1.018	1.012	1.019
Ti	0.000	0.001	0.000		0.000	0.000	0.000	0.000	0.000	0.000	0.000	0.000	0.000	0.000	0.000
Al	0.001	0.000	0.000		0.000	0.000	0.000	0.000	0.000	0.000	0.000	0.000	0.000	0.000	0.000
Cr	0.000	0.000	0.001		0.000	0.000	0.000	0.000	0.000	0.000	0.000	0.000	0.000	0.000	0.000
Fe	0.183	0.187	0.195		0.181	0.171	0.192	0.197	0.183	0.197	0.191	0.193	0.193	0.193	0.192
Mn	0.002	0.003	0.003		0.003	0.003	0.003	0.003	0.003	0.003	0.003	0.004	0.003	0.004	0.003
Mg	1.819	1.839	1.821		1.782	1.801	1.770	1.769	1.793	1.775	1.778	1.771	1.768	1.779	1.767
Ca	0.001	0.000	0.000		0.000	0.001	0.000	0.000	0.000	0.000	0.000	0.000	0.000	0.000	0.000
Ni	0.007	0.007	0.008		0.007	0.007	0.008	0.009	0.007	0.008	0.008	0.006	0.007	0.007	0.006
Mg no	0.909	0.908	0.903		0.908	0.913	0.902	0.900	0.907	0.900	0.903	0.902	0.902	0.902	0.902
Fo	90.76	90.63	90.22		90.61	91.15	90.05	89.86	90.59	89.85	90.16	90.01	90.01	90.04	90.06

Notes: cations calculated on the basis of 6 oxygens. Dun=dunite, Harz*= II-Type harzburgite, Trans: Transitional between dunite and harzburgite, Dep. Harz: opx depleted II-Type harzburgite, + olivine close to a spinel grain.

Table 3. Representative electron microprobe analyses of unaltered spinels from I-Type harzburgite, dunite and wehrlite and results of slightly altered spinels from dunite of the Aburrá Ophiolite.

Rock Sample	Harz JJ1396p1	Harz JJ1396p2	Dun AC52Ep1	Dun AC52Ep4	Wehr P21120p1	Wehr P21120p2	Dun AC52502p4	Dun AC52E3	Dun AC5204p2	Dun AC52502p1
SiO ₂	0.09	0.06	0.01	0.03	0.10	0.07	0.08	0.05	0.09	0.07
TiO ₂	0.09	0.12	0.35	0.11	0.23	0.21	0.29	0.07	0.38	0.23
Al ₂ O ₃	40.01	38.34	30.96	31.24	38.86	40.57	28.69	26.16	24.57	22.98
Cr ₂ O ₃	29.50	31.06	35.36	34.47	27.51	27.02	34.09	40.28	38.45	39.59
Fe ₂ O ₃	0.00	0.00	2.88	4.02	0.58	0.00	4.94	2.60	5.70	4.56
FeO	15.10	15.47	17.28	16.98	20.54	19.35	20.09	20.59	19.32	21.28
MgO	14.97	14.43	12.75	12.83	11.38	12.32	10.58	9.77	10.81	8.93
MnO	0.23	0.21	0.18	0.18	0.31	0.23	0.32	0.15	0.35	0.32
NiO	0.09	0.11	0.10	0.10	0.12	0.10	0.08	0.05	0.14	0.06
ZnO			0.23	0.31				0.78		
Total	100.08	99.80	100.10	100.27	99.62	99.87	99.16	100.50	99.80	98.02
Si	0.021	0.014	0.003	0.006	0.024	0.016	0.019	0.012	0.023	0.018
Ti	0.016	0.021	0.063	0.019	0.041	0.036	0.054	0.013	0.070	0.045
Al	10.691	10.368	8.691	8.748	10.692	11.008	8.307	7.608	7.187	6.951
Cr	5.288	5.633	6.658	6.475	5.076	4.917	6.620	7.856	7.545	8.030
Fe ³⁺	0.000	0.000	0.516	0.718	0.101	0.000	0.913	0.483	1.064	0.881
Fe ²⁺	2.863	2.967	3.442	3.374	4.010	3.724	4.127	4.247	4.009	4.565
Mg	5.060	4.935	4.527	4.544	3.960	4.229	3.877	3.593	3.999	3.415
Mn	0.045	0.041	0.036	0.037	0.061	0.046	0.066	0.032	0.075	0.070
Ni	0.016	0.019	0.020	0.020	0.022	0.019	0.016	0.011	0.028	0.013
Zn			0.040	0.055				0.142		
Mg#	0.639	0.625	0.568	0.574	0.497	0.532	0.484	0.458	0.499	0.428
Cr#	0.331	0.352	0.434	0.425	0.322	0.309	0.443	0.508	0.512	0.536
Fe ³⁺ #	0.000	0.000	0.033	0.045	0.006	0.000	0.058	0.030	0.067	0.056

Notes: Cations calculated on the basis of 32 oxygens. Blanks =not determined. Harz= I-Type harzburgite, Dun=dunite, Wehr= wehrlite.

Table 4. Representative electron microprobe analyses of altered spinel from II-Type harzburgite, dunites and metamorphic peridotites of the Aburrá Ophiolite.

Rock Sample	Harz* AC22B1	Harz* AC53A	A.Perid AC53Jp1	Harz* AC52C5	Harz* AC52E10	Harz* AC521651	Harz* AC5219252	Dun AC5226541	M.Perid AC59B3	M.Perid AC19B2	M.Perid AC19B3	M.Perid AC35A5
SiO ₂	0.09	0.02	0.10	0.16	0.04	0.21	0.24	0.10	0.07	0.018	0.02	0.00
TiO ₂	0.28	0.73	1.15	0.15	0.45	0.11	0.29	0.33	0.10	0.224	0.14	0.25
Al ₂ O ₃	1.38	2.86	0.14	3.32	2.68	3.21	2.79	2.92	0.05	0.053	0.04	0.06
V ₂ O ₃	n.a	0.33	n.a	0.77	n.a	n.a	n.a	n.a	0.052	0.20	0.12	
Cr ₂ O ₃	62.82	56.34	20.84	58.25	59.15	61.44	59.81	61.91	10.91	15.213	5.41	6.91
Fe ₂ O ₃	2.97	7.73	36.83	5.19	4.47	3.14	3.74	2.66	45.30	44.484	48.89	48.71
FeO	27.64	27.66	36.01	28.14	26.44	27.34	26.53	26.60	37.95	37.453	42.06	41.47
MgO	2.42	3.03	0.81	3.01	3.08	3.01	3.18	3.43	1.64	1.748	0.89	1.21
MnO	0.73	0.89	0.43	0.95	0.44	0.72	0.65	0.60	0.33	0.535	0.03	0.29
NiO	0.06	0.09	0.43	0.07	0.02	0.02	0.23	0.05	0.69	0.920	1.07	0.79
ZnO	n.a	0.65	n.a	0.67	0.52				0.107	0.05	0.00	
Total	98.38	100.32	96.75	100.69	97.29	99.22	97.46	98.60	97.03	100.81	98.79	99.82
Si	0.026	0.005	0.032	0.046	0.012	0.062	0.072	0.028	0.021	0.005	0.005	0.001
Ti	0.063	0.157	0.269	0.033	0.099	0.025	0.064	0.072	0.022	0.050	0.032	0.057
Al	0.479	0.968	0.052	1.119	0.933	1.095	0.967	1.001	0.020	0.019	0.015	0.021
V	0.062			0.145					0.000	0.010	0.041	0.024
Cr	14.676	12.803	5.111	13.151	13.832	14.041	13.922	14.213	2.655	3.563	1.301	1.642
Fe ³⁺	0.661	1.672	8.599	1.116	0.995	0.682	0.828	0.581	10.501	9.922	11.208	11.021
Fe ²⁺	6.832	6.650	9.342	6.722	6.542	6.609	6.532	6.460	9.773	9.281	10.712	10.426
Mg	1.066	1.299	0.374	1.280	1.359	1.299	1.397	1.486	0.751	0.772	0.404	0.541
Mn	0.182	0.218	0.113	0.230	0.110	0.176	0.162	0.147	0.086	0.134	0.008	0.074
Ni	0.014	0.022	0.108	0.017	0.004	0.005	0.054	0.012	0.170	0.219	0.263	0.192
Zn	0.138			0.142	0.113				0.000	0.023	0.011	0.000
Mg#	0.135	0.163	0.038	0.160	0.172	0.164	0.176	0.187	0.071	0.077	0.036	0.049
Cr#	0.968	0.930	0.990	0.922	0.937	0.928	0.935	0.934	0.993	0.995	0.989	0.988
Fe ³⁺ #	0.042	0.108	0.625	0.073	0.063	0.043	0.053	0.037	0.797	0.735	0.895	0.869

Cations calculated on the basis of 32 oxygens. Harz*= II-Type harzburgite, A.Perid=peridotite with amphibole aggregates, Dun=dunite, M. Perid=metamorphic basal peridotite.

2.6.3. Pyroxenes

Orthopyroxene was analysed in I-Type harzburgite and clinopyroxene in wehrlite, (Table 5). Primary orthopyroxene is classified as enstatite, bearing Mg# = 0.92, Al₂O₃ from 2.80 to 3.23 wt%, Cr₂O₃ between 0.62 and 0.80 wt% and TiO₂ values vary between 0.04 and 0.07.

Clinopyroxene is classified as diopside, (Table 5). There are small chemical differences between larger isolated grains and those irregularly distributed around the olivine grains. The first ones exhibit almost constant Mg# (~0.91), Al₂O₃ content ranging from 4.03 to 4.08 %, TiO₂ values ranging from 1.05 to 1.07, Cr₂O₃ content varies from 0.90 to 0.93 and the Na₂O values are 0.59-0.70. The second type displays Mg# content ranging from 0.91 to 0.92, the Al₂O₃ content ranging from 2.92 to 3.69 %, the TiO₂ values are 0.66-0.90 and the Cr₂O₃ values are 0.58-0.75 clustered between 0.72 and 0.75) and the Na₂O content ranges from 0.56 to 0.67.

Table 5. Representative microprobe analyses of pyroxenes from peridotites of the Aburrá Ophiolite.

Rock Sample	I-Type Harz JJ1396p4px	Wehr P21120p31	Wehr P21120p3ra
SiO ₂	55.71	52.03	52.97
TiO ₂	0.07	1.07	0.79
Al ₂ O ₃	3.23	4.03	3.56
Cr ₂ O ₃	0.80	0.93	0.75
Fe ₂ O ₃	0.20	0.00	0.00
FeO	4.90	2.76	2.39
MnO	0.10	0.09	0.09
NiO	0.13	0.00	0.01
MgO	34.06	15.24	15.71
CaO	0.51	22.65	23.34
Na ₂ O	0.03	0.70	0.67
Total	99.73	99.50	100.28
Si	1.920	1.908	1.923
Al ^{IV}	0.080	0.092	0.077
Al ^{VI}	0.052	0.083	0.076
Ti	0.002	0.029	0.022
Cr	0.022	0.027	0.021
Fe ³⁺	0.005	0.000	0.000
Mg	1.751	0.833	0.850
Ni	0.004	0.000	0.000
Fe ²⁺	0.141	0.085	0.073
Mn	0.003	0.003	0.003
Ca	0.019	0.890	0.908
Na	0.002	0.050	0.047
Mg#	0.925	0.908	0.921
Em.	91.24	46.01	46.38
Fs	7.77	4.83	4.10
Wo	0.99	49.16	49.52

Cations calculated on the basis of 6 oxygens.

2.6.4. Amphibole

Amphibole in harzburgites and in almost all peridotite samples corresponds to tremolite, which is here considered to be a metamorphic mineral. The amphibole in the metamorphic basal peridotite is not stoichiometric because the Si in T site is above 8.00 (see samples AC19B and AC35A in Table 5). Two explanations can account for this anomalous composition since analytical problems have been ruled out. One is the chemical modification of the amphiboles due to alteration processes, such as a talcification. The other possibility is the existence of a complex lamellar intergrowth of amphiboles and pyroboles. To test any of these alternatives it is necessary an investigation by transmission electron microscopy which was not carried out during this research.

Amphibole in wehrlite is classified as high-Ti red-brown kaersutite ($Ti \sim 0.51$, $Al^{IV} > 1.5$) and titanian pargasite ($0.39 < Ti < 0.49$) and low-Ti pale green-colorless tremolite ($Ti < 0.01$, $Al^{IV} < 1.5$). In high-Ti amphiboles the $(Na+K)_A$ content is between 0.74 and 0.80.

Table 6. Representative electron microprobe analyses of amphiboles from the peridotites of the Aburrá Ophiolite.

Rock	Harz	Harz*	Harz*	Harz*	Harz*	Harz*	Harz*	M.Perid	M.Perid	M.Perid	Wehr	Wehr	Wehr
Sample	JJ1396	AC22B	AC53A2	AC53J	AC52C	AC52E	AC52 2654	AC59B	AC19B	AC35A	P21120 535	P21120 527	P21120 537
SiO ₂	55.73	54.81	55.53	57.53	57.95	57.28	58.23	56.82	59.11	59.30	42.16	41.71	56.53
TiO ₂	0.12	0.04	0.15	0.01	0.01	0.00	0.02	0.01	0.03	0.01	4.68	3.59	0.04
Al ₂ O ₃	2.54	2.46	2.88	1.11	1.08	0.62	0.37	0.46	0.13	0.10	13.03	14.17	1.02
Cr ₂ O ₃	1.11	0.58	0.48	0.09	0.54	0.15	0.12	0.07	0.03	0.01	1.39	1.22	0.07
FeO	1.37	1.81	1.95	2.11	1.94	1.88	1.77	1.63	1.00	0.98	4.09	3.94	2.86
MnO	0.02	0.05	0.05	0.027	0.06	0.10	0.08	0.09	0.06	0.06	0.07	0.04	0.03
MgO	21.89	22.54	22.50	22.94	23.57	23.90	23.45	23.61	24.09	23.99	15.58	15.76	22.12
CaO	13.03	12.75	11.35	12.99	11.29	12.92	12.55	13.15	12.75	12.48	11.96	11.91	12.98
Na ₂ O	0.56	1.18	1.16	0.69	0.52	0.39	0.32	0.40	0.08	0.05	3.18	3.29	0.50
K ₂ O	0.02	0.01	0.02	0.05	0.02	0.01	0.01	0.05	0.01	0.03	0.05	0.19	0.01
Total	96.38	96.23	96.08	97.55	96.98	97.26	96.93	96.28	97.26	97.02	96.18	95.82	96.15
Si	7.733	7.644	7.699	7.884	7.936	7.867	7.989	7.868	8.042	8.076	6.079	6.033	7.887
Al ^{IV}	0.267	0.356	0.301	0.116	0.064	0.133a	0.011	0.132b	0.000	0.000	1.921	1.967	0.113
Al ^{VI}	0.148	0.048	0.170	0.063	0.110	0.000	0.050	0.000	0.020	0.016	0.292	0.448	0.054
Ti	0.013	0.004	0.016	0.001	0.001	0.000	0.002	0.001	0.003	0.001	0.508	0.390	0.004
Cr	0.122	0.064	0.052	0.010	0.059	0.016	0.013	0.007	0.003	0.001	0.158	0.139	0.008
Fe ³⁺	0.000	0.065	0.113	0.023	0.017	0.101	0.016	0.057	0.000	0.000	0.245	0.237	0.016
Fe ²⁺	0.159	0.146	0.114	0.219	0.205	0.083	0.186	0.076	0.114	0.111	0.250	0.242	0.318
Mn	0.003	0.006	0.006	0.003	0.007	0.012	0.010	0.010	0.006	0.007	0.008	0.005	0.004
Mg	4.528	4.685	4.651	4.687	4.812	4.883	4.796	4.874	4.886	4.871	3.350	3.398	4.601
Ca	1.937	1.906	1.687	1.907	1.656	1.897	1.845	1.951	1.858	1.821	1.847	1.846	1.941
Na	0.149	0.320	0.313	0.182	0.139	0.104	0.086	0.108	0.021	0.014	0.888	0.922	0.134
K	0.003	0.002	0.004	0.008	0.003	0.002	0.002	0.008	0.001	0.005	0.009	0.035	0.001
Mg#	0.966	0.970	0.976	0.955	0.959	0.983	0.963	0.985	0.977	0.978	0.930	0.934	0.935

^a Includes Fe³⁺ 0.032, ^b Includes Fe³⁺ 0.056. Cations calculated on the basis of 23 O. Harz= I-Type harzburgite, Harz*= II-Type harzburgite, M.Perid=metamorphic basal peridotite, Wehr= wehrlite.

2.6.5 Chlorite

Chlorite in II-Type harzburgite, dunite bands within II-Type harzburgite and peridotite with amphibole aggregates exhibit SiO₂ contents ranging between 26.95 and 34.40 wt % (Table 7) and Fe/(Fe+Mg) ratio below 0.06. Most of chlorite has composition of penninite and in lesser proportion of clinochlore and sheridanite.

Table 7. Representative electron microprobe analyses of chlorite from peridotites of the Aburrá Ophiolite

Rock Sample	Dunite AC52B31E	Dunite AC52E3A	Harz* AC52E12A	A. Perid. AC53J3
SiO ₂	31.55	26.95	33.61	34.40
TiO ₂	0.04	0.12	0.03	0.01
Al ₂ O ₃	16.18	21.09	11.69	13.71
Cr ₂ O ₃	1.99	3.30	2.77	0.66
FeO	2.62	3.18	3.05	3.58
MgO	33.79	31.13	34.12	33.53
MnO	0.03	0.00	0.04	0.02
NiO	0.00	0.00	0.00	0.00
CaO	0.01	0.02	0.30	0.01
Na ₂ O	0.05	0.00	0.01	0.02
K ₂ O	0.04	0.00	0.00	0.02
H ₂ O	12.56	12.36	12.41	12.57
Total	98.84	98.14	98.04	98.53
Si	6.018	5.227	6.491	6.559
Al ^{IV}	1.982	2.773	1.509	1.441
Sum Z	8.000	8.000	8.000	8.000
Al ^{VI}	1.656	2.048	1.151	1.639
Ti	0.005	0.018	0.004	0.001
Mg	9.609	9.002	9.821	9.529
Fe ²⁺	0.417	0.515	0.493	0.570
Ni	0.000	0.000	0.000	0.000
Mn	0.004	0.000	0.007	0.004
Ca	0.001	0.004	0.062	0.002
Na	0.018	0.000	0.004	0.006
K	0.011	0.000	0.000	0.005

Cations calculated on the basis of 28 O. Dun=dunite, Harz*=II-Type harzburgite, A.Perid=peridotite with amphibole aggregates

2.6.6 Ni-Fe-S mineral assemblage

Ni-Fe-S minerals were analysed only in one dunite sample (AC52B3). The identified minerals are: Fe-Ni sulphide (pentlandite), Ni sulphide (millerite) and Ni-Fe alloy (awaruite) (Table 8). The analysed grains consist of a pentlandite core, which is surrounded by awaruite and/or millerite rims. The Ni/Fe atomic ratio of pentlandite ranges from 0.72 to 0.90. The Co content of pentlandite is low.

Pentlandite is interpreted as primary sulphide, whereas the textural relationships between this sulphide and millerite and Ni-Fe alloy suggest that the present assemblages have formed between the primitive Fe-Ni-S component of dunites and serpentinizing fluids.

Table 8. Representative microprobe analyses of Fe-Ni-S mineral assemblages from one dunite of the Aburrá Ophiolite.

Rock Mineral	Dunite				
	Pn AC52B3 P1core	Pn AC52B3 P4core	Aw AC52B3 P4rim2	Pn AC52B3 P4_2core	Mi AC52B3 P4_2rim
Fe(wt%)	35.16	36.64	22.15	33.10	2.96
Ni	29.43	28.22	76.68	31.38	61.51
Co	0.86	0.82	0.17	0.69	0.03
Cu	0.00	0.02	0.26	0.48	5.43
S	34.57	34.23	1.35	34.29	32.35
As	0.00	0.02	0.00	0.00	0.00
Se	0.01	0.02	0.03	0.03	0.06
Te	0.00	0.05	0.04	0.03	0.01
Total	100.03	100.01	100.68	100.01	102.35
Fe(at%)	28.31	29.56	22.75	26.74	2.45
Ni	22.54	21.65	74.92	24.11	48.39
Co	0.66	0.62	0.16	0.53	0.02
Cu	0.00	0.01	0.24	0.34	3.94
S	48.50	48.11	2.41	48.25	46.60
As	0.00	0.01	0.00	0.00	0.00
Se	0.01	0.01	0.02	0.02	0.04
Te	0.00	0.02	0.02	0.01	0.00
Total	100.02	100.01	100.52	100.01	101.45
Ni/Fe	0.80	0.73	3.29	0.90	19.75

Pn=pentlandite, AW=awaruite, Mi=millerite

2.7. Discussion

2.7.1. Origin of peridotites

Origin of harzburgite

Harzburgite has traditionally been interpreted as depleted, refractory residue produced by partial melting of mantle lherzolite and cpx-bearing harzburgite (Coleman, 1977). Harzburgite (I-Type JJ1396 and II-Type AC52A) exhibits depleted residual signature in terms of its modal composition due to the lack of primary cpx (or its alteration relics). It also exhibits low whole rock major and trace elements content (Al_2O_3 , TiO_2 , CaO , Sc and V, not shown in this paper), suggesting that they are residues of partial melting.

When compared to the calculated curves for near-fractional melting of spinel peridotite (Figures 4 and 6) the compositions of the I-Type harzburgite are consistent with 15-17% near

fractional melting of spinel peridotite. II-Type harzburgite samples could not be plotted in this diagram because their spinel is too altered.

We interpret the I-Type harzburgite as a refractory residue after medium degree of melting; however a detailed study of trace and REE elements is necessary to define if such rocks are simple residues or if they were affected by other mantle processes.

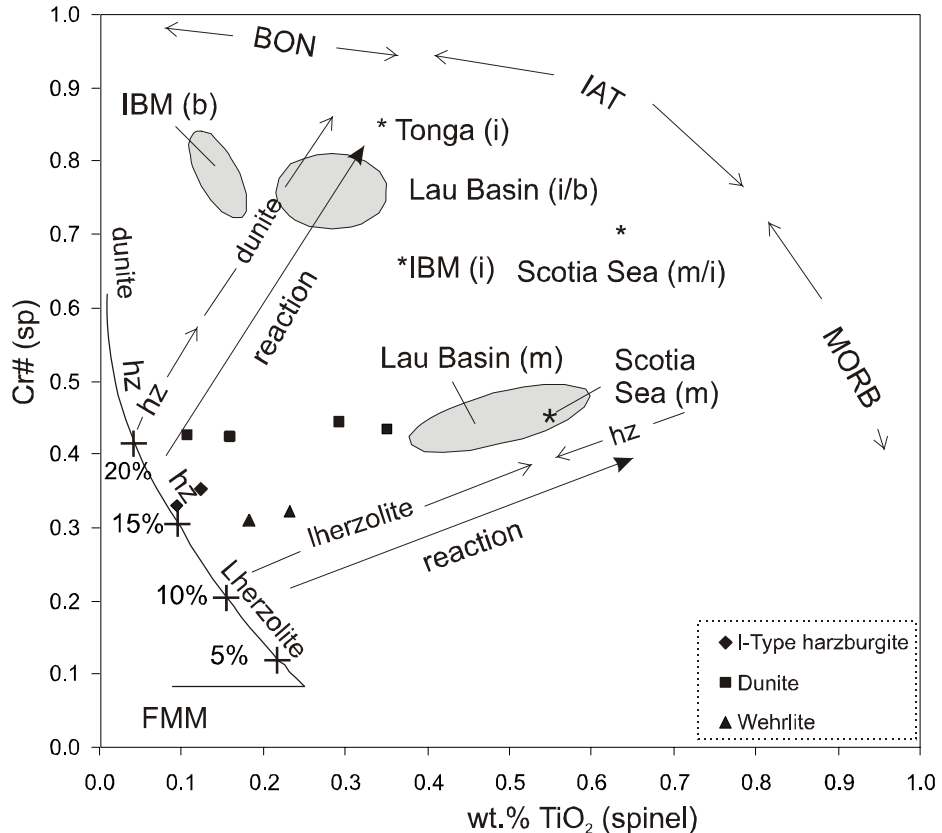


Figure 6. Plot of Cr# against TiO_2 for chrome spinel (Pearce et al. 2000). The diagram discriminates between partial melting trends and melt±mantle interaction trends. Subscripts m, i and b refer to MORB, island arc tholeiite and boninite chemistries, respectively, of the arc ± basin lava spinel reference data.

Origin of dunite

Two origins of dunite bodies have been proposed, particularly for transition-zone dunites: a cumulate origin (Coleman, 1977; Malpas, 1978) and a residual origin (Girardeau and Nicolas, 1981; Nicolas and Prinzhofer, 1983; Kelemen, 1990; Kelemen et al., 1995; Zhou et al., 1996). The residual dunite, also known as replacive or reactive dunite, is formed after extensive partial melting of lherzolite or harzburgite or by melt-rock interaction. They can be originated from a combined process of dissolution of pyroxenes in the peridotite and olivine accumulation from the melt (Kelemen, 1990; Kelemen et al., 1995).

The dunite bands of the Medellín Ultramafic Massif exhibits many features that may indicate a replacive, or residual origin after melt-peridotite interaction. Such evidence is as follows:

(1) The gradational contact between harzburgites and dunites characterized by the decreasing in the orthopyroxene content, i.e. modal layering. The occurrence of opx-depleted harzburgite suggests that the harzburgite was also partially affected by percolating melts.

(2) The morphological change of chromian spinel from holly-leaf and anhedral in harzburgite (Figure 3c) to euhedral and rounded in dunite (Figure 3e). Idiomorphism of chromian spinel can be produced by reaction between a preexisting spinel and a percolating magma (Leblanc et al., 1980; Matsumoto and Arai, 2001). The change in shape is accompanied by variations in the spinel composition (Kelemen et al., 1995).

(3) Spinel from dunite are enriched in TiO_2 in relation to those of the I-Type harzburgite. The increase in TiO_2 in dunite spinels must be a consequence of TiO_2 transfer from the impregnating mafic melt to dunite chromium spinel (Allan and Dick, 1996; Cannat et al., 1997). On the other hand the heterogeneous TiO_2 distribution inside some analysed spinel grains suggests that probably equilibrium between the percolating melt and the spinel was not achieved.

(4) Dunite exhibits high and nearly constant Mg# of olivine indicating that these rocks are not cumulates. Mg# values of olivine from dunite are only slightly higher than those in adjacent harzburgite. This feature can be produced by melt/rock reaction (Kelemen, 1990). The observed higher Mg# and lower NiO wt% in dunite (compared to the harzburgite) can be explained using an incongruent melting model of orthopyroxene as proposed by Kubo (2002).

(5) Some dunites exhibit higher content of intergranular sulphide grains than harzburgites. The analysed dunite sample carries up to 600 ppm S, which is considered as strongly sulfur-enriched, whereas the II-type harzburgite sample contains 200 ppm S. Lorand (1987, 1988) interpreted the sulphide enrichment in peridotites of the Transition Zone of the Bay of Islands and the Oman ophiolites as a metasomatic process resulting of percolation of a sulfur-saturated basaltic magma through the residual dunites. According to Luguet et al. (2008) during reactions between melt and wall-rock involving pyroxenitic components sulphides, because their low solidi, are among the first components to be transferred into the surrounding metasomatized wall-rock.

It is interpreted that most part of the dunite bands within harzburgite in the Medellín Ultramafic Massif are residual in origin due to melt-rock interaction processes, although the occurrence of cumulate dunite portions can not be ruled out. Coarse, equigranular textures of

dunites possibly result from syntectonic recrystallization during plastic deformation as interpreted by Nicolas and Prinzhofer (1983) in dunite of other ophiolites. This explanation can account for the intercalation of harzburgite with porphyroclastic microstructures and dunite with equigranular microstructures.

Evidence points to the assumption that the bands of dunite were initially irregular or discordant in relation to harzburgite. They probably became parallel to the foliation of harzburgite through plastic deformation in the upper mantle. A very similar harzburgite-dunite banding was studied by Braun and Kelemen (2002) who interpreted dunite as conduits for melt extraction from the shallow mantle. Thus the banding in the outcrop AC52 does not correspond to a layering produced by accumulation process.

Simultaneously with the formation of replacive dunite a SiO₂-rich secondary melt is generated and this can be later mixed with a subsequently supplied primitive MORB. This process allows magmas to become chromium-saturated and to promote spinel crystallization. This mechanism has been proposed to explain the formation of podiform chromitites (Arai and Yurimoto, 1994; Zhou et al., 1994). It is postulated that the large spinel grains which occur in trails within dunite bands from outcrop AC52 probably were formed via this process. Pyroxenite generation may also be achieved via a combined process of magma mixing and local melt-rock interaction that produce orthopyroxenites dykes which intrude dunite and harzburgite (e.g. Varfalvy et al., 1997). These processes can explain the occurrence of ultramafic dykes within peridotites from the Perico Sector (AC53).

Origin of wehrlite

Wehrlitic bodies have been described on the top of the mantle-crust transition and in the crustal section of different ophiolites around the world (Benn et al., 1988; Nicolas 1989). Wehrlite in the Transition Zone of ophiolites has been interpreted as resulting from pervasive impregnation of residual dunite by basaltic magma (Nicolas and Prinzhofer, 1983). Wehrlite in the crustal section is considered as intrusions originated from a crystal-melt mixture rooted in the Transition Zone (Benn et al., 1988). They represent a significantly different melt from those responsible for the formation of the gabbroic rocks (Juteau et al., 1988). They exhibit a crystallization sequence which is different from that of the gabbroic rocks and their genesis is not clear yet (Koepke et al. 2005).

Wehrlite of the Los Balsos sector (P2, P3) occurs relatively close (80-110 m) of metagabbros, but it is not possible to establish if wehrlite is intrusive in the mafic rocks. Recognition based on the composition and microstructures of the Los Balsos wehrlite as part

of Transition Zone or from the lower crust also was not successful. As pointed by several authors (e.g. Boudier and Nicolas, 1995; Jousselin and Nicolas, 2000) such differentiation is often difficult because composition and texture of wehrlitic intrusions are very similar in composition and texture of undeformed impregnated dunites of the Transition Zone.

In the Los Balsos wehrlite impregnation microstructures defined by clinopyroxene and probably by brown amphibole (kaersutite and titanian pargasite) together with low Ni contents and low Mg# values suggest that these rocks are impregnated dunites resulting from peridotite-melt interaction at a high melt/rock ratio. Moreover, the occurrence of some olivine grains with sub-structures could indicate that these olivine grains are xenocrysts, where deformation predates crystallization of the melt (Nicolas and Prinzhofer, 1983).

A notorious feature of these samples is the abundance of brown amphibole. The origin of the brown amphibole in wehrlite is uncertain. It could be igneous (Arai and Matsukage, 1996), or could be formed by subsolidus reaction of igneous minerals with H₂O (Cannat and Casey, 1995). The amphibole origin is related to the source of the water (Bazylev et al., 2001). The relationship between brown amphibole and olivine and clinopyroxene and the high Ti contents of kaersutite and pargasite in the Aburrá wehrlite samples suggest an origin of amphibole by crystallization from residual magma where fluids were concentrated. The brown amphibole found in the impregnated peridotites of the Canyon Mountain ophiolite was interpreted in this way by Misseri and Boudier (1985).

The melt responsible for these impregnations was sulphur-saturated, as is shown by the sulphur enrichment (1400 ppm) and the occurrence of Cu-Ni-Fe sulphides, associated with the clinopyroxene in wehrlite.

2.7.2. Primary spinel composition and nature of the percolating melts

The composition of primary accessory spinel in peridotites is widely used as a petrogenetic indicator in ophiolites (e.g. Dick and Bullen, 1984). In the Al₂O₃ versus TiO₂ plot the unaltered spinels lie in the overlap region of mid-ocean ridge (MORB) peridotite and suprasubduction zone (SSZ) peridotite (Figure 7a). According to the TiO₂ content (Figure 7b) spinel of dunite was partially re-equilibrated with a relatively Ti-rich magma (back-arc basin or MORB-like magma) and fresh spinel from wehrlite probably crystallized from a similar magma (melt) type. As can be observed in Figure 6 some points of the Aburrá dunite plot close to the MORB field from the Lau Basin. This suggests that these samples originated by interaction of a MORB-like melt with mantle that had experienced a significant (~20%) degree of partial melting.

The geochemical nature of the melt could be mid-ocean ridge basalts (MORB)-type or back-arc basin basalts (BABB)-type because both have similar contents of TiO_2 , Al_2O_3 and S (Wilson, 1989; Dick and Bullen, 1984; Lorand, 1988). It is not possible to be sure that the fluids that interacted with harzburgite which form the dunite bands were of the same kind of those that impregnated the upper peridotites that generated wehrlite.

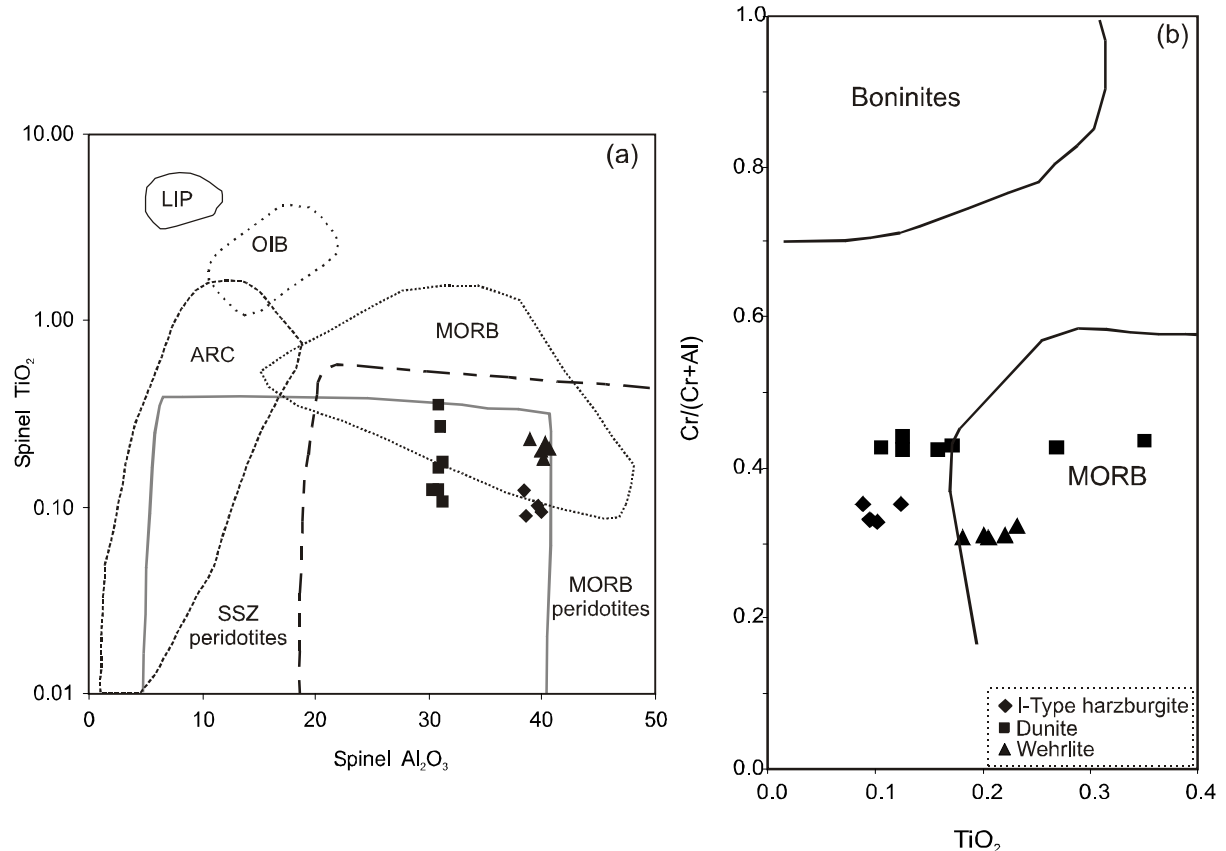


Figura 7. (a) TiO_2 - Al_2O_3 diagram showing the compositions of fresh accessory spinels of the ultramafic rocks. Fields are from Kamenetsky et al. (2001). LIP, large igneous provinces; OIB, ocean island basalts; MORB, mid-ocean ridge basalts; MORB peridotite, sub-basaltic, ocean crust peridotite; ARC, volcanic arc rocks; SSZ peridotite, suprasubduction zone peridotite. (b) Boninites and MORB fields are from Arai (1992).

Studies on wehrlites of ophiolites demonstrated that they were in equilibrium with normal MORB melts, but the order of crystallization in this type of rock (olivine - clinopyroxene - plagioclase) is different to that expected in typical MORB systems (olivine-plagioclase-clinopyroxene) (e.g. Koga et al., 2001). This difference in crystallization sequence may be ascribed to the occurrence of water in the magma, as is shown experimentally that in water-rich systems plagioclase crystallization is suppressed (Koga et al., 2001; Koepke et al., 2005;

Feig et al., 2006). Another evidence of the high water activity in these melts is the occurrence of pargasite as a primary phase (Feig et al., 2006).

In the case of the wehrlites of the Aburrá Ophiolite the occurrence of clinopyroxene and primary amphibole suggests that the fluids responsible for the impregnation probably consisted of two components: a MORB type melt modified by an aqueous (hydrous) fluid component. The aqueous fluids may be magmatic or hydrothermal. Magmatic fluids are released from MORB-type melts after a high degree of crystallization, whereas hydrothermal fluids are seawater-derived and heated by the still hot gabbroic cumulate pile (Koepke et al., 2005).

2.7.3. Tectonic implications

The I-Type harzburgite probably represents a residue from ~15 to 17% of partial melting (Figures 4 and 6), but these values are not diagnostic enough to determine the original tectonic setting in which such melting occurred. It is widely accepted that 15-20% degree of melting is common for uppermost mantle lithosphere formed by decompression melting at the axial zone of a mid-ocean ridge segment, at a sub-arc or at a marginal basin (Pearce et al. 2000). In Figure 8a the I-Type harzburgite plots within the Suprasubduction peridotites field of Ishii et al. (1992), and in Figure 8b the I-Type harzburgite plots on the edge of Mariana Trough peridotites field of Ohara et al. (1996, 2002), which represent peridotites from a back-arc basin.

According to Boudier and Nicolas (1995) the limit between the harzburgitic mantle and the Transition Zone of the ophiolites is characterized by progressive upward increase in frequency of dunite bands and discordant veins within the harzburgite, and simultaneous decrease in the orthopyroxene fraction of the harzburgite. The upper boundary of the Transition Zone corresponds to the base of the continuous layered gabbro unit, but this limit between the mantle and the oceanic crust is often difficult to establish (Nicolas and Prinzhöfer, 1983; Jousselin and Nicolas, 2000).

The abundance of dunite and orthopyroxene-depleted harzburgite, together with the evidence of reactions such as orthopyroxene dissolution reaction, clinopyroxene impregnation, and furthermore the occurrence of podiform chromitites indicate that most parts of the ultramafic portion of the Aburrá ophiolite represent the Transition Zone of the ophiolite. The sectors of banded harzburgite-dunite probably correspond to the lower or intermediate portion of the Transition Zone, whereas wehrlite probably represents the upper part of the Transition Zone and the limit with the mafic crust. So far, typical cumulate

peridotites of the mantle-crust limit have not been recognized in the Aburrá ophiolite. Spinel in dunite lie on the overlap sector of the edge of the back-arc basin peridotites field and in the lower part of the fore-arc peridotites field, however the Cr# values in these spinels are more typical of those observed in spinels from back-arc basin peridotites (Cr# <0.53 - Ohara et al., 1996). The results of this study suggest that the peridotite of the Transition Zone of this ophiolite were formed through interactions processes between a MORB-like magma and pre-existing oceanic crust.

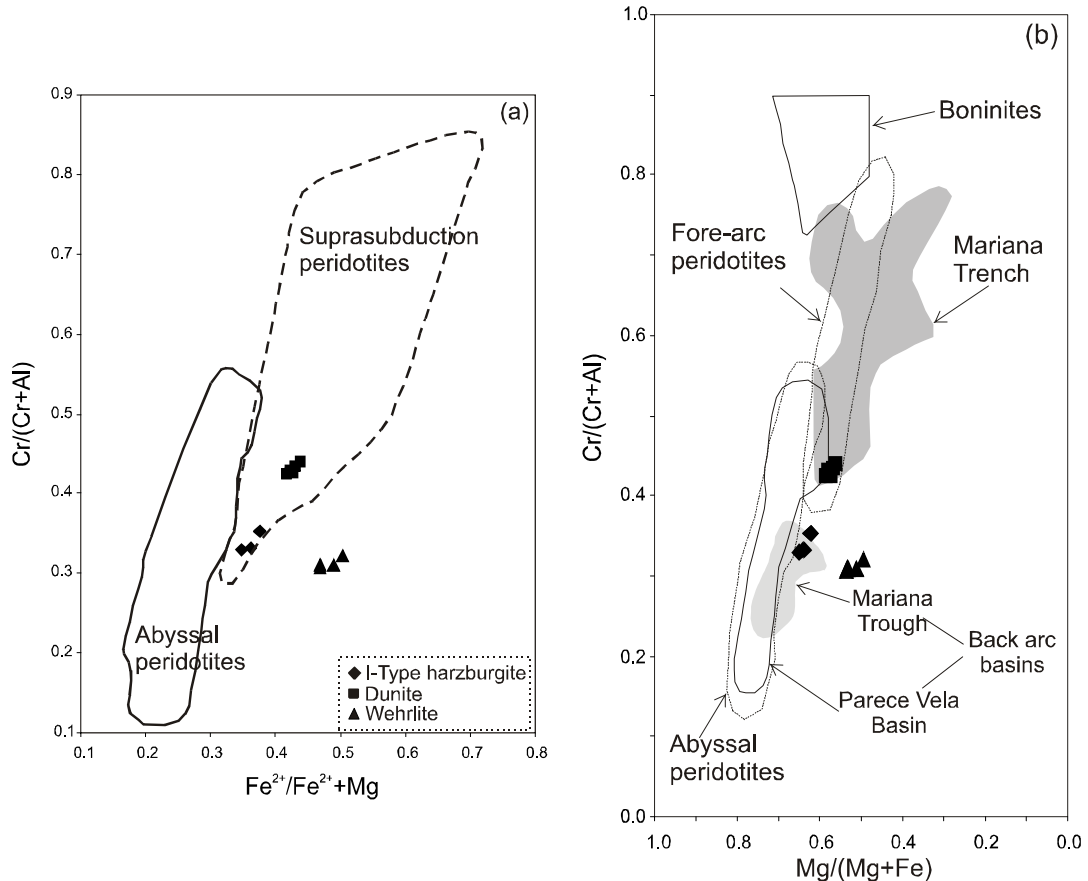


Figura 8. (a) Compositions of unaltered spinels from ultramafic rocks of the Aburrá ophiolite. Field of spinels from mid-ocean ridge peridotites after Dick and Bullen (1984); field of spinels from suprasubduction peridotites after Ishii et al. (1992). (b) Plot of Cr# against Mg# for spinel in peridotite of Aburrá ophiolite. Fields for abyssal peridotites and boninites are from Dick and Bullen (1984); fields for Mariana Trench and fore-arc peridotites are given by Ohara and Ishii (1998); fields of Mariana Trough and Parece Vela Basin (back-arc basins) are from Ohara et al. (1996, 2002).

Since Iherzolites have not been found in the mantle section of the ophiolite and considering the mineralogical and chemical composition of rocks in the Medellín ultramafic

massif, the ophiolite may be classified as of Harzburgite-type in the sense of Boudier and Nicolas (1985).

According to the data and interpretations presented here, we believe that the Aburrá peridotite represents mantle formed and affected by melts possibly in a back-arc basin.

2.8. Concluding remarks

Based on the presented data and interpretations we conclude the following:

The ultramafic section of the Aburrá ophiolite is not as compositionally homogeneous as previously interpreted. Although the massifs are made up mainly of dunite, they also contain opx-depleted harzburgite and minor harzburgite, chromitites, ultramafic dykes and wehrlite.

I-Type harzburgite is probably the only preserved member of the lower mantle in this ophiolite. It is residue of moderate (intermediate) extents (15-20%) of partial melting at an ocean ridge. These rocks would represent the first evolution stage of the ophiolite.

II-Type harzburgite, dunite, chromitites and wehrlite seem to represent the Transition Zone of the ophiolite. Dunite bands within harzburgite are residual probably resulting from the reaction between a MORB-like melt and the host harzburgite. Wehrlite results from the interaction of residual peridotite with a hydrous melt (MORB melt + high water content hydrous fluid). These would correspond to a second stage of evolution of the peridotite.

We suggest that the Aburrá ultramafic massif represents a portion of back-arc oceanic lithosphere.

Acknowledgements

This work was supported by CNPq/Grant no. 141622/03-2 to A.M. Correa-M. The authors thank O. Ordóñez-Carmona, M. Weber and J.J. Restrepo (Universidad Nacional de Colombia-Medellín) for field assistance. We would also like to thank J.J. Restrepo for a harzburgite sample and for the unpublished data he communicated to us, and to P. Angel of the Solingral Company for the drill cores of the wehrlite samples. We are also grateful to U. Martens for microprobe analyses of the P2-11.20 sample at Stanford University. The first author acknowledges F. Boudier and A. Tommasi (Université Montpellier) and M. da G. da Silva (Universidade Federal da Bahia) for valuable discussions. We are also grateful to Tereza Brod for suggestions to improve the manuscript.

References

- Allan, J.F., Dick, H.J.B., 1996. Cr-rich spinels as a tracer for melt migration and melt wall rock interaction in the mangle: Hess Deep, leg 147, Sci. Res. Ocean Drill. Prog. 147, 157-172.
- Alvarez, J., 1982. Tectonitas dunitas de Medellín, Departamento de Antioquia, Colombia. Informe 1986, Ingeominas. Medellín. 62 p.
- Alvarez, J., 1985. Ofiolitas e evolución tectónica del Occidente Colombiano. Informe 1988, INGEOMINAS, Medellín, 30 p.
- Alvarez, J., 1987. Mineralogía y química de los depósitos de cromita podiforme de las dunitas de Medellín, Departamento de Antioquia, Colombia. Boletín Geológico de Ingeominas 33(1-3), 33-46.
- Arai, S., 1992. Chemistry of chromian spinel in volcanic rocks as a potential guide to magma chemistry. Mineralogical Magazine 56, 173-184.
- Arai, S., 1994. Characterization of spinel peridotites by olivine-spinel compositional relationships: review and interpretation. Chemical Geology 113, 191-204.
- Arai, S., Matsukage, J.H., 1996. Petrology of gabbro-troctolite-peridotite complex from Hess Deep, equatorial Pacific: implications for mantle-melt interaction within the oceanic lithosphere. In Mével, C., Gillis, K.M., Allan, J.F., and Meyer, P.S. (Eds.), Proc. ODP, Sci. Results, 147: College Station, TX (Ocean Drilling Program), 135-155.
- Arai, S., Yurimoto, H., 1994. Podiform chromitites in the Tari-Misaka ultramafic complex, southwestern Japan, as mantle-melt interaction products. Econ. Geol. 85, 1279-1288.
- Bazylev, B.A., Silantyev, S.A., Dick, H.J.B., Kononkova, N.N., 2001. Magmatic amphiboles and micas in oceanic peridotites and some specific features of the related magmas: 15~MAR Fracture Zone. Russian Journal of Earth Sciences 3(3), 219-234.
- Benn, K., Nicolas, A., Reuber, I., 1988. Mantle-crust transition zone and origin of wehrlitic magmas: Evidence from the Oman. Tectonophysics 151, 75-85.
- Botero, G., 1963. Contribución al conocimiento de la zona central de Antioquia. Anales Facultad de Minas (Medellín) 57. 101 p.
- Boudier, F., Nicolas, A., 1985. Harzburgite and Iherzolite subtypes in ophiolitic and oceanic environments. Earth and Planet. Sci. Lett. 76, 84-92.
- Boudier, F., Nicolas, A., 1995. Nature of the Moho transition zone in the Oman ophiolite. Journal of Petrology 36(3), 777-796.

- Braun, M.G., Kelemen, P.B., 2002. Dunite distribution in the Oman Ophiolite: Implications for melt flux through porous dunite conduits, *Geochem. Geophys. Geosyst.* 3 (11), 8603, doi:10.1029/2001GC000289.
- Cannat, M., Casey, J.F., 1995. An ultramafic lift at the Mid-Atlantic Ridge: Successive stages of magmatism in serpentined peridotites from the 15_N region. In: Vissers R.L.M. and Nicolas A. (Eds.), *Mantle and Lower Crust Exposed in Oceanic Ridges and in Ophiolites*. Norwell, Mass. Kluwer Acad., pp. 5-34.
- Cannat, M., Chatin, F., Whitechurch, H., Ceuleneer, G., 1997. Gabbroic rocks trapped in the upper mantle at the Mid-Atlantic Ridge. In: Karson, J.A., Cannat, M., Miller, D.J., Elthon, D. (Eds.), *Proceedings of the Ocean Drilling Program, Scientific Results*, 153. Ocean Drilling Program, College Station, TX, 243-264.
- Case, J.E., Barnes, J., Paris, G., Gonzalez, H., Viña, A., 1973. Trans-Andean geophysical profile, southern Colombia. *Geological Society of America Bulletin* 84, 2895-2904.
- Case, J.E., Duran, S.L.G., López, A., Moore, W.R., 1971. Tectonic investigations on western Colombia and eastern Panama. *Geological Society of America Bulletin* 82, 2685-2712.
- Coleman, R.G., 1977. *Ophiolites-Ancient Oceanic Lithosphere? Minerals and Rocks*, Springer-Verlag, 12, 229 p.
- Correa, A.M., Martens, U., 2000. Caracterización geológica de las anfibolitas de los alrededores de Medellín. Trabajo Dirigido de Grado (Unpublished), Facultad de Minas, Universidad Nacional de Colombia, 363p.
- Correa, A.M., Nilson, A.A., 2003. Dunitas de Medellín y Metagabros de El Picacho: Posibles Fragmentos de Ofiolita Subtipo Harzburgita, Tipo Zona de Supra-Subducción In: IX Congreso Colombiano de Geología, Resumenes, pp. 46-47.
- Correa, A.M., Pimentel, M.M., Armstrong, R., Laux, J.E., Ordoñez-Carmona, O., 2005. Edad U-Pb SHRIMP y características isotópicas Nd y Sr del granito de la Iguaná, Antioquia. In: X Congreso Colombiano de Geología, Bogotá. Memorias, CD ROM.
- Dick, H.J.B., Bullen, T., 1984. Chromian spinel as a petrogenetic indicator in abyssal and Alpine-type peridotites and spatially associated lavas. *Contr. Mineral. Petrol.* 86, 54-76.
- Droop, G.T.R., 1987. A general equation for estimating Fe^{3+} concentrations in ferromagnesian silicates and oxides from microprobe analyses, using stoichiometric criteria. *Min. Mag.* 51, 431-435.
- Feig, S., Koepke, J., Snow, J., 2006. Effect of water on tholeiitic basalt phase equilibria - an experimental study under oxidizing conditions. *Contrib. Miner. Petrol.* 152:5, 611-638.

- Feininger, T., Barrero, D., Castro, N., 1972. Geología de Antioquia y Caldas (Subzona II-B) Boletín Geológico de Ingeominas 20 (2), 1-173.
- Geominas, Ltda., 1975. Proyecto cromitas. Informe final. 39p.
- Girardeau, J., Nicolas, A., 1981. Structures in two of the Bay of Islands (Newfoundland) ophiolite massifs: a model for oceanic crust and upper mantle. *Tectonophysics* 77, 1-34.
- Ishii, T., Robinson, P.T., Maekawa, N., Fiske, R., 1992. Petrological studies of peridotites from diapiric serpentinite seamounts in the Izu-Ogasawara-Mariana forearc, Leg 125. In: Fryer, P., Pearce, J.A., Stokking, L.R. et al. (Eds.), *Proceedings of the Ocean Drilling Program, Scientific Results, 125: College Station, TX (Ocean Drilling Program)*, 445-485. doi:10.2973/odp.proc.sr.125.129.1992.
- Jousselin, D., Nicolas, A., 2000. The Moho transition zone in the Oman ophiolite-relation with wehrlites in the crust and dunites in the mantle. *Mar. Geophys. Res.* 21, 229-241.
- Juteau, T., Ernewein, M., Reuber, I., Whitechurch, H., Dahl, R., 1988. Duality of magmatism in the plutonic sequence of the Sumail nappe, Oman, *Tectonophysics*, 151, 107-135.
- Kamenetsky, V.S., Crawford, A.J., Meffre, S., 2001. Factors controlling chemistry of magmatic spinel: an empirical study of associated olivine, Cr-spinel and melt inclusions from primitive rocks. *Journal of Petrology* 42, 655-671.
- Kelemen, P.B., 1990. Reaction between ultramafic rock and fractionating basaltic magma, I. Phase relations, the origin of calc-alkaline magma series, and the formation of discordant dunite. *J. Petrol.* 31, 51-98.
- Kelemen, P.B., Shimizu, N., Salters, V.J.M., 1995. Extraction of MORB from the mantle by focused flow of melt in dunite channels. *Nature* 375, 747-753.
- Kerr, A.C., Marriner, G.F., Tarney, J., Nivia, A., Saunders, A.D., Thirlwall, M.F., Sinton, C.W., 1997. Cretaceous Basaltic Terranes in Western Colombia: Elemental, Chronological and Sr-Nd Isotopic Constraints on Petrogenesis. *Journal of Petrology* 38, 677-702.
- Koepke, J., Feig, S.T., Snow, J., 2005. Late-stage magmatic evolution of oceanic gabbros as a result of hydrous partial melting: evidence from the ODP Leg 153 drilling at the Mid-Atlantic Ridge. *Geochem. Geophys. Geosyst.* 6, 2004GC000805.
- Koga, K.T., Kelemen, P.B., Shimizu, N., 2001. Petrogenesis of the crustmantle transition zone and the origin of lower crustal wehrlite in the Oman ophiolite. *Geochem. Geophys. Geosyst.* 2, 2000GC000132.

- Kubo, K., 2002. Dunite formation processes in highly depleted peridotite: case study of the Iwanaidake Peridotite, Hokkaido, Japan. *Journal of Petrology* 43, 423–448.
- Leake, B.E., Woolley, A.R., Arps, C.E.S., Birch, W.D., Gilbert, M.C., Grice, J.D., Hawthorne, F.C., Kato, A., Kisch, H.J., Krivovichev, V.G., Linthout, K., Laird, J., Mandarino, J.A., Maresch, W.V., Nickel, E.H., Rock, N.M.S., Schumacher, J.C., Smith, D.C., Stephenson, N.C.N., Ungaretti, L., Whittaker, E.J.W., Youzhi, G., 1997. Nomenclature of amphiboles: Report of the Subcommittee on Amphiboles of the International Mineralogical Association, Commission on New Minerals and Mineral Names. *American Mineralogist* 82, 1019–1037.
- Leblanc, M., Dupuy, C., Cassard, D., Moutte, J., Nicolas, A., Prinzhofer, A., Rabinovitch, M., Routhier, P., 1980. Essai sur la genèse des corps podiformes de chromitite dans les péridotites ophiolitiques: Etude des chromites de Nouvelle-Caledónie et comparaison avec celles de Méditerranée orientale. In: Panayiotou, A. (Ed.), Ophiolites. Proceedings International Ophiolite Symposium, Cyprus, 1979. Geol Surv Dept, Cyprus Nicosia, pp 691-701.
- Leblanc, M., Nicolas, A., 1992. Ophiolitic chromitites. *Chronique de la Recherche Minière* 507, 3-25.
- Lorand, J.P., 1987. Cu-Fe-Ni mineral assemblages in upper-mantle peridotites from the Table Mountain and Blow-Me Down Mountain ophiolite massifs (Bay of Islands area, Newfoundland): Their relationships with fluids and silicate melts. *Lithos* 20, 59-76.
- Lorand, J.P., 1988. Fe-Ni-Cu sulfides in tectonite peridotites from the Maqsad district, Sumail ophiolite, southern Oman: implications for the origin of the sulfide component in the oceanic upper mantle. *Tectonophysics* 151, 57-73.
- Luguet, A., Pearson, D.G., Nowell, G.M., Dreher, S.T., Coggon, J.A., Spetsius, Z.V., Parman, S.W., 2008. Enriched Pt-Re-Os Isotope Systematics in Plume Lavas Explained by Metasomatic Sulfides. *Science* 319, 453-456, doi: 10.1126/science.1149868.
- Malpas, J., 1978. Magma generation in upper mantle, field evidence from ophiolite suites, and application to generation of oceanic lithosphere. *Philosophical Transactions of the Royal Society of London, Series A* 288, 527–545.
- Matsumoto, I., Arai, S., 2001. Morphological and chemical variations of chromian spinel in dunite-harzburgite complexes from the Sangun zone (SW Japan): implications for mantle/melt reaction and chromitite formation processes. *Mineralogy and Petrology* 73(4), 305-323.

- Maya, H.M., Gonzalez, H., 1996. Unidades litodémicas de la cordillera Central de Colômbia. Boletín Geológico de Ingeominas 35 (2-3), 43-57.
- McCourt, W.J., Aspden, J.A., Brook, M., 1984. New geological and geochronological data from the Colombian Andes: continental growth by multiple accretion. J. Geol. Soc. London. 141, 831-845.
- Misseri, M., Boudier, F., 1985. Structures in the Canyon Mountain ophiolite indicate an Island arc intrusion. Tectonophysics 120, 191-209.
- Monsalve, B.I., 1996. Evaluación geológica de las cromitas al NNW de Medellín. Trabajo Dirigido de grado (Unpublished), Facultad de Minas, Universidad Nacional de Colombia (Medellín). 88 p.
- Morimoto, N., 1989. Nomenclature of pyroxenes. Canadian Mineralogist 27, 143-156.
- Nicolas, A., 1989. Structures of Ophiolites and Dynamics of Oceanic Lithosphere. Petrology and Structural Geology. Vol. 4. Kluwer Academic Publishers, Dordrecht. 367 p.
- Nicolas, A., Prinzhofner, A., 1983. Cumulative or residual origin for the transition zone in ophiolites. Structural evidence. J. Petrol. 24, 188-206.
- Ohara, Y., Ishii, T., 1998. Peridotites from the southern Mariana forearc: Heterogeneous fluid supply in mantle wedge. The Island Arc 7, 541-558.
- Ohara, Y., Kasuga, S., Ishii, T., 1996. Peridotites from the Parece Vela Rift in the Philippine Sea upper mantle material exposed in an extinct backarc basin. Proceedings Japan Acad. 72, 118–123.
- Ohara, Y., Stern, R.J., Ishii, T., Yurimoto, H., Yamazaki, T., 2002. Peridotites from the Mariana Trough: first look at the mantle beneath an active back-arc basin. Contributions to Mineralogy and Petrology 143, 1-18.
- Ordóñez-Carmona, O., 2001. Caracterização Isotópica Rb-Sr e Sm-Nd dos Principais Eventos Magmáticos nos Andes Colombianos. Unpublished Ph.D. thesis, Instituto de Geociências, Universidade de Brasília. 176 p.
- Ordóñez-Carmona, O., Pimentel, M.M., 2001. Consideraciones geocronológicas e isotópicas del Batolito Antioqueño. Revista de la Academia Colombiana de Ciencias Exatas, Físicas y Naturales 25(94), 27-35.
- Pearce, J.A., Barker, P.F., Edwards, S.J., Parkinson, I.J., Leat, P.T., 2000. Geochemistry and tectonic significance of peridotites from the South Sandwich arc-basin system, South Atlantic. Contrib. Mineral. Petrol. 139, 36-53.

- Proenza, J., Escayola, M.P. Ortiz, F., Pereira, E., Correa, A.M., 2004. Dunite and associated chromitites from Medellin (Colombia). 32nd Int. Geol. Congr.Abs. Vol., pt. 1, abs 1-1, p.507.
- Rendón, D.A., 1999. Cartografía y caracterización de las unidades geológicas del área urbana de Medellín. Trabajo Dirigido de Grado (Unpublished), Facultad de Minas, Universidad Nacional de Colombia (Medellín). 113 p.
- Restrepo, J.J., 2005. Anfibolitas & Anfibolitas del Valle de Aburrá. In: X Congreso Colombiano de Geología, Memórias, CD-ROM.
- Restrepo, J.J., Frantz, J.C., Ordóñez-Carmona, O., Correa, A.M., Martens, U., Chemale, F., 2007. Edad triásica de formación de la Ofiolita de Aburrá, flanco occidental de la cordillera Central. In: XI Congreso Colombiano de Geología. Memorias. CD-ROM.
- Restrepo, J.J., Toussaint, J.F. 1973. Obducción Cretácea en el occidente Colombiano. Publicación Especial de Geología U. Nal., Medellín 3, 1-26.
- Restrepo, J.J., Toussaint, J.F. 1982. Metamorfismos superpuestos en la Cordillera Central de Colombia. V Congreso Latinoamericano de Geología, Actas. 3, pp. 505-512.
- Restrepo, J.J., Toussaint, J.F. 1984. Unidades litológicas de los alrededores de Medellín. In: I Conferencia sobre riesgos geológicos del Valle de Aburrá, Soc. Col. de Geol. Memoria 1, 1-26.
- Restrepo, J.J., Toussaint, J.F.; González, H.; Cordani, U.; Kawashita, K.; Linares, E., Parica, C., 1991. Precisiones geocronológicas sobre el occidente colombiano. Simposio sobre magmatismo andino y su marco tectónico. Memorias, I. Manizalez, p. 1-22.
- Rodriguez, G., González, H., Zapata, G. 2005. Geología de la Plancha 147 Medellín Oriental, Departamento de Antioquia. Ingeominas. 303 p.
- Toussaint, J.F., Restrepo, J.J., 1976. Modelos orogénicos de tectónica de placas en los Andes Colombianos. Boletín de Ciencias de la Tierra, Universidad Nacional de Colombia (Medellín), 1, p. 1-47.
- Varfalvy, V., Hebert, R., Bedard, J.H., Lafleche, M.R., 1997. Petrology and geochemistry of pyroxenite dikes in upper mantle peridotites of the North Arm Mountain massif, Bay of Islands ophiolite, Newfoundland: implications of the genesis of boninitic and related magmas. Canadian Mineralogist 35, 543-570.
- Vinasco, C.J., Cordani, U.G., González, H., Weber, M., Pelaez, C., 2006. Geochronological, isotopic, and geochemical data from Permo-Triassic granitic gneisses and granitoids of the Colombian Central Andes. Journal of South American Earth Sciences 21, 355-371.
- Wilson, M., 1989. Igneous petrogenesis. Londres: Unwin Hyman, 466 p.

- Zhou, M.-F., Robinson, P.T., Bal, W.-J., 1994 Formation of podiform chromites by melt/rock interaction in the upper mantle. *Mineralium Deposita* 28, 98-101.
- Zhou, M.-F., Robinson P.T., Malpas, J., Edwards, S.J., Qi, L., 2005. REE and PGE Geochemical Constraints on the Formation of Dunites in the Luobusa Ophiolite, Southern Tibet. *Journal of Petrology* 46(3), 615-639.
- Zhou, M.-F., Robinson, P.T., Malpas, J., Li, Z., 1996. Podiform chromitites in the Luobusa ophiolite (Southern Tibet): Implications for mantle-melt interaction and chromite segregation. *Journal of Petrology* 37, 3-21.

CAPÍTULO 3.

THE CHROMITE DEPOSITS OF THE ABURRÁ OPHIOLITE, COLOMBIAN ANDES: CONSTRAINTS FROM MINERAL CHEMISTRY AND Re-Os ISOTOPES

A.M. Correa, A.A. Nilson

Instituto de Geociências, Universidade de Brasília, Brasília-DF, 70910-900, Brazil.

E-mail: anamacor@unb.br

R.S.C. de Brito

*CPRM-Serviço Geológico do Brasil. SGAN-Quadra 603 - Conjunto J - Parte A - 1º andar,
Brasília-DF, 70830-030, Brazil*

J.C. Marques

*Departamento de Geologia, Instituto de Geociências, Universidade Federal do Rio Grande
do Sul, Av. Bento Gonçalves 9500, Porto Alegre-RS, 91509-900, Brazil*

R.W. Carlson

*Department of Terrestrial Magnetism, Carnegie Institution of Washington, 5241 Broad
Branch Road, NW Washington, DC 20015, USA*

Abstract

The Aburrá Ophiolite in the Central Cordillera of the Colombian Andes hosts the only known podiform chromite deposits of Colombia. The mantle in the ophiolite is of HOT-Harzburgite-Ophiolite-Type. The chromite ores occur within the Transition Zone of the ophiolite, mainly as concordant small podiform bodies. Most of the chromitites are massive to minor disseminated, except in one deposit located in the southernmost part of the southern sector where chromitites are nodular, disseminated, chain and banded. Typically the orebodies are surrounded by sheared dunite envelopes, which show sharp or transitional boundaries to harzburgite host rocks. Only in one deposit satellite stringers of chromite ore extend into the wall rocks. The chromitites consist of Al-rich spinel with variable Cr# [Cr/(Cr+Al), 0.34-0.53] and Mg# [Mg/(Mg+Fe²⁺), 0.69-0.75] values.

The negative initial γ Os of harzburgite indicates that it is a lithospheric mantle melt residue. The negative initial γ Os of massive chromitite is compatible with a parental magma derived from Re-depleted lithospheric mantle source. The Os isotopic characteristics of dunite and coarse-grained disseminated chromitite indicate addition of radiogenic Os, probably during melt-peridotite interaction processes.

Reactions between host harzburgite and percolating melts with composition varying between mid-ocean ridge basalt (MORB) and back-arc basalt (BABB) types coupled with magma mixing probably played an important role in the formation of most chromitite bodies in the Aburrá Ophiolite within a back- arc environment.

Keywords: *podiform chromitite, melt-rock interaction, MORB - BABB melts, Re-Os isotopes*

3.1. Introduction

Ophiolitic chromitites comprise irregular masses of chromite ores which generally have limited lateral extension; they are also known as podiform chromitites. In spite of that they are not considered as world class chromite deposits as compared to stratiform chromitites from layered intrusions, they are valuable petrogenetic indicators in the study of ophiolite petrogenesis.

These chromite bodies occur mainly in the transition zone of ophiolites and according to their structural relationships with respect to the host peridotites they can be classified as concordant, subconcordant and discordant pods (Cassard et al. 1981).

The chemical composition, the origin and the tectonic environment of formation of the ophiolitic chromitites have been subject of numerous researches, but nevertheless many questions still remain unclear. The occurrence either as high-Al chromitites or high-Cr chromitites has been ascribed to their environment of formation (Dick and Bullen 1984; Zhou and Robinson 1997), to the position of chromitites in the mantle sequence (Neary and Brown 1979; Leblanc and Violette 1983), and to the degree of melt-rock interaction at different levels within the mantle (Proenza et al. 2002; Rollinson 2005). It is currently widely accepted that the main mechanism of the chromitites formation and their dunite envelopes is the interaction between parental magma and peridotite in the uppermost mantle (Arai 1980; Kelemen et al. 1995; Arai and Yurimoto 1994; Zhou et al. 1996; Matsumoto and Arai 2001; Zhou et al. 2005). It is recognized that ophiolitic chromitites originated in environments related to subduction zones (Pearce et al. 1984; Roberts 1988; Zhou et al. 1996; Zhou and Robinson 1997; Matveev and Ballhaus 2002; Proenza et al. 2002; Zhou et al. 2005). However the discovery of some small podiform bodies in modern mid-ocean ridges (Arai and Matsukage 1996, 1998; Abe 2003) underlines the possible formation of podiform chromite not only in tectonic settings related to supra-subduction zones.

The Aburrá Ophiolite in the Central Cordillera of the Colombian Andes contains the only known occurrence of podiform-type chromitites recognized in Colombia. The chromite deposits are small (~20.000 tons of ore) and are associated with dunite. Most of them were exploited during the 1970's and 1980's for the glass and metallurgical industries. Mining activities were reactivated in the last years when small mines and quarries have been opened in the northern and southern bodies. Although these occurrences are of reduced economic importance, they are useful as a tool to understand their genesis and the evolution of the Aburrá Ophiolite. The aim of this paper is to present new field, petrographic, geochemical and the first Re-Os systematic data about the Aburrá Ophiolite chromitites and their host peridotites, discuss a possible mechanism for the formation of chromite pods, propose a paleotectonic setting for their formation and for the origin of the ophiolite.

3.2. Previous work

Mineral exploration activities for chromite in the Medellín area were carried out mainly in the southern sector during the 1970's, (Geominas 1975). Alvarez (1987) describes the mineral, textural and chemical composition of chromitite samples from two occurrences of the southern sector and identified cumulus textures that confirmed the ophiolitic nature of the ultramafic massif. The author also proposed that the chromitites and their host dunites formed

in the lower part of the transition zone of an ophiolite. The chromitites would be the product of magmatic accumulation in pockets or in narrow magmatic interconnected chambers that would lead basaltic magma to the overlying expanding crust. Monsalve (1996) describes a podiform chromite deposit located in the northern sector, evaluated its reserves and mentioned that it is associated to the transition zone of an ophiolite, and Quintero and Delgado (1998) concluded that these chromitites are appropriate for refractory use. Correa and Nilson (2003) proposed that the presence of chromitite and harzburgite indicates that the Aburrá Ophiolite formed within a supra-subduction zone environment. Mineral chemistry studies carried out on chromitites of the southern and northern sectors by Martinez et al. (2004) indicate that chromite from the chromitite and accessory spinels of the peridotites exhibit alteration evidence and that only the core of the chromitites still have primary composition useful as petrogenetic indicators. Proenza et al. (2004) suggest that the ophiolite was generated in a supra-subduction environment of a back arc zone and conclude that chromitites are PGE-depleted, which is typical of most of the Al-rich chromitites of ophiolite complexes, while dunites are PGE-rich and exploration target for such elements. Ortíz et al. (2004) report for the first time the occurrence of PGE in the Medellín dunite and provide some exploration guides for the detection of their minerals in this ophiolite.

3.3. Geological Setting

According to Restrepo and Toussaint (1988) the “Colombian West” extends from the Otú-Pericos Fault, to the east, to the western margin of the country (Fig. 1a). It consists of a mosaic of allochthonous terranes accreted to the South American Plate since the Upper Cretaceous until the Miocene (Toussaint and Restrepo 1989, 1994); almost all of oceanic affinity, except the Tahami Terrane. One part of the oceanic terranes consist of ophiolite fragments believed to be Triassic to Cretaceous in age (Restrepo and Toussaint 1973; Alvarez 1982; González 1980), whereas the other part are oceanic plateau and island arcs fragments of Cretaceous age (Kerr et al. 1997; Alvarez 1987b).

In contrast, the Tahami Terrane consists of schists, gneisses, migmatites, derived from continental sources, amphibolites and subordinated basic granulites that were grouped as the Central Cordillera Polymetamorphic Complex (Restrepo and Toussaint 1982). It exhibits evidence of several metamorphic events that occurred during the Devonian-Carboniferous and Permian-Triassic (Restrepo and Toussaint 1982; Ordóñez-Carmona 2001; Vinasco et al. 2006).

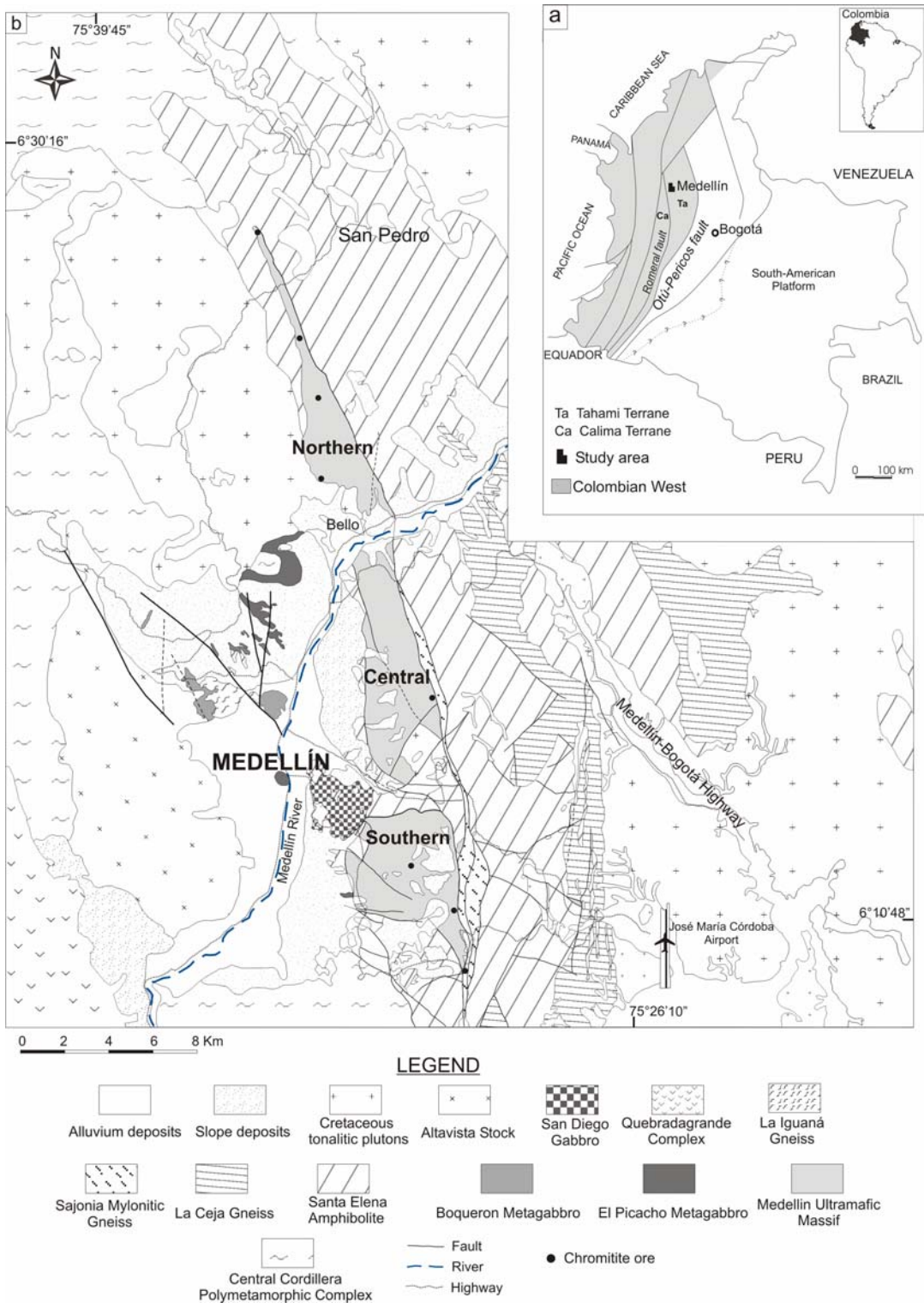


Fig. 1. (a) Geological sketch of the “Colombian West” showing the Tahami (Ta) and Calima (Ca) Terranes (Toussaint and Restrepo 1989; Ordóñez-Carmona 2001). (b) Geological map of the Medellín area showing the Medellín Ultramafic Massif separated in three sectors (Northern, Central and Southern Sectors). Chromite deposits are pointed out as black points. Modified from Botero (1963), Rendón (1999), Correa and Martens (2000), González (2001), Rodríguez et al. (2005).

The ophiolites in the Colombian Andes are exposed mainly in the western flank of the Central Cordillera, closely associated to the Romeral Fault System, and, to a lesser extent, within the axial zone of the cordillera northernmost part (Restrepo and Toussaint 1973; Alvarez 1985).

The Aburrá Ophiolite occurs in the northwestern sector of the Central Cordillera, to the east of the Romeral Fault System. It is located at the western border of the Tahami Terrane close to the limit with the oceanic Calima Terrane, and crops out in the city of Medellín and surrounding towns (Fig. 1). It contains parts of both the mantle and crustal section (Correa and Martens 2000, Correa et al. 2005).

The mantle section, informally known as Medellín Dunite (Restrepo and Toussaint 1984) or Medellín Ultramafic Massif (Correa et al. 2008) crops out in three ultramafic bodies locally named as Southern, Central and Northern Sectors (Fig. 1). The three bodies define a discontinuous 35 km long, 0.2 to 0.5 km wide, N10-20°W trending belt. The dominant rock is dunite with subordinate orthopyroxene-depleted harzburgite, harzburgite and podiform chromitite. The degree of serpentinization is variable. Only the basal peridotite, near the contact with amphibolite, is strongly deformed, probably related to the emplacement of the ophiolite. Dunite occurs as extensive bodies, also surrounding the chromitites, and as milimetric to centimetric bands within harzburgite. The last type is exposed in one outcrop in the southeastern portion of the study area, and is interpreted as a reaction zone that might have formed by melt/rock interaction within the Moho Transition Zone of the ophiolite. The mantle section of the ophiolite is of harzburgite-type and most of the ultramafic bodies outcropping in the area have been interpreted as the Moho Transition Zone of the ophiolite (Correa et al. 2008).

The plutonic section is made up of El Picacho and Boquerón Metagabbros, the later was previously known as Boquerón Amphibolite (Correa and Martens 2000). It consists of fairly layered and isotropic metagabbros respectively that occur as isolated blocks mainly in the northwestern sector of the city of Medellín and those of the El Picacho type also occur in the southeastern sector, close to the ultramafic rocks. These rocks present intense dislocation and hydrothermal metamorphism that modified the primary mineral assemblage, but without obliteration of the original igneous structures. The contact between the mafic and ultramafic rocks was not observed in outcrops.

The volcanic portion of the ophiolite is probably represented by the Santa Elena Amphibolite (Restrepo 2005) over which the ultramafic bodies lie in fault contact. Two metasedimentary units are associated with the amphibolite and comprise the La Ceja Gneiss

and the Sajonia mylonitic gneiss. The amphibolite was initially considered as part of the cordillera continental basement, but has been recently reinterpreted as a MORB oceanic crust (Correa and Martens 2000; Restrepo 2005; Pereira et al. 2006) of unknown age that probably belongs to the Aburrá Ophiolite.

The faulted contact between peridotite and amphibolite is characterized by chlorite and tremolite schists (Restrepo and Toussaint 1973; Alvarez 1982) and by a set of amphibolite, garnet amphibolite and mylonite gneiss that could be the metamorphic sole of the ophiolite (Correa et al. 2008b; Rodríguez et al. 2005). The time of formation and emplacement of the amphibolite have not been clearly constrained. Restrepo and Toussaint (1973) and Alvarez (1982) interpret the peridotite as Triassic or Jurassic and emplaced during the Cretaceous, while Restrepo (2003, 2005) and Pereira et al. (2006) consider the ophiolite as Devonian, Carboniferous or Permian and emplaced during the Permio-Triassic orogeny. We obtained a 217 ± 0.4 Ma U-Pb concordant age from a plagiogranite dyke in the metagabbro section, interpreted as the age of syn-oceanic deformation of the mafic crust, thus indicating that the minimum age for generation of the oceanic crust is Upper Triassic (Correa et al. 2008b), and Restrepo et al. (2007) report a 228 ± 0.9 Ma U-Pb age for a partially rodingitized gabbro pegmatite. On the other hand, the ophiolite is intruded by trondhjemites of the Jurassic La Iguaná Gneiss (Correa et al. 2005b) and by the rocks of the Cretaceous Antioquean Batholith (e.g., Ordóñez-Carmona and Pimentel 2001).

3.4. Field relationships

3.4.1 Chromite deposits

Chromite deposits in the Aburrá Ophiolite occur within all three peridotite bodies (Fig. 1), but only those of the Southern and Northern Sectors (Fig. 2 and 3) have been mined and studied to some extent. It occurs as pods, lenses and disseminated schlieren (Geominas 1975; Alvarez 1987; Monsalve 1996).

Chromite deposits of the Southern Sector

In the Southern Sector, Geominas (1975) identified 27 mineralized sites, 17 corresponding to outcrops and 10 to eluvial deposits (Fig. 2). The main features of the in situ chromitite deposits from the Southern Sector are summarized in Table 1. Three areas contain relevant chromite mineralization and comprise the Patio Bonito (P), El Carmelo (C) and El Chagualo (CH), among which Patio Bonito is the leading producing site. According to

Geominas (1975) most of the ore bodies are centimetric to metric pods, which are presumably fault controlled. The chromitite seams are steeply dipping towards the west.

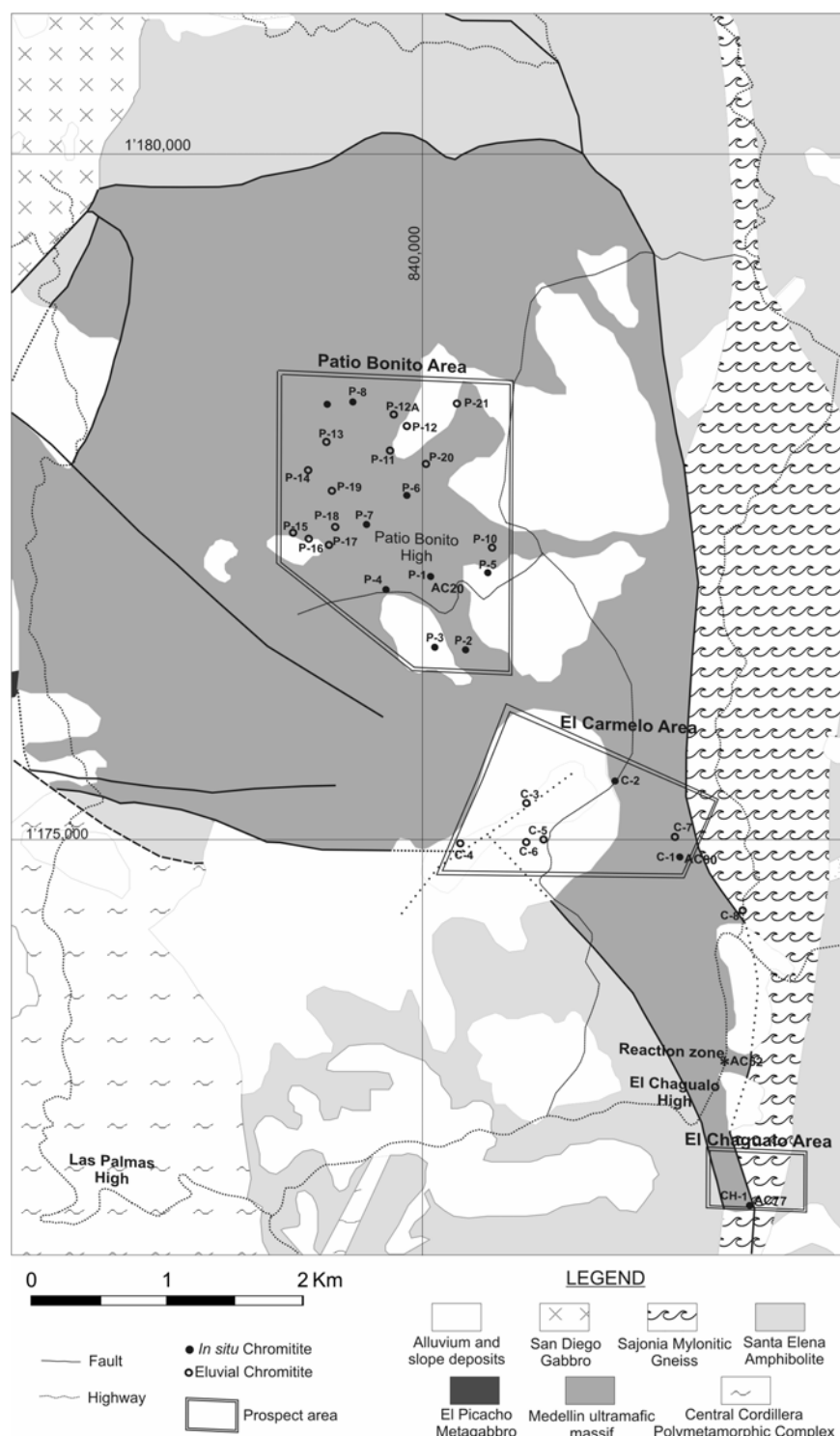


Fig. 2. Geologic map of the Southern Sector of the Medellín Ultramafic Massif, showing three areas with chromitite occurrences, the location of the reaction zone and sampling sites (AC20, AC52, AC77 and AC80). Modified after Geominas (1975), Rodríguez et al. (2005). P, C and CH stand for Geominas (1975) samples.

Most podiform chromitites bodies of this sector are lenses in sharp contact with the enclosing dunite and concordant to subconcordant with the foliation of the host peridotite. In the El Chagualo deposit, the chromite body is lense-shaped, extends fine satellite stringers into the wallrock (Geominas 1975), and appears to be discordant.

Table 1. Main characteristics of the *in situ* chromite deposits of the Aburrá Ophiolite. After Geominas (1975), Monsalve (1996) and this study.

	Southern Sector			Northern Sector	
Ocurrences/ Prospects	Pátio Bonito/ P-1 a P-9	El Carmelo/ C-1 e C-2	El Chagualo/ CH-1	Don Jaime/ Ja-1 e Ja-2	Don Jesus/ Je-1 a Je-4
Relative Importance	P-1 Great P-2 a P-9 medium and less	Great	Great	Medium	Medium
Bearing/Shape	P-1 fusiform body 15 x 3 m. N10°W/vertical P-2 a P-9: veins aprox. thickness 0.20m. P4: N15°E/80°W P7: N65°W/90	C-1: 3 fusiform bodies 5 x 0.40 m, N20°W/68W P-2 a P-9: veins aprox. thickness 0.20m. P4: N15°E/80°W P7: N65°W/90	CH-1 lensoid body with chromite stringers toward wallrock 3 x 1 a 3.5 m N45°W	Ja-1 Lensoid/ concordant 4 x 1 x 10m N5W/40-50E Other small occurrences, probably subconcordant	Je-1 Lensoid/ concordant 16 x 1.5 x 0.8-1.5 m N30W/35E Je-2 Stone line, pod-like 5x <1m Je-3 lensoid Je-4 lensoid/ concordant 20 x 4m N40W
Texture of chromitites	Massive, pseudoclastic, Disseminated	Massive fairly sheared, nodular	Nodular, disseminated, banded, chain- textured	Massive	Massive pseudoclastic, disseminated
Gangue /fracture filling minerals	Chlorite Uvarovite, carbonate, limonite, talc, tremolite	Chlorite Small faults filling by amphibole	Olivine, chlorite, serpentine, magnesite	Chlorite	Chlorite

Je-1: Betsabé Quarry, Je-2: Aníbal Quarry, Je-3: Reinaldo Quarry, Je-4: Ildebrando Quarry

Eluvial chromite deposits are scarce, small and proximal to the primary ores (Geominas 1975). Chromite pebbles, gravels and blocks also occur in stone lines, locally known as “chromite line”, lying between lateritized peridotite and a volcanic ash layer. Eluvial horizons have been an important chromite exploration guide in the region.

Chromite deposits of the Northern Sector

In the Northern Sector the podiform chromitite (Fig. 1 and 3) occurs in Niquía (C-Niq), Loma de Meneses (Je-Don Jesus deposit), Cerezales (Ja-Don Jaime deposit) and San Pedro (CSP).

The pods are lens-like or fuse-shaped. At the Don Jaime and Don Jesus deposits, the chromitites occur as concordant pods in sharp contact with sheared and strongly serpentinized dunite (Monsalve 1996; this study) (Fig. 4a). The main features of these deposits are shown in Table 1. The C-Niq and CSP chromitites are not well characterized structurally. The Don Jaime deposit has been partially mined, and according to Monsalve (1996) its reserves are as large as 90 metric tons. The Don Jesus deposit was investigated in this study. The ore bodies are currently mined in an artisanal manner in several sites, such as the Betsabé quarry, a pod-like body, the Aníbal quarry, which is exploited both from primary mineralization and a stone line, and the Reinaldo and Ildebrando quarries, both in primary mineralization.

Most of the orebodies are within highly sheared and fractured dunite (Geominas 1975; Monsalve 1996; this work). At the Patio Bonito deposit, the dunite is intensely fractured and serpentinized, and at the Betsabé quarry the chromite body is in sharp contact with a 1.2 m thick sheared dunite envelope, which in turn is in sharp contact with a harzburgite. During our field investigations in the El Carmelo and El Chagualo deposits, the enveloping dunite was not found; Geominas (1975) describes them as strongly chloritized.

3.4.2 The reaction zone peridotites

These peridotites occur in the southernmost part of the Southern Sector, in an outcrop between El Carmelo and El Chagualo deposits (Fig. 2), closer to the last one. The outcrop consists of alternating, 0.5 cm to 1.0 m thick bands of dunite and harzburgite (Fig. 4b), in grading contacts given by the decrease in orthopyroxene content from harzburgite to dunite. Some of the dunites contain narrow, discontinuous bands of chromite. These banded rocks are similar to those described by Braun and Kelemen (2002) from the Oman Ophiolite and by Zhou et al. (2005) from the Luobusa Ophiolite (Tibet), which have been interpreted as evidence of melt-rock interaction.

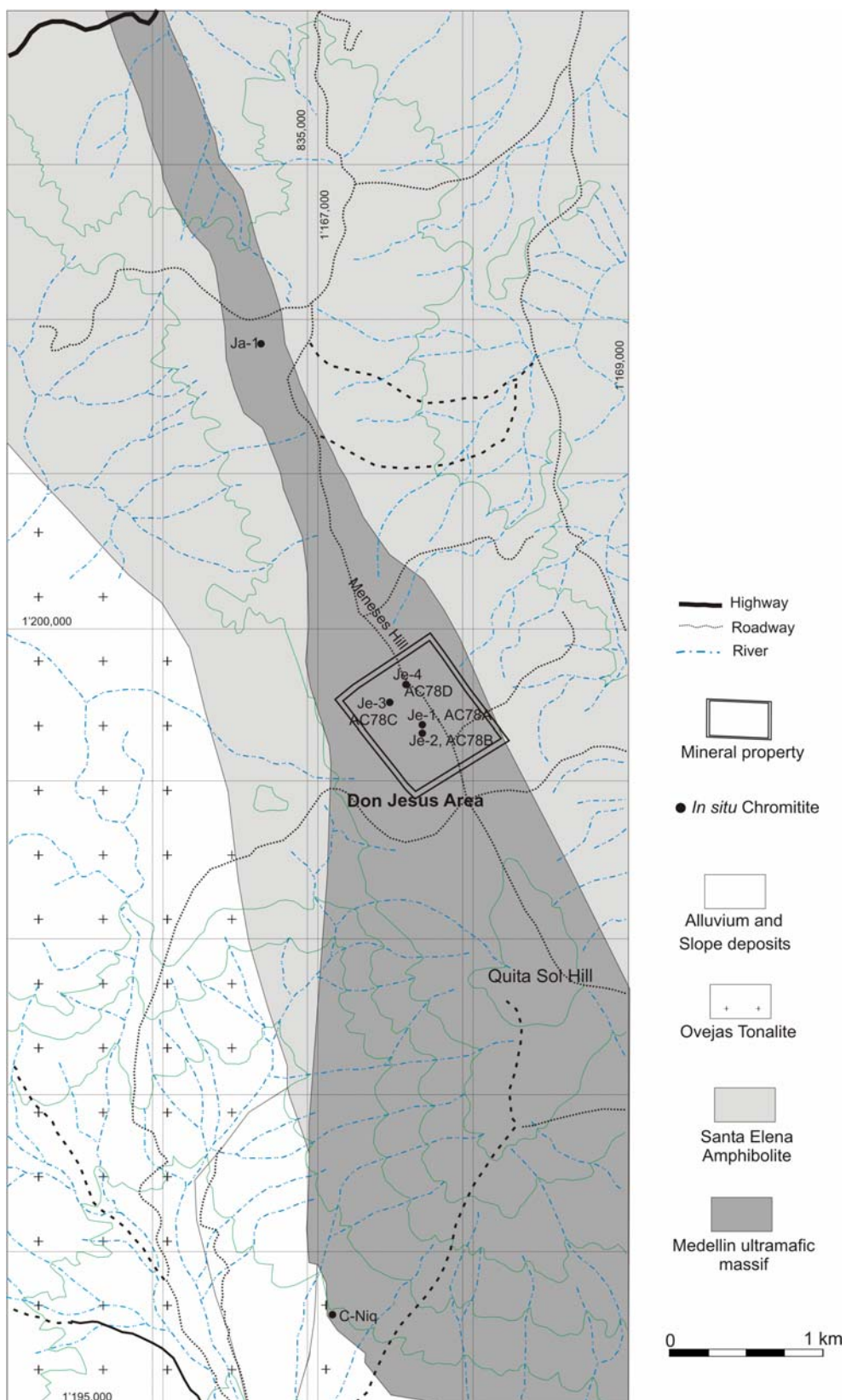


Fig. 3. Geologic map of the Northern ultramafic body. Locations of main occurrences of chromitites and some studied samples (AC78A to AC78D, C-Niq).

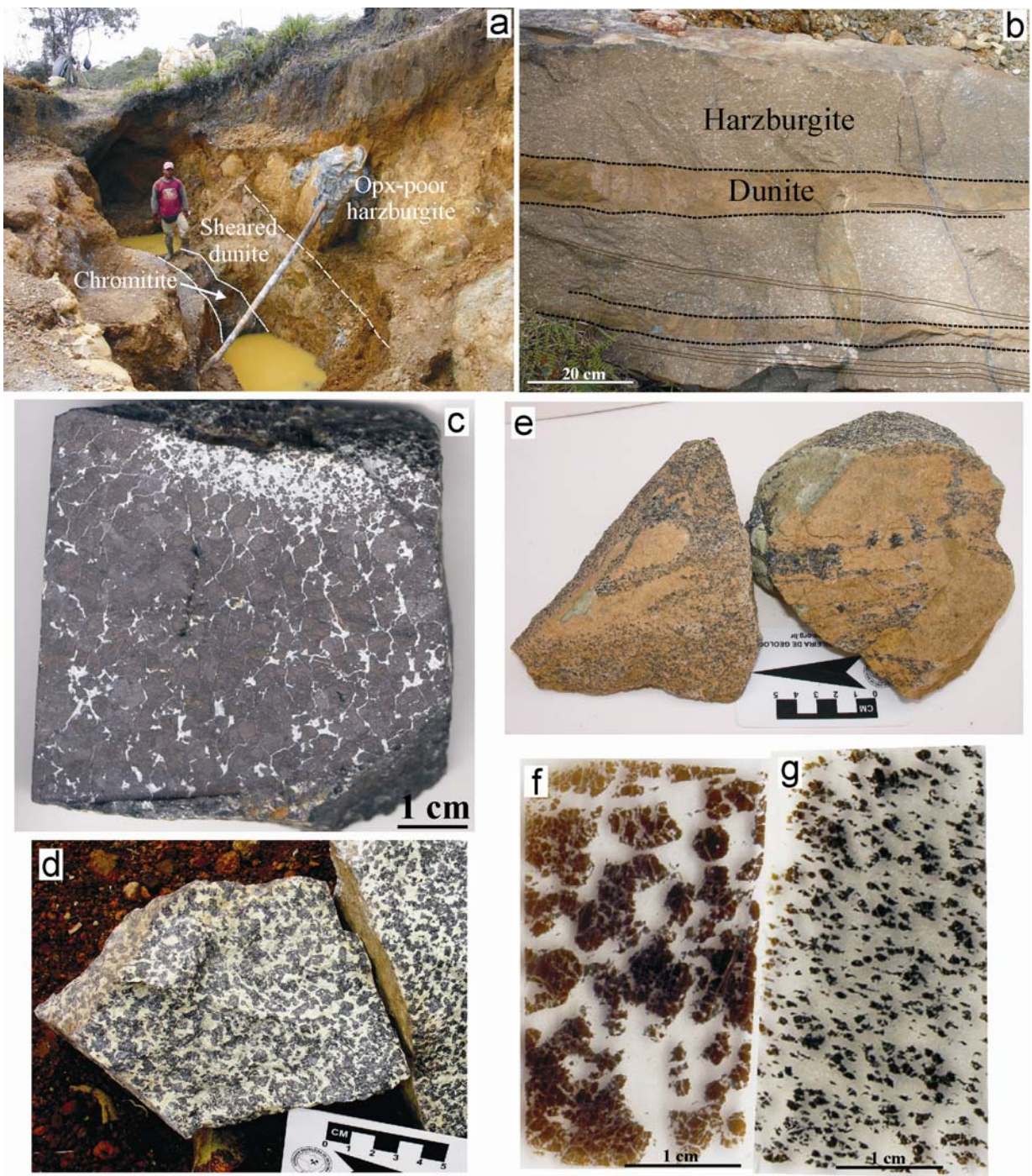


Fig. 4. Field and hand specimen photographs. (a) Chromitite body with envelope of sheared dunite surrounded by opx-depleted harzburgite of the Don Jesus deposit. (b) Dunite bands within harzburgite in a reaction zone. (c) Massive chromitite with clot of disseminated chromitite of the Pátio Bonito deposit. (d) Coarse-grained disseminated chromitite. (e) Fine-grained disseminated chromitite. (f) Nodular chromitite. (g) Chain chromitite. (d) to (g) are from samples of the El Chagualo deposit.

3.5. Samples and analytical methods

Representative samples (15) of chromitites and host peridotites were selected for mineral chemistry studies from the Pátio Bonito, El Chagualo, El Carmelo, San Pedro, Niquía and Don Jesus deposits. All samples were studied under transmitted and reflected light microscope.

Four samples were also selected for Re/Os isotopic studies. They were: two samples, one of harzburgite and one of dunite from the reaction zone, and two chromite concentrates from chromitites, one massive from the Patio Bonito and another coarse-grained disseminated chromitite from El Chagualo deposit.

3.5.1. Mineral chemistry

Mineral electron microprobe analyses were carried out at the Geosciences Institutes of the Universities of Brasília, São Paulo and Montpellier. At the University of Brasília, analyses were performed using a CAMECA SX-50 microprobe operating at 15 kV accelerating voltage and 20 nA sample current. The beam size varied between 2 and 5 µm and the counting time 10 s. At the University of São Paulo, the mineral analyses were obtained with a JEOL JXA-8600 Superprobe, using an accelerating voltage of 15 kV, a beam current of 20 nA, and counting time of 10 s for major elements and 50 s for trace elements. The beam size was of 1 µm for oxides analyses and of 5 µm for silicate analyses. At the Laboratoire de Tectonophysique (Université Montpellier II, France) the data were obtained using a CAMECA SX-100 microprobe operating at 20 kV, 10 nA, beam size of 1-5 µm and counting time between 10 and 50 s. In all cases natural and synthetic standards were used.

The samples analyzed in Brasilia were AC20A, AC20F, AC20I, AC20L, C-Niq and CSP. The samples analyzed in São Paulo were AC77A, AC77B, AC77C, AC78B, AC80B1 and AC80B2. The samples analyzed in Montpellier were AC20M, AC20L and AC78C1.

Fe^{3+} content of spinel was calculated according to the charge balance equation of Droop (1987). Representative mineral compositions are shown in Tables 2 to 5.

3.5.2. Re-Os method

The preliminary preparation for Re-Os analyses was performed at the Universidade Federal do Rio Grande do Sul (Brazil). The whole-rock samples were reduced to <200 mesh powders using ceramic crucible. Chromite concentrates were obtained in a four-stage process. First, the chromitite samples were crushed by hand using ceramic tools, to a diameter when most of the grains were free of silicate. The clean grains were then washed with deionized

water, dried and magnetically separated first by hand and then in an Isodynamic Frantz separator. Further purification was obtained by hand-picking under a binocular microscope. The pure chromite concentrate was then comminuted to less than 200 mesh in a ceramic pestle.

Re-Os analytical procedures

The Re-Os analyses were carried out at the Department of Terrestrial Magnetism of the Carnegie Institution of Washington, USA, following the procedures described by Carlson et al. (1999). A weighed amount of sample powder was added to a Pyrex Carius tube (Shirey and Walker 1995) kept at low temperature in a dry-ice-methanol slurry, and mixed with a weighed quantity of mixed ^{185}Re - ^{190}Os tracer solution, followed by acid dissolution with 2 ml concentrated HCl and 4 ml concentrated HNO₃. After freezing of the mixture, the Carius tube was sealed, allowed to slowly warm up to room temperature, followed by placing it into a steel explosion shield and heated in an oven to 240° C for 48 hours. All chromite samples were completely dissolved and produced a clear deep green solution. After cooling to room temperature, the Carius tubes were again frozen in dry-ice-methanol and their tops cracked open. The frozen solutions were then transferred to 50 ml centrifuge tubes and added with 3 ml of CCl₄. Oxidized OsO₄ was extracted 3 times into CCl₄ (a total of 9 ml CCl₄). With each step, the CCl₄ solution was removed with a pipette and added to a teflon beaker containing 4 ml concentrated HBr to reduce the OsO₄ to a non-volatile dissolved in the HBr. After 1 hour, the CCl₄ was pipetted and discarded and the HBr dried under a heat lamp. The Os was further purified by microdistillation (Roy-Barman and Allègre 1994) and dried. The dry Os sample was dissolved in 30 microliters of a 12N H₂SO₄ and CrO₃ mixture, transferred to the cap of 7 ml teflon conical beaker to which 20 microliters of concentrated HBr was placed to its bottom. The inverted beaker was placed on a hot plate at 80° C for 2 hours to distil the oxidized Os into the HBr. The HBr solution was evaporated to dryness under heat lamp and then loaded to Pt filaments. Twenty micrograms of BaNO₃ was added to the filament that was loaded into the mass spectrometer.

Re remained in the aqua-regia solution, which was transferred to a 15 ml beaker and dried under heat lamp. The dry sample was dissolved in 10 ml 1N HCl, centrifuged and loaded on an anion exchange column. Re was retained on the column while the rest of the sample eluted in 1N HCl followed by 0.8N HNO₃. Re was then eluted with 4N HNO₃. This solution was dried under heat lamp, dissolved in 0.1N HNO₃ and placed onto a small anion column. After eluting 0.1N HNO₃, the Re was eluted with 8N HNO₃. This solution was dried

under heat lamp, dissolved in a solution containing 20 micrograms of BaNO₃, loaded onto Pt filaments which were placed in the mass spectrometer.

OsO₃-and ReO₄- mass spectrometry data were obtained in a Finnigan™ Triton thermal ionization mass spectrometer, using Faraday cups. Concentration uncertainties for whole rock Re-Os analyses generally range from 1-5% because of inhomogeneous distribution of the trace phases containing these elements. Re/Os ratios in standard solutions can be determined to a precision of 0.1%. Blanks for Re and Os were both 1 ± 0.5 picograms. Os blank corrections were insignificant for all samples. Re interference in Os was corrected for both chromite separated samples using a determined ¹⁸⁷Re/¹⁸⁵Re ratio (=0.15 to 0.17).

3.6. Petrography

3.6.1. Chromitites

Massive and disseminated chromitites are the most common types in the studied deposits (Geominas 1975; Alvarez 1987; Monsalve 1996) (Fig. 4 c), but in the El Chagualo deposit additional structures occur as foliation and pull-apart fractures, which are produced by relatively high temperature deformation. Primary silicates in the matrix of the chromitites are preserved only in the samples of the El Chagualo area.

Massive chromitites consist of more than 80 vol % anhedral, mostly 2-7 mm, seldom corroded chromite. The chromite grains interstices and fractures are filled with chlorite. Some chromitites have pseudoclastic texture, in the sense of Ahmed (1984), and probably correspond to samples with deformed occluded silicate texture. Individual chromite grains have a dark-gray, smooth or fractured core and light-gray, corroded rims of ferrichromite in contact with chlorite. The alteration of chromite into ferrichromite is more evident in pseudoclastic and disseminated chromitites of the Patio Bonito deposit.

Solid inclusions of olivine, serpentine (former olivine) and Fe-Ni sulphides occur in few chromite grains. Fluid inclusions are present in many chromite grains in samples from the Pátio Bonito, Niquía, San Pedro and Don Jesus deposits. The inclusions occur mainly in trails that are likely secondary, and as scarce isolated probably primary, and some are two-phase and three-phase inclusions. Tiny exsolutions needles of probably rutile or ilmenite are present in some of the grains. Rare hematite and sulfide grains occur either in the interstices of the chromite grains or within chlorite of the fractures.

Disseminated chromitites contain 20-80 vol % of chromite grains scattered in a chlorite matrix, and are in general smaller (<1mm) than those in the massive chromitites. The

disseminated type usually occurs as clots within massive chromitites (Fig. 4c), or as part of silicate-rich layers, locally grading into massive chromitite, or as individual horizons.

All samples from the El Chagualo deposit differ from the other deposits by containing preserved olivine and coarse- and fine-grained, disseminated, chain-textured, banded and folded chromite. Coarse-grained disseminated variety consists of polygonal and nearly spherical chromite grains in an olivine-rich matrix (Fig. 4d). Some portions of samples display a nodular texture (Fig. 4f), locally known as “leopard” chromite (Geominas 1975), that resembles the dismembered nodular chromitite described by Nicolas (1989). The chromite grains are 2-8 mm in size and mainly unaltered. Olivine grains are in the average 1.25 mm and partially serpentinized. Chlorite and serpentine are hydrothermal alteration products and surround the chromite grains. The fine-grained disseminated variety also differs from the other deposits because chromite is scattered in a matrix of well preserved olivine (Fig. 4e). Slightly banded varieties consist of discontinuous, locally folded, alternating chromite-rich and olivine-rich bands within dunite. In the disseminated portions, anhedral, chromite grains are 1.5 mm in diameter and have concave borders that enclose less than 1.0 mm olivine grains suggesting a chain texture (Fig. 4g). Chlorite occurs in the contact between chromite and olivine grains. The chromite grains of the El Chagualo deposit are less altered than those of the other chromitite deposits.

3.6.2. Surrounding peridotites

The dunite envelope of some chromite deposits was not observed due to the large rubble tailings of exploitation activity, or to the dense vegetation and deep weathering of the mined areas or removal during mining activities in the past. Thus, the herein described peridotites are from samples collected near the ore bodies.

Dunites are composed of 3 x 5 mm elongated olivine crystals parallel to the spinel crystals. Many of the olivine grains exhibit kink-bands and undulose extinction. Accessory chromite is subhedral to euhedral, and in the El Carmelo deposit it ranges from less than 1 vol % up to 10 vol %. In some samples it is elongated and always surrounded by a chlorite halo. In the Patio Bonito deposit, the peridotite is completely serpentinized and contains tremolite, disseminated magnetite, tiny grains of native copper and veinlets of carbonate. In most samples, chromite is porous, whereas in the Patio Bonito area it has a smooth surface.

Orthopyroxene depleted harzburgites surrounding the dunites have a porphyroclastic texture and contain olivine, bastite and talc pseudomorphs after orthopyroxene (5 vol %), spinel and tremolite.

3.6.3. Reaction zone

The harzburgite of the reaction zones have a porphyroclastic texture and consist of olivine (80-90 %), bastite, talc and tremolite as pseudomorphs after orthopyroxene (10-20 %), spinel (<1%) and traces of sulfides. Foliation is due to flattened and oriented chromite. Olivine is 1 to 5 mm with wavy extinction and subgrain boundaries. The original shape of the orthopyroxene seems porphyroclastic (2.5 x 4.5 mm) to anhedral. Spinel is 0.5 x 1.0 mm, holly-leaf to anhedral and surrounded with chlorite. Locally the harzburgite grades into Opx-depleted harzburgite and dunite with decreasing quantity of pyroxene.

The dunites are medium to coarse-grained and consist of olivine (98-99%), less flattened and coarser (3mm x 3.75 mm) than that of the adjacent harzburgite, spinel (1-2%), and less than 2% of secondary talc, tremolite and chlorite. The dunites are in general richer in sulfides than the adjacent harzburgites. The sulfide grains vary from anhedral (0.075 x 0.25 mm) to euhedral (0.25 x 0.35 mm).The spinel grains are usually subhedral to euhedral (0.9 mm x 0.85 mm) and have a chlorite halo. Dunites and harzburgites are variably serpentinized.

Some petrographic features suggest interaction between harzburgite and percolating melts. The observed grading from harzburgite to orthopyroxene-depleted harzburgite-dunite indicates that the harzburgites were percolated by melts which partially dissolved the orthopyroxene (opx-depleted harzburgite) or may have promoted its entire removal to produce dunite. Such process may also explain the idiomorphism of chromian spinel in dunite, which could be produced by reaction between a preexisting spinel and a percolating magma (Leblanc et al. 1980; Matsumoto and Arai 2001).

3.7. Mineral chemistry

3.7.1 Chromitites

Ore composition

Most chromite grains are compositionally homogeneous, with no significant difference between cores and rims, except in fine altered rims and along fractures of some pseudoclastic chromitites from the Patio Bonito deposit.

The Cr# [Cr/(Cr+Al)] vs Mg# [Mg/(Mg+Fe²⁺)] diagram (Fig. 5a) clearly shows that the Aburrá chromite lies within the field of ophiolitic chromitites. Although all samples are Al-rich, the Cr# (<60) allows to distinguish three groups.

Group 1 comprises the chromite samples from the Patio Bonito and Niquía deposits. Its Cr# varies between 0.50 and 0.53 and the Mg# from 0.70 to 0.74. There is no significant compositional difference between the coarse-grained chromite from the massive portions and

the fine-grained chromite from disseminated portions. TiO_2 contents are generally less than 0.23 wt%, except for the sample from the Niquía deposit, where TiO_2 lies between 0.25 and 0.30 wt%. The Fe_2O_3 content ranges between 1.53 and 2.98 wt%, MnO between 0.19 and 0.49 wt%, ZnO is in general less than <0.13%, except for one analysis of Niquía that yield 0.23 wt%, and the NiO contents are less than 0.31 wt%. No significant compositional variations of chromite have been detected within a single deposit.

Group 2 includes the chromite samples from the San Pedro, Don Jesus and El Carmelo deposits. The Cr# of samples of this group varies between 0.40 and 0.50 (0.42 to 0.49), the Mg# ranges from 0.72 to 0.78. TiO_2 contents are generally less than 0.12 wt % in San Pedro Deposit and less than 0.29 in the El Carmelo and Don Jesus deposits. The Fe_2O_3 contents ranges between 1.13 and 2.14 wt%, MnO between 0.03 and 0.34 wt%, ZnO is in general less than 0.13%, and NiO is less than 0.28 wt%.

Group 3 consists of the chromite samples from the El Chagualo deposit. There are slight variations in the composition of chromite from coarse-grained disseminated to the chain-textured samples. The Cr# is less than 0.40 in both types, with 0.37-0.38 in the coarse-grained chromite, and 0.34-0.36 in the chain chromite. The Mg# in the coarse-grained disseminated chromitite varies from 0.73 to 0.75, TiO_2 is less than 0.12 wt%, Fe_2O_3 ranges between 1.67 and 2.33 wt%, MnO is less than 0.13 wt%, ZnO is less than 0.10%, and the NiO less than 0.23 wt%. The Mg# in the chain-textured chromitite lies between 0.70 and 071, TiO_2 is less than 0.21 wt%, Fe_2O_3 ranges between 2.71 and 3.41 wt%, MnO is less than 0.12 wt%, ZnO less than <0.16%, and NiO less than 0.19 wt%.

In the Cr# vs TiO_2 diagram (Fig. 5b) the samples plot in different fields and their distribution does not agree with the above described groups. All samples from Niquía and Don Jesus deposits lie in the MORB field, and those from the Patio Bonito and San Pedro deposits plot in the field of the Al-rich chromitites of the Ságua de Táamo district of Cuba. The El Carmelo and El Chagualo chromite compositions plot outside any field of the diagram, except two samples from each deposit which lie in the MORB field.

In some pseudoclastic chromitites of the Patio Bonito deposit, the chromite grains with wide altered rims, the core has primary chromite whilst the altered rims are richer in Cr and Fe^{2+} and depleted in Al and Mg (Fig. 5c). This is attributed to re-equilibration during hydrothermal alteration and formation of chlorite.

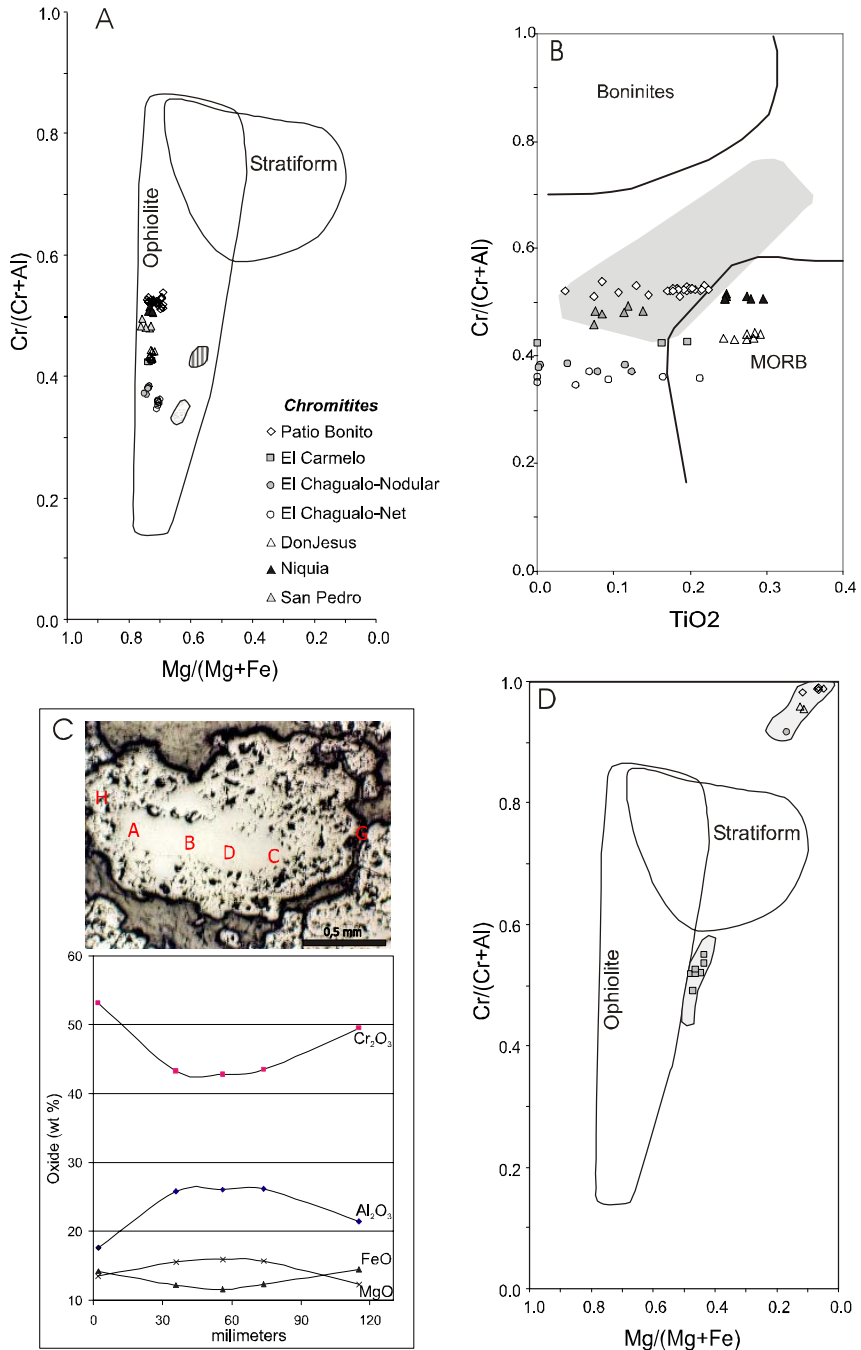


Fig. 5. Variation diagrams for composition of chromite from the Aburrá chromitites and hot peridotite. (a) Cr#[Cr/(Cr+Al)] versus Mg#[Mg/(Mg+Fe)] for primary spinel of chromitites. The ophiolite and stratiform fields are from Leblanc and Nicolas (1992). Field with dots: composition of spinel in mantle harzburgite; field with lines: composition of spinel in dunite. (b) Cr-number versus TiO₂ variations seen in chromite of chromitites with respect to some tectonic settings. Boninites and MORB fields are from Arai (1992); grey field: chromites of Sagua de Tánamo (Cuba) after Proenza et al. (1999). (c) Photomicrograph of a zoned chromite grain with altered borders from pseudoclastic chromitite and profile of compositional data across the grain. (d) Cr#[Cr/(Cr+Al)] versus Mg#[Mg/(Mg+Fe)] for altered accessory spinel of the host peridotites.

Table 2. Representative analyses (wt %) of primary chromites from chromitites of the Aburrá Ophiolite.

Sector Deposit	South								North		
	Patio Bonito				El Carmelo		El Chagualo		Don Jesús	Niquía	San Pedro
Sample	AC20F4B Massive	AC20L1C Massive	AC20M-2 Coarse Mas	AC20M-1 Fine Dis	AC20I4C Pseud.	AC80B1 Massive	AC77A1C Coarse Dis	AC77C7B Fine Dis	AC78C1 Massive	NIQUIA3D Massive	CSP2D Massive
SiO ₂	0.00	0.00	0.08	0.08	0.00	0.04	0.01	0.00	0.07	0.03	0.00
TiO ₂	0.21	0.19	0.20	0.18	0.21	0.00	0.04	0.05	0.27	0.25	0.11
Al ₂ O ₃	26.31	27.11	26.51	26.77	26.31	33.05	36.31	37.47	32.77	27.52	29.13
Cr ₂ O ₃	42.95	42.26	43.84	43.11	42.31	36.15	33.74	29.47	36.73	41.69	39.98
V ₂ O ₃	0.13	0.17			0.26					0.23	0.24
Fe ₂ O ₃	2.97	1.90	1.53	1.62	2.98	1.86	1.67	3.52	1.39	1.73	2.18
FeO	10.37	12.07	10.38	11.48	10.55	10.90	11.22	12.11	11.44	10.94	10.01
MgO	16.58	15.45	16.79	16.06	16.43	16.95	17.25	16.56	16.79	16.30	16.85
MnO	0.44	0.49	0.21	0.24	0.36	0.03	0.12	0.12	0.18	0.42	0.34
ZnO	0.07	0.09			0.12	0.03	0.10	0.14		0.00	0.14
CaO	0.00	0.01	0.00	0.00	0.00	0.00	0.00	0.00	0.01	0.00	0.00
NiO	0.20	0.15	0.13	0.13	0.10	0.14	0.21	0.19	0.20	0.06	0.21
Total	100.22	99.88	99.67	99.66	99.63	99.15	100.66	99.63	99.85	99.16	99.18
Si	0.000	0.000	0.018	0.018	0.001	0.009	0.002	0.000	0.017	0.007	0.000
Al	7.338	7.609	7.406	7.503	7.381	9.030	9.672	10.064	8.921	7.714	8.089
Ti	0.037	0.033	0.036	0.032	0.038	0.000	0.007	0.009	0.048	0.044	0.020
Cr	8.035	7.956	8.212	8.105	7.962	6.626	6.027	5.309	6.707	7.838	7.445
Fe ³⁺	0.529	0.341	0.273	0.291	0.533	0.324	0.283	0.604	0.242	0.310	0.387
V	0.020	0.026			0.041					0.036	0.037
Mg	5.851	5.485	5.931	5.696	5.832	5.860	5.812	5.626	5.783	5.780	5.918
Fe ²⁺	2.053	2.403	2.058	2.283	2.099	2.113	2.120	2.308	2.209	2.176	1.973
Zn	0.013	0.017			0.021	0.005	0.017	0.023		0.000	0.023
Mn	0.087	0.099	0.043	0.048	0.073	0.005	0.023	0.022	0.035	0.084	0.068
Ca	0.000	0.002	0.000	0.000	0.000	0.000	0.000	0.000	0.002	0.001	0.000
Ni	0.037	0.029	0.024	0.025	0.019	0.026	0.038	0.034	0.036	0.011	0.040
Mg#	0.74	0.70	0.74	0.71	0.74	0.74	0.73	0.71	0.72	0.73	0.75
Cr#	0.52	0.51	0.53	0.52	0.52	0.42	0.38	0.35	0.43	0.50	0.48
Fe ³⁺ #	0.03	0.02	0.02	0.02	0.03	0.02	0.02	0.04	0.02	0.02	0.02

Cation proportion on the basis of 32 oxygens. Mg# = Mg/(Mg+Fe²⁺); Cr# = Cr/(Cr+Al).

Table 3. Representative analyses (wt %) of altered spinels. Profile of a chromite grain in chromitite AC20I showing chemical changes from fresh core to altered rim, and composition of altered accessory spinel in hosting peridotites.

Sample	Chromite from chromitite							Acc. spinel from peridotite		
	AC20I1B	AC20I1C	AC20I1D	AC20I1E	AC20I1F	AC20I1G	AC20I1H	AC20A1B	AC80B21C	AC78BE4B
SiO ₂	0.04	0.02	0.03	0.00	0.07	0.04	0.01	0.00	0.05	0.04
TiO ₂	0.20	0.22	0.18	0.22	0.18	0.06	0.04	0.35	0.28	0.77
Al ₂ O ₃	26.13	25.79	26.08	26.25	26.29	17.60	21.47	0.19	22.27	1.52
Cr ₂ O ₃	43.53	43.22	42.79	42.75	43.86	53.15	49.54	24.86	35.86	52.26
V ₂ O ₃	0.22	0.15	0.16	0.17	0.20	0.27	0.18	0.13		
Fe ₂ O ₃	2.06	2.65	2.90	0.00	0.21	1.37	0.00	37.23	10.71	12.75
FeO	11.99	11.96	11.33	12.28	13.73	13.81	14.42	34.36	20.91	28.47
MgO	15.63	15.50	15.91	14.19	14.28	13.48	12.31	1.51	9.52	2.35
MnO	0.41	0.44	0.43	0.35	0.51	0.51	0.41	0.57	0.21	0.54
ZnO	0.00	0.07	0.11	0.07	0.04	0.04	0.18	0.31	0.36	0.61
CaO	0.00	0.00	0.00	0.01	0.00	0.02	0.01	0.03	0.01	0.01
NiO	0.20	0.21	0.17	0.14	0.20	0.03	0.09	0.59	0.15	0.08
Total	100.40	100.24	100.10	96.43	99.56	100.36	98.65	100.13	100.33	99.39
Si	0.009	0.004	0.007	0.000	0.016	0.010	0.003	0.000	0.012	0.012
Al	7.324	7.255	7.318	7.663	7.471	5.174	6.354	0.066	6.620	0.526
Ti	0.035	0.039	0.033	0.041	0.033	0.011	0.008	0.079	0.052	0.170
Cr	8.184	8.154	8.053	8.370	8.360	10.482	9.831	5.863	7.148	12.150
Fe ³⁺	0.369	0.476	0.520	0.000	0.038	0.257	0.000	8.360	2.033	2.822
V	0.034	0.024	0.025	0.028	0.032	0.045	0.029	0.025	0.000	0.000
Mg	5.541	5.517	5.649	5.240	5.132	5.013	4.609	0.671	3.578	1.028
Fe ²⁺	2.384	2.388	2.257	2.542	2.769	2.881	3.027	8.573	4.410	7.001
Zn	0.000	0.013	0.019	0.013	0.006	0.007	0.033	0.068	0.068	0.132
Mn	0.083	0.089	0.087	0.073	0.103	0.108	0.087	0.145	0.044	0.135
Ca	0.000	0.000	0.000	0.002	0.000	0.006	0.002	0.009	0.004	0.004
Ni	0.037	0.041	0.033	0.028	0.039	0.006	0.017	0.141	0.031	0.019
Mg#	0.70	0.70	0.71	0.67	0.65	0.64	0.60	0.07	0.45	0.13
Cr#	0.53	0.53	0.52	0.52	0.53	0.67	0.61	0.99	0.52	0.96
Fe ³⁺ #	0.02	0.03	0.03	0.00	0.00	0.02	0.00	0.59	0.13	0.18

Cation proportion on the basis of 32 oxygens. Mg# = Mg/(Mg+Fe²⁺); Cr# = Cr/(Cr+Al).

Table 4. Representative analyses (wt %) of olivine from chromitites and host peridotites.

Samle	Olivine from chromitite			Olivine from host peridotite			
	AC77A0I3B	AC77COI6A	AC20M3ISa	AC20A5B	AC80B2OI1CB	AC77BOI1cA	AC78BOI4B
SiO ₂	41.61	41.16	40.31	41.35	39.80	40.56	40.56
TiO ₂	0.00	0.00	0.01	0.00	0.02	0.12	0.04
Al ₂ O ₃	0.00	0.001	0.25	0.00	0.00	0.00	0.02
Cr ₂ O ₃	0.00	0.05	0.94	0.00	0.00	0.01	0.02
FeO	4.84	5.87	2.67	9.42	8.69	8.92	9.26
MnO	0.09	0.09	0.05	0.14	0.11	0.10	0.12
MgO	53.01	52.55	55.19	49.22	51.22	49.90	49.74
CaO	0.00	0.00	0.01	0.02	0.03	0.00	0.02
NiO	0.38	0.47	0.91	0.44	0.42	0.40	0.22
Total	99.93	100.18	100.33	100.57	100.28	100.00	99.99
Si	1.000	0.994	0.967	1.006	0.975	0.994	0.994
Ti	0.000	0.000	0.000	0.000	0.000	0.002	0.001
Al	0.000	0.000	0.007	0.000	0.000	0.000	0.000
Cr	0.000	0.001	0.018	0.000	0.000	0.000	0.000
Fe	0.097	0.118	0.054	0.192	0.178	0.183	0.190
Mn	0.002	0.002	0.001	0.003	0.002	0.002	0.002
Mg	1.900	1.891	1.973	1.784	1.869	1.822	1.817
Ca	0.000	0.000	0.000	0.000	0.001	0.000	0.000
Ni	0.007	0.009	0.018	0.009	0.008	0.008	0.004
Mg/(Mg+Fe*)	0.951	0.941	0.974	0.903	0.913	0.909	0.905
Fo	95.03	94.02	97.31	90.17	91.20	90.79	90.43

Cation proportions on the basis of 4 oxygens.

Associated silicates

The composition of olivine in nodular chromitite varies from Fo94.9 to Fo95.2 and the NiO content ranges between 0.35 and 0.42 wt%, whilst in that of chain chromitite varies from Fo93.9 to Fo94.5 and the NiO from 0.40 to 0.47 wt%. The Fo and NiO content in olivine included in chromite is Fo97.3 and 0.91 wt%, respectively (Table 4).

Chlorite interstitial to chromite has SiO₂ contents between 28.03 and 30.70 wt % and Fe/(Fe+Mg) ratio below 0.04. Most of the chlorite has the composition of clinochlore, but sheridanite also occurs. One chlorite inclusion in chromite has SiO₂ content of 37.09 wt % and Fe/(Fe+Mg) ratio of 0.05, corresponding to penninite.

Table 5. Representative analyses of chlorite from chromitites and host peridotites.

Sample	Chromitites			Host peridotite
	AC20M2	AC80B1	AC77C	AC80B2
SiO ₂	30.91	28.37	37.09	30.09
TiO ₂	0.03	0.07	0.28	0.00
Al ₂ O ₃	20.89	20.93	19.41	17.61
Cr ₂ O ₃	2.12	1.53	1.60	0.63
FeO	1.32	1.15	2.11	2.73
MgO	31.67	31.70	24.60	32.78
MnO	0.02	0.00	0.02	0.02
NiO	0.00	0.00	0.00	0.00
CaO	0.01	0.00	0.04	0.02
Na ₂ O	0.02	0.00	0.00	0.02
K ₂ O	0.00	0.01	0.00	0.02
F	0.00	0.02	0.00	0.05
Cl	0.00	0.01	0.00	0.00
H ₂ O	12.81	12.31	12.78	12.25
Total	99.79	96.09	97.93	96.22
Si	5.783	5.519	6.956	5.877
Al	4.606	4.799	4.290	4.054
Ti	0.005	0.010	0.039	0.000
Mg	8.833	9.194	6.876	9.545
Fe ²⁺	0.206	0.187	0.331	0.447
Ni	0.000	0.000	0.000	0.000
Mn	0.003	0.000	0.003	0.003
Ca	0.001	0.000	0.008	0.005
Na	0.006	0.000	0.000	0.006
K	0.000	0.002	0.000	0.005
OH	16.000	15.985	16.000	15.971
F	0.000	0.010	0.000	0.029
Cl	0.000	0.005	0.000	0.000

Cations calculated on the basis of 28 oxygens.

3.7.2. Surrounding peridotites

Accessory chromite from the peridotites plots outside of the ophiolitic chromite field (Fig. 5d), indicating that it does not preserve a primary composition, but underwent alteration to chromian magnetite with Cr# of 0.98 and Mg# of 0.05 to 0.1 (Table 3).

The Fo and NiO contents of olivine from most of these peridotites are 90.0-91.5 and 0.37-0.48 wt%, respectively, except for a opx-depleted harzburgite, where the NiO content is between 0.18 and 0.25 wt % (Table 4). Chlorite has SiO₂ content between 30.09 and 31.34 and Fe/(Fe+Mg) below 0.05, which classifies it as clinochlore.

3.7.3. Reaction zone

The mineral chemistry data of these rocks are presented in a paper by Correa et al. (2008) and only the main compositional characteristics of rocks from the reaction zone are given below.

Olivine from the dunite bands are richer in Fo (90.15-90.88) than that of the harzburgite portions (Fo=89.53-90.02), whereas the NiO content is slightly higher in the harzburgites (0.36-0.45 wt%, with most values between 0.37 and 0.39) than those in the dunites (0.31-0.40 wt%, most close to 0.36%). Chromite from the dunite has Cr# ranging from 0.42 to 0.45 and Mg# from 0.48 to 0.58. TiO₂ varies from 0.11 to 0.35 wt % and NiO from 0.07 to 0.12 wt%. Altered chromite from dunites and harzburgites has Cr# from 0.93 to 0.97 and Mg# from 0.13 to 0.16. Chlorite is mainly penninite, but sheridanite and clinochlore also occur. The sulfide of the dunite is pentlandite altered to millerite and to awaruite. Correa et al. (2008) has a more complete description and the mineral chemistry analyses.

Distinct modal compositions ascribed to melt-rock interaction obviously have a dramatic effect on bulk rock chemical variations and mineral chemistry of essential and accessory minerals within harzburgites and dunites. Olivine from dunites depicts slightly higher Mg# value than those from adjacent harzburgites, which according to Kelemen (1990), could be produced by melt/rock reaction. On the other hand the higher Mg# and lower NiO wt% content in dunites can be explained using an incongruent orthopyroxene melting model as proposed by Kubo (2002). The higher TiO₂ content of the spinels in the dunite must be a consequence of titanium transfer from the impregnating mafic melt to the chromium spinel of the dunite (Allan and Dick 1996; Cannat et al. 1997). It is also observed that dunite bands exhibits higher S content than the host harzburgite which may favors the idea that dunite portions were percolating with a sulfur-saturated magma.

3.8. Re-Os systematic

Os concentration ranges from 1.96 to 4.35 ppb, Re from 0.0513 to 1.3138 ppb, and the ¹⁸⁷Os/¹⁸⁸Os isotopic ratios from 0.1190 to 0.1361 (Table 6).

The $^{187}\text{Os}/^{188}\text{Os}$ ratio in harzburgite is 0.1190, which is within the range of the isotopic values observed in other peridotitic massifs (0.115-0.130, e.g. Reisberg and Lorand 1995; Saal et al. 2001), whereas in the dunites it is higher (0.1361) than the observed in worldwide peridotites.

Table 6. Re-Os systematic results of chromitites and peridotites from Aburrá Ophiolite.

Sample	Rock	Unit	Re(ppb)	Os(ppb)	$^{187}\text{Re}/^{188}\text{Os}$	$\pm 2\text{ S.E}$ (absolute)	$^{187}\text{Os}/^{188}\text{Os}$	$^{187}\text{Os}/^{188}\text{Os}$ (220 Ma)	γOs_i (T=0.22 Ga)
AC 20F	Chromitite-massive	Patio Bonito	0.0849	1.9645	0.2083	0.0024	0.1240	0.12325	-3.7
AC 77F	Chromitite-coar. diss.	El Chagualo	0.2296	3.8566	0.2871	0.0025	0.1318	0.13077	2.2
AC 52H	Depleted Harzburgite (WR)	Reaction zone	0.0513	4.3546	0.0567	0.0011	0.1190	0.11884	-7.2
AC 52D	Dunite (WR)	Reaction zone	1.3138	2.7203	2.3305	0.0022	0.1361	0.12756	-0.3

The $^{187}\text{Os}/^{188}\text{Os}$ ratio in chromite from two chromitite deposits varies from 0.12402 to 0.13182, with an average of 0.1279 ± 0.0039 (2σ), which agrees well with the average of worldwide podiform chromitites ($^{187}\text{Os}/^{188}\text{Os}$: 0.12809 ± 0.00085 2σ ; Walker et al. 2002). It lies within the average error of the Troodos ophiolite chromitites (0.1284 ± 0.0021 2σ ; Büchl et al. 2004), but it is lower than the estimated value for the primitive upper mantle ($^{187}\text{Os}/^{188}\text{Os}$: 0.1296 ± 0.0008 2σ ; Meisel et al. 2001), somewhat higher than estimates for the chondritic reservoir ($^{187}\text{Os}/^{188}\text{Os}$: 0.1260 ± 0.0013 ; Walker et al. 2002) and for the Mayarí-Baracoa ophiolitic belt chromitites (0.1259 ± 0.0019 2σ ; Gerville et al. 2005).

Initial $^{187}\text{Os}/^{188}\text{Os}$ ratios were calculated at 220 Ma, the presumed age of the ophiolite, are shown in Table 6 and plotted in Fig. 6. γOs , the percent deviation from chondrite at a given time (Shirey and Walker 1998), as also calculated to 220 Ma. The γOs value for massive chromitite of Patio Bonito is slightly negative ($\gamma\text{Os} = -3.7$), whereas in the coarse-grained disseminated chromitite from El Chagualo deposit it is slightly positive (2.2). The orthopyroxene depleted harzburgite from the reaction zone has negative γOs (-7.2), while in the dunite it is higher γOs (-0.3). The negative γOs indicates subchondritic or unradiogenic Os in the peridotites and one chromitite of the Aburrá Ophiolite, and the positive γOs indicates suprachondritic or radiogenic Os of one chromitite sample.

The unradiogenic harzburgite yield a TMA (mantle extraction) age ca. 1.65 Ga and a model Re-depletion age ca. 1.46 Ga. The age of other samples was not calculated because the Re-Os composition is disturbed and, therefore, would not yield a geologically meaningful age (Becker et al. 2001; Frei and Jensen 2003).

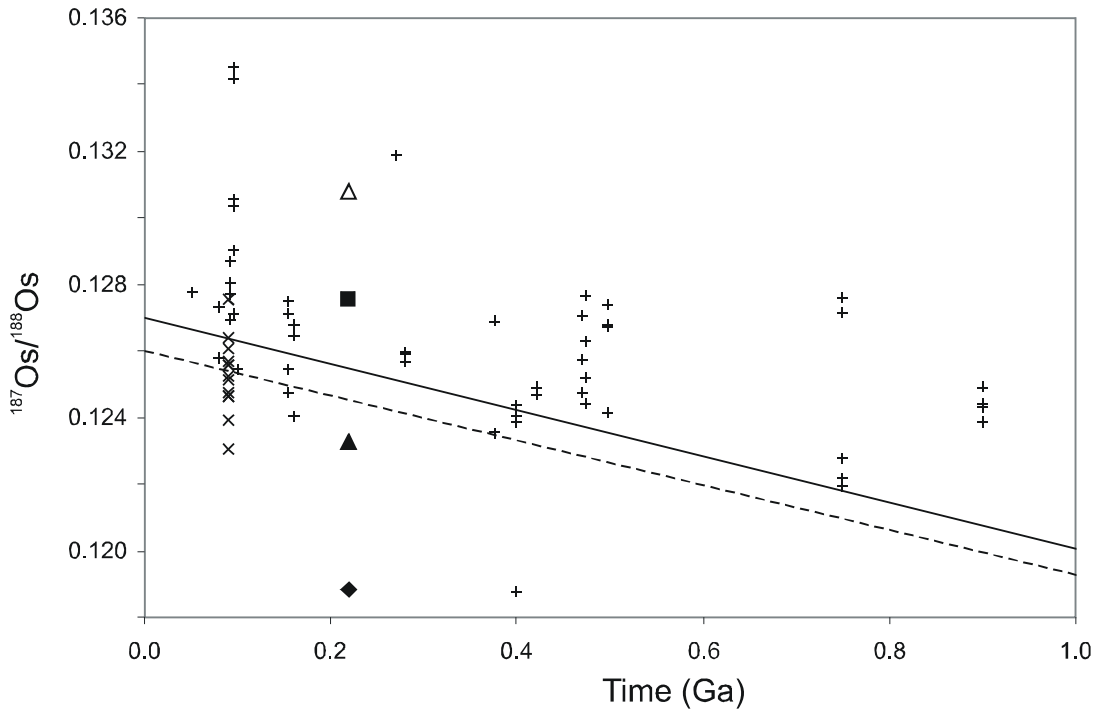


Fig. 6. $^{187}\text{Os}/^{188}\text{Os}$ ratios of the Aburrá samples, plotted with $^{187}\text{Os}/^{188}\text{Os}$ ratios from other studies. The solid line represents the Mantle projection (Shirey and Walker 1998). The dashed line shows the chondritic projection. Samples of Aburrá Ophiolite: Triangles= chromitites, black diamond: harzburgite, black square: dunite. Crosses: chromitite samples analyzed by Walker et al. (2002); x:chromitite samples analyzed by Gervilla et al. (2005).

3.9. Discussion

The concordant to subconcordant chromite ores with deformed magmatic structures are dominant in the Aburrá Ophiolite. Only one discordant pod was found in which chromitite has preserved nodular and chain structures, regarded as primary by many authors (e.g. Thayer 1969; Greenbaum 1977). The structural differences have been attributed to the time-lag between the formation of the pods and the plastic flow in the Moho Transition Zone. The concordant and subconcordant pods should be emplaced during solid-state flow and the discordant emplaced after plastic deformation (Nicolas 1989).

3.9.1. Constraints on chromitites composition

The Aburrá chromitites are of the high-aluminum type, similar to refractory-grade chromitites (Cr_2O_3 from 30 to 40 wt %, Al_2O_3 between 25 and 32 wt %, $\text{FeO} < 15$ wt % and $\text{Al}_2\text{O}_3 + \text{Cr}_2\text{O}_3 > 58$ wt %), which commonly occur in the uppermost part of the upper mantle of ophiolites.

The primary composition of the Aburrá chromite considering most of the ores is homogeneous at the scale of a pod, but there are slight compositional differences among the deposits. Patio Bonito and Niquía chromitites have higher Cr# (see Fig. 5a) than those of the San Pedro, Don Jesús, El Carmelo and El Chagualo deposits. The last one has the lowest Cr/Cr+Al ratio and also shows chemical differences between the coarse-grained and the fine-grained disseminated chromite.

Cr-Al compositional variations among chromite ores can be explained by (1) a decrease of the Cr/Cr+Al ratio as a function of chromite crystallization with decreasing temperature (Roeder and Reynolds 1991) in response to progressive decrease of Cr activity in the melt; (2) mixing between a fractionated melt and a relatively primitive magma (e.g. Rolinson 2005); and (3) subsolidus reequilibrium during hydrothermal alteration (e.g. Kimball 1990). According to process (1) the Patio Bonito and Niquía chromitites probably formed prior to the San Pedro, Don Jesus, El Carmelo and El Chagualo chromitites. Tegyey (1990) states that in chromitites at the top of harzburgites and in stratiform deposits of the Oman ophiolite, the Cr/Cr+Al ratio decreases upwards due to fractional crystallization. Thus, the lower Cr# of the El Chagualo ore may indicate that their chromite crystallized in an upper structural level than in the other deposits, but all in the transition zone of the ophiolite. However, if during a basaltic melt cooling only chromite and olivine are crystallizing, chromite will be progressively depleted in Cr and Mg, enriched in Fe, without significant change in Al. Therefore, the increase in Al of some chromitites (El Carmelo, Don Jesus and El Chagualo) probably reflects the effect of melt-rock interaction or the influx of other type of magma, rather than fractional crystallization of the already differentiated melt from which the other chromitites precipitated. Both the progress of melt-rock interaction and the input of new melt batches that react with differentiated melt promote magma mixing, resulting in a melt with a different composition.

On the other hand, the compositional differences between nodular and disseminated chromite in the El Chagualo deposit may also be attributed to different modal proportions of chromite and olivine and subsolidus re-equilibrium.

Olivine from chromitites of the El Chagualo deposit and an inclusion in massive chromitite is highly forsteritic, as typically occurs in olivine of ophiolitic chromitites. The very high forsterite nature of olivine and its compositional variation are best explained by Mg-Fe postmagmatic/subsolidus exchange. Under declining temperature, diffusion in the solid state allows the exchange of Mg^{2+} for Fe^{2+} between silicates and chromite (Irvine 1965; Roeder et al. 1979). During such exchange reaction in chromitite, the high modal proportion of chromite buffers the Mg loss of chromite to the interstitial olivine (Roberts and Neary 1993), leading to the formation of hyper-magnesian olivine (Lehmann 1983).

Parental magma composition

Experimental studies demonstrate that chromite is a high sensitive petrogenetic indicator and can be used to constrain the composition of the melt from which it segregated. Maurel and Maurel (1982) show that the Al content of spinel can be related to that of the melt by the following formula:

$$(Al_2O_3)_{Sp} = 0.035 (Al_2O_3)^{2.42} \text{liquid } (Al_2O_3 \text{ in wt\%})$$

The equation was obtained from experiments carried out at 1 atm total pressure and between 1180°C and 1300°C, at oxygen fugacities between 10^{-7} and 10^{-9} atm. It is valid for (Al_2O_3) liq values between 8 and 18 %.

It is also possible to constrain the FeO/MgO ratio of the melt using the formula of Maurel (1984, cited by Augé 1987).

$$\ln(FeO/MgO)_{Sp} = 0.047 - 1.07 YAl_{Sp} + 0.64 YFe^{3+}_{Sp} + \ln(FeO/MgO)_{liq}$$

where $YAl_{Sp} = Al/(Al + Cr + Fe^{3+})$ and $YFe^{3+}_{Sp} = Fe^{3+}/(Al + Cr + Fe^{3+})$.

According to Augé (1987) such FeO/MgO ratio calculations must be carried out in the case of nearly monomineralic chromitite in order to avoid the effects of subsolidus reequilibrium between olivine and spinel which varies the Fe and Mg content.

The calculations were applied to the Aburrá chromitites and are given in Table 7. One would argue that results must be used with caution considering the possibility of chemical modifications of chromite, especially of those related to changes of Al_2O_3 content, due to hydrothermal alteration which promoted chlorite formation. Nevertheless the mineral chemistry data used for such calculations were taken from analysis from the cores of chromite grains which were undoubtedly preserved from the hydrothermal alteration that took place in the borders of grains. Thus the results reported here can be considered as giving an approximated idea of spinel parental magma composition. Such calculations have

previously been applied to chromitites of several ophiolites and of Archean ultramafic massifs (Augé 1987; Orberger et al. 1995; Zhou et al. 1996; Melcher et al. 1997; Proenza et al. 2004; Mondal et al. 2006) (Table 7).

Table 7. Calculations of Al₂O₃ content and FeO/MgO ratio of the parental melts in equilibrium with the Aburrá chromitite bodies.

	Al ₂ O ₃ liquid	FeO/MgO liquid
Aburrá Chromitites		
Patio Bonito massive	15.3-15.8	0.63-0.75
Niquía massive	15.6-15.7	0.68-0.72
San Pedro massive	15.9-16.5	0.66-0.69
Don Jesús	16.7-16.9	
El Carmelo massive	16.9-17.0	0.72-0.76
El Chagualo coarse disseminated	17.5-17.6	
El Chagualo fine disseminated	17.7-17.8	
Oman chromitite ¹	11.4-16.4	0.62
Nan Uttaradit chromitite ²	11.6-12.0	
Kempirsai chromitites ³		
MOF	9.0-10.6	0.3-0.5
BAT	13.5-16.7	0.8-1.0
Tehuitzingo chromitite ⁴	15.3	
Boninite ⁵	10.6-14.4	0.7-1.4
MORB ⁵	15	1.2-1.6
BABB southern Mariana Trough ⁶	16.5	1.23
BABB East Scotia Sea ⁷	14.5-17.9	1.0-1.23

¹Augé (1987); ²Orberger et al. (1995); ³Melcher et al. (1997); ⁴Proenza et al. (2004b); ⁵Wilson (1989); ⁶Gribble et al. (1996); ⁷Saunders and Tarney (1979)

The Al₂O₃ contents of the parent liquids for all the Aburrá chromitites show variation and suggest that there were two types of melts. When compared to the compositions of primitive magma of different tectonic settings, one group of the Aburrá chromitites may have precipitated from normal mid-ocean ridge basalt (MORB) melts and another probably crystallized from back-arc basalt (BABB) melt.

The mineral chemistry data and the theoretical calculations for the parental melt composition for Aburrá chromitites are consistent with the observed worldwide ophiolitic chromitites, in which the high-Al or low-Cr (Cr# <60) chromitites formed in equilibrium with tholeiitic melts (Zhou and Robinson 1997) of MORB or BABB types (Dick and Bullen 1984; Proenza et al. 1999). On the other hand, high-Cr chromitites, so far absent in the Aburrá Ophiolite formed in equilibrium with boninitic melts (Zhou and Robinson 1997).

3.9.2. Re-Os constraints

The Os isotopic composition of the Aburrá Ophiolite peridotites and chromitites is heterogeneous.

During mantle partial melting Re behaves mildly incompatible, whereas Os remains in the refractory residue (Walker et al. 1988, Pearson et al. 1995), thus the $^{187}\text{Os}/^{188}\text{Os}$ of peridotites only changes when these residual peridotites interact with melts that may contain significant radiogenic Os. It is thus expected that during stages of successive partial melting and melt extraction the residual peridotite would become Re-depleted, yielding negative initial γOs . The observed strongly negative γOs (-7.2) of the studied harzburgite is consistent with its residual nature after melting of the lithospheric mantle peridotites, and the negative γOs (-3.7) of the massive chromitite suggests an origin related to this Re-depleted lithospheric mantle (Lambert et al. 1994). On the other hand, the Os isotopic characteristics of the dunite and coarse-grained disseminated chromitite, in comparison to harzburgite and massive chromitite suggest addition of radiogenic Os.

The variation of Re and Os content and the Os isotopic composition between harzburgite and dunite are not consistent with a residual nature of the latter. One possible explanation for such compositional extreme variation in samples from the same outcrop may be the influence of local melt-rock reaction processes. Several studies have shown that this can modify the Os isotopic composition at small scales (e.g. Rehkämper et al. 1999; Becker et al. 2001), as recorded in peridotites of different tectonic settings (Brandon et al. 1999; Godard et al. 2001). During melt percolation, Os was removed and the γOs of the dunite shifted to more radiogenic values, as compared to the adjacent harzburgite. Correa et al. (2008) evidenced that these dunites resulted from melt-rock reaction, when they were metasomatised with sulfides by a basalt melt. The high Re content in these dunites can be related to the abundance of sulfides. The coarse-grained disseminated chromitites probably also resulted from a similar melt-rock interaction process and, in this case, chromite crystallized from a percolating magma enriched in radiogenic Os, similar to what has been described in the Troodos complex chromites (Büchl et al. 2004).

3.9.3. Origin of the chromitites

It has been proposed that chromitites from ophiolites are produced in the upper mantle as a result of melt-rock interaction processes (e.g. Zhou et al. 1994, 1998; Arai 1998), which explains not only the origin of chromitites but also the enveloping dunites, as well as some

dunite bodies of ophiolites (Nicolas and Prinzhofer 1983; Kelemen et al. 1995; Zhou et al. 1996, 2005). The melt-rock interaction model is based on the principle that at low pressures the reaction of parental basaltic magma with the host peridotites consumes the orthopyroxene and may precipitate olivine. The resultant melt will have a higher content of silica and will move from the olivine-chromite cotectic into the chromite crystallization field. In addition to the melt-rock interaction, other processes such as fractionation, melt migration and magma mixing may have been effective for the chromitite genesis (Zhou et al. 1996), thus explaining the chemical and textural variations in the studied deposits. According to Matsumoto and Arai (2001), the formation of monomineralic chromite aggregates takes place where the melt conduits are large and the interaction is high.

The Aburrá Ophiolite peridotites have field, textural and some chemical evidences of melt-rock interaction such as replacive dunites and impregnated peridotites (Correa et al. 2008). This petrologic process, which has occurred in the whole area, is also probably responsible for the chemical differences observed in chromitites from several ores and point out that the melt-rock interaction has played an important role in the formation of the chromitites.

3.9.4. Tectonic setting implications

The tectonic setting for the formation of chromitite is still controversial (e.g. Lago et al. 1982; Roberts 1988, Zhou and Robinson 1997). It has been experimentally demonstrated that chromitite formation needs water-rich primitive melts saturated in olivine and chromite (e.g. Matveev and Balhaus 2002). Such conditions are common in subduction-related environments, one reason for many authors favors the model for chromitite genesis in supra-subduction zones (e.g. Pearce et al. 1984; Arai and Abe 1994, Matveev and Balhaus 2002; Zhou et al. 2005). According to Zhou and Robinson (1997), it is expected that chromitites also occur in arc and back-arc environments because of the widespread melt-rock interaction due to reaction of refractory or mildly refractory melts with the old lithospheric mantle. Since melt-rock reactions are not significant in mature spreading ridges, chromitites would not be expected to form in such environments (Zhou and Robinson 1997). However, studies demonstrate that podiform chromitites also occur in modern mid-ocean ridges (Arai and Matsukage 1996, 1998; Abe 2003). In any case, hydrated mineral inclusions have been observed and underline the importance of hydrous phases in the crystallization of chromite, and show that hydrated conditions can be reached also in mid ocean ridges (Kelemen et al. 2004). Therefore, the podiform chromitites can be originated in both large oceans and

subduction-related settings (Arai 1997; Kelemen et al. 2004). On the other hand, high-Al chromitite is thought to form in back-arc basin (Zhou and Robinson 1997) or in mid ocean ridges (Dick and Bullen 1984; Arai and Matsukage 1998).

The composition of the Aburrá chromitites is similar to the high-Al chromitites of several worldwide ophiolites, such as those of the Coto Block in the Zambales Ophiolite Complex in the Philippines, interpreted as formed in a transitional mid-ocean ridge-island arc (MOR-IA) environment (Yumul and Balce 1994), the Sangun zone in Japan interpreted as MORB or back-arc basalt type (Matsumoto et al. 1997) and the Moa-Baracoa, Cuba, interpreted as crystallized in a evolved back arc basin (Proenza et al. 1999). In Fig. 5b, part of the studied chromite plots in the MORB field, while another in the Al-rich chromites field of the Sagua de Tánamo district, Cuba, and of Tehuitzingo, Mexico, interpreted as formed in back-arc environment (Proenza et al., 1999, 2004b), whereas another group fall outside any specific field. Thus, the similarity of the Aburrá chromitites with those of Cuba and Mexico, coupled with the evidence of BABB parental melts suggest that they formed in a back-arc basin rather than in mature spreading ridges.

3.10. Conclusions

The Aburrá Ophiolite contains Al-rich chromitites hosted by dunite and by orthopyroxene depleted harzburgite. The orebodies are mainly concordant to subconcordant.

The chemical composition of the chromitites indicates that they derived from at least two different parental magmas. The Patio Bonito, Niquía and San Pedro chromitites seem to be formed by crystallization of mafic melts, probably of MORB composition, whereas chromitites from Don Jesús, El Carmelo and El Chagualo deposits probably crystallized from mafic melts with BABB affinity. The Re-Os data presented here also suggest two different sources of Os for the ores.

Results from this study indicate that some peridotites had experienced several stages of reaction with percolating melts. The banded dunite-harzburgite rocks represent portions of high permeability and the dunite bands represent zones of Re-enriched melt percolation. At least part of the chromitites crystallized owing to chrome saturation in the percolating melts after interaction with peridotites.

All the chromitites were formed in the Transition Zone of the ophiolite and are possibly related to a back-arc basin environment.

Acknowledgments

This study was financially supported by the Conselho Nacional de Desenvolvimento Científico e Tecnológico - CNPq (Brazil) grant (#141622/03-2) to A.M. Correa-M. The authors wish to thank H. González for two chromitite samples, and M. Diaz for introducing the first author to the Don Jesús and El Carmelo chromitite deposits. We also would like to acknowledge Dr. Hardy Jost for the review and valuable suggestions to the original manuscript.

References

- Abe N (2003) Petrological insights of the first recovered chromitites from Site 1271, ODP Leg 209, MAR 15.N. Eos Trans AGU 84 (46): abstract V11E-0533
- Ahmed Z (1984) Stratigraphic and textural variations in the chromite composition of the ophiolitic Sakhakot-Qila Complex, Pakistan. Econ Geol 79: 1334-1359
- Allan JF, Dick HJB (1996) Cr-rich spinels as a tracer for melt migration and melt-wall rock interaction in the mangle: Hess Deep, leg 147. In: Mével C, Gillis KM, Allan JF, Meyer PS (eds.) Proc. ODP, Sci. Results, 147: College Station, TX (Ocean Drilling Program), pp 157-172
- Alvarez J (1982) Tectonitas dunitas de Medellín, Departamento de Antioquia, Colombia. Ingeominas, Informe 1986, Medellín, 62 p
- Alvarez J (1985) Ofiolitas y evolución tectónica del occidente Colombiano. Ingeominas, Informe 1988, Medellín, 30 p
- Alvarez J (1987) Mineralogía y química de los depósitos de cromita podiforme de las dunitas de Medellín. Departamento de Antioquia, Colombia. Boletín Geológico de Ingeominas 33: 33-46
- Alvarez J (1987 b) Geología del Complejo Ofiolítico de Pácora y cuencas relacionadas de arcos de islas. Ingeominas Departamento de Bogotá, Colombia. Informe 2027, pp 1-87
- Arai S (1980) Dunite-harzburgite-chromitite complexes as refractory residue in the Sangun-Yamaguchi zone, western Japan. J Petrol 21: 141-165
- Arai S (1992) Chemistry of chromian spinel in volcanic rocks as a potential guide to magma chemistry. Miner Magazine 56: 173-184
- Arai S (1997) Origin of podiform chromitites. J of Asian Earth Sci 15: 303-10
- Arai S (1998) Comments of the paper ‘Primitive basaltic melts included in podiform chromites from the Oman ophiolite’ by P. Schiano et al. Earth and Planet Sci Lett 156: 117-119

- Arai S, Abe N (1994) Podiform chromitite in the arc mantle: Chromitite xenoliths from the Takashima alkali basalt, Southwest Japan arc. *Miner Deposita* 29: 434-8
- Arai S, Matsukage JH (1996) Petrology of gabbro-troctolite-peridotite complex from Hess Deep, equatorial Pacific: implications for mantle-melt interaction within the oceanic lithosphere. In: Mével C, Gillis KM, Allan JF, Meyer PS (eds.) *Proc. ODP, Sci. Results*, 147: College Station, TX (Ocean Drilling Program), pp 135-155
- Arai S, Matsukage JH (1998) Petrology of a chromitites micropod from Hess Deep, equatorial Pacific: A comparison between abyssal and alpine-type podiform chromitites. *Lithos* 43: 1-14
- Arai S, Yurimoto H (1994) Podiform chromitites in the Tari-Misaka ultramafic complex, southwestern Japan, as mantle-melt interaction products. *Econ Geol* 85: 1279-1288
- Augé TH (1987) Chromite deposits in the northern Oman ophiolite: Mineralogical constraints. *Miner Deposita* 22: 1-10
- Becker H, Shirey SB, Carlson RW (2001) Effects of metal percolation on Re-Os systematics of peridotites from Paleozoic convergent plate margin. *Earth Planet Sci Lett* 188: 107-121
- Botero G (1963) Contribución al conocimiento de la zona central de Antioquia. *Anales Facultad de Minas*, No. 57. Medellín, 101 p
- Brandon AD, Norman MD, Walker RJ, Morgan JW (1999) ^{186}Os - ^{187}Os systematics of Hawaiian picrites. *Earth Planet Sci Lett* 174: 25-42
- Braun MG, Kelemen PB (2002) Dunite distribution in the Oman Ophiolite: Implications for melt flux through porous dunite conduits. *Geochem Geophys Geosyst* 3: 8603, DOI 10.1029/2001GC000289
- Büchl A, Brügmann G, Batanova V (2004) Formation of podiform chromitite deposits: implications from PGE abundances and Os isotopic compositions of chromites from the Troodos complex, Cyprus. *Chem Geol* 208: 217-232
- Cannat M, Chatin F, Whitechurch H, Ceuleneer G (1997) Gabbroic rocks trapped in the upper mantle at the Mid-Atlantic Ridge. In: Karson JA, Cannat M, Miller DJ, Elthon D (eds.) *Proceeding of the Ocean Drilling Program, Scientific Results*, 153: College Station, TX (Ocean Drilling Program), pp 243-264
- Carlson RW, Pearson DG, Boyd FR ,Shirey SB, Irvine G, Menzies AH, Gurney JJ (1999) Re-Os systematics of Litospheric peridotites : implications for litosphere formation and preservation. In: Gurney JJ, Pascoe MD, Richardson SH (eds.) *Proceedings of 7th International Kimberlite Conference*. Cape Town: Red Roof Design, pp 99-108

- Cassard D, Rabinovitch M, Nicolas A, Moutte J, Leblanc M, Prinzhofe A (1981) Structural classification of chromite pods in southern New Caledonia. *Econ Geol* 76: 805-831
- Correa AM, Martens, U (2000) Caracterización geológica de las anfibolitas de los alrededores de Medellín. BsC thesis (Unpublished), Facultad de Minas, Universidad Nacional de Colombia, Medellín, 363p
- Correa AM, Nilson AA (2003) Dunitas de Medellín y Metagabros de El Picacho: Posibles Fragmentos de Ofiolita Subtipo Harzburgita, Tipo Zona de Supra-Subducción. In: IX Congreso Colombiano de Geología, Medellín, Resumenes, pp 46-47
- Correa AM, Martens U, Restrepo JJ, Ordóñez-Carmona O, Pimentel MM (2005) Subdivisión de las metamorfitas básicas de los alrededores de Medellín (Colombia). *Revista de la Academia Colombiana de Ciencias Exatas, Físicas y Naturales*. XXIX (112): 325-344
- Correa AM, Pimentel MM, Armstrong R, Laux JE, Ordoñez-Carmona O (2005b) Edad U-Pb Shrimp y características isotópicas Nd y Sr del granito de la Iguaná, Antioquia. In: X Congreso Colombiano de Geología, Bogotá. Memorias, CD ROM
- Correa AM, Nilson A, Pimentel M (2008). The nature of the ultramafic section of the Aburrá Ophiolite, Medellín region, Colombian Andes. (Submitted to Journal of South American Earth Sciences)
- Dick HJB, Bullen T (1984) Chromian spinel as a petrogenetic indicator in abyssal and Alpine-type peridotites and spatially associated lavas. *Contr Mineral Petrol* 86: 54-76
- Droop GTR (1987) A general equation for estimating Fe^{3+} concentrations in ferromagnesian silicates and oxides from microprobe analyses, using stoichiometric criteria. *Min Magazine* 51: 431-435
- Frei R, Jensen BK (2003) Re-Os, Sm-Nd isotope- and REE systematics on ultramafic rocks and pillow basalts from the Earth's oldest oceanic crustal fragments (Isua Supracrustal Belt and Ujaragssuit nunât area, W Greenland. *Chem Geol* 196: 163-191
- Geominas Ltda (1975) Proyecto cromitas. Informe final, pp 1-39
- Gerville F, Proenza JA, Frei R, Gonzalez-Jimenez JM, Garrido CJ, Meibom A, Diaz-Martínez R, Lavaut W (2005) Distribution of Platinum-group elements and Os isotopes in chromite ores from Mayari-Baracoa Ophiolite Belt (eastern Cuba). *Contrib Mineral Petrol* 150: 589-607
- Godard M, Alard O, Lorand J, Burton KW (2001) Tracking Melt-Rock Reaction Using Os Isotopes: Maqsad Diapir (Oman Ophiolite) *Eos Trans. AGU*, 82(47): abstract V22A-1008
- González, H (1980) Geología de las planchas 167 (Sonsón) y 187 (Salamina). *Boletín Geológico de Ingeominas*, 23 (1): 1-174

- González H (2001) Mapa Geológico del Departamento de Antioquia. Geología, recursos minerales y amenazas potenciales Escala 1:400.000. Memoria Explicativa, Ingeominas, 240 p
- Greenbaum D (1977) The chromitiferous rocks of the Troodos ophiolite complex, Cyprus. Econ Geol 72: 1175-1194
- Gribble RF, Stern RJ, Bloomer SH, Stuben D, O'Hearn T, Newman S (1996) MORB mantle and subduction components interact to generate basalts in the Southern Mariana Trough back-arc basin. Geochim Cosmochim Acta 60: 2153-2166
- Irvine TN (1965) Chromian spinel as a petrogenetic indicator: Part 1. Can J Earth Sci 2: 648-672
- Kelemen PB (1990) Reaction between ultramafic rock and fractionating basaltic magma, I. Phase relations, the origin of calc-alkaline magma series, and the formation of discordant dunite. J Petrol 31: 51-98.
- Kelemen PB, Shimizu N, Salters VJM (1995) Extraction of MORB from the mantle by focused flow of melt in dunite channels. Nature 375: 747-753
- Kelemen PB, Kikawa E, Miller DJ et al (2004) Proceedings of the Ocean Drilling Program, Initial Reports, 209 (SITE 1271): College Station, TX (Ocean Drilling Program), 129 p DOI:10.2973/odp.proc.ir.209.106.2004
- Kerr AC, Marriner GF, Tarney J, Nivia A, Saunders AD, Thirlwall MF, Sinton CW (1997) Cretaceous Basaltic Terranes in Western Colombia: Elemental, chronological and Sr-Nd Isotopic Constraints on Petrogenesis. J Petrol 38: 677-702
- Kimball KL (1990) Effects of hydrothermal alteration on the compositions of chromian spinels. Contributions to Mineralogy and Petrology 105: 337-346
- Kubo K (2002) Dunite formation processes in highly depleted peridotite: case study of the Iwanaidake Peridotite, Hokkaido, Japan. Journal of Petrology 43: 423-448.
- Lago NL, Rabinowicz M, Nicolas A. (1982) Podiform chromite orebodies: a genetic model. J Petrol 23: 103-125
- Lambert DD, Walker RJ, Morgan JW, Shirey SB, Carlson RW, Zientek ML, Lipin BR, Koski MS, Cooper RL (1994) Re-Os and Sm-Nd isotope geochemistry of the stillwater complex, Montana: implications for petrogenesis of the J-M reef. J Petrol. 35: 1717-1735
- Leblanc M, Nicolas A, (1992) Ophiolitic chromitites. Chronique de la Recherche Minière 507: 3-25
- Leblanc M, Viollete JF (1983) Distribution of aluminium-rich and chromium-rich chromite pods in ophiolite peridotites. Econ Geol 78: 293-301

- Leblanc M, Dupuy C, Cassard D, Moutte J, Nicolas A, Prinzhofe A, Rabinovitch M, Routhier P (1980) Essai sur la genèse des corps podiformes de chromitite dans les périclases ophiolitiques: Etude des chromites de Nouvelle-Caledónie et comparaison avec celles de Méditerranée orientale. In: Panayiotou A (ed) Ophiolites. Geol Surv Dept, Cyprus Nicosia, pp 691-701
- Lehmann J (1983) Diffusion between olivine and spinel: Application to geothermometry. Earth Planet Sci Lett 64: 123-138
- Martinez AMC, Nilson AA, Brito RSC (2004) Discriminantes químicos entre espinélicos primários e secundários aplicados ao complexo ofiolítico de Aburrá no setor norte da Cordilheira Central da Colômbia. In: XLII Congresso Brasileiro de Geologia, Anais, S 25: 365
- Matsumoto I, Arai S (2001) Morphological and chemical variations of chromian spinel in dunite-harzburgite complexes from the Sangun zone (SW Japan): implications for mantle/melt reaction and chromitite formation processes. Mineral Petrol 73: 305-323
- Matsumoto I, Arai S, Yamauchi H (1997) High-Al podiform chromitites in dunite-harzburgite complexes of the Sangun zone, central Chugoku district, Southwest Japan. J Asian Earth Sci 15(2-3): 295-302
- Matveev S, Ballhaus C (2002) Role of water in the origin of podiform chromitite deposits. Earth Planet Sci Lett 203: 235-243
- Maurel C, Maurel P (1982) Etude expérimentale de la distribution de l'aluminium entre bain silicaté basique et spinelle chromifère. Implications pétrogénétiques : teneur en chrome des spinelles. Bull Minéral 105: 197-202
- Meisel T, Walker RJ, Irving AJ, Lorand JP (2001) Osmium isotopic compositions of mantle xenoliths: a global perspective. Geochim Cosmochim Acta 65: 1311-1323
- Melcher F, Grum W, Simon G, Thalhammer TV, Stumpf EF (1997) Petrogenesis of the Ophiolitic Giant Chromite Deposits of Kempirsai, Kazakhstan: a Study of Solid and Fluid Inclusions in Chromite. J Petrol 38: 1419-1458
- Mondal SK, Li C, Ripley EM, Feei R (2006) The genesis of Archaean chromitites from the Nuasahi and Sukinda massifs in the Singhbhum Craton, Índia. Precambrian Res 148: 45-66
- Monsalve BI (1996) Evaluación geológica de las cromitas al NW de Medellín. BsC thesis (Unpublished), Facultad de Minas, Universidad Nacional de Colombia, Medellín, 88 p
- Neary CR, Brown MA (1979) Chromites from Al'Ays Complex, Saudi Arabia and the Semail Complex, Oman: Evolution and Mineralization of the Arabian Nubian Shield.

Jedah, Saudi Arabia. King Abudulaziz University, Institute of Arabian Geologist Bull 2: 193-205

Nicolas A (1989) Structures of Ophiolites and Dynamics of Oceanic Lithosphere. Petrol Struct. Geol 4 Kluwer Academic Publishers, Dordrecht p 367

Nicolas A, Prinzhofner A (1983) Cumulative or residual origin for the transition zone in ophiolites: Structural evidence. J Petrol 24: 188-206

Orberger B, Lorand JP, Girardeau J, Merciera JCC, Pitragool S (1995) Petrogenesis of ultramafic rocks and associated chromitites in the Nan Uttaradit ophiolite, Northern Thailand. Lithos 35: 153-182

Ordóñez-Carmona (2001) Caracterização Isotópica Rb-Sr e Sm-Nd dos Principais Eventos Magmáticos nos Andes Colombianos. Unpubl PhD thesis, Universidade de Brasília, 176 p

Ordóñez-Carmona O, Pimentel MM (2001) Consideraciones geocronológicas e isotópicas del Batolito Antioqueño. Revista de la Academia Colombiana de Ciencias Exatas, Físicas y Naturales 25: 27-35

Ortíz, F, Gaviria AC, Parra N, Arango JC, Ramírez G (2004) Guías Geológicas para Localización de Metales Preciosos en las Ofiolitas del Occidente de Colombia. In: Pereira E, Castroviejo R, Ortiz F (eds.) Complejos ofiolíticos en IBEROAMÉRICA guías de prospección para metales preciosos, pp 169-199

Pearce JA, Lippard SJ & Roberts S (1984) Characteristics and tectonic significance of supra-subduction zone ophiolites. In: Kokelaar BP, Howells MF (eds.) Marginal Basin Geology. Geol Soc Lond Spec Pub 16, pp 77-94

Pearson DG, Shirey SB, Carlson RW, Boyd FR, Pokhilenko NP, Shimizu N (1995) Re-Os, Sm-Nd and Rb-Sr isotope evidence for thick Archaean lithospheric mantle beneath the Siberian craton modified by multistage metasomatism. Geochim Cosmochim Acta 59: 959-977

Pereira O, Ortiz F, Prichard H (2006) Contribución al conocimiento de las Anfibolitas y Dunitas de medellín (Complejo Ofiolítico de Aburrá). Dyna 149: 17-30

Proenza J, Gervilla F, Melgarejo JC, Bodinier JL (1999) Al- and Cr- rich chromitites from de Mayarí-Baracoa Ophiolitic Belt (eastern Cuba): Consequence of interaction between volatile-rich melts and peridotite in suprasubduction mantle. Econ Geol 94: 547-566

Proenza J, Gervilla F, Melgarejo JC (2002). Los depósitos de cromita en complejos ofiolíticos: discusión de un modelo de formación a partir de las particularidades de las cromitas de Cuba Oriental. Bol. Soc. Española de Mineralogía 25: 97-128

- Proenza J, Escayola MP, Ortiz F, Pereira E, Correa AM (2004) Dunite and associated chromitites from Medellín (Colombia). 32nd Int. Geol. Congr. Abs. Vol., pt. 1, abs 1-1: 507
- Proenza JA, Ortega-Gutiérrez F, Camprubí A, Tritlla J, Elías-Herrera M, Reyes-Salas M (2004b) Paleozoic serpentinite-enclosed chromitites from Tehuitzingo (Acatlán Complex, southern Mexico): a petrological and mineralogical study. *J South Amer Earth Sci* 16: 649-666
- Quintero CA, Delgado E (1998) Caracterización química y mineralogica de las cromitas de la zona de Bello y San Pedro (Departamento de Antioquia). *Revista Colombiana de Química* 27: 51-60
- Rehkämper M, Halliday AN, Alt J, Fitton JG, Zipfel J, Takazawa E (1999) Non-chondritic platinum-group element ratios in abyssal peridotites petrogenetic signature of melt percolation?. *Earth Planet Sci Lett* 172: 65-81
- Reisberg L, Lorand J P (1995) Longevity of subcontinental mantle lithosphere from Os isotope and PGE systematics in orogenic peridotite massifs. *Nature* 376: 59-162
- Rendón DA (1999) Cartografía y caracterización de las unidades geológicas del área urbana de Medellín. BsC thesis (Unpublished), Facultad de Minas, Universidad Nacional de Colombia, Medellín, 113 p.
- Restrepo JJ (2003) Edad de generación y emplazamiento de ofiolitas en la cordillera Central: un replanteamiento (resumen). In: *Memorias IX Congreso Colombiano de Geología*, Medellín, Resumenes, pp 48-49
- Restrepo JJ (2005) Anfibolitas & Anfibolitas del Valle de Aburrá. In: *X Congreso Colombiano de Geología*, Bogotá-Colombia. Memórias, CD-ROM
- Restrepo JJ, Toussaint JF (1973) Obducción Cretácea en el occidente Colombiano. Publicación Especial de Geología U. Nal., Medellín 3, 1-26
- Restrepo JJ, Toussaint JF (1982) Metamorfismos superpuestos en la Cordillera Central de Colombia. In: *Actas del V Congreso Latinoamericano de Geología*. 3: 505-512
- Restrepo JJ, Toussaint JF (1984) Unidades litológicas de los alrededores de Medellín. In: I Conferencia sobre riesgos geológicos del Valle de Aburrá, Soc Col de Geol Memoria 1, pp 1-26
- Restrepo JJ, Toussaint JF (1988) Terranes and continental accretion in the Colombian Andes. *Episodes* 11:189-193
- Restrepo JJ, Frantz JC, Ordóñez-Carmona O, Correa AM, Martens U, Chemale F (2007) Edad triásica de formación de la Ofiolita de Aburrá, flanco occidental de la cordillera Central. In: *XI Congreso Colombiano de Geología*. Memorias. CD-ROM

- Roberts S (1988) Ophiolitic chromitite formation: a marginal basin phenomenon?. *Econ Geol* 83: 1034-1036
- Roberts S, Neary C (1993) Petrogenesis of ophiolitic chromitite. In: Prichard HM, Alabaster T, Harris NBW, Neary CR (eds.) *Magmatic Processes and Plate Tectonics*. Geol Soc, London, Spec Publications 76, pp 257-272
- Rodríguez G, González H, Zapata G (2005) *Geología de la Plancha 147 Medellín Oriental, Departamento de Antioquia*. Ingeominas, 303 p
- Roeder PL, Reynolds I (1991) Crystallization of chromite and chromium solubility in basaltic melts. *J Petrol* 32: 909-934
- Roeder PL, Campbell IH, Jamieson HE (1979) Re-evaluation of the olivine-spinel geothermometer. *Contrib Mineral Petrol* 68: 325-334
- Rollinson H (2005) Chromite in the mantle section of the Oman ophiolite: A new genetic model. *The Island Arc* 14(4): 542-550
- Roy-Barman M, Allègre CJ (1994) $^{187}\text{Os}/^{186}\text{Os}$ ratios in mid-oceanic ridge basalts and abyssal peridotites. *Geochim Cosmochim Acta* 58: 5043-5054
- Saal AE, Takazawa E, Frey FA, Shimizu N, Hart SR (2001) Re-Os isotopes in the Horoman peridotite: Evidence for refertilization? *J Petrol* 42: 25-37
- Saunders AD, Tarney J (1979) The geochemistry of basalts from a back-arc spreading centre in the East Scotia Sea. *Geochim Cosmochim Acta* 43: 555-572
- Shirey SB, Walker RJ (1995) Carius tube digestion for low-blank rhenium-osmium analysis. *Anal Chem* 67: 2136-2141
- Shirey SB, Walker RJ (1998) The Re-Os isotope system in cosmochemistry and high-temperature geochemistry. *Ann Rev Earth Planet Sci* 26: 423-500
- Tegyey M (1990) *Ophiolite and Metamorphic Rocks of the Oman Mountains: A petrographic Atlas*. Ministry of Petroleum and Minerals, 156 p
- Thayer TP (1969) Gravity differentiation and magmatic re-emplacement of podiform chromite deposits. In: Wilson HDB (ed.) *Magmatic Ore Deposits: a Symposium*. USA, Econ. Geol. (Monograph 4) pp 132-146.
- Toussaint JF, Restrepo JJ (1989) Acreciones sucesivas en Colombia: Un Nuevo modelo de evolución geológica. V Congreso Colombiano de Geología. Bucaramanga, Tomo I, pp 127-146
- Toussaint JF, Restrepo JJ (1994) The Colombian Andes during Cretaceous times. In: Salfity JA (ed.) *Cretaceous tectonics of the Andes*. Vieweg & Sohn, Wiesbaden, pp 61-100

- Vinasco CJ, Cordani UG, González H, Weber M, Pelaez C (2006) Geochronological, isotopic, and geochemical data from Permo-Triassic granitic gneisses and granitoids of the Colombian Central Andes. *J South Amer Earth Sci* 21: 355-371
- Walker RJ, Shirey SB, Stecher O (1988) Comparative Re-Os, Sm-Nd, Rb-Sr and trace element systematics for Archaen komatiite flows from Munro Township, Abitibi, Ontario. *Earth Planet Sci Lett* 87: 1-12
- Walker R, Richard HM, Ishiwatari A, Pimentel MM (2002) The osmium isotopic composition of convecting upper mantle deduced from ophiolite chromites. *Geochim Cosmochim Acta* 66: 329-345
- Wilson M (1989). Igneous petrogenesis. Londres: Unwin Hyman, 466 p
- Yumul GPJ, Balce GR (1994) Supra-subduction zone ophiolites as favorable hosts for chromitite, platinum and massive sulfide. *J Southeast Asian Earth Sci* 10: 65-79
- Zhou M-F, Robinson PT (1997) Origin and tectonic setting of podiform chromite deposits. *Econ Geol* 92: 259-262
- Zhou M-F, Robinson PT, Bal W-J (1994) Formation of podiform chromites by melt/rock interaction in the upper mantle. *Mineral Deposita* 28: 98-101
- Zhou, M-F, Robinson PT, Malpas J, Li Z (1996) Podiform chromitites in the Luobusa ophiolite (Southern Tibet): Implications for mantle-melt interaction and chromite segregation. *J Petrol* 37: 3-21
- Zhou M-F, Sun M, Keays RR, Kerrich RW (1998) Controls on platinum-group elemental distributions of podiform chromitites: a case study of high-Cr and high-Al chromitites from Chinese orogenic belts. *Geochim Cosmochim Acta* 62: 677-688
- Zhou M.-F, Robinson PT, Malpas, J Edwards SJ, Qi L (2005) REE and PGE Geochemical Constraints on the Formation of Dunites in the Luobusa Ophiolite, Southern Tibet. *J Petrol* 46: 615-639

CAPÍTULO 4.

AGE AND PETROGENESIS OF THE METAMAFIC ROCKS OF THE MEDELLÍN AREA, COLOMBIAN CENTRAL CORDILLERA: CONSTRAINTS ON THEIR RELATIONSHIPS WITH THE ABURRÁ OPHIOLITE

Ana María Correa Martínez

Instituto de Geociências, Universidade de Brasília, Brasília, Brazil. CEP 70910900
anamacor@unb.br

Márcio M. Pimentel

Instituto de Geociências, Universidade de Brasília, Brasília, Brazil. CEP 70910900
marcio@unb.br

Ariplínio A. Nilson

Instituto de Geociências, Universidade de Brasília, Brasília, Brazil. CEP 70910900
aanilson@unb.br

Abstract

Metagabbros and amphibolites occurring in the region around the city of Medellín in the Central Cordillera of the Colombian Andes have been recognized as the remnants of oceanic crust. The El Picacho Metagabbro consists of variable sheared rocks which locally exhibit preserved igneous features, such as cumulus textures and magmatic layering. The Boquerón rocks preserve coarse-grained isotropic gabbros and varied-textured portions. Both units display evidence of shearing and oceanic hydration at decreasing temperatures and a subsequent static oceanic recrystallization under low pressure regime. These metamorphic processes started at higher temperatures in the El Picacho rocks than in Boquerón. Plagiogranites nested within El Picacho metagabbros exhibit characteristics which indicate origin related to hydrous partial melting of the metagabbros in the oceanic environment. The Santa Elena amphibolites are plagioclase - and amphibole - bearing, fine-grained rocks which probably correspond to recrystallized basalts.

The major -and minor-element geochemistry of the metamafic rocks indicate that some alteration of the original compositions has taken place. Nevertheless certain elements have had an immobile behavior and thus, reflect the original igneous abundances. Chondrite-normalized REE patterns of the El Picacho rocks are similar to those of tholeiitic cumulates and similar to gabbroic cumulates of ophiolites, whereas the patterns of Boquerón and Santa Elena rocks are similar to those of mid-ocean ridge basalt (MORB). U-Pb age in zircon of plagiogranite indicates a minimum age for the ophiolite of 216.6 ± 0.36 Ma. The neodymium isotopic characteristics are similar for all mafic rocks and are typical of depleted oceanic rocks, indicating derivation of the original magmas from depleted mantle. In terms of their initial Sr and Nd isotopic compositions the El Picacho metagabbros, the Boquerón metagabbros and the Santa Elena amphibolites plot within or close to the back-arc or island arc field. Geochemical and isotopic data, together with the present-day geologic context, support the hypothesis that they are cogenetic (N-MORB)-derived magmatic rocks and this indicates that the tectonic setting of formation was probably within a back-arc basin.

Keywords: metamafic-rocks, plagiogranite, ocean-floor metamorphism, U-Pb age, Sr-Nd isotopes, MORB-BABB magmas, ophiolite emplacement, Colombian Andes

4.1. Introduction

Metamorphosed oceanic mafic plutonic and volcanic rocks constitute a major part of ophiolite complexes in many orogenic belts worldwide. The recognition of the original tectonic setting of their protoliths is very important to assess the kind of oceanic crust in which the mafic rocks were formed and to model the tectonic processes involved in the evolution of the region in which they occur.

It has been demonstrated that ocean-floor metamorphism may operate in both shallow and deeper parts of oceanic crust, as deep as the crust-mantle boundary (Manning et al., 2000; Nicolas et al., 2003). Evidences of oceanic metamorphism in many ophiolites remain recognizable if they have not been obliterated by deformation/recrystallization during ophiolite emplacement or during subsequent regional metamorphism (Mével et al., 1978; Girardeau and Mével, 1982; Mével and Cannat, 1991; Berger et al., 2005).

In the northwestern flank of the Colombian Central Cordillera, within and in the vicinities of the city of Medellín, metamorphosed mafic rocks representing dismembered fragments of one or various sectors of oceanic crust are exposed. They are associated with ultramafic rocks -the Medellín Dunite (Restrepo and Toussaint, 1984) or Medellín Ultramafic Massif (this study)- and are locally associated with metasedimentary rocks. The mafic rocks were traditionally grouped in the so-called Medellín Amphibolite unit (Restrepo and Toussaint, 1984; Restrepo, 1986) and were interpreted as portions of an oceanic basin upon which sediments were deposited (Echeverría, 1973). Recent study carried out by Correa and Martens (2000) led to the identification of metagabbroic bodies within the amphibolite unit. These bodies were informally named El Picacho Metagabbro and Boquerón Amphibolite (Correa and Martens, 2000). Restrepo (2005) suggested that the informal name Medellín Amphibolite should not be used anymore and proposed the name Santa Elena Amphibolite for the metamafic rocks which occur to the east of the ultramafic rocks. Although the Santa Elena Amphibolite unit has been studied in greater detail (Botero, 1963; Restrepo and Toussaint, 1984; Restrepo, 1986; Correa and Martens, 2000) than the Boquerón Amphibolite and the El Picacho Metagabbro, still very little is known about the origin and metamorphic evolution of these mafic rocks. Additionally, the age, stratigraphic and petrological relationships between the three metamafic units are not well constrained. It has been suggested that the El Picacho Metagabbro, together with the Medellín Dunite, is part of the Aburrá Ophiolitic Complex (Correa and Martens, 2000; Correa et al., 2005). On the other hand, the genetic relationships between the Boquerón and Santa Elena amphibolites with the ophiolite remain unclear. These amphibolites may be part of the Palaeozoic metamorphic basement of the Central Cordillera,

older than the ophiolite (Botero, 1963; Rodríguez et al., 2005) or they may represent the upper part of the ophiolite (Restrepo, 1986; Pereira and Ortíz, 2003).

In this paper, we present new field, mineralogical and geochemical evidence, combined with geochronological and isotopic data of metamafic rocks of the Medellín area. We report for the first time the occurrence of plagiogranites and metasomatites within the El Picacho Metagabbro unit and the zircon U-Pb age of one sample of the plagiogranites. The purposes of the study are to constrain the origin and metamorphic evolution of the different metamafic rock types and their tectonic significance. We also discuss the possibility that the three metamafic units, the El Picacho Metagabbro, the Boquerón Metagabbro and the Santa Elena Amphibolite, represent different dismembered parts of the Aburrá Ophiolite.

4.2. Geological context

The Central Cordillera of the Colombian Andes comprises the area between the Magdalena inter-Andean valley, to the east, and the Cauca inter-Andean valley, to the west. It consists of four lithotectonic belts, one located east of the Otú-Pericos Fault and the three remaining to the west of the fault (Figure 1a). The first unit corresponds to the eastern flank of the Cordillera and represents part of the Precambrian sialic basement of the Northern Andes (Restrepo and Tousaint, 1988). The three western lithotectonic belts are separated from each other by different segments of the Romeral Fault System (Maya and González, 1995) and are, from east to west: (i) the Central Cordillera Polymetamorphic Complex (Restrepo and Toussaint, 1982) also known as the Cajamarca Complex (Maya and González, 1995), (ii) the Quebradagrande Complex (Botero, 1963; Maya and González, 1995) and (iii) the Arquia Complex (Restrepo and Toussaint, 1975; Maya and González, 1995) (Figure 1a). The polymetamorphic belt is composed mainly by Paleozoic to Early Mesozoic continental rocks (Restrepo et al., 1991). The two remaining belts are made up of oceanic rocks forming the Cretaceous Quebradagrande Complex (e.g. González, 1980) and the Palaeozoic (McCourt et al. 1984) or Cretaceous (Restrepo and Toussaint, 1975) Arquía Complex.

The study area is located in the northwestern sector of the Central Cordillera in the Central Cordillera Polymetamorphic Complex. It comprises the eastern and northern part of the Aburrá Valley in which the city of Medellín is located (Figure 1)

The main lithological units recognized in the Medellín region are (Figure 1b) (1) Palaeozoic - Triassic metamorphic rocks, including gneisses, migmatites, granulites and amphibolites; (2) ultramafic and mafic bodies that may represent parts of an ophiolite segment of possible Triassic age; (3) Cretaceous plutonic rocks of mainly intermediate to acid

composition; and (4) Neogene detrital sedimentary cover. The metamorphic rocks were originally grouped into the Ayurá-Montebello Group (Botero, 1963) which is also included in the Central Cordillera Polymetamorphic Complex (Figure 1b). Rodríguez et al. (2005) mapped them as part of the El Retiro and Cajamarca complexes. They have been considered to be part of the Palaeozoic basement of the Cordillera. With the exception of the amphibolites, all metamorphic bodies were derived from continental crust sources (Ordóñez-Carmona, 2001; Vinasco et al., 2006). The last orogenic metamorphic event recorded in these units is attributed to a Permian - Triassic continent-continent collision, (Toussaint and Restrepo, 1976; Vinasco et al., 2006).

Studies on the amphibolites from this region indicated some important differences between them which imply that not all belong to the same geological unit. The main amphibolite bodies of the region are the Medellín Amphibolite and associated paragneiss (Restrepo and Toussaint, 1984) of unknown age; the Caldas Amphibolite of Devonian age (Restrepo and Toussaint, 1977) and the El Retiro Amphibolite of Triassic age (Restrepo, 1986, Ordóñez-Carmona, 2001, Vinasco et al. 2001). The last two amphibolite units are not discussed in this paper.

Recent studies have differentiated several subunits within the former Medellín Amphibolite and associated paragneiss as follows: (1) El Picacho Metagabbro, the Boquerón Amphibolite and the Las Peñas Paragneiss (Correa and Martens, 2000); (2) the Santa Elena Amphibolite (Restrepo, 2005); (3) the Sajonia mylonitic Gneiss and the La Ceja Gneiss (Rodríguez et al., 2005) (Figure 1b). According to Correa and Martens (2000) and Correa et al. (2005) the metabasic units differ in the compositional and metamorphic characteristics.

The ultramafic bodies of the area were grouped into the Medellín Dunite (Restrepo and Toussaint, 1984) or the Medellín Ultramafic Massif in this study (Figure 1b) and were early interpreted as part of the mantle section of an ophiolite (Restrepo and Toussaint, 1973; Alvarez, 1982). According to Correa and Martens (2000), the Aburrá Ophiolitic Complex consists of such ultramafic rocks as well as of mafic rocks of the El Picacho Metagabbro. The ophiolite was possibly formed in a suprasubduction environment (Correa and Nilson, 2003) such as a back-arc basin (Proenza et al., 2004; Correa and Nilson, submitted).

The ultramafic bodies lie along a faulted contact with the amphibolites of the Santa Elena unit and the gneisses of the Sajonia Mylonitic Gneiss. Part of the metamafic units was intruded by the Jurassic La Iguaná Orthogneiss (Correa et al., 2005b). All the units mentioned above were intruded by Cretaceous plutons (e.g. the Antioquean Batholith, the Ovejas Tonalite, the Altavista Stock and the San Diego Gabbro).

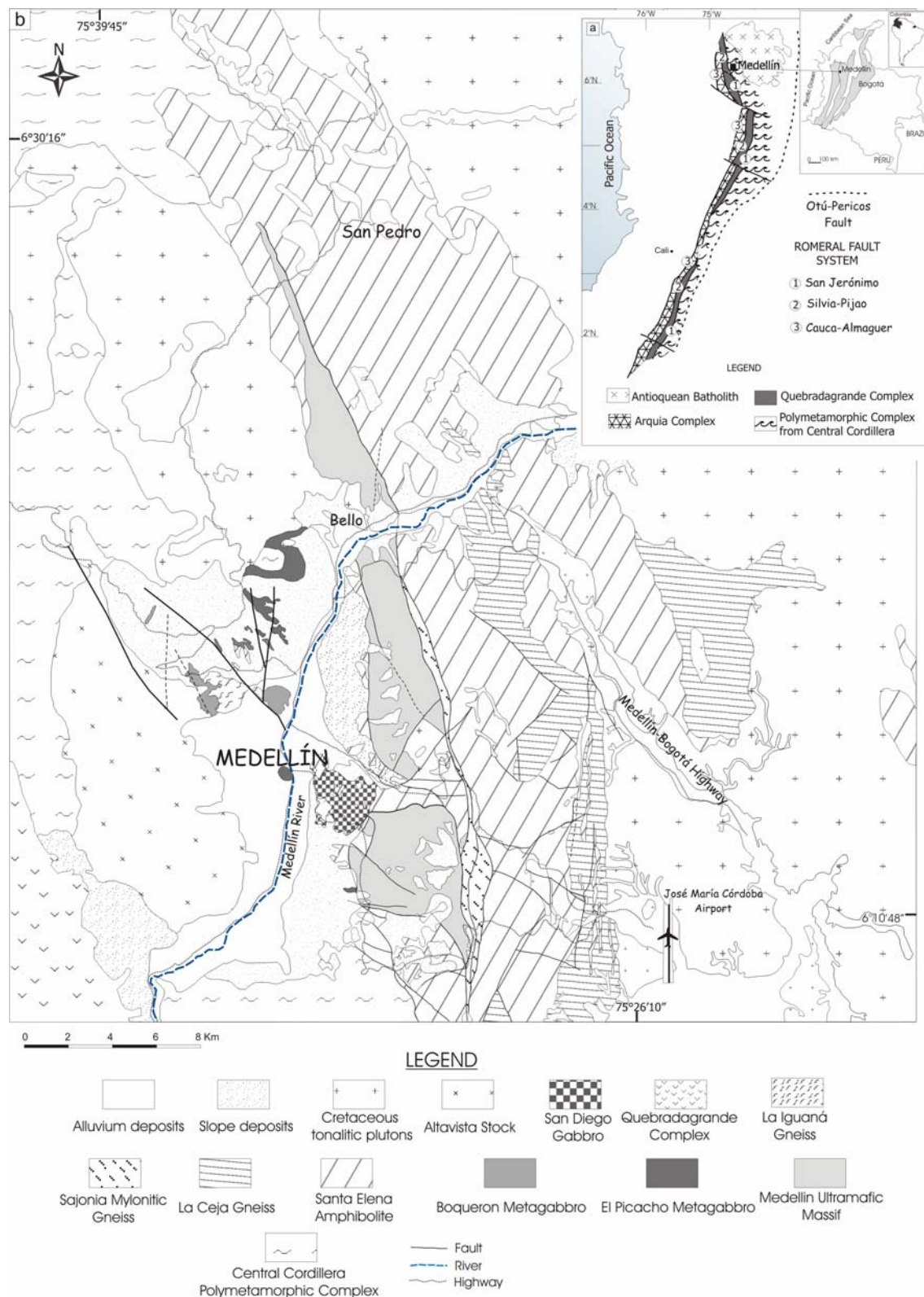


Figure 1. (a) Geological sketch of the Colombian Central Cordillera showing the main lithotectonic belts (Modified from Nivia et al. 1996). (b) Geological map of the Medellín area showing the various metamorphic bodies. Modified from: Botero (1963), Rendón (1999), Correa and Martens (2000), Rodríguez et al. (2005).

4.3. Nomenclature, field occurrence and petrography

The local names for the studied units are: the El Picacho Metagabbro and associated plagiogranite, the Boquerón Metagabbro and the Santa Elena Amphibolite.

This work is focused on metagabbroic and plagiogranitic rocks, however representative samples of the amphibolites were also investigated. The samples labeled as CMK were previously sampled by A.M. Correa and U. Martens in 1999 and 2000.

4.3.1. El Picacho Metagabbro

The name El Picacho Metagabbro unit is used in this study in the same sense as in Correa and Martens (2000). The main outcrops of the El Picacho metagabbro are shown in Figures 1b and 2. In addition to the exposures of gabbroic rocks described by Correa and Martens (2000), other small occurrences have also been recognized. They occur in the El Volador hill (AC06); the northern part of the study area, north of Bello (AC22), in the vicinities of San Pedro (AC58, AC59) and in the Loma de Menezes sector (AC78). With the exception of the El Volador hill samples, in all these exposures metagabbro occurs in close spatial association with ultramafic rocks. Leucocratic rocks, occurring within the metagabbros and classified as both plagiogranite and metasomatite, were recognized for the first time in the Picacho sector (AC32). Felsic veinlets also occur in the metagabbros of the El Nutibara Hill (AC05).

4.3.1.1. Metagabbros

These rocks locally display a discrete igneous layering, consisting of alternance of mesocratic and leucocratic bands. In some localities, modal layering and grading occur and suggest that these gabbros represent cumulates. A discontinuous foliation overprints the magmatic layering, parallel or slightly oblique to it. Both layering and foliation are displaced by numerous shear zones.

Deformation is heterogeneous and characterized by the alternance of high and low strain zones even in outcrops. According to the intensity of shearing and recrystallization, several rock types can be defined such as undeformed metagabbros (Figure 3A, B), flaser gabbros (Figure 3C), mylonites and highly sheared gabbros.

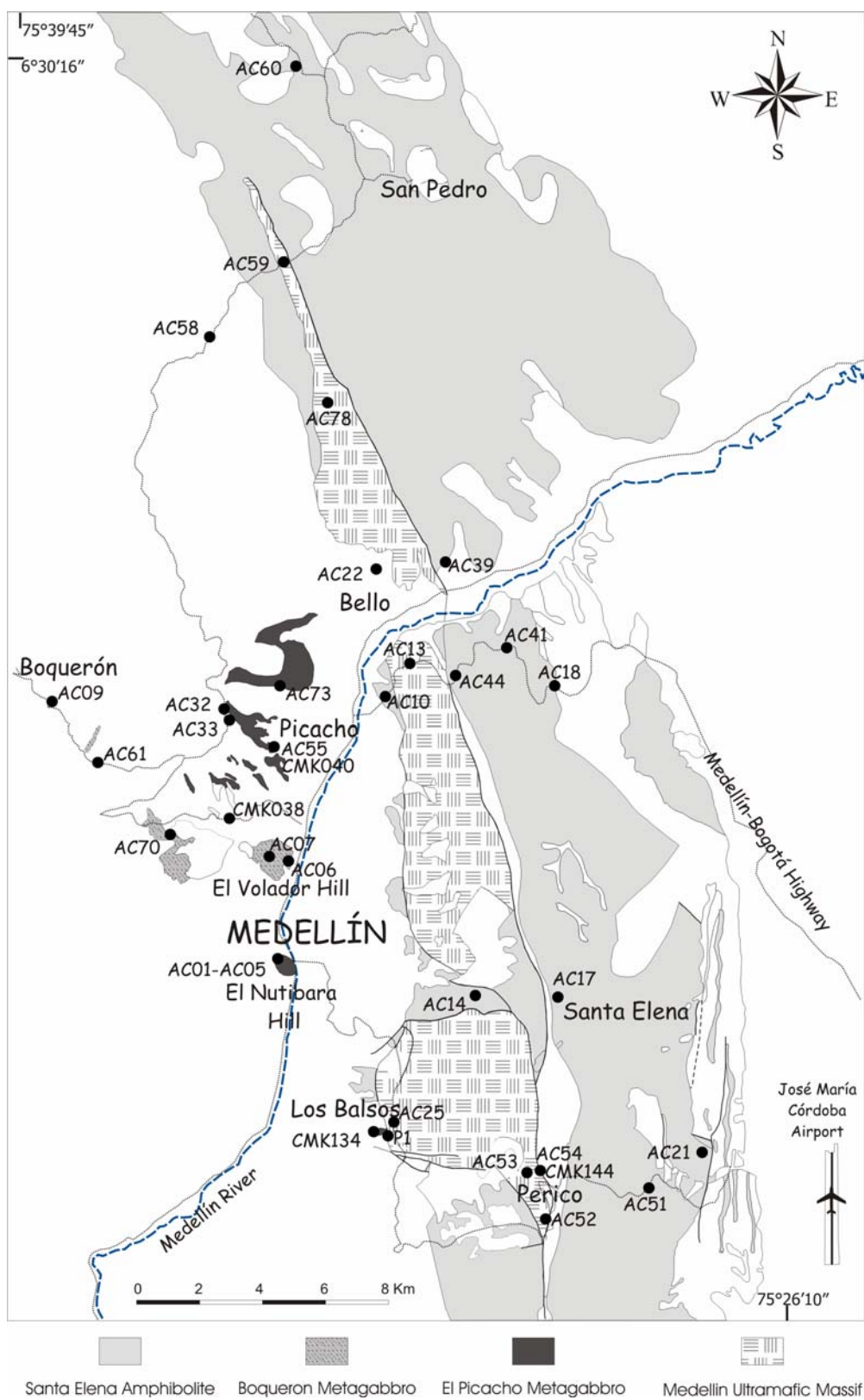


Figure 2. Sketch map of the occurrences of metamorphic-rocks in the Medellín area, showing the location of the sampling sites.

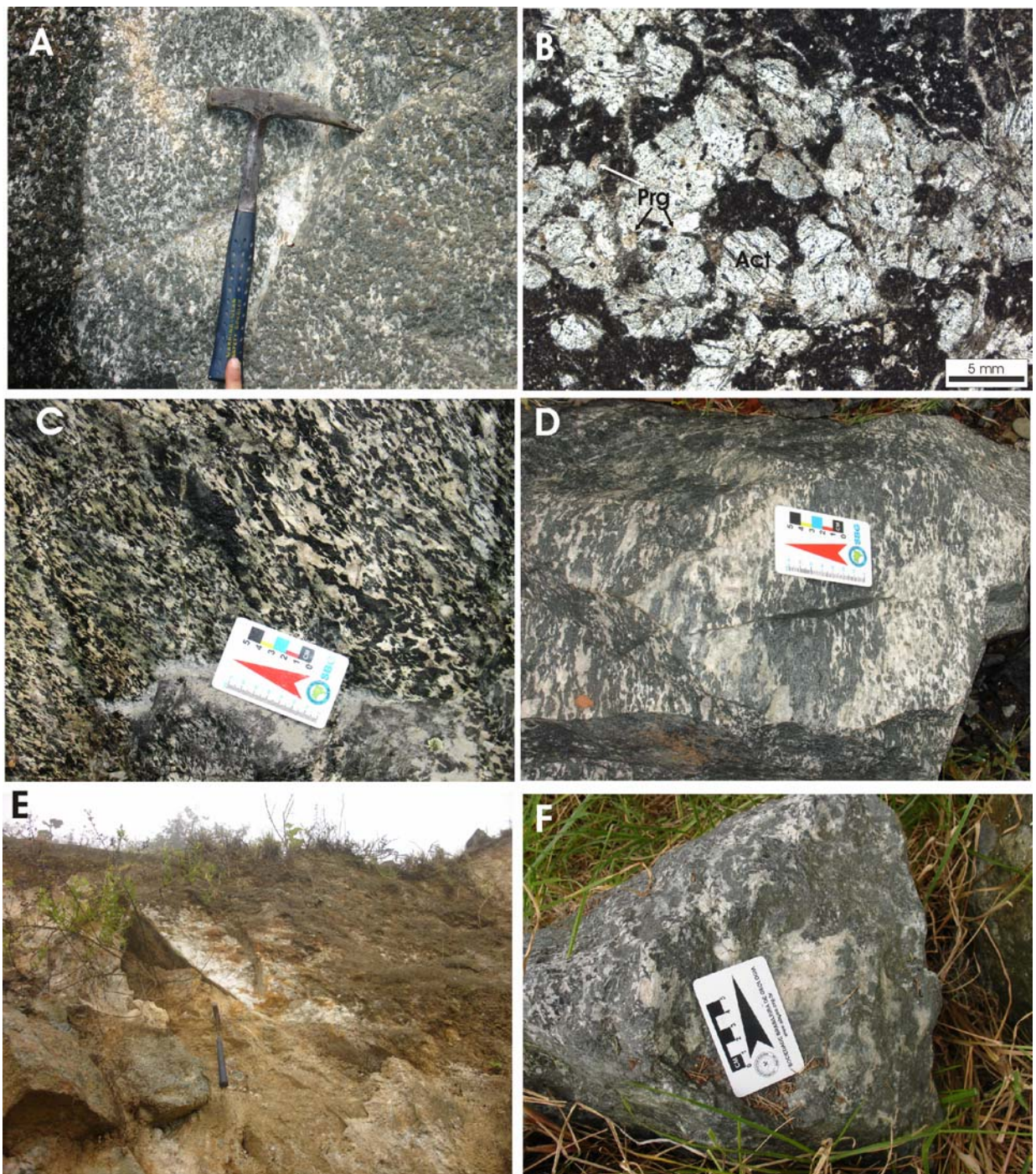


Figure 3. Mesoscopic and microscopic features of the El Picacho metagabbros and other associated rocks. A. Undeformed metagabbro showing igneous structure. B. Cumulus-textured gabbro; light crystals: actinolite-Act (former clinopyroxene), dark areas: saussuritized plagioclase, small brown grains: pargasite-Prg. C. Flaser gabbro. D. Deformed gabbro with plagiogranite segregations. E. Plagiogranite dike. F. Pale pink rodingite patch within a metagabbro.

Undeformed gabbros exhibit fine-to coarse-grained gabbroic texture and also display a discrete compositional micro layering. Some samples show preserved cumulus textures (Figure 3B). In most of the studied specimens the igneous mineral assemblage was almost totally recrystallized, however they preserve the original gabbro textures. Microfractures occasionally filled with clinozoisite, are common. The mylonites vary from protomylonites to ultramylonites, depicting mylonitic lineation and foliation.

The primary magmatic mineralogy probably consisted of clino- and orthopyroxene, plagioclase, olivine and magmatic brown amphibole. The metamorphic mineralogy consists of several types of amphiboles, clinopyroxene neoblasts, recrystallized plagioclase, clinozoisite, zoisite, epidote and chlorite. The magmatic clinopyroxene has been totally replaced by green amphibole and fine-grained recrystallized clinopyroxene. Plagioclase locally exhibits relict magmatic features such as Carlsbad twinning, but it normally shows recrystallization in polygonal subgrains with albite twinning. Plagioclase may be intensely saussuritized (Figure 3B). In some samples pyroxene (now amphibole) and plagioclase show graphic intergrowth, suggesting cotectic crystallization of the two phases.

The highly deformed rocks do not preserve relict structures or textures. They consist of fine-grained amphibole aligned parallel to shear bands, with recrystallized and saussuritized grains of plagioclase. Chlorite occurs in bands alternating with amphibole-rich bands or as small flakes crosscutting the foliation.

The mylonitized rocks that occur near ultramafic outcrops in the Perico sector (AC54 and CMK144) consist of bands made up by amphibole probably corresponding to former pyroxenitic bands, alternating with mylonitic amphibolite bands which probably represent previous gabbroic portions.

4.3.1.2 Plagiogranites

The plagiogranite often occurs as light-colored patches (Figure 3D), pockets and centimetric to metric dikes (Figure 3E) and are moderately to highly altered. In the Nutibara hill, the plagiogranite occurs in veinlets oblique to the foliation of the mafic rock. The plagiogranite consists of plagioclase, quartz and minor amphibole, rutile and zircon. The plagiogranite of the El Picacho sector are inequigranular rocks made of coarse-grained plagioclase and quartz, lacking an evident igneous structure. Plagioclase is anhedral and is locally altered to clinozoisite. Quartz exhibits undulose extinction and subgrains. Rutile exhibits alteration rim probably made up by leucoxene. Amphibole is light-green and usually occurs as fibrous aggregates. On the other hand, plagiogranite of the Nutibara hill consists of

fine-grained quartz and plagioclase. Textural relationships suggest that the veinlets were developed after the deformation of the mafic rock and before the static recrystallization responsible for the fibrous amphiboles.

4.3.1.3 Garnet-epidote-plagioclase metasomatite (or Rodingite-like rock)

Rodingite-like rocks are white to light-pink, aphanitic rocks, forming sparse centimetric patches within the metagabbros (Figure 3D). It consists of plagioclase and aggregates of clinozoisite, zoisite, chlorite and garnet.

4.3.2 Boquerón Metagabbro

The name *Boquerón Metagabbro* is proposed in this work to substitute *Boquerón amphibolite* of Correa and Martens (2000) and Correa et al. (2005). This is based on the fact that these rocks typically exhibit igneous primary gabbroic macrostructures as discussed below.

In this research we have been able to establish that the metagabbros outcropping to the west of the La Iguaná Gneiss are of the Boquerón type. The Boquerón metagabbro is intruded by granitoids of the La Iguaná Gneiss, as pointed out by Rodríguez and Sanchez (1987) and Rendón (1999). Both units were mylonitized along the intrusive contact. Rocks from both the El Picacho and Boquerón Metagabbros occur in the El Volador Hill but the precise spatial distribution and the relationships between them are not clear.

El Boquerón metagabbros tend to be isotropic, contain pegmatitic portions and lack magmatic layering (Figure 4a). These gabbros may be classified into two groups according to the degree of deformation: (i) slightly deformed gabbros and (ii) gabbroic mylonites (Figure 4B). The slightly deformed gabbros preserve igneous granular hypidiomorphic texture and display evidence of shearing and significant static recrystallization. Primary magmatic mineralogy consists of clinopyroxene, plagioclase, variable proportions of ilmenite (~1 vol% to ~5 vol%) and apatite (trace to ~1 vol%) and minor zircon. Only small relicts of magmatic clinopyroxene are preserved. Metamorphic mineralogy consists of amphibole, recrystallized polygonal plagioclase, titanite, clinozoisite, zoisite and quartz. Three types of amphibole were recognized: (1) green to brownish replacing magmatic clinopyroxene, (2) colorless to pale-green replacing pyroxene or in rims around green amphibole, and (3) blue-green fibrous amphibole in rims around other amphiboles and in disordered aggregates in the rock. Plagioclase is variably recrystallized and altered. In some samples it shows polygonal texture and in others the primary plagioclase grains were replaced by subgrains and exhibits a high

degree of saussuritization. Mylonitized metagabbros vary from protomylonite to ultramylonite and consist of amphibole rich bands alternating with plagioclase-rich bands with quartz ribbons, ilmenite, titanite and apatite. Amphibole is oriented and plagioclase is highly polygonized which probably corresponds to early recrystallized porphyroclasts previous to mylonitization.



Figure 4. Macroscopic appearance of Boquerón metagabbros. A. Varitextured gabbro showing isotropic and pegmatitic structure. B. Mylonitized gabbro.

4.3.3 Santa Elena Amphibolite

This unit has been studied by many previous workers (Botero, 1963; Restrepo and Toussaint, 1984; Restrepo, 1986; Correa and Martens, 2000, Rodríguez et al., 2005, Restrepo, 2005). The only new occurrence of a garnet amphibolite reported in this study is exposed on the Medellín-Bogotá Highway approximately 300 m east of the contact between peridotites and amphibolites. The studied samples correspond to amphibolite and garnet amphibolites. Two types of amphibolites are recognized: the first exhibits a nematoblastic texture (AC39, Figure 2), and the second presents granoblastic texture (AC51). Compositional banding formed by the alternance of amphibole-rich and plagioclase-rich bands is recognized locally. Amphibolites are formed by green to brownish amphibole, plagioclase, and ilmenite, titanite, apatite, zircon as well as minor pyrite, chalcopyrite and pyrrhotite. Green amphibole defines the nematoblastic texture in which plagioclase is interstitial. Plagioclase is fresh in amphibole-rich bands and is highly saussuritized in plagioclase-rich bands. Titanite was formed at the expense of ilmenite. Brown amphibole in the granoblastic amphibolite is darker than in other amphibolites.

Garnet amphibolite exhibits nematoblastic to porphyroblastic textures with garnet porphyroblasts surrounded by plagioclase and amphibole; it also contains ilmenite, minor

amounts of quartz, rutile and zircon. Xenomorphic garnet porphyroblasts are medium-grained and mostly undeformed. They contain plagioclase, amphibole and rutile inclusions, indicating that they grew at the expense of the main assemblage.

4.4 Analytical Methods

4.4.1. Mineral chemistry

Mineral electron microprobe analyses were carried out at the Geosciences Institute of the University of Brasília and at the Laboratoire de Tectonophysique, University of Montpellier II. At the University of Brasília, analyses were performed using a CAMECA SX-50 microprobe operating at 15 kV accelerating voltage and 20 nA sample current. The beam size varied between 2 and 5 μm and the counting time 10 s. In Montpellier the data were obtained using a CAMECA SX-100 microprobe operating at 20 kV, 10 nA, beam size of 1-5 μm and counting time between 10 and 50 s.

Total iron was measured as FeO. The Fe^{3+} for amphibole was calculated from microprobe analyses following the recommendations of the I.M.A.C. Subcommittee on Amphiboles (Leake et al., 1997). Fe^{3+} content of garnet and ilmenite was calculated according to the charge balance equation of Droop (1987).

The samples analyzed in Brasilia were AC32A, AC33C, AC41A, AC44A, AC59A, CMK38B, CMK040A, CMK040D and CMK144 and those analyzed in Montpellier were AC25, AC51, AC61T and CMK38B.

4.4.2. Litogeochimistry

Only fresh samples were used for the major and trace elements and Sr-Nd isotope geochemistry. Sample preparation was carried out at the Geochronology Laboratory of the Geosciences Institute of the University of Brasília. Samples were pulverized in a tungsten carbide crushing equipment to less than 150 mesh. Whole-rock geochemical analyses were carried out at the ACME Analytical Laboratories Ltd. (Canada) using the 4A&B package. For major and most part of the trace elements, lithium metaborate/tetraborate fusion and subsequent dilute nitric acid digestion was used. For base metals (Cu, Ni, Pb, Zn) a sample aliquote was digested in aqua regia. Major elements and Sc were determined by inductively coupled plasma-emission spectrometry (ICP-OES) and all other trace elements were analyzed by inductively coupled plasma-mass spectrometry (ICP-MS). The following elements were additionally analyzed in a metagabbro sample: P, Hf, Nb, Ta, Cs, Rb, La, Th. These elements were determined using the package 1T-MS by ICP mass spectrometry following a 4-acid

digestion. Analytical methods are reported in the ACME web page (www.acmelab.com). Detection limits for elements are given in Table 5.

4.4.3. *U-Pb procedures*

Zircon concentrates were extracted from ca. 1 kg rock sample, using conventional gravimetric (DENSITEST®) and magnetic (Frantz isodynamic separator) techniques at the Geochronology Laboratory of the University of Brasília. Final purification was achieved by hand picking, using a binocular microscope.

Zircon fractions were dissolved in concentrated HF and HNO₃ (HF:HNO₃ = 4:1) using microcapsules in Parr-type bombs. A mixed ²⁰⁵Pb-²³⁵U spike was used. Chemical extraction followed standard anion exchange technique, using Teflon microcolumns, following the procedures modified from Krogh (1973). Pb and U were loaded together on single Re filaments with H₃PO₄ and Si gel, and isotopic analyses were carried out on a Finnigan MAT-262 multi-collector mass spectrometer equipped with secondary electron multiplier - ion counting, at the Geochronology Laboratory of the University of Brasília. Procedure blanks for Pb, at the time of analyses, were better than 10 pg. PBDAT (Ludwig 1993) and ISOPLOT-Ex (Ludwig 2001) was used for data reduction and age calculation. Errors for isotopic ratios shown in Table 7 are 2 σ .

4.4.4. *Sr-Nd procedures*

Sr-Nd isotopic analyses followed the method described by Gioia and Pimentel (2000) and were carried out at the Geochronology Laboratory of the University of Brasília. Nd and Sr isotopic analyses and Nd, Sm, Sr concentrations were analyzed on the same sample powder using a mixed ¹⁵⁰Nd-¹⁴⁹Sm spike. Rb and Sr concentrations were determined by inductively coupled plasma-mass spectrometry (ICP-MS) in the ACME Lab. Whole rock powders (ca. 50 mg for felsic rocks and ca. 80 mg for mafic rocks) were mixed with ¹⁴⁹Sm-¹⁵⁰Nd spike solution and dissolved in Savillex capsules. Sm and Nd extraction of whole-rock samples followed conventional cation exchange techniques, using Teflon columns containing LN-Spec resin (HDEHP - diethylhexil phosphoric acid supported on PTFE powder). Sm and Nd samples were loaded on Re evaporation filaments of double filament assemblies and the isotopic measurements were carried out on a multi-collector Finnigan MAT 262 mass spectrometer in static mode. Uncertainties for Sm/Nd and ¹⁴³Nd/¹⁴⁴Nd ratios are better than $\pm 0.2\%$ (1 σ) and $\pm 0.005\%$ (1 σ); respectively, based on repeated analyses of international rock standards BHVO-1 and BCR-1. ¹⁴³Nd/¹⁴⁴Nd ratios were normalized to ¹⁴⁶Nd/¹⁴⁴Nd of 0.7219

and the decay constant used was 6.54×10^{-12} a-1. T_{DM} values were calculated using DePaolo's (1981) model. Measured Sr isotopic ratios were normalized to $^{86}\text{Sr}/^{88}\text{Sr} = 0.1194$. Repeated measurements of the NBS 987 Sr standard resulted in $^{87}\text{Sr}/^{86}\text{Sr} = 0.710212 \pm 0.000036$ (2σ).

4.5. Mineral chemistry

4.5.1. Amphibole

Amphibole has been classified according to petrographic and compositional features. Representative amphibole compositions of the different metabasites are given in Table 1.

4.5.1.1. El Picacho metagabbros

The metagabbros contain five types of amphibole, four of them occur in almost all the analyzed samples, and one of them was identified in just one sample. The four types (Type I-Type IV) of amphibole are: red-brown to brown, green, colorless to pale green, and green-blue amphiboles. Red-brown and brown amphiboles occur in small grains within the green and pale green amphibole grains or among pale green amphibole aggregates. Colorless to pale green and green amphibole usually replaces pyroxene, whereas blue-green amphibole is fibrous, often forming rims around the previous two types. Pale brown amphibole of the Perico mylonite (Type V) occurs as oriented porphyroclasts surrounded by plagioclase and locally by small recrystallized clinopyroxene.

Type I. Red-brown amphibole occurs in metagabbros of the El Tesoro sector which are located close to wehrlites that also contain a similar amphibole. Brown amphibole occurs in metagabbros of all localities. Red-brown amphibole (Type Ia) is titanian pargasite ($\text{Ti} \sim 0.47$ a.p.f.u.), whereas the brown amphibole (Type Ib) is pargasite ($0.21 < \text{Ti} < 0.23$ a.p.f.u.) according to the classification of Leake et al. (1997) (Figure 5a). They exhibit high Al^{IV} contents (1.60-1.95 a.p.f.u.) and the $(\text{Na}+\text{K})_A$ content is 0.59 in red-brown amphiboles and 0.51-0.53 a.p.f.u. in brown amphiboles. Magnesium number [$\text{Mg}\# = \text{Mg}/(\text{Mg}+\text{Fe}^{2+})$] ranges from 67 to 72.

Type II. Green amphibole mostly exhibits compositions between pargasite and magnesiohornblende with subsidiary magnesiohastingsite compositions (Figure 5a, b). Pargasite and magnesiohastingsite show high Al^{IV} and $(\text{Na}+\text{K})_A$ contents (1.67-1.74 and 0.56-0.58 a.p.f.u., respectively). Magnesiohornblende presents lower Al^{IV} and $(\text{Na}+\text{K})_A$ contents

(0.58-0.68 and 0.11-0.12 a.p.f.u., respectively). Both types of amphibole have low Ti content (0.03-0.05 a.p.f.u.); Mg# ranges from 76 to 82.

Type III. Colorless to pale green amphibole is Al-poor actinolite (Figure 5b) and exhibits low contents of Al^{IV} and (Na+K)_A with values ranging between 0.1 and 0.5 and 0.01 and 0.1 a.p.f.u. respectively. Ti contents are also low (less 0.03 a.p.f.u.). In one sample (AC59A) amphibole with tremolitic composition was found.

Type IV. Green-blue amphibole exhibits compositions of pargasite and magnesiohornblende (Figure 5a, b). Pargasite has high Al^{VI} and (Na+K)_A contents (1.70-1.82 and 0.59 a.p.f.u. respectively). Some of the magnesiohornblende is Al-rich with high contents of Al^{VI} and (Na+K)_A (1.41-1.42 and 0.46 a.p.f.u., respectively) and some tend to be Al-poor, showing lower contents of Al^{VI} and (Na+K)_A (0.9-1.28 and 0.19-0.31 a.p.f.u., respectively). All these amphiboles are titanium poor with contents that range between 0.005 and 0.023 a.p.f.u. Mg# ranges from 56 to 72.

Type V. Pale brown amphibole of the Perico mylonite is classified as magnesiohornblende (Figure 5b). Al^{IV} content varies from 0.82 to 0.90 a.p.f.u., (Na+K)_A is low (0.27 – 0.31 a.p.f.u.) and Ti content is of 0.03 a.p.f.u. Mg# exhibit a narrow variation between 83 and 86.

4.5.1.2. Boquerón metagabbros

In the Boquerón metagabbros two types of amphibole are recognized: green-brownish and colorless to pale green.

Type I. Green-brownish amphibole corresponds to magnesiohornblende (Figure 5c). However there are compositional differences between the two analyzed samples. Sample CMK38B exhibits Al^{IV} contents (0.76-1.24 a.p.f.u.); (Na+K)_A is low (0.18 - 0.33 a.p.f.u.); Ti content is 0.10 – 0.11 a.p.f.u. and Si content ranges from 6.80 to 6.93 a.p.f.u.; Mg# ranges from 70 to 75. Sample AC61T exhibits slightly higher Al^{IV} and (Na+K)_A contents (1.23-1.34 and 0.33-0.36 a.p.f.u., respectively), lower contents of Ti and Si (0.07- 0.09 and 6.67-6.76 a.p.f.u., respectively), and lower Mg# values (55-57).

Type II. Colorless to pale green amphibole is actinolite (Figure 5c) characterized by low Al^{IV} contents (0.04-0.32 a.p.f.u.), (Na+K)_A ranging from 0.002 to 0.08 a.p.f.u. and Ti values from 0.002 to 0.010 a.p.f.u..

Table 1. Representative microprobe analyses of amphibole.

Type	El Picacho Metagabbro								Boquerón Metagabbro				Santa Elena Amphibolite				
	Ia AC25	Ib CMK040 A	Ib AC32A	II AC33C	III CMK040 A	IV CMK040 A	IV CMK40D	V CMK144 B	II	II	II	III	AC41	AC44	AC44	AC51	AC51
Sample	Ti-Prg	Prg	Prg	Mg-Hbl	Act	Prg	Mg-Hbl	Mg-Hbl	CMK38B	CMK38B	AC61T	CMK38B	Mg-Hbl	Mg-Hbl	Ts	Mg-Hbl	Mg-Hbl
Name	Ti-Prg	Prg	Prg	Mg-Hbl	Act	Prg	Mg-Hbl	Mg-Hbl	Mg-Hbl	Mg-Hbl	Mg-Hbl	Act	Mg-Hbl	Mg-Hbl	Ts	Mg-Hbl	Mg-Hbl
SiO ₂	41.44	43.06	43.19	51.07	51.64	42.45	48.40	49.60	48.28	49.95	45.72	53.97	45.87	46.48	43.84	45.02	47.09
TiO ₂	4.31	1.86	0.47	0.37	0.21	0.08	0.17	0.31	1.02	0.49	0.83	0.07	0.73	0.77	0.65	1.59	1.01
Al ₂ O ₃	14.12	13.41	14.84	6.44	4.31	14.52	8.86	8.13	9.45	6.52	10.74	2.80	10.35	10.21	14.43	9.98	8.58
Cr ₂ O ₃	0.64	0.34	0.84	0.07	0.09	0.19	0.03	0.17	0.09	0.07	0.01	0.01	0.04	0.05	0.02	0.03	0.03
FeO	9.71	10.59	8.01	10.56	11.24	16.19	12.47	6.85	11.67	10.20	16.46	11.56	14.92	15.86	16.95	17.89	16.81
MnO	0.17	0.12	0.16	0.23	0.26	0.22	0.12	0.10	0.19	0.22	0.26	0.26	0.18	0.25	0.18	0.38	0.34
MgO	12.45	12.87	14.56	15.49	15.10	9.73	13.74	17.35	14.20	15.46	10.28	15.94	11.67	11.27	9.45	9.87	10.95
CaO	12.14	11.13	11.36	11.59	12.36	11.84	11.04	12.17	10.71	12.49	11.80	12.63	11.86	10.45	9.78	11.30	11.39
Na ₂ O	2.13	2.20	2.46	0.92	0.43	2.10	1.20	1.34	1.42	0.90	1.32	0.34	1.66	0.96	1.38	1.62	1.35
K ₂ O	0.46	0.30	0.16	0.06	0.04	0.22	0.13	0.09	0.07	0.07	0.08	0.02	0.24	0.26	0.39	0.09	0.08
Total	97.58	95.86	96.03	96.81	95.67	97.53	96.16	96.10	97.10	96.36	97.51	97.60	97.51	96.55	97.06	97.78	97.65
<i>Based on 23 O</i>																	
Si	6.060	6.343	6.265	7.323	7.538	6.298	7.044	7.092	6.931	7.244	6.757	7.722	6.751	6.856	6.455	6.691	6.943
AlIV	1.940	1.657	1.735	0.677	0.462	1.702	0.956	0.908	1.069	0.756	1.243	0.278	1.249	1.144	1.545	1.309	1.057
AlVI	0.493	0.670	0.802	0.411	0.280	0.835	0.563	0.462	0.529	0.358	0.627	0.194	0.546	0.631	0.960	0.440	0.434
Ti	0.474	0.206	0.051	0.040	0.023	0.009	0.019	0.033	0.110	0.054	0.092	0.008	0.081	0.085	0.071	0.178	0.112
Cr	0.074	0.040	0.096	0.007	0.010	0.022	0.004	0.019	0.010	0.008	0.002	0.001	0.005	0.006	0.002	0.003	0.004
Fe ³⁺	0.000	0.214	0.304	0.224	0.006	0.266	0.347	0.154	0.386	0.088	0.191	0.063	0.176	0.338	0.457	0.272	0.251
Fe ²⁺	1.188	1.096	0.674	1.048	1.366	1.754	1.182	0.668	1.027	1.152	1.853	1.322	1.667	1.633	1.651	1.964	1.833
Mn	0.021	0.015	0.019	0.028	0.032	0.028	0.015	0.012	0.023	0.027	0.033	0.032	0.023	0.031	0.022	0.047	0.042
Mg	2.715	2.827	3.148	3.312	3.286	2.153	2.981	3.699	3.038	3.342	2.266	3.401	2.560	2.477	2.075	2.186	2.407
Ca	1.902	1.756	1.765	1.781	1.933	1.881	1.721	1.864	1.647	1.940	1.868	1.935	1.870	1.651	1.542	1.799	1.800
Na	0.605	0.628	0.690	0.255	0.123	0.603	0.338	0.370	0.395	0.252	0.379	0.095	0.473	0.274	0.393	0.467	0.386
K	0.086	0.056	0.029	0.011	0.008	0.041	0.024	0.017	0.012	0.014	0.016	0.003	0.046	0.048	0.073	0.018	0.015
XMg	0.70	0.72	0.82	0.76	0.71	0.55	0.72	0.85	0.75	0.74	0.55	0.72	0.61	0.60	0.56	0.53	0.57

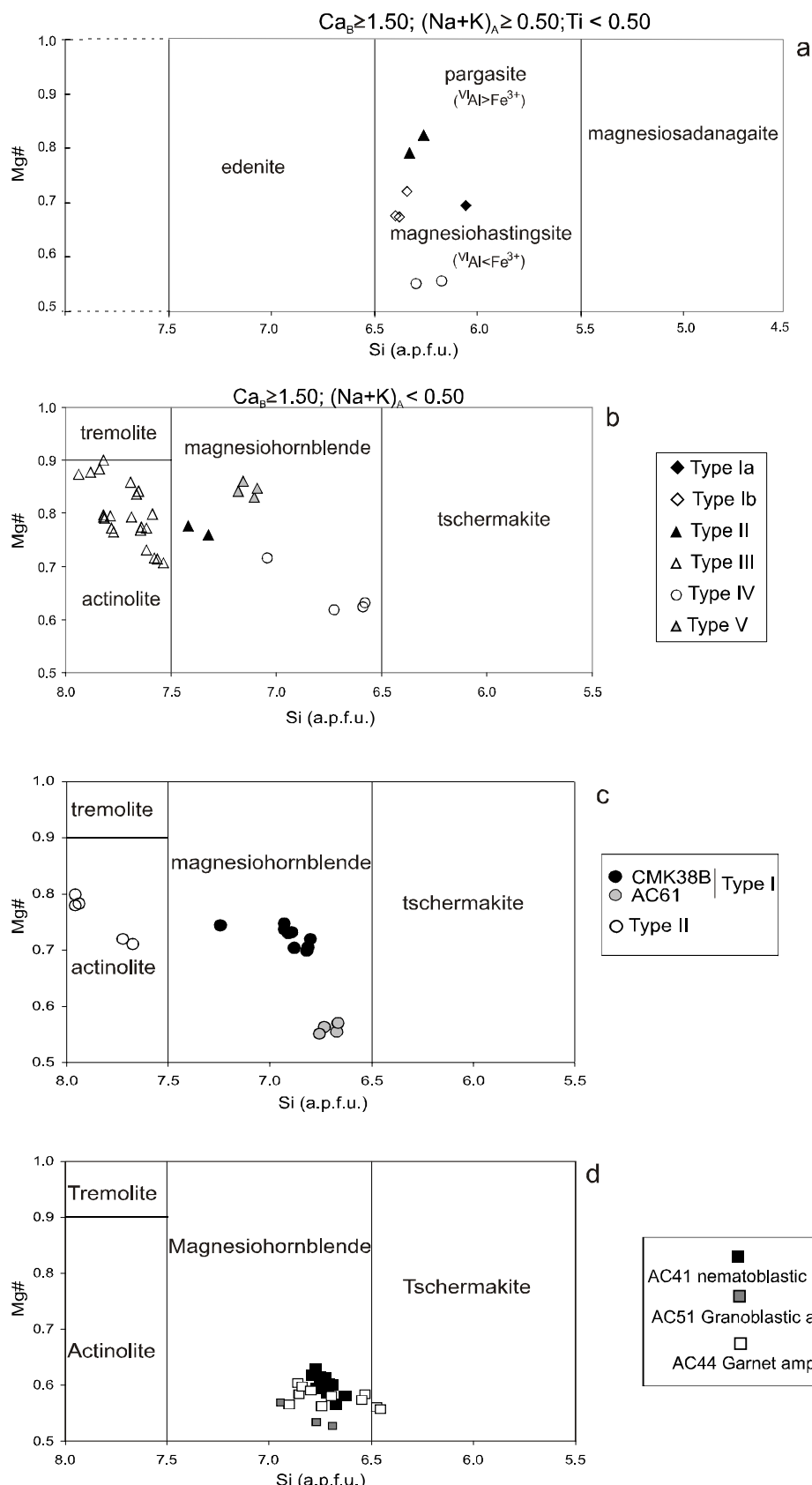


Figure 5. Compositional variations for amphiboles of metamorphic rocks (classification diagram after Leake et al., 1997). (a) and (b) Amphiboles from El Picacho metagabbros. (c) Amphiboles from Boquerón metagabbros. (d) Amphiboles from Santa Elena amphibolites.

4.5.1.3. Santa Elena amphibolites

Amphiboles in nematoblastic and granoblastic amphibolites are classified as magnesiohornblende (Figure 5d) which have Al^{IV} and $(\text{Na}+\text{K})_A$ contents ranging from 1.06 to 1.37 and from 0.28 to 0.49 a.p.f.u., respectively. Granoblastic amphibole exhibits slightly higher Ti contents (0.11-0.16 a.p.f.u.) and lower Mg# values (53-57) when compared with the nematoblastic amphibole (0.06-0.08 a.p.f.u. and 57-63, respectively). Amphibole in garnet amphibolite is mainly magnesiohornblende with subsidiary tschermakite (Figure 5d). Al^{IV} contents range from 1.10 to 1.55 and they exhibit lower $(\text{Na}+\text{K})_A$ and Ti contents (0.13-0.27 and 0.07- 0.11a.p.f.u., respectively).

4.5.2. Plagioclase

Representative compositions of plagioclase are shown in Table 2.

4.5.2.1 El Picacho metagabbros

Plagioclase in El Picacho metagabbros exhibits a wide spectrum of composition. Hydrothermal alteration obliterated the primary textural features of plagioclase, thus the following classification is based only on the compositional characteristics.

Group I. Plagioclase with composition between labradorite and bytownite (An_{60} to An_{89}). Probably corresponds to relict igneous compositions

Group II. Secondary calcic plagioclase with An_{90-96} composition.

Group III. Secondary plagioclase with andesine and labradorite compositions (An_{29-69}).

Group IV. Plagioclase from the Perico mylonite (CMK144) which was completely recrystallized, exhibits homogeneous compositions (Oligoclase An_{27-29}).

4.5.2.2. Boquerón metagabbros

In these rocks the igneous plagioclase corresponds to labradorite, with compositions from An_{50} to An_{67} , whereas the metamorphic plagioclase is oligoclase to andesine (An_{25} to An_{40}).

4.5.2.3. Santa Elena amphibolites

Plagioclase in the nematoblastic and granoblastic amphibolites is andesine (An_{32} to An_{43}). Plagioclase composition in the garnet amphibolite ranges from oligoclase (An_{24-27}) to andesine (An_{30-35}).

Table 2. Representative microprobe analyses of plagioclase of the El Picacho Metagabbro, Boquerón Metagabbro and Santa Elena Amphibolite.

Sample	El Picacho Metagabbro									
	AC25	AC33C	CMK40D	CMK40D	CMK40D	CMK040A	CMK40D	CMK40D	AC59A	CMK144
SiO ₂	45.49	46.99	46.74	50.60	53.56	60.00	45.88	45.30	43.66	61.01
TiO ₂	-	0.00	0.00	0.00	0.00	0.00	0.00	0.00	0.00	0.00
Al ₂ O ₃	35.10	34.64	34.83	32.31	30.46	25.00	35.86	36.21	36.28	24.16
Fe ₂ O ₃	0.01	0.01	0.14	0.01	0.08	0.06	0.02	0.16	0.05	0.00
BaO	-	0.00	0.00	0.00	0.00	0.00	0.00	0.00	0.00	0.18
CaO	17.71	16.39	15.59	12.95	11.16	6.16	16.60	17.23	19.51	5.72
Na ₂ O	1.45	1.48	1.71	3.40	4.63	8.26	1.00	0.47	0.34	8.56
K ₂ O	0.01	0.03	0.02	0.04	0.03	0.07	0.01	0.02	0.00	0.04
Total	99.77	99.53	99.08	99.31	99.92	99.55	99.36	99.38	99.83	99.66
Based on 8 O										
Si	2.098	2.157	2.153	2.306	2.414	2.683	2.110	2.086	2.022	2.723
Al	1.908	1.874	1.891	1.736	1.618	1.318	1.944	1.965	1.980	1.271
Fe ³⁺	0.000	0.000	0.005	0.000	0.003	0.002	0.001	0.005	0.002	0.000
Ti	-	0.000	0.000	0.000	0.000	0.000	0.000	0.000	0.000	0.000
Na	0.130	0.132	0.153	0.301	0.404	0.716	0.089	0.042	0.031	0.741
Ca	0.875	0.806	0.769	0.632	0.539	0.295	0.818	0.850	0.968	0.273
K	0.001	0.001	0.001	0.002	0.002	0.004	0.001	0.001	0.000	0.002
Ba	-	0.000	0.000	0.000	0.000	0.000	0.000	0.000	0.000	0.003
X _{An}	87.04	85.84	83.30	67.62	57.03	29.07	90.12	95.22	96.91	26.81
X _{Or}	0.08	0.16	0.12	0.24	0.20	0.40	0.06	0.11	0.00	0.51
X _{Ab}	12.88	14.01	16.58	32.14	42.77	70.52	9.82	4.67	3.09	72.68

Table 2. continued

	Boquerón Metagabbro					Santa Elena Amphibolite				
	CMK38B	CMK38B	AC61T	AC61T	CMK38B	AC41	AC41	AC44	AC44	AC51
SiO ₂	52.09	54.62	56.08	61.03	62.29	57.06	58.72	59.73	62.53	59.82
TiO ₂	0.00	0.00			0.00	0.00	0.00	0.00	0.00	0.00
Al ₂ O ₃	31.60	30.17	28.34	25.02	24.48	27.61	25.57	26.58	24.38	25.86
Fe ₂ O ₃	0.08	0.18	0.09	0.05	0.07	0.04	0.02	0.17	0.08	0.04
BaO	0.00	0.00			0.01	0.00	0.00	0.00	0.15	
CaO	12.80	10.70	10.39	6.37	5.04	9.32	7.43	6.92	5.02	6.77
Na ₂ O	3.45	4.58	5.80	7.96	8.14	6.69	7.77	7.27	8.56	8.00
K ₂ O	0.04	0.04	0.04	0.05	0.03	0.07	0.10	0.05	0.12	0.06
Total	100.06	100.29	100.75	100.49	100.06	100.79	99.61	100.72	100.84	100.56
Based on 8 O										
Si	2.352	2.445	2.504	2.698	2.749	2.543	2.636	2.638	2.748	2.652
Al	1.681	1.592	1.491	1.304	1.273	1.450	1.353	1.384	1.263	1.351
Fe ³⁺	0.003	0.006	0.003	0.002	0.002	0.001	0.001	0.006	0.003	0.001
Ti	0.000	0.000	0.000	0.000	0.000	0.000	0.000	0.000	0.000	0.000
Na	0.302	0.397	0.502	0.683	0.696	0.578	0.676	0.623	0.729	0.688
Ca	0.619	0.513	0.497	0.302	0.238	0.445	0.357	0.327	0.236	0.322
K	0.002	0.002	0.002	0.003	0.002	0.004	0.006	0.003	0.007	0.004
Ba	0.000	0.000	0.000	0.000	0.000	0.000	0.000	0.000	0.003	0.000
X _{An}	67.07	56.24	49.62	30.56	25.45	43.32	34.38	34.35	24.22	31.76
X _{Or}	0.22	0.23	0.23	0.29	0.23	0.37	0.55	0.29	0.94	0.35
X _{Ab}	32.71	43.53	50.15	69.15	74.32	56.31	65.07	65.36	74.84	67.90

4.5.3. Garnet

Representative garnet analyses of garnet amphibolite (AC44) are in Table 3. The complete range of garnet compositions is almandine 59-65 %, pyrope 6-10.5%, grossular 19 - 24.5 % and spessartine 2.5 -12 %. Garnet exhibits a subtle chemical zonation from core to rim in Mg, Mn, Fe and Ca (Table 3).

4.5.4. Ilmenite

Representative ilmenite analyses from amphibolite (AC41) and garnet amphibolite (AC44) are shown in Table 3. Ilmenite in amphibolite consists of ilmenite (94.3-94.8 %), pirofanite (4.5-5 %) and geikelite (0.4-0.6 %). Ilmenite in garnet amphibolite consists of: ilmenite (97.3 %), pirofanite (2.0 %) and geikelite (0.6 %).

Table 3. Representative microprobe analyses of garnet and ilmenite of Santa Elena Amphibolite.

Sample	AC44	Garnet						Ilmenite	
		rim- A	core-B	rim-C	rim-D	core-E	rim-F	AC41	AC44
SiO ₂		38.13	37.48	37.71	37.93	36.84	37.94	0.06	0.04
TiO ₂		0.14	0.77	0.13	0.07	0.15	0.16	52.83	52.80
Al ₂ O ₃		21.25	21.11	20.93	21.08	20.76	21.20	0.01	0.02
Cr ₂ O ₃		0.00	0.01	0.00	0.02	0.00	0.00	0.03	0.01
FeO		27.55	26.17	27.41	27.98	26.82	26.70	43.79	46.02
MnO		3.67	5.25	3.91	3.70	5.37	4.11	2.13	0.95
MgO		1.69	1.48	1.65	1.77	1.42	1.61	0.16	0.17
CaO		8.10	8.04	8.25	7.73	7.98	8.52	0.16	0.01
Total		100.54	100.31	100.00	100.28	99.35	100.24	99.16	100.02
<i>Based on 12 O</i>									
Si		3.022	2.987	3.011	3.019	2.980	3.017	0.003	0.002
Al		1.985	1.983	1.970	1.977	1.979	1.987	0.001	0.001
Ti		0.009	0.046	0.008	0.004	0.009	0.009	2.021	2.002
Cr		0.000	0.001	0.000	0.001	0.000	0.000	0.001	0.001
Fe ³⁺		0.000	0.000	0.019	0.013	0.015	0.000	0.000	0.000
Fe ²⁺		1.826	1.744	1.812	1.849	1.800	1.775	1.862	1.940
Mn		0.246	0.354	0.264	0.250	0.368	0.277	0.092	0.040
Mg		0.200	0.175	0.197	0.210	0.172	0.190	0.012	0.013
Ca		0.688	0.686	0.706	0.659	0.691	0.726	0.009	0.000
X _{Alm}		61.7	58.9	60.8	62.3	59.4	59.8	Ilmenite	94.3
X _{Prp}		6.8	5.9	6.6	7.1	5.7	6.4	Pirofanite	4.6
X _{Sps}		8.3	12.0	8.9	8.4	12.1	9.3	Geikelite	0.6
X _{Grs}		23.2	23.2	22.8	21.5	22.1	24.4		0.6

4.6. Geothermobarometry

The El Picacho and Boquerón gabbros contain different generations of amphibole and plagioclase, suggesting that the whole rock did not reach equilibrium during metamorphism. On the other hand, amphibole and plagioclase of the mylonitized banded rock of the El Picacho unit (CMK144) and all analyzed samples of the Santa Elena unit exhibit a narrow compositional interval, indicating that these rocks achieved metamorphic equilibrium.

Temperature estimates

Temperature estimation was carried out with the thermometer of Otten (1984) based on Ti content of amphibole. This thermometer comprises two segments: (1) for $T > 970^{\circ}\text{C}$, $T(\text{°C}) = 273 \times (\text{Ti}/23\text{ O}) + 877$; (2) for $T < 970^{\circ}\text{C}$, $T(\text{°C}) = 1,204 \times (\text{Ti}/23\text{ O}) + 545$; where $\text{Ti}/23\text{ O}$ is the number of Ti cations per unit formula (23 oxygens). This thermometer was applied also to the amphiboles from amphibolites and the results are summarized in Table 4.

Table 4. Estimated temperatures in the metamafic rocks.

Unit Sample/Amphibole	<u>Ti in Amp</u> Otten (1984)	<u>Pl-Amp</u> Holland and Blundy (1994)
El Picacho		
AC25 / Red-brown	1006	~980
CMK040A / Brown	793-825	
AC32,33, CMK040A Brown, green	582-607	
AC25, 32, 33, 59A	546-578	
CMK040A, D Pale green		
CMK040A, D Blue-green	550-573	
CMK144 Pale brown	582-587	560
Boquerón		
CMK38B Green-brown	610-678	
AC61 Green-brown	628-656	
CMK38B Colorless	547-557	
Santa Elena		
AC41 Green-brown	612-659	651-676 (P=2) 661-677 (P=5)
AC51 Brown-greenish	680-759	655-666 (P=2) 654-658 (P=5) 507-563 (P=2)
AC44 Green-brown	628-675	518-585 (P=5) 531-614 (P=9) 542-635 (P=12)

The plagioclase-amphibole geothermometer “B” of Holland and Blundy (1994), based on the $\text{NaSi} \leftrightarrow \text{CaAl}$ exchange reaction, was applied to two metagabbros devoid of quartz. One is a metagabbro (AC25) which presumably preserves the original igneous composition and the other corresponding to a mylonite (CMK144) that achieved metamorphic equilibrium. Due to the absence of mineral pairs suitable to determine the pressure, this parameter was assumed to be 2 kbar. This value has been also suggested by other authors (e.g. Girardeau and Mével 1982; Giguère et al. 2003).

The Otten (1984) thermometer for the red-brown amphibole (AC25) indicates temperatures of approximately 1000 °C, whereas the temperature obtained from the Holland and Blundy (1994) thermometer for the same sample is 980°C and lies outside of the range of temperature for this thermometer (500 - 900 °C), but suggests high metamorphic temperatures for the sample. These results indicate that the high temperatures are indicative of the late magmatic stage of the original gabbros. Temperatures obtained in other amphiboles of the El Picacho rocks suggest amphibole crystallization at decreasing temperatures from values as high as ~825°C, down to lower temperatures of ~550 °C.

Temperatures obtained by the Otten (1984) thermometer for the Boquerón rocks show a narrower range when compared with the El Picacho, but also indicates the formation of different generations of amphiboles at decreasing temperatures between ~680°C and ~550 °C.

The plagioclase-amphibole geothermometer “A” based on the $\text{NaAl} \leftrightarrow \text{Si}$ exchange reaction of Holland and Blundy (1994) was applied to compositionally appropriate amphibole-plagioclase pairs of the Santa Elena amphibolites. Calculations were carried out at different pressure values (Table 4).

For the nematoblastic amphibolite (AC41) the Otten (1984) thermometer gives temperatures between 610° and 650°C, whereas the Holland and Blundy (1994) thermometer yields slightly higher temperatures of 650°-680°C. Contrary to that in the granoblastic amphibolite (AC51) the Otten thermometer yields higher temperatures (680°-760°C) than the Holland and Blundy thermometer (650°-670°C)

The results for garnet amphibolite obtained by using the Otten (1984) and Holland and Blundy (1994) temperatures are between 520° and 680°C

Pressure estimates

The pressure of metamorphism of the amphibolites was estimated using the partitioning of Al in amphiboles as suggested by Raase (1974). $\text{Al}^{\text{VI}}/\text{Al}^{\text{IV}}$ ratios of the samples (Figure 6) show that almost all analyses cluster around the boundary separating amphiboles from low

pressure regimes ($P < 5$ kbar) from those formed in high pressure regimes ($P > 5$ kbar). However it is evident that the garnet amphibolites lie above that boundary indicating that they were metamorphosed under higher pressure ($P > 5$ kbar).

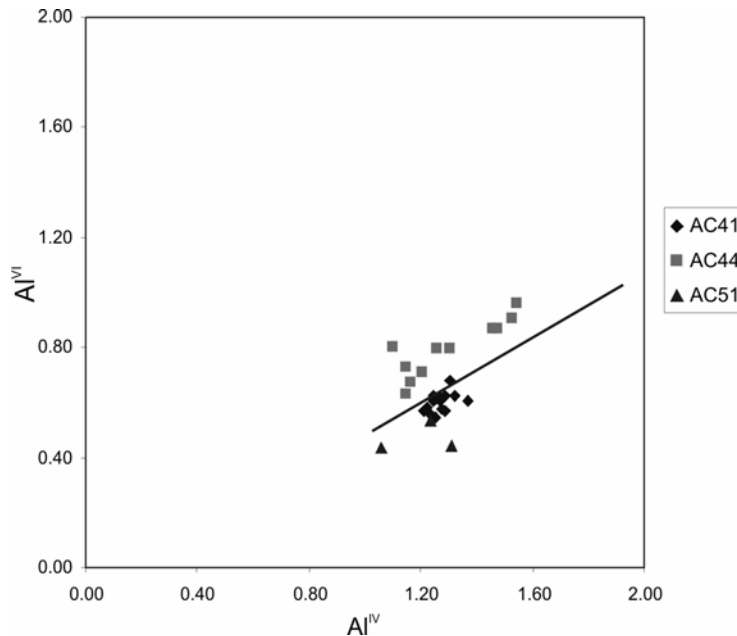


Figure 6. Plot of Al^{VI} vs Al^{IV} for amphibole of Santa Elena amphibolites. The line shown separates amphiboles formed at $P > 5$ kbar (above the line) from those formed at $P < 5$ kbar (Raase 1974).

Two geobarometers calibrated by Kohn and Spear (1990) which may be used to estimate the pressure for the assemblage garnet+amphibole+plagioclase+quartz were applied to the garnet amphibolite. For pressure estimation two values of temperatures 500 and 650 °C were used. The estimated pressure is 6.5 - 9.0 kbar.

4.7. Geochemistry

Whole rock composition of the different rock types is given in Tables 5 and 6. It has been demonstrated that during hydrothermal alteration or metamorphism some elements are mobile, mainly silica and alkalis and the incompatible elements which belong to the low-field-strength (LFS) group such as Cs, Sr, K, Rb and Ba (e.g. Rollinson, 1993). Also low temperature interaction between seawater and basalts produces enrichment of LFS as well as of ^{87}Sr and U (e.g. Saunders and Tarney, 1984). On the other hand the elements generalized as relatively immobile are those of the high-field-strength (HFS) group such as Sc, Y, Th, Zr, Hf, Ti, Nb, Ta, P and rare earth elements (REE). Contrary to the relative immobility documented for light rare earth elements (LREE) during low-grade metamorphic processes

(e.g. Hermann et al., 1974), other studies have shown that under very low grade metamorphic and seafloor weathering conditions ($T < 150$ °C, and high H₂O/rock ratios) some LREE may be selectively mobilized (Ludden and Thompson, 1979; Humphris, 1984). To avoid the influence of probable element mobility in the petrological interpretations the discussion will be focused on the elements considered as relatively immobile.

The whole rock compositions of the different rock types studied are given in Tables 5 and 6. Mg-numbers (Mg# = molar Mg/[Mg+Fe²⁺]) are in the interval between 0.77 and 0.88 for the El Picacho metagabbros and of 0.63 and 0.13 for plagiogranite and rodingite, respectively. MgO contents in the metagabbros are high, varying mostly between 9.36% and 14.94%. TiO₂ concentrations are low in all samples (0.02% - 0.35%), whereas P₂O₅ concentrations are very low (below 0.02%). Plagiogranite and metasomatite have SiO₂ content of 71.66% and 55.37%, respectively. In the normative Ab-An-Or diagram of Barker (1979) (not shown) the plagiogranite plots in the trondhjemite field.

High Mg# values observed in the El Picacho metagabbros suggest that these rocks are cumulates. Other evidence for the cumulate character of the El Picacho metagabbros is low K₂O, P₂O₅ and TiO₂ contents (Seifert et al. 1996). Similarly, one Boquerón metagabbro sample (CMK38B) has high Mg# suggesting that it also could represent crystal fractionation processes.

The Boquerón metagabbros and the Santa Elena amphibolites have Mg# values in the intervals between 0.58 - 0.72 and 0.54 - 0.64, respectively. MgO contents are similar in rocks of both units (6.18-8.69%) and are considerably lower than those of the El Picacho metagabbros. TiO₂ and P₂O₅ concentrations in Boquerón rocks are higher than those in the El Picacho. TiO₂ contents range from 0.61% to 2.26% and P₂O₅ contents range from 0.06 to 0.26%. The higher TiO₂, P₂O₅, V and Mn values in the Boquerón metagabbros and in the Santa Elena amphibolites are compatible with the presence of ilmenite (almost completely transformed to titanite) and apatite.

Table 5. Major elements (wt%) and trace elements (ppm) composition of the El Picacho metagabbros and associated plagiogranite and metasomatite.

		AC32A	AC33D	CMK 040A	CMK 040C	AC58	AC59A	AC53C	AC05	CMK 134	AC32B	AC32B3
Rock	d.l	m-ga	m-ga	m-ga	m-ga	m-ga	m-ga	m-ga	m-ga	m-ga	pg	msom
SiO ₂	0.04	47.29	50.92	47.95	46.2	47.52	49.36	48.91	50.99	47.78	71.66	55.37
TiO ₂	0.01	0.21	0.27	0.3	0.12	0.19	0.19	0.2	0.35	0.17	0.07	0.02
Al ₂ O ₃	0.03	14.33	15.45	17.15	24.24	18.56	15.38	16.53	16.18	20.5	17.32	24.4
Fe ₂ O ₃ ^T	0.04	5.96	5.79	7.37	3.13	4.26	4.12	4.87	4.75	4.21	0.15	0.77
MnO	0.01	0.1	0.11	0.11	0.05	0.07	0.08	0.09	0.09	0.07	0.01	0.08
MgO	0.01	14.92	10.21	10.67	6.06	11.02	13.02	11.28	9.51	9.36	0.11	0.05
CaO	0.01	14.34	14.75	12.79	16.77	15.54	15.02	15.57	14.69	15.33	1.05	15.02
Na ₂ O	0.01	0.95	1.45	1.86	1.03	1.05	1.02	1.28	1.98	1.09	6.24	2.4
K ₂ O	0.02	0.05	0.03	0.05	0.05	0.06	0.04	0.02	0.04	0.12	0.06	n.d
P ₂ O ₅	0.01	0.004**	n.d	n.d	0.02	n.d	n.d	n.d	0.02	n.d	n.d	0.02
Cr ₂ O ₃	0.00	0.1	0.03	0.09	0.11	0.11	0.16	0.06	0.21	0.1	0.002	n.d
LOI	0.10	1.6	0.8	1.5	2.2	1.4	1.2	0.8	1.2	1.1	3.2	1.9
SUM		99.86	99.82	99.85	99.98	99.79	99.6	99.62	100.01	99.84	99.87	100.03
FeO*		4.55	4.42	5.63	2.39	3.25	3.15	3.72	3.63	3.21	0.11	0.59
Mg#		0.85	0.80	0.77	0.82	0.86	0.88	0.84	0.82	0.84	0.63	0.13
Sc	1	38	45	30	17	32	39	33	48	23	1	n.d
V	5	145	189	139	64	112	215	149	170	95	n.d	18
Cr		684.5	198.5	588.6	725.5	752.9	1108.8	376.45	1423.6	684.5	13.7	n.d
Co	0.5	77.6	74.7	74.7	67.3	76.8	86.4	70.3	61.6	64.1	19.7	31.9
Ni	0.1	60.7	9.3	66.3	37.8	42.5	87.2	63.6	24.4	55	114.6	1.1
Cu	0.1	147	45.7	28.9	1.1	31.7	70.6	118.8	41.4	27.1	28.5	12.7
Zn	1	8	4	13	4	5	5	4	4	7	8	3
Ga	0.5	8.7	12.5	12.3	14.1	10.7	8.8	10	10.1	10.8	9.4	26.1
Rb	0.5	n.d	1.1	n.d	0.8	1	1.3	n.d	n.d	2.2	n.d	n.d
Sr	0.5	109.4	146.5	147.4	409.3	122.4	90.8	86.7	100.3	113.5	91.7	205.7
Ba	0.5	8.4	11.7	7	9.3	19.5	8.3	8.3	4.1	25.6	31.1	5.3
Th	0.1	0.1**	0.1	n.d	n.d	n.d	n.d	n.d	n.d	0.3	n.d	0.1
U	0.1	n.d	n.d	n.d	n.d	n.d	n.d	n.d	n.d	n.d	n.d	0.1
Pb	0.1	0.3	0.6	0.4	0.5	0.8	0.4	0.3	0.2	2.1	0.2	0.4
Y	0.1	6	8.6	7.7	3	5.2	6.4	5.8	9.2	5.3	2	2.5
Zr	0.5	4.1	4.2	7.1	2.2	4.6	3.4	4.3	9.1	6.5	21.4	0.9
Hf	0.5	0.19**	n.d	n.d	n.d	n.d	n.d	n.d	n.d	n.d	n.d	n.d
Nb	0.5	0.10**	n.d	n.d	n.d	n.d	n.d	n.d	n.d	n.d	n.d	0.1
Ta	0.1	0.1**	n.d	n.d	0.1	n.d	n.d	n.d	0.1	0.1	0.2	0.1
Cs	0.1	n.d	n.d	n.d	n.d	n.d	n.d	n.d	n.d	0.2	n.d	0.1
La	0.5	n.d	n.d	0.5	n.d	n.d	n.d	n.d	0.5	0.8	1.2	2.8
Ce	0.5	0.7	0.9	1.6	0.6	0.7	0.5	0.7	1.3	2.3	3.5	0.9
Pr	0.02	0.15	0.19	0.26	0.15	0.14	0.13	0.15	0.3	0.28	0.25	0.26
Nd	0.4	0.9	1.2	1.8	0.7	0.9	1.1	1	1.5	1.3	0.9	1.2
Sm	0.1	0.5	0.7	0.6	0.5	0.4	0.4	0.4	0.7	0.5	0.2	0.18
Eu	0.05	0.3	0.38	0.4	0.28	0.29	0.32	0.28	0.41	0.29	0.18	0.24
Gd	0.05	0.66	1.16	1.14	0.58	0.76	0.77	0.75	1.37	0.78	0.37	0.35
Tb	0.01	0.16	0.2	0.2	0.04	0.14	0.17	0.14	0.24	0.14	0.06	0.04
Dy	0.05	1.05	1.37	1.25	0.4	0.95	1.1	1	1.55	0.77	0.33	0.2
Ho	0.05	0.22	0.31	0.31	0.12	0.21	0.23	0.23	0.38	0.19	0.08	0.04
Er	0.05	0.67	0.94	0.83	0.29	0.57	0.71	0.64	1	0.54	0.19	0.12
Tm	0.05	0.08	0.12	0.12	n.d	0.08	0.09	0.08	0.16	0.08	n.d	0.02
Yb	0.05	0.63	0.77	0.78	0.27	0.48	0.63	0.52	0.78	0.52	0.15	0.09
Lu	0.01	0.08	0.11	0.11	0.04	0.07	0.1	0.08	0.12	0.08	0.03	0.01

^T Total iron as Fe₂O₃. FeO* was calculated treating all iron as FeO and assuming that FeO/(FeO+Fe₂O₃) = 0.85. Mg# based on FeO = 0.85. FeOt. d.l: detection limit, m-ga: metagabbro, pg: plagiogranite, msom: metasomatite. n.d: not detected (below detection limit). **elements obtained with other analytical method (see text).

Table 6. Major elements (wt%) and trace elements (ppm) composition of the Boquerón metagabbros and Santa Elena amphibolites.

Sample Rock	CMK-038B	AC-61	AC09	AC70A	AC-41A	AC-51	AC 44A	AC 44S
	m-ga	m-ga	m-ga	m-ga	am	am	g-am	f-am
SiO ₂	50.05	48.25	54.65	50.73	48.38	48.71	49.71	53.3
TiO ₂	0.61	2.13	1.03	1.53	1.26	2.01	2.26	1.82
Al ₂ O ₃	16.01	13.41	14.49	14.6	15.33	13.6	13.98	15.54
Fe ₂ O ₃ ^T	7.81	13.08	8.99	9.29	10.54	13.3	13.35	9.1
MnO	0.12	0.19	0.13	0.12	0.15	0.23	0.18	0.11
MgO	8.69	7.85	6.18	7.12	8.02	7.14	6.83	4.62
CaO	13.21	11.68	10.27	11.75	12.19	10.54	9.32	8.61
Na ₂ O	2.09	2.11	3.03	3	2.68	3.18	2.6	2.61
K ₂ O	0.06	0.08	0.07	0.24	0.28	0.08	0.18	0.12
P ₂ O ₅	0.06	0.18	0.09	0.15	0.08	0.18	0.26	0.44
Cr ₂ O ₃	0.06	0.01	0.02	0.04	0.03	0.02	0.01	0.03
LOI	1	0.8	0.9	1.4	0.8	0.6	1.3	3.6
SUM	99.77	99.77	99.853	99.97	99.74	99.59	99.98	99.9
FeO*	5.96	9.99	6.87	7.09	8.05	10.16	10.19	6.95
Mg#	0.72	0.58	0.62	0.64	0.64	0.56	0.54	0.54
Sc	37	48	32	33	41	47	42	40
V	201	430	253	283	333	431	414	386
Cr	410.68	75.29	157.43	273.68	205.34	102.67	95.82	205.34
Co	81.7	88.1	85.6	42.5	65.9	92.7	77.5	126.9
Ni	31.7	13.2	12.8	16.4	17.2	22.4	21.4	64.5
Cu	20	1.5	2.4	4.1	38.6	52.3	9.4	83.2
Zn	11	18	12	5	13	23	21	133
Ga	13.7	18.4	15.8	16	21.8	19	20.9	18.1
Rb	n.d	n.d	0.7	1.3	4.6	0.5	1.1	1.6
Sr	126.5	110.6	180.6	275.2	91.6	101.9	79.1	216.1
Ba	16.2	25.8	19	93.9	10.2	8.4	25.9	160.4
Th	n.d	0.3	0.3	0.9	n.d	n.d	0.6	0.7
U	n.d	0.2	n.d	0.4	n.d	n.d	0.3	2.3
Pb	0.2	0.2	0.1	0.4	0.2	0.1	0.2	1.3
Y	14.4	48.6	24.9	41.9	31	45.7	55.3	39.5
Zr	62.1	104.9	88.3	123.3	65.5	100.5	154.8	136.5
Hf	1.5	3.1	2.5	3.7	2	3.1	5	3.4
Nb	0.5	3.4	1.5	3.7	1.4	1.7	6.6	11.9
Ta	n.d	0.3	0.2	0.3	0.1	0.3	0.5	1.2
Cs	n.d	n.d	n.d	0.1	n.d	n.d	n.d	n.d
La	1.3	5.2	2.8	5.9	2.2	3.5	6.7	10.6
Ce	3	14.1	7	15.4	6.4	11.2	21	24.7
Pr	0.56	2.41	1.26	2.54	1.27	2.1	3.3	3.56
Nd	3.2	15.4	6.7	13.9	7.4	13.1	17.2	16.9
Sm	1.2	4.8	2.4	4.37	2.7	4.3	5.7	5
Eu	0.49	1.81	0.98	1.38	1.15	1.68	1.79	1.88
Gd	1.86	6.99	3.48	5.59	4.23	6.26	6.95	6.04
Tb	0.36	1.26	0.62	1.13	0.79	1.23	1.36	1.03
Dy	2.27	7.62	4.38	6.83	4.98	7.41	9.45	6.66
Ho	0.51	1.7	0.93	1.45	1.15	1.62	2.03	1.39
Er	1.5	5.09	2.7	4.21	3.35	5.06	5.67	3.96
Tm	0.23	0.73	0.41	0.65	0.47	0.73	0.86	0.63
Yb	1.46	4.59	2.22	4	2.67	4.5	5.19	3.4
Lu	0.24	0.7	0.37	0.57	0.43	0.74	0.86	0.57

^T Total iron as Fe₂O₃. FeO* was calculated treating all iron as FeO and assuming that FeO/(FeO+Fe₂O₃) = 0.85. Mg# based on FeO = 0.85 FeOt. m-ga: metagabbro, am: amphibolite, g-am: garnet amphibolite, f-am: feldspathic amphibolite. n.d: not detected (below detection limit).

The chondrite-normalized REE patterns of the El Picacho gabbros (Figure 7a,b) are typical of tholeiitic cumulates. Most samples exhibit depletion in the LREE ($\text{La}_{\text{N}}/\text{Yb}_{\text{N}} < 0.64$) and are characterized by a positive Eu anomaly (Figure 7a), attributed to plagioclase accumulation. These patterns are similar to those of the layered gabbros of the Oman ophiolite (e.g. Pallister and Knight, 1981). In some samples (AC05, CMK040A, CMK134) LREE depletion is less intense (Figure 7b). The plagiogranite shows chondrite-normalized REE patterns with low LREE contents, lower than 10x the chondrite, and a moderate relative enrichment of the LREE. It also presents a positive Eu-anomaly (Figure 7c). The metasomatite displays REE pattern which is rather similar to that of the plagiogranite (Figure 8c). Plagiogranite and metasomatite carry similar content of HREE to one metagabbro (CMK040C) (Figure 7c).

The Boquerón metagabbros and the Santa Elena amphibolites display parallel nearly flat REE patterns, no Eu anomaly (Figures 7d, e) and slight, but distinctive, LREE depletion ($\text{La}_{\text{N}}/\text{Yb}_{\text{N}} = 0.89-1.48$ in Boquerón and $0.78-1.29$ in Santa Elena) . The increase in REE concentrations is accompanied by the decrease in Mg# (except for the mylonitized metagabbro-AC70A, which also shows a small negative Eu anomaly). The mean REE contents of Boquerón metagabbros are slightly higher than those of El Picacho metagabbros and some plot within the field of Oman varitextured or upper gabbros (Figure 7e). The Santa Elena amphibolites have chondrite-normalized REE patterns and abundances similar to those of N-MORB and to the Oman lavas and dikes (Figure 7e). With the exception of sample (CMK038B), all samples of the Boquerón and Santa Elena units seem to represent liquid compositions.

Primitive mantle-normalized trace element abundances for El Picacho metagabbros are shown in Figure 8. In general, abundances of the immobile REEs and HFSEs are low, similar to the primitive mantle, to layered gabbros from the Oman ophiolite (MacLeod and Yaouancq, 2000) and to cumulate gabbros of Hole 900A (Seifert et al., 1996) (Figure 8). The spidergram suggests that some samples may have been enriched in LILE by hydrous solutions.

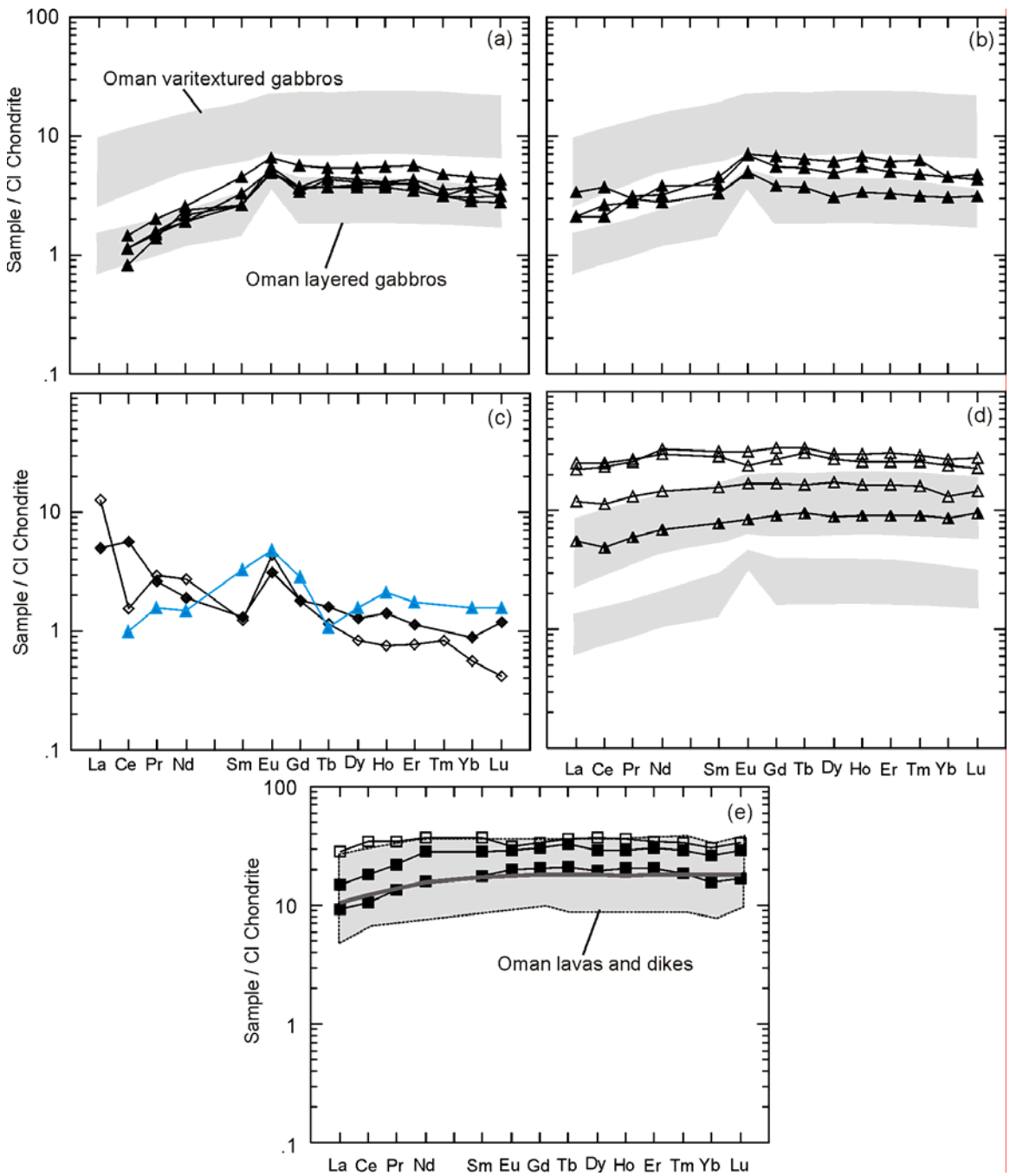


Figure 7. Chondrite-normalized rare earth element abundances of mafic rocks, plagiogranite and rodingite. (a) and (b) El Picacho metagabbros. (c) plagiogranite: black diamond, metasomatite: open diamond, metagabbro CMK040C: blue triangle. (d) Boquerón metagabbros. (e) Santa Elena amphibolites. Thick line in (e) represents the N-MORB composition from Sun and McDonough (1989). Grey fields in (a), (b) and (d): compositional range of Oman gabbros (data from MacLeod and Yaouancq, 2000); grey field in (e) is the compositional range of Oman lavas and dikes (compiled by Kelemen et al., 1997).

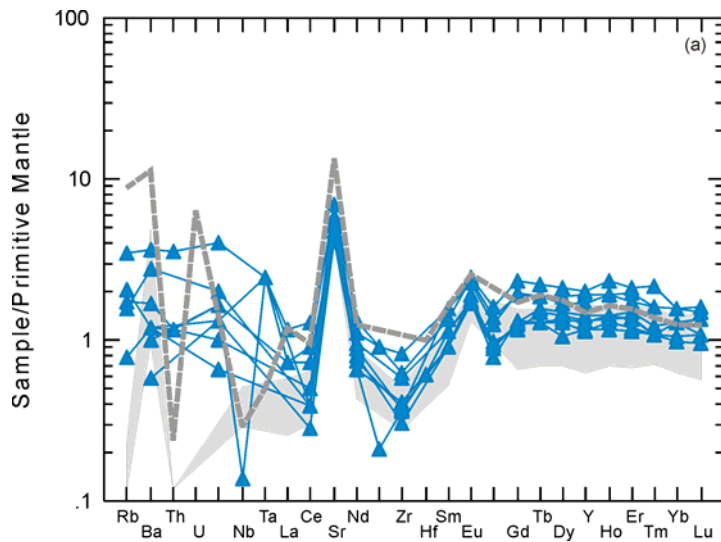


Figure 8. Primitive mantle (Sun and McDonough, 1989) normalized trace element abundances of El Picacho metagabbros (blue triangles). Grey field represents layered and massive gabbros from the Oman ophiolite (MacLeod and Yaouancq, 2000). Broken line represents the average composition of cumulate gabbros sampled in Hole 900A (Seifert et al., 1996). Concentrations of the immobile REEs and HFSEs are similar to those of the primitive mantle, indicating very little magma retention, and enrichment in the LILE (Rb, Ba, K, and Sr) in some samples.

Primitive mantle-normalized trace element abundances for Boquerón metagabbros are displayed on Figures 9A, B. We can observe a broad pattern that resembles a N-MORB type with the remarkable disturbance of LILE concentration, given by the positive Sr anomalies and irregular shapes for various peaks. This suggests remobilization of LILE from somewhere else that might have partitioned to hydrothermal solutions that might have added U, Th, Ba and Rb to the gabbros. Garnet amphibolite exhibits a pattern approximately parallel to N-MORB, but it is 10 times enriched denoting that it might be an evolved magma from original N-MORB Boquerón magma.

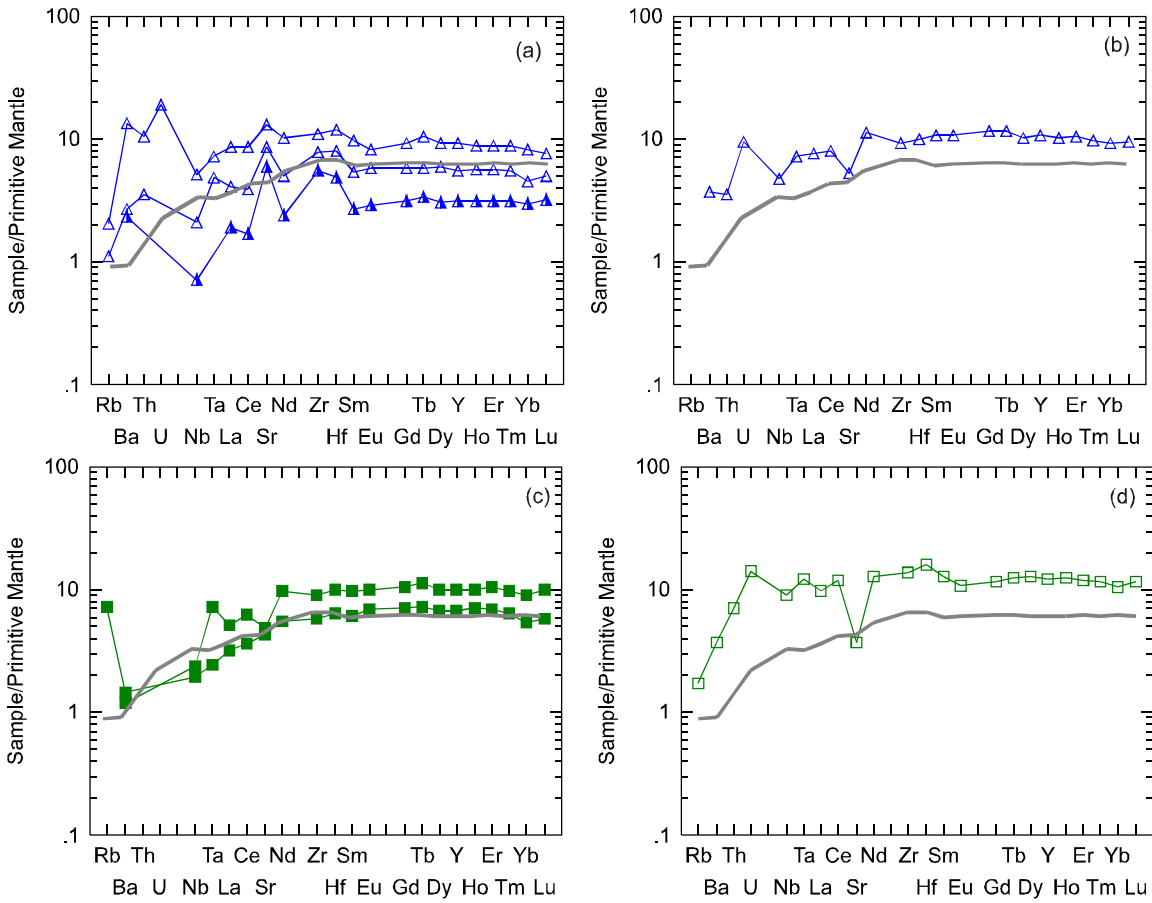


Figure 9. Primitive mantle-normalized trace element contents of Boquerón metagabbros (A-B) and Santa Elena amphibolites (C-D). Grey line: N-MORB. Primitive mantle and N-MORB of Sun and McDonough (1989).

The MORB signature of the Boquerón metagabbros and Santa Elena amphibolites is confirmed by tectonomagmatic discrimination diagrams (Figure 10).

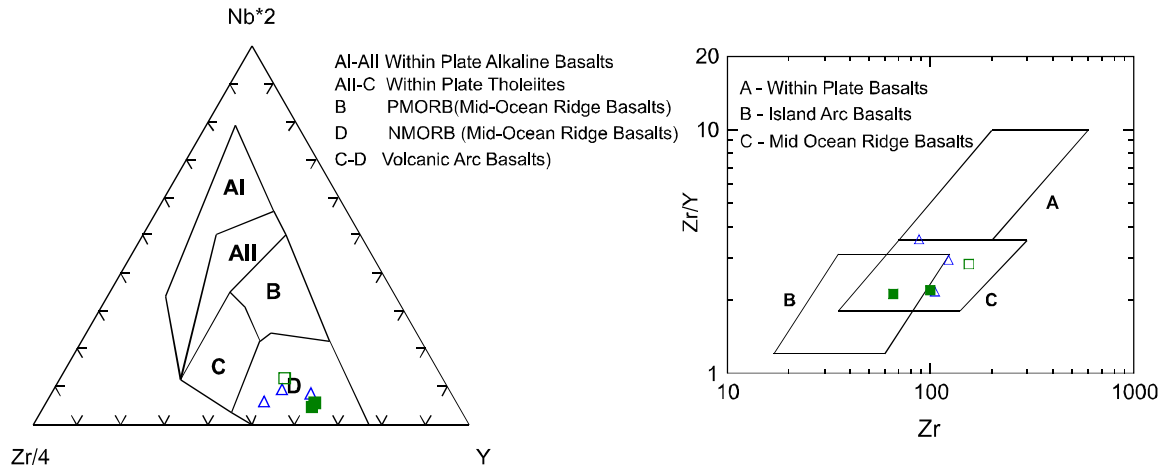


Figure 10. Selected tectonomagmatic discrimination diagrams for Boquerón metagabros and Santa Elena amphibolites. (a) Meschede, 1986. (b) Pearce and Norry, 1979.

4.8. Zircon U-Pb age

Zircon grains in sample AC28A are euhedral light pink, some with spherical football shaped (Figure 11). They vary in size from 0.15 mm to 1.25 mm. The U-Pb results for four zircon fractions from plagiogranite (Table 7) reveal the age of 216.6 ± 0.4 Ma (Figure 12).



Figure 11. Photograph of euhedral zircon grains from plagiogranite.

Table 7. U-Pb isotopic data for the El Picaho plagiogranite.

Sample Fraction	Size (mg)	U (ppm)	Pb (ppm)	$^{206}\text{Pb}/^{204}\text{Pb}$	$^{207}\text{*Pb}/^{235}\text{U}$	(pct)	$\text{Pb206}^*\text{ U238}$
AC 32B							
E11	0.200	197.28	6.8901	811.6991	0.228542	0.752	0.034289
E14	0.191	172.61	5.9242	6306.823	0.238558	0.168	0.034178
10	0.262	153.44	5.2929	7559.459	0.24363	0.556	0.034308
11	0.190	170.91	6.45	463.2405	0.236946	1.4	0.034554
Sample Fraction	(pct)	Correl. Coeff. (rho)	$\text{Pb207}^*\text{ Pb206}^*$	(pct)	$\text{Pb206}^*\text{ U238 Age}$	$\text{Pb207}^*\text{ U235 Age}$	$\text{Pb207}^*\text{ Pb206}^*\text{ Age}$
AC 32B							
E11	0.64	0.8631	0.048341	0.38	217.34	208.99	115.97
E14	0.164	0.978	0.050624	0.035	216.64	217.24	223.72
10	0.549	0.9893	0.051503	0.081	217.46	221.39	263.4
11	0.815	0.5939	0.049734	1.13	218.98	215.92	182.59

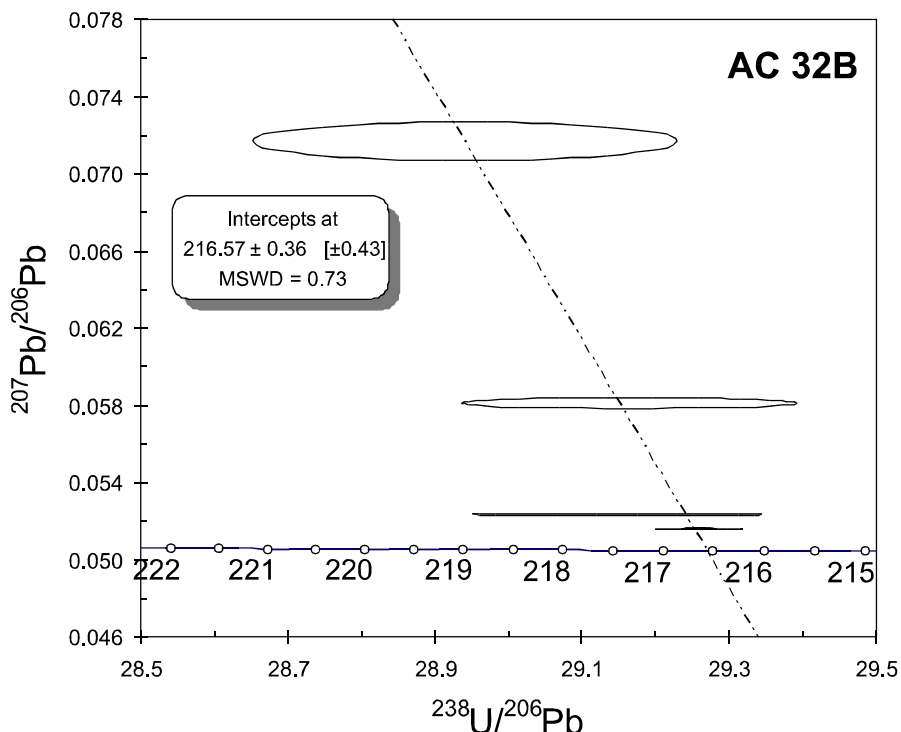


Figure 12. Tera-Wasserburg concordia diagram for the plagiogranite of the El Picacho unit.

4.9. Sr-Nd Isotopic compositions

Sr and Nd whole rock isotopic data are shown in Table 8. Initial $^{87}\text{Sr}/^{86}\text{Sr}$ ratios (calculated for an age of 220 Ma) are distinctively low in the mafic rocks, varying between 0.70329 and 0.70344 in the El Picacho metagabbros, between 0.70292 and 0.70334 in the Boquerón metagabbros and between 0.70336 to 0.70392 in the Santa Elena amphibolites. The plagiogranite presents a slightly higher initial $^{87}\text{Sr}/^{86}\text{Sr}$ (0.70444). $^{147}\text{Sm}/^{144}\text{Nd}$ ratios for the mafic rocks are high, mostly ranging from 0.20 to 0.29, which is typical of depleted oceanic rocks. ϵ_{Nd} values calculated for 220 Ma are shown in Table 8. Initial ϵ_{Nd} values are +4.2 to +8.7 for El Picacho metagabbros, +3.4 for the plagiogranite, +6.1 to +8.3 for Boquerón metagabbros and +7.2 to +8.3 for Santa Elena amphibolites, confirming derivation of the original magmas from depleted mantle. The depleted model age (T_{DM}) for the plagiogranite is 670 Ma.

In terms of their initial Sr and Nd isotopic compositions (Figure 13), El Picacho metagabbros, Boquerón metagabbros and Santa Elena amphibolites plot within or close to the back-arc or island arc field, with initial $^{87}\text{Sr}/^{86}\text{Sr}$ ratios which are shifted to higher values possibly due to seawater alteration. The plagiogranite sample shows very different isotopic compositions when compared with the mafic rocks, with higher Sr and lower Nd initial isotopic ratios.

Table 8. Sr and Sm-Nd data for the El Picacho Metagabbro and plagiogranite sample, the Boquerón Metagabbro and the Medellin Amphibolite.

Unit/ Sample	Sm (ppm)	Nd (ppm)	$^{147}\text{Sm}/^{144}\text{Nd}$	$^{143}\text{Nd}/^{144}\text{Nd}$	T _{DM} (Ga)	$\epsilon_{\text{Nd(T)}}$	Sr (ppm)	$^{87}\text{Sr}/^{86}\text{Sr}$	$^{87}\text{Rb}/^{86}\text{Sr}$	$\epsilon_{\text{Sr(T)}}$
El Picacho metagabbro										
AC32A	0.459	0.963	0.2878	0.513213±14	-	+8.7	109.4	0.703468±2	0.00793	-11.3
AC33C	0.635	1.368	0.2804	0.513159±9	-	+7.8				
AC33E	0.412	0.917	0.2715	0.513124±13	-	+7.4				
CMK040A	0.665	1.60	0.2513	0.513146±16	-	+8.4				
CMK040C	0.261	0.70	0.2253	0.513067±8	-	+7.6				
AC58	0.438	1.028	0.2576	0.513112±13	-	+7.5	122.4	0.70336±7	0.02363	-13.6
AC06B	0.997	2.881	0.2093	0.513074±7	-	+8.2				
AC05	0.7655	1.75	0.2639	0.512948±16	-	+4.2				
AC32B	0.217	0.915	0.1433	0.512740±23	0.67	+3.4	91.0	0.704483±2	0.01271	+2.8
Boquerón metagabbro										
CMK038A	1.21	3.257	0.2246	0.512985±12	-	+6.1	134.3	0.702957±1	0.01292	-18.8
AC61	4.932	14.188	0.2101	0.513081±6	-	+8.3	110.6	0.70338±2	0.013074	-12.8
Santa Elena amphibolite										
AC41A	2.695	7.15	0.2279	0.513054±33	-	+7.2	91.6	0.70437±4	0.14525	-4.6
AC44A	5.6	17.309	0.1956	0.513059±8	-	+8.3	79.1	0.70349±2	0.04022	-12.5

The epsilon values calculated for an age of 220 Ma except for AC32 B for which was calculated for an age of 217 Ma. AC32B: plagiogranite sample. AC44A: garnet amphibolite. Error of the measured ratios is the in run precision, given as 2s in the last two digits.

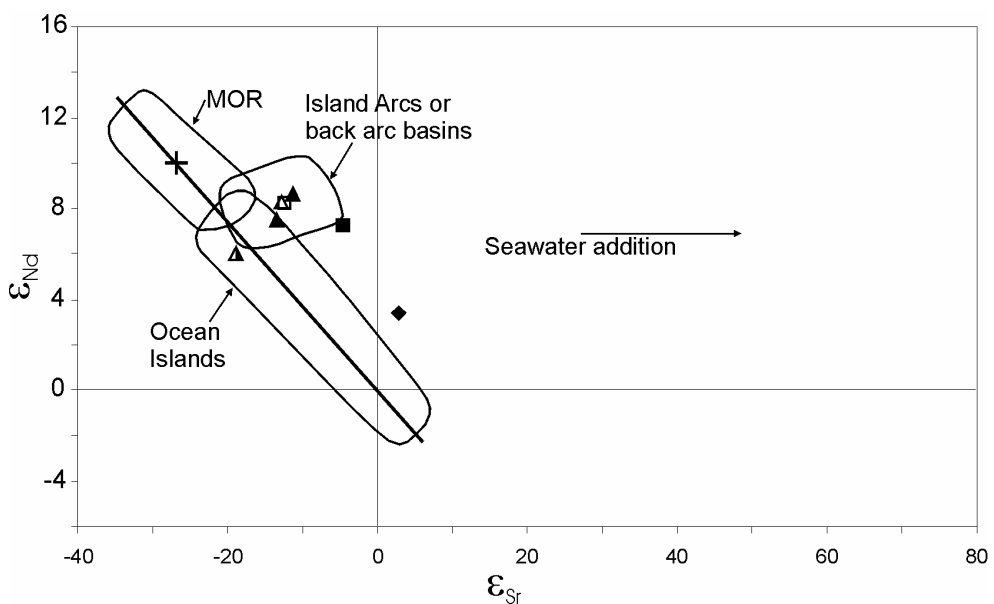


Figure 13. Initial ϵ_{Nd} and ϵ_{Sr} values for metagabbros, amphibolites and plagiogranite. Cross: ϵ_{Nd} average of the present-day MORB. Symbols: Filled triangle: El Picacho gabbros, filled diamond: plagiogranite, open triangle: Boquerón gabbros, partially filled triangle: Boquerón sample CMK38B, filled square: amphibolite, open square: garnet amphibolite.

4.10. Discussion

4.10.1 Constraints on the origin of the mafic rocks

The poorly preserved magmatic layering and cumulus textures observed in El Picacho metagabbros, as well as the observed minor abundance of oxide minerals (e.g. Natland and Dick, 1996) are evidence for a cumulate origin for these gabbros. The low contents of K₂O, TiO₂, P₂O₅ and other incompatible elements also support the cumulate nature of the gabbros and indicate little trapped magma retention. The magmatic paragenesis probably consisted mainly of plagioclase, clinopyroxene, orthopyroxene in variable proportions and locally olivine and Ti-rich amphibole (described as Type-Ia). The initial mineral association was strongly re-equilibrated under low-P at decreasing temperature from high-T to medium-T. Thus plagioclase and Ti-pargasite are the only two primary minerals remaining in the gabbros. The high Ti content in El Picacho pargasite suggests that it represents a late-magmatic product resulting of precipitation from highly evolved silicate liquid or fractionationated magmatic fluids, instead of formed by solid state reaction of igneous minerals with seawater derived fluids (Tribuzio et al. 2000). The major elements contents from amphibole yield high temperatures of ~1000°C, which probably correspond to its temperature of crystallization. This amphibole plots close to the magmatic amphibole field (Figure 14A). A similar Ti-rich amphibole was identified in a wehrlite occurring near metagabbros. This evidence suggests a common late-magmatic process for upper mantle and lower crust.

The protolith of Boquerón metagabbros was an isotropic gabbro with different proportions of igneous ilmenite (up to 5%) and apatite (<1%) indicating that the gabbros crystallized at lower temperatures than El Picacho gabbro and that were generated from a more fractionated magma than that of El Picacho. The chemistry of these rocks probably represents liquid compositions; nevertheless some of these gabbros may contain a significant proportion of cumulate phases. The protoliths of Santa Elena amphibolite were mainly basaltic lavas but also gabbros similar to those of Boquerón may occur.

4.10.2. Constraints on metamorphism

El Picacho metagabbros exhibit evidence of shearing and static recrystallization. The amphiboles show a wide variation in Si, Al and Ti in a single thin section, suggesting crystallization over a range of temperatures from values as high as ~825°C, down to lower temperatures of ~550 °C. Pargasite (Type Ib) is the highest temperature amphibole, probably formed at the initial shearing and hydrothermal alteration stage promoted by solid state

reactions between igneous minerals and seawater-derived fluids. Other amphiboles such as magnesiohornblende and actinolite might have formed at lower temperatures and as a result of that a new generation of pargasite and magnesiohornblende were formed at successive lower temperatures.

It is also possible to identify evidences of hydrothermal alteration and static recrystallization in the Boquerón rocks, which occurred at decreasing temperatures over an approximate range of ~680 and 550°C. This unit exhibits a mylonitization event superimposed to the previous metamorphic paragenesis.

Deformed and static recrystallized gabbros of similar structural and compositional characteristics have been dredged by the Ocean Drilling Program (ODP) in many sites of modern oceanic crust (e.g. Bonatti et al., 1975; Manning and MacLeod, 1996; Gaggero and Cortesogno, 1997) and also in older ophiolites (Figure 14). These amphibolitized gabbros of ophiolites have been interpreted as indicators of metamorphic events occurred in the oceanic crust (e.g. Girardeau and Mével, 1982; Berger et al., 2005).

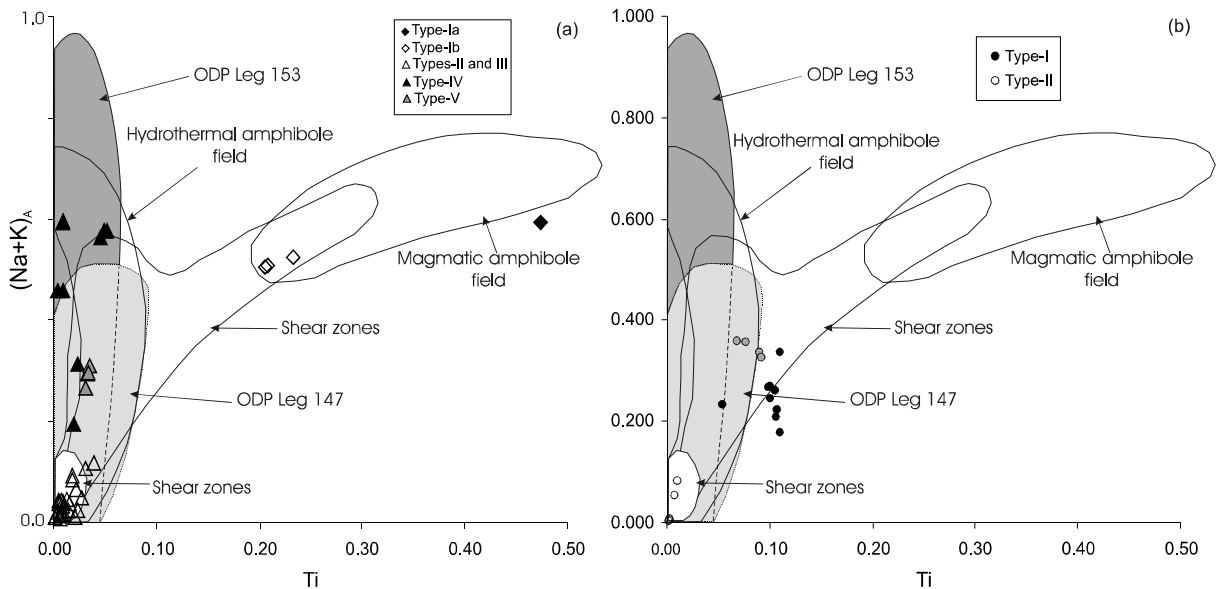
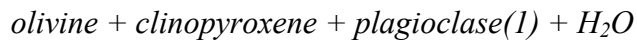


Figure 14. Na^+/K^+ versus Ti diagram for amphiboles. (a) amphiboles from El Picacho metagabbros, (b) amphiboles from Boquerón metagabbros). The compositional domains for magmatic amphibole field, shear zones and hydrothermal amphibole field are of Girardeau and Mével (1982) and those for ODP legs 147 and 153 are compiled by Berger et al. (2005).

Some mineralogical features observed in the metagabbros of the El Picacho unit are similar to those described by Koepke et al. (2004) as related to partial melting. These authors determined experimentally that during the hydrous partial melting of a variety of natural

gabbros, under pressure of 200 Mpa and at temperatures between 900 and 1000 °C the following reaction takes place:



The new plagioclase (2) is anorthite-enriched compared to that of the protolith due to the water-saturated conditions.

Although in the El Picacho gabbros orthopyroxene relicts and the textural relations were obliterated by hydrothermal alteration, other three possible products of a partial melting still remain in some samples such as: pargasite, An-rich plagioclase and plagiogranite melts. Therefore it is possible to assume that El Picacho metagabbros underwent hydrous partial melting during high-temperature hydrothermal alteration, probably at temperatures above 800° C according to the geothermometry data obtained from pargasite.

The Santa Elena Amphibolite, on the other hand, exhibits a stronger strain rate given the more recrystallized pattern than the metagabbroic units. Such amphibolites exhibit typical characteristics of rocks that achieved metamorphic equilibrium in a narrow range of pressure and temperature. Nevertheless the geothermobarometric data indicate differences in the temperatures of recrystallization of the various amphibolites. The granoblastic amphibolite shows the highest temperatures and probably related to the thermal effect of granite intrusions. The nematoblastic and granoblastic amphibolites were recrystallized to pressure below 5 kbar, whereas the garnet amphibolite recrystallized to higher pressures. This difference can be ascribed to the proximity of the garnet amphibolite to the contact with ultramafic bodies, suggesting that this amphibolite probably belongs to the metamorphic sole of the ophiolite.

4.10.3. The origin of the plagiogranites and the age of syn-oceanic deformation

The main mechanisms for plagiogranite generation in ophiolites are (1) differentiation of subalkaline basaltic magma (Coleman and Peterman, 1975); (2) partial melting of basic rocks (e.g., Gerlach et al., 1981; Pedersen and Malpas, 1984; Koepke et al., 2004), commonly related to high-temperature shear zones (e.g., Flagler and Spray, 1991); and (3) melting below the ophiolite nappe (Boudier et al., 1998). Studies of Koepke et al. (2004, 2005 and 2007), on the petrogenesis of oceanic plagiogranites within the deep oceanic crust have demonstrated that the partial melting triggered by water-rich fluids is a very common process in the deep ocean crust of modern ridges and ophiolites. The hydrous partial melting as a consequence of

the hydrothermal alteration is an important mechanism for generation of oceanic plagiogranites (Koepke et al. 2004, 2007).

The TiO₂ content is a key chemical parameter for discriminating between the different mechanisms of plagiogranite generation (Koepke et al., 2007). On the basis of its very low TiO₂ content, the plagiogranite of the El Picacho unit would be the product of anatexis and not fractional crystallisation from a MORB magma. The plagiogranites investigated here may be, therefore, the product of partial melting of the gabbros during syn-oceanic hydrothermal alteration or during obduction of the ophiolite. Moreover, the field relationships suggest that cumulate gabbros were the probable parent of the original plagiogranite magma.

As discussed above, the metagabbros exhibit evidence of partial melting under hydrous conditions and such process may be related to the origin of the plagiogranite melts. In the products of reaction (1) the hydrous melt has a composition which is equivalent to that of oceanic plagiogranites. However the isotopic characteristics of the plagiogranite, at a first approach, indicate that the original plagiogranite melt is not a simple product of remelting of the ophiolitic mafic rocks.

Two possibilities are proposed for the source of plagiogranites that can account for their isotopic composition:

(1) If the El Picacho metagabbros represent the source for the plagiogranites, then the partial remelting of gabbro must have occurred under low melting rates, allowing the melting of hydrated phases with high Rb/Sr ratio and lower Sm/Nd ratios. If this is true small amounts of plagiogranite melts would be generated in this way carrying high ⁸⁷Sr/⁸⁶Sr values and low ¹⁴³Nd/¹⁴⁴Nd values.

(2) The plagiogranites could be the product of simultaneous melting of ophiolitic mafic rocks and underlying continental rocks during ophiolite emplacement.

Considering that the plagiogranite melts were formed during shearing and high-T hydrothermal metamorphism of the basal gabbros then its U-Pb age indicates the time of deformation of the lower oceanic crust of the ophiolite at approximately 216.6 ± 0.36 Ma and represents a minimum age for the ophiolite.

4.11. Conclusions

The El Picacho metagabbros preserve igneous textures and chemical composition consistent with origin as cumulate rocks in small magma chambers of lower oceanic crust. The Boquerón rocks also preserve gabbroic textures and their chemistry indicates crystallization from a N-MORB type magma, which was more fractionated than the El

Picacho gabbros parent magma. In the Santa Elena amphibolites the igneous textures were obliterated, however their igneous composition is preserved and indicates that these rocks represent liquid basaltic compositions.

The El Picacho and Boquerón metagabbros both record and preserve the deformational and hydrothermal evolution through time of lower oceanic layer under low pressures ($P < 2$ kbar). Shearing and oceanic hydration at high temperatures and a subsequent static oceanic recrystallization were the main deformation and recrystallization processes. These processes operated at temperatures ranging from granulite to greenschist facies in El Picacho unit, and from amphibolite facies down to greenschist facies in the Boquerón unit.

The oceanic hydrothermal metamorphism probably was the mechanism responsible for production of plagiogranites within El Picacho metagabbros. The Boquerón rocks additionally record a later mylonitization process. The Santa Elena amphibolites, on the other hand, are more deformed probably due to intra-oceanic thrusting, nappe stacking and obduction of the ophiolite.

From the chemical and isotopic points of view the three mafic units can be correlated and may be considered as components of the same oceanic crust of an unique ophiolite. El Picacho Metagabbro represents the lower gabbros, Boquerón corresponds to the upper gabbros and Santa Elena is the lava and/or dike portion. This association was formed before 217 (216.6 ± 0.4) Ma in a back-arc basin.

Acknowledgments

This work is part of Correa's Ph.D. thesis and was financed by the Conselho Nacional de Desenvolvimento Científico e Tecnológico - CNPq (Brazil) grant (#141622/03-2). We thank O. Ordóñez for field assistance and P. Angel for samples of metagabbros from the Los Balsos sector (P1). We are also grateful to Reinaldo Brito for critical reading of the manuscript.

References

- Alvarez, J. 1982. Tectonitas dunitas de Medellín, Departamento de Antioquia, Colombia. Informe 1986 de Ingeominas, Medellín. 62 p.
- Barker, F. 1979. Trondjemites: Definition, environment and hypothesis of origin. In: Barker F. (ed). Trondjemites, Dacite and Related Rocks. Elsevier, Amsterdam, pp. 1-12.
- Berger, F., Femenias, O., Mercier J.C.C., Demaiffe, D. 2005. Ocean-floor hydrothermal metamorphism in the Limousin ophiolites (western French Massif Central): evidence of a rare preserved Variscan oceanic marker. *J. metamorphic Geol.* 2005, 23: 795–812.
- Bonatti, E., Honnorez, J., Kirst, P., Radicati, F. 1975. Metagabbros from the Mid-Atlantic Ridge at 06°N: contact-hydrothermal dynamic metamorphism beneath the axial valley. *J. Geol.* 83: 61-78.
- Botero, G. 1963. Contribución al conocimiento de la zona central de Antioquia. *Anales Facultad de Minas*, No. 57. Medellín, 101 p.
- Boudier, F., Ceuleneer, G., Nicolas, A. 1988. Shear zones, thrusts and related magmatism in the Oman ophiolite: initiation of thrusting on an oceanic ridge. *Tectonophysics* 151: 275-296.
- Coleman, R.G., Peterman, Z.E. 1975. Oceanic plagiogranite. *Journal of Geophysical Research*. 80: 1099-1108.
- Correa, A.M., Martens, U. 2000. Caracterización geológica de las anfibolitas de los alrededores de Medellín. BsC thesis (Unpublished), Facultad de Minas, Universidad Nacional de Colombia, Medellín, 363p.
- Correa, A.M., Martens, U., Restrepo, J.J., Ordóñez-Carmona, O., Pimentel, M.M. 2005. Subdivisión de las metamorfitas básicas de los alrededores de Medellín (Colombia). *Revista de la Academia Colombiana de Ciencias Exatas, Físicas y Naturales*. V. XXIX 112: 325-344.
- Correa, A.M., Nilson, A.A. 2003. Dunitas de Medellín y Metagabros de El Picacho: Posibles Fragmentos de Ofiolita Subtipo Harzburgita, Tipo Zona de Supra-Subducción. In: IX Congreso Colombiano de Geología, Medellín, Memorias pp 46 – 47.
- Correa, A.M., Nilson, A.A. (submitted). The Nature of the Ultramafic Section of the Aburrá Ophiolite, Medellín region, Colombian Andes. Submitted to *Journal of South American Earth Sciences*.
- Correa, A.M., Pimentel, M.M., Armstrong, R., Laux, J.E., Ordoñez-Carmona, O. 2005b. Edad U-Pb Shrimp y características isotópicas Nd y Sr del granito de la Iguaná, Antioquia. In: X Congreso Colombiano de Geología, Bogotá. Memorias, CD ROM.

- DePaolo, D.J. 1981. Neodymium isotopes in the Colorado Front Range and crust-mantle evolution in the Proterozoic. *Nature*: 291: 193 – 196.
- Droop, G.T.R. 1987. A general equation for estimating Fe³⁺ concentrations in ferromagnesian silicates and oxides from microprobe analyses, using stoichiometric criteria. *Min. Mag.* 51, 431-435.
- Echeverría, L.M. 1973. Zonación de las rocas metamórficas del valle de Aburrá y sus alrededores. *Anales de la Facultad de Minas* 58: 30-56.
- Flagler, P.A., Spray, J.G. 1991. Generation of plagiogranite by amphibolite anatexis in oceanic shear zones. *Geology* 19: 70-73.
- Gaggero, L., Cortesogno L. 1997 Metamorphic evolution of oceanic gabbros: recrystallization from subsolidus to hydrothermal conditions in the MARK area (ODP Leg 153). *Lithos* 40: 105-131.
- Gerlach, D.C., Leeman, W.P., Ave' Lallement, H.G. 1981. Petrology and geochemistry of plagiogranite in the Canyon Mountain ophiolite, Oregon, *Contrib. Mineral. Petrol.* 72: 82–92.
- Giguère, E., Hébert, R., Beaudoin, G., Bédard, J.H., Berclaz, A. 2003. Hydrothermal circulation and metamorphism in crustal gabbroic rocks of the Bay of Islands ophiolite complex, Newfoundland, Canada: evidence from mineral and oxygen isotope geochemistry. In: Dilek, Y., Robinson, P.T. (Eds.) *Ophiolites in Earth History*. Spec. Publ. Geol. Soc. London 218: 369-400.
- Gioia, S.M.C.L., Pimentel, M.M. 2000. The Sm-Nd Isotopic Method in the Geochronology Laboratory of the University of Brasília. *Anais da Academia Brasileira de Ciências* 72(2): 219-245.
- Girardeau, J., Mével, C. 1982. Amphibolitized sheared gabbros from ophiolites as indicators of the evolution of the oceanic crust: Bay of Islands, Newfoundland. *Earth and Planetary Science Letters* 61: 151-165.
- González, H. 1980 Geología de las planchas 167 (Sonsón) y 187 (Salamina), *Boletín Geológico de Ingeominas* 23, 174 p.
- Hermann, A.G., Potts, M.J., Knake, D. 1974 Geochemistry of the REE in spilites from the oceanic and continental crust. *Contrib. Mineral. Petrol.* 44: 1-16.
- Holland, T., Blundy, J. 1994. Non-ideal interactions in calcic-amphiboles and their bearing on amphibole-plagioclase thermometry. *Contrib. Mineral. Petrol.* 116: 433-447.
- Humphris, S.E. 1984. The mobility of REE in the crust. In: P. Henderson (Editor), *Rare Earth Element Geochemistry*. Elsevier, Amsterdam, pp. 9:17-28.

- Kelemen, P. B., Koga, K., Shimuzu, N. 1997. Geochemistry of gabbro sills in the crust-mantle transition zone of the Oman ophiolite: implications for the origin of the oceanic lower crust. *Earth Planet. Sci. Lett.* 146: 475-488.
- Koepke, J., Feig, S.T., Snow, J., Freise, M. 2004. Petrogenesis of oceanic plagiogranites by partial melting of gabbros: an experimental study. *Contrib. Miner. Petrol.* 146: 414-432.
- Koepke, J., Feig S.T., Snow, J. 2005. Hydrous partial melting within the lower oceanic crust. *Terra Nova.* 17: 286–291.
- Koepke, J., Berndt, J., Feig, S.T., Holtz, F. 2007. The formation of SiO₂-rich melts within the deep oceanic crust by hydrous partial melting of gabbros. *Contrib Mineral Petrol* 153: 67–84. DOI 10.1007/s00410-006-0135-y.
- Kohn, M.J., Spear, F.S. 1990. Two new geobarometers for garnet amphibolites o with applications to southeastern Vermont. *Amer. Mineralogist*, 75:89-96.
- Krogh, T.E. 1973. A low-contamination method for hydrothermal decomposition of zircon and extraction of U and Pb for isotopic age determinations. *Geochim. Cosmochim. Acta* 37: 485-494.
- Leake, B.E., Woolley, A.R., Arps, C.E.S., Birch, W.D., Gilbert, M.C., Grice, J.D., Hawthorne, F.C., Kato, A., Kisch, H.J., Krivovichev, V.G., Linthout, K., Laird, J., Mandarino, J.A., Maresch, W.V., Nickel, E.H., Rock, N.M.S., Schumacher, J.C., Smith, D.C., Stephenson, N.C.N., Ungaretti, L., Whittaker, E.J.W., Youzhi, G. 1997. Nomenclature of amphiboles: Report of the Subcommittee on Amphiboles of the International Mineralogical Association, Commission on New Minerals and Mineral Names. *American Mineralogist* 82: 1019–1037.
- Ludden, J.N., Thompson, G. 1979. An evaluation of the behaviour of REE during the weathering of sea floor basalt. *Earth Planet. Sci. Lett.* 43:85-92.
- Ludwig, K.R. 1993. Isoplot - a plotting and regression program for radiogenic isotope data. Version 2.70. June 9, 1993: revision. U.S.G.S. Open-File Report, n. 91-445. 42 p.
- Ludwig, K.R. 2001. Squid 1.02. A user's manual. BGC Special Publ. 2., Berkeley, 19p.
- MacLeod, C.J., Yaouancq, G. 2000. A fossil melt lens in the Oman ophiolite: Implications for magma chamber processes at fast spreading ridges. *Earth Planet. Sci. Lett.* 176: 357-373.
- Manning, C.E., MacLeod, C.J. 1996. Fracture-controlled metamorphism of Hess Deep gabbros, Site 894: constraints on the roots of mid-ocean-ridge hydrothermal systems at fast-spreading centers. In: Mével, C., Gillis, K.M., Allan, J.F., and Meyer, P.S. (Eds.), *Proc. ODP, Sci. Results*, 147: College Station, TX (Ocean Drilling Program), 189-212.

- Manning, C.E., MacLeod, C.J., Weston, P.E. 2000. Lower-crustal cracking front at fast-spreading ridges: evidence from the East Pacific Rise and the Oman ophiolite. *Journal of the Geological Society, London* 349: 261-272.
- Maya, H.M., González, H. 1995. Unidades litodémicas en la cordillera Central de Colombia. *Boletín Geológico de Ingeominas* 35 (2-3), 43-57.
- McCourt, W.J., Aspden, J.A., Brook, M. 1984. New geological and geochronological data from the Colombian Andes: continental growth by multiple accretion. *J. Geol. Soc. London*. 141: 831-845.
- Mével, C., Caby, R., Kienast, J-R. 1978. Amphibolite facies conditions in the oceanic crust: example of amphibolitized flaser-gabbro and amphibolites from the Chenaillet ophiolite massif (Hautes Alpes, France). *Earth and Planetary Science Letters* 39: 98-108.
- Mével, C., Cannat, M. 1991. Lithospheric stretching and hydrothermal processes in oceanic gabbros from slow-spreading ridges. In: Peters, T.J., Nicolas, A. & Coleman, R.G. (eds) *Ophiolitic Genesis and Evolution of the Oceanic Lithosphere*. Kluwer Academic, Dordrecht, 293-312.
- Meschede, M. 1986. A method of discriminating different types of mid-ocean ridge and continental tholeiites with Nb-Zr-Y diagrams. *Chem. Geol.* 56, 207-218.
- Natland, J.H., Dick, H.J.B. 1996. Melt migration through high-level gabbroic cumulates of the East Pacific Rise at Hess Deep: the origin of magma lenses and the deep crustal structure of fast-spreading ridges. In: C. Mével C et al. (eds), *Proc. ODP, Scientific Results*, 147, Ocean Drilling Program, College Station, 21-58.
- Nicolas, A., Mainprice, D., Boudier, F. 2003. High temperature seawater circulation through the lower crust of ocean-ridges-a model derived from the Oman ophiolites. *Journal of Geophysical Research on line first*. <http://www.agu.org/pubs/current/jb/>, 108(B8), 2372.
- Nivia, A., Giselle, M., Andrew, K. 1996. El Complejo Quebradagrande una posible cuenca marginal intracratónica del Cretáceo Inferior en la cordillera Central de los Andes Colombianos. In: VII Congreso Colombiano de Geología, Memorias I: 108-123.
- Ordóñez-Carmona, O. 2001. Caracterização Isotópica Rb-Sr e Sm-Nd dos Principais Eventos Magmáticos nos Andes Colombianos. Ph.D (Unpublished), Universidade de Brasília. 176 p.
- Otten, M.T. 1984. The origin of brown hornblende in the Artfjallet gabbro and diorites. *Contrib. Mineral Petrol.* 86:189-199.
- Pallister, J.S., Knight, R.J. 1981. Rare earth element geochemistry of the Samail Ophiolite near Ibra, Oman. *J. Geophysical Research* 86: 2673-2687.

- Pearce, J.A., Norry, N.J. 1979. Petrogenetic implications of Ti, Zr, Y, and Nb variations in volcanic rocks. *Contrib. Mineral. Petrol.* 69: 33-47.
- Pedersen, R.B., Malpas, J. 1984. The origin of oceanic plagiogranites from the Karmoy ophiolite, western Norway. *Contributions to Mineralogy and Petrology*. 88: 36-52.
- Pereira, E., Ortíz, F. 2003. Contribución al conocimiento de las anfibolitas y dunitas de Medellín (Complejo Ofiolítico de Aburrá)-resumen. In: *Memorias IX Congreso Colombiano de Geología*. Medellín, pp. 207.
- Proenza, J., Escayola, M.P., Ortiz, F., Pereira, E., Correa, A.M. 2004. Dunite and associated chromitites from Medellín (Colombia). *32nd Int. Geol. Congr. Abs. Vol.*, pt. 1, abs 1-1:507.
- Raase, P. 1974. Al and Ti contents of hornblende, indicators of pressure and temperature of regional metamorphism. *Cont. Mineral Petrol.* 45: 231-236.
- Rendón, D.A. 1999. Cartografía y caracterización de las unidades geológicas del área urbana de Medellín. BsC thesis (Unpublished), Facultad de Minas, Universidad Nacional de Colombia, Medellín, 113 p.
- Restrepo, J.J. 1986. Metamorfismo en el sector norte de la Cordillera Central de Colombia. Medellín: Universidad Nacional, Facultad de Ciencias, 276 p.
- Restrepo, J.J. 2005. Anfibolitas & Anfibolitas del Valle de Aburrá. In: *X Congreso Colombiano de Geología*, Bogotá-Colombia. Memorias CD ROM.
- Restrepo, J.J., Toussaint, J.F. 1973. Obducción Cretácea en el occidente Colombiano. Publicación Especial, Geología No.3. Centro de Publicaciones U-N, Medellín. 26 p.
- Restrepo, J.J., Toussaint, J.F. 1975. Edades radiométricas de algunas rocas de Antioquia, Colombia. Publ. Esp. Geol. Universidad Nacional de Colombia, Medellín, 6: 1-24.
- Restrepo, J.J., Toussaint, J. F. 1977. Anfibolitas granatíferas de Caldas, Antioquia. Boletín Ciencias de la Tierra, Universidad Nacional de Colombia, Sede de Medellín, 2: 147-154.
- Restrepo, J.J., Toussaint, J.F. 1982. Metamorfismos superpuestos en la Cordillera Central de Colombia. In *Actas del V Congreso Latinoamericano de Geología*. 3: 505-512.
- Restrepo, J.J., Toussaint, J.F. 1984. Unidades litológicas de los alrededores de Medellín. In: 1^a conferencia sobre riesgos geológicos del Valle de Aburrá. Memorias, 1-26.
- Restrepo, J.J., Toussaint, J.F. 1988. Terranes and continental accretion in the Colombian Andes. *Episodes* 11(3): 189-193.
- Restrepo, J.J., Toussaint, J.F., González, H., Cordani, U., Kawashita, K., Linares, E., Parica, C. 1991. Precisiones geocronológicas sobre el occidente colombiano. En: *Simposio sobre magmatismo andino y su marco tectónico*. Memorias, Tomo I. Manizalez, pp. 1-22.

- Rodríguez, G., Sánchez, F. 1987. Petrografía y petroquímica del plutón de Altavista, zona central. BsC thesis (Unpublished), Facultad de Minas, Universidad Nacional de Colombia Medellín. 180 p.
- Rodríguez, G., González, H., Zapata, G. 2005. Geología de la Plancha 147 Medellín Oriental, Departamento de Antioquia. Ingeominas. 303 p.
- Rollinson, H.R. 1993. Using Geochemical Data: Evaluation, Presentation, Interpretation. Longman, London. 352p.
- Saunders, A.D., Tarney, J. 1984. Geochemical characteristics of basaltic volcanism within back arc basins. In Kokelaar B.P. and Howells MF. Eds) Marginal basin geology, Spec. Publ. Geol. Soc. London 16:59-76.
- Seifert, K., Gibson, I., Weis, D., Brunotte, D. 1996. Geochemistry of metamorphosed cumulate gabbros from hole 900A, Iberia Abyssal Plain. In: Whitmarsh, R.B., Sawyer, D.S., Klaus, A., and Masson, D.G. (Eds.), *Proc. ODP, Sci. Results*, 149: College Station, TX (Ocean Drilling Program), 471–488.
- Sun, S.-S., McDonough, W.F. 1989. Chemical and isotopic systematics of oceanic basalts: implications for mantle composition and processes. In: Saunders, A.D., Norry, M.J. (Eds.) Magmatism in the Ocean Basins. Spec. Publ. Geol. Soc. London 42: 313–345.
- Toussaint, J.F., Restrepo, J.J. 1976. Modelos orogénicos de téctonica de placas en los Andes Colombianos. Boletín Ciencias de la Tierra. Universidad Nacional de Colombia, Sede Medellín 1.
- Tribuzio, R., Tiepolo, M., Thirlwall, M.F. 2000. Origin of titanian pargasite in gabbroic rocks from the Northern Apennine ophiolites (Italy): insights into the late-magmatic evolution of a MOR-type intrusive sequence Earth and Planetary Science Letters 176: 281-293.
- Vinasco, C.J., Cordani, U.G., Vasconcelos, P. 2001. $^{40}\text{Ar}/^{39}\text{Ar}$ dates in the Central Cordillera of Colombia: evidence for an upper Triassic regional tectonomagmatic event. In: III Simposio Sudamericano de Geología Isotópica, Pucón - Chile.
- Vinasco, C.J., Cordani, U.G., González, H., Weber, M., Peláez, C. 2006. Geochronological, isotopic, and geochemical data from Permo-Triassic granitic gneisses and granitoids of the Colombian Central Andes. Journal of South American Earth Sciences 21: 355–371.

CAPÍTULO 5. DISCUSSÕES E MODELO EVOLUTIVO.

5.1 Características do ofiolito da área do Vale de Aburrá

A unidade Dunito de Medellín era considerada na área de estudo como a única componente de um ofiolito desmembrado (Restrepo & Toussaint 1973, 1974, Alvarez 1982). Posteriormente, Restrepo (1986) afirmou que seria factível que dunitos (Dunito de Medellín) e anfibolitos (Anfibolito de Medellín) fizessem parte da mesma seqüência ofiolítica. Esta última interpretação também foi sugerida por Pereira & Ortíz (2003). Correa & Martens (2000) definiram o “Complexo Ofiolítico de Aburrá” como composto pelo Dunito de Medellín e o Metagabro de El Picacho. Na definição destes autores não ficaram claramente incluídas outras unidades de anfibolitos como os de Medellín e Boquerón.

Na área de estudo quase todos os elementos essenciais de um ofiolito são encontrados de acordo com o estabelecido pela Conferência Penrose de 1972, ou seja: o peridotito de manto tectonizado, parte da zona de transição do ofiolito, rochas máficas plutônicas e vulcânicas e rochas sedimentares metamorfisadas.

Os dados de geologia de campo, geoquímicos e de isótopos radiogênicos apontam para a relação consangüínea das rochas máficas. A unidade Metagabro de El Picacho representa rochas cumuláticas, o Metagabro de Boquerón corresponde a rochas plutônicas formadas por cristalização fracionada e o Anfibolito de Santa Elena corresponde a rochas vulcânicas, embora a possibilidade de existir protolitos plutônicos nesta unidade não seja descartada. Assim, os cumulatos de El Picacho podem ser comparados com os gabros basais de outros ofiolitos, os gabros de Boquerón seriam os equivalentes dos gabros isotrópicos e varitexturados, e a unidade de anfibolito seria equivalente à porção de basaltos e possivelmente também à parte dos gabros superiores de ofiolitos.

Até o presente momento não foi reconhecido no campo enxame de diques que é comum em muitos ofiolitos. Existem várias explicações para a falta do enxame de diques: (i) não se formou originalmente, (ii) existe, mas sua identificação é dificultada em função da deformação e metamorfismo, ou (iii) existiu, mas foi tectonicamente desmembrado dos outros componentes durante alojamento tectônico ou durante processos de deformação posteriores.

As unidades de rochas metassedimentares que são o Gnaisse Milonítico de Sajonia e parte do Gnaisse de La Ceja corresponderiam às seqüências sedimentares depositadas por sobre as rochas vulcânicas do edifício ofiolítico.

É importante notar que as unidades de anfibolitos e gnaisses foram interpretadas por vários autores como unidades mais antigas que o ofiolito, as quais tinham sido colocadas,

metamorfisadas e erodidas antes do alojamento das rochas ultramáficas (Restrepo & Toussaint 1973, Rodríguez et al. 2005).

Com base nas evidências geoquímicas e isotópicas de Sr-Nd disponíveis, os anfibolitos investigados podem ser considerados como representantes da crosta máfica superior do ofiolito. Porém são necessários ainda dados geocronológicos adicionais nos anfibolitos e rochas metassedimentares para estabelecer a relação cronológica com as outras unidades do ofiolito.

Redefinição do ofiolito

Neste trabalho o Complexo Ofiolítico de Aburrá (Correa & Martens 2000) é re-definido como Ofiolito de Aburrá composto pelas seguintes unidades: Maciço ultramáfico de Medellín, Metagabros de El Picacho e Boquerón, Anfibolito de Medellín, Gnaissé milonítico de Sajonia e Gnaissé de La Ceja (excluindo os gnaisses e migmatitos da região de El Retiro).

O ambiente de geração

Todas as unidades mencionadas apresentam características geoquímicas compatíveis com origem em uma bacia de retro-arco.

A idade de geração

Estudos relacionados com o Ofiolito de Aburrá realizados nos últimos anos apontavam a geração do ofiolito no Paleozóico, no oceano Rheic (Pereira & Ortíz 2003) sendo que a obdução provavelmente ocorreu no Paleozóico Superior, durante o ciclo orogênico Varisquiano (Pereira & Ortíz 2003) ou durante a orogenia Permo-Triássica (Restrepo 2005).

Na área de estudo, Restrepo et al. (2007) obtiveram idade de 228 Ma em zircão de gabro pegmatítico que é aqui interpretado como um gábro parcialmente rodingitizado. Essa idade pode indicar o momento da serpentinação em ambiente oceânico e o instante da formação da crosta oceânica representada pelo ofiolito.

No presente estudo foi obtida a idade de 217 ($216,6 \pm 0,36$) Ma em zircão de um plagiogranito. Este valor é interpretado como a idade de metamorfismo oceânico com cislhamento e alteração hidrotermal da crosta oceânica que produziu fusão parcial dos cumulatos máficos e consequente geração de plagiogranitos.

Correa & Martens (2000) e Correa et al. (2005a) correlacionam os anfibolitos da região de Medellín com aqueles da região de El Retiro. No entanto, os anfibolitos de El Retiro foram metamorfizados há 230 Ma e se a interpretação feita neste trabalho sobre a idade do ofiolito e

a relação genética dos anfibolitos com o ofiolito é correta, então há 230 Ma o protólito dos anfibolitos de Medellín ainda não tinha se formado. Sendo assim, os anfibolitos de ambas as regiões não podem ser correlacionados.

O alojamento

Se os anfibolitos formam a parte superior da litosfera oceânica ou também se fossem um pouco mais antigos, a relação espacial atual em que peridotitos estão sobre os anfibolitos seria resultado de alojamento intra-oceânico, produzido por descolamento e empurrão inicial ao longo de dorsal oceânica que permitiria a colocação de parte do manto sobre a crosta oceânica (Figura 4). Este seria modelo análogo àquele proposto para o alojamento do ofiolito de Omã (Boudier et al. 1988, 2007).

Assim, as unidades mais próximas à base dos peridotitos representariam a sola metamórfica do ofiolito durante o alojamento intra-oceânico. Porém, até agora não foi encontrada sola metamórfica de gradiente invertido e também não tem sido possível determinar até onde chega a porção de rochas da sola. Em seguida, todo o conjunto de rochas ultramáficas+máficas+sedimentares teria sido colocado tectonicamente por obdução (?) ou acresção (?) na borda continental. O contato resultante deste último evento definiria uma sutura que até hoje não foi identificada no campo.

Uma questão que ainda não é bem entendida é porque a porção de anfibolitos e rochas metassedimentares está mais deformada do que as rochas ultramáficas e máficas plutônicas, as quais preservam bem o metamorfismo de fundo oceânico. O alojamento intra-oceânico explica a formação da sola sub-ofiolítica, mas esta geralmente atinge espessuras até de 500 m. Na área estudada anfibolitos + rochas metassedimentares exibem espessura aparente de vários quilômetros. Uma possibilidade é que a espessura atual destas unidades represente o resultado de duplicação tectônica. Outra possibilidade é a de que estas unidades tenham sido metamorfisadas em uma zona de subducção durante o deslocamento inicial do futuro ofiolito e depois o material subductado foi exumado e acrescido à base do ofiolito durante o empurrão progressivo contra a margem continental, tal como proposto por Searle & Malpas (1982) para as rochas de solas metamórficas ofiolíticas. Algumas explicações para essa deformação mais intensa nas unidades a leste dos corpos ultramáficos estão mencionadas no final do item 5.3.

Um *stock* de trondjemitos deformados conhecido como Gnaisse de La Iguaná ocorre próximo às unidades Metagabros de Boquerón e El Picacho, sendo que os trondjemitos intrudem as rochas de Boquerón. Os dados preliminares indicam que o corpo intrusivo deriva

de uma fonte máfica-ultramáfica com aporte de material continental. A idade de cristalização é de ca. 180 Ma (Correa et al. 2005b).

Uma proposta preliminar para explicar a relação dos trondjemitos de La Iguaná com as rochas maficas do ofiolito é que o stock trondjemítico tenha se formado devido à fusão parcial de rochas do manto ou dos gabros inferiores do ofiolito durante o processo de seu alojamento na borda continental. Se esta hipótese for verdadeira, então a obdução do ofiolito sobre o continente ocorreu há cerca de 180 Ma.

5.2 Correlação com outros complexos da região e proposta de modelo evolutivo

A falta de informação petrográfica, geoquímica, isotópica e geocronológica detalhada da maior parte dos conjuntos maficos e ultramáficos da Cordilheira Central da Colômbia dificulta a correlação e elaboração de modelos geológicos evolutivos destes conjuntos. Outra dificuldade na correlação das rochas ofiolíticas de Aburrá com as outras que se encontram a oeste é a presença do sistema de falhas de Romeral. As rochas de Aburrá afloram a leste da falha, enquanto que os outros conjuntos estão dentro do sistema de falhas. Porém, considerando as idades triássicas obtidas recentemente no ofiolito de Aburrá (neste trabalho; Restrepo et al., 2007) e o registro de idades também triássicas nas rochas maficas do Complexo Máfico-Ultramáfico de Heliconia (Vinasco et al., 2001), é possível fazer pelo menos uma correlação temporal. Deste modo, apresentamos uma proposta preliminar de correlação geológica das rochas de Aburrá com outras unidades maficas e ultramáficas da borda oeste da Cordilheira Central.

As unidades de rochas maficas e ultramáficas que existem a oeste do ofiolito de Aburrá e aproximadamente na mesma latitude são os complexos Quebradagrande, Heliconia e Arquia. As principais características destas unidades estão descritas no Capítulo 1 e a seguir estão sumarizadas as características que são importantes para a correlação e para o modelo evolutivo:

- (i) Complexo Quebradagrande: representa unidade vulcâno-sedimentar de afinidade oceânica e idade cretácea. Possivelmente representa uma bacia de retroarco ensílico (Nivia et al., 1996, 2006), desenvolvida há aproximadamente 145-100 Ma e fechada devido à abertura do Atlântico Sul e ao alojamento de uma parte do platô oceânico Colombiano-Caribenho há cerca de 120-100 Ma. Segundo (Nivia et al., 1996) esta unidade também pode representar parte de um arco de ilhas;

(ii) Complexo Máfico-Ultramáfico de Heliconia: consiste em rochas ultramáficas e de gabros e dioritos. Segundo Montoya & Peláez (1993) os peridotitos e gabros fazem parte de um ofiolito, enquanto que a relação genética entre os dioritos e as outras rochas não é clara. Restrepo & Toussaint (1974), González (1980) e Nivia et al. (1996) sugerem que essas rochas, por eles consideradas parte do Complexo Ofiolítico do Cauca, são cogéneticas com as do Complexo Quebradagrande. Porém, baseados nas idades Ar-Ar do gábro (230+/-3 Ma e 224+/-2 Ma) e de diorito (238+/-1 Ma e 232+/-1.6 Ma) do Complexo Heliconia, Vinasco et al. (2001) argumentam que o complexo ofiolítico associado geograficamente com o sistema de falhas Romeral é pelo menos triássico. Os mesmos autores concluem que as unidades máficas plutônicas e ultramáficas não poderiam ser contemporâneas com a seqüência vulcânica básica do Complexo Quebradagrande do Eo-Cretáceo. Giraldo et al. (2007) apresentam dados preliminares de geoquímica de um diorito e um gábro do Complexo de Heliconia e sugerem que estas rochas exibem características de ambiente tipo MORB com alguma afinidade de arco de ilhas. Estes autores argumentam que, embora as rochas de Heliconia apresentem semelhanças geoquímicas com as rochas metamáficas de Boquerón e Santa Elena, não é possível fazer uma correlação direta entre estas unidades devido à posição estrutural das mesmas;

(iii) Complexo Arquía: consiste em conjunto de rochas máficas e sedimentares metamorfisadas na fácie xisto verde a anfibolito, com fatias de rochas ultramáficas associadas. McCourt et al. (1984) propuseram modelo evolutivo, considerando as rochas do complexo Arquía como parte de um arco e de ante-arco desenvolvido no Paleozóico (há 340-350 Ma). Entretanto, a idade deste complexo ainda é desconhecida: o complexo é paleozóico para vários autores (McCourt et al. 1984, Aspden et al. 1987, Nivia et al. 2006) e cretáceo para outros (Restrepo & Toussaint 1975, Toussaint & Restrepo, 1989). De acordo com Vinasco et al. (2003), as idades triássicas do Stock de Cambumbia, e do gábro e diorito do Complexo de Heliconia definem o limite mínimo para a idade do grupo Arquía. Restrepo & Toussaint (1984) afirmam que o Anfibolito de Medellín (hoje conhecido com o nome de Santa Elena) e paragnasses associados que anteriormente eram considerados como de idade paleozóica exibem idades K-Ar 100 Ma, indicando que as rochas em questão são Cretáceas. Além disso, propõem

que os anfibolitos e paragnaisse associados podem representar um conjunto alóctone, com origem e idade semelhante às do Grupo Arquía.

A correlação do ofiolito de Aburrá com as rochas dos Complexos Heliconia e Arquía é, portanto, proposta. Propomos que o Complexo Arquía representa parte de uma região de ante-arco e arco, o complexo de Heliconia provavelmente corresponde a uma parte de arco e retro-arco, enquanto que o ofiolito de Aburrá representa uma bacia de retro-arco. Neste modelo, as porções de ante-arco e arco começaram a se desenvolver um pouco antes da região de retro-arco. Este sistema oceânico teria se desenvolvido entre o final do Triássico Médio e o começo do Triássico superior.

O modelo evolutivo proposto inclui os seguintes estágios:

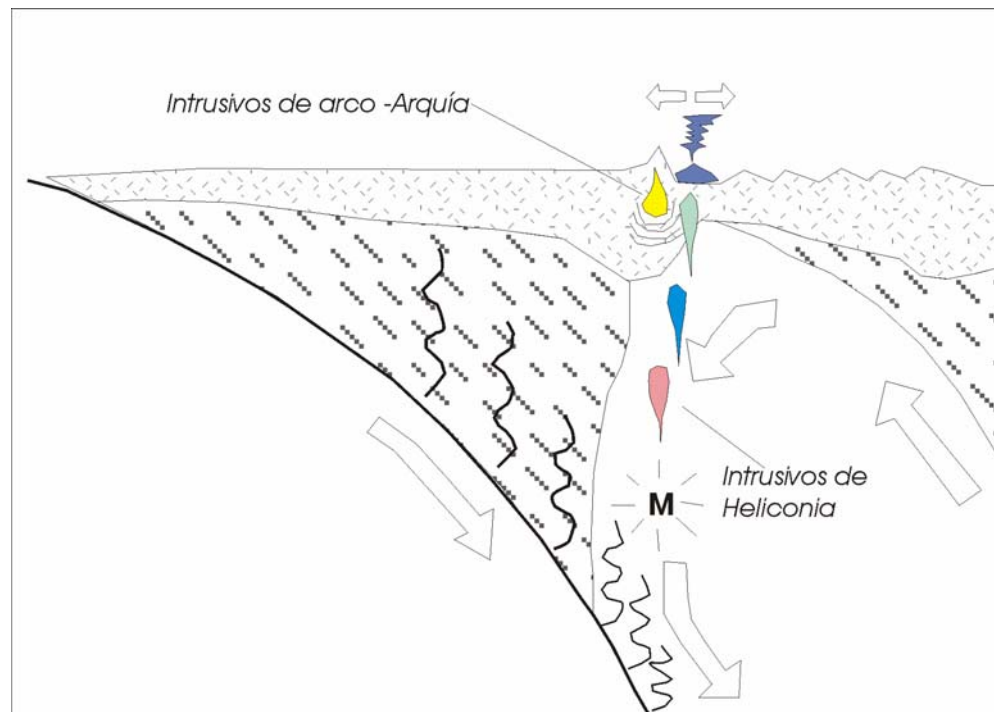
1. Metamorfismo permo-triássico resultante da colisão continente-continente durante a formação do supercontinente Pangea. Dentre as unidades metamórficas geradas nesta orogenia estão as rochas de El Retiro, os xistos de Ancón e os gnaisses e *stocks* graníticos. Vinasco et al. (2006) distinguem várias etapas desta orogênese: (a) colisão há 280 Ma, (b) magmatismo sin-tectônico há cerca de 250 Ma, gerando gnaisses graníticos, (c) colapso do orógeno e começo da ruptura do super-continente com magmatismo tardi-tectônico há cerca de 230 Ma evidenciado por *stocks* graníticos; as unidades geradas neste estágio conformam o terreno Tahamí no sentido de Toussaint & Restrepo (1989, 1994) ou o Complexo Polimetamórfico da Cordilheira Central, excluindo o Anfibolito de Santa Elena, o Gnaisse milonítico de Sajonia, e a maior parte do Gnaisse de La Ceja.

2. Contemporaneamente à etapa final do processo anterior, ou seja, no início da distensão inicia-se o desenvolvimento de um sistema oceânico relacionado com zonas de subducção e é gerada uma região de ante-arco (Complexo Arquía), arco (Complexos Arquía e Heliconia) e, logo em seguida, a de retro-arco (Complexo Heliconia e Ofiolito de Aburrá) como é mostrado na Figura 1.

O conjunto oceânico representaria um sistema de arco e bacias oceânicas equivalente aos existentes atualmente no Pacífico ocidental e na porção sul do oceano Atlântico, dentre outros. Como exemplo destes sistemas encontra-se a região do mar das Filipinas que evoluiu por meio de vários processos de formação de arco, rifteamento e expansão de retro-arco (Karig 1971) desde o Eoceno até hoje (Taylor et al. 1992). Nessa região o Palau-Kyushu Ridge e o West Mariana Ridge são arcos remanescentes separados pela bacia de retro-arco

Parece-Vela e Shikoku, sistema que foi ativo durante o Mioceno. O sistema atual está representado pelos arcos Izu-Bonin e Mariana e pelo retro-arco Mariana Trough. Outro exemplo de sistemas ante-arco, arco e retro-arco atuais é o conjunto de bacia-arco South Sandwich e a bacia de retro-arco East Scotia na porção sul do oceano Atlântico.

a) Há ~240-230 Ma



b). Há ~230-217 Ma

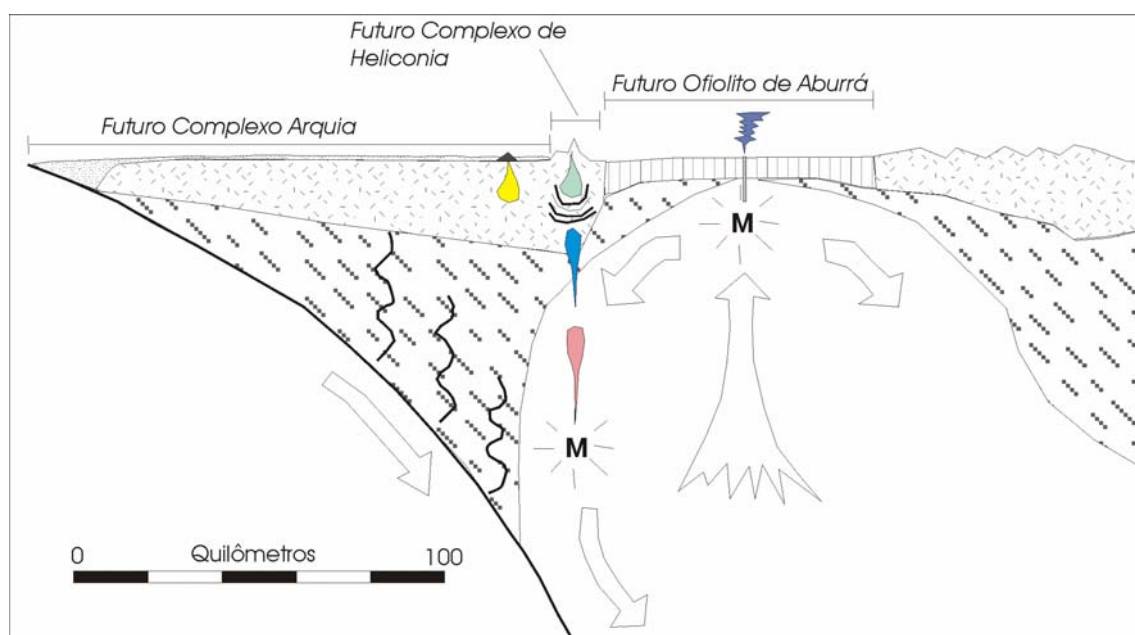


Figura 1. Proposta de modelo evolutivo dos complexos máficos e ultramáficos de Aburrá, Heliconia e Arquia. Desenho adaptado de Gribble et al. (1998).

O vulcanismo de retro-arco no Pacífico ocidental resulta da separação de um terreno de arco em uma bacia em expansão (Karig 1971, Hawkins et al. 1984 *in* Taylor et al. 1992). Isto implica que a atividade do arco é anterior à de bacia de retro-arco. A relação temporal da atividade magmática entre pares arco e bacias de retro-arco modernos tem sido discutida na literatura. Gribble et al. (1998) revisam e discutem este aspecto e encontram que para alguns autores a atividade magmática do arco é interrompida ou diminui quando ocorre o magmatismo de retro-arco, enquanto para outros existe sincronismo magmático no arco e no retro-arco.

Esta diferença temporal na atividade magmática do arco e do retro-arco permite explicar as diferenças geocronológicas existentes entre o Complexo de Heliconia e o ofiolito de Aburrá, indicando que as rochas de Heliconia estariam mais perto da porção de arco ou no eixo do arco e originaram-se um pouco antes das rochas máficas de Aburrá.

Não sabemos em que mar Triássico as unidades em questão foram formadas. Uma pergunta que surge ao momento de fazer uma correlação mais regional é a seguinte: em que posição paleogeográfica encontrava-se a bacia oceânica onde se formou o ofiolito ou o sistema de ante-arco – arco e retro-arco entre 238 Ma e 217 Ma com relação às rochas metamórficas e magmáticas de afinidade continental geradas durante a orogenia Permo-Triássica?. Não existe informação suficiente para estabelecer a posição deste sistema oceânico com relação ao conjunto continental gerado no estágio No. 1 descrito acima. Dois modelos podem ser aventados:

a) A bacia oceânica teria se desenvolvido adjacente ao terreno Tahami no Triássico Superior, por expansão de oceanos intra-pangeanos. Baseados em reconstruções apresentadas por outros autores, Cardona et al. (2006) propõem o terreno Tahamí a uma latitude vários graus a norte e leste da sua posição atual, aproximadamente no que hoje é o mar Caribe na frente do território Venezuelano (Figura 2a). Um ponto contrário a essa possibilidade é que não existem modelos claros que expliquem como o terreno Tahami migrou dessa posição no Triássico até sua posição atual.

b) Outra alternativa seria um conjunto oceânico formado no oceano Panthalassa (Oceano proto-Pacífico) perto da margem de Pangea (Figura 2b). Neste caso seria possível correlacionar os ofiolitos triássicos da Cordilheira Central da Colômbia com o ofiolito da península Vizcaíno na parte sul da Baixa California (México). O ofiolito da península Vizcaíno é interpretado como formado em zona de supra-subducção e tem idade de 221 ± 2 Ma (Kimbrough & Moore, 2003).

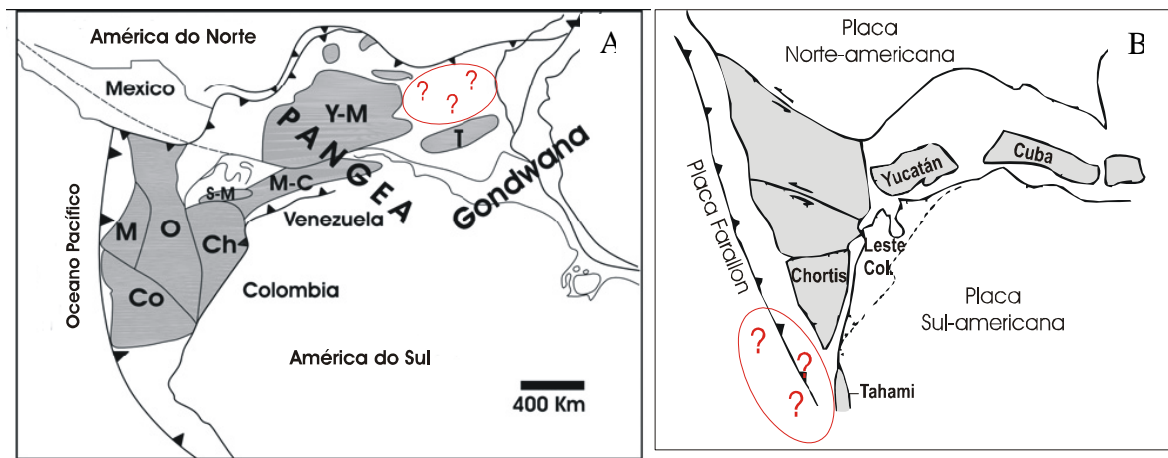


Figura 2. Modelos de reconstrução paleogeográfica dos Andes do Norte, América Central e da região Caribe no Permo-Triássico. a) Reproduzido de Cardona et al. (2006). Terrenos: T=Tahamí, Ch=Chibcha, M-C=Mérida Caparo, Co=Chortis, Y-M=Yucatán-Maya, O=Oaxaquia, M=Mixteca. b) Esquema para começos do Triássico reproduzido de Toussaint (1995). As elipses vermelhas com sinais de interrogação mostram as possíveis regiões onde ocorreram os sistemas oceânicos triássicos em discussão.

3. Alguns milhões de anos depois o regime de distensão muda para compressão e induz o alojamento intra-oceânico, colocando rochas ultramáficas e máficas plutônicas sobre rochas vulcânicas e sedimentares (Figura 3a) e consequente deformação de parte dos basaltos e sedimentos de fundo oceânico.

O conjunto oceânico aproxima-se do continente e é gerada uma zona de subducção (Figura 3b), supostamente de baixo ângulo, pois não produziu magmatismo, já que não existe registro magmático nos conjuntos de afinidade continental entre 215 e 180 Ma. Nessa zona de subducção são deformados basaltos e sedimentos para gerar as unidades de anfibolitos, gnaisses e xistos.

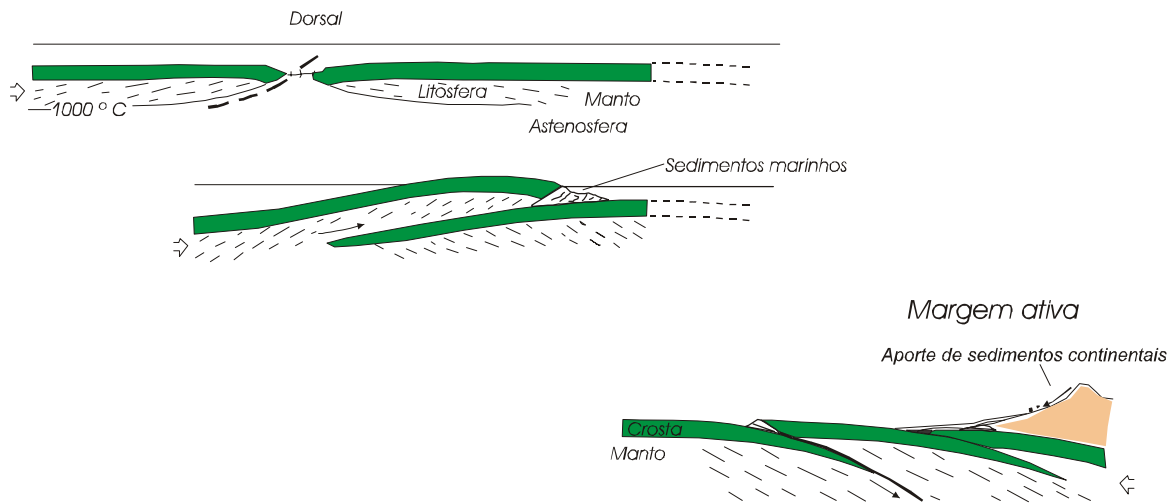


Figura 3. Proposta de modelo de alojamento intra-oceânico das unidades de Aburrá e aproximação do conjunto oceânico da borda continental.

4. No Jurássico (~180 Ma) possivelmente ocorreu o alojamento do conjunto ocêânico (Arquia, Heliconia e Aburrá) na borda continental representada pelas rochas formadas no estágio 1 (Figura 4). Esse alojamento parece ter sido de diferente natureza em várias partes, podendo ter correspondido à obdução (ou colisão) em algumas e à acresção em outras. A obdução típica de ofiolitos Tethyanos pode ter sido o mecanismo dominante durante o alojamento do ofiolito de Aburrá, enquanto a acresção em margem ativa, comum dos ofiolitos Cordilheiranos, pode ter sido mais importante no alojamento dos outros conjuntos (Heliconia e Arquia). Um modelo semelhante foi proposto por Restrepo & Toussaint (1973). Neste momento pode ter começado a zona de subducção que deu origem ao magmatismo Jurássico que hoje aflora no flanco leste da Cordilheira Central (Figura 5).

Há ~180 Ma

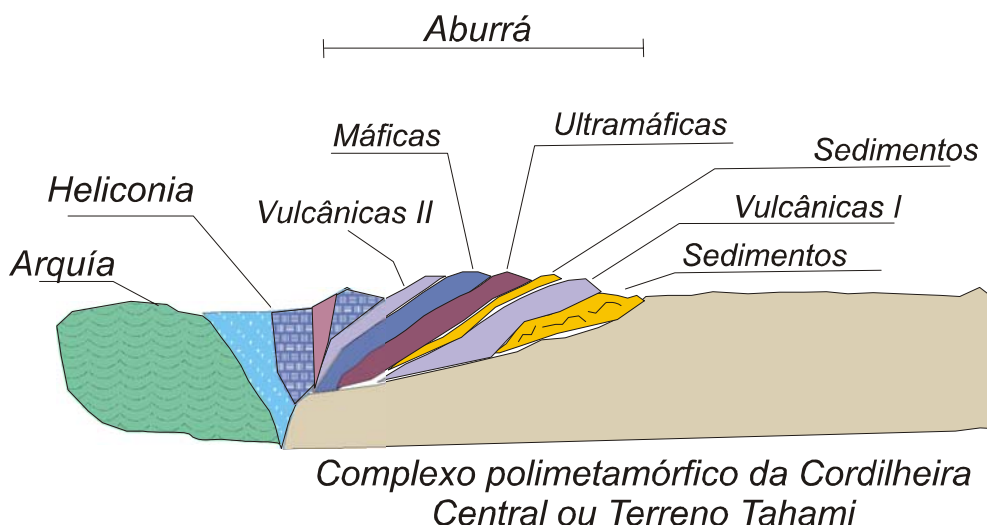


Figura 4. Esquema de alojamento dos complexos máfico-ultramáficos triássicos na borda continental. Neste modelo o Ofiolito de Aburrá teve alojamento colisional, enquanto os complexos Arquía e Heliconia foram alojados por acresção.

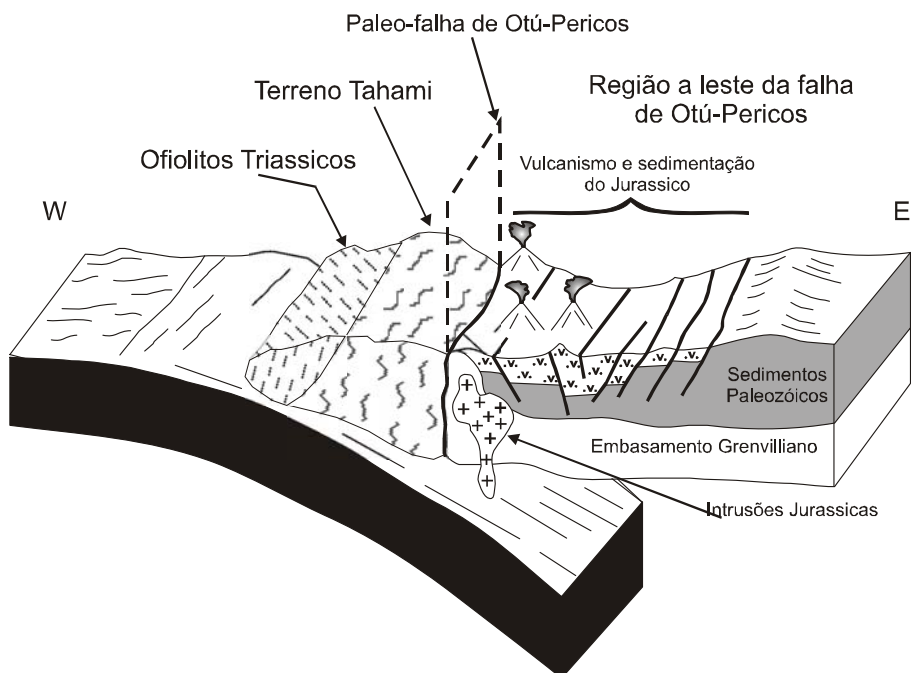


Figura 5. Esquema mostrando a zona subdução no Jurássico após alojamento dos complexos ofiolíticos triássicos no Terreno Tahami. A representação também mostra magmatismo provocado por essa subducción e o desenvolvimento da bacia de retro arco ensiálica na região do Rio Magdalena. Modificado de Toussaint & Restrepo (1994) e Ordóñez-Carmona (2001).

5. No início do Cretáceo inicia-se processo distensional que vai desagregar essa margem com rochas de afinidade oceânica já continentalizadas e parte do embasamento continental, dando origem a uma bacia marginal. O eixo de expansão ocorre entre os atuais conjuntos de Aburrá e Heliconia. Durante o Cretáceo inferior, na bacia marginal, desenvolve-se o Complexo Quebradagrande como proposto por Nivia et al. (1996, 2006) (Figura 6) e há deformação nas rochas dos complexos máficos-ultramáficos triássicos.

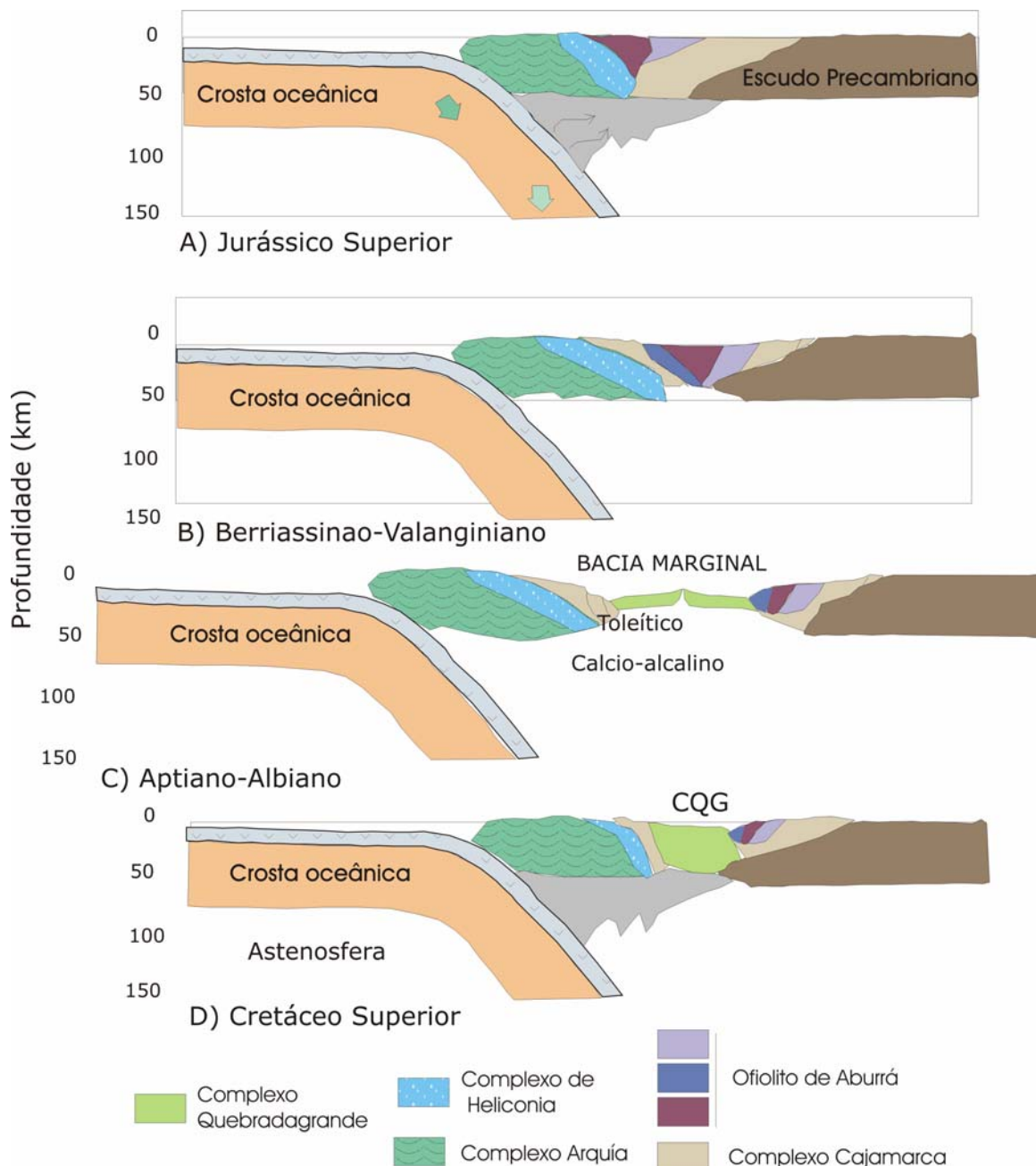


Figura 6. Diagrama esquemático que propõe a evolução da bacia marginal do Complexo Quebradagrande (CQG) e sua relação espacial com os complexos máfico-ultramáficos triássicos e o Terreno Tahami. Modificado de Nivia et al. (1996, 2006).

Neste momento de fechamento da bacia do Quebradagrande e nova compressão dos complexos da borda continental são geradas várias falhas importantes que limitam as diferentes unidades, tais como a Falha San Jerônimo, a Falha Amagá (no setor norte da Cordilheira, a oeste de Medellín) e a Falha Silvia-Pijao (Figura 7).

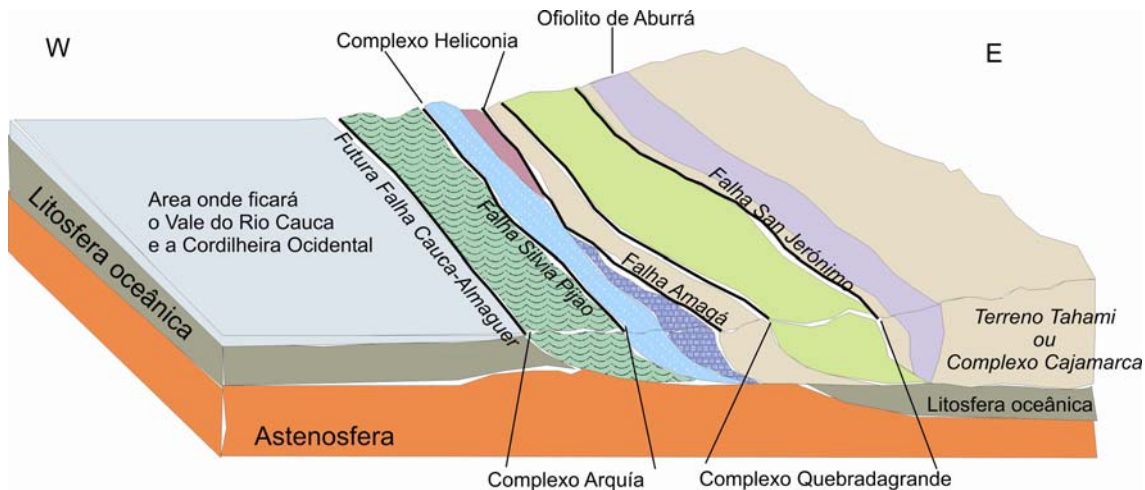


Figura 7. Representação esquemática da configuração da borda continental na porção NW da América do Sul no final do Cretáceo Inferior. Modificado de Naranjo (2001).

5. No final do Cretáceo Inferior acontece o choque da placa Pacifica contra a Placa Sul-americana e o alojamento da parte mais antiga do platô oceânico Colombiano-Caribenho. Em consequência, forma-se a sutura definida pela falha Cauca-Almaguer com deformação do Complexo Arquía, bem como as rochas de alta pressão. Nova deformação em todos os complexos máficos-ultramáficos triássicos e cretáceos também resulta desse processo.

Um argumento contrário a este modelo é que o Complexo de Heliconia não está tão deformado quanto o Complexo Arquía. Porém, Toussaint (1993) explica que as diferenças indicam uma gênese posterior para as rochas pouco deformadas ou ainda que essas rochas tenham sido preservadas do metamorfismo por estarem em nível estrutural superior ou mesmo afastadas das regiões de colisão. A segunda explicação é mais consistente com o modelo proposto no presente trabalho.

6. O início de uma zona de subducção a oeste da nova margem continental resulta em magmatismo de arco continental do Cretáceo Superior com a formação do Batólito Antioqueno na porção norte da Cordilheira Central.

O modelo proposto aqui tem algumas semelhanças com o modelo de McCourt et al. (1984) que considera uma região de arco e ante-arco, mas difere grandemente no tempo e local de geração deste sistema de arco.

Implicações para o significado do Sistema de Falhas de Romeral e nos modelos de terrenos:

O Sistema de Falhas de Romeral foi identificado desde os trabalhos de Case et al. (1971, 1973) como uma estrutura que separa dois grandes domínios com anomalias gravimétricas de Bouguer contrastantes. Os resultados geofísicos desses autores junto com a geologia mostraram que a leste da zona de falhas o embasamento é composto de crosta continental, enquanto a oeste o embasamento consiste em material de origem oceânica.

O sistema está composto por três traços de falhas principais, de leste para oeste (Maya & González 1995): Falha San Jerónimo, Falha Silvia-Pijao e Falha Cauca-Almaguer.

De maneira mais específica, a falha Cauca-Almaguer tem sido considerada por muitos autores o limite entre rochas metamórficas paleozóicas de afinidade continental e terrenos cretáceos acrescidos, de caráter oceânico (McCourt et al. 1984, Aspden & McCourt 1986; Aspden et al. 1987). Toussaint (1996) discute que o sistema de falhas de Romeral não é a sutura ou limite entre o domínio continental e oceânico e sim um sistema de dispersão. Este sistema pode, portanto, corresponder a uma sutura cretácea, mas não é o limite entre os dois grandes domínios, muito embora seja importante anotar que existe material oceânico a leste da falha, sugerindo a existência de uma sutura anterior.

Na medida em que novos dados geológicos são adquiridos na região é necessário reavaliar os modelos e interpretações pre-existentes. É preciso fazer uma análise mais detalhada do Sistema de Falhas Romeral porque este parece não representar um conjunto homogêneo e cada um dos seus componentes pode ter um significado geológico diferente. Algumas considerações são feitas a seguir:

1. Em escala continental, o sistema pode ser considerado como o limite de duas zonas, uma com embasamento continental e a outra com embasamento oceânico.
2. Na escala regional, entretanto, não é correto afirmar que o sistema separa materiais de afinidade oceânica daqueles de afinidade continental, uma vez que a leste do sistema de falhas estão expostas rochas de origem oceânica. O mesmo erro é cometido quando se considera falha Cauca-Almaguer (a mais ocidental do Sistema) como o limite entre rochas metamórficas paleozóicas de afinidade continental e terrenos cretáceos de caráter oceânico.

3. A falha Cauca-Almaguer é uma sutura do Cretáceo inferior como interpretado por McCourt et al. (1984). Porém nossa interpretação da falha difere da interpretação dos autores mencionados anteriormente porque a falha não coloca em contato materiais cretáceos com paleozóicos e sim materiais cretáceos com rochas do Mesozóico Inferior (triássicas).

4. A existência de rochas de afinidade oceânica a leste da falha Cauca-Almaguer implica que deve existir outra sutura que colocou em contato as rochas de afinidade oceânica com as de afinidade continental. Onde está esta sutura?

Qual é então o significado das falhas Silvia-Pijao e San Jerônimo?

Trabalhos recentes sobre o Complexo Quebradagrande (Nivia et al. 1996, 2006) têm mostrado que este complexo possivelmente formou-se em bacia marginal ensíatica, desenvolvida na margem do continente durante o Cretáceo Inferior. Acolhendo essa interpretação no modelo proposto no presente trabalho, as duas falhas do sistema de falhas de Romeral (San Jerônimo e Silvia-Pijao) representariam os limites da bacia marginal do Complexo Quebradagrande. Se o modelo aqui proposto for plausível, então o contato entre o domínio oceânico triássico com as rochas de afinidade continental permo-triássicas deve corresponder a uma zona de sutura, da qual ainda não se tem registro na bibliografia.

No modelo de terrenos da Colômbia (Toussaint & Restrepo 1989, 1994) as rochas oceânicas a leste de San Jerônimo são incluídas no Terreno Calima. Toussaint (1996) também anota que possivelmente o mega-Terreno Calima com embasamento oceânico consista em materiais oceânicos de diferentes proveniências e, portanto, o megaterreno consista em vários terrenos. Ordóñez-Carmona (2001) fez uma subdivisão do antigo Terreno Calima em dois terrenos: para uma porção preservou o nome Calima e para outra deu o nome de Terreno Embera. O Terreno Calima, de acordo com Ordóñez-Carmona (2001), inclui grande parte da Formação Amaime, mas com relação aos Complexos Arquía e Quebradagrande, o autor não deixa claro a qual terreno estes pertencem, ou seja, se ao Terreno Tahami ou Calima.

Como demonstrado por Nivia et al. (1996, 2006), o Complexo Quebradagrande não tem afinidade genética com Amaime. Deste modo propomos que se chame de Terreno Calima as unidades a oeste da falha Cauca-Almaguer, enquanto aquelas a leste da falha, que são de afinidade oceânica e idade triássica, que antes faziam parte do Calima, sejam excluídas deste terreno e agrupadas em um outro terreno. Este pode corresponder em grande parte ao Terreno Cauca-Romeral de Etayo et al. (1986).

6. RECOMENDAÇÕES

A seguir estão relacionadas sugestões para futuros trabalhos de pesquisa para responder uma série de questionamentos ainda pendentes em relação à evolução tectônica da região investigada. Assim julga-se necessário:

- (i) Realizar mapeamento detalhado do maciço ultramáfico; para tal sugere-se aproveitar todos os furos de sonda que foram feitos para o projeto de microzonificação sísmica da cidade bem como os testemunhos de furos disponíveis em empresas de consultoria. É importante prestar atenção no reconhecimento dos harzburgitos que ainda conservam ortopiroxênio e, ao estudar o flanco oeste do corpo ultramáfico, identificar os setores onde existe wehrlito;
- (ii) Realizar estudos estruturais de detalhe nas rochas ultramáficas para determinar possíveis padrões de fluxo do manto e/ou estruturas diapíricas;
- (iii) Tentar estabelecer as relações entre os corpos de wehrlito e as outras rochas ultramáficas e entre os wehrlitos e os metagabros, visando identificar se eles representam diques ou corpos intrusivos um pouco mais extensos;
- (iv) Realizar um estudo de isótopos estáveis nas rochas ultramáficas para identificar a origem dos fluidos responsáveis pelas diferentes fases de hidratação, ou seja, diferenciar se foram fluidos procedentes da água do mar, metamórficos e/ou meteóricos.
- (v) Executar perfis ao longo dos corpos de anfibolitos e realizar amostragem sistemática destinada a estudos geotermobarométricos, para caracterizar o metamorfismo e/ou metamorfismos.
- (vi) Determinar porque os anfibolitos e gnaisses estão mais deformados do que os peridotitos e metagabros.
- (vii) Investigar a relação entre a (extensa) unidade de anfibolitos e a unidade de rochas metamórficas que afloram na região de El Retiro.
- (viii) Estudar o contato peridotitos - anfibolitos e detalhar as características da sola metamórfica. Determinar a extensão da mesma e sua relação com a unidade maior de anfibolitos.
- (ix) Estudar a proveniência e datar rochas metassedimentares de Las Peñas e o gnaisse milonítico de Sajonia. Comparar suas fontes com aquelas das rochas paraderivadas de Las Palmas e El Retiro.

- (x) Desenvolver estudos petrológicos e geocronológicos dos conjuntos máfico-ultramáficos de Heliconia, Arquia e Yarumal e estabelecer as relações entre estas unidades e o Ofiolito de Aburrá. Determinar se as rochas de Arquia e Heliconia faziam parte de um ambiente de arco e ante-arco no Triássico, contemporâneo com a porção de retro-arco representada pelas rochas máficas e ultramáficas da região de Aburrá.
- (xi) Situar o Ofiolito de Aburrá no contexto dos complexos ofiolíticos do Caribe, América Central, e da borda oeste da América do Norte.

REFERÊNCIAS BIBLIOGRÁFICAS

- ALVAREZ, J. 1982. Tectonitas dunitas de Medellín, Departamento de Antioquia, Colombia. Informe 1986 de Ingeominas, Medellín. 62 p.
- ALVAREZ, J. 1983. Geología de la cordillera Central y el occidente colombiano y Petroquímica de los intrusivos granitoides mesocenozoicos. Ingeominas. *Boletín Geológico* **26**: (2) 175 p.
- ALVAREZ, J. 1985. Ofiolitas e evolución tectónica del Occidente Colombiano. Inf. 1988, INGEOMINAS, Medellín, 30 p.
- ALVAREZ, J. 1987. Mineralogía y química de los depósitos de cromita podiforme de las dunitas de Medellín, Departamento de Antioquia, Colombia. *Boletín Geológico* **33**: (1-3), 33-46.
- ALVAREZ, W. 1967. Geology of the Simarua and Carpintero areas, Guajira peninsula, Colombia. Disertación presentada en candidatura para el grado de Doctor en Filosofía, Princeton University. 147 p.
- ANONYMOUS. 1972. Penrose Field Conference on ophiolites. *Geotimes* **17**: 24-25.
- ARDILA, R. 1986. Petrografía de las rocas metamórficas de El Retiro- Antioquia. Medellín. Tesis de grado (inédita). Universidad Nacional, Facultad de Minas.
- ASPDEN, J.A. & MCCOURT, W.J. 1986. Mesozoic oceanic terrane in the central Andes of Colombia. *Geology* **14**: 415-418.
- ASPDEN, J.A. & MCCOURT, W.J. & BROOK, M. 1987. Geometrical Control of subduction-related magmatism: the Mezozoic and Cenozoic plutonic history of Western Colombia. *Journal of the Geological Society of London* **144**: 893-905.
- BECCALUVA, L., COLTORTI, M., GIUNTA, G. & SIENA, F. 2004. Tethyan vs. Cordilleran ophiolites: a reappraisal of distinctive tectono-magmatic features of supra-subduction complexes in relation to the subduction mode. *Tectonophysics* **393**: 163– 174.
- BOTERO, G. 1963. Contribución al conocimiento de la zona central de Antioquia. *Anales Facultad de Minas*, No. **57**. Medellín, 101 p.
- BOUDIER F., CEULENEER G., & NICOLAS A. 1988. Shear zones, thrusts and related magmatism in the Oman ophiolite: initiation of thrusting on an oceanic ridge. *Tectonophysics* **151**:275–296.
- BOUDIER F., NICOLAS A., PARRISH, R. R., WATERS D. J., SEARLE, M. P. 2007. Comment on “dating the geologic history of Oman’s Semail ophiolite: insights from U-Pb geochronology” by C. J. Warren. *Contrib Mineral Petrol* (2007) **154**:111–113.
- BOURGOIS, J., TOUSSAINT, J.F., GONZALEZ, H., AZEMA, J., CALLE, B., DESMET, A., MURCIA, L.S., ACEVEDO, A.P., PARRA, E. & TOURNON, J. 1987. Geological history of the Cretaceous ophiolitic complexes of NW South America (Colombian Andes). *Tectonophysics* **143**, 307-327.

- BOURGOIS, J., TOUSSAINT, J.F., GONZALEZ, H., ORREGO, A., AZEMA, J., CALLE, B., DESMET, A., MURCIA, L.S., PABLO, A., PARRA, E., TOURNON, J. 1985. Les Ophiolites des Andes de Colombie: Évolution Structurale et Signification Géodynamique. Symposium Paris: "Géodynamique des Caraïbes". Technip., Paris, pp. 475-493.
- CARDONA, A. M., CORDANI U.G., MACDONALD.W.D. 2006. Tectonic correlations of pre-Mesozoic crust from the northern termination of the Colombian Andes, Caribbean region. *Journal of South American Earth Sciences* **21**: 337–354.
- CARLSON, R.W., PEARSON, D.G., BOYD, F.R., SHIREY, S.B., IRVINE, G., MENZIES, A.H., GURNEY, J.J. 1999. Re-Os systematics of lithospheric peridotites: implications for lithosphere formation and preservation. Proc. 7th. Int. Kimberlite Conf., J.J. Gurny, J.L. Gurny, M.D. Pascoe, S.H. Richardson (eds.), Red Roof Design, Cape Town, p. 99-108.
- CASE, J.E., DURAN, S.L.G., LÓPEZ, A. & MOORE, W.R. 1971. Tectonic investigations on western Colombia and eastern Panama. *Geological Society of America Bulletin* **82**, 2685-2712.
- CASE, J.E., BARNES, J., PARIS, G., GONZALEZ, I.H. & VIÑA, A. 1973. Trans-Andean geophysical profile, southern Colombia. *Geological Society of America Bulletin* **84**, 2895-2904.
- CHICANGANA, G.E. VARGAS J., C., KAMMER, A. & MOLANO, J.C. 2004. Mesozoic to Cenozoic evolution of the Romeral Suture at the Northwestern South America Margin: 32nd Int. Geol. Congr.Abs. Vol., pt. 2, abs 1-1, p.1346.
- COLEMAN, R.G. 1971. Plate tectonic emplacement of upper mantle peridotites along continental edges. *Journal of Geophysical Research* **76**, 1212-1222.
- CONSTANTINOU, G. 1980. Metallogenesis associated with the Troodos Ophiolite. In: A. Panayiotou (ed.), Ophiolites, Proceedings, Intern. Ophiolite Symp. Cyprus, 1979, p. 663-674.
- CORREA A.M. & MARTENS, U. 2000. *Caracterización geológica de las anfibolitas de los alrededores de Medellín*. Facultad Nacional de Minas, Universidad Nacional de Colombia, Medellín, Trabajo Dirigido de Grado-Inédito, 363 p.
- CORREA A.M., MARTENS, U.C, RESTREPO, J.J., ORDÓÑEZ, O., PIMENTEL, M.M. 2005a. Subdivisión de las metamorfitas básicas de los alrededores de Medellín (Colombia). *Revista de la Academia Colombiana de Ciencias Exactas, Físicas y Naturales*. V. XXIX (112), 325-344.
- CORREA A.M., PIMENTEL, M.M. ARMSTRONG, R. LAUX, J.E. ORDÓÑEZ-CARMONA, O. 2005b. Edad U-Pb Shrimp y características isotópicas Nd y Sr del granito de la Iguaná, Antioquia. In: X Congreso Colombiano de Geología, Bogotá-Colombia. Memórias em CD.
- CORREA A.M., PIMENTEL, M.M., RESTREPO A., J.J., NILSON, A.A., ORDONEZ C., O., MARTENS K., U., LAUX, J., JUNGES, S. 2006. U-Pb Zircon ages and Nd-Sr isotopes of the Altavista Stock and the San Diego Gabbro: New insights on Cretaceous arc magmatism in the Colombian Andes. In: V- SSAGI V SOUTH AMERICAN SYMPOSIUM ON ISOTOPE GEOLOGY, Punta del Este, Uruguay. Short Papers V-SSAGI. Buenos Aires: IDEA GRAFICA. pp. 84 – 86.

- DEWEY, J.F. 1976. Ophiolite obduction. *Tectonophysics* **31**, 93-120.
- DILEK, Y. 2003. Ophiolite pulses, mantle plumes and orogeny. In: Dilek, Y. & Robinson, P.T. (eds) *Ophiolites in Earth History*. Geological Society, London, Special Publication, 218, 9-19.
- DROOP G.T.R. 1987. A general equation for estimating Fe³⁺ concentrations in ferromagnesian silicates and oxides from microprobe analyses, using stoichiometric criteria. *Min. Mag.* **51**, 431-435.
- ECHEVERRÍA, L.M., 1973. Zonación de las rocas metamórficas del valle de Aburrá y sus alrededores. *Anales de la Facultad de Minas* **58**, 30-56.
- ESTRADA, A. 1967. Asociación magmática básica del Nechí. Tesis de grado (Inédita). Facultad de Minas, Medellín. 88 p.
- ESTRADA-CARMONA, J., 2003. Caracterización geológica de las rocas metamórficas en los alrededores de la cuchilla Las Peñas. Universidad Nacional, Facultad de Minas, Medellín. Tesis de grado (inédita). 91 p.
- ETAYO, F. et al. 1986. Mapa de terrenos geológicos de Colombia. *Publicación Geológica Especial, Ingeominas* **14**, 1-235.
- FEININGER, T. 1980. Eclogite and related high pressure regional metamorphic rocks from the Andes of Ecuador. *Journal of Petrology* **21**, 107-140.
- FEININGER, T. 1982. Glaucomphane schist in the Andes at Jambaló, Colombia. *Canadian Mineralogist* **20**, 41-47.
- FEININGER, T. & BOTERO, G. 1982. The Antioquian Batholith, Colombia. *Publicación Geológica Especial Ingeominas*. Bogotá. **12**, 1-50.
- GEOMINAS, LTDA. 1975. Proyecto cromitas. Informe final. 39p.
- GIGUERE, E., HEBERT, R., BEAUDOIN, G., BEDARD, J.H. & BERCLAZ, A. 2003. Hydrothermal circulation and metamorphism in crustal gabbroic rocks of the Bay of Islands ophiolite complex, Newfoundland, Canada: evidence from mineral and oxygen isotope geochemistry. In: Dilek, Y. & Robinson, P.T. (eds) *Ophiolites in Earth History*. Geological Society, London, Special Publication, 218. 369-400.
- GIOIA, S.M.C.L. & PIMENTEL, M.M. 2000. The Sm-Nd Isotopic Method in the Geochronology Laboratory of the University of Brasília. *Anais da Academia Brasileira de Ciências* **72**(2), 219-245.
- GIRALDO, M. I., VINASCO C. J., WEBER, M. 2007. Esquema Geodinámico de la Parte Nor-Occidental de la Cordillera Central de Colombia. *Memorias XI Congreso Colombiano de Geología*, Bucaramanga.
- GÓMEZ, A., MORENO, M. & PARDO, A. 1995. Edad y origen de “Complejo metasedimentario de Aranzazu-Manizales” en los alrededores de Manizales (Departamento de Caldas, Colombia). *Geología Colombiana* **19**, 83-93.

- GONZÁLEZ, H. 1976. Geología del Cuadrángulo J-8 (Sonsón). Ingeominas. Informe 1704. 421 p. Medellín.
- GONZÁLEZ, H. 1980. Geología de las planchas 167 (Sonsón) y 187 (Salamina). *Boletín Geológico INGEOMINAS*, **23**(1), 174p.
- GONZALEZ, H. 1997. Mapa geológico del Departamento de Antioquia, escala 1:400.000. Memoria Explicativa. Ingeominas, Informe 2199, Santafé de Bogotá. 232 p.
- GONZÁLEZ, H. 2001. Mapa Geológico del Departamento de Antioquia. Geología, recursos minerales y amenazas potenciales. Escala 1:400.000. Memoria Explicativa. Ingeominas, 240 p.
- GRIBBLE R.F., STERN, R.F., NEWMAN, S., BLOOMER S. H. & O'HEARN, T. 1998. Chemical and Isotopic Composition of Lavas from the Northern Mariana Trough: Implications for Magma genesis in Back-arc Basins *Journal of Petrology* Volume 39: 1: 125–154.
- GROSSE, E. 1926. El Terciario Carbonífero de Antioquia. D. Reimer. E. Vohsen, Berlín. 361 p.
- JAMIESON, R.A. 1986. P-T paths from high temperature shear zones beneath ophiolites. *J. metam. Geol.* **4**:3-22.
- KARIG, D.E. 1971. Structural history of the Mariana island arc system. *Geological Society of America Bulletin*, **82**: 323-344.
- KERR, A.C., MARRINER, G.F., TARNEY, J., NIVIA, A., SAUNDERS, A.D., THIRLWALL, M.F., SINTON, C.W. 1997. Cretaceous Basaltic Terranes in Western Colombia: Elemental, Chronological and Sr-Nd Isotopic Constrains on Petrogenesis. *Journal of Petrology* **38**: 677-702.
- KERR, A.C., TARNEY, J., MARRINER, G.F., NIVIA, A., SAUNDERS, A.D., KLAVER, G.T. 1996. The geochemistry and tectonic setting of late Cretaceous Caribbean and Colombian volcanism. *Journal of South American Earth Sciences* **9**: 111–120.
- KIMBROUGH, D.L., & MOORE, T.E. 2003. Ophiolite and volcanic arc assemblages on the Vizcaíno Peninsula and Cedros Island, Baja California Sur, México: Mesozoic forearc lithosphere of the Cordilleran magmatic arc, *in* Johnson, S.E., Paterson, S.R., Fletcher, J.M., Girty, G.H., Kimbrough, D.L., and Martín-Barajas, A., eds., Tectonic evolution of northwestern México and the southwestern USA: Boulder, Colorado, Geological Society of America Special Paper 374.
- KLEIN, E.M. & LAGMUIR, C.H. 1987. Global correlations of ocean ridge basalt chemistry with axial depth and crustal thickness. *J. geophys. Res.* **92**: 8089-8115.
- KROGH TE. 1973. A low-contamination method for hydrothermal decomposition of zircon and extraction of U and Pb for isotopic age determinations. *Geochim. Cosmochim. Acta* **37**, 485-494.
- KROGH, T.E. & DAVIS, G.L. 1975. The production and preparation of ^{205}Pb for use as a tracer for isotope dilution analysis. *Carnegie Inst. Washington Yearb.*, **74**: 416-417.
- LEAKE, B.E., WOOLLEY, A.R., ARPS, C.E.S., BIRCH, W.D., GILBERT, M.C., GRICE, J.D., HAWTHORNE, F.C., KATO, A., KISCH, H.J., KRIVOVICHEV, V.G., LINTHOUT, K., LAIRD, J., MANDARINO, J.A.,

- MARESCH, W.V., NICKEL, E.H., ROCK, N.M.S., SCHUMACHER, J.C., SMITH, D.C., STEPHENSON, N.C.N., UNGARETTI, L., WHITTAKER, E.J.W., YOZHI, G. 1997. Nomenclature of amphiboles: Report of the Subcommittee on Amphiboles of the International Mineralogical Association, Commission on New Minerals and Mineral Names. *American Mineralogist* **82**: 1019–1037.
- LUDWIG, K.R. 2003. Isoplot 3.00 A geochronological toolkit for Microsoft Excel. Berkeley Geochronology Center. Special Publication No. 4.
- MACHADO, J. & SALAZAR, K. 2000. Caracterización petrográfica y geoquímica del Stock de San Diego. Medellín, Tesis de grado (inédita). Universidad Nacional, Facultad de Minas. 100 p.
- MAYA, H.M. & GONZALEZ, H. 1995. Unidades litodémicas en la cordillera Central de Colombia. *Boletín Geológico. INGEOMINAS* **35**: 43-57.
- MCCOURT, W.J., ASPDEN, J.A. & BROOK, M. 1984. New geological and geochronological data from the Colombian Andes: continental growth by multiple accretion. *J. Geol. Soc. London*. **141**: 831-845.
- MCCOURT, W.J. & FEININGER, T. 1984. High pressure metamorphic rocks in the Central Cordillera of Colombia. *Brit. Geol. Surv. Rep. Series*. **16/1**: 28-35.
- MEJÍA V. M. & DURANGO, J.R. 1981. Geología de las lateritas niquelíferas de Cerro Matoso. *Bol. de Geología- UIS*, **15**:(29): 117-123.
- MÉVEL, C. & CANNAT, M. 1991. Lithospheric stretching and hydrothermal processes in oceanic gabbros from slow-spreading ridges. In: Peters, TJ., Nicolas, A. & Coleman, R.G. (eds) Ophiolitic Genesis and Evolution of the Oceanic Lithosphere. Kluwer Academic, Dordrecht, 293-312.
- MILLWARD, D., MARRINER, G., & SAUNDERS, A.D. 1984. Cretaceous tholeiitic volcanic rocks from the Western Cordillera of Colombia. *Journal of the Geological Society, London* **141**: 847–860.
- MIYASHIRO, A. 1973. The Troodos ophiolite complex was probably formed in an island arc. *Earth and Planetary Science Letters* **19**: 218-224.
- MOJICA, J., PATARROYO, P., CAMARGO, G. & ARÉVALO, O.J. 2001. Sedimentitas del Aptiano Tardío en el Flanco Occidental de la Cordillera Central, Río Lejos, Pijao, Quindío-Colombia. In: VIII Congreso Colombiano de Geología, *Memorias em CD* (Estratigrafia, trabalho 6).
- MONTOYA, T. 1987. Petrografía y petroquímica del plutón de Altavista, zona norte. Facultad de Minas, Universidad Nacional de Colombia Medellin. Tesis de grado-inédita.
- MONTOYA, D. & PELÁEZ, I. 1993. Ultramafitas y rocas relacionadas de Heliconia, Antioquia. Tesis de grado (inédita). Facultad de Minas, Universidad Nacional, Medellín. 223p.
- MOORES, E.M. 1982. Origin and emplacement of ophiolites. *Rev. Geophys. Space Physics* **20**: 735-760.
- MOORES, E.M, & TWISS, R.J. 1995. Tectonics. W.H. Freeman and Co., 415 p.
- MORIMOTO, N. 1989. Nomenclature of pyroxenes. *Canadian Mineralogist* **27**: 143-156.

- NARANJO J. L.H. 2001. Modelo de Evolucion Morfotectonica del Sistema de Fallas de Romeral entre Pereira (Risaralda) y Filadelfia (Caldas). In Memórias VIII Congreso Colombiano de Geología. Manizalez-Colombia.
- NIVIA, A. 1987. Geochemistry and origin of the Amaime and Volcanic Sequences, Southwestern Colombia: Unpublished Master of Philosophy thesis. University of Leicester, Leicester, UK, 163 p.
- NIVIA, A. 1993. Evidencias de obducción en el Complejo Ultramáfico de Bolívar. In: VI Congreso Colombiano de Geología, *Memorias I*: 63-79.
- NIVIA, A. 1996. El Complejo Estructural Dagua, registro de deformación de la Provincia Litosférica Oceánica Cretácea Occidental en un prisma acrecionario. In: VII Congreso Colombiano de Geología, *Memorias I*: 54-67.
- NIVIA, A. & GÓMEZ, J. 2005. El Gabro Santa Fe de Antioquia y la Cuarzodiorita Sabanalarga, una propuesta de nomenclatura litoestratigráfica para dos cuerpos plutónicos diferentes agrupados previamente como Batolito de Sabanalarga en el Departamento de Antioquia, Colombia. In: X Congreso Colombiano de Geología, Bogotá-Colombia. Memórias em CD.
- NIVIA, A., GISELLE M. & ANDREW, K. 1996. El Complejo Quebradagrande una posible cuenca marginal intracratónica del Cretáceo Inferior en la cordillera Central de los Andes Colombianos. In: VII Congreso Colombiano de Geología, *Memorias I*: 108-123.
- NIVIA, A., GISELLE M., ANDREW, K. & TARNEY, J. 2006. The Quebradagrande Complex: A Lower Cretaceous ensialic marginal basin in the Central Cordillera of the Colombian Andes. *Journal of South American Earth Sciences* **21**: 423 – 436.
- O'HANLEY D.S. 1996. Serpentinites. Records of Tectonic and Petrological History, Oxford Monographs on Geology and Geophysics, v. 34, Oxford University Press, New York - Oxford, 1-277.
- ORDÓÑEZ-CARMONA, O. 2001. Caracterização Isotópica Rb-Sr e Sm-Nd dos Principais Eventos Magmáticos nos Andes Colombianos. Instituto de Geociências, Universidade de Brasília. Tese de Doutorado-Inédita. 176 p.
- ORDÓÑEZ-CARMONA,O. & PIMENTEL M.M. 2001. Consideraciones geocronológicas e isotópicas del Batolito Antioqueño. *Revista de la Academia Colombiana de Ciencias Exactas, Físicas y Naturales* **25**(94): 27-35.
- ORDÓÑEZ-CARMONA,O. & PIMENTEL M.M. 2002. Preliminary Sr and Nd Isotopic and Geochronological Study of the Puquí Complex, Colombian Andes. *Journal of the South American Earth Sciences* **15**: 173-182.
- ORDÓÑEZ-CARMONA,O., PIMENTEL, M.M., CORREA M, A.M., MARTENS K, U. & RESTREPO A, J.J. 2001. Edad Sm/Nd del metamorfismo de alto grado de El Retiro (Antioquia). Memórias VIII Congreso Colombiano de Geología. Manizalez-Colombia.

- ORREGO, A. CEPEDA, H. & RODRÍGUEZ, G.I. 1980. Esquistos glaucofánicos em el área de Jambaló. *Geol. Norandina* **10**: 161-202.
- PEARCE, J.A., LIPPARD, S.J. & ROBERTS, S. 1984. Characteristics and tectonic significance of supra-subduction zone ophiolites. In: Kokelaar, B.P. & Howells, M.F. (eds) Marginal Basin Geology. Geological Society, London, Special Publications, 16: 77-94.
- PEREIRA, E. & ORTIZ, F. 2003. Contribución al conocimiento de las anfibolitas y dunitas de Medellín (Complejo Ofiolítico de Aburrá)-resumen. In: Memorias IX Congreso Colombiano de Geología. Medellín, p. 207.
- PÉREZ, A.G. 1967. Determinación de la edad absoluta de algunas rocas de Antioquia por métodos radioactivos. *Revista Dyna*, **84**: 27-31.
- PIMENTEL, M.M., DANTAS E.L., FUCK, R.A., AMSTRONG, R 2003. SHRIMP and conventional U-Pb age, Sm-Nd isotopic characteristics and tectonic significance of the K-rich Itapuranga suíte in Goiás, Central Brazil. *Acad. Bras. Ciencias*, **75**(1): 97-108.
- PRECIADO L. M. & VÁSQUEZ, H. J. 1987. Petrografía y petroquímica del plutón de Altavista, zona sur. Tesis de grado (inédita), Facultad de Minas, Universidad Nacional de Colombia Medellin.
- PRINZHOFER, A. & ALLEGRE, C.J. 1985. Residual peridotites and the mechanism of partial melting. *Earth and Planetary Science Letters* **74**: 251-265.
- RENDÓN, D. A. 1999. Cartografía y caracterización de las unidades geológicas del área urbana de Medellín. Universidad Nacional, Facultad de Minas, Medellín. Tesis de grado (inédita). 113 p.
- RESTREPO, J.J. 1986. Metamorfismo en el sector norte de la Cordillera Central de Colombia. Medellín: Universidad Nacional, Facultad de Ciencias, 276 p.
- RESTREPO, J. J. 2003. Edad de generación y emplazamiento de ofiolitas en la Cordillera Central: un replanteamiento (resumen). En: Memorias IX Congreso Colombiano de Geología. Medellín: 48-49.
- RESTREPO, J.J. 2005. Anfibolitas & Anfibolitas del Valle de Aburrá. In: X Congreso Colombiano de Geología, Bogotá-Colombia. Memórias em CD.
- RESTREPO, J.J., FRANTZ, J.C., ORDÓÑEZ-CARMONA, O., CORREA, A.M., MARTENS, U., CHEMALE, F. 2007. Edad triásica de formación de la Ofiolita de Aburrá, flanco occidental de la cordillera Central. In: Memorias XI Congreso Colombiano de Geología, Bucaramanga.
- RESTREPO, J.J. & TOUSSAINT, J.F. 1973. Obducción Cretácea en el occidente Colombiano. *Publicación Especial, Geología* No.3. Centro de Publicaciones U-N, Medellín. 26 p.
- RESTREPO, J.J. & TOUSSAINT, J.F. 1974. Obducción Cretácea en el occidente Colombiano. *Anales de la Facultad de Minas*, **58**: 73-105.
- RESTREPO, J.J. & TOUSSAINT, J.F. 1975. Edades radiométricas de algunas rocas de Antioquia, Colombia. *Publ. Esp. Geol.* Universidad Nacional de Colombia, Medellín, **6**: 1-24.

- RESTREPO, J.J. & TOUSSAINT, J.F. 1982. Metamorfismos superpuestos en la Cordillera Central de Colombia. In *Actas del V Congreso Latinoamericano de Geología*. **3**: 505-512.
- RESTREPO, J.J. & TOUSSAINT, J.F. 1984. Unidades litológicas de los alrededores de Medellín. In: 1^a conferencia sobre riesgos geológicos del Valle de Aburrá. *Memorias*, 1-26.
- RESTREPO, J.J. & TOUSSAINT, J.F. 1988. Terranes and continental accretion in the Colombian Andes. *Episodes* **11**(3): 189-193.
- RESTREPO, J.J. & TOUSSAINT, J.F. 1989. Terrenos alóctonos en los Andes Colombianos: explicación de algunas paradojas. V Congreso Colombiano de Geología. Bucaramanga, Tomo I, 92-107.
- RESTREPO, J.J.; TOUSSAINT, J.F.; GONZÁLEZ, H.; CORDANI, U.; KAWASHITA, K.; LINARES, E.; PARICA, C. 1991. Precisiones geocronológicas sobre el occidente colombiano. En: Simposio sobre magmatismo andino y su marco tectónico. *Memorias*, Tomo I. Manizalez, p. 1-22.
- RICO, H. 1965. Estudio geológico en Santa Rosa de Osos y municipios vecinos. Trabajo Dirigido de Grado (Inédito), Facultad de Minas, Universidad Nacional de Colombia, Medellín, 106 p.
- RODRIGUEZ, G., GONZÁLEZ, H. & ZAPATA, G. 2005. Geología De La Plancha 147 Medellín Oriental, Departamento de Antioquia. Ingeominas. 303 p.
- RODRIGUEZ, G. & SANCHEZ, F. 1987. Petrografía y petroquímica del plutón de Altavista, zona central. Tesis de grado (inédita), Facultad de Minas, Universidad Nacional de Colombia Medellin.
- SEARLE, MP. & MALPAS J. 1982. Petrochemistry and origin of sub-ophiolitic metamorphic and related rocks in the Oman Mountains. *Journal of the Geological Society, London*, **139**:235-48.
- SEPÚLVEDA, L., 2003. Ultramafitas del Cabo de la Vela y rocas gabróicas asociadas. Tesis de grado (inédita), Facultad de Minas, Universidad Nacional de Colombia, Sede Medellín. 113 p.
- SHERVAIS, J.W. 2001. Birth, death, and resurrection: The life cycle of suprasubduction zone ophiolites. *Geochem. Geophys. Geosyst.*, **2**, doi:10.1029/2000GC000080.
- TAMAYO, L.M. 1984. Análisis y mediciones de miniestructuras en la anfibolita del Grupo Ayurá-Montebello. Tesis de grado (inédita), Facultad de Minas, Universidad Nacional de Colombia, Medellín.
- TAYLOR, R.N., MURTON, B. J.2 & NESBIT, R.W. 1992. Chemical transects across intra-oceanic arcs: implications for the tectonic setting of ophiolites In: Parson, L. M., Murton, B. J., Browning, P. (eds), *Ophiolites and their Modern Oceanic Analogues*. Geological Society Special Publication No. **60**:117-132.
- TOUSSAINT, J.F. 1993. Evolución Geológica de Colombia – Precámbrico y Paleozoico. Ed : Univ. Nac. Medellín. Tomo1 : 229p.
- TOUSSAINT, J.F. 1995. Evolución Geológica de Colombia – Triássico y Jurásico. Ed : Univ. Nac. Medellín. Tomo 2 : 94p.

- TOUSSAINT, J. F. 1996. Evolución Geológica de Colombia 3: Cretácico. Universidad Nacional, Facultad de Minas, Medellín. 277p.
- TOUSSAINT, J.F. & RESTREPO, J.J. 1976. Modelos orogénicos de téctonica de placas en los Andes Colombianos. Boletín Ciencias de la Tierra. Universidad Nacional de Colombia, Sede Medellín 1, p. 1-47.
- TOUSSAINT, J.F. & RESTREPO, J.J. 1978. Edad K/Ar de dos rocas básicas del flanco noroccidental de la Cordillera Central. Publicación especial de Geología, Universidad Nacional, 17: 1-1.
- TOUSSAINT, J.F. & RESTREPO, J.J. 1987. Collages de Megaterrenos alóctonos en la Cordillera central de Colombia. Memorias Seminario Gerardo Botero. Medellín, 1-12.
- TOUSSAINT, J.F. & RESTREPO, J.J. 1989. Acreciones sucesivas en Colombia: Un Nuevo modelo de evolución geológica. V Congreso Colombiano de Geología. Bucaramanga, Tomo I, 127-146.
- TOUSSAINT, J.F. & RESTREPO, J.J. 1994. The Colombian Andes during Cretaceous time. In: Cretaceous Tectonics of the Andes. Ed; Vieweg & Sohn, Wiesbaden: 61-100.
- VAKANJAC, B. & LLICH, M. 1980. Non-metallics in the ultramafites of the ophiolite complex of Yugoslavia. In: A. Panayiotou (ed.), Ophiolites, Proceedings, Intern. Ophiolite Symp. Cyprus, 1979, p. 722-726.
- VINASCO, C.J., CORDANI, U.G., VASCONCELOS, P. 2001. $^{40}\text{Ar}/^{39}\text{Ar}$ dates in the Central Cordillera of Colombia: evidence for an upper Triassic regional tectonomagmatic event. In: III Simposio Sudamericano de Geología Isotópica, Pucón - Chile.
- VINASCO, C., CORDANI, U., GONZÁLEZ, H., VASCONCELOS, P. & LIU, D. 2003. Tectonomagmatic evolution of the northern part of the Central Cordillera of Colombia using Ar-Ar and U-Pb Shrimp methodologies (resumen). In: Memorias IX Congreso Colombiano de Geología. Medellín: 57-58.
- VINASCO, C.J., CORDANI, U.G., GONZÁLEZ, H., WEBER, M., & PELAEZ, C. 2006. Geochronological, isotopic, and geochemical data from Permo-Triassic granitic gneisses and granitoids of the Colombian Central Andes. *Journal of South American Earth Sciences* **21**: 355–371.
- WAKABAYASHI, J. & DILEK, Y. 2003. What constitutes “emplacement” of an ophiolite?: Mechanisms and relationship to subduction initiation and formation of metamorphic soles. In: Dilek, Y. & Robinson, P.T. (eds) Ophiolites in Earth History. Geological Society, London, Special Publication, 218: 427-447.
- WEBER, M., CARDONA, A., PANIAGUA, F. & SEPÚLVEDA, L. 2004. Complejo máfico-ultramáfico del Cabo de la Vela, península de la Guajira, Colombia: Registro oceánico de la separación de Norte y Sudamérica. Libro de resúmenes, IV Reunión Nacional de Ciencias de la Tierra, 202.
- WILLIAMS, H. & SMYTH, W. R. 1973. Metamorphic aureoles beneath ophiolite suites and Alpine peridotites: tectonic implications with west Newfoundland examples. *American Journal of Science* **273**: 594–621.

ANEXOS

ANEXO 1

ARTIGO PUBLICADO

SUBDIVISIÓN DE LAS METAMORFITAS BÁSICAS DE LOS ALREDEDORES DE MEDELLÍN – CORDILLERA CENTRAL DE COLOMBIA

por

Ana María Correa M.¹, Uwe Martens², Jorge Julián Restrepo A.³,
Oswaldo Ordóñez-Carmona⁴ & Marcio Martins Pimentel⁵

Resumen

Correa A.M., U. Martens, J. J. Restrepo, O. Ordóñez-Carmona & M. Martins.: Subdivisión de las metamorfitas básicas de los alrededores de Medellín – Cordillera Central de Colombia. Rev. Acad. Colomb. Cienc. **29** (112): 325-344. 2005. ISSN 0370-3908.

Las características encontradas en las metamorfitas básicas que afloran en los alrededores de la ciudad de Medellín permiten diferenciar al menos dos grupos principales: uno compuesto por grandes cuerpos de metabasaltos anfibolíticos sin texturas reliquia que corresponden a la mayor parte de la unidad *Anfibolitas de Medellín* y otro grupo formado por cuerpos menos extensos de plutones bandeados y metamorfizados, los cuales constituyen los *Metagabros de El Picacho*. Los metagabros se metamorfizaron hidrotermalmente en facies esquisto verde - anfibolita baja y corrientemente presentan estructuras miloníticas y están relacionados espacialmente con las Dunitas de Medellín, conformando, junto con éstas, el *Complejo Ofiolítico de Aburrá*.

Palabras clave: Anfibolitas, gabros bandeados, Medellín, El Picacho, Cordillera Central, Colombia.

- ¹ Facultad de Minas, Universidad Nacional de Colombia. A.A. 1027 Medellín – Colombia, Instituto de Geociencias – Universidad de Brasilia – Brasil. CEP 70910-900. Correo electrónico: anamacor@unb.br
- ² Facultad de Minas, Universidad Nacional de Colombia. A.A. 1027 Medellín – Colombia, Centro Universitario del Norte, Universidad de San Carlos de Guatemala. Correo electrónico: uwe.martens@geoguate.net
- ³ Facultad de Minas, Universidad Nacional de Colombia. A.A. 1027 Medellín – Colombia. Correo electrónico: jrestrep@epm.net.co
- ⁴ Facultad de Minas, Universidad Nacional de Colombia. A.A. 1027 Medellín – Colombia. Correo electrónico: oordonez@unalmed.edu.co
- ⁵ Instituto de Geociencias – Universidad de Brasilia – Brasil. CEP 70910-900.

Abstract

Based on the features discovered in metamorph rocks from Medellin, two different rock units may be identified. One of them, *Medellín Amphibolites*, is an extensive amphibolitic body that shows no relics of its metavolcanic protolith and is frequently associated with metasediments. We redefine this unit as not enclosing banded metagabbros, which should be regarded as a separate lithostratigraphic unit that we designate *El Picacho Metagabbros*. El Picacho Metagabbros show greenschist- to lower-amphibolite-facies parageneses, conspicuous mylonitic structure, no relation to metasediments, and spatial association to the Medellin Dunite. We propose that these gabbros and peridotites constitute the *Aburrá Ophiolitic Complex*.

Key words: Amphibolites, banded gabbros, Medellín, El Picacho, Central Cordillera, Colombia.

Geología regional

El basamento metamórfico del eje de la cordillera Central en los alrededores de Medellín está compuesto por metabasitas y gneises de alto grado, asociados con esquistos de bajo grado (Botero, 1963; Echeverría, 1973; Restrepo & Toussaint, 1984). Botero (1963) agrupó estas rocas dentro del Grupo Ayurá – Montebello, que fue subdividido por Echeverría (1973) en la Zona Ayurá para el conjunto de alto grado, y la Zona Montebello para el de grado bajo. Restrepo & Toussaint (1982; véase también Restrepo *et al.*, 1991), al identificar varios metamorfismos superpuestos en las metamorfitas de la cordillera, eventos Devónico-Carbonífero, Pérmico-Triásico, y Cretácico, proponen renombrar la unidad como Complejo Polimetamórfico de la Cordillera Central. En efecto, trabajos geocronológicos recientes con el sistema U-Pb Shrimp, apoyan la idea del carácter polimetamórfico de la unidad (Ordóñez, 2001; Vinasco *et al.*, 2003).

El complejo incluye cuerpos mayores de anfibolitas (Figura 1) que se agrupan bajo el nombre de Anfibolitas de Medellín (Restrepo & Toussaint, 1984) por su ubicación cercana a dicha ciudad. Dataciones de tales rocas, como las obtenidas por Restrepo *et al.* (1991), sirvieron de fundamento para proponer un evento metamórfico cretácico; se sugirió que las metabasitas serían correlacionables con las rocas del Complejo Arquía, correspondiendo a la parte básica de una ofiolita que se habría metamorfoseado en una zona de subducción cretácica (Toussaint, 1996). McCourt *et al.* (1984) estudiaron rocas del Complejo Arquía más al sur, y no concuerdan con una edad cretácica para el metamorfismo, sino que la consideran paleozoica o anterior. Dataciones recientes Ar-Ar de las Anfibolitas de Medellín (Martens & Dunlap, 2003) indican que las edades cretácicas obtenidas se deben a perturbaciones térmicas producidas por la intrusión de grandes plutones mesozoicos como el Batolito Antioqueño; la edad de metamorfismo sería más antigua, posiblemente dentro del lapso Pérmico-Triásico.

Al norte y oriente del valle de Aburrá yace la Dunita de Medellín, una unidad ultramáfica elongada que contiene cuerpos menores de harzburgita (Figura 1), en contacto tectónico, generalmente subhorizontal, con las anfibolitas de Medellín (Restrepo & Toussaint, 1974; Álvarez, 1987). El emplazamiento de las rocas ultramáficas probablemente ocurrió entre el Triásico y el Cretácico (Restrepo & Toussaint, 1974 y 1978; Álvarez, 1987) aunque propuestas más recientes sugieren que el emplazamiento pudo darse antes o durante la orogenia Pérmico-Triásica (Restrepo, 2003). En la literatura hay referencias en las que se plantea que tanto las anfibolitas como las ultramafitas pertenecen a una ofiolita desmembrada (Álvarez, 1987; Toussaint, 1996), sin que al momento se hayan señalado otras litologías en los alrededores de Medellín que puedan formar parte de tal.

Otros cuerpos geológicos importantes en la parte septentrional de la cordillera Central son los intrusivos mesozoicos de composición básica a intermedia, dentro de los que se destaca el Batolito Antioqueño, del cual se han obtenido edades de enfriamiento del sistema K/Ar en biotita entre ~ 65 y 90 Ma. Al oriente de Medellín el batolito es intrusivo en anfibolitas y gneises de alto grado, y posiblemente también en los cuerpos ultramáficos (Restrepo & Toussaint, 1984; Álvarez, 1987), limitando al Cretácico Tardío la edad mínima del metamorfismo de las anfibolitas y del emplazamiento de las ultramafitas.

Objetivo

Varios autores han advertido diferencias considerables en las anfibolitas que afloran en los alrededores de Medellín (valle de Aburrá) y han dejado duda sobre la conveniencia de agruparlas en una sola unidad litoestratigráfica (Restrepo, 1986; INGEOMINAS, 1996; Rendón, 1999). Las diferencias son especialmente notables entre las metabasitas que yacen en las vertientes oriental y occidental del valle.

Este trabajo tiene como objeto presentar una subdivisión de las metamorfitas básicas que afloran en los alrededores de Medellín en dos unidades principales, con base en las notables diferencias estructurales, petrográficas y geoquímicas que presentan, y proponer un origen particular para cada una. Se verá que en la zona hay grandes

cuerpos anfibolíticos que no tienen estructuras reliquia y que se interpretan como metabasaltos, y cuerpos menos extensos de metagabros bandeados, que constituyen una unidad más que puede ser integrada dentro de una posible ofiolita desmembrada en los alrededores del valle de Aburrá.

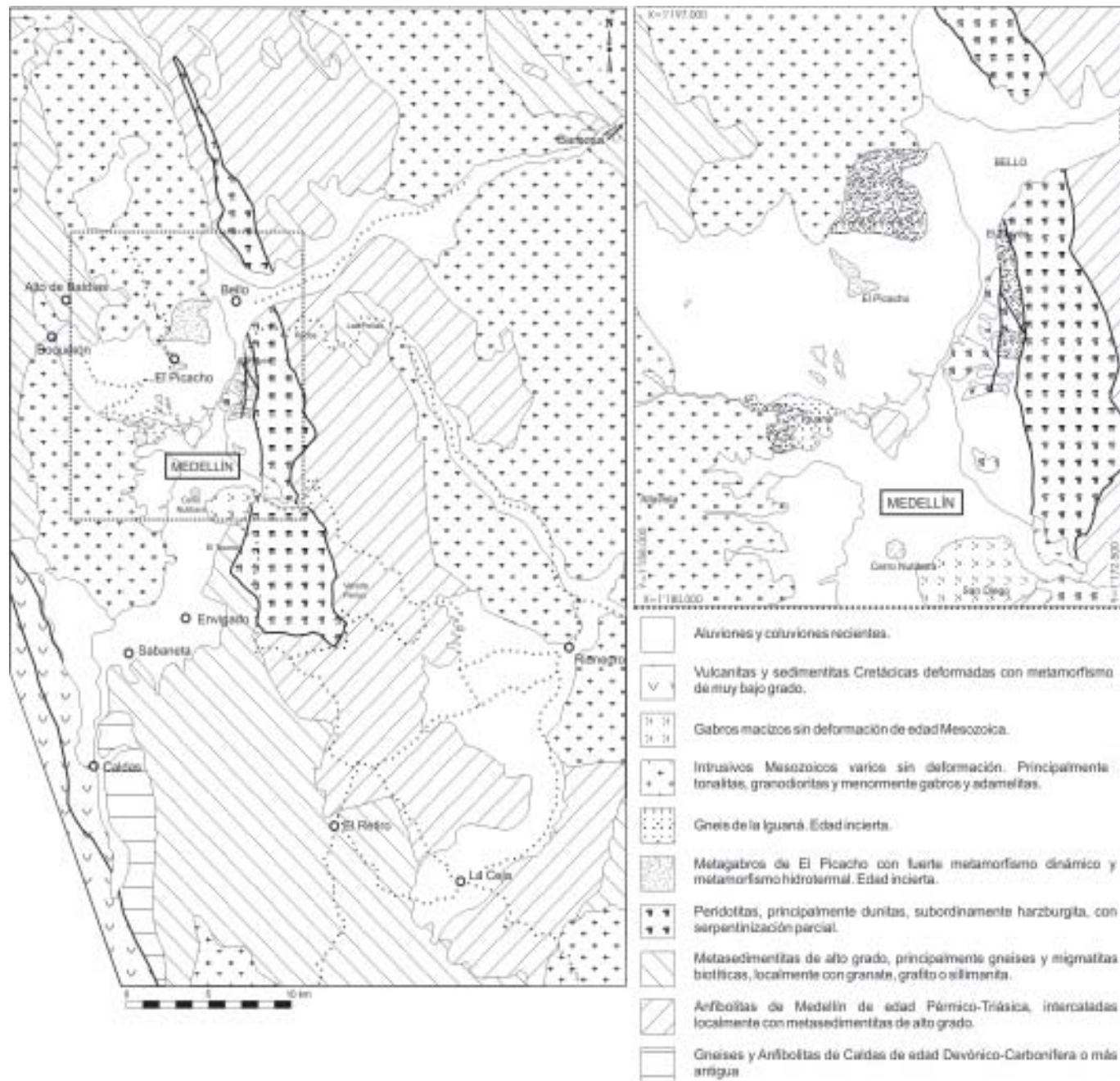


Figura 1. Mapa geológico de los alrededores de la ciudad de Medellín. Adaptado de Botero (1963), Ingeominas (1997), Rendón (1999), Estrada (2003)

Este trabajo se desarrolló principalmente como tesis de grado en la Facultad de Minas de la Universidad Nacional, Sede Medellín.

Metagabros de El Picacho

Los *Metagabros de El Picacho* se definen como una nueva unidad en la litoestratigrafía de los alrededores de Medellín. Estas rocas afloran en el cerro El Picacho y sus alrededores (sector noroccidental de Medellín; Figura 1), en el cerro Nutibara (centro de la ciudad), sector de El Tesoro (oriente), autopista Medellín Bogotá y barrio El Playón (nororiente). Se encuentra además gran cantidad de bloques de metagabros en los extensos depósitos de vertiente al occidente de Medellín; en menor cantidad existen bloques dispersos en la vereda Perico al oriente de la ciudad. A diferencia de las Anfibolitas de Medellín, los Metagabros de El Picacho afloran como cuerpos aislados, de menor tamaño y no están asociados con paragneises.

Características mineralógicas y estructurales

La paragénesis mineral está representada por minerales primarios y secundarios, siendo estos últimos los más abundantes. Los minerales primarios son clinopiroxeno y plagioclasa. Los minerales secundarios son anfíboles, plagioclasa y en menor cantidad cuarzo, epidota, y ocasionalmente opacos (Tabla 1).

El clinopiroxeno es anhedral, en granos pequeños, de incoloro a verde claro. Los clinoanfíboles ocurren en cristales prismáticos medios con bordes irregulares, cuyo pleocroísmo varía de incoloro a verde muy claro, y en agregados aciculares a fibrosos finos (Figura 2a), con pleocroísmo de verde claro a verde azulado. Este mineral reemplaza a un máfico anterior, un piroxeno y quizás otro anfíbol primario. La plagioclasa está intensamente sausuritizada, lo que indica que la plagioclasa original tenía un componente cálcico importante. No fue posible determinar su composición por el método Michel Lévy. Los granos son anhedrales de bordes completamente irre-

Tabla 1. Composición mineralógica de los Metagabros de El Picacho y Anfibolitas de Medellín, Boquerón y El Retiro analizadas en lámina delgada.

Muestra	Unidad ¹	Hbl	Act/Trm	Pl	Qtz	Bt	Grt	CPx	Tnt	Opacos	Chl	Ep	Cc	Ap	Zrn
CMK004A	A.M.	50		40	5				3					Acc.	?
CMK 015	A.M. ²	45		40						3	2	2		Acc.	Acc.
CMK 021	A.M. ²	60		20	15					3				?	?
CMK 022A	A.M.	55		30	10				3	Acc.	<2	<2			Acc.
CMK 023	M.P.		45	45				?				10			
CMK 028A	M.P.		60	40						Acc.		<2			
CMK 028B	M.P.		50	48						Acc.		2			
CMK 030	A.M.	55		40	3				2	Acc.				Acc.	Acc.
CMK 033A	A.M.	35		35	5			20	Acc.	Acc.		<2			
CMK 033B	A.M.	40		50					5						Acc.
CMK 034A	A.M. ²	65		25	5	3	<2		<2	2				Acc.	Acc.
CMK 034C	A.M. ²	65		25	5				<2	3	<2	<2		Acc.	Acc.
CMK 038A	A.B.	50		35	10				3	2					
CMK 039	A.B.	50		35	10				4	Acc.					
CMK 040A	M.P.		55	40				1		Acc.		4			
CMK 042A	A.B.	55		35	13				1	Acc.					
CMK 042B	A.B.	60		35					2	2				Acc.	
CMK 044	M.P.?	50		40				1		8					
CMK045	A.R.	50		40				5	Acc.	5				Acc.	Acc.
CMK 046	A.M.	65		15	10		Acc.		Acc.	2	<2			Acc.	Acc.
CMK057	A.R.	45		35	10				2	5	3			Acc.	
CMK 113A	A.M. ²	60	<2	30		3				3	<2	<2			Acc.
CMK 119D	A.M. ²	50		40		2			<2	3	<2	<2			
CMK 120A	A.M. ²	40		20	10		15	5	2	5	<2	<2	<2	Acc.	Acc.
CMK 141	A.M.	50		40	5				2						
CMK 144	M.P.	45		50					5						

¹ A.M. Anfibolita de Medellín; M.P. Metagabro de El Picacho; A.B. Anfibolita de Boquerón; A.R. Anfibolita de El Retiro.

² Anfibolitas intercaladas con metasedimentitas de alto grado.

gulares, aunque se conservan pequeños residuos de los cristales primarios.

Las estructuras de los metagabros de El Picacho son de dos clases: reliquias y metamórficas. Las estructuras reliquias de un protolito ígneo corresponden a bandeadimiento composicional y estructural. El bandeadimiento composicional está definido por la presencia de capas centimétricas a decimétricas, unas ricas en minerales ferromagnesianos y otras ricas en félidos. El bandeadimiento estructural se carac-

teriza por la alternancia de bandas de grano grueso a muy grueso con bandas de grano fino (Figura 2b).

En los planos perpendiculares a la lineación, donde es posible ver las estructuras originales, las rocas son faneríticas de grano grueso y localmente muy grueso (Figura 2c). Los anfíboles y agregados de éstos alcanzan 1.5 cm de largo y 1 cm de ancho, tienen desarrollo cristalino moderado, con exfoliación notable, mientras que la plagioclasa es de menor tamaño y en escala mesoscópica es anhedral.

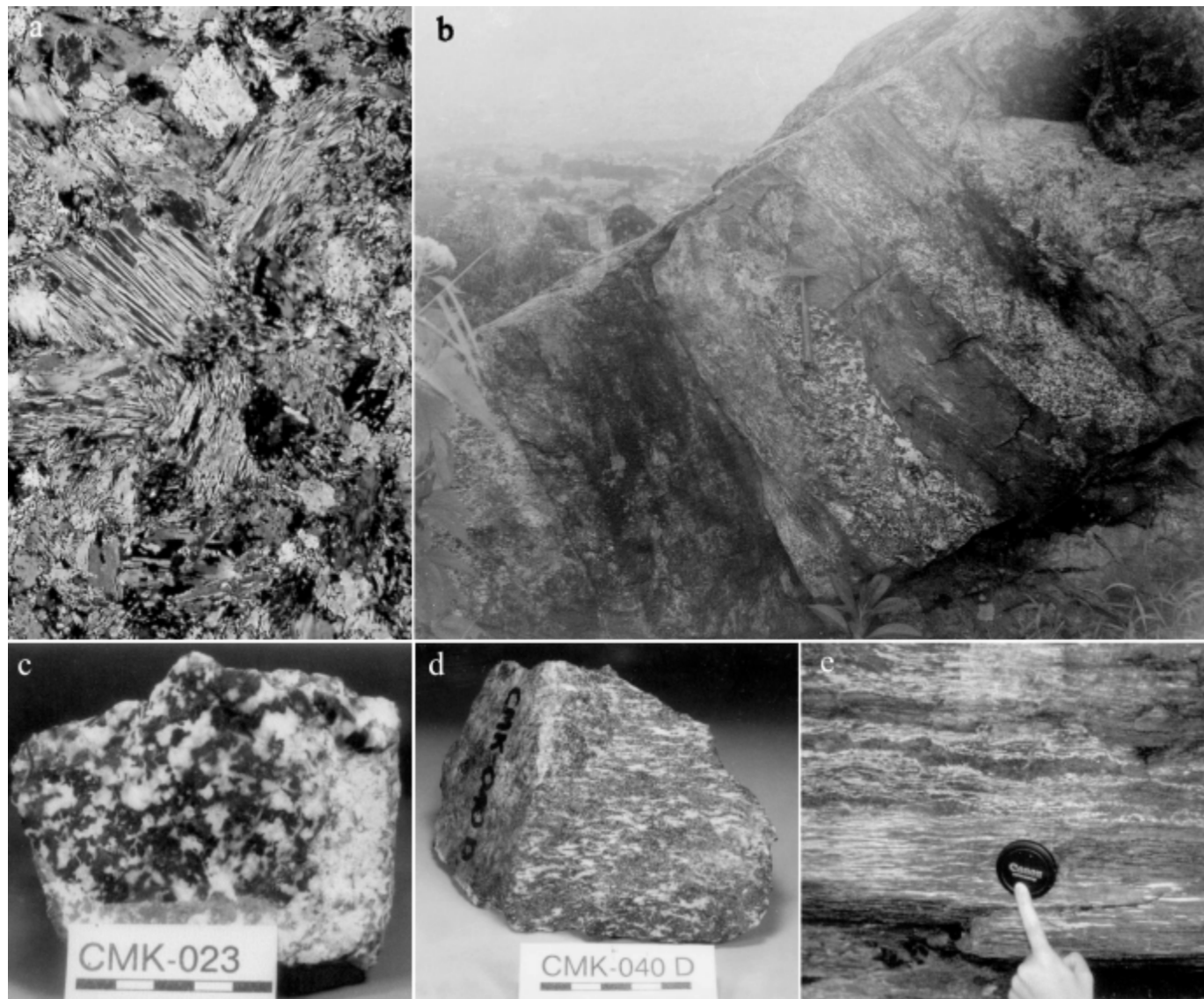


Figura 2. Fotografías de los Metagabros de El Picacho. (a) Fotomicrografía de la muestra CMK 040A, en los que se notan la textura de la roca y los anfíboles aciculares. (b) Bandeadimiento composicional y estructural del afloramiento en el cerro El Picacho (martillo mide 32 x 17 cm). (c) Corte perpendicular a la lineación de la muestra CMK 023, en los que aún se descubre la textura ígnea de la roca (cuadros de la escala miden 1 cm). (d) Textura de la muestra CMK 040D en plano paralelo a la lineación. (e) Afloramiento en la vereda Perico, en el que se notan los fuertes efectos dinámicos de la roca (tapa de cámara fotográfica mide 58 mm).

Las estructuras metamórficas se deben a deformación dinámica y entre las más comunes se encuentran: lineación fuerte por alargamiento (“stretching lineation”), “flasers”, pequeñas cintas félscicas replegadas de manera discontinua, pequeñas zonas de cizalla, y bandas que se abren y se cierran (“pinch and swell”). Con menor frecuencia se encuentra una fábrica LS. Estos rasgos permiten clasificar las muestras de algunos sectores como milonitas (Figura 2d).

En los bloques de la vereda Perico el espesor de las bandas es menor al original debido a los efectos dinámicos y es común la presencia de boudines (Figura 2e).

Además de las características propias de una deformación dinámica, los metagabros exhiben evidencias de alteración hidrotermal, que provocó reemplazamiento de los máficos por anfíboles aciculares posiblemente del tipo actinolita. A partir de la paragénesis actinolita + plagioclasa + epidota, se deduce que el metamorfismo pudo ocurrir en las facies esquisto verde o anfibolita baja (**Bucher & Frey**, 2002). La alteración hidrotermal pudo ocurrir en las etapas finales de la deformación como resultado de la circulación de fluidos en las zonas de cizallamiento o pudo ser también un evento térmico posterior al metamorfismo dinámico, ya que las relaciones estructurales indican que los anfíboles aciculares no presentan rasgos de deformación.

Protolito y nomenclatura de la unidad

El protolito de los metagabros de El Picacho correspondió a rocas ígneas plutónicas de composición básica, faneríticas, de grano grueso y equigranulares. Fueron rocas ígneas bandeadas. Dada la transformación mineralógica que sufrieron es difícil determinar con precisión el protolito específico de éstas. Sin embargo, debido a las características minerales y estructurales heredadas, es posible inferir que correspondieron a gabros y/o noritas.

La unidad Metagabros de El Picacho que aquí se propone, no se había señalado en la estratigrafía de la zona, porque las rocas que la conforman eran consideradas como parte de las Anfibolitas de Medellín en el sentido de **Restrepo & Toussaint** (1984). La propuesta del nombre tiene las siguientes justificaciones: “Metagabros” porque las rocas conservan bien las estructuras de una roca ígnea plutónica básica (recuerda a un gáboro), a pesar de los cambios inducidos por el metamorfismo dinámico e hidrotermal; “de El Picacho”, por ser en el cerro El Picacho donde se hallan los mejores afloramientos con las características reliquias del protolito.

Anfibolitas de Medellín

Al oriente de la ciudad de Medellín aflora un cuerpo elongado en dirección N-S compuesto por metabasitas de alto grado asociadas localmente con paquetes de esquistos y paragneises cuarzo-feldespáticos con biotita. Como se explicó antes, **Restrepo & Toussaint** (1984) consideraron estas metabasitas como parte fundamental de las *Anfibolitas de Medellín*, denominación que en esta publicación se toma en un sentido más restringido, al considerar aquellas metabasitas no asociadas con paragneises que afloran principalmente al occidente y norte de la ciudad como parte de los Metagabros de El Picacho.

El cuerpo metamórfico en consideración se extiende hacia el sur hasta los municipios de El Retiro y La Ceja, donde adicionalmente se han señalado migmatitas y granulitas. Hacia el norte el cuerpo metamórfico llega hasta el municipio de Belmira. La extensión en planta de la unidad comprende aproximadamente 72 km a lo largo y un ancho promedio de 6 km (Figura 1). Hay abundantes afloramientos de buen tamaño donde las anfibolitas se presentan frescas. Vale destacar aquellos de las carreteras Medellín-Bogotá, Santa Elena y Variante Palmas-Aeropuerto.

Características mineralógicas y estructurales

La asociación mineralógica típica en esta unidad es hornblenda + plagioclasa + esfena +/- cuarzo +/- opacos (ilmenita, sulfuros) con apatitos y circones muy pequeños como accesorios (Tabla 1, Figura 3a). Hay algunas variaciones en la composición mineralógica por la presencia de paquetes donde adicionalmente aparece granate o diópsido, los cuales corrientemente se encuentran donde hay metasedimentitas intercaladas. Éstas están compuestas por esquistos o gneises cuarzo-feldespáticos con biotita, que localmente contienen granate, sillimanita, grafito o moscovita. Recientemente se reportó cummingtonita en las anfibolitas de la cuchilla Las Peñas (**Estrada-Carmona**, 2003).

La hornblenda es x = amarillo claro, y = verde oliva, z = verde azuloso en el sector de Rodas, parte alta de Santa Elena y descenso a La Fe. El anfibol de las muestras tomadas en Las Peñas, variante al aeropuerto, quebrada El Guamo y carretera a la Ceja es pardo, lo cual se debe a un mayor contenido de Ti en el mineral (**Miyashiro**, 1994). La composición de la plagioclasa, medida ópticamente por el método Michel-Lévy varía entre An_{42} y An_{53} (andesina-labradorita), composición que es típica de la facies de anfibolitas (**Bucher & Frey**, 2002). En general, las plagioclásas son más cálidas donde los anfíboles tienen coloraciones más pardas.

Las asociaciones mineralógicas encontradas indican condiciones correspondientes a la facies de anfibolitas. La asociación plagioclasa ($\sim \text{An}_{30-50}$) + hornblenda +/- granate +/- biotita es característica de la parte central de esta facies, con temperatura mínima cercana a 600°C (Bucher & Frey, 2002). Donde el anfíbol es pardo, hay diópsido o donde la textura denota reducción del cociente área/volumen de los granos, las condiciones posiblemente fueron de facies anfibolita alta. Una muestra de la cuchilla Las Peñas (Figura 3d) con la paragénesis hornblenda + plagioclasa + granate + cuarzo + clinopiroxeno indica temperatura superior a 650°C, correspondiente a la transición entre la facies de anfibolitas y de granulitas. Debe anotarse que la estimación es válida para un gradiente barroviano que se ha verificado en las rocas del lugar pues allí el granate tiene primordialmente composición de almandino (Estrada-Carmona, 2003). Si bien las condiciones de presión y temperatura pudieron favorecer el desarrollo de granates, éstos son escasos en las Anfibolitas de Medellín, posiblemente porque el cociente FeO/MgO es insuficientemente alto (Miyashiro, 1994).

Macroscópicamente la unidad se caracteriza por la presencia de pocas bandas cuarzo-feldespáticas de espesor milimétrico a centimétrico, y por lineación sintectónica de anfíboles (foliación nematoblástica, Figura 3c).

El estudio microestructural de las Anfibolitas de Medellín permitió determinar el carácter polifásico-polimetamórfico (?) de las rocas, ya que se presentan al menos tres fases tectónicas. Las anfibolitas granatíferas tienen inclusiones alineadas o a modo de S dentro de los granates (D1) que son oblicuas en relación con la lineación externa a este mineral (D2). Las muestras tomadas en Copacabana y Rodas presentan crenulaciones cilíndricas (D3; Figura 3b) sobreimpuestas a las microestructuras anteriores. Estos resultados concuerdan con el estudio microestructural efectuado por Tamayo (1984) en la carretera Medellín-Bogotá.

Contacto con otras unidades

El contacto entre las Anfibolitas y las Dunitas de Medellín está bien representado en un tramo de 1,5 km de longitud en la autopista Medellín – Bogotá, sector de Rodas. Allí hay afloramientos decamétricos en los que se presenta una compleja asociación de anfibolitas, dunitas, esquistos talcosos, esquistos cloríticos localmente microplegados (Figura 3e) y esquistos actinolíticos, resultado de una mezcla tectónica. Ha habido consenso entre autores al considerar que la dunita reposa sobre la anfibolita debido a un cabalgamiento y que en muchos

sitios el contacto es subhorizontal (Restrepo & Toussaint, 1974; Álvarez, 1987).

Ya Botero (1963) había notado que el Batolito Antioqueño es intrusivo en las Anfibolitas de Medellín, lo cual se constata muy bien en la cuchilla las Peñas, donde se observan xenolitos de rocas foliadas dentro de la roca granítica. Además la intrusión genera migmatitas de inyección con aspecto brechoso en las metasedimentitas y anfibolitas de Las Peñas.

Todos los contactos entre anfibolitas y metasedimentitas que se observaron son concordantes. Generalmente, se pasa de manera transicional del cuerpo principal de anfibolitas a intercalaciones de metasedimentitas y anfibolitas. Ejemplos de ello se tienen en la carretera Alto de Las Palmas-Variante al Aeropuerto y en la cuchilla Las Peñas.

Anfibolitas de Boquerón

En la carretera que comunica a Medellín con el Occidente, a la altura del sitio conocido como El Boquerón, y en las quebradas Agua Fría y La Seca ubicadas cerca del lugar, afloran en pequeñas exposiciones, dada la cobertura de extensos depósitos de vertiente, un conjunto de anfibolitas con rasgos muy peculiares, que aquí se propone denominar *Anfibolitas de Boquerón*. Dentro del depósito de vertiente las anfibolitas se presentan en bloques métricos y en ciertas áreas aparecen mezcladas con los bloques de los Metagabros de El Picacho.

Características mineralógicas y estructurales

Los minerales que componen las Anfibolitas de Boquerón son hornblenda + plagioclasa + esfena +/- cuarzo + opacos (Tabla 1), asociación diagnóstica de la facies de anfibolitas a presión baja o media.

La hornblenda es media a gruesa, anhedral a subhedral, y algunas contienen cristales finos y redondeados de plagioclasa. La fórmula de pleocroísmo x = crema, y = verde amarillento, z = verde azuloso, sugiere condiciones de la parte baja de la facies de anfibolitas. La plagioclasa se encuentra en agregados lenticulares o en bandas discontinuas que se abren y se cierran compuestas por granos finos, equidimensionales, con poligonización, aunque también se distinguen granos mayores muy sausuritzados con macla polisintética. La esfena es abundante y está íntimamente asociada con ilmenita. En cantidad moderada, se presenta la formación de minerales secundarios como anfíboles aciculares desordenados, epidota y clorita.

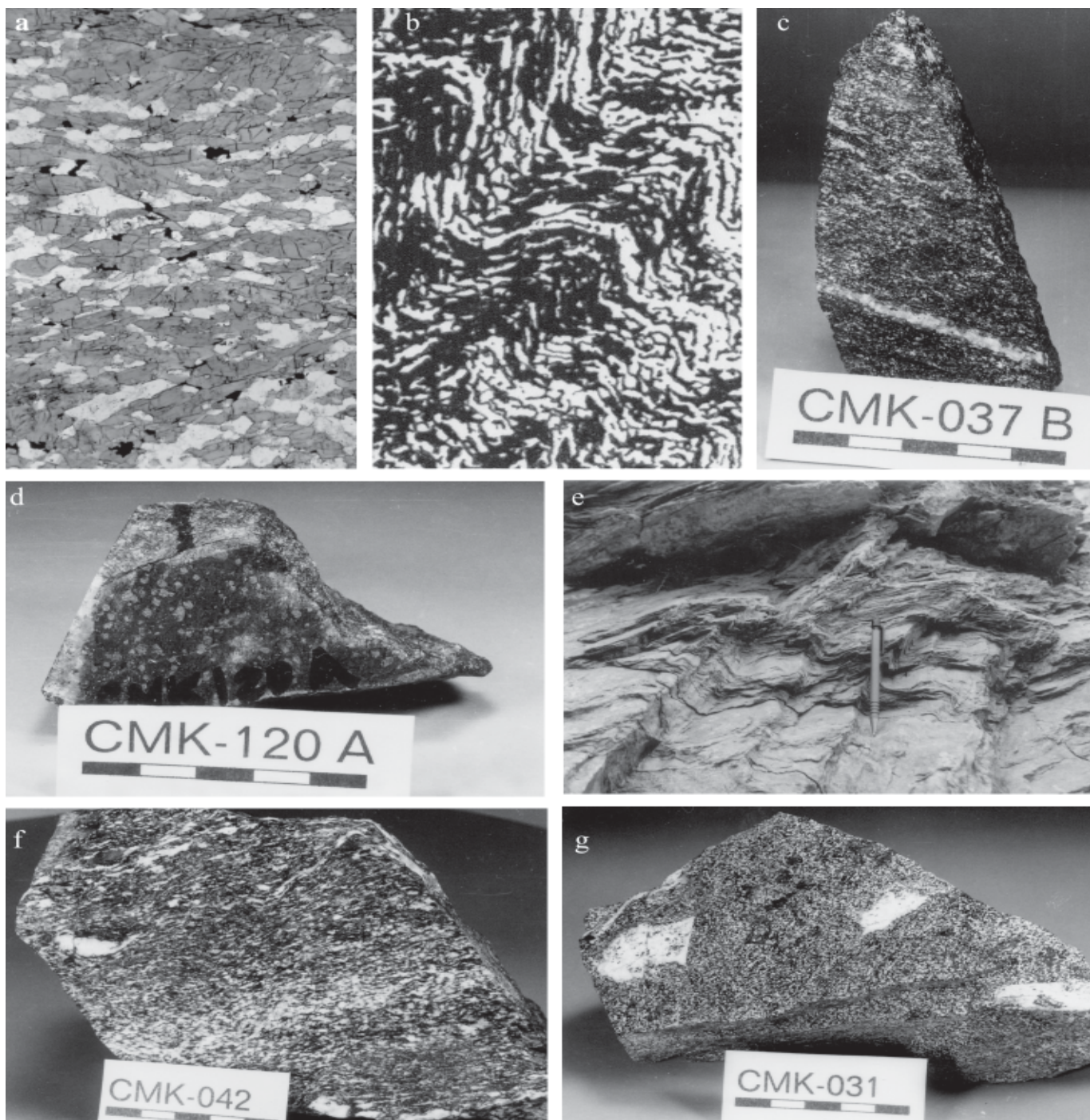


Figura 3. (a) Macrofotografía de una típica Anfibolita de Medellín tomada en el cuerpo principal al Este de Medellín (rectángulos de la escala miden 1 cm cada uno). (b) Dibujo de la crenulación de las Anfibolitas de Medellín en el sector de Rodas y Copacabana. (c) Anfibolita del cuerpo principal al Este de Medellín; se notan las bandas milimétricas de minerales felsicos. (d) Anfibolita granatífera del sector de Las Peñas; nótese la abundancia de granate y la menor intensidad en la foliación de la roca, en comparación con las otras muestras. (e) Esquistos de color verde muy plegados en la zona de contacto entre la Dunita y las Anfibolitas de Medellín.

A escala macroscópica se denota una intercalación de bandas milimétricas a centímetricas de grano medio donde la proporción de félscicos es más notable, y bandas de grano fino más máficas. De forma paralela al bandeamiento composicional hay esquistosidad y lineación por orientación de la hornblenda (Figura 3f).

Estas anfibolitas muestran rasgos de metamorfismo dinámico tales como bandas boudinadas, hornblendas ocelares (“augen”) y agregados lenticulares de félscicos. A escala microscópica existen bandas de hornblenda que se abren y se cierran, que en parte bordean agregados lenticulares félscicos, y determinan una textura anastomosada. Los cristales gruesos de hornblenda están doblados y exhiben extinción ondulatoria, y las plagioclasas, aunque alteradas, denotan estar dobladas y acuñadas. El cuarzo se presenta en agregados recristalizados dinámicamente en forma de cinta incipiente (“ribbon”).

Geoquímicamente, estas metabasitas guardan semejanza con las Anfibolitas de Medellín, especialmente en el contenido relativamente alto de Ti que se traduce en contenidos de esfena de hasta 4%. No obstante, las estructuras dinámicas recuerdan más a un cuerpo ígneo fanerítico deformado, rasgo semejante al encontrado en los Metagabros de El Picacho, cuya ubicación geográfica es cercana.

Contactos con otras unidades

Hay diques que intruyen las Anfibolitas de Boquerón cerca a la quebrada Seca, donde la metabasita presenta efectos térmicos que se atribuyen a la intrusión del Batolito de Ovejas, apófisis del Batolito Antioqueño, o del Stock de Altavista. Lamentablemente los contactos con las otras unidades adyacentes, como los Metagabros de El Picacho y las metasedimentitas de alto grado que afloran en el alto de Baldías, no fueron observados debido al gran depósito de vertiente que cubre la región.

Otros cuerpos de anfibolitas

Al norte de Boquerón, en el alto de Baldías, paquetes métricos a decamétricos de metasedimentitas, principalmente gneises cuarzo-feldespáticos con biotita, que localmente contienen granate o sillmanita, presentan al menos tres paquetes de anfibolitas intercaladas cuyo espesor puede llegar a 50 m. Se trata de anfibolitas con fuerte lineación, compuestas por hornblenda + plagioclasa +/- cuarzo +/- esfena. Algunas denotan efectos térmicos, certamente atribuibles a la intrusión del Batolito de Ovejas, con formación de albita y epidota, y modificación de la fábrica a una más desordenada.

Hacia el sur, las Anfibolitas de Medellín se extienden hasta los municipios de El Retiro y La Ceja, en donde es común encontrar algo de granate o diópsido; su mineralogía detallada se describe en la tabla 1. Allí las metabasitas se encuentran como paquetes intercalados con esquistos micáceos a veces grafíticos, gneises y migmatitas. Estas últimas son relativamente abundantes en el lugar. Una zona de extensión limitada presenta granulitas básicas y granofelsas.

Estructuralmente, las anfibolitas en El Retiro y La Ceja pueden ser casi macizas hasta fuertemente lineadas (foliación nematoblástica, Figura 3g), y pueden mostrar reducción del cociente área/volumen de los granos. Se intentó determinar en un corte en la carretera Las Palmas, si existía límite tectónico entre las Anfibolitas de Medellín y aquellas de El Retiro. Al no encontrar evidencias de tal, se propone simplemente una variación lateral que incluye zonas con abundantes migmatitas en El Retiro, estas últimas también presentes en otros sitios, como Las Peñas o Alto de las Palmas, pero no en tan copiosa cantidad.

Otro cuerpo que se estudió en el marco de este trabajo se encuentra ubicado en el municipio de Barbosa e incluye anfibolitas y metasedimentitas, principalmente esquistos cuarzo-micáceos con grafito. El cuerpo es alargado en dirección NW y está bordeado completamente por el intrusivo Batolito Antioqueño. Las características encontradas en Barbosa permiten proponer una correlación con las Anfibolitas de Medellín y sus metasedimentitas asociadas.

Debe mencionarse que en los alrededores del municipio de Caldas, hay cuerpos de anfibolitas, algunas muy granatíferas, y cuyas características mineralógicas y asociaciones son muy disímiles a las presentes en las Anfibolitas de Medellín y Metagabros de El Picacho. Las relaciones entre las metamorfitas en Caldas, que incluye gneises, anfibolitas granatíferas, esquistos biotíticos con granate y estaurolita, esquistos cuarzomoscovíticos de bajo grado en facies esquisto verde y migmatitas de alto grado al E, aún no se comprenden plenamente, aunque recientemente Montes (2003) propone una transición gradual del grado metamórfico de W a E. Por sus notables diferencias y complejidad, las anfibolitas señaladas no se han tenido en cuenta para este trabajo.

Geoquímica

Los análisis químicos que a continuación se discuten fueron realizados en el Instituto de Geociencias de la Universidad de Brasilia (Brasil), bajo el convenio

existente entre esa universidad y la Universidad Nacional de Colombia.

Se analizaron 19 muestras de roca total para elementos mayores y traza (los análisis representativos se presentan en las tablas 2 y 3). Las concentraciones de los elementos mayores en la forma de óxidos (excepto Na₂O y K₂O) y de los elementos traza fueron determinadas por espectrometría de emisión con plasma (ICP-AES). La concentración de Na₂O y K₂O se determinó usando un espectrómetro de absorción atómica Perkin Elmer. La concentración de volátiles fue determinada a través de métodos gravimétricos y la concentración de Fe ferroso por volumetría.

Es importante considerar la posible movilidad de los elementos químicos de las metamafitas debido a procesos post-ígneos. Aunque no existen criterios definitivos para establecer el comportamiento de los elementos durante metamorfismo y meteorización (**Grauch**, 1989), diversos autores (e.g. **Rollinson**, 1993) citan elementos móviles e inmóviles ante diferentes procesos. Entre los inmóviles

están: las tierras raras pesadas, Y, Zr, Ti, Nb, P, Al, Co, Ni, V y Cr. Con el fin de observar si las rocas en cuestión presentan alteraciones químicas significativas de los elementos mayores, se construyeron algunos diagramas de **Beswick & Soucie** (1978) (Figura 4). En los diagramas 4a, 4b y 4c las muestras están alineadas y definen tendencias, lo que sugiere que las rocas no sufrieron alteraciones post-mármaticas importantes de los elementos involucrados. En el gráfico 4d la dispersión de los puntos indica movilidad, así por ejemplo, Ca y Na se movilizaron en relación con el K. La dispersión existente en varios diagramas de variación (Figura 7) también sustenta la interpretación anterior y sugiere movilidad de otros elementos mayores.

Resultados analíticos

De acuerdo con los datos geoquímicos obtenidos y según lo muestran los diagramas Sílice vs. Álcalis Total (Figura 5a y 5b), los protolitos de las Anfibolitas de Medellín y El Retiro correspondieron a rocas de composición basáltica, con carácter subalcalino y de afinidad

Tabla 2. Análisis representativos de elementos mayores para muestras de los Metagabros de El Picacho, las Anfibolitas de Boquerón, Medellín y El Retiro.

Grupo	Muestra	SiO ₂	TiO ₂	Al ₂ O ₃	Fe ₂ O ₃	FeO	MnO	MgO	CaO	Na ₂ O	K ₂ O	P ₂ O ₅	PF	Total	# Mg
I	CMK-028A(AM-1)	49.65	0.46	14.85	0.77	5.16	0.10	11.87	12.02	2.30	0.36	0.05	1.77	99.36	64.60
	CMK-028B(AM-2)	44.72	0.29	21.07	1.55	2.87	0.06	8.65	15.61	1.37	0.28	0.05	2.63	99.15	64.60
	DM-2	46.76	0.26	16.51	1.65	5.19	0.09	12.77	12.34	1.87	0.24	0.03	1.35	99.06	63.26
	CMK-040	47.35	0.17	22.85	3.32	0.00	0.05	6.13	16.41	1.32	0.41	0.05	1.37	99.43	64.87
	CMK-101	47.47	0.60	15.04	6.30	0.00	0.11	13.57	13.81	1.66	0.41	0.06	0.52	99.55	68.29
II A	CMK-042A (AM-3)	52.77	1.19	13.89	1.17	7.83	0.15	7.47	9.79	3.33	0.28	0.12	1.03	99.02	43.07
	CMK-042B(AM-4)	48.99	1.45	16.63	1.09	8.84	0.14	6.64	8.14	4.15	0.32	0.16	1.89	98.44	37.83
	CMK-039(AM-6)	47.84	1.68	13.83	2.22	8.54	0.18	8.16	10.43	2.94	0.20	0.17	1.25	97.44	41.07
II B	CM-030A(AM-5)	48.61	1.71	15.61	1.53	7.80	0.17	8.87	9.94	3.66	0.32	0.09	0.81	99.12	46.52
	CMK-096B	48.20	1.77	16.34	8.91	0.00	0.18	10.41	8.45	3.09	0.57	0.14	0.39	98.45	53.88
	CMK-103	49.75	1.71	14.54	11.06	0.00	0.23	8.10	11.33	2.37	0.41	0.17	0.80	100.47	42.28
	CMK-105	51.10	1.70	13.90	9.16	0.00	0.15	8.93	10.11	3.30	0.41	0.12	0.88	99.76	49.36
	CMK-033A(AM-8)	44.98	0.97	18.86	1.09	7.64	0.16	7.45	14.62	2.37	0.48	0.12	2.06	100.80	43.74
	CMK-033B(AM-9)	48.61	1.40	14.78	1.85	7.43	0.14	8.80	11.01	3.11	0.20	0.14	1.72	99.19	46.54
	CMK-094	50.40	1.62	13.06	11.79	0.00	0.19	7.44	11.80	2.46	0.49	0.15	0.58	99.98	38.69
	CMK-074A	50.00	1.89	13.30	12.12	0.00	0.20	7.79	13.10	1.06	0.49	0.18	0.53	100.66	39.13
III	CMK-044(AM-7)	49.67	1.33	14.19	1.68	8.62	0.18	8.57	9.96	2.67	0.24	0.15	0.97	98.23	43.22
	CMK-045	48.85	2.43	11.22	2.1	11.94	0.23	6.65	10.26	2.68	0.57	0.22	0.19	98.69	30.22
	CMK-057	49.08	2.51	12.04	1.99	11.33	0.28	6.26	11.12	1.86	0.71	0.22	0.80	99.48	30.06

Óxidos expresados en porcentaje por peso (%). PF, pérdida por ignición.

Tabla 3. Análisis representativos de elementos traza para muestras de los Metagabros de El Picacho, las Anfibolitas de Boquerón, Medellín y El Retiro.

Grupo	Muestra	V	Ba	Sr	Nb	Zr	Y	La	Ce	Nd	Sm	Eu	Gd	Dy	Ho	Er	Yb
I	CMK-028A(AM-1)	148	39	101	6.0	67	10	2.60	6.60	5.80	2.40	0.57	3.20	2.30	0.72	1.70	1.20
	CMK-028B(AM-2)	72	23	168	7.0	135	6	3.60	7.00	4.60	2.30	0.53	2.00	1.50	0.50	1.20	0.83
	DM-2	97	775	110	6.0	7	6	0.00	0.00	0.00	0.00	0.00	0.00	0.00	0.00	0.00	0.00
	CMK-040	n.d.	25	337	n.d.	98	3	8.59	12.99	5.87	8.13	0.56	3.96	1.83	1.07	1.85	0.42
	CMK-101	n.d.	21	81	n.d.	164	13	5.81	10.12	6.47	8.00	0.85	4.79	3.66	1.60	3.08	1.32
II A	CMK-042A (AM-3)	210	49	130	9.0	41	21	3.60	10.40	8.40	4.20	0.88	5.60	4.20	1.10	3.20	2.50
	CMK-042B(AM-4)	204	67	214	10.0	48	26	3.80	9.10	8.00	3.00	0.97	6.50	5.30	1.00	3.40	3.10
	CMK-039(AM-6)	252	85	121	11.0	43	34	4.70	10.20	10.30	3.80	1.20	6.00	6.00	1.10	3.70	3.50
II B	CM-030A(AM-5)	231	41	114	16.0	148	24	2.20	5.60	6.10	1.80	0.83	5.10	4.20	0.93	2.70	2.60
	CMK-096B	n.d.	37	108	n.d.	45	33	6.17	14.25	11.49	9.66	1.39	6.51	6.41	2.08	4.52	3.01
	CMK-103	n.d.	52	198	n.d.	83	47	9.34	21.25	16.12	9.28	1.62	7.09	7.26	1.88	4.85	3.24
	CMK-105	n.d.	26	141	n.d.	106	32	4.93	11.77	11.15	7.10	1.17	4.65	5.52	1.44	3.84	2.58
	CMK-033A(AM-8)	198	58	164	8.0	98	21	3.30	5.20	4.90	2.00	0.95	4.60	4.00	0.68	2.30	2.20
	CMK-033B(AM-9)	203	36	121	9.0	69	24	3.10	6.80	7.70	2.70	1.00	5.50	4.70	0.87	2.90	2.70
	CMK-094	n.d.	55	118	n.d.	66	41	4.80	13.63	11.91	6.24	1.38	4.78	6.71	1.60	4.22	3.16
	CMK-074A	n.d.	62	144	n.d.	111	46	8.75	21.56	17.22	9.30	1.70	7.90	8.70	2.44	5.58	3.95
	CMK-044(AM-7)	196	88	185	12.0	71	22	5.20	12.40	9.60	2.80	1.10	6.10	4.50	0.84	2.80	2.70
III	CMK-045	n.d.	111	269	n.d.	129	49	15.37	35.00	23.66	15.09	2.49	10.57	10.14	2.6	6.16	4.27
	CMK-057	n.d.	154	243	n.d.	137	50	14.26	36.36	23.6	9.92	2.01	7.18	8.02	1.91	4.81	3.27

Elementos expresados en p.p.m. n.d.= no determinado.

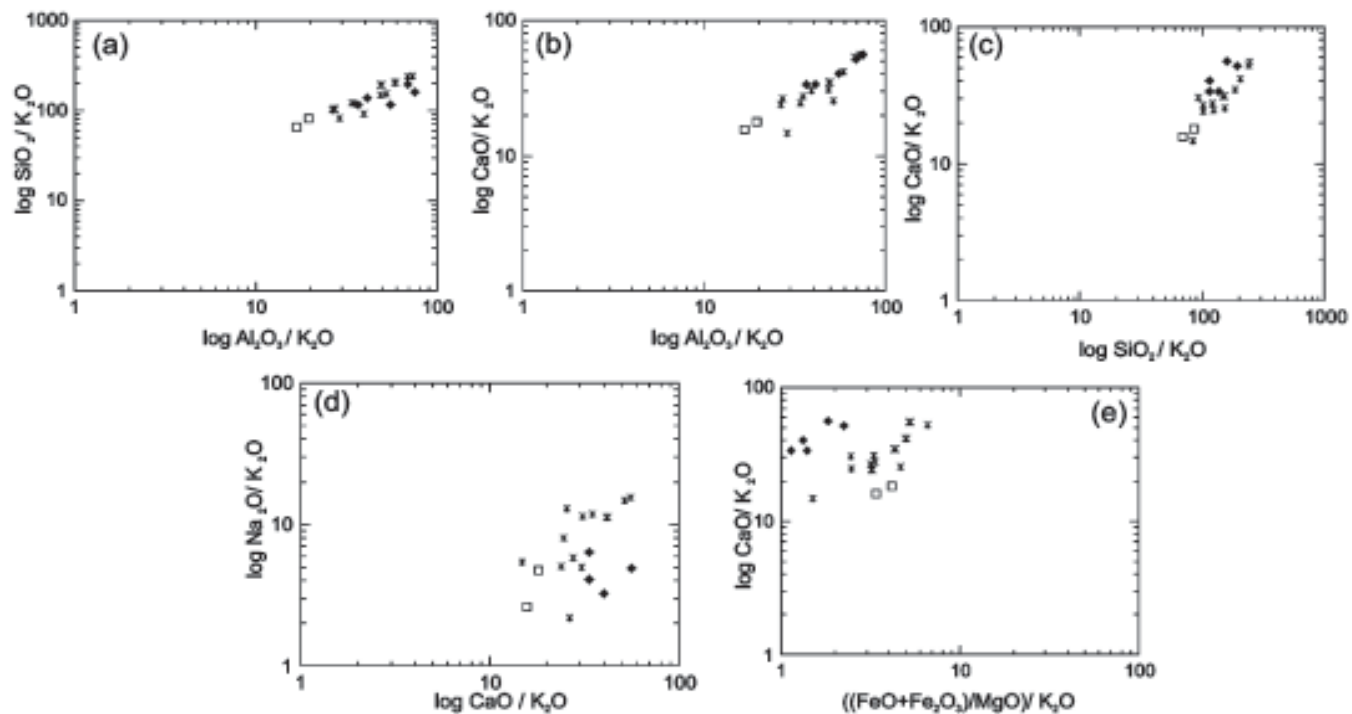


Figura 4. Diagramas de Beswick & Soucie (1978) para las metamorfitas básicas de los alrededores de Medellín. Símbolos: rombo lleno = metagabros de El Picacho, asterisco = anfibolitas de Medellín y Boquerón, cuadrado vacío = anfibolitas de El Retiro.

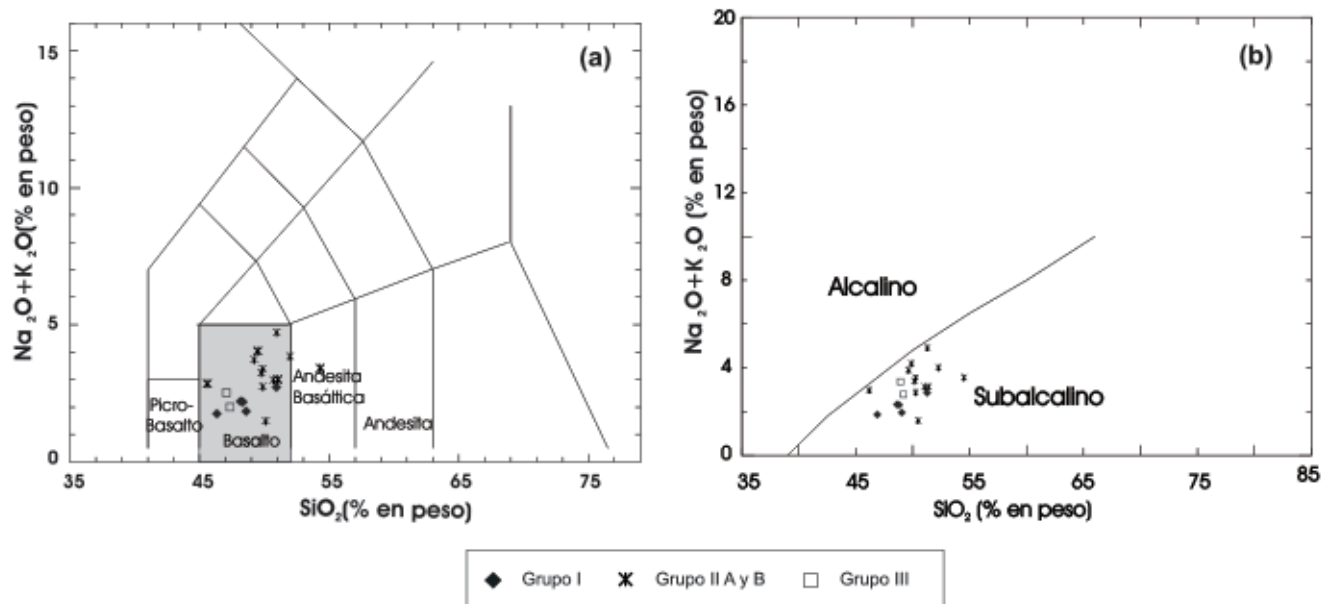


Figura 5. Diagrama sílice vs. álcalis total. (a) Diagrama según Le Bas *et al.* (1986) para clasificación de rocas volcánicas. (b) Campos alcalino y subalcalino de acuerdo con Irvine & Baragar (1971). Símbolos como en la figura 4

toleítica (Figura 6). Los protolitos de los metagabros de El Picacho fueron rocas gabroides (campo de basaltos en la figura 5a) de carácter subalcalino (Figura 5b).

Desde el punto de vista de los elementos mayores y traza es posible diferenciar tres grupos geoquímicos (ver

diagramas de variación de #Mg vs. otros elementos, en la figura 7): el Grupo I representa las características geoquímicas de la unidad Metagabros de El Picacho, el Grupo II incluye las muestras de las unidades Anfibolitas de Boquerón y de Medellín, y el Grupo III reúne las anfibolitas de El Retiro.

El Grupo I muestra una amplia variación de Al₂O₃ con valores desde 14.85 a 22.85, valores bajos de Fe₂O₃ (3.32 - 7.42), de MnO (0.5-0.11) y de TiO₂ (0.17-0.46). Estos valores de TiO₂ indican bajos contenidos de Ti en los piroxenos o anfíboles primarios y reflejan la ausencia o escasa presencia de ilmenita primaria.

Estas rocas presentan #Mg variables entre 63 y 69, mayores con respecto al Grupo II. El número de magnesio #Mg se calculó así: [100 x MgO/(MgO + Fe₂O₃*)], siendo Fe₂O₃* el hierro total.

Los patrones de tierras raras (Figura 8a) y multielementales (Figura 9a) son irregulares, y no muestran tendencias que sean típicas de algún ambiente tectónico.

El Grupo II, con relación al Grupo I, muestra poca variación de Al₂O₃ desde 13.30 a 16.34, de Fe₂O₃* (>de 8%) y de MnO (0.14-0.23). Este grupo tiene un contenido más alto de TiO₂, reflejo de la cantidad apreciable de esfena e ilmenita registradas en la petrografía. Los valores de #Mg son menores a los del Grupo I. La relación inversa entre el

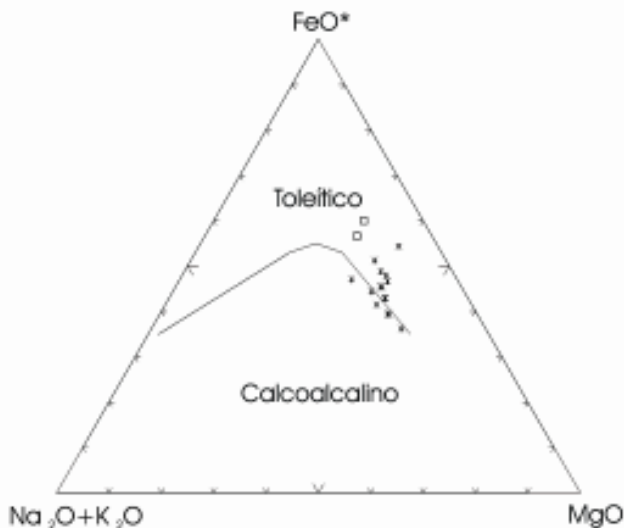


Figura 6. Diagrama AFM de Irvine & Baragar (1971) donde se observa la tendencia de cristalización toleíticas de las anfibolitas de Medellín, Boquerón y El Retiro. Símbolos como en la figura 4

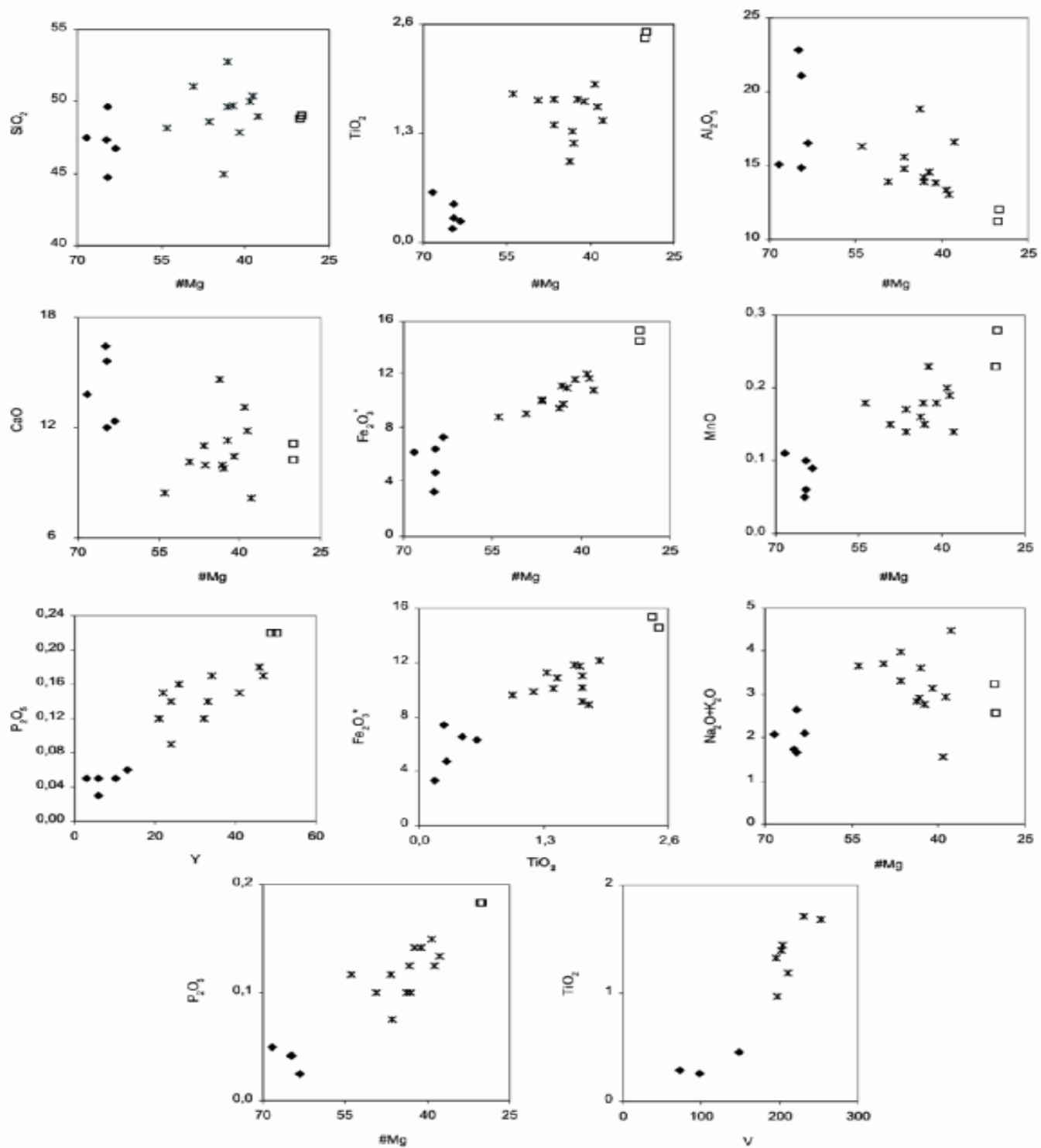


Figura 7. Diagramas de variación de #Mg con respecto a elementos mayores y diagramas entre algunos elementos traza. Símbolos como en la figura 4.

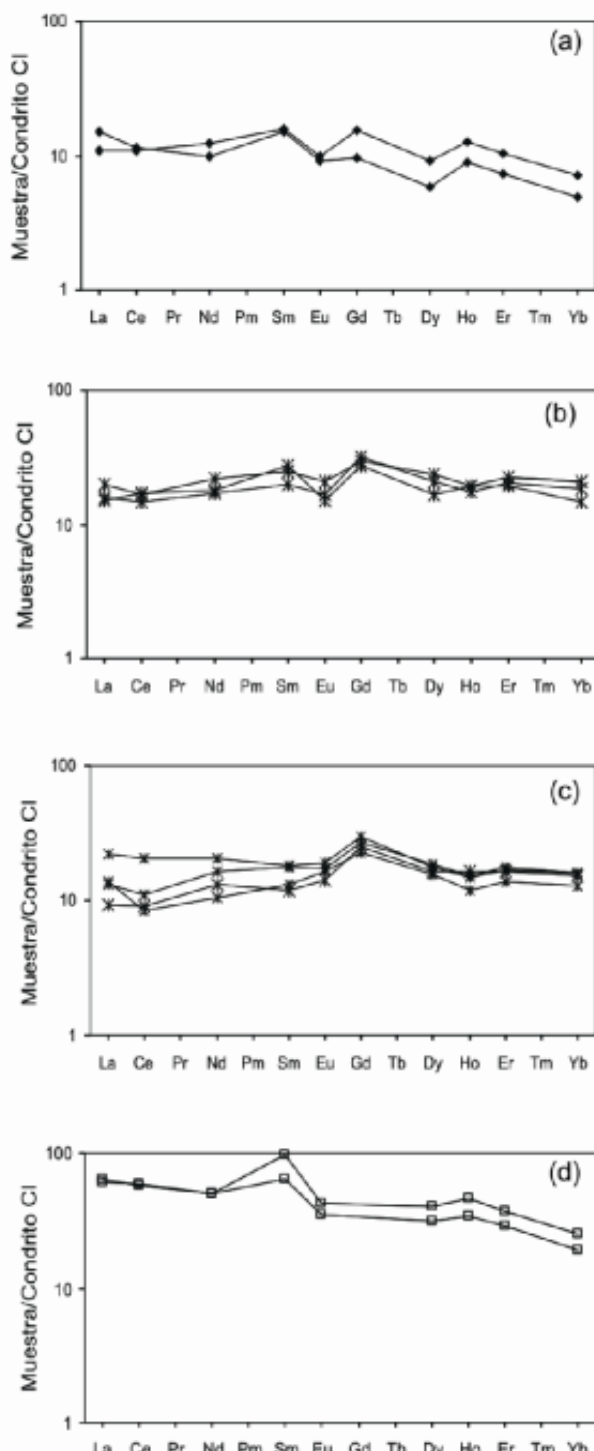


Figura 8. Patrones de elementos de las tierras raras de las unidades de metabasitas. (a)-Metagabros de El Picacho, (b)-Anfibolitas de Boquerón, (c)-Anfibolitas de Medellín, (d)-Anfibolitas de El Retiro. Valores normalizados contra el Condrito CI (**Sun & McDonough, 1989**).

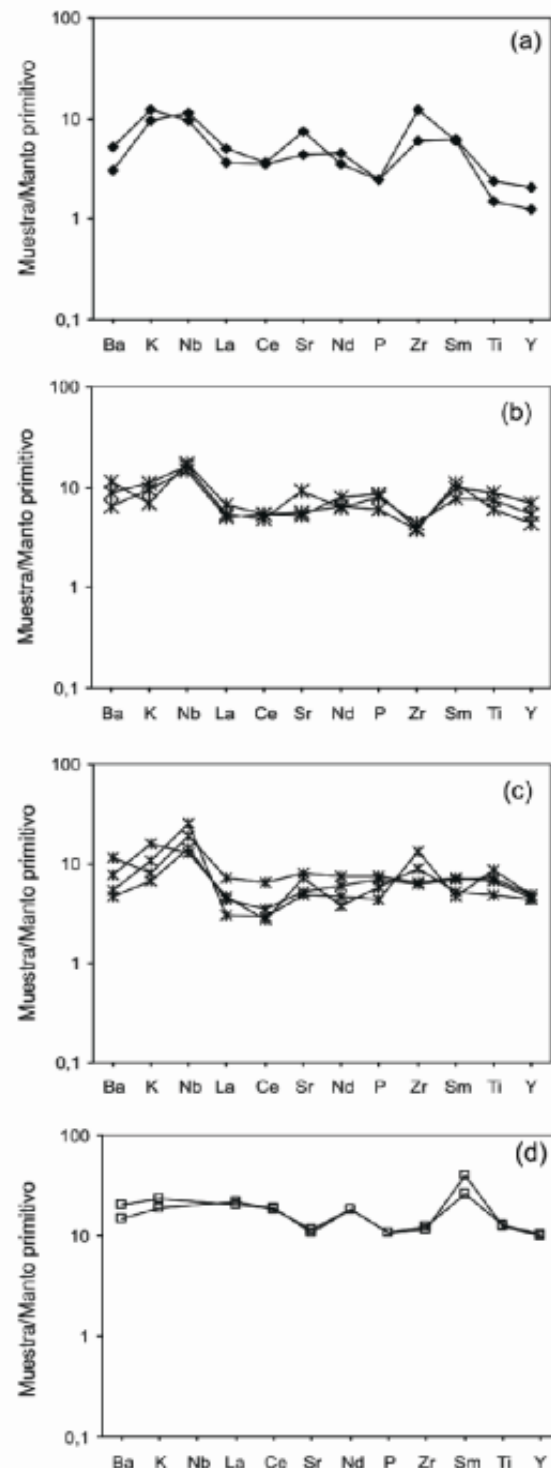


Figura 9. Diagramas multielementales de las unidades de metabasitas. (a)-Metagabros de El Picacho, (b)-Anfibolitas de Boquerón, (c)-Anfibolitas de Medellín, (d)-Anfibolitas de El Retiro. Valores normalizados con respecto al Manto primitivo (**Wood et al., 1979**).

MgO y el Fe_2O_3^* , SiO_2 y MgO, y proporcional entre SiO_2 y Fe_2O_3^* sugiere que los magmas protolitos de estas rocas siguieron tendencias de cristalización toleítica, conclusión también obtenida a partir del diagrama AFM (Figura 6).

Las tendencias encontradas en los diagramas #Mg vs. P_2O_5 y Y vs. P_2O_5 (Figura 7) sugieren cristalización de apatito. Los diagramas de TiO_2 contra Fe_2O_3 y V contra TiO_2 indican la existencia de minerales tales como ilmenita.

Al considerar los elementos traza no existen muchas diferencias entre las muestras de anfibolitas, sin embargo dividimos el Grupo II en A (Anfibolitas de Boquerón) y B (Anfibolitas de Medellín). En el Grupo II A los patrones de distribución de REE (Figura 8b) son relativamente paralelos y planos, mientras que el Grupo II B exhibe un patrón de tierras raras con tendencia levemente positiva (Figura 8c). Las anfibolitas de Boquerón muestran una leve anomalía negativa de Eu que se puede explicar por fraccionamiento de plagioclasa. Dicha anomalía no es clara en las Anfibolitas de Medellín. Los patrones multielementales (Figuras 9b y c) también son paralelos en ambos subgrupos, siendo la diferencia más notable la anomalía negativa de Zr en las muestras del II A y positiva en dos del IIB.

Los patrones de tierras raras y aquellos de los diagramas multielementales, para el Grupo II, están comprendidos entre los patrones citados para toleítas de arco de isla y MORB, para el campo propuesto entre N-MORB y E-MORB por **Wilson** (1989).

El Grupo III presenta valores menores de Al_2O_3 y mayores de Fe_2O_3^* y de MnO que los otros dos grupos. También es el grupo con más alto contenido de TiO_2 . Los valores bajos de MgO y de #Mg (~30) sugieren que el protolito de estas rocas se generaron de magmas parentales diferenciados o más evolucionados que las fuentes de los otros dos grupos.

Los patrones de tierras raras son paralelos con pendiente negativa (Figura 8d) indicando enriquecimiento de las tierras raras livianas en relación con las pesadas, siendo ésta una característica que diferencia este grupo de los otros dos. Este patrón guarda semejanza con el presentado por basaltos de cuencas tras-arco, basaltos de arco de isla o por E-MORB. El patrón exhibido en los diagramas multielementales (Figura 9d) muestra enriquecimiento de casi todos los elementos en aproximadamente 30 veces con relación al manto primitivo, excepto el Sm que presenta una anomalía positiva alta.

Con miras a tener más información sobre el ambiente tectónico de los protolitos de las anfibolitas, se elaboraron varios diagramas discriminantes (Figura 10), en los cuales las rocas estudiadas caen dentro del campo MORB.

Las muestras de metagabros no aparecen en los diagramas porque son rocas gruesogranulares resultado de diferenciación magmática que no representan magmas parentales; estos diagramas sólo se pueden usar para rocas que muestren la afinidad de los magmas originales.

Geocronología

En el desarrollo de este trabajo se intentaron llevar a cabo dataciones Sm-Nd isócrona de granate y roca total en anfibolitas granatíferas y esquistos granatíferos de la carretera a Santa Elena (sector de El Guamo), la carretera Medellín-Bogotá (sector de Las Peñas) y del alto de Baldías. Lamentablemente los resultados no fueron satisfactorios; en algunos casos el granate no concentró suficientemente las tierras raras, y en otros, los resultados obtenidos no pudieron correlacionarse cronológicamente con las edades que se conocen para el basamento de la cordillera Central. Como no hay pruebas internas en este tipo de datación, que además se fundamenta en una isócrona de dos puntos, se decidió descartarlos de los resultados. También se intentó elaborar una isócrona de rocas totales con muestras de las unidades principales que se identificaron, pero los puntos no presentan suficiente dispersión en la isócrona para calcular una edad ígnea confiable.

No existen al momento dataciones de los Metagabros de El Picacho. Muestras recolectadas en El Boquerón fueron analizadas por **Martens & Dunlap** (en prep.), quienes intentaron una datación con el sistema Ar-Ar en hornblendas. El espectro resultó de difícil interpretación y dudosa validez, con edades que oscilan entre ca. 100-145 Ma. Será necesario esperar un trabajo geocronológico serio y extenso para determinar confiablemente la edad de los Metagabros de El Picacho y las Anfibolitas de Boquerón. Las Anfibolitas de Medellín, por el contrario, se han datado en varias oportunidades (**Restrepo et al.**, 1991 y referencias contenidas allí; **Martens & Dunlap**, 2003). Las abundantes edades cretácicas obtenidas se deben a perturbaciones térmicas originadas durante la intrusión del voluminoso Batolito Antioqueño; el metamorfismo orogénico se dio antes, probablemente durante el lapso Pérmico-Triásico. Este resultado es concordante con las edades K/Ar 251 +/- 21 Ma y Sm/Nd 226 +/- 17 Ma obtenidas en las granulitas y granofelsas asociadas de El Retiro (**Restrepo et al.**, 1991; **Ordóñez et al.**, 2001), y las dos fechas Ar-Ar de ca. 230 Ma obtenidas por **Vinasco et al.** (2001) en anfibolitas recolectadas en El Retiro durante la ejecución de este trabajo. Como se planteó anteriormente, es probable que las metamorfitas de alto grado de este lugar pertenezcan a una misma unidad junto con las rocas de alto grado de Medellín y por eso la correlación cronológica se considera válida.

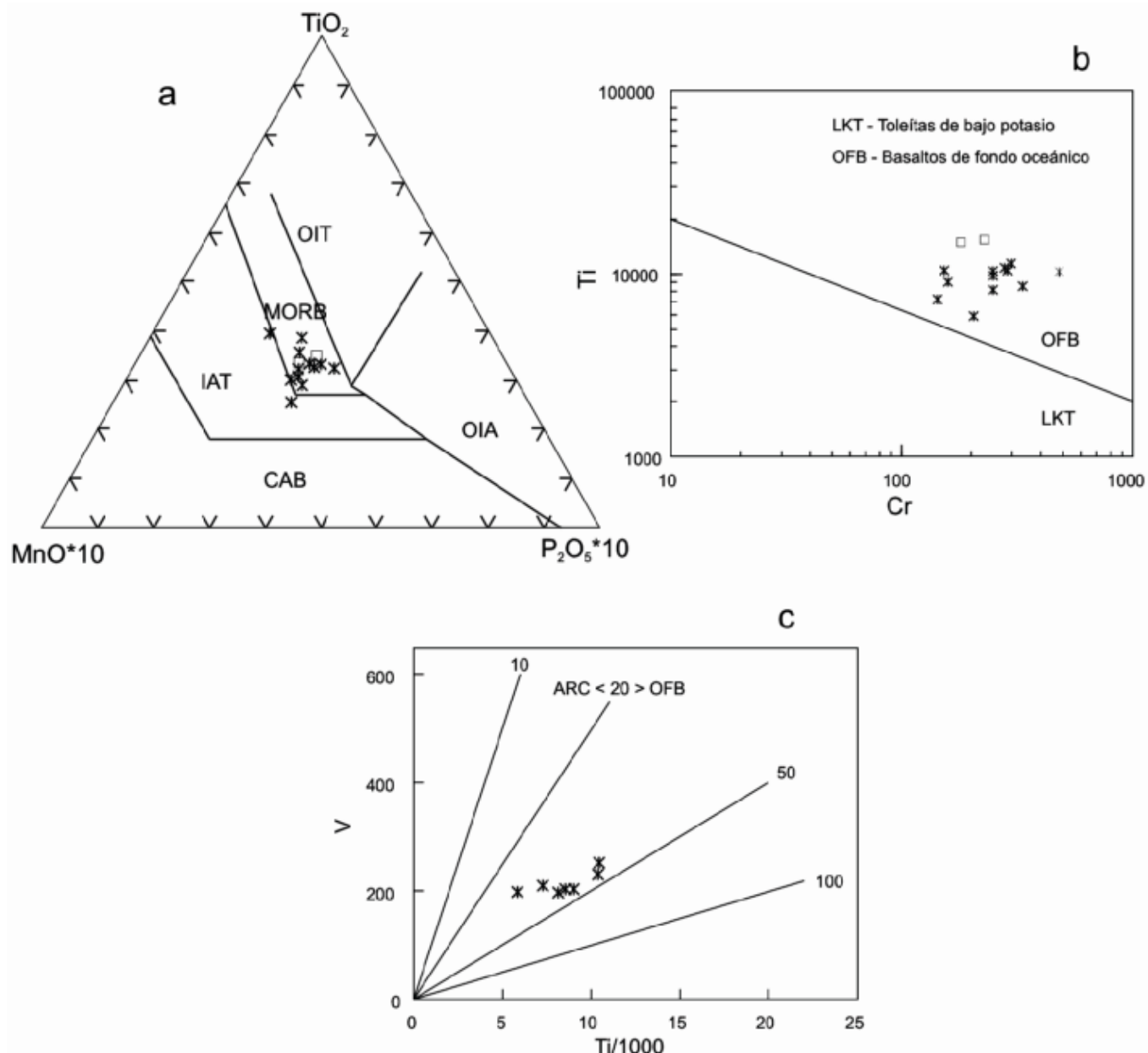


Figura 10. Diagramas discriminantes de ambientes tectónicos para las anfibolitas de Medellín, Boquerón y El Retiro. a) **Mullen** (1983). Campos: MORB-basaltos de dorsal medio-oceánica, OIT-toleítas de islas oceánicas, OIA- basaltos alcalinos de islas oceánicas, CAB-basaltos calcoalcalinos de arcos de isla, IAT-toleítas de arco de isla. b) **Pearce** (1975). c) **Shervais** (1982). Campos: ARC-basaltos de arco, OFB-basaltos de fondo oceánico. Símbolos como en la figura 4.

Discusión

Las notables diferencias geoquímicas, mineralógicas y estructurales descubiertas en las metabasitas de los alrededores de Medellín obligan a una subdivisión de éstas.

Los Metagabros de El Picacho muestran estructuras que revelan su protolito ígneo plutónico, como una unidad de gabros con estratificación ígnea. Este tipo de intrusiones bandeadas pueden presentarse en complejos estratificados (**Wager & Brown**, 1968) o como parte de la cámara magmática de ofiolitas (**Coleman**, 1977). Los va-

lores relativamente altos del #Mg indican que los magmas basálticos parentales eran poco evolucionados; sin embargo la información geoquímica es insuficiente para dar luz sobre el ambiente de formación y el tipo de manto del cual se derivaron. Como parte de un complejo ofiolítico, estas rocas se pudieron generar en varios ambientes como una dorsal medio-oceánica, una cuenca trasarco, una cuenca antearco, un arco de islas o un ‘plateau’ oceánico.

Los gabros fueron afectados por metamorfismo dinámico dúctil, que milonitizó variablemente las rocas. Éstas sufrieron posteriormente, o al final de la deformación dinámica, otro metamorfismo de tipo hidrotermal, a temperaturas correspondientes a la facies anfibolita. La alteración hidrotermal generó una disposición desordenada de anfíboles secundarios, principalmente clinoanfíboles verdes, que en algunas muestras están sobreimpuestos a la fábrica milonítica. Se propone que el metamorfismo dinámico se produjo durante el proceso de emplazamiento del fragmento de corteza oceánica sobre una corteza continental y el hidrotermal por la acción de fluidos y el calor residual de tal corteza.

Las Anfibolitas de Medellín, por su parte, no presentan texturas relictas de su protolito. El tamaño del cuerpo, la presencia de grafito en algunos paquetes de anfibolitas y la asociación local con metasedimentitas sin rocas calcáreas, sugiere un origen ígneo volcánico. La intercalación milimétrica a centimétrica de anfibolitas y metasedimentitas indica sedimentación y vulcanismo contemporáneos.

La geoquímica indica que se trata de metabasitas con una tendencia de cristalización toleítica y que la fuente pudo corresponder a un magma intermedio entre aquellos que generan los basaltos N-MORB y E-MORB. Los ambientes más probables de formación para esta unidad son una cuenca tras-arco o una dorsal oceánica con aporte de sedimentos continentales. En una cuenca tras-arco los basaltos generados pueden tener características geoquímicas similares a las de un MORB (**Wilson, 1989**). En el caso de que haya sido este el ambiente de generación, se trató de una cuenca evolucionada muy alejada de la zona de subducción, pues no se aprecian los rasgos geoquímicos propios de ésta, como anomalías negativas de Nb y enriquecimiento en tierras raras livianas.

El conjunto de basaltos y sedimentitas se metamorfizó en facies anfibolita durante un metamorfismo orogénico; no hay evidencias de metamorfismo hidrotermal o dinámico que afecte de manera global a la unidad. Si bien estas anfibolitas tienen fábrica lineal, ésta es por la disposición de los anfíboles columnares que sintectónicamente

crecieron disponiéndose de manera casi paralela (foliación nematoblástica), y no por un cizallamiento posterior a la formación de la metamorfita. No se descubre el anastomosamiento y las estructuras típicas de las rocas fuertemente deformadas dúctilmente. La mineralogía indica condiciones de metamorfismo de más alto grado que en los Metagabros de El Picacho, incluso en la transición de la facies de anfibolitas a la de granulitas.

Otra unidad importante, pero de limitada extensión, son las Anfibolitas de Boquerón, compuestas por metabasitas de grano medio en facies de anfibolita, posiblemente baja, que contienen abundante esfena. Las rocas tienen bandeo composicional, foliación en la que predomina la esquistosidad sobre la lineación, evidencias de metamorfismo dinámico y minerales secundarios como anfíboles aciculares desordenados, epidota y esfena. Los rasgos estructurales sugieren correlación con los Metagabros de El Picacho, pero su geoquímica es semejante a la de las Anfibolitas de Medellín.

Por otro lado, las anfibolitas de El Retiro comparten características de campo, petrográficas y de condiciones metamórficas con las Anfibolitas de Medellín, pero presentan algunas diferencias geoquímicas con éstas. Así, el #Mg es más bajo y los patrones de tierras raras muestran leve enriquecimiento en elementos de las tierras raras livianas lo que sugiere que el protolito correspondió a magmas parentales diferenciados o más evolucionados que las fuentes de las Anfibolitas de Medellín. No obstante es necesario realizar estudios geoquímicos detallados para determinar si esas variaciones geoquímicas se pueden explicar a través de un proceso de diferenciación magmática o si indican magmas diferentes para las Anfibolitas de Medellín y El Retiro. Aún se desconoce si los protolitos de estas anfibolitas estuvieron relacionados espacial y temporalmente.

La asociación en los alrededores de Medellín de las metabasitas descritas junto con cuerpos ultramáficos, invita a considerar la existencia de un complejo ofiolítico. Las ultramafitas, principalmente dunitas, provendrían del manto litosférico; los metagabros se habrían derivado de los gabros bandeados de una cámara magmática en la parte intermedia de la ofiolita; y las anfibolitas sin rasgos relictos que están asociadas a metasedimentitas serían la parte superior de la ofiolita, donde basaltos, doleritas y sedimentos se habrían metamorfizado bajo condiciones de alto grado. Incluso el límite tectónico que separa las unidades no sería de extrañar, ya que en muchos ejemplos de ofiolitas en el mundo, éstas se presentan desmembradas como bloques dispersos limitados tectónicamente (**anónimo, 1972**).

No obstante, es necesario ser precavidos con esta interpretación, ya que las características encontradas en los Metagabros de El Picacho y las Anfibolitas de Medellín, sugieren una historia metamórfica disímil para cada unidad. Los Metagabros de El Picacho tienen texturas ígneas relictuales, evidencias de cizallamientos fuertes y alteración hidrotermal que genera texturas desordenadas. Ninguno de estos rasgos está presente en las Anfibolitas de Medellín, que en cambio, presentan fábrica sintectónica de un metamorfismo orogénico, asociaciones minerales que indican alto grado incluso alcanzando la transición a la facies de granulitas, y una cantidad notablemente superior de esfenas.

Preferimos, por esto, proponer dos conjuntos principales: uno ofiolítico, compuesto por las ultramafitas y los metagabros, para el que se propone el nombre *Complejo Ofiolítico de Aburrá*, y otro, compuesto por las Anfibolitas de Medellín (*s.s.*) y los gneises de alto grado asociados.

Los conjuntos propuestos pueden extenderse para incluir otras litologías de los alrededores de la ciudad. El Gneis de la Iguaná (**Restrepo & Toussaint**, 1982), ubicado en el sector del mismo nombre (Figura 1), se ha correlacionado con gneises paleozoicos de la cordillera Central. En nuestra opinión debería estudiarse con más detalle para establecer si, por el contrario, hace parte del Complejo Ofiolítico de Aburrá. Este cuerpo corresponde a un granitoide milonitizado, de coloración clara, constituido principalmente por plagioclasa, cuarzo, feldespato potásico en la mayoría de muestras, poca biotita, grandes cristales de epidota, y zircón como accesorio, con una fábrica lineada-milonítica. Si bien su composición parece ser relativamente ácida, las estructuras que tiene son muy semejantes a aquellas presentes en los Metagabros de El Picacho, los cuales están asociados espacialmente con el gneis.

Hacia el sur, las Anfibolitas de Medellín y las metasedimentitas de alto grado se extienden a las poblaciones de El Retiro y La Ceja, pero allí no se han registrado, al momento, cuerpos de extensión considerable de ultramafitas o de metagabros. No se conoce ningún sistema de fallas importante que separe las unidades de este lugar de las Anfibolitas de Medellín, y en nuestra opinión, al menos las anfibolitas de uno y otro lugar, deberían considerarse un solo cuerpo. También hay una prolongación de las anfibolitas hacia el norte que llega al menos hasta Belmira.

Parece razonable incluir por grado metamórfico otros cuerpos metasedimentarios de alto grado, en conjunto con las Anfibolitas de Medellín y sus extensiones. Destacan las rocas del alto de Baldías, los gneises y migmatitas al

sur de Envigado, y las migmatitas en El Retiro. Ya **Echeverría** (1973) había propuesto una subdivisión semejante al definir la Zona La Ayurá, si bien su interpretación tiene significativas diferencias con la nuestra.

La información geocronológica que se tiene hasta el presente es insuficiente para determinar si las Anfibolitas de Medellín y los Metagabros de El Picacho conforman un único complejo ofiolítico contemporáneo que fue desmembrado. Con la información existente son concebibles dos escenarios. En uno, un fragmento basal de corteza oceánica y otro de manto litosférico de edad incierta (Dunita de Medellín + Metagabros de El Picacho) se emplazan sobre un extenso cinturón metamórfico, que incluye anfibolitas, después de que éste fue generado en un metamorfismo orogénico Pérmico-Triásico y antes de la intrusión del Batolito Antioqueño en el Cretácico. En este caso el Complejo Ofiolítico de Aburrá estaría formado exclusivamente por las ultramafitas y los metagabros bandeados de los alrededores de Medellín. Una segunda propuesta, desarrollada recientemente por **Restrepo** (2003), plantea un metamorfismo Pérmico-Triásico conjunto entre Anfibolitas y Dunitas de Medellín, durante el que no sólo ultramafitas y metagabros, sino también las Anfibolitas de Medellín, se habrían emplazado sobre un basamento metamórfico más antiguo.

Conclusión

En este estudio se descubrió que algunos cuerpos de metabasitas en los alrededores de Medellín corresponden a intrusiones ígneas bandeadas que fueron metamorfosadas dinámicamente, luego hidrotermalizadas, y cuya geoquímica, mineralogía y estructuras particulares, hacen necesario separarlas en una nueva unidad litoestratigráfica cuyo nombre se propone sea Metagabros de El Picacho. Estas metabasitas deben considerarse aparte de la unidad Anfibolitas de Medellín, compuesta por metavulcanitas y metasedimentitas subordinadas, y que se formaron durante un metamorfismo orogénico de alto grado.

Los Metagabros pueden agruparse junto con las Dunitas de Medellín en una unidad que aquí se define como Complejo Ofiolítico de Aburrá, y que corresponde a la parte basal de una corteza oceánica cuyo ambiente de generación aún no se conoce. Queda por verse si las Anfibolitas de Medellín hacen parte del mismo complejo, pues si bien puede tratarse de la parte superior de la ofiolita metamorfosada bajo condiciones de alto grado, hay muchas diferencias, especialmente en la sucesión y tipo de eventos metamórficos, que sugieren dos historias geológicas disímiles para cada unidad de metabasitas.

Los datos que actualmente se tienen de las Anfibolitas de Boquerón son insuficientes para dilucidar su origen, y su correlación es aún incierta. Las Anfibolitas de El Retiro se consideran extensiones laterales hacia el sur de las Anfibolitas de Medellín aunque sus rasgos geoquímicos y el tipo de metasedimentitas asociadas son un tanto disímiles.

La información geocronológica disponible indica que el metamorfismo de alto grado de las Anfibolitas de Medellín y de El Retiro se dio durante el lapso Pérmico-Triásico. La edad de los Metagabros de El Picacho, y en general, del Complejo Ofiolítico de Aburrá, no ha sido determinada. El emplazamiento del complejo ofiolítico pudo darse asociado con el metamorfismo Pérmico-Triásico citado, o bien, posteriormente.

Agradecimientos

Queremos agradecer al CIMEX y al Centro del Carbón de la Universidad Nacional de Colombia, Sede Medellín, y al laboratorio de trazas de fisión de la Universidad EAFIT (Medellín) por permitir la preparación de muestras, y a los laboratorios de Geoquímica y Geocronología de la Universidad de Brasilia (Brasil) por la ejecución de los análisis químicos. Agradecimiento especial a todos nuestros amigos, geólogos o no, por acompañarnos a las excursiones de campo. Al geólogo Álvaro Nivia por la ayuda brindada en la interpretación de los datos geoquímicos.

Los dos primeros autores agradecen especialmente a los profesores Jorge Julián Restrepo y Oswaldo Ordóñez-Carmona por la orientación del trabajo dirigido de grado que dio origen a este artículo.

Bibliografía

- Álvarez, J.**, 1987. Tectonitas dunitas de Medellín, departamento de Antioquia, Colombia. Boletín Geológico Ingeominas. **28** (3): 9-44.
- Anónimo**, 1972. Penrose Field Conference on ophiolites. Geotimes, **17** (12): 24-25.
- Beswick, A.E. & Soucie, G.**, 1978. A correction procedure for metasomatism in an Archean greenstone belt. Precambrian Res. **6**: 235-248.
- Botero, G.**, 1963. Contribución al conocimiento geológico de la zona central de Antioquia. En: Anales de la Facultad de Minas. (57): 1-101.
- Bucher, K. & Frey, M.**, 2002. Petrogenesis of metamorphic rocks. Springer Verlag, Berlin. 318 p.
- Coleman, R.G.**, 1977. Ophiolites. Ancient Oceanic Lithosphere? SpringerVerlag, Berlin. 229 p.
- Estrada-Carmona, J.**, 2003. Caracterización geológica de las rocas metamórficas en los alrededores de la cuchilla Las Peñas. Universidad Nacional, Facultad de Minas, Medellín. Tesis (inédita). 91 p.
- Echeverría, L.M.**, 1973. Zonación de las rocas metamórficas del valle de Aburrá y sus alrededores. En: Anales de la Facultad de Minas. (58): 30-56.
- Grauch, R.I.**, 1989. Rare earth elements in metamorphic rocks. En: Reviews in Mineralogy. **21**: 147-167.
- INGEOMINAS**, 1996. Memoria explicativa del mapa geológico generalizado del departamento de Antioquia. Escala 1:400.000. Medellín.
- _____, 1997. Mapa geológico generalizado del departamento de Antioquia. Escala 1:400.000. Medellín.
- Irvine, T. N. & Baragar, W. R.**, 1971. A guide to the chemical classification of the common volcanic rocks. En: Can. J. Earth Sci. **8**: 523-548
- Le Bas M. J., Le Maitre R. W., Streckeisen A. & Zanettin B.**, 1986 - A chemical classification of volcanic rocks based on the Total Alkali-Silica Diagram. J. Petrol., **27**: 745-750
- Martens, U. & Dunlap, W.J.**, 2003. Características del metamorfismo Cretácico del terreno Tahamí como se infiere a partir de edades Ar/Ar obtenidas en las Anfibolitas de Medellín, cordillera Central de Colombia (resumen). En: Memorias IX Congreso Colombiano de Geología. Medellín: 47-48.
- McCourt, W. J., Aspden, J. A. & Brook, M.**, 1984. New geological and geochronological data from the Colombian Andes: continental growth by multiple accretion. J. Geol. Soc. London. **141**: 831-845.
- Miyashiro, A.**, 1994. Metamorphic petrology. Oxford University Press, Londres. 404 p.
- Montes, L.F.**, 2003. Relación entre las metamorfitas de alto y bajo grado en el sur del valle de Aburrá. IX Congreso Colombiano de Geología, Medellín (resúmenes).
- Mullen, E. D.**, 1983. MnO/TiO₂/P₂O₅: a minor element discriminant for basaltic rocks of oceanic environments and its implications for petrogenesis. Earth and Planetary Science Letters **62**: 53-62.
- Ordóñez, O.**, 2001. Caracterização isotópica Rb-Sr e Sm-Nd dos principais eventos magmáticos nos Andes Colombianos. Tesis de Doctorado (inédita). Universidad de Brasilia. 176 p.
- _____. Pimentel, M., Correa, A.M., Martens, U., Restrepo, J.J., 2001. Edad Sm/Nd del metamorfismo de alto grado de El Retiro (Antioquia). En: VIII Congreso Colombiano de Geología, Manizales (C.D.).
- Pearce, J. A.**, 1975. Basalt geochemistry used to investigate past tectonic environments on Cyprus. Tectonophysics **25**: 41-67
- Rendón, D. A.**, 1999. Cartografía y caracterización de las unidades geológicas del área urbana de Medellín. Universidad Nacional, Facultad de Minas, Medellín. Tesis de grado (inédita).
- Restrepo, J. J.**, 1986. Metamorfismo en el sector norte de la Cordillera Central de Colombia. Universidad Nacional, Facultad de Ciencias, Medellín. 276 p.

- _____. 2003. Edad de generación y emplazamiento de ofiolitas en la cordillera Central: un replanteamiento (resumen). En: Memorias IX Congreso Colombiano de Geología. Medellín: 48-49.
- _____. & Toussaint, J. F., 1974. Obducción Cretácica en el Occidente Colombiano. Anales de la Facultad de Minas. (58): 73-105.
- _____. 1978. Edades radiométricas de algunas rocas de Antioquia, Colombia. Boletín de Ciencias de la Tierra. (5-6): 1-18.
- _____. 1982. Metamorfismos superpuestos en la Cordillera Central de Colombia. En: Actas del V Congreso Latinoamericano de Geología. 3: 505-512.
- _____. 1984. Unidades litológicas de los alrededores de Medellín. En: Conferencia sobre riesgos geológicos del valle de Aburrá: 1-26.
- Restrepo A. J.J., Toussaint, J.F., González, H., Cordani, U., Kawashita, K., Linares, E. & Parica, C.**, 1991. Precisiones geocronológicas sobre el Occidente Colombiano. En: Simposio sobre magmatismo andino y su marco tectónico. Manizales. 1: 1-21.
- Rollinson, H.**, 1993. Using geochemical data: evaluation, presentation, interpretation. Longman Group, Essex. 352p.
- Shervais, J.W.**, 1982. Ti-V plots and the petrogenesis of modern and ophiolitic lavas. Earth Planet. Science Lett., **59** (1): 101-118.
- Sun, S.-s., McDonough, W.F.**, 1989. Chemical and isotopic systematics of oceanic basalts: implications for mantle composition and processes. En: Saunders, A.D. & Norry, M.J. (eds.), Magmatism in the Oceanic Basins. Geological Society of America Special Publication **42**: 313 – 345.
- Tamayo, L.M.**, 1984. Análisis y mediciones de miniestructuras en la anfibolita del Grupo Ayurá-Montebello. Medellín, Universidad Nacional, Facultad de Minas. Tesis de grado (inédita).
- Toussaint, J. F.**, 1996. Evolución Geológica de Colombia 3: Cretácico. Universidad Nacional, Facultad de Minas, Medellín. 277p.
- Vinasco, C., Cordani, U., González, H., Vasconcelos, P., Liu, D.**, 2003. Tectonomagmatic evolution of the northern part of the Central Cordillera of Colombia using Ar-Ar and U-Pb Shrimp methodologies (resumen). En: Memorias IX Congreso Colombiano de Geología. Medellín: 57-58.
- Vinasco, C.J., Cordani, U.G., Vasconselos, P.**, 2001. 40Ar/39Ar dates in the Central Cordillera of Colombia: evidence for an upper Triassic regional tectonomagmatic event. En: III Simposio Sudamericano de Geología Isotópica, Pucón - Chile.
- Wager, L.R. & Brown, G.M.**, 1968. Layered igneous rocks. W.H. Freeman, San Francisco. 588 p.
- Wilson, M.**, 1989. Igneous petrogenesis. Chapman & Hall, Londres. 466 p.
- Wood, D.A., Tarney, J., Varet, J., Saunders, A.D., Bougault, H., Joron, J.-L., Treuil, M. and Cann, J.R.**, 1979. Geochemistry of basalts drilling in the North Atlantic by IPOD Leg 49: implications for mantle heterogeneity. Earth Planet. Sci. Lett., **42**: 77-97.

Recibido el 4 e octubre de 2004.

Aceptado para su publicación el 15 de junio de 2005.

ANEXO 2

TABELA DE LOCALIZAÇÃO DOS PONTOS

Anexo 2. Tabela de localização dos pontos

Ponto	Local	Rocha-Descrição	Sistema central		Sistema ocidental	
			Coordenada Norte	Coordenada Leste	Norte	Leste
AC-01	Cerro Nutibara, via da portaria da 65	Metagabro	1181443	833496	1181440	1165541
AC-02	Cerro Nutibara, via da portaria da 65	Metagabro e Dique	1181583	833496	1181580	1165540
AC-03	Cerro Nutibara, via da portaria da 65. 20 m antes divisória para Av.33	Metagabro e solo branco (leucogranito?)	1181702	833577	1181700	1165620
AC-04	Cerro Nutibara, via parte alta. Atrás do Cacique Nutibara	Metagabro e metagabro milonitizado. Passa uma falha	1181561	833776	1181560	1165820
AC-05	Cerro Nutibara, Calle 65	Metagabro com várias zonas de pequenas cisalhas	1181723	833427	1181720	1165470
AC-06A,B,C	Cerro El Volador, via de acesso.	Metagarbo com diferente nível de deformação	1181822	833557	1184820	1165600
AC-06D	Cerro El Volador, perto caixa de água	Metagabro	1181803	833487	1184800	1165530
AC-07	Cerro El Volador, parte alta. Equivale com CMK-103	Metagabro de Boquerón, ou anfibolito	1181874	833308	1184870	1165350
AC-08	Estrada a Boquerón perto da Quebrada Seca	Brecha intrusiva de Altavista	1190687	825848	1190640	1157840
AC-09	Estrada Boquerón, afloramento JJ	Metagabro de Boquerón milonitizado. Dique	1190453	825859	1190406	1157853
AC-10	Rodovia Medellín-Bogotá, Aprox 80 m depois de Restaurante Belvedere	Anfibolito	1190401	837376	1190420	1169370
AC-11	Rodovia Medellín-Bogotá, pequenas falhas das fotos	Anfibolito milonitisado	1190430	837387	1190450	1169380
AC-12	Rodovia Medellín-Bogotá, 50 m antes de Canteras de Colombia	Anfibolito milonitisado,	1190480	837407	1190500	1169400
AC-13	Rodovia Medellín-Bogotá,	Contato anfibolito-dunito, xistos verdes dobrados	1191197	837991	1191220	1169980
AC-14	Estrada Medellín-Santa Elena Perto de Bairro perigoso	Anfibolito	1180660	839360	1180691	1171409

Ponto	Local	Rocha-Descrição	Sistema central		Sistema occidental	
			Coordenada Norte	Coordenada Leste	Norte	Leste
AC-15	Estrada Medellín-Santa Elena, parte alta equivalente a CMK-096	Anfibolito	1181360	841490	1181403	1173535
AC-16	Estrada Medellín-Santa Elena, parte alta mais ao norte do anterior.	Anfibolito	1181185	841850	1181230	1173896
AC-17	Estrada Medellín-Santa Elena, parte alta mais ao norte do anterior.	Anfibolito	1181005	841912	1181050	1173960
AC-18	Rodovia Medellín-Bogotá	Contato anfibolito de Medellín-gnaisse Las Peñas	1190560	842450	1190609	1174443
AC-19	Rodovia Medellín-Bogotá	Peridotito milonitisado	1191218	837851	1191240	1169840
AC-20	Mina de Cromita de Patio Bonito	Cromitito, peridotito	1177054	840100	1177089	1172170
AC-21	Cantera Sajonia	Anfibolito	1175280	847770	1175358	1179850
AC-22	Quebrada Chagualones, Bello	Peridotito e metagabro cislhado	1195200	836000	1195211	1167966
AC-23	Convento de Las Clarizas	Anfibolito				
AC-24	Vía El Tesoro, carretera Las Palmas	Metagabro e dique básico	1176150	837000	1176167	1169075
AC-25	Las Palmas	Metagabro	1176421	837317	1176440	1169390
AC-26	Las Palmas 80 m antes do aviso Bienvenido a Medellín. Equivale a CMK-140	Peridotito	1176721	837338	1176740	1169410
AC-27	Las Palmas, antes da entrada para Cola Del Zorro	Peridotito	1178740	837530	1178760	1178760
AC-28	Cantera de Indural	Gnaisse de La Iguaná. E diques intermediários a básicos.	1185308	832627	1185300	1164650
AC-29	Estrada Medellín-San Pedro, um pouco após qda. La Loca	Granodiorito com enclaves	1190635	831453	1190620	1163445
AC-30	Estrada Medellín-San Pedro, cauce quebrada La Loca	Blocos rolados de metagabros e granitoides	1190545	831377	1190530	1163370

Ponto	Local	Rocha-Descrição	Sistema central		Sistema occidental	
			Coordenada Norte	Coordenada Leste	Norte	Leste
AC-31	Estrada Medellín-San Pedro, córrego abaixo do restaurante Jalisco	Blocos de metagabro	1190082	831834	1190070	1163830
AC-32	Estrada Medellín-San Pedro, afloramento de Jalisco	Metagabro in situ, deformação variável. Veios e diques de leucogranito	1189853	831985	1189842	1163982
AC-33	Estrada Medellín-San Pedro, entrada a Bairro Perigoso. Equivale a CMK-023	Bloco de metagabro com bandas centimétricas com diferente deformação. E dique básico	1189586	832027	1189575	1164025
AC-34	Estrada Medellín-San Pedro, entre AC-32 e AC-33	Metagabro cisalhado	1189651	832002	1189640	1164000
AC-35	Estrada a Central Hidroelétrica de Niquía	Peridotito com pequeno stockwork de magnesita	1193882	838806	1193910	1170780
AC-36	Estrada a Central Hidroelétrica de Niquía	Peridotito bandado	1193930	838856	1193958	1170785
AC-37	Estrada a Central Hidroelétrica de Niquía	Peridotito bandado	1194112	838823	1194140	1170795
AC-38	Estrada a Central Hidroelétrica de Niquía, cisalhamento	Peridotito cisalhado Contato com anfibolito	1194282	838799	1194310	1170770
AC-39	Estrada a Central, Hidroelétrica de Niquía, anfibolitos	Anfibolito	1194621	839034	1194650	1171003
AC-40	Rodovia Medellín-Bogotá, 500m após o pedágio.	Anfibolito	1192370	841280	1192412	1173262
AC-41	Rodovia Medellín-Bogotá, curva	Anfibolito com dobras, dique básico	1191735	839974	1191770	1171960
AC-42	Rodovia Medellín-Bogotá, após do augen gigante	Anfibolito	1191225	840011	1191260	1172000
AC-43	Rodovia Medellín-Bogotá, perto de Rodas, após da curva	Anfibolito	1191218	839571	1191250	1171560
AC-44	Rodovia Medellín-Bogotá, na frente de Rodas	Granada anfibolito, anfibolito	1191059	839450	1191090	1171440
AC-45	Rodovia Medellín-Bogotá,	Cloritito e actinolítito	1190550	839117	1190580	1171110

Ponto	Local	Rocha-Descrição	Sistema central		Sistema occidental	
			Coordenada Norte	Coordenada Leste	Norte	Leste
	antes da quebrada Rodas					
AC-46	Rodovia Medellín-Bogotá, entre AC-47 e AC-45	Cloritito e actinolítico	1190892	838929	1190920	1170920
AC-47	Rodovia Medellín-Bogotá, ao lado das linhas de transmissão, perto entrada Rodas	Contato entre anfibolito e peridotito. Dique de rocha pôrfídica. Zona de reação entre o dique e o peridotito	1191012	838810	1191040	1170800
AC-48	Rodovia Medellín-Bogotá, entre AC-19 e AC-47	Peridotito milonitzado	1191255	838371	1191280	1170360
AC-49	Vereda La Quiebra	Harzburgito pegmatoide. Cloritito, hornblendito, vermiculitito	1176046	847153	1176120	1179229
AC-50	Vereda La Quiebra	Harzburgito, veios félscicos	1175959	847229	1176034	1179306
AC50cis	Vereda La Quiebra, início zona de cisalha	Harzburgito cisalhado	1175999	847217	1176074	1179293
AC-51	Variante Aeroporto-Las Palmas. Equivale com CMK-141	Anfibolito	1174580	845050	1174642	1177134
AC-52	Variante Aeroporto-Las Palmas.	Harzburgito com bandas de dunito	1173208	842047	1173254	1174139
AC-53	Vereda Perico. Estrada em terra entre a varainte e El Alto El Chagualo	Harzburgito com bandas de dunito. Boudins de anfibolito no contato com a ultramáfica. Dique básico	1174533	842010	1174578	1174095
AC-53 Acima	Vereda Perico	Harzburgito com bandas de dunito, abundante clorita	1174643	841859	1174688	1173943
AC-53 Abaixo	Vereda Perico		1174532	841991	1174577	1174075
AC-54	Vereda Perico	Blocos enormes de metagabros	1174830	842282	1174877	1174364
AC-55	Cerro El Picacho, equivale com CMK-040	Metagabro	1189126	832999	1189120	1165000
AC-56	Quebrada La Miel, Caldas	Granada anfibolita	1160639	831313	1160625	1163475
AC-57	Estrada Medellín-San Pedro	Brecha metagabro	1190899	831859	1190886	1163850
AC-58	Estrada Medellín-San Pedro, perto a El Tambo	Blocos de metagabro na beira da estrada	1192159	831777	1192146	1163760
AC-59	Estrada Medellín-San	Peridotito in situ, blocos de	1203928	833807	1203927	1165722

Ponto	Local	Rocha-Descrição	Sistema central		Sistema occidental	
			Coordenada Norte	Coordenada Leste	Norte	Leste
	Pedro, casa Zulia	metagabro				
AC-60	Estrada a Belmira	Harzburgito grosso e médio, dunito. Contato falhado com anfibolito	1211049	834177	1211040	1166050
AC-61	Estrada a Boquerón, onde a estrada tem sempre problemas de instabilidade	Blocos rolados de metagabro de Boquerón	1188054	828394	1188022	1160402
AC-62	Quebrada Miserenga, ocidente		1195787	819905	1195705	1151868
AC-63						
AC-64	Complexo Quebradagrande, Pedra Negra		1197869	818398	1197778	1150350
AC-65	Carretera Anzá, Formação Barroso, Aflora. Pillow lavas		1192300	802886	1192120	1134873
AC-66	Estrada a Central Hidroelétrica de Niquia	Blocos rolados de olivina gabronorito e gábro	1193422	838799	1193450	1170775
AC-67						
AC-68	Córrego La Mina. Calazans	Gnaisse de La Iguaná	1184938	830895	1184920	1162920
AC-69	Bairro Calazans	Gnaisse de La Iguaná	1185719	830627	1185699	1162647
AC-70	Invasión Olaya Herrera II	Contato intrusivo do gnaisse de la Iguaná en metagabro de boquerón. Intercalação de bandas das duas unidades milonitisadas	1186064	830136	1186042	1162154
AC-71	Quebrada La Iguana perto do parque de San Cristóbal	Diorito de Altavista	1186048	827321	1186010	1159340
AC-72	Quebrada La Iguana via entre San Cristóbal e Juan XXIII	Dique aplítico en Altavista	1185953	828241	1185920	1160260
AC-73	Bairro Maruchenca, margem esquerda córrego La Loca	Metagabro in situ intemperizado. Dique máfico	1190398	834406	1190400	1166400
AC-74	Quebrada La Iguana, perto entrada do túnel.	Dioritos com enclaves de microdioritos-Stock de Altavista	1188148	825800	1188101	1157807
AC-75	Belén Altavista	Diorito com enclaves-Stock de Altavista	1180652	827275	1180614	1159325

Ponto	Local	Rocha-Descrição	Sistema central		Sistema ocidental	
			Coordenada Norte	Coordenada Leste	Norte	Leste
AC-76	San Antonio de Prado	Granito-Stock de Altavista	1178682	824172	1178627	1156234
AC-77	Depósito El Chagualo	Cromita disseminada grossa a quase nodular- Depósito El Chagualo	1172592	842312	1172639	1174407
AC-78 A	Depósito Loma Menezes Frente Betsabé	Cromita maciça e disseminada. Peridotitos. O contato entre o minério e o peridotito fresco é um peridotito intensamente cisalhado	1199379	835742	1199389	1167683
AC-78 B	Depósito Loma Menezes Frente Aníbal	Cromita eluvial e cromita maciça in situ	1199348	835745	1199358	1167686
AC-78 C	Depósito Loma Menezes Frente Reinaldo	Cromita maciça	1199511	835530	1199520	1167471
AC-78 D	Depósito Loma Menezes Frente Ildebrando, rocha ultramáfica	Peridotito	1199511	835711	1199521	1167652
AC-78 D2	Depósito Loma Menezes Frente Ildebrando, cromitito	Cromita maciça	1199637	835647	1199646	1167587
AC-79	Vereda Perico, perto escola	Peridotito	1176232	841744	1176276	1173818
AC-80	Depósito El Carmelo	Peridotito com abundante cromita disseminada	1175108	841645	1175151	1173726
AC-80 B	Depósito El Carmelo, frente Carmén	Cromita maciça e peridotito	1175111	841670	1175154	1173751
AC-81 A	Via perto a El Carmelo, afloramento falso	Peridotito cisalhado	1175418	841508	1175461	1173587
AC-81 B	Via perto a El Carmelo, afloramento grande	Peridotito e xistos cloríticos	1175529	841419	1175571	1173497
AC-82	Chácara Samarcanda, beira da estrada	Granito de Samarcanda	1177154	845298	1177218	1177368
AC-83 A	Afloramento de saprolito	Saprolito Granito de Samarcanda	1174917	846461	1174987	1178543
AC-83B	Cantera	Granito de Samarcanda e anfibolito	1175084	845852	1175151	1177934
PJ	Afloramento Peridotito, vereda El Plan	Peridotito	1178640	839550	1178672	1171611
CNI	Cromita Niquia	Depósito de cromita maciça	1195600	835030	1195606	1166993

Ponto	Local	Rocha-Descrição	Sistema central		Sistema ocidental	
			Coordenada Norte	Coordenada Leste	Norte	Leste
CSP	Cromita San Pedro	Depósito de cromita disseminada grossa	1206800	833450	1206796	1165348
P1	Urbanização Santa Maria de Los Balsos-El Tesoro	Metagabro. Testemunho de perfuração	1176076	837297	11760949	1169372
P2	Urbanização Santa Maria de Los Balsos-El Tesoro	Wehrlito. Testemunho de perfuração	1176015	837354	1176034	1169430
P3	Urbanização Santa Maria de Los Balsos-El Tesoro	Wehrlito. Testemunho de perfuração	1176123	837375	1176142	1169450
A	Depósito Don Jaime, TF de (Monsalve, 1996)	Cromita Maciça	1202060	834300	1202062	1166226
F			1199820	836630	1199835	1168569
I	Alto de Medina. Monsalve, 1996	Cromita diseminada.	1199700	835500	1199709	1167440
U	Monsalve, 1996	Dunita com grãos de cromita.	1199700	835400	1199708	1167340
JJ1396	Córrego Chupaderos	Blocos rolados de harzburgito	1179747	839052	1179776	1171107
JJ1342	San Diego, perto a Fonte de Sonolux	Diorito de San Diego	1180802	834956	1180807	1167005

ANEXO 3

RESULTADOS DE ANÁLISES DE QUÍMICA MINERAL

OLIVINA

Harzburgitos e peridotito com agregados de anfibólio

Amostra	JJ1396p5ol	JJ1396p5ol	Ac22B1oliv	Ac22B1oliv	1	2	Ac22B3oliv1	Ac22B3oliv2	Ac22B2oliv	AC53A4-A	AC53A4-B	AC53A4-C	AC53A4-D	AC53A6-B	AC53Jp1Olivine1a	AC53Jp1ol1ou	AC53Jp1oli1fine1	AC53Jp1oli1fine2	AC53Jp4oli1vinefine
SiO ₂	41.56	41.42	40.88	40.47	40.59	40.98	40.87	41.59	41.84	41.91	41.93	41.81	41.40	41.33	41.34	40.96	41.71		
TiO ₂	0.00	0.01	0.01	0.01		0.01											0.01	0.03	
Al ₂ O ₃	0.02	0.00	0.03	0.00	0.01			0.00	0.04	0.01	0.00	0.00	0.01				0.01	0.03	
Cr ₂ O ₃	0.03	0.00	0.00	0.00				0.03	0.00	0.04	0.03	0.05					0.02	0.01	
FeO	7.85	7.79	9.84	9.81	9.74	9.67	9.73	8.89	9.17	8.86	9.34	9.09	10.34	10.46	10.39	10.44	10.39		
MnO	0.11	0.14	0.17	0.15	0.16	0.15	0.16	0.05	0.08	0.03	0.09	0.12	0.15	0.17	0.18	0.20	0.15		
MgO	49.84	49.73	48.38	48.54	48.50	48.74	48.45	49.54	49.94	49.82	49.61	49.61	47.79	47.58	48.23	48.39	47.66		
CaO	0.00	0.01	0.01	0.00	0.00	0.00	0.00	0.00	0.00	0.00	0.00	0.02	0.01	0.00	0.01	0.00	0.00		
NiO	0.38	0.39	0.38	0.40	0.36	0.39	0.39	0.49	0.39	0.43	0.37		0.31	0.36	0.28	0.34	0.26		
	99.80	99.48	99.71	99.40	99.35	99.94	99.61	100.59	101.47	101.09	101.37	100.70	100.00	99.91	100.43	100.37	100.24		

Cations na base de 4 oxigênios

	JJ1396p5ol	JJ1396p5ol	Ac22B1oliv	Ac22B1oliv	1	2	Ac22B3oliv1	Ac22B3oliv2	Ac22B2oliv	AC53A4-A	AC53A4-B	AC53A4-C	AC53A4-D	AC53A6-B	AC53Jp1Olivine1a	AC53Jp1ol1ou	AC53Jp1oli1fine1	AC53Jp1oli1fine2	AC53Jp4oli1vinefine
Si	1.013	1.013	1.008	1.001	1.004	1.007	1.008	1.009	1.007	1.010	1.010	1.012	1.017	1.018	1.012	1.005	1.021		
Ti	0.000	0.000	0.000	0.000		0.000							0.000	0.000	0.000	0.000	0.000	0.001	
Al	0.001		0.001	0.000	0.000			0.000	0.001	0.000	0.000	0.000	0.000	0.000	0.000	0.000	0.001		
Cr	0.000		0.000	0.000				0.001	0.000	0.001	0.001	0.001	0.001	0.000	0.000	0.000	0.000		
Fe	0.160	0.159	0.203	0.203	0.201	0.199	0.201	0.180	0.185	0.179	0.188	0.184	0.212	0.215	0.213	0.214	0.213		
Mn	0.002	0.003	0.004	0.003	0.003	0.003	0.003	0.001	0.002	0.001	0.002	0.002	0.003	0.004	0.004	0.004	0.003		
Mg	1.810	1.812	1.777	1.790	1.787	1.784	1.780	1.791	1.791	1.790	1.781	1.788	1.750	1.746	1.759	1.770	1.739		
Ca	0.000	0.000	0.000	0.000	0.000	0.000	0.000	0.000	0.000	0.000	0.000	0.000	0.000	0.000	0.000	0.000	0.000		
Ni	0.007	0.008	0.008	0.008	0.007	0.008	0.008	0.009	0.008	0.008	0.008	0.007	0.000	0.006	0.007	0.006	0.005		
	2.994	2.995	2.999	3.006	3.003	3.001	3.000	2.991	2.993	2.989	2.989	2.988	2.989	2.989	2.994	3.001	2.983		
Mg/(Mg+Fe*)	0.919	0.919	0.898	0.898	0.899	0.900	0.899	0.909	0.907	0.909	0.904	0.907	0.892	0.890	0.892	0.892	0.891		
Fo	91.77	91.79	89.59	89.67	89.72	89.84	89.72	90.80	90.58	90.90	90.36	90.57	89.04	88.86	89.04	89.02	88.96		

Harzburgitos e dunitos da zona de reação

Amostra	AC52C4-A	AC52C4-A	AC52C4-C	AC52C4-D	AC52C4-E	AC52B31C	AC52B31D	AC52B34A	AC52B34B	AC52B33A	AC52B33B	AC52EOI2A
SiO ₂	41.63	41.47	42.16	41.56	41.47	41.16	41.48	40.86	41.27	40.45	41.16	40.76
TiO ₂												0.00
Al ₂ O ₃	0.00	0.00	0.00	0.00	0.00	0.00	0.02	0.00	0.00	0.00	0.04	0.03
Cr ₂ O ₃	0.00	0.00	0.00	0.00	0.00	0.01	0.00	0.00	0.00	0.00	0.04	0.00
FeO	9.66	10.00	9.73	9.85	9.89	9.15	9.50	9.15	8.98	8.96	9.15	8.96
MnO	0.07	0.15	0.16	0.14	0.10	0.08	0.13	0.10	0.17	0.11	0.12	0.10
MgO	49.05	48.71	49.31	49.29	49.32	49.03	49.49	48.92	49.29	49.31	50.03	49.91
CaO	0.00	0.02	0.01	0.01	0.00	0.00	0.01	0.01	0.01	0.01	0.00	0.04
NiO	0.36	0.39	0.47	0.43	0.37	0.27	0.34	0.31	0.35	0.36	0.40	0.35
	100.77	100.74	101.84	101.28	101.14	99.70	100.97	99.35	100.07	99.20	100.93	100.15

Cations na base de 4 oxigênios

	AC52C4-A	AC52C4-A	AC52C4-C	AC52C4-D	AC52C4-E	AC52B31C	AC52B31D	AC52B34A	AC52B34B	AC52B33A	AC52B33B	AC52EOI2A
Si	1.011	1.009	1.013	1.006	1.005	1.009	1.007	1.007	1.009	0.999	0.999	0.997
Ti												0.000
Al	0.000	0.000	0.000	0.000	0.000	0.000	0.001	0.000	0.000	0.000	0.001	0.001
Cr	0.000	0.000	0.000	0.000	0.000	0.000	0.000	0.000	0.000	0.000	0.001	0.000
Fe	0.196	0.204	0.195	0.199	0.200	0.188	0.193	0.189	0.184	0.185	0.186	0.183
Mn	0.001	0.003	0.003	0.003	0.002	0.002	0.003	0.002	0.003	0.002	0.002	0.002
Mg	1.774	1.767	1.766	1.777	1.781	1.792	1.790	1.796	1.795	1.815	1.810	1.819
Ca	0.000	0.001	0.000	0.000	0.000	0.000	0.000	0.000	0.000	0.000	0.000	0.001
Ni	0.007	0.008	0.009	0.008	0.007	0.005	0.007	0.006	0.007	0.007	0.008	0.007
	2.989	2.991	2.987	2.994	2.995	2.996	3.000	3.000	2.998	3.008	3.007	3.010
Mg/(Mg+Fe*)	0.901	0.897	0.900	0.899	0.899	0.905	0.903	0.905	0.907	0.907	0.907	0.909
Fo	89.99	89.53	89.88	89.78	89.80	90.45	90.15	90.40	90.57	90.64	90.58	90.76

OLIVINA

Harzburgitos e dunitos da zona de reação

Amostra	AC52EOI2B	AC52EOI2C	AC52EOI2D	AC52EOI1A	AC52EOI9A	AC52EOI9B	AC52EOI5A	AC52EOI5B	AC52EOI8A	AC52EOI12A	AC5204p4ol1
SiO ₂	39.81	39.96	40.77	40.64	40.22	40.46	40.29	40.44	40.51	40.49	41.41
TiO ₂	0.01	0.05	0.03	0.01	0.04	0.00	0.05	0.00	0.01	0.02	0.01
Al ₂ O ₃	0.01	0.03	0.02	0.01	0.01	0.01	0.00	0.02	0.00	0.01	0.00
Cr ₂ O ₃	0.00	0.00	0.00	0.02	0.00	0.02	0.00	0.02	0.04	0.00	0.01
FeO	8.60	8.76	8.80	8.75	9.15	9.02	9.87	9.64	9.52	9.91	8.84
MnO	0.17	0.11	0.12	0.12	0.15	0.11	0.10	0.10	0.14	0.21	0.16
MgO	50.53	50.06	49.91	50.36	50.44	50.74	49.91	49.92	49.98	49.96	48.72
CaO	0.00	0.01	0.00	0.02	0.00	0.03	0.01	0.02	0.00	0.00	0.01
NiO	0.38	0.35	0.35	0.36	0.37	0.37	0.36	0.35	0.39	0.33	0.38
	99.51	99.33	100.01	100.28	100.36	100.75	100.57	100.50	100.58	100.92	99.53

	AC52EOI2B	AC52EOI2C	AC52EOI2D	AC52EOI1A	AC52EOI9A	AC52EOI9B	AC52EOI5A	AC52EOI5B	AC52EOI8A	AC52EOI12A	AC5204p4ol1
Si	0.981	0.986	0.998	0.992	0.984	0.985	0.987	0.989	0.990	0.988	1.016
Ti	0.000	0.001	0.001	0.000	0.001	0.000	0.001	0.000	0.000	0.000	0.000
Al	0.000	0.001	0.001	0.000	0.000	0.000	0.000	0.000	0.000	0.000	0.000
Cr	0.000	0.000	0.000	0.000	0.000	0.000	0.000	0.000	0.001	0.000	0.000
Fe	0.177	0.181	0.180	0.179	0.187	0.184	0.202	0.197	0.195	0.202	0.181
Mn	0.004	0.002	0.003	0.002	0.003	0.002	0.002	0.002	0.003	0.004	0.003
Mg	1.856	1.841	1.820	1.832	1.839	1.842	1.821	1.820	1.821	1.816	1.782
Ca	0.000	0.000	0.000	0.001	0.000	0.001	0.000	0.000	0.000	0.000	0.000
Ni	0.007	0.007	0.007	0.007	0.007	0.007	0.007	0.007	0.008	0.006	0.007
	3.026	3.019	3.008	3.014	3.022	3.021	3.020	3.017	3.017	3.018	2.991
Mg/(Mg+Fe*)	0.913	0.911	0.910	0.911	0.908	0.909	0.900	0.902	0.903	0.900	0.908
Fo	91.12	90.95	90.88	91.01	90.63	90.83	89.92	90.13	90.22	89.79	90.61

OLIVINA

Harzburgitos e dunitos da zona de reação

Amostra	AC5204p4ol2	AC5204p1o	AC5204p3o	AC5204p3o	AC52165p2	AC52165p2	AC52165p2o	AC52165p3	AC52165p3	AC52165p3	AC52165p3	AC52165p4
		livine	livinefractur	livinefractur	olivine2a	olivine2bce	livine2coutra	olivine3bor	olivine3cen	olivine3cen	olivine3bor	olivine
		ada1	ada2		ntro	borda	da1	tro1	tro2	da2		
SiO ₂	41.55	41.39	41.68	41.61	41.16	41.50	41.99	41.19	41.25	41.44	41.59	41.05
TiO ₂		0.00	0.00	0.00	0.00	0.00	0.00	0.00	0.00	0.00	0.01	0.01
Al ₂ O ₃	0.00	0.01	0.02	0.01	0.01	0.00	0.00	0.01	0.00	0.01	0.00	0.02
Cr ₂ O ₃	0.00	0.00	0.01	0.02	0.00	0.01	0.01	0.02	0.00	0.00	0.00	0.00
FeO	8.82	8.38	8.84	8.62	9.45	9.39	9.28	9.62	9.58	9.62	9.48	9.58
MnO	0.16	0.16	0.16	0.12	0.15	0.15	0.14	0.16	0.15	0.13	0.15	0.17
MgO	47.84	49.42	47.68	48.47	48.62	48.46	48.56	49.17	47.88	48.46	47.57	48.26
CaO	0.01	0.02	0.03	0.02	0.00	0.00	0.01	0.00	0.00	0.01	0.01	
NiO	0.35	0.38	0.37	0.41	0.35	0.39	0.38	0.36	0.34	0.45	0.41	0.35
	98.72	99.75	98.80	99.26	99.74	99.90	100.36	100.53	99.20	100.11	99.22	99.43

Amostra	AC5204p4ol2	AC5204p1o	AC5204p3o	AC5204p3o	AC52165p2	AC52165p2	AC52165p2o	AC52165p3	AC52165p3	AC52165p3	AC52165p3	AC52165p4
		livine	livinefractur	livinefractur	olivine2a	olivine2bce	livine2coutra	olivine3bor	olivine3cen	olivine3cen	olivine3bor	olivine
		ada1	ada2		ntro	borda	da1	tro1	tro2	da2		
Si	1.027	1.012	1.029	1.022	1.011	1.017	1.023	1.005	1.019	1.015	1.026	1.012
Ti	0.000	0.000	0.000	0.000	0.000	0.000	0.000	0.000	0.000	0.000	0.000	0.000
Al	0.000	0.000	0.001	0.000	0.000	0.000	0.000	0.000	0.000	0.000	0.000	0.001
Cr	0.000	0.000	0.000	0.000	0.000	0.000	0.000	0.000	0.000	0.000	0.000	0.000
Fe	0.182	0.171	0.183	0.177	0.194	0.192	0.189	0.196	0.198	0.197	0.196	0.197
Mn	0.003	0.003	0.003	0.002	0.003	0.003	0.003	0.003	0.003	0.003	0.003	0.004
Mg	1.761	1.801	1.754	1.774	1.780	1.770	1.762	1.788	1.762	1.769	1.749	1.773
Ca	0.000	0.001	0.001	0.000	0.000	0.000	0.000	0.000	0.000	0.000	0.000	0.000
Ni	0.007	0.007	0.007	0.008	0.007	0.008	0.007	0.007	0.007	0.009	0.008	0.007
	2.980	2.995	2.978	2.985	2.996	2.991	2.985	3.001	2.988	2.993	2.982	2.994
Mg/(Mg+Fe*)	0.906	0.913	0.906	0.909	0.902	0.902	0.903	0.901	0.899	0.900	0.899	0.900
Fo	90.47	91.15	90.42	90.81	90.02	90.05	90.18	89.95	89.76	89.86	89.79	89.82

OLIVINA

Harzburgitos e dunitos da zona de reação

Amostra	AC52502p2	AC52502p2	AC52502p3	AC52502p3	AC52502p3o		AC521925p	AC521925p	AC521925p	AC521925p	AC521925p	AC521925p	AC522654p
	olivine1a	olivine1b	olivine1a	olivine2a	livine2bmes	mograo	1olivine	3oliv1a	3oliv1b	3oliv1c	4oliv1a	4oliv1b	2olivine1
SiO ₂	41.11	41.23	41.50	41.17	41.02	41.21	41.36	41.38	41.08	41.21	41.30	41.15	
TiO ₂	0.00	0.00	0.00	0.00	0.02	0.00	0.00	0.01	0.02	0.00	0.02	0.01	
Al ₂ O ₃	0.00	0.00	0.02	0.00	0.01	0.00	0.01	0.02	0.00	0.00	0.00	0.01	
Cr ₂ O ₃	0.00	0.00	0.02	0.00	0.00	0.00	0.00	0.01	0.00	0.02	0.02	0.00	
FeO	8.92	8.81	8.90	9.04	9.03	9.58	9.48	9.51	9.52	9.60	9.51	9.27	
MnO	0.14	0.12	0.14	0.13	0.13	0.16	0.16	0.14	0.13	0.16	0.14	0.15	
MgO	48.95	49.03	49.17	48.99	49.26	48.43	48.27	48.53	48.82	48.52	48.64	48.46	
CaO	0.01		0.02	0.01	0.01		0.01	0.00			0.01	0.01	
NiO	0.36	0.35	0.36	0.36	0.34	0.41	0.37	0.38	0.37	0.39	0.37	0.39	
	99.50	99.54	100.12	99.71	99.81	99.78	99.66	99.97	99.93	99.90	100.00	99.45	

	AC52502p2	AC52502p2	AC52502p3	AC52502p3	AC52502p3o		AC521925p	AC521925p	AC521925p	AC521925p	AC521925p	AC521925p	AC522654p
	olivine1a	olivine1b	olivine1a	olivine2a	livine2bmes	mograo	1olivine	3oliv1a	3oliv1b	3oliv1c	4oliv1a	4oliv1b	2olivine1
Si	1.010	1.012	1.013	1.010	1.006	1.013	1.017	1.014	1.008	1.012	1.012	1.013	
Ti	0.000	0.000	0.000	0.000	0.000	0.000	0.000	0.000	0.000	0.000	0.000	0.000	
Al	0.000	0.000	0.001	0.000	0.000	0.000	0.000	0.001	0.000	0.000	0.000	0.000	
Cr	0.000	0.000	0.000	0.000	0.000	0.000	0.000	0.000	0.000	0.000	0.000	0.000	
Fe	0.183	0.181	0.182	0.185	0.185	0.197	0.195	0.195	0.195	0.197	0.195	0.191	
Mn	0.003	0.003	0.003	0.003	0.003	0.003	0.003	0.003	0.003	0.003	0.003	0.003	
Mg	1.793	1.793	1.788	1.791	1.800	1.774	1.768	1.772	1.785	1.775	1.776	1.778	
Ca	0.000	0.000	0.000	0.000	0.000	0.000	0.000	0.000	0.000	0.000	0.000	0.000	
Ni	0.007	0.007	0.007	0.007	0.007	0.008	0.007	0.007	0.007	0.008	0.007	0.008	
	2.997	2.995	2.994	2.997	3.001	2.995	2.991	2.993	2.999	2.996	2.994	2.994	
Mg/(Mg+Fe*)	0.907	0.908	0.908	0.906	0.907	0.900	0.901	0.901	0.901	0.900	0.901	0.903	
Fo	90.59	90.73	90.65	90.49	90.56	89.86	89.92	89.96	90.01	89.85	89.98	90.16	

OLIVINA

Harzburgitos e dunitos da zona de reação

Amostra	AC522654p 2olivine2ho mogenea	AC522654p 6olivine1	AC522654p 6olivine2	AC522654p5	AC522654p 3olivine	AC522654p 3olivine2
SiO ₂	42.09	41.21	41.56	41.29	41.21	41.44
TiO ₂	0.01	0.00	0.00	0.01	0.00	0.01
Al ₂ O ₃	0.00	0.00	0.00	0.00	0.00	0.00
Cr ₂ O ₃	0.02	0.00	0.00	0.00	0.00	0.00
FeO	8.96	9.34	9.43	9.23	9.41	9.35
MnO	0.14	0.18	0.15	0.14	0.17	0.14
MgO	48.72	48.18	48.44	48.90	48.62	48.22
CaO		0.00	0.00	0.01	0.00	
NiO	0.38	0.33	0.36	0.28	0.36	0.32
	100.32	99.25	99.93	99.86	99.77	99.47

	AC522654p 2olivine2ho mogenea	AC522654p 6olivine1	AC522654p 6olivine2	AC522654p5	AC522654p 3olivine	AC522654p 3olivine2
Si	1.024	1.016	1.018	1.011	1.012	1.019
Ti	0.000	0.000	0.000	0.000	0.000	0.000
Al	0.000	0.000	0.000	0.000	0.000	0.000
Cr	0.000	0.000	0.000	0.000	0.000	0.000
Fe	0.182	0.193	0.193	0.189	0.193	0.192
Mn	0.003	0.004	0.003	0.003	0.004	0.003
Mg	1.766	1.771	1.768	1.785	1.779	1.767
Ca	0.000	0.000	0.000	0.000	0.000	0.000
Ni	0.007	0.006	0.007	0.006	0.007	0.006
	2.983	2.990	2.989	2.994	2.995	2.987
Mg/(Mg+Fe*)	0.906	0.902	0.902	0.904	0.902	0.902
Fo	90.50	90.01	90.01	90.28	90.04	90.06

Amostra	Wehrlito													
	P22OI465A	P22OI466B	P22OI467C	P22OI468D	P22OI469E	P22OI Dark Core470	P22OI Dark Core471	P22OI Dark Core472	P22OI Core Rim473	P22OI Core Rim474	P22OI Core Rim475	P22OI Core Rim476	P22OI Core Rim477	P22OI Core Rim478
SiO ₂	40.23	40.26	40.65	40.58	40.08	40.43	40.53	40.42	40.39	40.74	40.34	40.45	40.72	40.38
TiO ₂	0.00	0.00	0.00	0.00	0.00	0.00	0.00	0.01	0.01	0.00	0.02	0.00	0.00	0.01
Al ₂ O ₃	0.04	0.06	0.05	0.05	0.04	0.04	0.01	0.05	0.05	0.04	0.05	0.03	0.02	0.03
Cr ₂ O ₃	0.00	0.00	0.00	0.00	0.02	0.00	0.02	0.00	0.00	0.00	0.00	0.00	0.00	0.04
FeO	12.15	12.37	12.07	12.34	15.71	12.16	12.09	12.20	12.15	12.11	12.18	12.17	12.19	12.58
MnO	0.19	0.21	0.14	0.17	0.26	0.16	0.18	0.26	0.15	0.23	0.18	0.23	0.17	0.21
MgO	46.14	46.28	46.07	46.15	43.51	45.95	45.85	45.74	45.98	46.30	46.14	46.07	46.47	45.94
CaO	0.00	0.00	0.00	0.00	0.00	0.00	0.00	0.00	0.00	0.00	0.00	0.00	0.00	0.00
NiO	98.75	99.17	98.98	99.29	99.62	98.74	98.68	98.69	98.74	99.42	98.91	98.95	99.58	99.20

Cations na base de 4 oxigênios														
	P22OI465A	P22OI466B	P22OI467C	P22OI468D	P22OI469E	P22OI Dark Core470	P22OI Dark Core471	P22OI Dark Core472	P22OI Core Rim473	P22OI Core Rim474	P22OI Core Rim475	P22OI Core Rim476	P22OI Core Rim477	P22OI Core Rim478
Si	1.008	1.006	1.015	1.011	1.012	1.013	1.015	1.014	1.012	1.013	1.009	1.011	1.011	1.009
Ti	0.000	0.000	0.000	0.000	0.000	0.000	0.000	0.000	0.000	0.000	0.000	0.000	0.000	0.000
Al	0.001	0.002	0.001	0.001	0.001	0.001	0.000	0.001	0.002	0.001	0.001	0.001	0.001	0.001
Cr	0.000	0.000	0.000	0.000	0.000	0.000	0.000	0.000	0.000	0.000	0.000	0.000	0.000	0.001
Fe	0.255	0.258	0.252	0.257	0.332	0.255	0.253	0.256	0.255	0.252	0.255	0.254	0.253	0.263
Mn	0.004	0.004	0.003	0.004	0.006	0.003	0.004	0.006	0.003	0.005	0.004	0.005	0.004	0.005
Mg	1.723	1.723	1.713	1.714	1.637	1.715	1.711	1.709	1.716	1.716	1.720	1.716	1.719	1.711
Ca	0.000	0.000	0.000	0.000	0.000	0.000	0.000	0.000	0.000	0.000	0.000	0.000	0.000	0.000
Ni	0.000	0.000	0.000	0.000	0.000	0.000	0.000	0.000	0.000	0.000	0.000	0.000	0.000	0.000
	2.991	2.993	2.985	2.988	2.987	2.987	2.984	2.986	2.987	2.986	2.990	2.988	2.988	2.990
Mg/(Mg+Fe*)	0.871	0.870	0.872	0.869	0.832	0.871	0.871	0.870	0.871	0.872	0.871	0.871	0.872	0.867
Fo	86.95	86.76	87.05	86.79	82.92	86.92	86.95	86.73	86.94	86.99	86.93	86.87	87.00	86.48

Amostra	Wehrliito																
	P22OICore Rim479	P22OICore Rim480	P22OICore Rim481	P22OICore Rim482	P22OICore Rim483	P22OIRim4 84	P22OIRim4 85	P22OIRim4 86	TestOnOI5 16	P23Zoned OI528	P23Zoned OI529	P23Zoned OI530	P23Zoned OI531	P23Zoned OI532	P21120p4Si l2a		
SiO ₂	39.77	39.69	39.37	39.41	39.19	39.68	39.98	40.01	40.07	40.35	40.43	40.21	40.21	40.04	40.76		
TiO ₂	0.00	0.03	0.00	0.00	0.00	0.00	0.00	0.00	0.00	0.00	0.03	0.00	0.01	0.03	0.01		
Al ₂ O ₃	0.05	0.04	0.05	0.04	0.03	0.06	0.08	0.07	0.04	0.03	0.06	0.05	0.02	0.03	0.01		
Cr ₂ O ₃	0.02	0.01	0.00	0.00	0.00	0.00	0.00	0.00	0.04	0.00	0.00	0.03	0.00	0.00	0.00		
FeO	14.46	16.25	16.44	16.06	16.44	16.66	16.91	17.07	12.23	12.13	12.42	12.06	12.23	13.40	13.16		
MnO	0.28	0.30	0.31	0.35	0.34	0.37	0.29	0.36	0.18	0.14	0.22	0.14	0.17	0.24	0.21		
MgO	44.62	43.01	43.01	43.32	43.41	42.19	42.01	41.60	47.00	46.48	46.59	46.61	46.22	44.90	45.48		
CaO	0.00	0.00	0.00	0.00	0.00	0.03	0.01	0.01	0.00	0.00	0.00	0.00	0.00	0.02	0.01		
NiO															0.25		
	99.20	99.32	99.18	99.18	99.41	99.00	99.29	99.12	99.56	99.13	99.76	99.10	98.86	98.67	99.87		
P22OICore Rim479 P22OICore Rim480 P22OICore Rim481 P22OICore Rim482 P22OICore Rim483 P22OIRim4 84 P22OIRim4 85 P22OIRim4 86 TestOnOI5 16 P23Zoned OI528 P23Zoned OI529 P23Zoned OI530 P23Zoned OI531 P23Zoned OI532 P21120p4Si l2a																	
Si	1.004	1.008	1.003	1.003	0.997	1.013	1.018	1.021	0.997	1.007	1.004	1.004	1.007	1.010	1.016		
Ti	0.000	0.001	0.000	0.000	0.000	0.000	0.000	0.000	0.000	0.000	0.001	0.000	0.000	0.000	0.000		
Al	0.002	0.001	0.001	0.001	0.001	0.002	0.002	0.002	0.001	0.001	0.002	0.002	0.001	0.001	0.000		
Cr	0.000	0.000	0.000	0.000	0.000	0.000	0.000	0.000	0.001	0.000	0.000	0.001	0.000	0.000	0.000		
Fe	0.305	0.345	0.350	0.342	0.350	0.356	0.360	0.364	0.255	0.253	0.258	0.252	0.256	0.283	0.274		
Mn	0.006	0.006	0.007	0.007	0.007	0.008	0.006	0.008	0.004	0.003	0.005	0.003	0.004	0.005	0.004		
Mg	1.678	1.629	1.634	1.643	1.647	1.606	1.594	1.582	1.744	1.728	1.725	1.734	1.725	1.688	1.689		
Ca	0.000	0.000	0.000	0.000	0.000	0.001	0.000	0.000	0.000	0.000	0.000	0.000	0.000	0.001	0.000		
Ni	0.000	0.000	0.000	0.000	0.000	0.000	0.000	0.000	0.000	0.000	0.000	0.000	0.000	0.000	0.005		
	2.995	2.990	2.996	2.996	3.002	2.986	2.981	2.978	3.002	2.993	2.994	2.995	2.993	2.989	2.989		
Mg/(Mg+Fe*)	0.846	0.825	0.823	0.828	0.825	0.819	0.816	0.813	0.873	0.872	0.870	0.873	0.871	0.857	0.860		
Fo	84.35	82.24	82.06	82.47	82.17	81.52	81.31	80.96	87.09	87.10	86.78	87.19	86.91	85.43	85.84		

OLIVINA

Peridotitos metamorfizados

Amostra	AC19B3-B	AC19B3-C	AC19B3-F	AC19B3-G	AC19B5-A	AC19B5-B	AC35A5-D	AC35A4-C	AC35A4-D	AC59bp5ol	AC59bp6ol
SiO ₂	41.88	42.31	41.88	42.17	42.73	42.23	42.41	42.49	42.16	41.91	41.51
TiO ₂	0.02									0.02	0.02
Al ₂ O ₃	0.02	0.01	0.01	0.01	0.01	0.02	0.00	0.00	0.00		0.00
Cr ₂ O ₃	0.02	0.00	0.00	0.00	0.02	0.01	0.06	0.03	0.00	0.01	0.00
FeO	7.12	5.94	6.28	6.72	5.80	6.74	6.26	6.18	6.26	7.44	7.38
MnO	0.22	0.09	0.12	0.19	0.14	0.16	0.14	0.08	0.05	0.22	0.24
MgO	50.53	52.24	51.54	51.26	52.33	51.11	51.89	51.86	51.79	50.23	51.30
CaO	0.04	0.02	0.04	0.00	0.01	0.01	0.04	0.01	0.00	0.01	0.00
NiO		0.35	0.35	0.48	0.31	0.26	0.40	0.32	0.31	0.41	0.37
	99.84	100.96	100.21	100.84	101.34	100.53	101.20	100.97	100.57	100.26	100.82

Cations na base de 4 oxigênios

Amostra	AC19B3-B	AC19B3-C	AC19B3-F	AC19B3-G	AC19B5-A	AC19B5-B	AC35A5-D	AC35A4-C	AC35A4-D	AC59bp5ol	AC59bp6ol
Si	1.013	1.008	1.008	1.011	1.013	1.014	1.010	1.013	1.010	1.015	1.001
Ti	0.000									0.000	0.000
Al	0.000	0.000	0.000	0.000	0.000	0.001	0.000	0.000	0.000	0.000	0.000
Cr	0.000	0.000	0.000	0.000	0.000	0.000	0.001	0.001	0.000	0.000	0.000
Fe	0.144	0.118	0.126	0.135	0.115	0.135	0.125	0.123	0.125	0.151	0.149
Mn	0.004	0.002	0.003	0.004	0.003	0.003	0.003	0.002	0.001	0.004	0.005
Mg	1.822	1.855	1.848	1.831	1.849	1.828	1.842	1.842	1.848	1.813	1.844
Ca	0.001	0.001	0.001	0.000	0.000	0.000	0.001	0.000	0.000	0.000	0.000
Ni	0.000	0.007	0.007	0.009	0.006	0.005	0.008	0.006	0.006	0.008	0.007
	2.986	2.992	2.992	2.989	2.986	2.986	2.989	2.987	2.990	2.992	3.006
Mg/(Mg+Fe*)	0.927	0.940	0.936	0.932	0.941	0.931	0.937	0.937	0.936	0.923	0.925
Fo	92.46	93.92	93.49	92.97	94.02	92.95	93.52	93.66	93.60	92.11	92.30

Peridotitos hospedeiros de cromititos

Amostra	Patio Bonito						El Chagualo							
	AC20A1-C	AC20A1-E	AC20A2-A	AC20A3-G	AC20A5-A	AC20A5-B	AC77BOl4A	AC77BOl4B	AC77BOl5A	AC77BOl5B	AC77BOl5C	AC77BOl5D	AC77BOl5E	AC77BOl1cA
SiO ₂	41.65	42.02	42.09	41.75	41.48	41.35	40.29	40.49	40.62	40.74	40.50	40.62	40.56	40.56
TiO ₂							0.01	0.00	0.00	0.00	0.01	0.02	0.00	0.12
Al ₂ O ₃	0.00	0.01	0.01	0.00	0.01	0.00	0.02	0.00	0.00	0.01	0.01	0.00	0.02	0.00
Cr ₂ O ₃	0.00	0.03	0.02	0.00	0.00	0.00	0.00	0.02	0.00	0.04	0.00	0.00	0.00	0.01
FeO	9.19	9.65	9.52	9.48	9.29	9.42	8.74	8.97	8.91	8.42	9.44	8.98	8.45	8.92
MnO	0.12	0.24	0.15	0.18	0.17	0.14	0.11	0.14	0.08	0.14	0.12	0.09	0.14	0.10
MgO	48.77	49.60	49.16	48.98	49.19	49.22	48.99	48.89	50.00	49.70	49.51	49.57	49.26	49.90
CaO	0.02	0.01	0.05	0.00	0.00	0.02	0.00	0.03	0.00	0.01	0.00	0.01	0.01	0.00
NiO	0.48	0.42	0.34	0.43	0.43	0.44	0.36	0.36	0.41	0.40	0.40	0.38	0.40	0.40
	100.22	101.96	101.34	100.82	100.56	100.57	98.51	98.90	100.02	99.45	99.98	99.66	98.84	100.00
<hr/>														
Cations na base de 4 oxigênios														
AC20A1-C	AC20A1-E	AC20A2-A	AC20A3-G	AC20A5-A	AC20A5-B	AC77BOl4A	AC77BOl4B	AC77BOl5A	AC77BOl5B	AC77BOl5C	AC77BOl5D	AC77BOl5E	AC77BOl1cA	
Si	1.015	1.009	1.015	1.013	1.008	1.006	1.001	1.003	0.995	1.001	0.995	0.999	1.003	0.994
Ti	0.000	0.000	0.000	0.000	0.000	0.000	0.000	0.000	0.000	0.000	0.000	0.000	0.000	0.002
Al	0.000	0.000	0.000	0.000	0.000	0.000	0.001	0.000	0.000	0.000	0.000	0.000	0.000	0.000
Cr	0.000	0.001	0.000	0.000	0.000	0.000	0.000	0.000	0.000	0.001	0.000	0.000	0.000	0.000
Fe	0.187	0.194	0.192	0.192	0.189	0.192	0.181	0.186	0.183	0.173	0.194	0.185	0.175	0.183
Mn	0.002	0.005	0.003	0.004	0.004	0.003	0.002	0.003	0.002	0.003	0.002	0.002	0.003	0.002
Mg	1.771	1.775	1.766	1.770	1.782	1.784	1.814	1.804	1.825	1.820	1.813	1.816	1.815	1.822
Ca	0.000	0.000	0.001	0.000	0.000	0.000	0.000	0.001	0.000	0.000	0.000	0.000	0.000	0.000
Ni	0.009	0.008	0.007	0.008	0.008	0.009	0.007	0.007	0.008	0.008	0.008	0.008	0.008	0.008
	2.985	2.991	2.985	2.987	2.991	2.994	3.006	3.004	3.013	3.006	3.013	3.009	3.005	3.012
Mg/(Mg+Fe*)	0.904	0.902	0.902	0.902	0.904	0.903	0.909	0.907	0.909	0.913	0.903	0.908	0.912	0.909
Fo	90.33	89.94	90.05	90.03	90.25	90.17	90.80	90.53	90.83	91.19	90.23	90.69	91.08	90.79

OLIVINA

Peridotitos hospedeiros de cromititos

Amostra	El Carmelo						Don Jesus				
	AC80B2OI1cA	AC80B2OI3A	AC80B2OI2A	AC80B2OI1CB	AC80B2OI1CC	AC80B2OI2B	AC78BOI1A	AC78BOI1B	AC78BOI1C	AC78BOI4A	AC78BOI4B
SiO ₂	40.58	40.52	40.80	39.80	40.77	40.80	40.85	40.76	40.76	40.22	40.56
TiO ₂	0.00	0.00	0.03	0.02	0.00	0.06	0.01	0.00	0.00	0.00	0.04
Al ₂ O ₃	0.01	0.00	0.01	0.00	0.02	0.00	0.01	0.00	0.00	0.01	0.02
Cr ₂ O ₃	0.00	0.00	0.02	0.00	0.00	0.03	0.00	0.00	0.06	0.01	0.02
FeO	8.46	8.75	8.49	8.69	8.18	8.35	9.40	8.78	9.69	9.13	9.26
MnO	0.17	0.11	0.13	0.11	0.12	0.11	0.14	0.13	0.15	0.12	0.12
MgO	50.37	50.35	50.54	51.22	49.91	50.69	49.34	49.47	49.74	49.47	49.74
CaO	0.03	0.03	0.00	0.03	0.01	0.01	0.02	0.01	0.00	0.00	0.02
NiO	0.39	0.37	0.37	0.42	0.39	0.40	0.18	0.22	0.20	0.25	0.22
	100.01	100.12	100.40	100.28	99.38	100.45	99.95	99.37	100.59	99.19	99.99
Si	0.993	0.991	0.994	0.975	1.001	0.993	1.001	1.002	0.995	0.994	0.994
Ti	0.000	0.000	0.001	0.000	0.000	0.001	0.000	0.000	0.000	0.000	0.001
Al	0.000	0.000	0.000	0.000	0.000	0.000	0.000	0.000	0.000	0.000	0.000
Cr	0.000	0.000	0.000	0.000	0.000	0.001	0.000	0.000	0.001	0.000	0.000
Fe	0.173	0.179	0.173	0.178	0.168	0.170	0.193	0.180	0.198	0.189	0.190
Mn	0.004	0.002	0.003	0.002	0.002	0.002	0.003	0.003	0.003	0.002	0.002
Mg	1.837	1.836	1.835	1.869	1.826	1.838	1.801	1.812	1.809	1.821	1.817
Ca	0.001	0.001	0.000	0.001	0.000	0.000	0.000	0.000	0.000	0.000	0.000
Ni	0.008	0.007	0.007	0.008	0.008	0.008	0.004	0.004	0.004	0.005	0.004
	3.015	3.016	3.013	3.033	3.006	3.013	3.002	3.002	3.009	3.011	3.009
Mg/(Mg+Fe*)	0.914	0.911	0.914	0.913	0.916	0.915	0.903	0.909	0.901	0.906	0.905
Fo	91.23	91.02	91.26	91.20	91.46	91.43	90.20	90.82	90.01	90.51	90.43

OLIVINA

Cromititos

Amostra	El Chagualo nodular										El Chagualo em rede						Inclusão AC20M3ISa
	AC77AOI1A	AC77AOI1B	AC77AO11C	AC77A012A	AC77A012B	AC77A012C	AC77A013A	AC77A013B	AC77A013C	AC77COI2A	AC77COI2B	AC77COI2C	AC77COI4A	AC77COI4B	AC77COI6A		
SiO ₂	41.28	41.68	41.53	41.61	41.67	41.62	41.96	41.61	41.78	40.86	41.17	41.49	41.67	41.71	41.16	40.31	
TiO ₂	0.00	0.01	0.00	0.02	0.00	0.09	0.00	0.00	0.05	0.00	0.04	0.00	0.00	0.05	0.00	0.01	
Al ₂ O ₃	0.01	0.00	0.01	0.02	0.00	0.00	0.01	0.00	0.00	0.01	0.01	0.02	0.04	0.02	0.00	0.25	
Cr ₂ O ₃	0.04	0.00	0.01	0.05	0.00	0.03	0.00	0.00	0.02	0.00	0.00	0.00	0.04	0.01	0.05	0.94	
FeO	4.88	4.75	5.05	4.69	4.64	4.89	4.56	4.84	4.78	5.48	5.94	5.77	5.53	5.90	5.87	2.67	
MnO	0.07	0.07	0.06	0.06	0.09	0.07	0.08	0.09	0.06	0.06	0.10	0.05	0.10	0.10	0.09	0.05	
MgO	53.22	53.46	53.16	53.69	53.67	53.70	52.57	53.01	53.18	53.48	52.75	52.12	52.81	52.07	52.55	55.19	
CaO	0.00	0.00	0.01	0.03	0.02	0.00	0.00	0.00	0.00	0.01	0.00	0.00	0.00	0.02	0.00	0.01	
NiO	0.36	0.40	0.40	0.35	0.37	0.42	0.36	0.38	0.36	0.40	0.46	0.44	0.44	0.42	0.47	0.91	
Total	99.85	100.37	100.23	100.51	100.46	100.82	99.54	99.93	100.23	100.30	100.46	99.89	100.62	100.29	100.18	100.33	
Cations na base de 4 oxigênios																	
AC77AOI1A	AC77AOI1B	AC77AO11C	AC77A012A	AC77A012B	AC77A012C	AC77A013A	AC77A013B	AC77A013C	AC77COI2A	AC77COI2B	AC77COI2C	AC77COI4A	AC77COI4B	AC77COI6A	AC20M3ISa		
Si	0.994	0.998	0.997	0.994	0.996	0.993	1.010	1.000	1.001	0.984	0.992	1.003	0.999	1.004	0.994	0.967	
Ti	0.000	0.000	0.000	0.000	0.000	0.002	0.000	0.000	0.001	0.000	0.001	0.000	0.000	0.001	0.000	0.000	
Al	0.000	0.000	0.000	0.001	0.000	0.000	0.000	0.000	0.000	0.000	0.000	0.000	0.001	0.000	0.000	0.007	
Cr	0.001	0.000	0.000	0.001	0.000	0.001	0.000	0.000	0.000	0.000	0.000	0.000	0.001	0.000	0.001	0.018	
Fe	0.098	0.095	0.101	0.094	0.093	0.098	0.092	0.097	0.096	0.110	0.120	0.117	0.111	0.119	0.118	0.054	
Mn	0.001	0.001	0.001	0.001	0.002	0.001	0.002	0.002	0.001	0.001	0.002	0.001	0.002	0.002	0.001	0.001	
Mg	1.910	1.907	1.902	1.912	1.912	1.910	1.886	1.900	1.899	1.919	1.893	1.877	1.887	1.868	1.891	1.973	
Ca	0.000	0.000	0.000	0.001	0.001	0.000	0.000	0.000	0.000	0.000	0.000	0.000	0.001	0.000	0.000	0.000	
Ni	0.007	0.008	0.008	0.007	0.007	0.008	0.007	0.007	0.007	0.008	0.009	0.009	0.008	0.008	0.009	0.018	
	3.012	3.010	3.011	3.011	3.013	2.997	3.007	3.005	3.023	3.016	3.006	3.009	3.003	3.015	3.038		
Mg/(Mg+Fe)	0.951	0.952	0.949	0.953	0.954	0.951	0.954	0.951	0.952	0.946	0.941	0.942	0.944	0.940	0.941	0.974	
Fo	95.04	95.18	94.88	95.28	95.29	95.07	95.28	95.03	95.14	94.50	93.97	94.11	94.35	93.92	94.02	97.31	

GRANADA

Granada anfibolito

	AC445-A	AC445-B	AC445-B	AC445-D	AC445-E	AC445-F	AC442-A	AC442-B	AC442-C	AC442-D	AC442-E	AC442-F
SiO ₂	38.13	37.48	37.71	37.93	36.84	37.94	38.26	37.92	37.95	38.17	38.62	38.10
TiO ₂	0.14	0.77	0.13	0.07	0.15	0.16	0.13	0.14	0.08	0.13	0.08	0.15
Al ₂ O ₃	21.25	21.11	20.93	21.08	20.76	21.20	21.45	21.33	21.11	21.32	21.73	21.18
Cr ₂ O ₃	0.00	0.01	0.00	0.02	0.00	0.00	0.04	0.00	0.04	0.06	0.00	0.03
Fe ₂ O ₃	0.00	0.00	0.31	0.22	0.24	0.00	0.00	0.00	0.03	0.00	0.00	0.00
FeO	27.55	26.17	27.14	27.78	26.61	26.70	28.70	28.29	27.27	28.14	28.69	28.04
MnO	3.67	5.25	3.91	3.70	5.37	4.11	1.05	2.88	3.79	1.65	2.51	3.05
MgO	1.69	1.48	1.65	1.77	1.42	1.61	2.34	2.01	1.86	2.24	2.62	2.15
CaO	8.10	8.04	8.25	7.73	7.98	8.52	8.27	7.16	7.67	8.57	6.57	7.34
Total	100.54	100.31	100.03	100.30	99.37	100.24	100.25	99.72	99.79	100.27	100.82	100.04

Cations na base de 12 oxigênios

Si	3.022	2.987	3.011	3.019	2.980	3.017	3.022	3.023	3.028	3.019	3.032	3.028
Al _{IV}	0.000	0.013	0.000	0.000	0.020	0.000	0.000	0.000	0.000	0.000	0.000	0.000
Sum Z	3.022	3.000	3.011	3.019	3.000	3.017	3.022	3.023	3.028	3.019	3.032	3.028
Al _{VI}	1.985	1.969	1.970	1.977	1.959	1.987	1.997	2.004	1.985	1.987	2.011	1.984
Cr	0.000	0.001	0.000	0.001	0.000	0.000	0.002	0.000	0.002	0.004	0.000	0.002
Fe ³⁺	0.000	0.000	0.019	0.013	0.015	0.000	0.000	0.000	0.002	0.000	0.000	0.000
Ti	0.009	0.046	0.008	0.004	0.009	0.009	0.007	0.008	0.005	0.008	0.005	0.009
Sum Y	1.994	2.016	1.997	1.995	1.983	1.996	2.007	2.012	1.993	1.998	2.016	1.994
Mg	0.200	0.175	0.197	0.210	0.172	0.190	0.276	0.239	0.221	0.264	0.307	0.254
Fe ²⁺	1.826	1.744	1.812	1.849	1.800	1.775	1.896	1.886	1.820	1.861	1.884	1.864
Mn	0.246	0.354	0.264	0.250	0.368	0.277	0.070	0.195	0.256	0.111	0.167	0.205
Ca	0.688	0.686	0.706	0.659	0.691	0.726	0.700	0.612	0.656	0.726	0.552	0.625
Sum X	2.960	2.959	2.979	2.967	3.030	2.968	2.942	2.931	2.952	2.961	2.910	2.948

Xalm	61.7	58.9	60.8	62.3	59.4	59.8	64.4	64.4	61.6	62.8	64.7	63.2
Xpy	6.8	5.9	6.6	7.1	5.7	6.4	9.4	8.1	7.5	8.9	10.5	8.6
Xsp	8.3	12.0	8.9	8.4	12.1	9.3	2.4	6.6	8.7	3.7	5.7	7.0
Xuv	0.0	0.0	0.0	0.1	0.0	0.0	0.1	0.0	0.1	0.2	0.0	0.1
Xand	0.0	0.0	0.9	0.7	0.7	0.0	0.0	0.0	0.1	0.0	0.0	0.0
gro+and+uv	23.2	23.2	23.7	22.2	22.8	24.4	23.8	20.9	22.2	24.5	19.0	21.2
Xgro	23.2	23.2	22.8	21.5	22.1	24.4	23.7	20.9	22.0	24.3	19.0	21.1
	100.0	100.0	100.0	100.0	100.0	100.0	100.0	100.0	100.0	100.0	100.0	100.0

PIROXÊNIO

Rochas ultramáficas											Máfica
	Harzburgito			Wehrlito							Metagabro
Amostra	JJ1396p3	JJ1396p3px2	JJ1396p4px	P21120p2	P21120p31	P21120p32	P21120p33	P21120p3ra	P21120p41a	P21120p41b	CMK38BAC
SiO ₂	55.66	57.64	55.71	52.05	52.87	52.55	52.87	52.97	52.33	52.03	55.42
TiO ₂	0.04	0.07	0.07	0.82	0.67	0.66	0.90	0.79	1.05	1.07	0.07
Al ₂ O ₃	2.85	2.80	3.23	3.66	2.92	3.09	3.69	3.56	4.08	4.03	8.91
Cr ₂ O ₃	0.73	0.62	0.80	0.72	0.58	0.73	0.74	0.75	0.90	0.93	0.00
Fe ₂ O ₃	0.00	0.00	0.20	0.45	0.00	0.00	0.00	0.00	0.00	0.00	0.00
FeO	5.21	5.18	4.90	2.40	2.70	2.67	2.68	2.39	2.87	2.76	7.37
MnO	0.15	0.13	0.10	0.09	0.09	0.12	0.11	0.09	0.12	0.09	0.21
NiO	0.09	0.08	0.13	0.03	0.04	0.01	0.03	0.01	0.02	0.00	0.03
MgO	33.93	33.46	34.06	15.72	15.94	16.09	15.80	15.71	15.44	15.24	12.81
CaO	0.38	0.33	0.51	23.03	23.09	22.67	22.91	23.34	22.18	22.65	9.33
Na ₂ O	0.04	0.01	0.03	0.63	0.56	0.58	0.64	0.67	0.59	0.70	4.90
K ₂ O	0.00	0.01	0.01	0.00	0.00	0.00	0.00	0.00	0.00	0.01	0.07
Total	99.09	100.33	99.74	99.60	99.45	99.17	100.36	100.28	99.57	99.50	99.12
Cations na base de 6 oxigênios											
	JJ1396p3	JJ1396p3px2	JJ1396p4px	P21120p2	P21120p31	P21120p32	P21120p33	P21120p3ra	P21120p41a	P21120p41b	CMK38BAC
Si	1.932	1.983	1.920	1.904	1.936	1.928	1.920	1.923	1.919	1.908	1.996
AlIV	0.068	0.017	0.080	0.096	0.064	0.072	0.080	0.077	0.081	0.092	0.004
Sum T	2.000	2.000	2.000	2.000	2.000	2.000	2.000	2.000	2.000	2.000	2.000
AlVI	0.049	0.097	0.052	0.062	0.062	0.062	0.078	0.076	0.095	0.083	0.375
Ti	0.001	0.002	0.002	0.023	0.019	0.018	0.024	0.022	0.029	0.029	0.002
Cr	0.020	0.017	0.022	0.021	0.017	0.021	0.021	0.021	0.026	0.027	0.000
Fe ³⁺	0.000	0.000	0.005	0.012	0.000	0.000	0.000	0.000	0.000	0.000	0.000
Mg	1.755	1.716	1.751	0.857	0.870	0.880	0.855	0.850	0.844	0.833	0.688
Ni	0.003	0.002	0.004	0.001	0.001	0.000	0.001	0.000	0.001	0.000	0.001
Fe ²⁺	0.151	0.149	0.141	0.073	0.083	0.082	0.081	0.073	0.088	0.085	0.222
Mn	0.004	0.004	0.003	0.003	0.003	0.004	0.003	0.003	0.004	0.003	0.006
Ca	0.014	0.012	0.019	0.903	0.906	0.891	0.891	0.908	0.871	0.890	0.360
Na	0.002	0.001	0.002	0.045	0.040	0.041	0.045	0.047	0.042	0.050	0.343
K	0.000	0.000	0.000	0.000	0.000	0.000	0.000	0.000	0.000	0.000	0.003
Sum M	2.000	2.000	2.000	2.000	2.000	2.000	2.000	2.000	2.000	2.000	2.000
Total	4.000	4.000	4.000	4.000	4.000	4.000	4.000	4.000	4.000	4.000	4.000
Mg #	0.921	0.920	0.925	0.921	0.913	0.915	0.913	0.921	0.906	0.908	0.756
En.	91.18	91.24	91.24	46.37	46.76	47.39	46.71	46.38	46.72	46.01	53.90
Fs	8.09	8.12	7.77	4.79	4.58	4.61	4.62	4.10	5.07	4.83	17.88
Wo	0.74	0.64	0.99	48.84	48.66	47.99	48.66	49.52	48.22	49.16	28.21

ANFIBÓLIO

	Rochas ultramáficas														
	JJ1396p6a mph1	JJ1396p6 amph2	Ac22B1 amp1	Ac22B1a mp2	AC59B	ac59bp2	AC19B1A	AC19B1B	AC19B3A	AC19B4B	AC19B4C	AC19B4A	AC35A6A	AC35A6C	AC35A6D
SiO ₂	57.25	55.73	56.21	54.81	58.45	56.82	59.11	59.74	59.30	60.01	59.74	59.67	59.30	59.30	58.90
TiO ₂	0.05	0.12	0.06	0.04		0.01	0.03	0.00	0.00	0.00	0.03	0.00	0.04	0.01	0.00
Al ₂ O ₃	1.67	2.54	2.11	2.46	0.28	0.46	0.13	0.17	0.11	0.08	0.26	0.07	0.07	0.10	0.09
Fe ₂ O ₃															
Cr ₂ O ₃	0.74	1.12	0.29	0.58	0.06	0.07	0.03	0.00	0.00	0.06	0.05	0.02	0.00	0.01	0.00
FeO	1.45	1.37	1.79	1.81	1.04	1.63	1.00	1.12	0.99	1.07	1.16	0.99	1.02	0.98	1.17
MnO	0.07	0.02	0.06	0.05	0.02	0.09	0.06	0.00	0.00	0.03	0.06	0.02	0.00	0.06	0.05
ZnO															
MgO	22.05	21.89	22.91	22.54	23.29	23.61	24.09	24.10	23.68	23.95	23.97	23.86	23.73	23.99	23.34
CaO	12.89	13.03	12.68	12.75	13.40	13.15	12.75	12.62	12.25	12.36	12.08	12.32	12.14	12.48	12.10
Na ₂ O	0.39	0.56	1.18	1.18	0.21	0.40	0.08	0.10	0.06	0.08	0.16	0.00	0.02	0.05	0.08
K ₂ O	0.01	0.02	0.02	0.01	0.01	0.05	0.01	0.03	0.01	0.00	0.06	0.00	0.01	0.03	0.00
F	0.00	0.00	0.00	0.00											
Cl	0.00	0.00	0.00	0.00											
Total 1	96.58	96.38	97.31	96.23	96.75	96.28	97.26	97.87	96.40	97.65	97.56	96.94	96.33	97.02	95.73
Cations normalizados na base de 23 oxigênios															
Si	7.896	7.733	7.729	7.644	8.000	7.868	8.042	8.070	8.114	8.111	8.086	8.116	8.116	8.076	8.121
AlIV	0.104	0.267	0.271	0.356	0.000	0.076	0.000	0.000	0.000	0.000	0.000	0.000	0.000	0.000	0.000
Fe ³⁺						0.056									
Sum T	8.000	8.000	8.000	8.000	8.000	8.000	8.042	8.070	8.114	8.111	8.086	8.116	8.116	8.076	8.121
AlVI	0.168	0.148	0.071	0.048	0.046	0.000	0.020	0.026	0.017	0.012	0.041	0.011	0.011	0.016	0.014
Fe ³⁺	0.000	0.000	0.064	0.065	0.110	0.057	0.000	0.000	0.000	0.000	0.000	0.000	0.000	0.000	0.000
Ti	0.005	0.013	0.006	0.004	0.000	0.001	0.003	0.000	0.000	0.000	0.003	0.000	0.004	0.001	0.000
Cr	0.081	0.122	0.031	0.064	0.006	0.007	0.003	0.000	0.000	0.007	0.005	0.002	0.000	0.001	0.000
Mg	4.533	4.528	4.698	4.685	4.752	4.874	4.886	4.854	4.829	4.825	4.837	4.839	4.841	4.871	4.797
Fe ²⁺	0.167	0.159	0.130	0.133	0.010	0.061	0.088	0.120	0.114	0.121	0.114	0.112	0.117	0.110	0.135
Zn	0.000	0.000	0.000	0.000	0.000	0.000	0.000	0.000	0.000	0.000	0.000	0.000	0.000	0.000	0.000
Mn	0.008	0.003	0.000	0.000	0.003	0.000	0.000	0.000	0.000	0.003	0.000	0.002	0.000	0.000	0.006
Sum C	4.962	4.973	5.000	5.000	4.924	5.000	5.000	5.000	4.960	4.968	5.000	4.966	4.974	5.000	4.952
Mg	0.000	0.000	0.000	0.000	0.000	0.000	0.000	0.000	0.000	0.000	0.000	0.000	0.000	0.000	0.000
Fe ²⁺	0.000	0.000	0.011	0.013	0.000	0.015	0.026	0.007	0.000	0.000	0.017	0.000	0.000	0.001	0.000
Zn	0.000	0.000	0.000	0.000	0.000	0.000	0.000	0.000	0.000	0.000	0.000	0.000	0.000	0.000	0.000
Mn	0.000	0.000	0.007	0.006	0.000	0.010	0.006	0.000	0.000	0.000	0.007	0.000	0.000	0.007	0.000
Ca	1.905	1.937	1.868	1.906	1.965	1.951	1.858	1.826	1.795	1.789	1.752	1.795	1.779	1.821	1.788
Na	0.094	0.063	0.113	0.076	0.035	0.024	0.021	0.025	0.016	0.022	0.041	0.000	0.006	0.014	0.022
Sum B	2.000	2.000	2.000	2.000	2.000	2.000	1.911	1.857	1.811	1.811	1.817	1.795	1.786	1.843	1.810
Na	0.011	0.086	0.201	0.244	0.020	0.084	0.000	0.000	0.000	0.000	0.000	0.000	0.000	0.000	0.000
K	0.002	0.003	0.004	0.002	0.002	0.008	0.001	0.006	0.002	0.001	0.010	0.000	0.002	0.005	0.000
Sum A	0.013	0.090	0.206	0.246	0.022	0.092	0.001	0.006	0.002	0.001	0.010	0.000	0.002	0.005	0.000

			Rochas ultramáficas												
			P23Amp 525	P23Amp 526	P23Amp 527	P24bAmp5 33	P24bAmp5 34	P24bAmp 535	P24bAm p536	P24bAmp 537	P24aAmp5 39	P24aAmp5 40	P24aAmp5 41	P24aAmp5 542	P21Cpx 543
AC35A4D AC35AA															
SiO ₂	59.75	59.58	41.61	41.73	41.71	42.19	41.84	42.16	56.90	56.53	41.90	42.21	41.82	56.10	56.44
TiO ₂	0.02	0.06	3.61	3.59	3.59	4.59	4.65	4.68	0.05	0.04	4.59	4.60	4.52	0.02	0.01
Al ₂ O ₃	0.12	0.08	13.56	13.85	14.17	13.15	13.05	13.03	0.96	1.02	13.52	13.52	13.49	1.19	1.15
Fe ₂ O ₃															
Cr ₂ O ₃	0.03	0.02	1.12	1.19	1.22	1.49	1.36	1.39	0.08	0.07	1.28	1.37	1.29	0.12	0.07
FeO	1.24	1.00	3.84	3.86	3.94	3.85	4.08	4.09	2.87	2.86	3.92	3.97	4.08	2.63	2.51
MnO	0.04	0.04	0.09	0.00	0.04	0.03	0.10	0.07	0.08	0.03	0.03	0.07	0.07	0.04	0.01
ZnO															
MgO	24.40	23.81	15.82	15.97	15.76	15.50	15.46	15.58	22.25	22.12	15.59	15.81	15.93	22.47	22.59
CaO	11.30	12.35	11.66	11.80	11.91	11.95	11.95	11.96	13.28	12.98	11.92	11.99	11.89	13.20	13.36
Na ₂ O	0.05	0.04	3.31	3.26	3.29	3.24	3.11	3.18	0.52	0.50	3.19	3.24	3.30	0.50	0.50
K ₂ O	0.01	0.03	0.15	0.17	0.19	0.06	0.06	0.05	0.03	0.01	0.05	0.07	0.05	0.01	0.02
F															
Cl															
Total 1	96.96	97.00	94.76	95.42	95.82	96.04	95.66	96.18	97.02	96.15	95.99	96.86	96.44	96.29	96.66
Si	8.114	8.105	6.080	6.055	6.033	6.087	6.067	6.079	7.862	7.887	6.047	6.042	6.017	7.819	7.837
AlIV	0.000	0.000	1.920	1.945	1.967	1.913	1.933	1.921	0.138	0.113	1.953	1.958	1.983	0.181	0.163
Fe ³⁺															
Sum T	8.114	8.105	8.000	8.000	8.000	8.000	8.000	8.000	8.000	8.000	8.000	8.000	8.000	8.000	8.000
AlVI	0.019	0.013	0.414	0.424	0.448	0.322	0.298	0.292	0.019	0.054	0.347	0.322	0.304	0.015	0.025
Fe ³⁺	0.000	0.000	0.233	0.233	0.237	0.231	0.246	0.245	0.109	0.016	0.236	0.237	0.244	0.044	0.009
Ti	0.002	0.006	0.397	0.392	0.390	0.498	0.507	0.508	0.005	0.004	0.498	0.495	0.489	0.002	0.001
Cr	0.003	0.002	0.129	0.137	0.139	0.170	0.155	0.158	0.008	0.008	0.146	0.155	0.147	0.014	0.008
Mg	4.939	4.830	3.446	3.456	3.398	3.334	3.343	3.350	4.584	4.601	3.353	3.374	3.418	4.670	4.676
Fe ²⁺	0.036	0.113	0.238	0.238	0.242	0.236	0.251	0.250	0.224	0.317	0.240	0.242	0.250	0.255	0.281
Zn	0.000	0.000	0.000	0.000	0.000	0.000	0.000	0.000	0.000	0.000	0.000	0.000	0.000	0.000	0.000
Mn	0.000	0.005	0.012	0.000	0.005	0.004	0.012	0.008	0.009	0.000	0.004	0.009	0.008	0.000	0.000
Sum C	5.000	4.968	4.870	4.878	4.860	4.794	4.812	4.812	4.958	5.000	4.823	4.834	4.861	5.000	5.000
Mg	0.000	0.000	0.000	0.000	0.000	0.000	0.000	0.000	0.000	0.000	0.000	0.000	0.000	0.000	0.000
Fe ²⁺	0.105	0.000	0.000	0.000	0.000	0.000	0.000	0.000	0.000	0.001	0.000	0.000	0.000	0.008	0.001
Zn	0.000	0.000	0.000	0.000	0.000	0.000	0.000	0.000	0.000	0.000	0.000	0.000	0.000	0.000	0.000
Mn	0.004	0.000	0.000	0.000	0.000	0.000	0.000	0.000	0.000	0.004	0.000	0.000	0.000	0.005	0.001
Ca	1.644	1.800	1.825	1.835	1.846	1.847	1.857	1.847	1.966	1.941	1.843	1.838	1.832	1.971	1.988
Na	0.012	0.011	0.175	0.165	0.154	0.153	0.143	0.153	0.034	0.054	0.157	0.162	0.168	0.016	0.009
Sum B	1.765	1.811	2.000	2.000	2.000	2.000	2.000	2.000	2.000	2.000	2.000	2.000	2.000	2.000	2.000
Na	0.000	0.000	0.763	0.751	0.768	0.754	0.733	0.735	0.105	0.080	0.735	0.738	0.751	0.118	0.125
K	0.001	0.005	0.027	0.031	0.035	0.011	0.011	0.009	0.005	0.001	0.010	0.013	0.010	0.002	0.004
Sum A	0.001	0.005	0.790	0.782	0.803	0.764	0.743	0.745	0.110	0.081	0.744	0.751	0.761	0.120	0.129

		Rochas ultramáficas								
	P21Cpx 544	AC77BAnf1 IA	AC77BAnf1 1B	AC77BAnf1 cA	AC77BAnf1 1cB	AC77BAnf1 C	AC77BAnf1 f4A	AC78BAnf1 A	AC78BAnf1 B	AC78BAnf1 C
SiO ₂	54.66	55.56	56.57	53.52	54.88	56.00	53.80	56.77	57.76	56.36
TiO ₂	0.08	0.00	0.01	0.00	0.00	0.00	0.00	0.04	0.03	0.00
Al ₂ O ₃	3.03	1.27	0.55	2.84	2.09	1.10	2.51	1.02	0.76	1.42
Fe ₂ O ₃										
Cr ₂ O ₃	0.15	0.31	0.12	0.97	0.92			0.14	0.12	
FeO	3.29	1.30	1.69	1.77	1.87	1.72	1.95	1.75	1.95	1.88
MnO	0.09	0.03	0.08	0.02	0.03	0.03	0.04	0.05	0.08	0.04
ZnO										
MgO	22.35	23.48	23.24	22.94	22.93	23.67	22.46	23.30	23.19	23.05
CaO	12.87	13.31	13.08	13.30	12.93	12.80	12.84	13.03	12.97	12.95
Na ₂ O	1.21	0.51	0.26	0.94	0.73	0.46	0.90	0.63	0.54	0.71
K ₂ O	0.05	0.00	0.02	0.03	0.00	0.04	0.04	0.03	0.01	0.01
F						0.03	0.00			0.06
Cl						0.01	0.01			0.01
Total 1	97.78	95.76	95.61	96.34	96.38	95.86	94.54	96.76	97.40	96.46
Si	7.542	7.764	7.902	7.502	7.656	7.809	7.627	7.841	7.910	7.805
AlIV	0.458	0.209	0.091	0.470	0.343	0.181	0.373	0.159	0.090	0.195
Fe ³⁺										
Sum T	8.000	7.973	7.992	7.971	7.999	7.990	8.000	8.000	8.000	8.000
AlVI	0.034	0.000	0.000	0.000	0.000	0.000	0.045	0.006	0.032	0.036
Fe ³⁺	0.161	0.000	0.000	0.000	0.000	0.000	0.115	0.035	0.057	0.063
Ti	0.008	0.000	0.001	0.000	0.000	0.000	0.000	0.004	0.003	0.000
Cr	0.017	0.034	0.013	0.108	0.102	0.000	0.000	0.015	0.013	0.000
Mg	4.597	4.892	4.838	4.793	4.769	4.920	4.747	4.798	4.735	4.760
Fe ²⁺	0.183	0.074	0.147	0.099	0.129	0.080	0.093	0.142	0.159	0.141
Zn	0.000	0.000	0.000	0.000	0.000	0.000	0.000	0.000	0.000	0.000
Mn	0.000	0.000	0.000	0.000	0.000	0.000	0.000	0.000	0.000	0.000
Sum C	5.000	5.000	5.000	5.000	5.000	5.000	5.000	5.000	5.000	5.000
Mg	0.000	0.000	0.000	0.000	0.000	0.000	0.000	0.000	0.000	0.000
Fe ²⁺	0.037	0.077	0.050	0.109	0.089	0.121	0.024	0.026	0.007	0.013
Zn	0.000	0.000	0.000	0.000	0.000	0.000	0.000	0.000	0.000	0.000
Mn	0.010	0.003	0.009	0.003	0.003	0.004	0.004	0.006	0.009	0.005
Ca	1.902	1.920	1.941	1.889	1.907	1.875	1.950	1.929	1.903	1.921
Na	0.050	0.000	0.000	0.000	0.000	0.000	0.022	0.040	0.081	0.061
Sum B	2.000	2.000	2.000	2.000	2.000	2.000	2.000	2.000	2.000	2.000
Na	0.274	0.137	0.070	0.256	0.197	0.124	0.225	0.130	0.062	0.129
K	0.009	0.000	0.004	0.005	0.000	0.007	0.008	0.005	0.001	0.001
Sum A	0.284	0.209	0.089	0.369	0.222	0.167	0.233	0.135	0.063	0.130

	Rochas ultramáficas											
	AC52	AC52C3-A	AC52C3-B	AC52C3-C	AC52CP1	AC53A2-A	AC53A2-D	AC53A2-E	AC53A2-F	AC53A3-A	AC52EAnf1 2B	AC522654p 5amphibole 2
SiO ₂	59.29	58.93	57.95	59.89	59.56	55.53	57.43	58.03	56.00	55.03	57.28	58.23
TiO ₂	0.00	0.05	0.01	0.00	0.00	0.15	0.13	0.05	0.14	0.16	0.00	0.02
Al ₂ O ₃	0.25	0.51	1.08	0.20	0.28	2.88	1.01	0.21	2.54	2.81	0.62	0.37
Fe ₂ O ₃												
Cr ₂ O ₃	0.06	0.16	0.54	0.00	0.06	0.48	0.37	0.05	1.02	0.67	0.15	0.12
FeO	1.98	2.21	1.94	1.74	1.92	1.95	1.81	1.61	1.69	1.89	1.88	1.77
MnO	0.07	0.07	0.06	0.04	0.12	0.05	0.07	0.00	0.00	0.03	0.10	0.09
ZnO												
MgO	23.82	23.82	23.57	23.85	23.88	22.50	23.04	23.27	22.48	22.24	23.90	23.45
CaO	12.30	11.55	11.29	12.20	12.26	11.35	11.46	11.73	11.26	11.73	12.92	12.55
Na ₂ O	0.25	0.36	0.52	0.23	0.24	1.16	0.81	0.32	0.94	1.37	0.39	0.33
K ₂ O	0.01	0.02	0.02	0.01	0.01	0.02	0.01	0.02	0.03	0.02	0.01	0.01
F											0.00	
Cl											0.00	
Total 1	98.02	97.67	96.98	98.14	98.32	96.08	96.14	95.29	96.11	95.95	97.26	96.93
Cations normalizados na base de 23 oxigênios												
Si	7.996	8.000	7.936	8.081	8.041	7.699	7.932	8.066	7.750	7.666	7.853	7.989
AlIV	0.004	0.000	0.064	0.000	0.000	0.301	0.068	0.000	0.250	0.334	0.101	0.011
Sum T	8.000	8.000	8.000	8.081	8.041	8.000	8.000	8.066	8.000	8.000	7.954	8.000
AlVI	0.035	0.081	0.110	0.031	0.044	0.170	0.097	0.034	0.165	0.127	0.000	0.050
Fe ³⁺	0.223	0.072	0.017	0.000	0.000	0.113	0.071	0.000	0.098	0.110	0.107	0.016
Ti	0.000	0.005	0.001	0.000	0.000	0.016	0.014	0.005	0.014	0.016	0.000	0.002
Cr	0.006	0.017	0.059	0.000	0.006	0.052	0.040	0.005	0.112	0.074	0.016	0.013
Mg	4.736	4.820	4.812	4.798	4.807	4.648	4.744	4.822	4.612	4.617	4.876	4.796
Fe ²⁺	0.000	0.006	0.001	0.171	0.143	0.000	0.035	0.134	0.000	0.055	0.000	0.122
Zn	0.000	0.000	0.000	0.000	0.000	0.000	0.000	0.000	0.000	0.000	0.000	0.000
Mn	0.000	0.000	0.000	0.000	0.000	0.000	0.000	0.000	0.000	0.000	0.000	0.000
Sum C	5.000	5.000	5.000	5.000	5.000	5.000	5.000	5.000	5.000	5.000	5.000	5.000
Mg	0.052	0.000	0.000	0.000	0.000	0.003	0.000	0.000	0.027	0.000	0.010	0.000
Fe ²⁺	0.000	0.173	0.204	0.025	0.074	0.114	0.103	0.053	0.098	0.056	0.108	0.064
Zn	0.000	0.000	0.000	0.000	0.000	0.000	0.000	0.000	0.000	0.000	0.000	0.000
Mn	0.008	0.008	0.007	0.004	0.014	0.006	0.008	0.000	0.000	0.004	0.012	0.010
Ca	1.777	1.680	1.656	1.763	1.774	1.687	1.696	1.746	1.670	1.750	1.870	1.845
Na	0.066	0.095	0.133	0.059	0.062	0.191	0.193	0.086	0.205	0.191	0.000	0.081
Sum B	1.903	1.957	2.000	1.851	1.923	2.000	2.000	1.885	2.000	2.000	2.000	2.000
Na	0.000	0.000	0.006	0.000	0.000	0.122	0.024	0.000	0.048	0.178	0.104	0.005
K	0.001	0.004	0.003	0.002	0.002	0.004	0.002	0.004	0.005	0.004	0.002	0.002
Sum A	0.001	0.004	0.009	0.002	0.002	0.125	0.026	0.004	0.053	0.182	0.134	0.008

	Rochas ultramáficas						
	AC521925p 1amp	AC52Cp31 a	AC52Cp32 a	AC53Jp2a mp1a	AC53Jp2a mp1b outro grao	AC53Jp2a mp1c outro grao	AC53Jp3a mph
SiO ₂	58.67	57.91	58.57	57.97	57.53	57.92	57.64
TiO ₂	0.02	0.01	0.00	0.03	0.01	0.05	0.01
Al ₂ O ₃	0.22	0.29	0.66	0.96	1.11	1.05	0.96
Fe ₂ O ₃							
Cr ₂ O ₃	0.00	0.09	0.20	0.04	0.10	0.06	0.06
FeO	2.03	1.72	1.92	1.81	2.11	1.86	1.88
MnO	0.08	0.10	0.10	0.05	0.03	0.05	0.04
ZnO							
MgO	23.22	23.51	23.18	23.02	22.94	22.87	22.91
CaO	12.94	12.74	12.65	13.31	12.99	13.20	13.22
Na ₂ O	0.19	0.22	0.37	0.44	0.69	0.61	0.54
K ₂ O	0.01	0.01	0.00	0.03	0.05	0.03	0.04
F	0.00	0.00	0.00	0.00	0.00	0.00	0.00
Cl	0.00	0.00	0.00	0.00	0.00	0.00	0.00
Total 1	97.37	96.59	97.66	97.66	97.55	97.70	97.30
Si	8.000	7.976	7.984	7.922	7.884	7.916	7.913
AlIV	0.000	0.024	0.016	0.078	0.116	0.084	0.087
Sum T	8.000	8.000	8.000	8.000	8.000	8.000	8.000
AlVI	0.035	0.023	0.090	0.076	0.063	0.085	0.069
Fe ³⁺	0.135	0.029	0.002	0.000	0.023	0.000	0.000
Ti	0.002	0.001	0.000	0.003	0.001	0.005	0.001
Cr	0.000	0.010	0.022	0.004	0.010	0.006	0.007
Mg	4.720	4.827	4.711	4.691	4.687	4.660	4.689
Fe ²⁺	0.098	0.110	0.175	0.206	0.216	0.213	0.216
Zn	0.000	0.000	0.000	0.000	0.000	0.000	0.000
Mn	0.010	0.000	0.000	0.000	0.000	0.000	0.004
Sum C	4.999	5.000	5.000	4.980	5.000	4.970	4.986
Mg	0.000	0.000	0.000	0.000	0.000	0.000	0.000
Fe ²⁺	0.000	0.058	0.042	0.000	0.003	0.000	0.000
Zn	0.000	0.000	0.000	0.000	0.000	0.000	0.000
Mn	0.000	0.012	0.012	0.006	0.003	0.006	0.000
Ca	1.890	1.880	1.848	1.948	1.907	1.932	1.944
Na	0.049	0.050	0.098	0.046	0.086	0.062	0.056
Sum B	1.939	2.000	2.000	2.000	2.000	2.000	2.000
Na	0.000	0.010	0.001	0.072	0.096	0.099	0.086
K	0.002	0.001	0.000	0.005	0.008	0.005	0.008
Sum A	0.002	0.011	0.001	0.077	0.104	0.104	0.094

Metagabros de El Picacho																
	AC25p2a mph2	CMK040A P2C	CMK040P 2D	CMK040A P3A	CMK040P 2B	AC32A15- A	AC32A15- B	AC33C5-A	CMK040A P2E	AC25p2a mph1	CMK040A P1A	CMK040A P1C	CMK040A P4K	CMK040A P2A	CMK040A P6C	CMK040A P6E
SiO ₂	41.44	42.98	44.30	43.06	43.06	42.57	43.19	51.07	51.91	54.18	54.48	54.79	53.18	53.12	54.83	54.39
TiO ₂	4.31	2.08	1.91	1.86	0.45	0.41	0.47	0.37	0.29	0.17	0.07	0.07	0.08	0.05	0.07	0.13
Al ₂ O ₃	14.12	13.36	14.14	13.41	11.37	14.74	14.84	6.44	5.77	3.05	1.97	2.52	3.23	4.18	3.34	3.34
Fe ₂ O ₃	0.64	0.24	0.26	0.34	0.42	0.62	0.84	0.07	0.15	0.18	0.13	0.05	0.06	0.03	0.03	0.08
FeO	9.71	10.83	10.86	10.59	12.22	7.93	8.01	10.56	8.53	7.00	8.71	8.72	8.71	8.67	6.55	7.59
MnO	0.17	0.15	0.13	0.12	0.15	0.15	0.16	0.23	0.13	0.22	0.32	0.20	0.21	0.26	0.18	0.17
ZnO	0.01	0.04	0.00	0.07					0.00		0.01	0.09	0.06	0.06	0.01	0.00
MgO	12.45	12.48	12.69	12.87	14.36	14.38	14.56	15.49	16.58	18.84	18.01	18.21	17.14	17.48	19.26	18.71
CaO	12.14	11.11	11.18	11.13	11.69	11.42	11.36	11.59	12.37	12.70	11.85	11.59	12.11	11.63	11.99	12.10
Na ₂ O	2.13	2.08	2.20	2.20	1.99	2.25	2.46	0.92	0.74	0.51	0.28	0.37	0.42	0.55	0.58	0.49
K ₂ O	0.46	0.27	0.30	0.30	0.38	0.12	0.16	0.06	0.04	0.04	0.02	0.00	0.05	0.04	0.04	0.01
F	0.00	0.00	0.00	0.00	0.12		0.00		0.24	0.00	0.00	0.00	0.00	0.16	0.00	0.00
Cl	0.00	0.01	0.03	0.02	0.01		0.03		0.04	0.00	0.03	0.03	0.02	0.01	0.04	0.02
Total 1	97.58	95.59	98.04	95.88	96.28	94.59	96.06	96.81	96.78	96.90	95.87	96.63	95.28	96.23	96.90	97.03
-O≡F	0.00	0.00	0.00	0.05	0.00	0.00	0.00	0.10		0.00	0.00	0.00	0.07	0.00	0.00	0.00
-O≡Cl	0.00	0.01	0.00	0.00	0.00	0.01	0.00	0.01		0.01	0.01	0.00	0.00	0.01	0.00	0.00
Total	95.58	98.03	95.88	96.23	94.59	96.05	96.81	96.67		95.87	96.62	95.28	96.16	96.89	97.03	
Cations normalizados na base de 23 oxigênios																
Si	6.060	6.383	6.398	6.343	6.330	6.264	6.265	7.323	7.416	7.656	7.819	7.787	7.689	7.590	7.695	7.662
AlIV	1.940	1.617	1.602	1.657	1.670	1.736	1.735	0.677	0.584	0.344	0.181	0.213	0.311	0.410	0.305	0.338
Sum T	8.000	8.000	8.000	8.000	8.000	8.000	8.000	8.000	8.000	8.000	8.000	8.000	8.000	8.000	8.000	8.000
AlVI	0.493	0.721	0.805	0.670	0.300	0.821	0.802	0.411	0.387	0.163	0.152	0.209	0.240	0.295	0.246	0.216
Fe ³⁺	0.000	0.000	0.000	0.214	0.695	0.308	0.304	0.224	0.001	0.084	0.039	0.046	0.090	0.105	0.110	0.129
Ti	0.474	0.232	0.208	0.206	0.050	0.045	0.051	0.040	0.031	0.019	0.007	0.007	0.009	0.006	0.008	0.013
Cr	0.074	0.028	0.030	0.040	0.049	0.072	0.096	0.007	0.017	0.020	0.015	0.006	0.007	0.003	0.009	
Mg	2.715	2.763	2.732	2.827	3.147	3.156	3.148	3.312	3.531	3.969	3.854	3.858	3.695	3.724	4.029	3.929
Fe ²⁺	1.188	1.256	1.225	1.044	0.759	0.598	0.599	1.007	1.017	0.744	0.933	0.874	0.959	0.868	0.605	0.704
Zn	0.000	0.000	0.000	0.000	0.000	0.000	0.000	0.000	0.000	0.000	0.000	0.000	0.000	0.000	0.000	0.000
Mn	0.021	0.000	0.000	0.000	0.000	0.000	0.000	0.000	0.015	0.001	0.000	0.000	0.000	0.000	0.000	0.000
Sum C	4.965	5.000	5.000	5.000	5.000	5.000	5.000	5.000	5.000	5.000	5.000	5.000	5.000	5.000	5.000	5.000
Mg	0.000	0.000	0.000	0.000	0.000	0.000	0.000	0.000	0.000	0.000	0.000	0.000	0.000	0.000	0.000	0.000
Fe ²⁺	0.000	0.088	0.087	0.052	0.072	0.077	0.074	0.042	0.000	0.000	0.074	0.117	0.006	0.065	0.056	0.063
Zn	0.000	0.001	0.005	0.000	0.007	0.000	0.000	0.000	0.000	0.000	0.001	0.010	0.007	0.007	0.001	0.000
Mn	0.000	0.018	0.015	0.015	0.019	0.018	0.019	0.028	0.001	0.025	0.038	0.023	0.026	0.031	0.021	0.020
Ca	1.902	1.767	1.730	1.756	1.841	1.801	1.765	1.781	1.893	1.923	1.822	1.765	1.876	1.780	1.802	1.826
Na	0.098	0.125	0.163	0.177	0.062	0.104	0.142	0.149	0.106	0.052	0.064	0.085	0.086	0.117	0.120	0.090
Sum B	2.000	2.000	2.000	2.000	2.000	2.000	2.000	2.000	2.000	2.000	2.000	2.000	2.000	2.000	2.000	2.000
Na	0.507	0.474	0.453	0.451	0.506	0.539	0.549	0.106	0.098	0.087	0.014	0.016	0.032	0.037	0.038	0.045
K	0.086	0.051	0.055	0.056	0.071	0.023	0.029	0.011	0.008	0.008	0.004	0.000	0.010	0.007	0.007	0.003
Sum A	0.593	0.525	0.507	0.506	0.577	0.562	0.578	0.118	0.106	0.095	0.018	0.016	0.042	0.045	0.047	

Metagabros de El Picacho																
	CMK040A P5A	CMK040A P5B	CMK40D2 2-F	CMK40D2 2-F	CMK40D2 2-I	CMK40D2 9-A	CMK40D2 9-B	CMK40D2 A	AC32A14- AC33C1-A	AC33C1-B	AC33C1- C	AC33C3-B	AC59A1A	AC59A2E	AC59A3A	CMK040A P1D
SiO ₂	51.64	52.44	52.62	52.98	54.89	53.84	55.37	56.79	53.56	55.84	53.83	55.22	55.49	56.45	56.21	44.17
TiO ₂	0.21	0.17	0.13	0.15	0.06	0.07	0.09	0.06	0.22	0.10	0.26	0.19	0.04	0.01	0.05	0.08
Al ₂ O ₃	4.31	3.44	5.20	4.70	2.99	5.02	2.32	1.49	3.96	2.35	4.09	2.71	1.71	1.29	1.86	11.87
Fe ₂ O ₃																
Cr ₂ O ₃	0.09	0.14	0.06	0.00	0.14	0.09	0.04	0.03	0.11	0.05	0.12	0.09	0.00	0.31	0.09	0.02
FeO	11.24	11.08	11.36	11.64	9.66	9.33	9.06	5.30	9.45	8.95	9.66	9.55	5.22	5.26	4.30	14.47
MnO	0.26	0.16	0.09	0.28	0.13	0.32	0.30	0.06	0.12	0.16	0.20	0.19	0.09	0.08	0.11	0.27
ZnO	0.00	0.01											0.00	0.03	0.01	0.00
MgO	15.10	15.78	15.32	15.41	17.47	16.78	18.51	20.69	17.18	18.60	16.94	17.91	20.52	20.55	20.99	11.43
CaO	12.36	12.35	11.33	11.60	11.59	10.40	10.72	11.75	11.54	11.64	11.81	11.49	12.47	12.91	13.18	11.89
Na ₂ O	0.43	0.45	0.51	0.55	0.36	0.83	0.66	0.32	0.42	0.35	0.58	0.36	0.21	0.16	0.24	1.67
K ₂ O	0.04	0.05	0.03	0.03	0.07	0.04	0.03	0.05	0.02	0.04	0.08	0.03	0.03	0.02	0.02	0.10
F	0.24	0.00											0.00	0.00	0.00	0.00
Cl	0.05	0.00											0.01	0.00	0.01	0.02
Total 1	95.95	96.07	96.66	97.33	97.36	96.71	97.10	96.54	96.57	98.07	97.57	97.73	95.78	97.07	97.06	95.99
-O≡F	0.10	0.00	0.00	0.00	0.00	0.00	0.00	0.00	0.00	0.00	0.00	0.00	0.00	0.00	0.00	0.00
-O≡Cl	0.01	0.00	0.00	0.00	0.00	0.00	0.00	0.00	0.00	0.00	0.00	0.00	0.00	0.00	0.00	0.01
Total	95.84	96.07	96.66	97.33	97.36	96.71	97.10	96.54	96.57	98.07	97.57	97.73	95.78	97.07	97.06	95.99
Si	7.538	7.619	7.566	7.580	7.774	7.646	7.819	7.936	7.643	7.816	7.617	7.782	7.837	7.880	7.820	6.579
AlIV	0.462	0.381	0.434	0.420	0.226	0.354	0.181	0.064	0.357	0.184	0.383	0.218	0.163	0.120	0.180	1.421
Sum T	8.000	8.000	8.000	8.000	8.000	8.000	8.000	8.000	8.000	8.000	8.000	8.000	8.000	8.000	8.000	8.000
AlVI	0.280	0.208	0.448	0.372	0.272	0.486	0.205	0.181	0.308	0.204	0.300	0.232	0.121	0.093	0.125	0.664
Fe ³⁺	0.006	0.090	0.053	0.098	0.008	0.039	0.076	0.000	0.062	0.025	0.095	0.017	0.050	0.019	0.023	0.338
Ti	0.023	0.019	0.014	0.016	0.006	0.008	0.010	0.007	0.024	0.011	0.027	0.021	0.004	0.001	0.005	0.009
Cr	0.010	0.016	0.007	0.000	0.016	0.010	0.005	0.003	0.013	0.005	0.014	0.010	0.000	0.034	0.010	0.002
Mg	3.286	3.417	3.285	3.288	3.690	3.553	3.898	4.310	3.655	3.882	3.573	3.763	4.320	4.277	4.353	2.537
Fe ²⁺	1.366	1.251	1.194	1.226	1.008	0.905	0.807	0.500	0.939	0.873	0.990	0.957	0.505	0.576	0.477	1.449
Zn	0.000	0.000	0.000	0.000	0.000	0.000	0.000	0.000	0.000	0.000	0.000	0.000	0.000	0.001	0.000	0.000
Mn	0.030	0.000	0.000	0.000	0.000	0.000	0.000	0.000	0.000	0.000	0.000	0.000	0.000	0.000	0.006	0.000
Sum C	5.000	5.000	5.000	5.000	5.000	5.000	5.000	5.000	5.000	5.000	5.000	5.000	5.000	5.000	5.000	5.000
Mg	0.000	0.000	0.000	0.000	0.000	0.000	0.000	0.000	0.000	0.000	0.000	0.000	0.000	0.000	0.000	0.000
Fe ²⁺	0.000	0.008	0.121	0.072	0.128	0.165	0.189	0.119	0.128	0.150	0.060	0.151	0.062	0.019	0.000	0.027
Zn	0.000	0.001	0.000	0.000	0.000	0.000	0.000	0.000	0.000	0.000	0.000	0.000	0.000	0.003	0.000	0.000
Mn	0.002	0.020	0.011	0.034	0.016	0.038	0.036	0.007	0.014	0.018	0.024	0.023	0.010	0.010	0.007	0.034
Ca	1.933	1.921	1.746	1.777	1.759	1.582	1.622	1.760	1.764	1.745	1.791	1.734	1.887	1.930	1.964	1.897
Na	0.065	0.051	0.122	0.116	0.097	0.215	0.153	0.086	0.094	0.087	0.125	0.092	0.041	0.038	0.029	0.042
Sum B	2.000	2.000	2.000	2.000	2.000	2.000	2.000	1.973	2.000	2.000	2.000	2.000	2.000	2.000	2.000	2.000
Na	0.057	0.076	0.019	0.035	0.003	0.014	0.027	0.000	0.022	0.009	0.034	0.006	0.017	0.006	0.036	0.442
K	0.008	0.010	0.005	0.005	0.012	0.007	0.005	0.008	0.003	0.007	0.015	0.004	0.006	0.003	0.003	0.018
Sum A	0.065	0.086	0.024	0.039	0.015	0.021	0.032	0.008	0.025	0.016	0.048	0.011	0.023	0.010	0.039	0.460

Metagabros de El Picacho

	CMK040A 4E	CMK040A P4I	CMK040A P6G	CMK40D2 2-A	CMK40D2 2-E	CMK1441 A	CMK1441 B	CMK1444 A	CMK1444 B
SiO ₂	44.59	41.01	42.45	48.40	45.29	49.81	49.99	49.42	49.60
TiO ₂	0.04	0.08	0.08	0.17	0.21	0.29	0.30	0.33	0.31
Al ₂ O ₃	10.65	14.39	14.52	8.86	10.66	7.67	7.66	8.04	8.13
Fe ₂ O ₃									
Cr ₂ O ₃	0.02	0.07	0.19	0.03	0.00	0.06	0.05	0.15	0.17
FeO	16.91	17.14	16.19	12.47	16.32	6.33	6.39	6.45	6.85
MnO	0.14	0.24	0.22	0.12	0.14	0.07	0.12	0.13	0.10
ZnO	0.07	0.00	0.01			0.00	0.00	0.00	0.00
MgO	11.42	9.35	9.73	13.74	11.24	17.65	17.38	17.27	17.35
CaO	11.57	11.87	11.84	11.04	10.67	12.08	12.30	12.53	12.17
Na ₂ O	1.72	2.06	2.10	1.20	1.47	1.25	1.33	1.30	1.34
K ₂ O	0.16	0.09	0.22	0.13	0.15	0.08	0.07	0.06	0.09
F	0.00	0.04	0.08			0.00	0.00	0.16	0.00
Cl	0.04	0.01	0.04			0.00	0.00	0.00	0.02
Total 1	97.32	96.34	97.66	96.16	96.15	95.28	95.60	95.82	96.12
-O≡F	0.00	0.02	0.03	0.00	0.00	0.00	0.00	0.07	0.00
-O≡Cl	0.01	0.00	0.01	0.00	0.00	0.00	0.00	0.00	0.00
Total	97.31	96.32	97.61	96.16	96.15	95.28	95.60	95.76	96.12
Si	6.588	6.178	6.298	7.044	6.724	7.156	7.180	7.103	7.092
AlIV	1.412	1.822	1.702	0.956	1.276	0.844	0.820	0.897	0.908
Sum T	8.000	8.000	8.000	8.000	8.000	8.000	8.000	8.000	8.000
AlVI	0.442	0.733	0.835	0.563	0.589	0.455	0.476	0.465	0.462
Fe ³⁺	0.606	0.514	0.266	0.347	0.510	0.153	0.067	0.026	0.154
Ti	0.005	0.009	0.009	0.019	0.023	0.031	0.033	0.035	0.033
Cr	0.003	0.008	0.022	0.004	0.000	0.007	0.006	0.017	0.019
Mg	2.515	2.099	2.153	2.981	2.487	3.782	3.722	3.700	3.699
Fe ²⁺	1.429	1.637	1.716	1.086	1.391	0.572	0.697	0.749	0.633
Zn	0.000	0.000	0.000	0.000	0.000	0.000	0.000	0.000	0.000
Mn	0.000	0.000	0.000	0.000	0.000	0.000	0.000	0.008	0.000
Sum C	5.000	5.000	5.000	5.000	5.000	5.000	5.000	5.000	5.000
Mg	0.000	0.000	0.000	0.000	0.000	0.000	0.000	0.000	0.000
Fe ²⁺	0.082	0.033	0.038	0.096	0.148	0.038	0.005	0.000	0.035
Zn	0.007	0.000	0.001	0.000	0.000	0.000	0.000	0.000	0.000
Mn	0.018	0.030	0.028	0.015	0.017	0.009	0.015	0.008	0.012
Ca	1.831	1.916	1.881	1.721	1.696	1.859	1.892	1.930	1.864
Na	0.062	0.021	0.052	0.168	0.138	0.095	0.088	0.062	0.090
Sum B	2.000	2.000	2.000	2.000	2.000	2.000	2.000	2.000	2.000
Na	0.429	0.580	0.552	0.171	0.285	0.252	0.282	0.300	0.280
K	0.030	0.017	0.041	0.024	0.029	0.014	0.013	0.011	0.017
Sum A	0.459	0.597	0.593	0.194	0.314	0.266	0.295	0.311	0.297

Metagabros de Boquerón

	CMK38BA	CMK38B3B	CMK38B3C	CMK38BAV	CMK38B3A	CMK38B3B	CMK38B3F	CMK38Bp1 0amph1	CMK38Bp1 0amph2	CMK38Bp10amp hverdeescuro1	CMK38Bp10amp hverdeescuro2
SiO ₂	47.32	47.78	48.07	47.80	48.28	47.36	47.01	56.12	55.92	46.92	49.95
TiO ₂	0.98	0.93	0.98	0.93	1.02	0.97	0.90	0.02	0.03	1.00	0.49
Al ₂ O ₃	10.42	9.54	9.82	9.84	9.45	9.30	10.29	1.02	1.13	10.09	6.52
Fe ₂ O ₃											
Cr ₂ O ₃	0.00	0.05	0.00	0.09	0.09	0.07	0.10	0.02	0.04	0.05	0.07
FeO	12.28	11.46	11.73	12.54	11.67	11.31	12.48	8.18	8.83	11.81	10.20
MnO	0.21	0.21	0.19	0.19	0.19	0.16	0.16	0.24	0.24	0.21	0.22
ZnO											
MgO	13.65	14.20	13.92	13.47	14.20	13.93	13.33	18.20	17.86	13.51	15.46
CaO	11.21	11.56	11.02	11.22	10.71	10.88	11.21	12.94	12.84	11.93	12.49
Na ₂ O	1.47	1.38	1.41	1.42	1.42	1.42	1.44	0.13	0.15	1.44	0.90
K ₂ O	0.08	0.07	0.09	0.10	0.07	0.09	0.12	0.01	0.02	0.09	0.07
F								0.00	0.00	0.00	0.00
Cl								0.00	0.00	0.00	0.00
Total 1	97.62	97.17	97.24	97.60	97.10	95.49	97.03	96.88	97.05	97.07	96.36
Cations normalizados na base de 23 oxigênios											
Si	6.802	6.890	6.908	6.882	6.931	6.929	6.813	7.954	7.937	6.817	7.244
AlIV	1.198	1.110	1.092	1.118	1.069	1.071	1.187	0.046	0.063	1.183	0.756
Sum T	8.000	8.000	8.000	8.000	8.000	8.000	8.000	8.000	8.000	8.000	8.000
AlVI	0.567	0.512	0.572	0.551	0.529	0.533	0.570	0.125	0.127	0.545	0.358
Fe ³⁺	0.345	0.269	0.321	0.303	0.386	0.311	0.320	0.000	0.000	0.175	0.088
Ti	0.105	0.100	0.106	0.100	0.110	0.107	0.099	0.002	0.003	0.110	0.054
Cr	0.000	0.005	0.000	0.011	0.010	0.008	0.012	0.003	0.004	0.006	0.008
Mg	2.925	3.052	2.981	2.892	3.038	3.037	2.880	3.846	3.779	2.927	3.342
Fe ²⁺	1.058	1.061	1.020	1.143	0.927	1.004	1.119	0.969	1.048	1.236	1.151
Zn	0.000	0.000	0.000	0.000	0.000	0.000	0.000	0.000	0.000	0.000	0.000
Mn	0.000	0.000	0.000	0.000	0.000	0.000	0.000	0.029	0.028	0.000	0.000
Sum C	5.000	5.000	5.000	5.000	5.000	5.000	5.000	4.974	4.989	5.000	5.000
Mg	0.000	0.000	0.000	0.000	0.000	0.000	0.000	0.000	0.000	0.000	0.000
Fe ²⁺	0.085	0.060	0.079	0.073	0.100	0.078	0.083	0.000	0.000	0.029	0.000
Zn	0.000	0.000	0.000	0.000	0.000	0.000	0.000	0.000	0.000	0.000	0.000
Mn	0.026	0.025	0.023	0.023	0.023	0.020	0.020	0.000	0.000	0.026	0.027
Ca	1.726	1.785	1.697	1.731	1.647	1.704	1.740	1.966	1.953	1.857	1.940
Na	0.163	0.130	0.201	0.172	0.230	0.197	0.158	0.034	0.040	0.087	0.033
Sum B	2.000	2.000	2.000	2.225	2.000	2.000	2.000	2.000	1.993	2.000	2.000
Na	0.246	0.255	0.192	0.225	0.165	0.205	0.246	0.000	0.000	0.319	0.219
K	0.015	0.013	0.016	0.019	0.012	0.016	0.021	0.002	0.003	0.017	0.014
Sum A	0.261	0.269	0.209	0.244	0.178	0.221	0.268	0.002	0.003	0.335	0.233

Metagabros de Boquerón

	CMK38Bp10a mphfibroso	CMK38Bp10a mphfibroso2	CMK38Bp6 pl2	AC61Tp1a mp1	AC61Tp1a mp4	AC61Tp1a mp4bclaro	AC61Tp1a mph3
SiO ₂	53.97	53.09	55.78	45.72	45.17	45.33	45.72
TiO ₂	0.07	0.09	0.02	0.81	0.69	0.62	0.83
Al ₂ O ₃	2.80	3.29	1.05	10.92	11.45	11.83	10.74
Fe ₂ O ₃							
Cr ₂ O ₃	0.01	0.02	0.04	-0.02	0.02	0.06	0.01
FeO	11.56	11.40	8.89	16.34	16.49	15.70	16.46
MnO	0.26	0.22	0.25	0.28	0.29	0.23	0.26
ZnO							
MgO	15.94	15.54	17.51	10.52	10.21	10.53	10.28
CaO	12.63	12.66	12.93	11.73	11.73	11.83	11.80
Na ₂ O	0.34	0.40	0.10	1.38	1.42	1.44	1.32
K ₂ O	0.02	0.02	0.01	0.09	0.09	0.10	0.08
F	0.00	0.00	0.00	0.00	0.00	0.00	0.00
Cl	0.00	0.00	0.00	0.00	0.00	0.00	0.00
Total 1	97.60	96.73	96.60	97.77	97.55	97.67	97.51
Si	7.722	7.676	7.957	6.728	6.673	6.665	6.757
AlIV	0.278	0.324	0.043	1.272	1.327	1.335	1.243
Sum T	8.000	8.000	8.000	8.000	8.000	8.000	8.000
AlVI	0.194	0.237	0.134	0.622	0.666	0.715	0.627
Fe ³⁺	0.063	0.017	0.000	0.229	0.236	0.205	0.191
Ti	0.008	0.010	0.003	0.090	0.077	0.069	0.092
Cr	0.001	0.002	0.004	0.000	0.002	0.007	0.002
Mg	3.401	3.350	3.725	2.307	2.249	2.308	2.266
Fe ²⁺	1.322	1.362	1.061	1.751	1.771	1.697	1.822
Zn	0.000	0.000	0.000	0.000	0.000	0.000	0.000
Mn	0.012	0.022	0.031	0.000	0.000	0.000	0.000
Sum C	5.000	5.000	4.958	5.000	5.000	5.000	5.000
Mg	0.000	0.000	0.000	0.000	0.000	0.000	0.000
Fe ²⁺	0.000	0.000	0.000	0.040	0.041	0.038	0.030
Zn	0.000	0.000	0.000	0.000	0.000	0.000	0.000
Mn	0.020	0.005	0.000	0.035	0.036	0.029	0.033
Ca	1.935	1.961	1.977	1.850	1.857	1.863	1.868
Na	0.045	0.034	0.023	0.075	0.066	0.070	0.069
Sum B	2.000	2.000	2.000	2.000	2.000	2.000	2.000
Na	0.050	0.079	0.005	0.318	0.341	0.341	0.310
K	0.003	0.003	0.001	0.017	0.017	0.019	0.016
Sum A	0.054	0.082	0.007	0.335	0.357	0.359	0.326

	Anfibolitos													
	ANFIBOLIO1	ANFIBOLIO1PA RTELIMPA	ANFI1C3	ANF2BOR 1	ANF2CENT RO	ANF2BOR2	ANPX?	ANF3PT1	ANF3PT2	ANF4PT1	ANF4PT2	ANF4PT3	ANF3PT3	ANF3PT4
SiO ₂	46.28	45.83	46.26	45.99	45.69	45.09	45.90	45.55	45.87	45.30	45.89	45.89	46.06	45.64
TiO ₂	0.51	0.61	0.53	0.86	0.59	0.72	0.60	0.53	0.73	0.71	0.51	0.54	0.74	0.52
Al ₂ O ₃	10.28	10.73	10.73	10.31	10.68	11.39	10.84	11.45	10.35	11.19	10.78	10.91	10.42	11.03
Fe ₂ O ₃														
Cr ₂ O ₃	0.03	0.00	0.06	0.03	0.07	0.08	0.03	0.00	0.04	0.12	0.08	0.02	0.04	0.10
FeO	14.77	14.81	14.93	14.82	15.02	15.36	14.34	14.58	14.92	15.16	14.82	14.72	14.09	14.85
MnO	0.24	0.26	0.25	0.21	0.25	0.28	0.25	0.23	0.18	0.16	0.19	0.17	0.19	0.16
ZnO	0.06	0.00	0.06	0.00	0.07	0.07	0.00	0.01	0.00	0.00	0.03	0.11	0.00	0.00
MgO	11.82	11.57	11.60	11.48	11.37	11.03	11.78	11.34	11.67	10.95	11.54	11.63	11.99	11.47
CaO	11.81	11.98	11.74	12.04	11.94	11.97	11.68	11.82	11.86	11.77	11.41	11.66	11.74	11.72
Na ₂ O	1.57	1.61	1.64	1.59	1.63	1.78	1.52	1.75	1.66	1.56	1.58	1.61	1.52	1.71
K ₂ O	0.12	0.15	0.12	0.27	0.16	0.23	0.15	0.19	0.24	0.31	0.16	0.20	0.18	0.18
F	0.00	0.61	0.09	0.00	0.33	0.05	0.33	0.00	0.00	0.57	0.00	0.10	0.00	0.10
Cl	0.00	0.01	0.00	0.02	0.00	0.02	0.01	0.04	0.00	0.01	0.00	0.00	0.00	0.00
Total 1	97.48	98.18	98.01	97.61	97.80	98.07	97.42	97.50	97.51	97.79	96.99	97.57	96.95	97.47
-O≡F	0.00	0.26	0.04	0.00	0.14	0.02	0.14	0.00	0.00	0.24	0.00	0.04	0.00	0.04
-O≡Cl	0.00	0.00	0.00	0.00	0.00	0.00	0.00	0.01	0.00	0.00	0.00	0.00	0.00	0.00
Total	97.48	97.92	97.97	97.61	97.66	98.04	97.27	97.49	97.51	97.55	96.99	97.53	96.95	97.43
Cations normalizados na base de 23 oxigênios														
Si	6.791	6.715	6.757	6.771	6.722	6.631	6.734	6.695	6.751	6.678	6.756	6.730	6.777	6.711
AlIV	1.209	1.285	1.243	1.229	1.278	1.369	1.266	1.305	1.249	1.322	1.244	1.270	1.223	1.289
Sum T	8.000	8.000	8.000	8.000	8.000	8.000	8.000	8.000	8.000	8.000	8.000	8.000	8.000	8.000
AlVI	0.569	0.567	0.604	0.560	0.574	0.605	0.607	0.678	0.546	0.621	0.626	0.616	0.583	0.622
Fe ³⁺	0.219	0.033	0.198	0.107	0.099	0.155	0.151	0.154	0.176	0.030	0.265	0.209	0.196	0.181
Ti	0.056	0.067	0.059	0.095	0.066	0.080	0.066	0.059	0.081	0.078	0.057	0.059	0.082	0.058
Cr	0.003	0.000	0.007	0.004	0.008	0.010	0.003	0.000	0.005	0.014	0.009	0.003	0.005	0.012
Mg	2.586	2.528	2.525	2.521	2.493	2.419	2.577	2.485	2.560	2.407	2.532	2.543	2.629	2.515
Fe ²⁺	1.567	1.783	1.607	1.713	1.753	1.731	1.596	1.624	1.632	1.840	1.511	1.570	1.506	1.613
Zn	0.006	0.000	0.000	0.000	0.007	0.000	0.000	0.000	0.000	0.000	0.000	0.000	0.000	0.000
Mn	0.030	0.033	0.000	0.000	0.000	0.000	0.000	0.000	0.000	0.010	0.000	0.000	0.000	0.000
Sum C	5.000	4.978	5.000	5.000	5.000	5.000	5.000	5.000	5.000	5.000	5.000	5.000	5.000	5.000
Mg	0.000	0.000	0.000	0.000	0.000	0.000	0.000	0.000	0.000	0.000	0.000	0.000	0.000	0.000
Fe ²⁺	0.035	0.000	0.027	0.008	0.000	0.009	0.018	0.020	0.035	0.000	0.059	0.034	0.039	0.039
Zn	0.000	0.000	0.006	0.000	0.001	0.007	0.000	0.001	0.000	0.000	0.003	0.012	0.000	0.000
Mn	0.000	0.000	0.031	0.026	0.031	0.035	0.031	0.029	0.023	0.010	0.024	0.021	0.024	0.020
Ca	1.856	1.880	1.837	1.899	1.881	1.886	1.835	1.861	1.870	1.858	1.800	1.832	1.850	1.846
Na	0.109	0.120	0.099	0.066	0.087	0.063	0.116	0.089	0.073	0.132	0.114	0.100	0.087	0.095
Sum B	2.000	2.000	2.000	2.000	2.000	2.000	2.000	2.000	2.000	2.000	2.000	2.000	2.000	2.000
Na	0.337	0.338	0.366	0.388	0.377	0.445	0.315	0.410	0.400	0.313	0.336	0.358	0.346	0.391
K	0.023	0.028	0.022	0.050	0.030	0.044	0.027	0.036	0.046	0.058	0.030	0.038	0.033	0.033
Sum A	0.360	0.366	0.388	0.438	0.407	0.489	0.342	0.446	0.446	0.371	0.366	0.396	0.379	0.425

Anfibolitos												AC51Ampver de	AC51Amp2m arrom	AC51Amp2m arrom2
	AC448-A	AC448-B	AC448-C	AC448-G	AC448-J	AC448-K	AC448-L	AC447-C	AC447-D	AC447-E	AC447-F			
SiO ₂	45.35	44.43	46.48	46.10	46.61	46.51	46.08	43.99	44.43	43.84	45.72	45.35	45.02	47.09
TiO ₂	0.84	0.64	0.77	0.96	0.69	0.80	0.83	0.62	0.71	0.65	0.74	1.41	1.59	1.01
Al ₂ O ₃	12.06	13.52	10.21	10.80	10.82	10.57	11.02	14.05	13.38	14.43	11.83	10.04	9.98	8.58
Fe ₂ O ₃														
Cr ₂ O ₃	0.00	0.03	0.05	0.03	0.03	0.03	0.02	0.00	0.03	0.02	0.08	0.03	0.03	0.03
FeO	16.17	16.48	15.86	15.99	16.34	16.01	16.02	16.99	16.52	16.95	16.86	17.07	17.89	16.81
MnO	0.13	0.14	0.25	0.18	0.18	0.14	0.22	0.22	0.21	0.18	0.22	0.36	0.38	0.34
ZnO														
MgO	10.32	10.05	11.27	10.64	10.94	11.11	10.73	9.48	9.84	9.45	10.26	9.87	9.87	10.95
CaO	10.11	9.98	10.45	9.16	9.97	10.26	10.32	10.06	10.10	9.78	9.75	11.16	11.30	11.39
Na ₂ O	1.22	1.41	0.96	0.96	1.04	1.11	1.13	1.41	1.34	1.38	1.11	1.54	1.62	1.35
K ₂ O	0.37	0.36	0.26	0.31	0.26	0.30	0.28	0.44	0.38	0.39	0.30	0.09	0.09	0.08
F												0.00	0.00	0.00
Cl												0.00	0.00	0.00
Total 1	96.58	97.02	96.55	95.13	96.87	96.82	96.65	97.27	96.94	97.06	96.85	96.90	97.78	97.65
-O≡F	0.00	0.00	0.00	0.00	0.00	0.00	0.00	0.00	0.00	0.00	0.00			
-O≡Cl	0.00	0.00	0.00	0.00	0.00	0.00	0.00	0.00	0.00	0.00	0.00			
Total	96.58	97.02	96.55	95.13	96.87	96.82	96.65	97.27	96.94	97.06	96.85			
Si	6.767	6.691	6.943	6.696	6.529	6.856	6.899	6.852	6.839	6.793	6.471	6.545	6.455	6.742
AlIV	1.233	1.309	1.057	1.304	1.471	1.144	1.101	1.148	1.161	1.207	1.529	1.455	1.545	1.258
Sum T	8.000	8.000	8.000	8.000	8.000	8.000	8.000	8.000	8.000	8.000	8.000	8.000	8.000	8.000
AlVI	0.534	0.440	0.434	0.794	0.870	0.631	0.803	0.727	0.671	0.708	0.906	0.868	0.960	0.798
Fe ³⁺	0.224	0.272	0.251	0.363	0.475	0.338	0.181	0.309	0.341	0.350	0.483	0.443	0.457	0.330
Ti	0.158	0.178	0.112	0.094	0.070	0.085	0.108	0.076	0.089	0.092	0.069	0.079	0.071	0.082
Cr	0.000	0.003	0.004	0.000	0.003	0.006	0.004	0.004	0.003	0.002	0.000	0.004	0.002	0.009
Mg	2.196	2.186	2.407	2.271	2.201	2.477	2.373	2.397	2.435	2.358	2.078	2.161	2.075	2.255
Fe ²⁺	1.889	1.921	1.792	1.479	1.380	1.462	1.531	1.487	1.461	1.490	1.463	1.446	1.435	1.526
Zn	0.000	0.000	0.000	0.000	0.000	0.000	0.000	0.000	0.000	0.000	0.000	0.000	0.000	0.000
Mn	0.000	0.000	0.000	0.000	0.000	0.000	0.000	0.000	0.000	0.000	0.000	0.000	0.000	0.000
Sum C	5.000	5.000	5.000	5.000	5.000	5.000	5.000	5.000	5.000	5.000	5.000	5.000	5.000	5.000
Mg	0.000	0.000	0.000	0.000	0.000	0.000	0.000	0.000	0.000	0.000	0.000	0.000	0.000	0.000
Fe ²⁺	0.028	0.044	0.041	0.170	0.191	0.171	0.296	0.226	0.180	0.151	0.166	0.166	0.215	0.239
Zn	0.000	0.000	0.000	0.000	0.000	0.000	0.000	0.000	0.000	0.000	0.000	0.000	0.000	0.000
Mn	0.046	0.047	0.042	0.017	0.017	0.031	0.023	0.023	0.017	0.027	0.028	0.026	0.022	0.027
Ca	1.785	1.799	1.800	1.599	1.571	1.651	1.469	1.570	1.615	1.630	1.586	1.594	1.542	1.540
Na	0.141	0.110	0.117	0.214	0.221	0.148	0.212	0.181	0.187	0.192	0.220	0.214	0.221	0.194
Sum B	2.000	2.000	2.000	2.000	2.000	2.000	2.000	2.000	2.000	2.000	2.000	2.000	2.000	2.000
Na	0.304	0.357	0.269	0.136	0.179	0.126	0.067	0.116	0.128	0.131	0.183	0.167	0.173	0.124
K	0.017	0.018	0.015	0.070	0.067	0.048	0.058	0.048	0.056	0.053	0.083	0.071	0.073	0.056
Sum A	0.322	0.375	0.284	0.206	0.246	0.174	0.126	0.163	0.184	0.184	0.266	0.238	0.246	0.180

CLORITA

Dunito e Harzburgito

	AC52B31A	AC52B31B	AC52B31E	AC52Eclo5 a	AC52EPx1 2A	AC52EClo3 A	AC52EClo3 C	AC5204p1c hlorite	AC52165p1 chlorite	AC52502p4 chlorite	AC521925p 2chlor	AC522654p 1chlorite
SiO ₂	31.38	32.05	31.55	32.02	33.61	26.95	33.14	29.54	34.31	33.22	34.35	33.83
TiO ₂	0.07	0.05	0.04	0.03	0.03	0.12	0.00	0.02	0.01	0.03	0.05	0.04
Al ₂ O ₃	15.88	13.74	16.18	14.24	11.69	21.09	12.69	17.81	14.51	16.30	14.14	14.65
Cr ₂ O ₃	0.89	1.22	1.99	1.82	2.77	3.30	2.07	1.32	2.17	0.50	2.14	1.28
FeO	2.69	2.89	2.62	2.27	3.05	3.18	2.44	2.92	2.49	2.47	2.53	2.24
MgO	34.21	34.45	33.79	33.24	34.12	31.13	34.79	32.94	32.81	32.38	32.93	33.73
MnO	0.03	0.00	0.03	0.00	0.04	0.00	0.02	0.02	0.02	0.01	0.01	0.00
NiO	0.00	0.00	0.00	0.00	0.00	0.00	0.00	0.00	0.00	0.00	0.00	0.00
CaO	0.01	0.00	0.01	0.00	0.30	0.02	0.01	0.02	0.01	0.02	0.02	0.01
Na ₂ O	0.06	0.05	0.05	0.00	0.01	0.00	0.00	0.00	0.03	0.01	0.03	0.00
K ₂ O	0.03	0.01	0.04	0.01	0.00	0.00	0.00	0.01	0.01	0.01	0.02	0.00
F	0.00	0.00	0.00	0.00	0.00	0.00	0.00	0.00	0.00	0.00	0.00	0.00
Cl	0.00	0.02	0.00	0.01	0.00	0.00	0.00	0.00	0.00	0.00	0.00	0.00
H ₂ O	12.44	12.30	12.56	12.23	12.41	12.36	12.42	12.31	12.66	12.52	12.63	12.61
Total	97.70	96.78	98.84	95.86	98.04	98.14	97.59	96.90	99.03	97.47	98.85	98.39
-O≡F												
-O≡Cl												
Total	97.70	96.78	98.84	95.86	98.04	98.14	97.59	96.90	99.03	97.47	98.85	98.39

Cations normalizados na base de 28 oxigênios

	Clinochlore	Penninite	Clinochlore	Penninite	Penninite	Sheridanite	Penninite	Clinoclore	Penninite	Penninite	Penninite	Penninite
Si	6.045	6.243	6.018	6.274	6.491	5.227	6.395	5.755	6.494	6.360	6.517	6.432
AlIV	1.955	1.757	1.982	1.726	1.509	2.773	1.605	2.245	1.506	1.640	1.483	1.568
Sum Z	8.000	8.000	8.000	8.000	8.000	8.000	8.000	8.000	8.000	8.000	8.000	8.000
AlVI	1.650	1.396	1.656	1.563	1.151	2.048	1.281	1.843	1.731	2.036	1.678	1.713
Ti	0.010	0.007	0.005	0.004	0.004	0.018	0.000	0.003	0.001	0.004	0.008	0.005
Mg	9.824	10.003	9.609	9.710	9.821	9.002	10.008	9.564	9.260	9.240	9.314	9.557
Fe2+	0.434	0.470	0.417	0.372	0.493	0.515	0.393	0.475	0.394	0.395	0.401	0.356
Ni	0.000	0.000	0.000	0.000	0.000	0.000	0.000	0.000	0.000	0.000	0.000	0.000
Mn	0.004	0.000	0.004	0.000	0.007	0.000	0.004	0.003	0.004	0.002	0.002	0.001
Ca	0.002	0.000	0.001	0.000	0.062	0.004	0.002	0.005	0.002	0.003	0.003	0.002
Na	0.024	0.019	0.018	0.002	0.004	0.000	0.000	0.000	0.013	0.002	0.009	0.001
K	0.008	0.003	0.011	0.003	0.000	0.000	0.000	0.001	0.003	0.003	0.004	0.000
Sum Y	11.955	11.900	11.722	11.655	11.543	11.587	11.688	11.895	11.407	11.686	11.420	11.635
OH	16.000	15.995	16.000	15.998	16.000	16.000	16.000	16.000	16.000	16.000	16.000	16.000
F	0.000	0.000	0.000	0.000	0.000	0.000	0.000	0.000	0.000	0.000	0.000	0.000
Cl	0.000	0.005	0.000	0.002	0.000	0.000	0.000	0.000	0.000	0.000	0.000	0.000

Peridotito	Peridotitos hospedeiros dos cromititos					Cromititos						
	AC53Jp3br u1a	AC77BClo4 A	AC77BClo4 B	AC80B2clo r1c	AC78Bclo4 a	AC20M2Ch Iorite	AC20M2Ch Iorite2	AC77ARclo r1a	AC77ARclo r2a	AC77Cclor 2b	AC77Cclor 5a	AC77C2Inc I1b
SiO ₂	34.40	30.88	30.73	30.09	31.34	30.91	29.04	30.70	29.88	30.62	30.63	37.09
TiO ₂	0.01	0.04	0.00	0.00	0.00	0.03	0.02	0.07	0.05	0.00	0.00	0.28
Al ₂ O ₃	13.71	15.06	17.27	17.61	14.71	20.89	21.74	17.97	19.85	18.68	19.06	19.41
Cr ₂ O ₃	0.66	1.99	1.23	0.63	2.20	2.12	1.65	0.90	1.67	0.29	0.85	1.60
FeO	3.58	2.66	2.78	2.73	2.81	1.32	1.83	1.75	2.05	1.74	2.17	2.11
MgO	33.53	32.53	31.83	32.78	33.53	31.67	31.41	33.16	32.05	33.20	32.13	24.60
MnO	0.02	0.01	0.00	0.02	0.01	0.02	0.01	0.02	0.02	0.02	0.03	0.02
NiO	0.00	0.00	0.00	0.00	0.00	0.00	0.00	0.00	0.00	0.00	0.00	0.00
CaO	0.01	0.02	0.02	0.02	0.02	0.01	0.00	0.00	0.01	0.03	0.01	0.04
Na ₂ O	0.02	0.00	0.01	0.02	0.01	0.02	0.00	0.03	0.01	0.01	0.00	0.00
K ₂ O	0.02	0.02	0.00	0.02	0.02	0.00	0.00	0.02	0.01	0.02	0.00	0.00
F	0.00	0.10	0.03	0.05	0.01	0.00	0.00	0.00	0.07	0.04	0.00	0.00
Cl	0.00	0.01	0.00	0.00	0.00	0.00	0.00	0.00	0.00	0.04	0.00	0.00
H ₂ O	12.57	12.08	12.25	12.25	12.30	12.81	12.57	12.44	12.51	12.44	12.47	12.78
Total	98.53	95.40	96.14	96.22	96.95	99.79	98.26	97.05	98.15	97.11	97.35	97.93
-O≡F												
-O≡Cl												
Total	98.53	95.40	96.14	96.22	96.95	99.79	98.26	97.05	98.15	97.11	97.35	97.93
Si	6.559	6.101	6.004	5.877	6.108	5.783	5.537	5.916	5.709	5.884	5.887	6.956
AlIV	1.441	1.899	1.996	2.123	1.892	2.217	2.463	2.084	2.291	2.116	2.113	1.044
Sum Z	8.000	8.000	8.000	8.000	8.000	8.000	8.000	8.000	8.000	8.000	8.000	8.000
AlVI	1.639	1.607	1.981	1.931	1.485	2.389	2.421	1.998	2.179	2.114	2.202	3.246
Ti	0.001	0.006	0.000	0.000	0.000	0.005	0.002	0.010	0.007	0.000	0.000	0.039
Mg	9.529	9.582	9.272	9.545	9.741	8.833	8.930	9.527	9.131	9.511	9.203	6.876
Fe2+	0.570	0.439	0.454	0.447	0.457	0.206	0.291	0.283	0.327	0.279	0.348	0.331
Ni	0.000	0.000	0.000	0.000	0.000	0.000	0.000	0.000	0.000	0.000	0.000	0.000
Mn	0.004	0.002	0.000	0.003	0.002	0.003	0.001	0.003	0.002	0.004	0.004	0.003
Ca	0.002	0.005	0.004	0.005	0.004	0.001	0.001	0.000	0.002	0.006	0.003	0.008
Na	0.006	0.000	0.005	0.006	0.002	0.006	0.000	0.010	0.003	0.002	0.001	0.000
K	0.005	0.006	0.001	0.005	0.005	0.000	0.000	0.004	0.001	0.004	0.000	0.000
Sum Y	11.756	11.645	11.717	11.941	11.696	11.443	11.646	11.835	11.653	11.920	11.763	10.503
OH	16.000	15.935	15.983	15.971	15.996	16.000	16.000	16.000	15.959	15.962	15.999	16.000
F	0.000	0.060	0.017	0.029	0.004	0.000	0.000	0.000	0.041	0.027	0.001	0.000
Cl	0.000	0.005	0.000	0.000	0.000	0.000	0.000	0.000	0.000	0.012	0.000	0.000
Penninite	Clinochlore	Clinochlore	Clinochlore	Clinochlore	Clinochlore	Clinoclore	Sheridanite	Clinochlore	Clinochlore	Clinochlore	Clinochlore	Penninite

CLORITA

Cromititos

	AC80B1Rcl or2a	AC80B1Rcl or1b	CSP4A	CSP4B	CSP4C	CSP1A	CNIQUIA1 B	CNIQUIA1 D	CNIQUIA2 B	CNIQUIA1 A	AC78C1p1 chl
SiO ₂	28.37	28.03	31.13	31.17	31.28	30.14	30.92	28.37	27.26	28.01	30.02
TiO ₂	0.07	0.05	0.06	0.04	0.00	0.02	0.06	0.04	0.00	0.00	0.00
Al ₂ O ₃	20.93	22.79	18.61	17.61	18.17	20.10	14.95	21.17	23.96	21.59	20.63
Cr ₂ O ₃	1.53	1.59	1.04	1.47	0.19	0.95	2.06	0.85	1.13	1.51	0.11
FeO	1.15	1.37	1.08	1.23	1.45	1.27	1.04	1.17	1.03	1.43	0.99
MgO	31.70	31.18	35.06	35.12	34.95	34.69	34.42	32.91	32.41	32.45	32.41
MnO	0.00	0.00	0.02	0.03	0.02	0.03	0.01	0.00	0.00	0.00	0.00
NiO	0.00	0.00		0.09						0.12	0.04
CaO	0.00	0.00	0.00	0.01	0.00	0.00	0.00	0.01	0.02	0.00	0.00
Na ₂ O	0.00	0.00	0.00	0.01	0.00	0.00	0.03	0.06	0.00	0.04	0.01
K ₂ O	0.01	0.00	0.00	0.00	0.00	0.01	0.01	0.05	0.02	0.03	0.00
F	0.02	0.03	0.10	0.00	0.00	0.05	0.48	0.26	0.10	0.16	0.00
Cl	0.01	0.00	0.01	0.00	0.03	0.01	0.01	0.06	0.02	0.02	0.00
H ₂ O	12.31	12.48	12.77	12.74	12.69	12.80	12.08	12.35	12.58	12.42	12.48
Total	96.09	97.52	99.88	99.52	98.79	100.08	96.05	97.29	98.53	97.77	96.71
-O≡F		-0.04	0.00	0.00	-0.02	-0.20	-0.11	-0.04	-0.07		
-O≡Cl		0.00	0.00	-0.01	0.00	0.00	-0.01	0.00	0.00		
Total	96.09	97.52	99.93	99.52	98.80	100.10	96.25	97.42	98.58	97.84	

Si	5.519	5.376	5.817	5.866	5.907	5.631	6.021	5.447	5.172	5.373	5.764
AlIV	2.481	2.624	2.183	2.134	2.093	2.369	1.979	2.553	2.828	2.627	2.236
Sum Z	8.000	8.000	8.000	8.000	8.000	8.000	8.000	8.000	8.000	8.000	8.000
AlVI	2.318	2.527	1.916	1.773	1.950	2.056	1.452	2.237	2.528	2.253	2.432
Ti	0.010	0.007	0.008	0.006	0.000	0.003	0.008	0.005	0.000	0.000	0.001
Mg	9.194	8.917	9.769	9.852	9.839	9.663	9.995	9.420	9.165	9.281	9.276
Fe ²⁺	0.187	0.219	0.168	0.194	0.229	0.199	0.169	0.188	0.163	0.230	0.158
Ni	0.000	0.000	0.000	0.013	0.000	0.000	0.000	0.000	0.000	0.019	0.007
Mn	0.000	0.000	0.004	0.004	0.003	0.005	0.001	0.000	0.000	0.000	0.000
Ca	0.000	0.000	0.000	0.003	0.001	0.000	0.000	0.003	0.004	0.000	0.001
Na	0.000	0.000	0.000	0.002	0.000	0.001	0.010	0.023	0.000	0.016	0.005
K	0.002	0.001	0.000	0.000	0.000	0.002	0.003	0.011	0.005	0.007	0.000
Sum Y	11.712	11.671	11.864	11.847	12.023	11.929	11.638	11.888	11.865	11.805	11.880
OH	15.985	15.982	15.936	15.999	15.990	15.966	15.704	15.823	15.932	15.899	16.000
F	0.010	0.018	0.061	0.000	0.000	0.030	0.293	0.157	0.062	0.094	
Cl	0.005	0.000	0.003	0.001	0.010	0.004	0.003	0.020	0.006	0.007	
	Sheridanite	Sheridanite	Clinochlore	Clinochlore	Clinochlore	Clinochlore	Clinochlore	Sheridanite	Sheridanite	Sheridanite	clinoclore

PLAGIOCLÁSIO

Metagabros de El Picacho

Oxido	AC33C4-A	AC33C4-B	AC33C4-C	AC33C4-D	AC33C4-E	AC33C4-F	AC33C2-A	AC33C3P	CMK40D27-A	CMK40D27-B	CMK40D28-A	CMK40D28-B	CMK40D28-C	CMK40D21-A
SiO ₂	47.43	53.87	54.16	46.99	47.20	53.62	47.53	47.63	45.88	45.17	52.60	49.51	50.60	44.95
TiO ₂	0.00	0.00	0.00	0.00	0.00	0.00	0.00	0.00	0.00	0.00	0.00	0.00	0.00	0.00
Al ₂ O ₃	34.60	30.11	30.23	34.64	34.58	30.24	34.69	34.09	35.86	36.37	31.27	29.81	32.31	36.09
Fe ₂ O ₃	0.05	0.04	0.01	0.01	0.03	0.05	0.14	0.10	0.02	0.07	0.04	1.78	0.01	0.11
BaO	0.00	0.00	0.00	0.00	0.01	0.04	0.01	0.00	0.00	0.07	0.00	0.01	0.00	0.00
SrO	0.07	0.07	0.00	0.00	0.00	0.00	0.00	0.00	0.00	0.00	0.03	0.12	0.00	0.00
CaO	16.25	11.54	11.06	16.39	15.88	11.49	16.40	15.49	16.60	17.58	11.88	14.12	12.95	17.24
Na ₂ O	2.01	4.75	4.81	1.48	1.45	4.77	1.85	2.10	1.00	0.61	4.14	3.39	3.40	0.67
K ₂ O	0.00	0.06	0.04	0.03	0.02	0.02	0.01	0.00	0.01	0.01	0.01	0.03	0.04	0.01
Total 1	100.41	100.44	100.32	99.53	99.17	100.24	100.63	99.40	99.36	99.88	99.97	98.77	99.31	99.06

Cations normalizados na base de 8 oxigênios

	AC33C4-A	AC33C4-B	AC33C4-C	AC33C4-D	AC33C4-E	AC33C4-F	AC33C2-A	AC33C3P	CMK40D27-A	CMK40D27-B	CMK40D28-A	CMK40D28-B	CMK40D28-C	CMK40D21-A
Si	2.162	2.419	2.430	2.157	2.170	2.414	2.161	2.187	2.110	2.075	2.373	2.298	2.306	2.079
Al	1.858	1.594	1.599	1.874	1.874	1.604	1.859	1.844	1.944	1.969	1.663	1.631	1.736	1.968
Fe ³⁺	0.002	0.001	0.000	0.000	0.001	0.002	0.005	0.003	0.001	0.002	0.001	0.062	0.000	0.004
Ti	0.000	0.000	0.000	0.000	0.000	0.000	0.000	0.000	0.000	0.000	0.000	0.000	0.000	0.000
Na	0.178	0.414	0.418	0.132	0.130	0.416	0.163	0.187	0.089	0.054	0.362	0.305	0.301	0.060
Ca	0.794	0.555	0.532	0.806	0.782	0.554	0.799	0.762	0.818	0.865	0.574	0.702	0.632	0.855
K	0.000	0.003	0.002	0.001	0.001	0.001	0.000	0.000	0.001	0.001	0.000	0.002	0.002	0.001
Ba	0.000	0.000	0.000	0.000	0.000	0.001	0.000	0.000	0.000	0.001	0.000	0.000	0.000	0.000
Sr	0.004	0.004	0.000	0.000	0.000	0.000	0.000	0.000	0.000	0.000	0.002	0.007	0.000	0.000
Total	4.997	4.991	4.981	4.972	4.958	4.992	4.988	4.983	4.962	4.967	4.976	5.008	4.977	4.965
Or	0.01	0.34	0.26	0.16	0.14	0.22	0.06	0.00	0.06	0.21	0.03	0.19	0.24	0.07
Ab	18.28	42.54	43.92	14.01	14.20	42.79	16.97	19.69	9.82	5.89	38.67	30.22	32.14	6.52
An	81.70	57.13	55.82	85.84	85.66	56.99	82.97	80.31	90.12	93.89	61.30	69.59	67.62	93.41

Metagabros de El Picacho

Oxido	CMK40D26-A	CMK40D23-CMK40D22-CMK40D22-CMK040AP CMK040AP CMK040AP CMK040P3 CMK040AP CMK040AP CMK040AP CMK040AP CMK040AP CMK040AP CMK040AP CMK040AP CMK040P3 CMK040AP													
		B	A	C	4H	4L	4N	3BR	C	3D	3E	3F	3G	H	3I
SiO ₂	46.74	44.85	53.56	45.30	44.16	54.32	55.94	60.00	44.32	45.08	55.69	51.59	47.75	44.56	51.48
TiO ₂	0.00	0.00	0.00	0.00	0.00	0.00	0.00	0.00	0.00	0.00	0.00	0.00	0.00	0.00	0.00
Al ₂ O ₃	34.83	34.31	30.46	36.21	35.62	28.42	27.21	25.00	35.26	35.38	27.69	31.00	35.57	35.25	31.66
Fe ₂ O ₃	0.14	0.11	0.08	0.16	0.22	0.10	0.04	0.06	0.03	0.01	0.03	0.05	0.03	0.04	0.04
BaO	0.00	0.00	0.00	0.00	0.07	0.00	0.00	0.00	0.00	0.04	0.19	0.00	0.00	0.04	0.00
SrO	0.04	0.00	0.00	0.00	0.00	0.00	0.00	0.00	0.00	0.00	0.00	0.00	0.00	0.00	0.00
CaO	15.59	16.18	11.16	17.23	18.52	10.42	9.66	6.16	18.29	18.11	9.63	13.14	16.76	18.42	13.39
Na ₂ O	1.71	1.25	4.63	0.47	0.61	5.68	6.48	8.26	0.83	1.26	6.00	3.94	1.74	0.79	3.96
K ₂ O	0.02	0.07	0.03	0.02	0.02	0.02	0.05	0.07	0.02	0.01	0.03	0.05	0.08	0.02	0.05
Total 1	99.08	96.77	99.92	99.38	99.21	98.96	99.39	99.55	98.76	99.88	99.26	99.77	101.93	99.12	100.58

	CMK40D26-A	CMK40D23-CMK40D22-CMK40D22-CMK040AP CMK040AP CMK040AP CMK040P3 CMK040AP CMK040AP CMK040AP CMK040AP CMK040AP CMK040AP CMK040P3 CMK040AP													
		B	A	C	4H	4L	4N	3BR	C	3D	3E	3F	3G	H	3I
Si	2.153	2.122	2.414	2.086	2.0536728	2.474	2.533	2.683	2.068	2.080	2.523	2.345	2.145	2.073	2.324
Al	1.891	1.913	1.618	1.965	1.953	1.525	1.452	1.318	1.939	1.924	1.479	1.661	1.883	1.932	1.684
Fe ³⁺	0.005	0.004	0.003	0.005	0.008	0.003	0.001	0.002	0.001	0.000	0.001	0.002	0.001	0.001	0.001
Ti	0.000	0.000	0.000	0.000	0.000	0.000	0.000	0.000	0.000	0.000	0.000	0.000	0.000	0.000	0.000
Na	0.153	0.115	0.404	0.042	0.055	0.501	0.569	0.716	0.075	0.112	0.527	0.347	0.152	0.072	0.346
Ca	0.769	0.820	0.539	0.850	0.923	0.508	0.468	0.295	0.915	0.895	0.468	0.640	0.807	0.918	0.648
K	0.001	0.004	0.002	0.001	0.001	0.001	0.003	0.004	0.001	0.000	0.002	0.003	0.004	0.001	0.003
Ba	0.000	0.000	0.000	0.000	0.001	0.000	0.000	0.000	0.000	0.001	0.003	0.000	0.000	0.001	0.000
Sr	0.002	0.000	0.000	0.000	0.000	0.000	0.000	0.000	0.000	0.000	0.000	0.000	0.000	0.000	0.000
Total	4.976	4.979	4.979	4.950	4.994	5.013	5.027	5.018	5.000	5.014	5.002	4.998	4.991	4.997	5.007
Or	0.12	0.44	0.20	0.11	0.23	0.11	0.29	0.40	0.11	0.11	0.50	0.29	0.46	0.18	0.30
Ab	16.58	12.20	42.77	4.67	5.64	49.60	54.68	70.52	7.60	11.14	52.72	35.08	15.74	7.22	34.74
An	83.30	87.35	57.03	95.22	94.13	50.29	45.03	29.07	92.29	88.75	46.78	64.63	83.79	92.61	64.96

Metagabros de El Picacho

Oxido	CMK040AP 3J	CMK040AP 3K	CMK040AP 6B	AC59A1C	AC59A1G	AC59A4A	AC59A4B	AC59A4C	AC59A2A	AC59A2B	CMK1442E	CMK1442F	CMK1442G	AC25p3pla 1
SiO ₂	45.85	52.29	48.80	43.11	42.98	43.00	44.17	42.77	43.66	42.85	61.01	60.34	60.25	45.49
TiO ₂	0.00	0.00	0.00	0.00	0.00	0.00	0.00	0.00	0.00	0.00	0.00	0.00	0.00	0.00
Al ₂ O ₃	33.76	29.42	33.34	35.37	35.95	35.30	35.32	35.61	36.28	35.66	24.16	24.77	24.32	35.10
Fe ₂ O ₃	0.00	0.06	0.08	0.01	0.01	0.00	0.01	0.03	0.05	0.03	0.00	0.00	0.00	0.01
BaO	0.11	0.12	0.00	0.00	0.10	0.04	0.00	0.07	0.00	0.00	0.18	0.00	0.00	0.01
SrO	0.00	0.00	0.00	0.00	0.00	0.00	0.00	0.00	0.00	0.00	0.00	0.00	0.00	0.00
CaO	17.02	11.65	15.79	18.86	19.16	19.07	18.55	19.42	19.51	19.01	5.72	6.09	5.82	17.71
Na ₂ O	1.52	5.03	2.24	0.54	0.29	0.55	0.78	0.28	0.34	0.32	8.56	8.28	8.37	1.45
K ₂ O	0.01	0.04	0.02	0.03	0.01	0.00	0.02	0.04	0.00	0.03	0.04	0.04	0.02	0.01
Total 1	98.26	98.61	100.28	97.91	98.50	97.96	98.85	98.20	99.83	97.90	99.66	99.51	98.79	99.77

	CMK040AP 3J	CMK040AP 3K	CMK040AP 6B	AC59A1C	AC59A1G	AC59A4A	AC59A4B	AC59A4C	AC59A2A	AC59A2B	CMK1442E	CMK1442F	CMK1442G	AC25p3pla 1
Si	2.143	2.403	2.221	2.035	2.018	2.031	2.061	2.017	2.022	2.023	2.723	2.696	2.710	2.098
Al	1.860	1.593	1.789	1.967	1.989	1.965	1.943	1.979	1.980	1.984	1.271	1.304	1.289	1.908
Fe ³⁺	0.000	0.002	0.003	0.000	0.000	0.000	0.000	0.001	0.002	0.001	0.000	0.000	0.000	0.000
Ti	0.000	0.000	0.000	0.000	0.000	0.000	0.000	0.000	0.000	0.000	0.000	0.000	0.000	0.000
Na	0.138	0.449	0.198	0.049	0.026	0.050	0.070	0.026	0.031	0.029	0.741	0.717	0.730	0.130
Ca	0.852	0.574	0.770	0.953	0.964	0.965	0.928	0.981	0.968	0.962	0.273	0.292	0.280	0.875
K	0.000	0.002	0.001	0.002	0.001	0.000	0.001	0.002	0.000	0.002	0.002	0.002	0.001	0.001
Ba	0.002	0.002	0.000	0.000	0.002	0.001	0.000	0.001	0.000	0.000	0.003	0.000	0.000	0.000
Sr	0.000	0.000	0.000	0.000	0.000	0.000	0.000	0.000	0.000	0.000	0.000	0.000	0.000	0.000
Total	4.996	5.025	4.983	5.007	5.000	5.012	5.003	5.007	5.003	5.000	5.013	5.011	5.011	5.013
Or	0.23	0.45	0.14	0.15	0.25	0.09	0.11	0.33	0.00	0.18	0.51	0.21	0.11	0.08
Ab	13.88	43.68	20.42	4.90	2.64	4.94	7.05	2.53	3.09	2.95	72.68	70.94	72.17	12.88
An	85.89	55.87	79.43	94.95	97.11	94.97	92.83	97.13	96.91	96.87	26.81	28.85	27.72	87.04

Meta gabros de Boquerón

Oxido	CMK38BPA	CMK38B6-A	CMK38B6-B	CMK38B6-C	CMK38B6-D	CMK38B6-E	CMK38B6-F	CMK38B5-A	CMK38B5-B	CMK38B5-C	CMK38B5-D
SiO ₂	46.01	50.52	52.09	52.55	57.40	46.43	59.86	54.62	62.29	59.00	48.64
TiO ₂	0.00	0.00	0.00	0.00	0.00	0.00	0.00	0.00	0.00	0.00	0.00
Al ₂ O ₃	35.89	32.48	31.60	30.75	28.38	33.14	27.02	30.17	24.48	26.16	33.66
Fe ₂ O ₃	0.11	0.06	0.08	0.20	0.04	0.13	0.05	0.18	0.07	0.07	0.09
BaO	0.00	0.00	0.00	0.01	0.00	0.00	0.01	0.00	0.01	0.06	0.00
SrO	0.00	0.00	0.00	0.01	0.00	0.00	0.00	0.00	0.00	0.00	0.00
CaO	18.02	13.73	12.80	12.00	7.64	15.16	7.38	10.70	5.04	7.04	14.68
Na ₂ O	1.00	3.74	3.45	4.36	7.96	2.03	7.13	4.58	8.14	6.89	2.50
K ₂ O	0.00	0.01	0.04	0.01	0.04	0.02	0.02	0.04	0.03	0.04	0.02
Total 1	101.04	100.53	100.06	99.88	101.46	96.90	101.47	100.29	100.06	99.26	99.58

Cations normalizados na base de 8 oxigênios

	CMK38BPA	CMK38B6-A	CMK38B6-B	CMK38B6-C	CMK38B6-D	CMK38B6-E	CMK38B6-F	CMK38B5-A	CMK38B5-B	CMK38B5-C	CMK38B5-D
Si	2.093	2.285	2.352	2.378	2.538	2.187	2.626	2.445	2.749	2.643	2.223
Al	1.924	1.732	1.681	1.640	1.479	1.840	1.397	1.592	1.273	1.381	1.813
Fe ₃	0.004	0.002	0.003	0.007	0.001	0.005	0.002	0.006	0.002	0.002	0.003
Ti	0.000	0.000	0.000	0.000	0.000	0.000	0.000	0.000	0.000	0.000	0.000
Na	0.089	0.328	0.302	0.383	0.682	0.185	0.606	0.397	0.696	0.599	0.222
Ca	0.878	0.665	0.619	0.582	0.362	0.765	0.347	0.513	0.238	0.338	0.719
K	0.000	0.000	0.002	0.001	0.002	0.001	0.001	0.002	0.002	0.002	0.001
Ba	0.000	0.000	0.000	0.000	0.000	0.000	0.000	0.000	0.000	0.001	0.000
Sr	0.000	0.000	0.000	0.000	0.000	0.000	0.000	0.000	0.000	0.000	0.000
Total	4.987	5.012	4.959	4.990	5.064	4.984	4.979	4.956	4.962	4.966	4.980
Or	0.01	0.03	0.22	0.10	0.19	0.13	0.17	0.23	0.23	0.33	0.10
Ab	9.16	33.03	32.71	39.65	65.24	19.45	63.52	43.53	74.32	63.70	23.54
An	90.83	66.94	67.07	60.25	34.57	80.42	36.32	56.24	25.45	35.96	76.36

Metagabros de Boquerón

Oxido	CMK38B6-G	CMK38BPX	CMK38Bp6pl	AC61Tp1pla1a	AC61Tp1pla1b	AC61Tp1pla1c	AC61Tp1plag3	AC61Tp1anffi
SiO ₂	44.93	48.17	58.31	56.08	60.48	59.72	61.03	55.33
TiO ₂	0.00	0.00						
Al ₂ O ₃	36.02	33.96	26.85	28.34	25.51	26.14	25.02	28.14
Fe ₂ O ₃	0.17	0.29	0.04	0.09	0.08	0.03	0.05	0.51
BaO	0.00	0.00						
SrO	0.00	0.00						
CaO	16.93	15.98	8.02	10.39	6.76	7.62	6.37	10.03
Na ₂ O	0.77	1.90	6.85	5.80	7.80	7.19	7.96	5.77
K ₂ O	0.00	0.00	0.04	0.04	0.05	0.05	0.05	0.04
Total 1	98.82	100.30	100.11	100.75	100.68	100.74	100.49	99.82

	CMK38B6-G	CMK38BPX	CMK38Bp6pl	AC61Tp1pla1a	AC61Tp1pla1b	AC61Tp1pla1c	AC61Tp1plag3	AC61Tp1anffi
Si	2.082	2.194	2.600	2.504	2.673	2.642	2.698	2.496
Al	1.967	1.823	1.411	1.491	1.329	1.363	1.304	1.496
Fe ₃	0.006	0.010	0.001	0.003	0.003	0.001	0.002	0.017
Ti	0.000	0.000	0.000	0.000	0.000	0.000	0.000	0.000
Na	0.069	0.168	0.592	0.502	0.669	0.617	0.683	0.504
Ca	0.841	0.780	0.383	0.497	0.320	0.361	0.302	0.485
K	0.000	0.000	0.003	0.002	0.003	0.003	0.003	0.002
Ba	0.000	0.000	0.000	0.000	0.000	0.000	0.000	0.000
Sr	0.000	0.000	0.000	0.000	0.000	0.000	0.000	0.000
Total	4.965	4.974	4.991	5.001	4.997	4.986	4.992	5.001
Or	0.00	0.00	0.26	0.23	0.26	0.28	0.29	0.24
Ab	7.58	17.73	60.56	50.15	67.46	62.88	69.15	50.87
An	92.42	82.27	39.18	49.62	32.29	36.83	30.56	48.89

Anfibolitos de Santa Elena

Oxido	P/ANFIBOL ITOCA	anfibolito											
		PLAGIOCL ASIO1MITA DE	PLAGIOCL ASIO1INFE RIOR	PLAGIOCL ASIO1BAIX O	PLAGIOCL ASIO1BAIX OREPETID O	PLAGIOCL ASIO2BOR DA1	PLAGIOCL ASIO2MITA DE	PLAGIOCL ASIO2MITA DE2	PLAGIOCL ASIO2INFE RIOR	PLAGIOCL ASIO3BOR DA1	PLAGIOCL ASI3CENT RO2	PLAG4PT1	PLAG4PT12
SiO ₂	58.73	58.72	58.10	58.87	59.34	58.33	58.81	58.61	58.71	57.76	58.06	59.36	59.52
TiO ₂	0.00	0.00	0.00	0.00	0.00	0.00	0.00	0.00	0.00	0.00	0.00	0.00	0.00
Al ₂ O ₃	26.41	25.57	26.98	26.40	26.37	27.12	26.61	26.63	26.53	26.77	26.76	26.17	26.00
Fe ₂ O ₃	0.03	0.02	0.01	0.08	0.13	0.05	0.11	0.01	0.00	0.04	0.03	0.02	0.11
BaO	0.00	0.00	0.01	0.00	0.09	0.00	0.00	0.03	0.00	0.17	0.00	0.00	0.07
SrO	0.00	0.00	0.00	0.02	0.00	0.00	0.00	0.00	0.00	0.00	0.00	0.00	0.00
CaO	8.16	7.43	8.75	8.08	8.02	8.68	8.29	8.43	8.05	8.59	8.48	7.52	7.77
Na ₂ O	7.52	7.77	6.93	7.47	7.71	7.22	7.32	7.15	7.32	6.98	7.16	7.65	7.71
K ₂ O	0.08	0.10	0.06	0.09	0.08	0.03	0.07	0.08	0.07	0.07	0.08	0.07	0.07
Total 1	100.94	99.61	100.86	101.01	101.74	101.43	101.22	100.93	100.67	100.38	100.56	100.79	101.24

Cations normalizados na base de 8 oxigênios

P/ANFIBOL ITOCA	PLAGIOCL ASIO1MITA DE	PLAGIOCL ASIO1INFE RIOR	PLAGIOCL ASIO1BAIX O	PLAGIOCL ASIO1BAIX OREPETID O	PLAGIOCL ASIO2BOR DA1	PLAGIOCL ASIO2MITA DE	PLAGIOCL ASIO2MITA DE2	PLAGIOCL ASIO2INFE RIOR	PLAGIOCL ASIO3BOR DA1	PLAGIOCL ASI3CENT RO2	PLAG4PT1	PLAG4PT12	
Si	2.606	2.636	2.581	2.609	2.614	2.579	2.602	2.600	2.608	2.582	2.587	2.631	2.631
Al	1.381	1.353	1.413	1.379	1.369	1.413	1.388	1.392	1.389	1.411	1.405	1.367	1.354
Fe ₃	0.001	0.001	0.000	0.003	0.004	0.002	0.004	0.000	0.000	0.001	0.001	0.001	0.004
Ti	0.000	0.000	0.000	0.000	0.000	0.000	0.000	0.000	0.000	0.000	0.000	0.000	0.000
Na	0.647	0.676	0.597	0.642	0.658	0.619	0.628	0.615	0.631	0.605	0.618	0.657	0.660
Ca	0.388	0.357	0.417	0.384	0.379	0.411	0.393	0.400	0.383	0.411	0.405	0.357	0.368
K	0.005	0.006	0.004	0.005	0.005	0.002	0.004	0.005	0.004	0.004	0.004	0.004	0.004
Ba	0.000	0.000	0.000	0.000	0.002	0.000	0.000	0.000	0.000	0.003	0.000	0.000	0.001
Sr	0.000	0.000	0.000	0.001	0.000	0.000	0.000	0.000	0.000	0.000	0.000	0.000	0.000
Total	5.029	5.029	5.012	5.023	5.031	5.024	5.019	5.013	5.015	5.016	5.021	5.016	5.022
Or	0.45	0.55	0.37	0.52	0.59	0.17	0.40	0.49	0.37	0.68	0.44	0.37	0.48
Ab	62.23	65.07	58.68	62.26	63.10	59.98	61.26	60.28	61.99	59.11	60.16	64.54	63.92
An	37.32	34.38	40.95	37.23	36.31	39.84	38.34	39.23	37.64	40.21	39.41	35.08	35.60

PLAGIOCLÁSIO

Anfibolitos de Santa Elena

anfibolitos								Granada anfibolito				
Oxido	PLAG4PT2	PLAG4PT3	PLAG4PT32	PLAG4PT4	AC51pla2	AC51pla1a	AC51pla1B	AC446-A	AC446-B	AC446-C	AC448-D	AC448-E
SiO ₂	58.44	57.38	57.06	58.37	59.67	59.82	60.43	59.29	61.33	60.94	59.87	59.02
TiO ₂	0.00	0.00	0.00	0.00				0.00	0.00	0.00	0.00	0.00
Al ₂ O ₃	27.25	27.71	27.61	26.88	26.38	25.86	25.92	26.48	25.28	25.56	26.27	26.90
Fe2O ₃	0.10	0.09	0.04	0.08	0.07	0.04	0.04	0.10	0.06	0.09	0.09	0.08
BaO	0.15	0.00	0.00	0.04				0.00	0.00	0.04	0.00	0.00
SrO	0.00	0.00	0.00	0.00				0.00	0.00	0.00	0.00	0.00
CaO	8.82	9.45	9.32	8.55	7.38	6.77	6.91	7.44	5.33	6.28	7.06	7.95
Na ₂ O	7.05	6.48	6.69	7.02	7.76	8.00	7.92	7.46	8.15	7.88	7.47	7.14
K ₂ O	0.05	0.05	0.07	0.08	0.07	0.06	0.07	0.09	0.87	0.15	0.08	0.04
Total 1	101.86	101.15	100.79	101.01	101.32	100.56	101.29	100.87	101.02	100.94	100.84	101.13
	PLAG4PT2	PLAG4PT3	PLAG4PT32	PLAG4PT4	AC441-H	AC441-H	AC441-H	AC446-A	AC446-B	AC446-C	AC448-D	AC448-E
Si	2.575	2.546	2.543	2.589	2.630	2.652	2.658	2.624	2.702	2.684	2.644	2.606
Al	1.415	1.449	1.450	1.405	1.370	1.351	1.344	1.381	1.313	1.327	1.367	1.400
Fe3	0.003	0.003	0.001	0.003	0.002	0.001	0.001	0.003	0.002	0.003	0.003	0.003
Ti	0.000	0.000	0.000	0.000	0.000	0.000	0.000	0.000	0.000	0.000	0.000	0.000
Na	0.602	0.557	0.578	0.603	0.663	0.688	0.676	0.640	0.696	0.673	0.640	0.612
Ca	0.417	0.449	0.445	0.406	0.348	0.322	0.326	0.353	0.251	0.296	0.334	0.376
K	0.003	0.003	0.004	0.004	0.004	0.004	0.004	0.005	0.049	0.008	0.004	0.002
Ba	0.003	0.000	0.000	0.001	0.000	0.000	0.000	0.000	0.000	0.001	0.000	0.000
Sr	0.000	0.000	0.000	0.000	0.000	0.000	0.000	0.000	0.000	0.000	0.000	0.000
Total	5.018	5.008	5.022	5.011	5.017	5.018	5.009	5.007	5.013	4.992	4.993	4.999
Or	0.50	0.26	0.37	0.49	0.38	0.35	0.39	0.53	4.92	0.94	0.45	0.22
Ab	58.83	55.22	56.31	59.46	65.29	67.90	67.22	64.13	69.85	68.77	65.41	61.77
An	40.67	44.53	43.32	40.05	34.33	31.76	32.40	35.35	25.22	30.29	34.14	38.01

PLAGIOCLÁSIO

Anfibolitos de Santa Elena

Granada anfibolito

Oxido	AC448-F	AC448-H	AC448-I	AC448-M	AC448-M1	AC441-A	AC441-B	AC441-C	AC441-D	AC441-E	AC441-G	AC441-F	AC441-H
SiO ₂	60.38	59.43	60.03	59.85	59.73	61.33	62.53	60.30	60.48	60.85	60.34	62.65	60.29
TiO ₂	0.00	0.00	0.00	0.03	0.00	0.00	0.00	0.00	0.00	0.00	0.00	0.00	0.00
Al ₂ O ₃	25.83	26.27	26.22	26.45	26.58	24.85	24.38	25.94	25.88	25.21	25.62	24.39	25.90
Fe ₂ O ₃	0.20	0.28	0.29	0.13	0.17	0.13	0.08	0.08	0.09	0.02	0.20	0.10	0.20
BaO	0.13		0.00		0.00	0.00	0.15	0.00	0.00	0.00	0.09	0.00	0.03
SrO	0.00		0.00		0.00	0.00	0.00	0.00	0.00	0.00	0.00	0.00	0.00
CaO	6.78	6.61	6.74	6.96	6.92	5.53	5.02	6.88	6.57	5.65	6.23	5.03	6.58
Na ₂ O	7.74	7.53	7.37	7.42	7.27	8.14	8.56	7.69	7.88	8.38	7.89	8.64	7.80
K ₂ O	0.10	0.05	0.06	0.08	0.05	0.08	0.12	0.08	0.10	0.10	0.07	0.12	0.09
Total 1	101.15	100.17	100.71	100.91	100.72	100.06	100.84	100.96	101.01	100.21	100.44	100.94	100.89

	AC448-F	AC448-H	AC448-I	AC448-M	AC448-M1	AC441-A	AC441-B	AC441-C	AC441-D	AC441-E	AC441-G	AC441-F	AC441-H
Si	2.661	2.641	2.651	2.640	2.638	2.717	2.748	2.659	2.665	2.696	2.673	2.748	2.661
Al	1.342	1.376	1.365	1.375	1.384	1.297	1.263	1.348	1.344	1.317	1.337	1.261	1.347
Fe ₃	0.007	0.009	0.010	0.004	0.006	0.004	0.003	0.003	0.003	0.001	0.007	0.003	0.007
Ti	0.000	0.000	0.000	0.001	0.000	0.000	0.000	0.000	0.000	0.000	0.000	0.000	0.000
Na	0.661	0.649	0.631	0.634	0.623	0.699	0.729	0.657	0.673	0.720	0.677	0.735	0.668
Ca	0.320	0.315	0.319	0.329	0.327	0.262	0.236	0.325	0.310	0.268	0.296	0.237	0.311
K	0.005	0.003	0.003	0.004	0.003	0.005	0.007	0.004	0.006	0.006	0.004	0.007	0.005
Ba	0.002	0.000	0.000	0.000	0.000	0.000	0.003	0.000	0.000	0.000	0.002	0.000	0.000
Sr	0.000	0.000	0.000	0.000	0.000	0.000	0.000	0.000	0.000	0.000	0.000	0.000	0.000
Total	4.998	4.992	4.979	4.988	4.980	4.984	4.988	4.997	5.001	5.008	4.996	4.990	4.999
Or	0.77	0.29	0.37	0.46	0.29	0.47	0.94	0.44	0.56	0.56	0.56	0.68	0.56
Ab	66.87	67.12	66.20	65.55	65.36	72.38	74.84	66.60	68.08	72.45	69.21	75.13	67.85
An	32.36	32.59	33.44	33.99	34.35	27.15	24.22	32.96	31.36	26.98	30.23	24.19	31.60

PLAGIOCLÁSIO

ESPINÉLIO

Cromititos

Amostra	AC20I1-A	AC20I1-B	AC20I1-C	AC20I1-D	AC20I1-E	AC20I1-F	AC20I1-G	AC20I1-H	AC20I4-A	AC20I4-B	AC20I4-C	AC20I4-D	AC20L3-C	AC20L3-E	AC20L3-F	AC20L3-F	AC20L1-B
SiO ₂	0.00	0.04	0.02	0.03	0.00	0.07	0.04	0.01	0.00	0.00	0.00	0.00	0.00	0.03	0.01	0.00	0.00
TiO ₂	0.18	0.20	0.22	0.18	0.22	0.18	0.06	0.04	0.18	0.23	0.21	0.20	0.04	0.07	0.15	0.11	0.09
Al ₂ O ₃	24.99	26.13	25.79	26.08	26.25	26.29	17.60	21.47	26.11	26.35	26.31	26.39	27.10	27.79	27.39	26.82	26.01
Cr ₂ O ₃	41.63	43.53	43.22	42.79	42.75	43.86	53.15	49.54	43.18	42.92	42.31	42.66	43.60	43.03	43.04	42.93	45.06
V ₂ O ₅	0.15	0.22	0.15	0.16	0.17	0.20	0.27	0.18	0.19	0.20	0.26	0.20	0.14	0.23	0.10	0.19	0.23
Fe ₂ O ₃	1.79	1.68	2.39	2.62	0.00	0.00	0.89	0.00	2.31	2.25	2.52	2.37	0.68	0.12	0.81	1.95	0.62
FeO	11.54	12.33	12.20	11.59	12.28	13.92	14.23	14.42	11.21	11.15	10.95	11.03	11.68	12.15	12.23	12.44	12.39
MgO	14.99	15.63	15.50	15.91	14.19	14.28	13.48	12.31	16.17	16.24	16.43	16.36	15.77	15.68	15.55	15.54	15.53
MnO	0.41	0.41	0.44	0.43	0.35	0.51	0.51	0.41	0.36	0.43	0.36	0.37	0.51	0.39	0.43	0.43	0.50
ZnO	0.00	0.00	0.07	0.11	0.07	0.04	0.04	0.18	0.09	0.13	0.12	0.11	0.11	0.12	0.07	0.03	0.00
CaO	0.00	0.00	0.00	0.00	0.01	0.00	0.02	0.01	0.02	0.00	0.00	0.00	0.00	0.01	0.00	0.01	0.01
NiO	0.18	0.20	0.21	0.17	0.14	0.20	0.03	0.09	0.21	0.18	0.10	0.10	0.06	0.22	0.13	0.19	0.11
Total	95.87	100.36	100.21	100.07	96.43	99.53	100.32	98.65	100.04	100.08	99.58	99.79	99.68	99.82	99.89	100.62	100.54

Fe₂O₃* Calculado por estequiometria

Ions normalizados na base de 32 oxigênios

Amostra	AC20I1-A	AC20I1-B	AC20I1-C	AC20I1-D	AC20I1-E	AC20I1-F	AC20I1-G	AC20I1-H	AC20I4-A	AC20I4-B	AC20I4-C	AC20I4-D	AC20L3-C	AC20L3-E	AC20L3-F	AC20L3-F	AC20L1-B
Si	0.000	0.009	0.004	0.007	0.000	0.016	0.010	0.003	0.000	0.000	0.001	0.000	0.000	0.007	0.002	0.000	0.000
Al	7.330	7.324	7.255	7.318	7.663	7.471	5.174	6.354	7.315	7.371	7.381	7.393	7.599	7.767	7.670	7.486	7.285
Ti	0.034	0.035	0.039	0.033	0.041	0.033	0.011	0.008	0.033	0.040	0.038	0.035	0.006	0.013	0.026	0.019	0.015
Cr	8.189	8.184	8.154	8.053	8.370	8.360	10.482	9.831	8.113	8.051	7.962	8.014	8.201	8.064	8.082	8.038	8.465
Fe ³⁺	0.336	0.301	0.429	0.470	0.000	0.000	0.167	0.000	0.414	0.401	0.452	0.425	0.122	0.022	0.145	0.348	0.112
V	0.025	0.034	0.024	0.025	0.028	0.032	0.045	0.029	0.030	0.031	0.041	0.032	0.022	0.035	0.016	0.029	0.036
Mg	5.563	5.541	5.517	5.649	5.240	5.132	5.013	4.609	5.732	5.747	5.832	5.797	5.593	5.542	5.507	5.487	5.502
Fe ²⁺	2.402	2.451	2.435	2.307	2.542	2.807	2.970	3.027	2.229	2.214	2.181	2.192	2.325	2.409	2.429	2.465	2.462
Zn	0.000	0.000	0.013	0.019	0.013	0.006	0.007	0.033	0.015	0.023	0.021	0.019	0.019	0.021	0.011	0.005	0.000
Mn	0.086	0.083	0.089	0.087	0.073	0.103	0.108	0.087	0.073	0.087	0.073	0.074	0.102	0.078	0.086	0.085	0.100
Ca	0.000	0.000	0.000	0.000	0.002	0.000	0.006	0.002	0.006	0.000	0.000	0.001	0.000	0.000	0.002	0.001	0.004
Ni	0.036	0.037	0.041	0.033	0.028	0.039	0.006	0.017	0.040	0.034	0.019	0.019	0.012	0.042	0.025	0.036	0.020
Total	24	24	24	24	24	24	24	24	24	24	24	24	24	24	24	24	24

Cromititos

Amostra	AC20L1-C	AC20F4-A	AC20F4-B	AC20F4-C	AC20F5-A	AC20F5-B	AC20F5-C	AC20F5-D	A	AC20M3I	AC20M3C	AC20M2C	AC20M2C	AC20M2C	AC20M1c	AC20M1c	
	Sb	hr	hrcentre1	hrpertoborda	hrborda1	hrborda2	hrc1	hrc2									
SiO ₂	0.00	0.00	0.00	0.00	0.02	0.01	0.00	0.03	0.00	0.06	0.07	0.08	0.09	0.78	8.31	0.06	0.08
TiO ₂	0.19	0.17	0.21	0.14	0.13	0.20	0.20	0.22	2.11	0.18	0.19	0.20	0.19	0.25	0.20	0.17	0.18
Al ₂ O ₃	27.11	26.52	26.31	26.28	25.79	26.45	26.74	26.66	23.02	26.91	26.93	26.51	26.87	14.49	12.98	26.88	26.77
Cr ₂ O ₃	42.26	43.00	42.95	43.97	43.42	43.36	43.89	43.59	43.95	44.32	43.91	43.84	43.90	48.43	41.63	43.26	43.11
V ₂ O ₅	0.17	0.19	0.13	0.17	0.18	0.09	0.16	0.18	0.07								
Fe ₂ O ₃	1.61	2.33	2.74	0.41	2.04	0.97	1.93	1.65	0.00	1.38	1.42	1.53	1.02	6.71	0.00	1.46	1.62
FeO	12.33	10.54	10.58	13.08	10.48	11.43	11.07	11.12	14.28	10.99	11.27	10.38	10.63	13.64	15.97	11.67	11.48
MgO	15.45	16.68	16.58	14.80	16.48	16.59	16.53	16.41	13.81	16.63	16.41	16.79	16.68	13.76	15.15	15.98	16.06
MnO	0.49	0.41	0.44	0.43	0.40	0.46	0.44	0.32	0.45	0.22	0.21	0.21	0.21	0.29	0.26	0.19	0.24
ZnO	0.09	0.04	0.07	0.13	0.00	0.00	0.03	0.10	0.06								
CaO	0.01	0.01	0.00	0.00	0.00	0.00	0.02	0.02	0.04	0.01	0.00	0.00	0.01	0.00	0.01	0.00	0.00
NiO	0.15	0.17	0.20	0.18	0.11	0.16	0.24	0.31	0.11	0.13	0.16	0.13	0.11	0.15	0.13	0.17	0.13
Total	99.85	100.06	100.20	99.59	99.04	100.51	101.23	100.60	97.91	100.82	100.57	99.67	99.71	98.50	94.63	99.85	99.66

Amostra	AC20L1-C	AC20F4-A	AC20F4-B	AC20F4-C	AC20F5-A	AC20F5-B	AC20F5-C	AC20F5-D	A	AC20M3I	AC20M3C	AC20M2C	AC20M2C	AC20M2C	AC20M1c	AC20M1c	
	Sb	hr	hrcentre1	hrpertoborda	hrborda1	hrborda2	hrc1	hrc2									
Si	0.000	0.000	0.000	0.000	0.004	0.001	0.000	0.007	0.000	0.013	0.017	0.018	0.021	0.199	2.146	0.015	0.018
Al	7.609	7.392	7.338	7.442	7.276	7.348	7.385	7.407	6.741	7.443	7.473	7.406	7.495	4.375	3.950	7.525	7.503
Ti	0.033	0.031	0.037	0.026	0.023	0.035	0.035	0.038	0.394	0.031	0.034	0.036	0.033	0.048	0.038	0.031	0.032
Cr	7.956	8.040	8.035	8.353	8.218	8.081	8.131	8.124	8.632	8.222	8.174	8.212	8.214	9.809	8.499	8.121	8.105
Fe ³⁺	0.289	0.415	0.488	0.074	0.367	0.172	0.340	0.294	0.000	0.245	0.251	0.273	0.182	1.295	0.000	0.261	0.291
V	0.026	0.029	0.020	0.026	0.028	0.014	0.024	0.029	0.011								
Mg	5.485	5.884	5.851	5.304	5.883	5.831	5.774	5.767	5.114	5.820	5.760	5.931	5.886	5.258	5.833	5.657	5.696
Fe ²⁺	2.455	2.086	2.093	2.628	2.099	2.254	2.170	2.191	2.968	2.156	2.219	2.058	2.104	2.922	3.449	2.317	2.283
Zn	0.017	0.006	0.013	0.024	0.001	0.000	0.005	0.017	0.011								
Mn	0.099	0.082	0.087	0.087	0.081	0.092	0.088	0.064	0.095	0.044	0.041	0.043	0.042	0.063	0.057	0.039	0.048
Ca	0.002	0.002	0.000	0.000	0.000	0.000	0.004	0.004	0.010	0.001	0.001	0.000	0.003	0.000	0.001	0.000	0.000
Ni	0.029	0.033	0.037	0.035	0.021	0.030	0.045	0.058	0.022	0.024	0.030	0.024	0.021	0.031	0.026	0.033	0.025
Total	24	24	24	24	24	24	24	24	24	24	24	24	24	24	24	24	24

Cromititos

Amostra	AC20M1c hrbord1	AC80B1R E1A	AC80B1R E1B	AC80B1R E1C	AC80B1R E1D	AC80B1R E1E	NIQUIA3A	NIQUIA3B	NIQUIA3C	NIQUIA3D	NIQUIA3E	NIQUIA4A	NIQUIA4B	CSP2A	CSP2B	CSP2C	CSP2D
SiO ₂	0.08	0.04	0.00	0.00	0.01	0.02	0.01	0.24	0.00	0.03	0.02	0.00	0.01	0.00	0.00	0.03	0.00
TiO ₂	0.16	0.00	0.14	0.14	0.16	0.20	0.27	0.25	0.25	0.25	0.30	0.28	0.25	0.09	0.12	0.14	0.11
Al ₂ O ₃	27.69	33.05	33.17	32.53	32.66	32.65	27.09	26.02	26.92	27.52	27.61	27.30	27.57	29.04	28.19	28.82	29.13
Cr ₂ O ₃	44.10	36.15	34.90	34.61	35.72	36.00	42.15	41.08	41.65	41.69	42.13	41.54	42.11	39.64	40.95	39.92	39.98
V ₂ O ₅		0.00	0.00	0.00	0.00	0.00	0.17	0.03	0.13	0.23	0.19	0.13	0.22	0.09	0.22	0.17	0.24
Fe ₂ O ₃	0.00	1.86	0.80	2.59	2.01	1.60	1.81	2.36	1.57	1.34	1.48	2.17	1.58	2.10	2.12	1.61	1.77
FeO	11.32	10.90	11.38	10.29	10.74	11.24	10.93	10.42	10.82	11.29	11.10	10.56	11.20	10.67	9.80	10.95	10.38
MgO	15.18	16.95	16.16	16.87	16.86	16.62	16.45	16.13	16.26	16.30	16.63	16.53	16.48	16.44	17.16	16.38	16.85
MnO	0.20	0.03	0.04	0.10	0.08	0.08	0.38	0.39	0.28	0.42	0.35	0.37	0.39	0.32	0.34	0.38	0.34
ZnO	0.03	0.06	0.04	0.05	0.02	0.02	0.08	0.08	0.00	0.00	0.23	0.02	0.00	0.06	0.00	0.14	
CaO	0.00	0.00	0.01	0.01	0.00	0.00	0.01	0.14	0.01	0.00	0.00	0.01	0.00	0.01	0.00	0.00	
NiO	0.12	0.14	0.19	0.21	0.22	0.19	0.14	0.11	0.08	0.06	0.04	0.13	0.12	0.28	0.23	0.17	0.21
Total	98.86	99.15	96.85	97.39	98.53	98.60	99.43	97.23	97.96	99.12	99.84	99.26	99.95	98.66	99.19	98.56	99.14

Amostra	AC20M1c hrbord1	AC80B1R E1A	AC80B1R E1B	AC80B1R E1C	AC80B1R E1D	AC80B1R E1E	NIQUIA3A	NIQUIA3B	NIQUIA3C	NIQUIA3D	NIQUIA3E	NIQUIA4A	NIQUIA4B	CSP2A	CSP2B	CSP2C	CSP2D
Si	0.020	0.009	0.000	0.000	0.003	0.004	0.002	0.057	0.000	0.007	0.004	0.000	0.001	0.000	0.000	0.007	0.000
Al	7.827	9.030	9.267	9.038	8.988	8.991	7.582	7.453	7.638	7.714	7.677	7.645	7.668	8.117	7.838	8.070	8.089
Ti	0.029	0.000	0.025	0.024	0.029	0.035	0.049	0.045	0.045	0.044	0.053	0.050	0.043	0.015	0.021	0.025	0.020
Cr	8.361	6.626	6.540	6.450	6.594	6.649	7.912	7.893	7.926	7.838	7.858	7.801	7.856	7.432	7.637	7.497	7.445
Fe ³⁺	0.000	0.324	0.143	0.460	0.353	0.281	0.324	0.431	0.284	0.240	0.263	0.388	0.281	0.375	0.377	0.288	0.315
V							0.026	0.005	0.021	0.036	0.029	0.021	0.035	0.015	0.035	0.027	0.037
Mg	5.429	5.860	5.712	5.929	5.870	5.789	5.824	5.845	5.834	5.780	5.848	5.856	5.800	5.813	6.037	5.802	5.918
Fe ²⁺	2.270	2.113	2.256	2.030	2.098	2.196	2.171	2.119	2.178	2.247	2.191	2.098	2.210	2.116	1.933	2.175	2.045
Zn		0.005	0.010	0.007	0.008	0.004	0.003	0.013	0.000	0.000	0.001	0.041	0.004	0.000	0.010	0.000	0.023
Mn	0.040	0.005	0.008	0.019	0.017	0.016	0.077	0.080	0.057	0.084	0.069	0.073	0.078	0.063	0.068	0.076	0.068
Ca	0.001	0.000	0.003	0.004	0.000	0.000	0.002	0.037	0.002	0.001	0.001	0.002	0.000	0.002	0.000	0.000	0.000
Ni	0.024	0.026	0.036	0.040	0.041	0.035	0.027	0.021	0.016	0.011	0.007	0.024	0.023	0.052	0.044	0.033	0.040
Total	24	24	24	24	24	24	24	24	24	24	24	24	24	24	24	24	24

Cromititos

Amostra	CSP3A	CSP3B	AC78C1p 1C1	AC78C1p 1pb1	AC78C1p 1agulinha	AC78C1p 1b1	AC78C1p 2I1	AC78C1p 2I2	AC78C1p 3c1	AC78C1p 4c1	AC78C1p 5c1	AC77ARE 1a	AC77ARE 1B
SiO ₂	0.01	0.00	0.07	0.08	6.32	0.06	0.09	0.09	0.06	0.07	0.07	0.05	0.03
TiO ₂	0.07	0.08	0.27	0.28	0.37	0.29	0.29	0.27	0.29	0.24	0.26	0.07	0.07
Al ₂ O ₃	30.81	29.01	32.77	32.26	28.65	18.92	31.65	31.96	31.94	32.33	32.76	36.33	35.63
Cr ₂ O ₃	38.63	40.19	36.73	36.65	31.74	39.43	37.58	37.58	37.42	36.76	36.67	31.88	31.30
V ₂ O ₅	0.15	0.12										0.00	0.00
Fe ₂ O ₃	1.76	1.91	1.39	1.90	0.00	12.75	1.72	1.13	1.27	2.14	2.13	2.33	4.20
FeO	9.19	9.59	11.44	11.06	11.03	11.55	11.14	11.61	11.28	11.02	11.24	10.39	9.67
MgO	17.77	17.18	16.79	16.91	16.64	15.19	16.87	16.60	16.72	17.01	17.05	17.55	17.98
MnO	0.32	0.33	0.18	0.21	0.20	0.30	0.19	0.18	0.19	0.19	0.21	0.10	0.10
ZnO	0.02	0.13										0.02	0.04
CaO	0.01	0.02	0.01	0.02	1.80	0.01	0.00	0.01	0.00	0.01	0.00	0.00	0.00
NiO	0.12	0.12	0.20	0.18	0.23	0.12	0.16	0.13	0.18	0.20	0.18	0.18	0.20
Total	98.86	98.67	99.85	99.56	96.99	98.60	99.67	99.56	99.34	99.97	100.55	98.90	99.23

Amostra	CSP3A	CSP3B	AC78C1p 1C1	AC78C1p 1pb1	AC78C1p 1agulinha	AC78C1p 1b1	AC78C1p 2I1	AC78C1p 2I2	AC78C1p 3c1	AC78C1p 4c1	AC78C1p 5c1	AC77ARE 1a	AC77ARE 1B
Si	0.003	0.000	0.017	0.018	1.490	0.014	0.020	0.022	0.015	0.016	0.015	0.011	0.008
Al	8.468	8.073	8.921	8.815	7.963	5.576	8.661	8.756	8.761	8.798	8.859	9.789	9.584
Ti	0.013	0.013	0.048	0.050	0.066	0.054	0.050	0.048	0.051	0.042	0.045	0.012	0.012
Cr	7.122	7.501	6.707	6.716	5.916	7.792	6.898	6.905	6.884	6.711	6.651	5.762	5.646
Fe ³⁺	0.309	0.339	0.242	0.332	0.000	2.399	0.300	0.198	0.222	0.372	0.368	0.401	0.722
V	0.023	0.019											
Mg	6.179	6.047	5.783	5.845	5.850	5.662	5.841	5.753	5.800	5.855	5.832	5.982	6.118
Fe ²⁺	1.792	1.893	2.209	2.144	2.175	2.414	2.163	2.256	2.195	2.128	2.157	1.986	1.846
Zn	0.004	0.023										0.004	0.007
Mn	0.063	0.065	0.035	0.042	0.040	0.063	0.037	0.035	0.037	0.038	0.040	0.020	0.020
Ca	0.003	0.004	0.002	0.004	0.456	0.002	0.000	0.001	0.000	0.003	0.001	0.000	0.000
Ni	0.022	0.022	0.036	0.034	0.044	0.025	0.031	0.024	0.035	0.037	0.032	0.034	0.037
Total	24	24	24	24	24	24	24	24	24	24	24	24	24

Cromititos

Amostra	AC77ARE	AC77CES															
	1CA	1CB	1CC	2A	2B	2C	2D	2E	p1A	p1B	p1C	p1D	p5A	p5B	p5C	p7A	p7B
SiO ₂	0.00	0.03	0.01	0.02	0.05	0.04	0.04	0.01	0.00	0.00	0.02	0.00	0.01	0.00	0.01	0.06	0.00
TiO ₂	0.08	0.00	0.04	0.14	0.12	0.00	0.12	0.00	0.09	0.21	0.17	0.00	0.03	0.00	0.00	0.00	0.05
Al ₂ O ₃	36.38	36.32	36.31	34.38	35.99	36.43	36.72	38.18	36.84	36.87	36.56	38.03	34.03	36.83	37.03	36.98	37.47
Cr ₂ O ₃	31.86	33.30	33.74	34.17	33.01	33.01	32.15	30.05	30.18	30.58	30.73	29.61	31.67	30.82	29.65	29.72	29.47
V ₂ O ₅	0.00	0.00	0.00	0.00	0.00	0.00	0.00	0.00	0.00	0.00	0.00	0.00	0.00	0.00	0.00	0.00	0.00
Fe ₂ O ₃	2.45	2.33	1.67	2.75	1.67	2.04	1.97	2.55	3.36	2.71	3.41	2.44	5.01	3.08	3.75	3.11	3.52
FeO	10.77	10.72	11.22	10.95	11.04	11.10	10.93	10.03	12.41	12.26	12.62	11.95	13.22	12.31	11.86	12.26	12.11
MgO	17.27	17.37	17.25	17.22	17.24	17.37	17.45	17.92	16.41	16.50	16.41	16.69	15.53	16.41	16.60	16.33	16.56
MnO	0.13	0.07	0.12	0.09	0.07	0.04	0.06	0.06	0.07	0.12	0.07	0.04	0.15	0.09	0.15	0.10	0.12
ZnO	0.04	0.04	0.10	0.06	0.08	0.00	0.07	0.09	0.05	0.10	0.14	0.03	0.17	0.16	0.09	0.07	0.14
CaO	0.01	0.00	0.00	0.01	0.00	0.01	0.00	0.02	0.00	0.02	0.00	0.00	0.01	0.00	0.00	0.00	0.00
NiO	0.23	0.19	0.21	0.15	0.15	0.18	0.15	0.16	0.18	0.18	0.15	0.14	0.15	0.15	0.20	0.16	0.19
Total	99.22	100.37	100.66	99.93	99.40	100.21	99.66	99.05	99.59	99.54	100.28	98.95	99.98	99.85	99.33	98.79	99.63

Amostra	AC77ARE	AC77CES															
	1CA	1CB	1CC	2A	2B	2C	2D	2E	p1A	p1B	p1C	p1D	p5A	p5B	p5C	p7A	p7B
Si	0.000	0.006	0.002	0.003	0.011	0.008	0.009	0.001	0.000	0.000	0.005	0.000	0.001	0.000	0.003	0.014	0.000
Al	9.795	9.685	9.672	9.281	9.690	9.724	9.829	10.184	9.928	9.931	9.812	10.233	9.297	9.906	9.982	10.025	10.064
Ti	0.014	0.001	0.007	0.025	0.020	0.000	0.021	0.000	0.016	0.037	0.028	0.000	0.006	0.000	0.000	0.000	0.009
Cr	5.754	5.956	6.027	6.185	5.960	5.910	5.772	5.377	5.456	5.525	5.531	5.344	5.803	5.561	5.360	5.404	5.309
Fe ³⁺	0.421	0.345	0.283	0.474	0.287	0.348	0.337	0.434	0.579	0.467	0.585	0.420	0.874	0.529	0.646	0.539	0.604
V																	
Mg	5.881	5.860	5.812	5.879	5.870	5.865	5.907	6.046	5.593	5.621	5.571	5.681	5.367	5.582	5.661	5.600	5.626
Fe ²⁺	2.058	2.093	2.120	2.098	2.110	2.102	2.075	1.898	2.373	2.344	2.403	2.282	2.564	2.349	2.268	2.358	2.308
Zn	0.007	0.006	0.017	0.009	0.013	0.001	0.012	0.015	0.008	0.017	0.023	0.005	0.029	0.027	0.014	0.011	0.023
Mn	0.025	0.014	0.023	0.017	0.013	0.008	0.011	0.011	0.014	0.022	0.014	0.007	0.029	0.017	0.030	0.019	0.022
Ca	0.003	0.000	0.000	0.001	0.000	0.002	0.000	0.005	0.000	0.004	0.000	0.001	0.002	0.000	0.000	0.001	0.000
Ni	0.042	0.035	0.038	0.028	0.027	0.032	0.028	0.029	0.033	0.033	0.028	0.026	0.028	0.028	0.037	0.029	0.034
Total	24	24	24	24	24	24	24	24	24	24	24	24	24	24	24	24	24

Espinélicos dos peridotitos hospedeiros dos cromititos

Amostra	Patio Bonito Deposit					El Chagualo		El Carmelo								Don Jesus	
	AC20A1-A	AC20A1-B	AC20A3-D	AC20A3-E	AC20A3-F	AC77BESp 4A	AC77BESp 4B	AC80B2Es p2D	AC80B2Es p1C	AC80B2ES p2A	AC80B2ES p1A	AC80B2ES p1B	AC80B2ES p2B	AC80B2ES p2C	AC78BE4A	AC78BE4B	
SiO ₂	0.02	0.00	0.03	0.31	0.00	0.07	3.51	0.09	0.05	0.01	0.00	0.85	0.04	0.04	0.10	0.04	
TiO ₂	0.40	0.35	0.44	0.32	0.34	0.10	0.04	0.16	0.28	0.26	0.35	0.26	0.24	0.29	0.66	0.77	
Al ₂ O ₃	0.22	0.19	0.17	0.19	0.14	3.28	6.47	23.17	22.27	22.00	23.12	23.06	21.02	22.80	1.62	1.52	
Cr ₂ O ₃	24.16	24.86	23.81	16.70	16.64	53.77	46.84	33.09	35.86	37.83	36.87	36.86	38.11	37.41	50.31	52.26	
V ₂ O ₅	0.22	0.13	0.17	0.17	0.27												
Fe ₂ O ₃	37.79	37.08	37.73	43.46	42.45	7.62	5.18	10.95	10.71	8.36	8.35	7.23	9.07	8.42	12.62	12.75	
FeO	35.43	34.50	35.20	36.34	38.10	25.71	24.64	19.72	20.91	20.94	19.65	20.56	21.00	20.17	28.11	28.47	
MgO	1.45	1.51	1.42	2.72	1.13	2.93	6.78	9.86	9.52	9.16	10.13	10.03	9.08	9.87	2.09	2.35	
MnO	0.54	0.57	0.54	0.43	0.34	0.38	0.42	0.17	0.21	0.18	0.26	0.26	0.23	0.23	0.48	0.54	
ZnO	0.17	0.31	0.35	0.14	0.10	0.43	0.37	0.33	0.36	0.30	0.30	0.29	0.25	0.34	0.53	0.61	
CaO	0.01	0.03	0.00	0.00	0.02	0.04	0.07	0.01	0.01	0.04	0.00	0.41	0.02	0.01	0.01	0.01	
NiO	0.64	0.59	0.57	0.74	0.71	0.03	0.06	0.17	0.15	0.16	0.15	0.17	0.14	0.15	0.08	0.08	
Total	101.05	100.11	100.41	101.52	100.22	94.36	94.40	97.69	100.33	99.23	99.17	99.97	99.18	99.73	96.60	99.39	

Ions normalizados na base de 32 oxigênios

Amostra	AC20A1-A	AC20A1-B	AC20A3-D	AC20A3-E	AC20A3-F	AC77BESp4	AC77BESp4	AC80B2Esp	AC78BE4A	AC78BE4B							
	Si	0.005	0.000	0.008	0.090	0.000	0.020	1.009	0.023	0.012	0.001	0.000	0.213	0.011	0.009	0.030	0.012
Al	0.077	0.066	0.060	0.067	0.049	1.175	2.189	7.001	6.620	6.618	6.881	6.797	6.356	6.775	0.578	0.526	
Ti	0.088	0.079	0.097	0.070	0.077	0.022	0.010	0.030	0.052	0.049	0.066	0.049	0.046	0.056	0.151	0.170	
Cr	5.647	5.863	5.603	3.849	3.937	12.943	10.634	6.705	7.148	7.632	7.360	7.288	7.728	7.455	12.043	12.150	
Fe ³⁺	8.410	8.326	8.456	9.539	9.563	1.746	1.121	2.112	2.033	1.606	1.587	1.362	1.751	1.599	2.876	2.822	
V	0.043	0.025	0.033	0.032	0.052	0.000	0.000	0.000	0.000	0.000	0.000	0.000	0.000	0.000	0.000	0.000	
Mg	0.641	0.671	0.630	1.180	0.503	1.330	2.905	3.767	3.578	3.487	3.815	3.740	3.473	3.709	0.942	1.028	
Fe ²⁺	8.761	8.607	8.765	8.861	9.535	6.548	5.918	4.226	4.410	4.469	4.150	4.301	4.506	4.253	7.118	7.001	
Zn	0.036	0.068	0.076	0.029	0.022	0.097	0.079	0.062	0.068	0.057	0.056	0.053	0.047	0.063	0.119	0.132	
Mn	0.134	0.145	0.135	0.106	0.085	0.099	0.103	0.036	0.044	0.038	0.056	0.054	0.049	0.050	0.123	0.135	
Ca	0.004	0.009	0.000	0.001	0.005	0.014	0.021	0.002	0.004	0.010	0.000	0.109	0.004	0.003	0.003	0.004	
Ni	0.153	0.141	0.136	0.174	0.170	0.006	0.014	0.034	0.031	0.032	0.030	0.034	0.028	0.029	0.018	0.019	
Total	24.000	24.000	24.000	24.000	24.000	24.000	24.000	24.000	24.000	24.000	24.000	24.000	24.000	24.000	24.000	24.000	

Harzburgitos

Amostra	JJ1396p1spi nela	JJ1396p1s pinelb	JJ1396p2s pinela	JJ1396p2s pinelb	Ac22B1chr1	Ac22B1chr2	AC53A-B	AC53A-C	AC53Jp1spin el1a
SiO ₂	0.09	0.06	0.11	0.06	0.11	0.09	0.00	0.02	0.10
TiO ₂	0.09	0.10	0.09	0.12	0.27	0.28	0.69	0.73	1.15
Al ₂ O ₃	40.01	39.67	38.57	38.34	1.49	1.38	2.27	2.86	0.14
Cr ₂ O ₃	29.50	29.00	31.33	31.06			0.36	0.33	
V ₂ O ₅					62.00	62.82	57.38	56.34	20.84
Fe ₂ O ₃	0.00	0.27	0.00	0.00	3.26	2.97	6.54	7.73	36.83
FeO	15.10	14.56	15.35	15.47	27.73	27.64	28.17	27.66	36.01
MgO	14.97	15.26	14.26	14.43	2.31	2.42	2.61	3.03	0.81
MnO	0.23	0.20	0.23	0.21	0.69	0.73	0.84	0.89	0.43
ZnO					0.01	0.01	0.01	0.02	0.00
					0.05	0.06	0.06	0.09	0.43
NiO	0.09	0.13	0.14	0.11			0.44	0.65	
Total	100.08	99.27	100.07	99.80	97.92	98.38	99.36	100.34	96.75

Ions normalizados na base de 32 oxigênios

Si	0.021	0.014	0.024	0.014	0.032	0.026	0.001	0.005	0.032
Al	10.691	10.662	10.410	10.368	0.060	0.063	0.150	0.157	0.269
Ti	0.016	0.018	0.015	0.021	0.522	0.479	0.781	0.968	0.052
Cr	5.288	5.228	5.672	5.633	0.000	0.000	0.070	0.062	0.000
Fe ³⁺	0.000	0.046	0.000	0.000	14.557	14.676	13.237	12.803	5.111
V					0.728	0.661	1.437	1.672	8.599
Mg	5.060	5.190	4.869	4.935	6.887	6.832	6.874	6.650	9.342
Fe ²⁺	2.863	2.777	2.939	2.967	1.024	1.066	1.133	1.299	0.374
Zn					0.172	0.182	0.209	0.218	0.113
Mn	0.045	0.040	0.045	0.041	0.004	0.002	0.002	0.007	0.000
					0.013	0.014	0.013	0.022	0.108
Ni	0.016	0.025	0.025	0.019	0.000	0.000	0.094	0.138	0.000
Total	24	24	24	24	24	24	24	24	24

Dunitos e harzburgitos

	AC52C6C	AC52C5A	AC52C5B	AC52EE sp1A	AC52EESp 1B	AC52EESp 1D	AC52EESp 1E	AC52EE Sp1F	AC52EEs p4A	AC52EE Sp4B	AC52EE Sp3B	AC52EE sp3D	AC52EES p5A	AC52EES p10A
SiO ₂	3.32	0.16	0.83	0.01	0.01	0.00	0.04	0.00	0.03	0.00	0.05	0.03	0.05	0.04
TiO ₂	0.12	0.15	0.15	0.35	0.27	0.16	0.13	0.17	0.11	0.13	0.07	0.20	0.19	0.45
Al ₂ O ₃	3.46	3.32	3.48	30.96	31.07	30.86	30.44	31.15	31.24	30.93	26.16	27.43	3.08	2.68
Cr ₂ O ₃	47.02	58.25	58.43	35.36	34.25	33.77	35.59	34.94	34.47	33.88	40.28	38.87	57.85	59.15
V ₂ O ₅	0.57	0.77	0.74	0.00	0.00	0.00	0.00	0.00	0.00	0.00	0.00	0.00	0.00	0.00
Fe ₂ O ₃	10.15	5.19	4.30	2.88	3.30	3.70	2.94	3.22	4.02	4.28	2.60	2.31	5.10	4.47
FeO	23.85	28.14	28.09	17.28	16.79	16.34	17.31	16.78	16.98	16.54	20.59	19.96	25.74	26.44
MgO	7.99	3.01	3.79	12.75	12.84	12.76	12.45	12.91	12.83	12.89	9.77	10.18	3.19	3.08
MnO	0.86	0.95	1.07	0.18	0.15	0.26	0.13	0.18	0.18	0.14	0.15	0.18	0.46	0.44
ZnO	0.54	0.67	0.44	0.23	0.18	0.30	0.25	0.19	0.31	0.28	0.78	0.92	0.50	0.52
CaO	0.01	0.00	0.02	0.02	0.06	0.00	0.00	0.00	0.02	0.01	0.02	0.00	0.01	0.00
NiO	0.00	0.07	0.05	0.10	0.07	0.10	0.10	0.11	0.10	0.12	0.05	0.07	0.04	0.02
Total	97.89	100.69	101.40	100.12	98.97	98.24	99.35	99.67	100.29	99.19	100.51	100.15	96.20	97.29

Ions normalizados na base de 32 oxigênios

Si	0.930	0.046	0.234	0.003	0.002	0.000	0.009	0.000	0.006	0.000	0.012	0.007	0.014	0.012
Al	1.144	1.119	1.154	8.691	8.795	8.801	8.631	8.762	8.748	8.746	7.608	7.939	1.083	0.933
Ti	0.025	0.033	0.031	0.063	0.049	0.029	0.023	0.031	0.019	0.023	0.013	0.036	0.042	0.099
Cr	10.411	13.151	12.980	6.658	6.503	6.460	6.769	6.592	6.475	6.426	7.856	7.545	13.639	13.832
Fe ³⁺	2.140	1.116	0.910	0.516	0.596	0.674	0.532	0.579	0.718	0.773	0.483	0.427	1.144	0.995
V	0.106	0.145	0.138	0.000	0.000	0.000	0.000	0.000	0.000	0.000	0.000	0.000	0.000	0.000
Mg	3.336	1.280	1.589	4.527	4.597	4.604	4.465	4.595	4.544	4.609	3.593	3.728	1.419	1.359
Fe ²⁺	5.588	6.722	6.601	3.442	3.371	3.306	3.482	3.349	3.374	3.319	4.247	4.100	6.421	6.542
Zn	0.111	0.142	0.092	0.040	0.032	0.053	0.045	0.034	0.055	0.050	0.142	0.167	0.109	0.113
Mn	0.205	0.230	0.255	0.036	0.029	0.054	0.026	0.037	0.037	0.029	0.032	0.037	0.116	0.110
Ca	0.004	0.000	0.007	0.006	0.014	0.001	0.000	0.000	0.005	0.002	0.004	0.000	0.002	0.000
Ni	0.000	0.017	0.011	0.020	0.013	0.019	0.019	0.021	0.020	0.023	0.011	0.014	0.010	0.004
Total	24	24	24	24	24	24	24	24	24	24	24	24	24	24

Dunitos e harzburgitos

	AC5204p1 spinel1	AC5204p1 spinel2	AC5204p2 spinel1	AC5204p2 spinel2	AC52165p1 spinel1a	AC52165p1 spinel1b	AC52165p1 spinel1c	AC52502p1 spinel1a	AC52502p1 spinel1b	AC52502p4 spinel1a	AC52502p4 spinel1b	AC52502p4 spinel1c
SiO ₂	0.05	0.06	0.09	0.04	0.21	0.16	0.35	0.08	0.07	0.06	0.08	0.07
TiO ₂	0.38	0.34	0.38	0.36	0.11	0.12	0.09	0.23	0.23	0.35	0.29	0.23
Al ₂ O ₃	23.85	23.49	24.57	25.04	3.21	3.71	3.94	20.84	22.98	28.51	28.69	24.89
Cr ₂ O ₃	38.89	38.79	38.45	37.42	61.44	59.48	59.23	41.40	39.59	34.51	34.09	38.21
V ₂ O ₅												
Fe ₂ O ₃	5.54	5.97	5.70	5.65	3.14	3.76	3.75	4.89	4.56	4.61	4.94	4.75
FeO	20.32	20.33	19.32	20.41	27.34	26.71	27.30	21.59	21.28	20.00	20.09	20.48
MgO	9.98	9.88	10.81	10.01	3.01	3.18	3.14	8.47	8.93	10.64	10.58	9.81
MnO	0.35	0.37	0.35	0.33	0.72	0.67	0.62	0.41	0.32	0.30	0.32	0.38
ZnO												
CaO	0.00	0.00	0.00	0.01	0.01	0.00	0.01	0.01	0.04	0.00	0.00	0.01
NiO	0.14	0.15	0.14	0.14	0.02	0.02	0.00	0.04	0.06	0.07	0.08	0.05
Total	99.51	99.37	99.81	99.40	99.23	97.80	98.42	97.97	98.06	99.04	99.16	98.87
Si	0.013	0.014	0.023	0.009	0.062	0.047	0.101	0.020	0.018	0.014	0.019	0.018
Al	7.052	6.970	7.187	7.376	1.095	1.279	1.348	6.386	6.951	8.266	8.307	7.375
Ti	0.072	0.064	0.070	0.067	0.025	0.025	0.021	0.046	0.045	0.065	0.054	0.043
Cr	7.715	7.721	7.545	7.392	14.041	13.739	13.580	8.510	8.030	6.710	6.620	7.593
Fe ³⁺	1.046	1.132	1.064	1.062	0.682	0.827	0.818	0.958	0.881	0.854	0.913	0.898
V	0.000	0.000	0.000	0.000	0.000	0.000	0.000	0.000	0.000	0.000	0.000	0.000
Mg	3.734	3.709	3.999	3.730	1.299	1.384	1.357	3.285	3.415	3.901	3.877	3.676
Fe ²⁺	4.265	4.280	4.009	4.264	6.609	6.527	6.621	4.694	4.565	4.114	4.127	4.305
Zn	0.000	0.000	0.000	0.000	0.000	0.000	0.000	0.000	0.000	0.000	0.000	0.000
Mn	0.075	0.079	0.075	0.069	0.176	0.166	0.153	0.090	0.070	0.062	0.066	0.080
Ca	0.000	0.000	0.001	0.003	0.004	0.000	0.002	0.002	0.012	0.000	0.001	0.002
Ni	0.028	0.030	0.028	0.028	0.005	0.006	0.000	0.009	0.013	0.013	0.016	0.011
Total	24	24	24	24	24	24	24	24	24	24	24	24

	AC521925p2 spinel1a	AC521925p2 spinel1b	AC522654p 1espinelioal terado1	AC522654p 1espinelioal terado2	AC522654p 1espinelioal terado3	AC52B3 1F	AC52B3 1G	AC52B3 2B	AC52B32C
SiO ₂	0.08	0.24	0.10	2.50	0.11	8.86	9.20	7.67	1.33
TiO ₂	0.34	0.29	0.33	0.38	0.39	0.18	0.21	0.41	0.42
Al ₂ O ₃	2.92	2.79	2.92	3.47	3.36	6.13	5.59	10.04	5.50
Cr ₂ O ₃	59.66	59.81	61.91	57.30	60.31	43.58	42.92	33.79	46.01
V ₂ O ₅						0.34	0.37	0.33	0.46
Fe ₂ O ₃	3.79	3.74	2.66	0.07	3.38	1.77	0.00	3.12	8.71
FeO	26.55	26.53	26.60	27.80	26.54	21.88	21.64	22.68	26.09
MgO	3.08	3.18	3.43	4.33	3.47	14.13	10.88	11.76	4.30
MnO	0.68	0.65	0.60	0.59	0.64	0.66	0.59	0.54	0.76
ZnO						0.44	0.20	0.29	0.45
CaO	0.02	0.01	0.00	0.01	0.00	0.04	0.05	0.00	0.08
NiO	0.07	0.23	0.05	0.10	0.03	0.01	0.04	0.02	0.11
Total	97.19	97.46	98.60	96.57	98.24	98.02	91.69	90.65	94.22
Si	0.022	0.072	0.028	0.728	0.033	2.299	2.591	2.133	0.394
Al	1.017	0.967	1.001	1.190	1.150	1.873	1.856	3.292	1.926
Ti	0.075	0.064	0.072	0.084	0.085	0.036	0.045	0.085	0.095
Cr	13.933	13.922	14.213	13.170	13.865	8.936	9.561	7.431	10.813
Fe ³⁺	0.844	0.828	0.581	0.016	0.740	0.346	0.000	0.653	1.950
V	0.000	0.000	0.000	0.000	0.000	0.058	0.068	0.061	0.090
Mg	1.356	1.397	1.486	1.879	1.505	5.464	4.570	4.879	1.905
Fe ²⁺	6.559	6.532	6.460	6.759	6.456	4.747	5.101	5.275	6.486
Zn	0.000	0.000	0.000	0.000	0.000	0.085	0.042	0.060	0.100
Mn	0.169	0.162	0.147	0.146	0.158	0.145	0.141	0.127	0.192
Ca	0.008	0.002	0.001	0.004	0.001	0.010	0.016	0.001	0.024
Ni	0.017	0.054	0.012	0.024	0.007	0.002	0.009	0.005	0.026
Total	24	24	24	24	24	24	24	24	24

Wehrlito

	P21120p1spinel1a	P21120p1spinel1b	P21120p2spinel1	P21120p2spinel2	P21120p2inclusion
SiO ₂	0.10	0.08	0.07	0.13	0.17
TiO ₂	0.23	0.22	0.21	0.20	0.18
Al ₂ O ₃	38.86	40.19	40.57	39.93	40.08
Cr ₂ O ₃	27.51	26.90	27.02	26.69	26.50
V ₂ O ₃					
Fe ₂ O ₃	0.58	0.00	0.00	0.11	0.06
FeO	20.54	20.02	19.35	19.22	19.29
MgO	11.38	11.67	12.32	12.19	12.26
MnO	0.31	0.29	0.23	0.27	0.27
ZnO					
CaO	0.05	0.03	0.02	0.08	0.01
NiO	0.12	0.12	0.10	0.14	0.11
Total	99.66	99.53	99.90	98.95	98.91

Ions normalizados na base de 32 oxigênios

Si	0.024	0.018	0.016	0.029	0.039
Al	10.692	10.995	11.008	10.945	10.979
Ti	0.041	0.039	0.036	0.035	0.032
Cr	5.076	4.935	4.917	4.907	4.868
Fe ³⁺	0.101	0.000	0.000	0.019	0.011
V					
Mg	3.960	4.038	4.229	4.227	4.248
Fe ²⁺	4.010	3.887	3.724	3.738	3.749
Zn					
Mn	0.061	0.058	0.046	0.053	0.053
Ca	0.012	0.008	0.006	0.019	0.001
Ni	0.022	0.022	0.019	0.026	0.020
Total	24	24	24	24	24

Peridotitos metamorfisados

Amostra	AC19B2-B	AC19B2-C	AC19B3-H	AC19B3-I	AC19B2-A	AC35A5-A	AC35A5-B	AC35A5-C	AC35A6-B	AC59bp3	AC59bp4
SiO ₂	0.78	0.02	0.02	0.03	0.018	0.01	0.01	0.00	0.01	0.07	0.09
TiO ₂	0.27	0.16	0.14	0.13	0.224	0.29	0.24	0.25	0.25	0.10	0.06
Al ₂ O ₃	0.26	0.04	0.04	0.00	0.053	0.04	0.06	0.06	0.01	0.05	0.05
Cr ₂ O ₃	25.25	8.64	5.41	5.30	15.213	6.89	6.84	6.91	6.91	10.91	9.69
V ₂ O ₅	0.13	0.06	0.20	0.16	0.052	0.18	0.16	0.12	0.13		
Fe ₂ O ₃	35.17	47.75	48.89	49.66	44.484	48.28	48.51	48.71	48.34	45.30	45.91
FeO	32.52	41.15	42.06	42.95	37.453	40.89	41.92	41.47	42.31	37.95	38.31
MgO	2.47	0.81	0.89	0.80	1.748	1.34	0.88	1.21	0.53	1.64	1.60
MnO	0.84	0.25	0.03	0.12	0.535	0.30	0.29	0.29	0.26	0.33	0.31
ZnO	0.22	0.10	0.05	0.00	0.107	0.12	0.09	0.00	0.08		
CaO	0.00	0.01	0.00	0.00	0.002	0.02	0.00	0.00	0.02	0.01	0.05
NiO	0.74	0.94	1.07	0.90	0.920	0.77	0.75	0.79	0.80	0.69	0.72
Total	98.65	99.94	98.79	100.03	100.809	99.12	99.76	99.82	99.63	97.04	96.79

Ions normalizados na base de 32 oxigênios

Si	0.233	0.007	0.005	0.008	0.005	0.004	0.002	0.001	0.004	0.021	0.029
Al	0.091	0.016	0.015	0.000	0.019	0.015	0.022	0.021	0.002	0.020	0.018
Ti	0.061	0.037	0.032	0.029	0.050	0.065	0.055	0.057	0.058	0.022	0.015
Cr	5.976	2.056	1.301	1.261	3.563	1.646	1.631	1.642	1.654	2.655	2.365
Fe ³⁺	7.928	10.826	11.208	11.252	9.922	10.990	11.014	11.021	11.019	10.501	10.670
V	0.025	0.013	0.041	0.032	0.010	0.036	0.032	0.024	0.025	0.000	0.000
Mg	1.103	0.364	0.404	0.358	0.772	0.606	0.394	0.541	0.238	0.751	0.735
Fe ²⁺	8.142	10.366	10.712	10.812	9.281	10.343	10.573	10.426	10.716	9.773	9.893
Zn	0.049	0.022	0.011	0.001	0.023	0.026	0.021	0.000	0.018	0.000	0.000
Mn	0.214	0.063	0.008	0.030	0.134	0.078	0.074	0.074	0.066	0.086	0.080
Ca	0.000	0.004	0.000	0.000	0.001	0.006	0.000	0.001	0.005	0.002	0.017
Ni	0.179	0.227	0.263	0.217	0.219	0.186	0.182	0.192	0.196	0.170	0.178
Total	24	24	24	24	24	24	24	24	24	24	24

ILMENITA

Anfibolitos

	ILM1PT1	ILM1PT2	ILM1PT3	ILM2PT1	ILM2PT2	ILM2PT3	AC448-N
SiO ₂	0.01	0.03	0.03	0.02	0.01	0.06	0.04
TiO ₂	52.18	51.99	52.08	53.55	53.50	52.83	52.80
Al ₂ O ₃	0.04	0.00	0.06	0.07	0.04	0.01	0.02
Cr ₂ O ₃	0.01	0.01	0.00	0.05	0.05	0.03	0.01
Fe ₂ O ₃	0.00	0.00	0.00	0.00	0.00	0.00	0.00
FeO	43.69	43.97	44.19	44.50	44.04	43.79	46.02
MnO	2.05	2.14	2.26	2.22	2.24	2.13	0.95
MgO	0.13	0.16	0.13	0.11	0.17	0.16	0.17
ZnO	-	-	-	-	-	-	0.00
CaO	0.09	0.06	0.09	0.06	0.06	0.16	0.01
NiO	-	-	-	-	-	-	0.01
Total	98.20	98.37	98.84	100.57	100.09	99.16	100.02

Cations na base de 6 oxigênios

	ILM1PT1	ILM1PT2	ILM1PT3	ILM2PT1	ILM2PT2	ILM2PT3	AC448-N
Si	0.000	0.002	0.001	0.001	0.000	0.003	0.002
Al	0.003	0.000	0.004	0.004	0.002	0.001	0.001
Ti	2.016	2.004	1.998	2.021	2.028	2.021	2.002
Cr	0.000	0.000	0.000	0.002	0.002	0.001	0.001
Fe ³⁺	0.000	0.000	0.000	0.000	0.000	0.000	0.000
V	0.000	0.000	0.000	0.000	0.000	0.000	0.000
Mg	0.010	0.012	0.010	0.008	0.013	0.012	0.013
Fe ²⁺	1.877	1.885	1.885	1.867	1.856	1.862	1.940
Zn	0.000	0.000	0.000	0.000	0.000	0.000	0.000
Mn	0.089	0.093	0.098	0.094	0.095	0.092	0.040
Ca	0.005	0.003	0.005	0.003	0.003	0.009	0.000
Ni	0.000	0.000	0.000	0.000	0.000	0.000	0.000
Total	4	4	4	4	4	4	4

COBRE NATIVO

SULFETOS

LIGA Fe-Ni

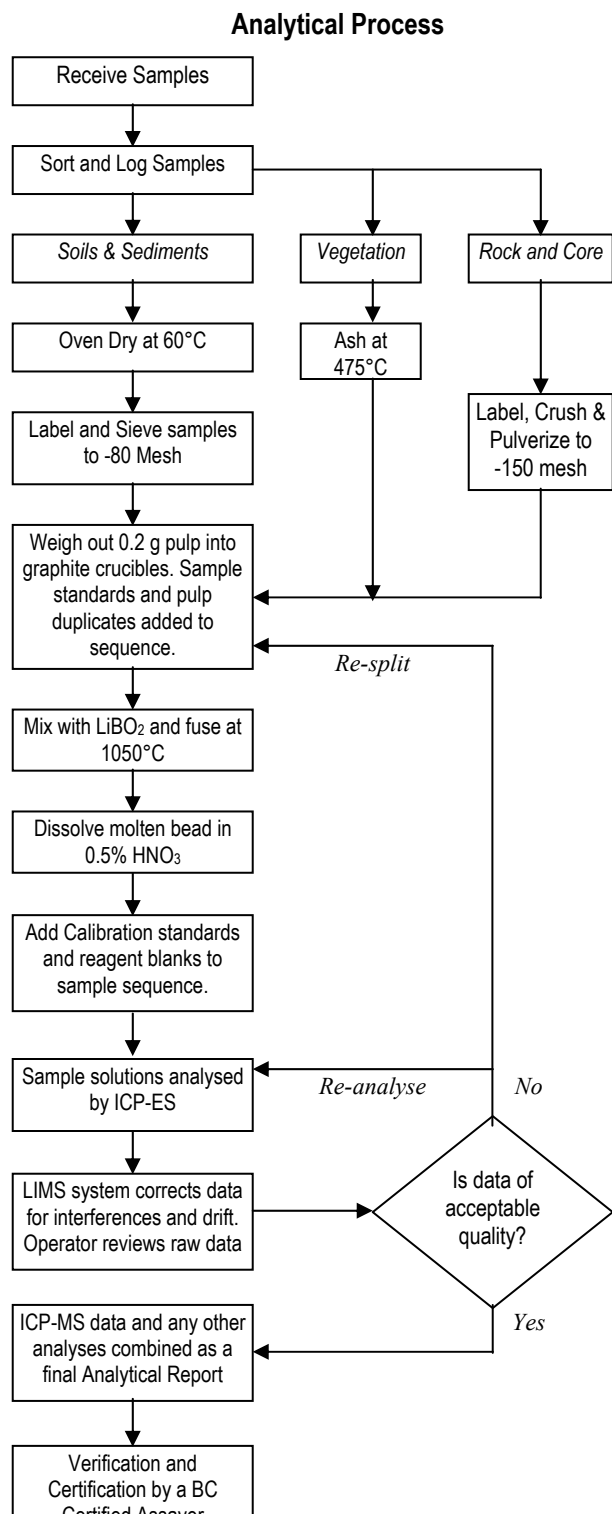
Litotipo	Harzburgito		Dunite										Cromitito			
Mineral	Cobre	cobre	Pn	Pn	?	Pn	Mi	Pn	Pn	?	Aw	AC20L	AC20L	AC20L	AC20L	
Amostra	AC20A3-AC20A3-	AC52B3	AC52B3	AC52B3	AC52B3	AC52B3	AC52B3	AC52B3	AC52B3	AC52B3	AC52B3	AC20L	AC20L	AC20L	AC20L	
No.			P1core	P4core	P4rim1	P4_2core	P4_2rim	P6core	P7core	P7rim	P4rim2	p4gra01	p4gra02	p4gra03a	p4gra03b	
Fe(wt%)	0.86	0.93	35.16	36.64	14.82	33.10	2.96	36.47	36.39	11.75	22.15	3.10	0.88	21.80	0.88	
Ni	0.06	0.07	29.43	28.22	74.36	31.38	61.51	27.49	27.97	73.50	76.68	58.05	57.50	43.03	61.43	
Co	0.03	0.00	0.86	0.82	0.28	0.69	0.03	0.69	0.81	0.04	0.17	0.09		0.29		
Cu	101.24	99.10	0.00	0.02	0.41	0.48	5.43	0.83	0.02	1.39	0.26	0.03		0.00		
S	0.07	0.01	34.57	34.23	14.98	34.29	32.35	34.44	34.66	14.92	1.35	38.72	41.48	34.83	37.68	
As	0.00	0.00	0.00	0.02	0.00	0.00	0.00	0.11	0.16	0.00	0.00		0.20		0.01	
Se			0.01	0.02	0.01	0.03	0.06	0.01	0.00	0.00	0.03	0.02	0.01	0.02	0.08	
Te			0.00	0.05	0.00	0.03	0.01	0.00	0.00	0.00	0.04		0.01	0.05		
Zn												0.01	0.00	0.01		
Total	102.26	100.10	100.03	100.01	104.85	100.01	102.35	100.03	100.00	101.59	100.68	100.04	100.08	100.03	100.07	
Fe(at%)	0.955	1.056	28.313	29.562	13.636	26.741	2.451	29.395	29.282	10.911	22.750	2.464	0.692	17.621	0.703	
Ni	0.066	0.071	22.543	21.655	65.098	24.114	48.392	21.076	21.409	64.896	74.918	43.862	42.755	33.087	46.768	
Co	0.027	0.000	0.657	0.624	0.242	0.531	0.020	0.530	0.616	0.033	0.165	0.067		0.223		
Cu	98.819	98.856	0.000	0.013	0.329	0.339	3.945	0.589	0.015	1.131	0.237	0.022		0.001		
S	0.133	0.017	48.498	48.113	24.008	48.254	46.599	48.354	48.585	24.122	2.413	53.579	56.485	49.051	52.528	
As	0.000	0.000	0.000	0.014	0.000	0.000	0.000	0.068	0.094	0.000	0.000		0.119		0.004	
Se			0.008	0.011	0.008	0.018	0.036	0.004	0.000	0.000	0.023	0.013	0.003	0.014	0.045	
Te			0.000	0.018	0.000	0.010	0.004	0.000	0.000	0.000	0.017		0.003	0.018		
Zn												0.008	0.001	0.006		
Total	100.000	100.000	100.019	100.010	103.320	100.006	101.446	100.015	100.001	101.092	100.522	100.014	100.058	100.021	100.048	
Ni/Fe			0.80	0.73	4.77	0.90	19.75	0.72	0.73	5.95	3.29				1.97	

ANEXO 4

MÉTODOS DE ANÁLISES QUÍMICOS DE ROCHA TOTAL

METHODS AND SPECIFICATIONS FOR ANALYTICAL PACKAGE

GROUP 4A - WHOLE ROCK ANALYSIS BY ICP-ES



Comments

Sample Preparation

All samples are dried at 60°C. Soil and sediment are sieved to -80 mesh (-177 µm). Moss-mats are disaggregated then sieved to yield -80 mesh material. Vegetation is pulverized or ashed (475°C). Rock and drill core is jaw crushed to 70% passing 10 mesh (2 mm), a 250 g riffle split is then pulverized to 95% passing 150 mesh (100 µm) in a mild-steel ring-and-puck mill.

Sample Digestion

A 0.2 g sample aliquot is weighed into a graphite crucible and mixed with 1.5 g of LiBO₂ flux. The flux/sample charge is heated in a muffle furnace for 15 minutes at 1050°C. The molten mixture is removed and immediately poured into 100 mL of 5% HNO₃ (ACS grade nitric acid in de-mineralised water). The solution is shaken for 2 hours then an aliquot is poured into a polypropylene test tube. Calibration standards, verification standards and reagent blanks are added to the sample sequence.

Sample Analysis

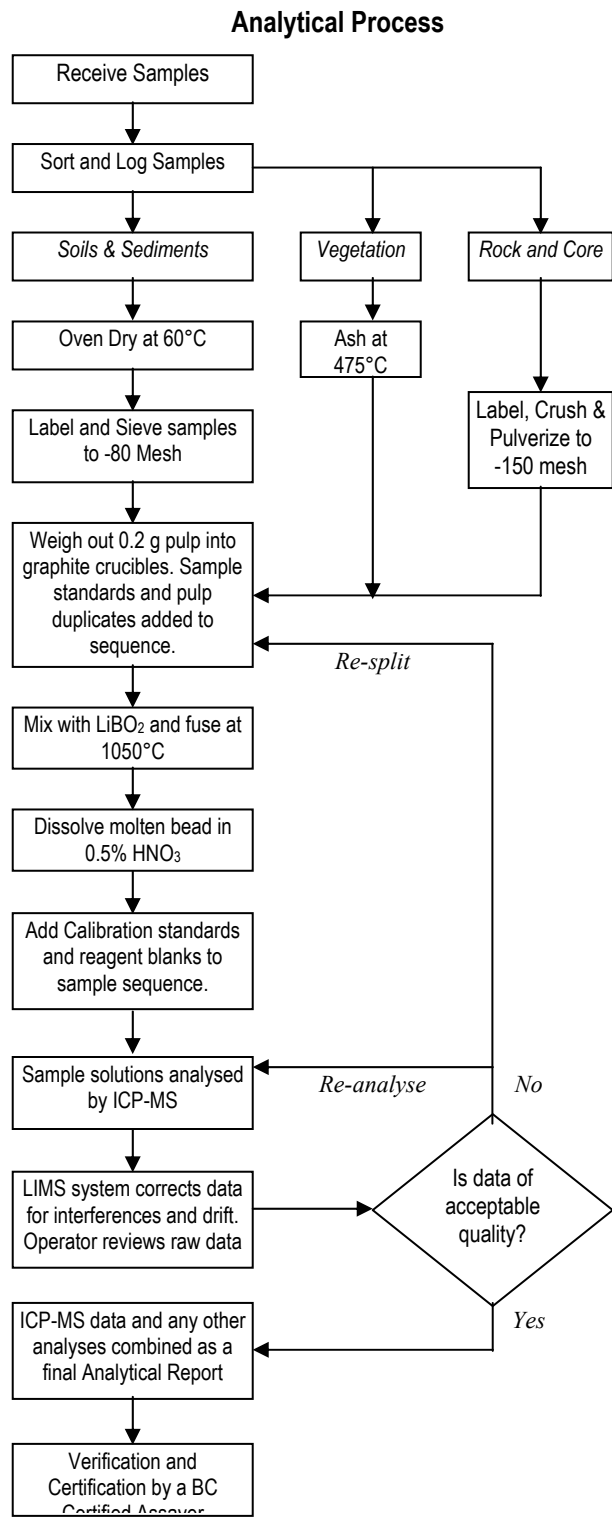
Sample solutions are aspirated into an ICP emission spectrometer (Jarrel Ash Atomcomp Model 975) for the determination of the basic package consisting of the following 18 major oxides and elements: SiO₂, Al₂O₃, Fe₂O₃, CaO, MgO, Na₂O, K₂O, MnO, TiO₂, P₂O₅, Cr₂O₃, Ba, Ni, Sr, Sc, Y and Zr. The extended package will also include: Ce, Co, Cu, Ta and Zn. A 1 g sample split is ignited for 90 minutes at 950°C, cooled in a desiccator then weighed with the difference expressed as percent Loss on Ignition (% LOI). A 0.1 g sample split is analysed for total Carbon and Sulphur by the LECO method.

Quality Control and Data Verification

An Analytical Batch (1 page) comprises 31 samples. QA/QC protocol incorporates a sample-prep blank (SI or G-1) carried through all stages of preparation and analysis as the first sample, a pulp duplicate to monitor analytical precision, a -10 mesh rejects duplicate to monitor sub-sampling variation (drill core only), two reagent blanks to measure background and aliquots of in-house Standard Reference Materials like STD SO-17 to monitor accuracy. STD SO-17 was certified in-house against 38 Certified Reference Materials including CANMET SY-4 and USGS AGV-1, G-2, GSP-2 and W-2.

Raw and final data undergo a final verification by a British Columbia Certified Assayer who signs the Analytical Report before it is released to the client. Chief Assayer is Clarence Leong, other certified assayers are Dean Toye, Jacky Wang and Ken Kwock.

METHODS AND SPECIFICATIONS FOR ANALYTICAL PACKAGE GROUP 4B - WHOLE ROCK TRACE ELEMENTS BY ICP-MS



Comments

Sample Preparation

All samples are dried at 60°C. Soil and sediment are sieved to -80 mesh (-177 µm). Moss-mats are disaggregated then sieved to yield -80 mesh sediment. Vegetation is pulverized or ashed (475°C). Rock and drill core is jaw crushed to 70% passing 10 mesh (2 mm), a 250 g riffle split is then pulverized to 95% passing 150 mesh (100 µm) in a mild-steel ring-and-puck mill.

Sample Digestion

A 0.2 g sample aliquot is weighed into a graphite crucible and mixed with 1.5 g of LiBO₂ flux. The flux/sample charge is heated in a muffle furnace for 15 minutes at 1050°C. The molten mixture is removed and immediately poured into 100 mL of 5% HNO₃ (ACS grade nitric acid in de-mineralised water). The solution is shaken for 2 hours then an aliquot is poured into a polypropylene test tube. Calibration standards, verification standards and reagent blanks are added to the sample sequence.

Sample Analysis

Sample solutions are aspirated into an ICP mass spectrometer (Perkin-Elmer Elan 6000) for the determination of the basic package consisting of the following 34 elements: Ba, Co, Cs, Ga, Hf, Nb, Rb, Sn, Sr, Ta, Th, Tl, U, V, W, Y, Zr, La, Ce, Pr, Nd, Sm, Eu, Gd, Tb, Dy, Ho, Er, Tm, Yb and Lu. A second sample split of 0.5 g is digested in Aqua Regia and analysed by ICP-MS (see Group 1DX) to determine: Au, Ag, As, Bi, Cd, Cu, Hg, Mo, Ni, Pb, Sb, Se, Tl and Zn.

Quality Control and Data Verification

An Analytical Batch (1 page) comprises 31 samples. QA/QC protocol incorporates a sample-prep blank (SI or G-1) carried through all stages of preparation and analysis as the first sample, a pulp duplicate to monitor analytical precision, a -10 mesh rejects duplicate to monitor sub-sampling variation (drill core only), two reagent blanks to measure background and aliquots of in-house Standard Reference Materials like STD SO-17 to monitor accuracy. STD SO-17 was certified in-house against 38 Certified Reference Materials including CANMET SY-4 and USGS AGV-1, G-2, GSP-2 and W-2.

Raw and final data undergo a final verification by a British Columbia Certified Assayer who signs the Analytical Report before it is released to the client. Chief Assayer is Clarence Leong, other certified assayers are Dean Toye, Jacky Wang and Ken Kwock.

LIMITES DE DETECÇÃO PARA OS MÉTODOS 4A e 4B.

	Group 4A	Group 4B	Upper limit
SiO ₂	0.04%	-	100%
Al ₂ O ₃	0.03	-	100%
Fe ₂ O ₃	0.04	-	100%
CaO	0.01	-	100%
MgO	0.01	-	100%
Na ₂ O	0.01	-	100%
K ₂ O	0.04	-	100%
MnO	0.01	-	100%
TiO ₂	0.01	-	100%
P ₂ O ₅	0.01	-	100%
Cr ₂ O ₃	0.001	-	100%
LOI	0.1	-	100%
C	0.01	-	100%
S	0.01%	-	100%
Au	-	0.5 ppb	100 ppm
Ag	-	0.1 ppm	100 ppm
As	-	1 ppm	10000 ppm
Ba	5 ppm	0.5 ppm	50000 ppm
Be	-	1 ppm	10000 ppm
Bi	-	0.1ppm	2000 ppm
Cd	-	0.1ppm	2000 ppm
Co	20 ppm*	0.5 ppm	10000 ppm
Cs	-	0.1 ppm	10000 ppm
Cu	20 ppm*	0.1ppm	10000 ppm
Ga	-	0.5 ppm	10000 ppm
Hf	-	0.5 ppm	10000 ppm
Hg	-	0.1 ppm	100 ppm
Mo	-	0.1 ppm	2000 ppm
Nb	20 ppm*	0.5 ppm	50000 ppm
Ni	20 ppm	0.1 ppm	10000 ppm

	Group 4A	Group 4B	Upper limit
Pb	-	0.1 ppm	10000 ppm
Rb	-	0.5 ppm	10000 ppm
Sb	-	0.1 ppm	2000 ppm
Sc	1 ppm	-	10000 ppm
Se	-	0.5 ppm	100 ppm
Sn	-	1 ppm	10000 ppm
Sr	10 ppm	0.5 ppm	50000 ppm
Ta	20 ppm*	0.1 ppm	50000 ppm
Th	-	0.1 ppm	10000 ppm
Tl	-	0.1 ppm	1000 ppm
U	-	0.1 ppm	10000 ppm
V	-	5 ppm	10000 ppm
W	-	0.1 ppm	10000 ppm
Y	10 ppm	0.1 ppm	50000 ppm
Zn	20 ppm*	1 ppm	10000 ppm
Zr	10 ppm	0.5 ppm	50000 ppm
La	-	0.5 ppm	50000 ppm
Ce	20 ppm*	0.5 ppm	50000 ppm
Pr	-	0.02 ppm	10000 ppm
Nd	-	0.4 ppm	10000 ppm
Sm	-	0.1 ppm	10000 ppm
Eu	-	0.05 ppm	10000 ppm
Gd	-	0.05 ppm	10000 ppm
Tb	-	0.01 ppm	10000 ppm
Dy	-	0.05 ppm	10000 ppm
Ho	-	0.05 ppm	10000 ppm
Er	-	0.05 ppm	10000 ppm
Tm	-	0.05 ppm	10000 ppm
Yb	-	0.05 ppm	10000 ppm
Lu	-	0.01 ppm	10000 ppm